Homogeneous Cr- and Co-mediated Selective Olefin Oligomerisation Catalysis

JASPREET KAUR SANGHERA

Homogeneous Cr- and Co-mediated Selective Olefin Oligomerisation Catalysis

Department of Chemistry, Durham University

Thesis submitted for the Degree of Doctor of Philosophy

By

Jaspreet Kaur Sanghera, M.Chem. (Dunelm)

January 2018

Statement of Originality

This thesis is based on work conducted by the author, in the Department of Chemistry at Durham University, during the period October 2013 to December 2017. All the work described in this thesis is original, unless otherwise acknowledged in the text or in the references. None of this work has been submitted for another degree in this or any other University.

Signed: 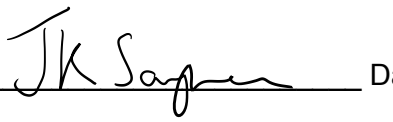 Date: 30/01/18

Dedication

This thesis is dedicated to my dear grandfather (Papa Ji), Bhajan Singh Sanghera. Papa Ji, you're my inspiration in everything that I do.

Abstract

This thesis investigates use of Cr/phosphanyl methanimine ligand (PCN, $Ph(PR_2)C{=}NAr$, R = alkyl group) combinations in selective ethylene *tri*-/*tetra*-merisation catalysis. Additionally, the use of the previously-reported linear α-olefin (LAO) dimerisation catalyst precursor $Cp^*Co(C_2H_4)P(OMe)_3$ (**4.5**) is further explored in 1-butene and 1-hexene dimerisation, in attempts to improve its reported low TON and low selectivity.

In Chapter 2 a description of the synthesis of variously-substituted PCN ligands **2.1**–**2.17** is given. A study of the coordination chemistry of a selection of these PCN ligands to Cr^0 revealed that both *mono*-(κ^1-P) and *bi*-dentate (κ^2-P,N) $[Cr(CO)_{4/5}(PCN)]$ complexes **2.18**–**2.19** and **2.22**-**2.25** were obtained, with the ratio of $[Cr(CO)_5(\kappa^1\text{-P-PCN})]$:$[Cr(CO)_4(\kappa^2\text{-P,N-PCN})]$ complexes present in the crude reaction mixtures being influenced by the steric bulk of the nitrogen substituent of the PCN ligand and reaction conditions. Cationic Cr^I-PCN complexes $[Cr(CO)_{4/5}(\kappa^1\text{-P or }\kappa^2\text{-P,N-PCN})]$ **2.26**–**2.30** and **2.32** were obtained *via* one-electron oxidation reactions of the corresponding Cr^0-PCN complexes with $Ag[Al\{OC(CF_3)_3\}_4]$. The synthesis of Cr^{III}-PCN complexes $[CrCl_3(THF)(\kappa^2\text{-P,N-PCN})]$ **2.34**-**2.37** was attempted, but proved successful only in two cases, complexes **2.36** and **2.37**.

Chapter 3 details the ethylene oligomerisation catalysis behaviour of the Cr^I and Cr^{III}-PCN complexes. In all cases, Cr^{III}/PCN-based ethylene *tri*-/*tetra*-merisation systems with high activities and selectivities were obtained, with the 1-octene:1-hexene ratios of these systems being influenced by the electronic properties of the phosphorus donor moiety and imine carbon substituents of the PCN ligands. The Cr^I-PCN complexes yielded low activity ethylene polymerisation systems; their poor performance is attributed to poisoning from CO liberated during reactions. It was found that using *in situ versus* preformed Cr^{III}-PCN complexes in ethylene oligomerisation catalysis improved the activities and selectivities towards 1-hexene and 1-octene production.

In Chapter 4, the effect of varying different solvents, temperatures, and activation methods in 1-butene/1-hexene dimerisation catalysis mediated by complex **4.5**/Brookhart's acid was assessed. In addition, complexes **4.15** and **4.16** (modified versions of complex **4.5**) were synthesised and found to perform worse in 1-butene/1-hexene dimerisation catalysis than complex **4.5** (in terms of activity and selectivity towards desired LAO dimer).

Chapters 5 and 6 describe all experimental data and supporting information.

Acknowledgments

Firstly I would like to thank my supervisor, Dr. Phil Dyer, for his constant support, encouragement, guidance and patience over the last four years. None of the work in this thesis would have been possible without him and it's been a pleasure to be able to work for him.

A big thanks must also go to Dr. Martin Hanton for taking time out of his busy schedule to help with the catalytic testing carried out at Sasol. In addition, I would like to thank David and John for all of their help with the catalytic testing at Sasol.

Thank you to the analytical services at Durham Chemistry Department, in particular the NMR services team (Dr. Alan Kenwright, Dr. Juan Aguilar Malavia, Ms Catherine Heffernan and Ms Raquel Belda-Vidal) and Dr. Andrei Bastanov for collecting the majority of the crystal data. The glassblowers within the Durham Chemistry Department, Aaron Brown and Malcolm Richardson, must also be thanked for fixing the multiple pieces of glassware that were broken during the "smashing" time I had in the lab. In addition, the EPSRC and Sasol are thanked for their funding which has enabled me to undertake this work.

During my PhD I've been fortunate enough to work alongside a long list of great masters students, PhD students, and post-docs in the Dyer group: Ben, Li Li, Dominikus, Luke, James, Jack, Anna, Michael L, Michael H, Stephen, Claire, Flora, Billy, Alex, and Sarah to name a few! Thank you all for your help, support and friendship over the last four years. Special thanks to James (not only for laying the groundwork for the PCN work, but for teaching me air-sensitive chemistry when I first started) and Stephen (for being my lab buddy on multiple occasions).

To Ben, Anna, Li Li, Beth, Sarah and Alex, thanks for all of the hot chocolates, laughs and sanity checks. Without your constant support and encouragement I wouldn't have made it through this PhD and am so grateful to have you in my life.

To my family, I don't think there are enough words to express my gratitude. Mum and Dad, without your hard work, support and encouragement I would never have been able to go to university, let alone do a PhD! Thank you for always being there, for your understanding and patience- I will forever be indebted to you. Raman, thank you for

being my biggest cheerleader. I never would have done this if it wasn't for the confidence you've always had in me. Bhabi, thanks for all the chats, all the meals (when I would finish work late), and most importantly of all for giving me a much-needed reminder of life outside of the PhD! Lastly, but by no means least, to my beautiful niece Ishneet thank you for all the smiles and cuddles which have helped me make it through to the end.

Table of Contents

Chapter 4: Investigating the Catalytic Dimerisation of Linear α-olefins to Yield Linear α-olefins

List of Abbreviations

General Abbreviations

acac	Acetylacetone
Ar	Aryl
ASAP	Atmospheric Solid Analysis Probe
BAO	Branched Alpha Olefin
b.p.	Boiling point
BP	British Petroleum
Bu	Butyl
°C	Degrees Celsius
CGC	Constrained geometry-type complex
COSHH	Control of Substances Hazardous to Health
Cp	Cyclopentadienyl
Cp*	Pentamethylcyclopentadienyl
Cy	Cyclohexyl
Cypent	Cyclopentyl
DCM	Dichloromethane
DMAO	TMA-depleted MAO
DME	1,2-Dimethoxyethane
DSC	Differential Scanning Calorimetry
2-EH	2-ethylhexanoate
EPR	Electron Paramagnetic Resonance
equiv.	Equivalent(s)
ESI	Electrospray ionisation
Et	Ethyl
Et_2O	Diethyl ether
FA	Fold Angle
FID	Free Induction Decay
Flu	Fluorenyl
GC	Gas Chromatography
GC-FID	Gas Chromatography-Flame Ionisation Detection
GC-MS	Gas Chromatography-Mass Spectrometry
GPC	Gel Permeation Chromatography
h	Hour(s)

HA	Hinge Angle
$HBAr_F^4$	Brookhart's acid
HDPE	High-density Polyethylene
HOMO	Highest Occupied Molecular Orbital
HTFT	High-temperature Fischer-Tropsch
Hz	Hertz
^{i}Bu	*iso*-Butyl
Ind	Indenyl
^{i}Pr	*iso*-Propyl
IR	Infra-Red
κ	Denticity
K	Kelvin
kcal	Kilocalorie
L	Generic 2 electron donor ligand
L_2X	Generic 5 electron donor ligand
LAO	Linear Alpha Olefin
LIO	Linear Internal Olefin
LLDPE	Linear Low-density Polyethylene
LTFT	Low-temperature Fischer-Tropsch
LUMO	Lowest Unoccupied Molecular Orbital
M	Generic Transition Metal (unless otherwise stated)
m-	*meta*-
Δ_{M-C}	Slip angle
m/*z*	Mass/charge ratio
MAO	Methylaluminoxane
Me	Methyl
MeCN	Acetonitrile
mL	Millilitre
MMAO	Modified methylaluminoxane
MMAO-3A	Modified methylaluminoxane, type 3A
mol	Mole
mmol	Millimole
MS	Mass Spectrometry
η	Hapticity
NMR	Nuclear Magnetic Resonance
o-	*ortho*-

OAc	Acetoxy
ORTEP	Oak Ridge Thermal Ellipsoid Plot
OTH	1-octene:1-hexene ratio
p-	*para*-
PCN	1-Phosphanyl methanimine
PE	Polyethylene
Ph	Phenyl
PIBAO	Partially Hydrolysed Tri-isobutylaluminium
PONA	Paraffins, Olefins, Naphthalenes and Aromatics
ppm	Parts per million
Py	Pyridyl
R	Generic alkyl or aryl group
RA	Rotation Angle
RSD %	Relative Standard Deviation as a % of the mean
RT	Room Temperature
SHOP	Shell Higher Olefins Process
T	Temperature
^{t}Bu	*tert*-Butyl
TEA	Triethylaluminium
THF	Tetrahydrofuran
TM	Transition Metal
TMA	Trimethylaluminium
TMS	Trimethylsilyl
TOF	Turn Over Frequency
TON	Turn Over Number
μ	Bridging ligand
μ_{eff}	Effective Magnetic Moment
UCC	Union Carbide Corporation
v	Absorbance
$\%V_{bur}$	Percentage buried volume
wt	Weight
XAS	X-ray Absorption Spectroscopy
XRD	X-ray Diffraction

NMR Spectroscopy Abbreviations

b	broad signal
COSY	Correlated Spectroscopy
δ	Chemical Shift (in ppm)
d	doublet
dd	doublet of doublets
dh	doublet of heptets
h	heptet
HMBC	Heteronuclear Multiple-bond Correlation
HSQC	Heteronuclear Single Quantum Coherence
J	Coupling constant
lb	Line broadening
m	multiplet
q	quartet
s	singlet
t	triplet
vbr	very broad signal
$v_{1/2}$	peak width at half-height

Chapter 1:
Introduction

The work in this thesis, which has been carried out in collaboration with Sasol Technology UK Ltd., details investigations into the synthesis and testing of catalyst precursors for the production of linear α-olefins (LAOs), in particular 1-hexene and 1-octene, by selective ethylene *tri-*/*tetra*-merisation catalysis and selective LAO dimerisation catalysis. This Chapter describes the literature precedent behind the work conducted in this thesis.

1.1. Commercial Importance of Linear α-Olefins (LAOs)

LAOs are unbranched hydrocarbons containing a terminal carbon-carbon double bond, with the general formula C_nH_{2n}. The demand for LAO materials is high (evidenced from the 8.26 billion dollar valuation of the global LAOs market size in 2016),[1] largely due to their use as commodity chemicals in a variety of applications as illustrated in Figure 1.1.

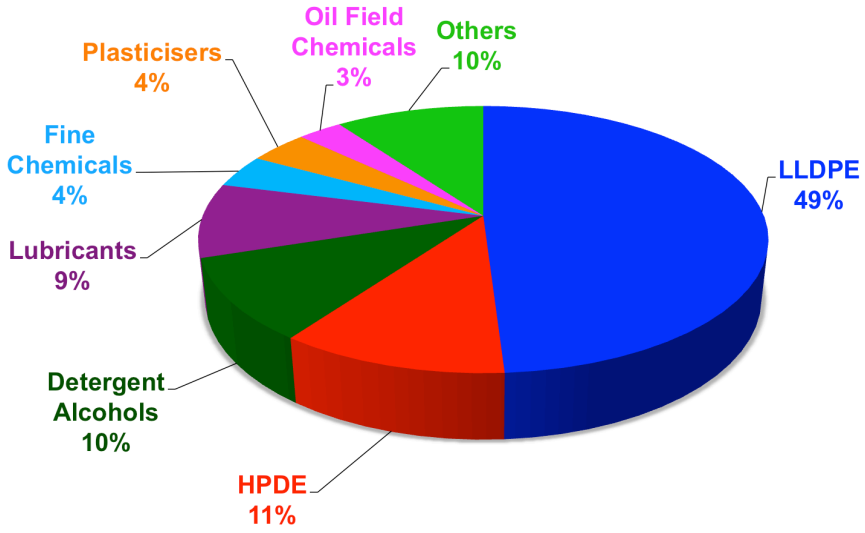

Figure 1.1: Commercial applications of LAOs, modified from Thammanayakatip 2017, where LLDPE = linear low-density polyethylene and HDPE = high-density polyethylene.[2]

The diverse range of applications of LAOs (Figure 1.1) is a function of the availability of different LAO chain lengths, since the number of carbons dictates their physical properties. Table 1.1 outlines the specific commercial applications corresponding to particular chain lengths of LAOs.

Table 1.1: Commercial applications of LAOs by chain length, modified from Breuil *et al.,* 2015.[3]

LAO chain length	Commercial application
C_4-C_8	Comonomers for the production of LLDPE and HDPE
C_6-C_{10}	Plasticiser alcohols
C_{10}-C_{20}	Surfactants/ Detergent alcohols
C_{14+}	Synthetic lubricants

As is evident from the data in Figure 1.1, the largest global applications of LAOs are as co-monomers in the production of linear low-density polyethylene (LLDPE) and high-density polyethylene (HDPE). Different amounts of 1-C_4, 1-C_6, and 1-C_8 are incorporated as co-monomers in HDPE and LLDPE; the former uses 2 – 4 % of co-monomer, the latter 8 – 10 %.[3] The widespread applications of LLDPE (commonly used for the manufacture of food packaging, toys, and wire and cable insulation) and HDPE (frequently used to make pipes, bottles and chemical containers) has resulted in a lucrative market for these materials, with global consumption of LLDPE of 30 million tons and that of HDPE, being 40 million tons in 2016.[2,4] Although 1-butene is the most used co-monomer in the formation of LLDPE (and to a lesser extent in HDPE), the use of 1-hexene and 1-octene as co-monomers is growing fast due to the superior properties of the resultant ethylene copolymers.[3] For example, employing 1-hexene in the formation of LLDPE generates a tougher and thinner film, which is more desirable for packaging applications than that produced through incorporation of 1-butene.[3] As a result, the high demand and popularity of 1-hexene and 1-octene as co-monomers for LLDPE and HDPE manufacture, means that the synthesis of these specific LAOs is of particular interest to industry.

1.2. Commercial Synthesis of LAOs

The synthesis of LAOs can be achieved through a variety of different routes, such as cracking and dehydrogenation of alkanes, dehydration of alcohols, ethylene oligomerisation, and from CO and H_2 *via* the Fischer-Tropsch process.[5] Since the latter two routes are the most commonly used commercially,[6] these will be considered in further detail in the next sections.

1.2.1. Ethylene oligomerisation processes

Shell, Ineos, and Chevron Phillips are currently the three major global suppliers of LAOs *via* ethylene oligomerisation.[1] These three companies use different catalysts and conditions (details summarized in Table 1.2) to transform ethylene into a mathematical distribution of LAOs ranging from C_4 to C_{30+} (the product distribution is considered in further detail in section 1.2.3), in addition to forming small amounts of internal olefins, alkanes and branched olefin side products.[7] Of the three ethylene oligomerisation processes listed in Table 1.2, the Shell Higher Olefins Process (SHOP) produces the greatest amount of LAOs (94 - 99 %, with greatest purity in the 1-hexene fraction).[7]

Table 1.2: Comparison of catalysts and process conditions in commercial ethylene oligomerisation processes, modified from Forestière *et al.*, 2009.[8]

Company	Process name	Catalyst	Process details
Chevron Phillips	Gulfene	$AlEt_3$ catalyst	• 175 – 290 °C, 2000 – 4000 psi ethylene • One-step process (same pot growth and termination steps)
Ineos	Ethyl	$AlEt_3$ catalyst	• 116 – 316 °C, 230 – 3,000 psi ethylene • Two-step process (separated growth and termination steps)
Shell	Shell Higher Olefins Process (SHOP)	Ni complex, *e.g.* 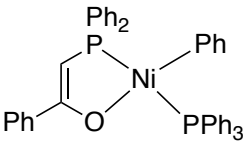 	• 80 – 120 °C, 1000 – 2,000 psi ethylene • Following ethylene oligomerisation, α-olefins of chain lengths $<C_{10}$ and $>C_{18}$ subjected to successive isomerisation and metathesis reactions to produce C_{10}-C_{18} linear internal olefins (to meet high demand of these materials in detergent applications).

(Space left blank intentionally)

The formation of LAOs *via* ethylene oligomerisation is believed to occur by the Cossee-Arlman mechanism, a simplified representation of which is shown in Scheme 1.1. [3,5] The first step of this mechanism involves coordination of ethylene to a vacant site on the metal centre, which is then followed by migratory insertion of ethylene into the metal-carbon bond.[5,9] Propagation of the growing LAO chain then occurs by sequential coordination and insertion (into the newly formed metal-carbon bond) of n ethylene molecules.[5,9] The free LAO chain is finally liberated in a termination step *via* β-hydride elimination (when a metal hydride is starting complex in Scheme 1.1) or β-hydride transfer between the growing LAO chain and ethylene monomer (when a metal alkyl is starting complex in Scheme 1.1); this regenerates the starting metal complex.[5,9] The rates of propagation and termination, which are influenced by the process conditions in ethylene oligomerisation (factors such as solvent, temperature, pressure, metal oxidation state, and nature of ligands on the metal), dictate the length of the LAO chain formed.[9] When the rate of termination is greater than that of propagation a dimer will form, while a polymer will be produced when a converse relation of the rates of termination and propagation is operative, and an oligomer will be generated in instances when similar rates of termination and propagation are exhibited.[9]

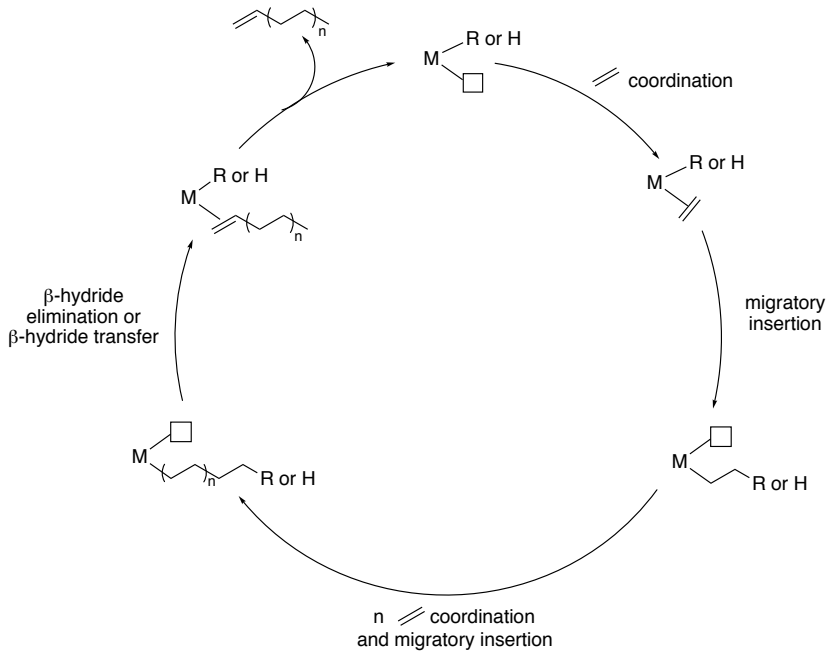

M = metal, R= alkyl group, □ = vacant coordination site

Scheme 1.1: Simplified version of Cossee-Arlman mechanism of ethylene oligomerisation, modified from Skupinska, 1991.[9]

1.2.2. Fischer-Tropsch process

Franz Fischer, Hans Tropsch and Helmut Pichler pioneered the Fischer-Tropsch Process in 1923.[10] Since then, the Fischer-Tropsch Process has evolved into one of

great commercial importance with the current global commercial operation of eight Fischer-Tropsch synthesis plants.[11] Sasol is currently the world-leading operator of the Fischer-Tropsch technology, running the largest Fischer-Tropsch plant with a capacity of 150,000 barrels per day.[12]

The Fischer-Tropsch process involves the catalytic conversion of syngas (a mixture of CO and H_2 generally obtained from reforming of natural gas, gasification of coal, or biomass) into a mixture of hydrocarbons (alkenes, alkanes and oxygenates).[11,13] The formation of the main hydrocarbon products obtained *via* the Fischer-Tropsch process, linear alkenes and alkanes, can simplistically be represented by Equations 1.1 and 1.2.[11,13] In contrast to ethylene oligomerisation that produces only even numbered olefins from a C_2 starting material, Fischer-Tropsch synthesis yields both odd- and even-numbered olefins due to the use of a C_1 starting material, namely CO.

$$2nH_2 + nCO \longrightarrow C_nH_{2n} + nH_2O$$

Equation 1.1: Conversion of syngas to alkenes *via* Fischer-Tropsch process.[11,13]

$$(2n + 1)H_2 + nCO \longrightarrow C_nH_{(2n+2)} + nH_2O$$

Equation 1.2: Conversion of syngas to alkanes *via* Fischer-Tropsch process.[11,13]

The Fischer-Tropsch process is industrially operated with heterogeneous Fe- or Co-based catalysts at high pressures (20 – 45 bar) and two different temperature ranges of 320 - 375 °C (classified as high temperature Fischer-Tropsch, HTFT) or 200 – 250 °C (classified as low temperature Fischer-Tropsch, LTFT).[13] The reaction conditions of the Fischer-Tropsch process, such as catalyst and temperature, dictate the product distribution, *e.g.* Fe-catalysed HTFT typically yields larger amounts of linear short-chained olefins (C_3 – C_{11}) than Fe- or Co-catalysed LFTF, which mainly produce waxes (C_{20+}).[13]

In spite of the Fischer-Tropsch process being a well-known and established industrial technology, even today its mechanism is still a matter of debate. The Fischer-Tropsch process is a surface chemistry reaction which is widely recognized to proceed via the general reaction sequence of: reactant adsorption – chain initiation – chain growth – product desorption – re-adsorption of reactive products and further reaction.[11,13] The main area of uncertainty lies within the nature of the monomers and chain initiators (different monomers proposed to be surface bound CH_2, enol or CO species), which impact the process of chain growth.[11,13] Nevertheless, Fischer-Tropsch is largely believed to operate by a dual mechanism, which consists of two incompatible

pathways (dissociative and associative routes).[13,14] For the Fe-catalysed Fischer-Tropsch process it has been proposed that the dissociative mechanism dominates at higher pressures of hydrogen, while the associative mechanism is prominent at higher pressures of CO.[14] The dissociative mechanism (Scheme 1.2) begins with dissociative chemisorption of CO and H_2, resulting in the formation of surface-bound {C}, {O} and {H} species.[13-15] The surface {O} and {H} species react to form water, while the surface {C} and {H} species react to generate methylene monomer species (CH_2), which subsequently undergo hydrogenation to yield {CH_3} moieties (the chain initiators).[13-15] Chain growth and propagation then proceed *via* consecutive incorporation of the {CH_2} surface species into the metal alkyl bond.[13-15] Finally, the major products of LAOs and linear alkanes are obtained by chain termination *via* β-hydride elimination or reduction of the growing alkyl chain with a surface hydride (as shown in Scheme 1.2).[13-15]

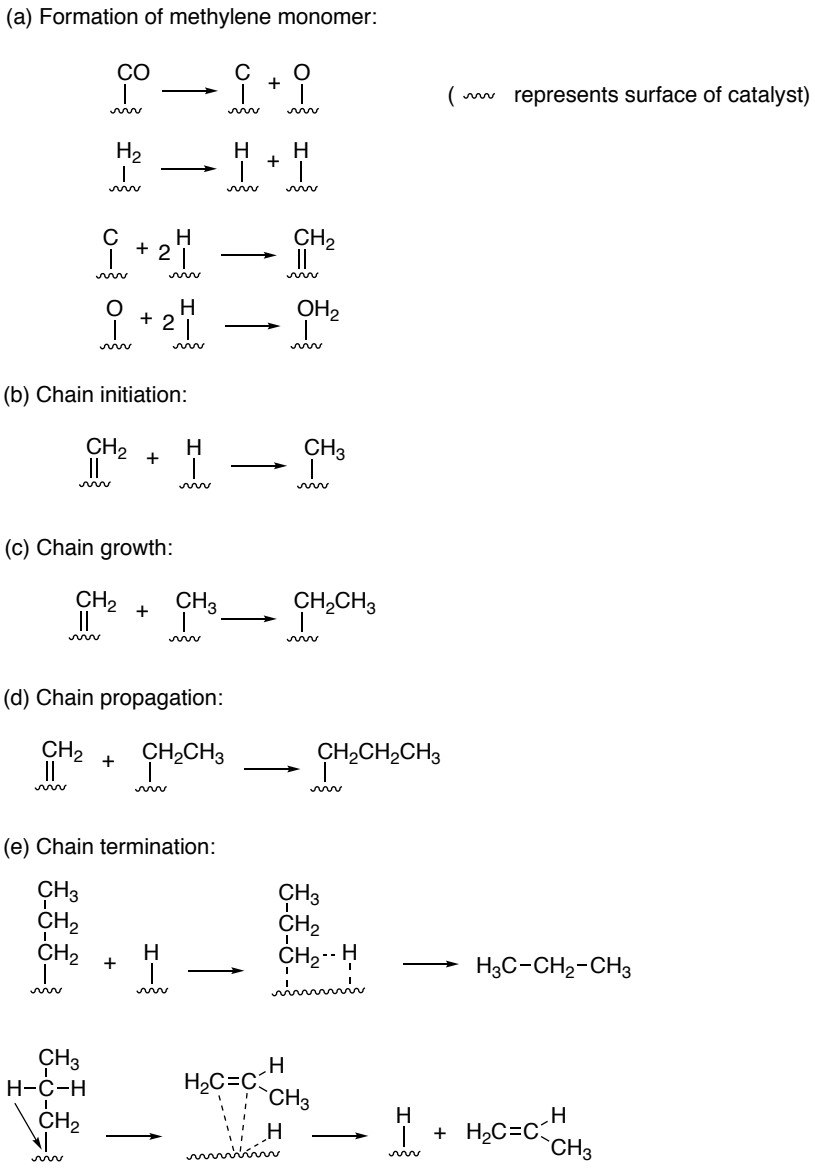

Scheme 1.2: Dissociative mechanism for the formation of LAOs and linear alkanes in Fischer Tropsch process, modified from Fontenelle *et al*., 2011.[15]

In contrast to the dissociative mechanism (Scheme 1.2), following chemisorption of CO and H_2, only H_2 undergoes dissociation in the associative pathway (Scheme 1.3).[13,14] Chain initiation then occurs by reactions between only surface-bound {CO} and {H}, resulting in the formation of $\{CH_3\}$.[13,14] Although the associative mechanism involves the same initiator species ($\{CH_3\}$) as its dissociative counterpart, the processes of chain growth and propagation are thought to proceed in a different manner *via* successive incorporation reactions of the {CO} surface species into the metal alkyl bond.[13,14] The last step of termination, yielding the major products of LAOs and linear alkanes, occurs in an analogous manner to that described for the dissociative mechanism.[13,14]

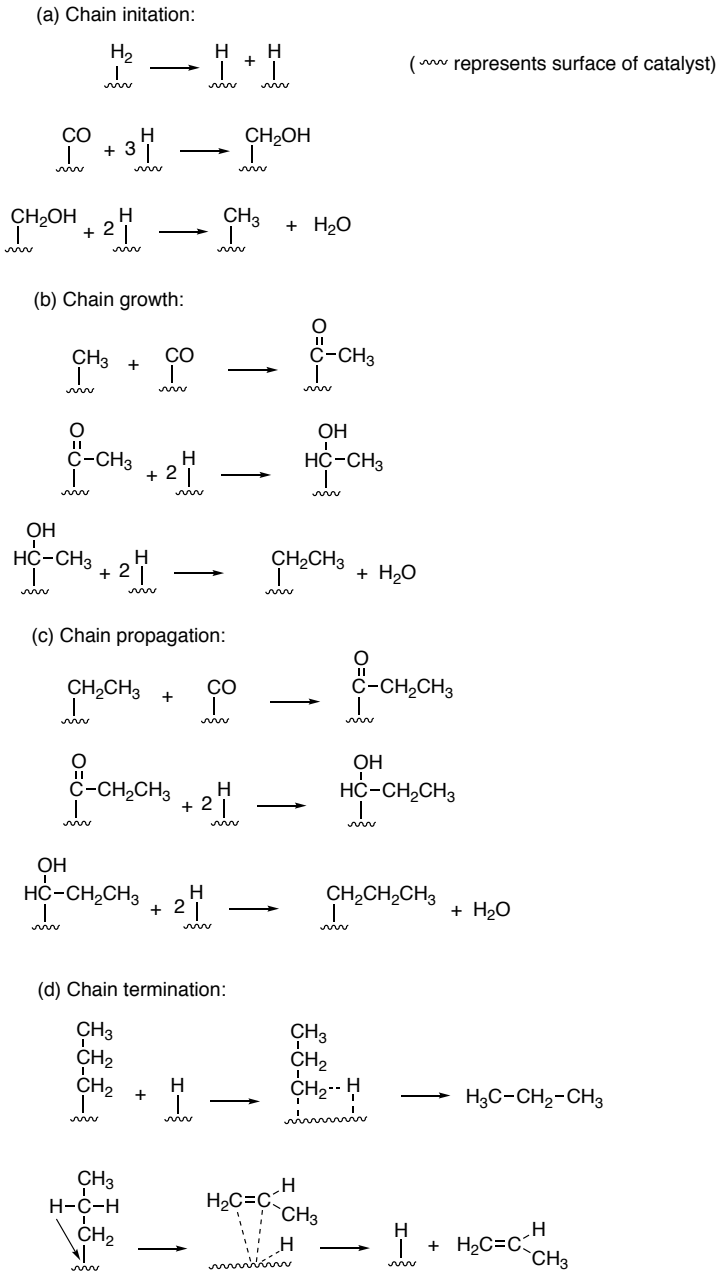

Scheme 1.3: Associative mechanism for the formation of LAOs and linear alkanes in Fischer Tropsch process, modified from Greener Fischer-Tropsch Processes for Fuels and Feedstocks, 2013.[13]

1.2.3. Consideration of LAO chain length distribution formed *via* ethylene oligomerisation and Fischer-Tropsch processes

The ethylene oligomerisation and Fischer-Tropsch processes described in sections 1.2.1 and 1.2.2, respectively, both produce a mathematical distribution of LAO products.[7,16] Specifically, a Schulz-Flory (also referred to as Anderson-Schulz-Flory) distribution of products is obtained via the Fischer-Tropsch and ethylene oligomerisation processes by Chevron Phillips and Shell, whilst a Poisson distribution is obtained for the Ineos ethylene oligomerisation process.[7,16] The Schulz-Flory distribution is an exponential decay function, which takes the form shown in Equation 1.3.[17,18] The most probable weight fraction distribution given in Equation 1.3 is derived on the basis that in the Fischer-Tropsch and Chevron Phillips/Shell's ethylene oligomerisation processes, following each consecutive insertion of the C_n unit into the growing hydrocarbon chain (with length n), there is the probability of chain propagation (α) or chain termination ($1 - \alpha$) occurring.[17,18] The form of Equation 1.3 implies that shorter chain length products are favoured over longer chain species, in line with the typical distribution of LAOs obtained via the Sasol operated Fischer-Tropsch process, displayed in Graph 1.1.[17,18]

$$W_n = n(1-\alpha)^2\alpha^{n-1}$$

Equation 1.3: Schulz-Flory most probable weight fraction distribution (W_n), where n = length of LAO chain, α = probability of propagation, and 1- α = probability of termination; modified from Flory *et al.*, 1936.[18]

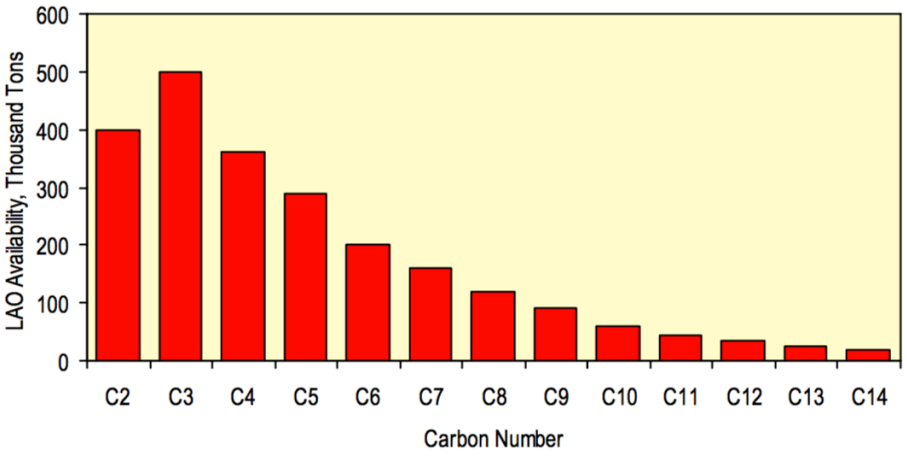

Graph 1.1: Schulz-Flory distribution of LAOs obtained *via* Sasol-operated Fischer-Tropsch process, figure modified from Nexant Chem Systems, PERP Report: Alpha Olefins, 2008.[19]

For the Ineos ethylene oligomerisation process it is argued that for alkyl groups possessing ≥2 carbon atoms, the length of the alkyl chain has little influence on the reactivity of the alkylaluminium bond towards ethylene.[20] Consequently, when the ethylene molecule is surrounded by a mixture of aluminium alkyls, the aluminium alkyl bond that reacts with ethylene is dictated by the Poisson statistical distribution given in

Equation 1.4.[20] In contrast to the Schulz-Flory distribution, the Poisson distribution exhibits a greater selectivity towards C_6 - C_{10} LAO products (evident upon comparing Graphs 1.1 and 1.2).

$$X_{(P)} = \frac{N^P e^{-N}}{P!}$$

Equation 1.4: Poisson statistical distribution for Ineos ethylene oligomerisation process, where $X_{(P)}$ = mole fraction of alkyl groups containing *P*-added ethylene groups and *N* = average moles of ethylene reacted (by growth reaction) per equivalent of alkylaluminium bonds; modified from Process Economics Program Report 12E: Linear Alpha Olefins, 2008.[20]

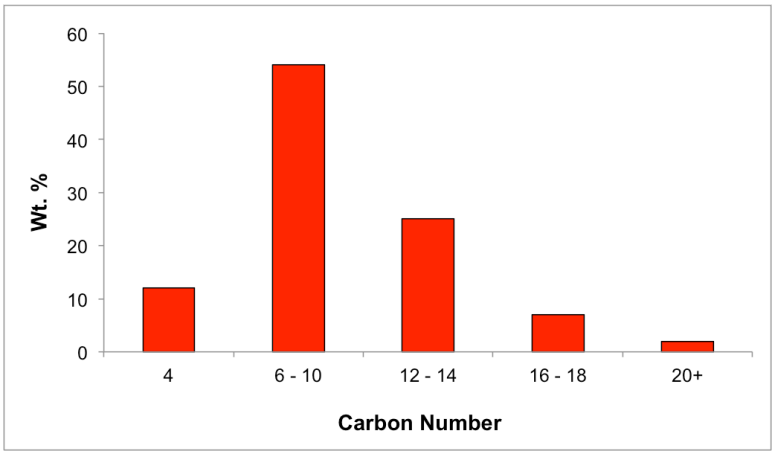

Graph 1.2: Typical Poisson distribution of LAOs obtained *via* the Ineos ethylene oligomerisation process; modified from Process Economics Program Report 12E: Linear Alpha Olefins, 2008.[20]

As a consequence of the commercial LAO synthesis processes (ethylene oligomerisation and Fischer-Tropsch) producing mixtures of LAOs, the supply of highly desirable LAO chain lengths, such as 1-hexene and 1-octene, by these methods does not match the market demand.[16] Furthermore, since a mixture of products is formed by the commercial LAO synthesis processes, costly separation techniques (such as distillation) are required to isolate 1-hexene and 1-octene as specific pure products. Thus, the continually growing demands for 1-hexene and 1-octene have sparked significant academic and industrial research into the development of selective ethylene oligomerisation processes for the synthesis of 1-hexene and 1-octene, in the last decade.[21] However, only a few commercial processes for the selective oligomerisation of ethylene to 1-hexene and/or 1-octene exist, namely those disclosed by Chevron Phillips (based on a Cr catalyst), Axens (Cr-based catalyst), and Mitsui (a Ti catalyst), in addition to Sasol's selective ethylene *tri*-/*tetra*-merisation system (based on Cr catalyst).[3]

In addition to the selective formation of 1-hexene and 1-octene by selective ethylene *tri*-/*tetra*-merisation, the dimerisation of 1-propene and 1-butene to 1-hexene and 1-

octene, respectively, would also be valuable synthetic routes. Indeed, Fischer-Tropsch processes produce large amounts of propene and 1-butene (evident from Graph 1.1), which often have restricted uses as there is a limit on the amount of short chain hydrocarbons that can be incorporated into motor gasoline.[22] Additionally, propene and 1-butene often require significant processing to upgrade their research octane numbers before becoming useful as fuels. Therefore the development of a homogeneous, transition-metal catalytic system that could selectively dimerise these underexploited, unsaturated carbon fractions into more useful 1-hexene and 1-octene would be of great economic value. Furthermore, industrial processes that are optimised to convert even-numbered olefins into commercial products cannot use the large amounts of odd-numbered olefins produced *via* Fischer-Tropsch synthesis; here, the implementation of a catalytic dimerisation system capable of converting the odd-numbered olefins to even-numbered olefins would be of great commercial value.

1.3. Thesis Aims

From the preceding sections it is evident that work still remains to be done towards the development of selective processes for the synthesis of 1-hexene and 1-octene to meet their continually growing commercial demand. In this vein, the objective of the work described in this thesis is two-fold. The first objective is to further research and develop the selective Cr/phosphanyl methanimine (PCN)-based ethylene *tri*-/*tetra*-merisation system developed previously by Dr. James Radcliffe in the Dyer group, in collaboration with Sasol (full details of this system and a brief literature review on ethylene *tri*-/*tetra*-merisation system are entailed in Chapter 2).[23,24] The second objective is to investigate the direct synthesis of LAOs, in particular 1-hexene and 1-octene, by catalytic dimerisation from their LAO monomers. In this vein, the literature system described by Broene *et al.,*[25] which dimerises 1-butene, 1-hexene and 1-octene to their respective LAO dimers using a $Cp^*Co(C_2H_4)(P(OMe)_3$ catalyst precursor and deficit of Brookhart's acid activator, will be investigated (full details of this system and a brief literature review on LAO dimerisation catalysis are entailed in Chapter 4).

Chapter 2 of this thesis details the synthesis and characterisation of novel PCN ligands for use in Cr/PCN-based ethylene *tri*-/*tetra*-merisation, in order to gain further insight into the effects of varying the C and P substituents of PCN ligands on ethylene oligomerisation catalysis. In addition, the synthesis and characterisation of novel Cr^0-PCN complexes and Cr^I-PCN complexes is outlined to obtain further understanding of the electronic properties of PCN ligands, as well as obtaining Cr^I-PCN complexes for

testing in ethylene oligomerisation catalysis. Finally, the synthesis attempts of a series of Cr^{III}-PCN complexes is reported.

In Chapter 3 the catalytic testing results of the PCN ligands, Cr^{I} and Cr^{III}-PCN complexes in ethylene oligomerisation is reported to evaluate their performance and obtain structure-activity relationships.

Finally, Chapter 4 of this thesis explores the effect(s) of varying a selection of catalysis conditions in 1-butene and 1-hexene dimerisation on the performance of Broene's catalyst precursor. Additionally, synthesis attempts of modified versions of Broene's catalyst precursor and testing of the modified catalyst precursors in 1-butene or 1-hexene dimerisation are reported, with a view to obtaining structure-activity relationships.

1.4. References

1 GVR Market Research Report "Alpha Olefin Market Analysis by Product, Application, Region, and Segment Forecasts," 2017.
2 C. Thammanayakatip, presented in Asia Petrochemical Industry Conference, 2017.
3 P. A. R. Breuil, L. Magna and H. Olivier-Bourbigou, *Catal. Lett.*, 2015, **145**, 173–192.
4 M. Chanda and S. K. Roy, *Industrial Polymers, Specialty Polymers, and Their Applications*, CRC Press, Taylor & Francis Group, Boca Raton, 2009.
5 F. Speiser, P. Braunstein and L. Saussine, *Acc. Chem. Res.*, 2005, **38**, 784–793.
6 *Sustainable Industrial Processes*, ed. F. Cavani, G. Centi, S. Perathoner and F. Trifiro, Wiley-VCH, Weinheim, 2009.
7 E. O. C. Greiner and Y. Inoguchi, CEH Marketing Research Report: Linear Alpha-Olefins, 2010**.**
8 A. Forestière, H. Olivier-Bourbigou and L. Saussine, *Oil Gas Sci. Technol.-Rev. IFP*, 2009, **64**, 649–667.
9 J. Skupinska, *Chem. Rev.*, 1991, **91**, 613–648.
10 F. Fischer and H. Tropsch, *Chem. Ber.*, 1923, **56**, 2428-2443
11 S. S. Ail and S. Dasappa, *Renew. Sust. Energ. Rev.*, 2016, **58**, 267–286.
12 R. L. Nersesian, *Energy Economics: Markets, History and Policy*, Routledge, Oxon, 2016.
13 *Greener Fischer-Tropsch Processes for Fuels and Feedstocks*, ed. P. M. Maitlis and A. de Klerk, Wiley-VCH, Germany, 2013.
14 J. Gaube and H. F. Klein, *J. Mol. Catal. A:Chem*, 2008, **283**, 60–68.
15 A. B. Fontenelle Jr. and F. A. N. Fernandes, *Chem. Eng. Technol.*, 2011, **34**, 963–971.
16 D. S. McGuinness, *Chem. Rev.*, 2011, **111**, 2321–2341.
17 G. V. Schulz, *Z. Phys. Chem. (B),* 1935, **30**, 379-398.
18 P. J. Flory, *J. Am. Chem. Soc.*, 1936, **58**, 1877–1885.
19 Nexant Chem Systems, PERP Report: Alpha Olefins, 2008.
20 Process Economics Program Report 12E: Linear Alpha Olefins, 2008
21 S. Härzschel, F. E. Kühn, A. Wöhl, W. Müller, M. H. Al-Hazmi, A. M. Alqahtani, B. H. Müller, N. Peulecke and U. Rosenthal, *Cat. Sci. Technol.*, 2015, **5**, 1678–1682.

22 A. de Klerk, *Green Chem.*, 2008, **10**, 1249–1279.
23 J. E. Radcliffe, A. S. Batsanov, D. M. Smith, J. A. Scott, P. W. Dyer and M. J. Hanton, *ACS Catal.*, 2015, **5**, 7095–7098.
24 J. E. Radcliffe, PhD Thesis, Durham University, 2015.
25 R. D. Broene, M. Brookhart, W. M. Lamanna and A. F. Volpe, *J. Am. Chem. Soc.*, 2005, **127**, 17194–17195.

Chapter 2:

Cr/Phosphanyl Methanimine (PCN) Ligand-based Ethylene *Tri*-/*Tetra*-merisation: Synthesis and Coordination Chemistry of PCN Ligands

2.1. Introduction

By way of introduction to the Cr/phosphanyl methanimine (PCN)-based selective ethylene *tri*-/*tetra*-merisation system explored in this Chapter and Chapter 3 of this thesis, a brief literature review on homogeneous Cr/P,N-ligand based ethylene *tri*-/*tetra*-merisation systems will be presented. As previously mentioned in Chapter 1, selective ethylene *tri*-/*tetra*-merisation has emerged as an area of significant academic and industrial research interest over the last decade (due to the important applications of 1-hexene and 1-octene as co-monomers in the syntheses of linear low-density polyethylene (LLDPE) and high-density polyethylene (HDPE)). The vast volume of academic and industrial research conducted on developing and understanding selective ethylene *tri*-/*tetra*-merisation systems has resulted in a number of excellent review articles summarising the open literature on this subject matter.[1-8] As such, the brief literature review detailed here will convey a short history of selective ethylene *tri*-/*tetra*-merisation chemistry before focusing on specific aspects of this area that relate to the Cr/PCN-based ethylene *tri*-/*tetra*-merisation system investigated in this thesis. Specifically, Cr/P,N-ligand based ethylene *tri*-/*tetra*-merisation literature systems will be reviewed, in addition to considering the mechanism, oxidation state, and role of activator in Cr-based ethylene *tri*-/*tetra*-merisation systems, before discussing the Cr/PCN-based ethylene *tri*-/*tetra*-merisation system investigated in this thesis.

2.1.1. Short history of Cr-based selective ethylene *tri*-/*tetra*-merisation

The landmark discovery of a catalytic ethylene trimerisation system, which paved the way for academic and industrial research into this and selective ethylene tetramerisation processes, was reported in 1967 by Manyik *et al.*[9] The formation of a small amount of 1-hexene was observed in ethylene polymerisation catalysed by Cr(2-EH)$_3$, which had been activated by partially hydrolysed *tri*-isobutylaluminium (PIBAO), with its formation being attributed to an ethylene trimerisation pathway.[9] The 1-hexene that had formed was found to subsequently co-polymerise with ethylene to afford a polymer with butyl side chains.[9] In addition to 1-hexene (the predominant oligomer), the formation of 1-butene, 1-octene, and 1-decene were also detected by chromatographic analysis of the solvent produced in the ethylene polymerisation reactions (catalysed by Cr(2-EH)$_3$ activated with PIBAO).[10] Interestingly, the rate of 1-hexene formation was found to be second order, with respect to ethylene, which led Manyik and co-workers to propose a metallacycle mechanism for ethylene trimerisation (discussed in further detail in section 2.1.3).[10] This contrasts with conventional first order polymerisation processes, which are believed to proceed *via* linear chain growth

Cosee-Arlmann mechanism (Chapter 1, Scheme 1.1).

2.1.1.1. Cr-pyrrole based selective ethylene trimerisation systems

Taking inspiration from the work of Manyik *et al.,*[9,10] workers at the Phillips Petroleum Company generated the first selective ethylene trimerisation system displaying 99 % selectivity towards hexene formation in the liquid fraction (of which 83 % selectivity was towards 1-hexene).[11,12] The selective ethylene trimerisation system employed comprised of a Cr pyrrolyl complex, which was activated with triethylaluminium (TEA).[11,12] Following a decade of ensuing research, by workers at the Phillips Petroleum Company, into varying features of the Cr pyrrolyl-based ethylene trimerisation system, such as ligand structure, activation protocol (using *in situ* formed Cr pyrrolyl complexes as opposed to preformed Cr pyrrolyl complexes), and molar ratio of starting materials, optimisation of the ethylene trimerisation system was achieved resulting in the system displayed in Scheme 2.1.[13,14] The optimised system exhibits a liquid fraction selectivity of 93 % towards 1-hexene, with an activity of 156,666 g/g Cr/h implementing 2,5-dimethyl pyrrole ligand and $AlEt_2Cl$, in addition to TEA activator.[14]

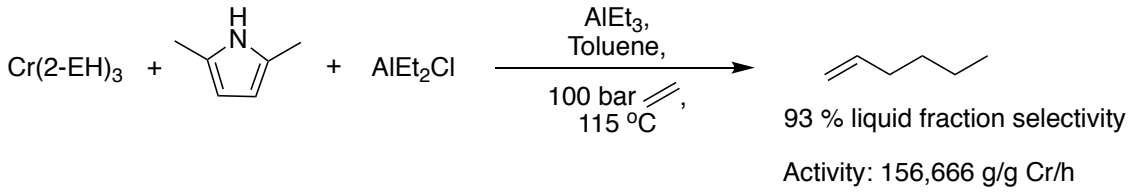

Scheme 2.1: Phillips selective ethylene trimerisation system patented in 1999.[14]

Further optimisation of the Phillips selective ethylene trimerisation system illustrated in Scheme 2.1 was attempted by a number of chemical companies, with the most significant improvements being that accomplished by Mitsubishi Chemical Corporation, which led to the commissioning of the world's first selective ethylene trimerisation plant in 2003 by Mitsubishi-Phillips. Workers at Mitsubishi Chemical Corporation observed that monitoring the ethylene:1-hexene ratio inside the reactor and utilising hexachloroethane solvent engendered a selective ethylene trimerisation process with unprecedented activity (3,780,000 g/g Cr/h, 95 % liquid fraction selectivity to 1-hexene, Scheme 2.2).[15]

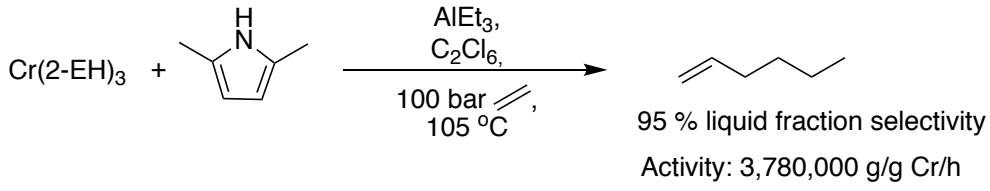

Scheme 2.2: Phillips-Mitsubishi selective ethylene trimerisation system patented in 1999.[15]

2.1.1.2. Cr diphosphinoamine(PNP)-based selective ethylene trimerisation systems

In 2002, British Petroleum Chemicals Limited (BP) reported a selective ethylene trimerisation system (Scheme 2.3) capable of achieving activities of one order of magnitude more than that found for the Phillips trimerisation system (Scheme 2.1), with an exceptionally high purity of 1-hexene in the hexene fraction of 99.9%.[16,17] The ethylene trimerisation system discovered by BP Chemicals Limited consists of $CrCl_3(THF)_3$, a diphosphinoamine ligand (PNP), and methylaluminoxane activator (MAO).[16,17]

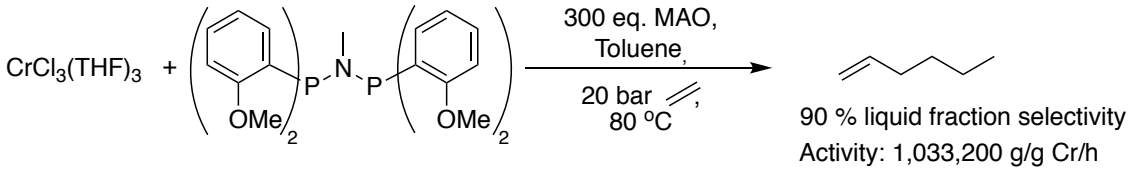

Scheme 2.3: Cr/PNP-based selective ethylene trimerisation system patented by BP Chemicals Limited in 2002.[16,17]

It was postulated in the work conducted by BP Chemicals Limited that two features of the PNP ligand are mandatory to obtain a species capable of catalysing selective ethylene trimerisation, when employed in conjunction with a Cr source and MAO activator.[16] The first requirement claimed was a nitrogen-based backbone, as ligands tested without nitrogen backbones were inactive in ethylene oligomerisation catalysis, when used in the presence of a Cr source and MAO activator.[16] The second factor believed to be a necessity was the presence of an OMe group at the *ortho*-positions of the P-aryl groups of the PNP ligand. This latter requirement was based on the finding that systems employing a Cr source, MAO activator and PNP ligands with *ortho*-Et (sterically analogous to PNP ligand with *ortho*-OMe substituted P-aryl groups) or *p*ara-OMe (electronically equivalent to PNP ligand with *ortho*-OMe substituted P-aryl groups) substituents on their P-aryl groups were inactive in ethylene oligomerisation catalysis.[16] The difference in the ethylene oligomerisation reactivity upon changing the nature and position of the P-aryl group substituent was attributed to the potential of the O atoms of the *ortho*-OMe substituted P-aryl groups to behave as a pendant donor group and bind the Cr centre of the catalytic species.[16] However, it was later shown in studies by Blann *et al*. that *ortho*-OMe substituted P-aryl groups are not a prerequisite for generating Cr/PNP-based selective ethylene trimerisation systems.[18,19]

2.1.1.3. Cr diphosphinoamine(PNP)-based selective ethylene tetramerisation systems

Bollmann *et al.*,[20,21] at Sasol Technology Limited, pursued further research into Cr/PNP-based selective ethylene trimerisation reported by BP chemicals (Scheme 2.3).[16,17] Here, Bollmann and co-workers found that varying the structure of the PNP ligand, catalysis temperature, and ethylene pressure switched the ethylene oligomerisation behavior from trimerisation to tetramerisation, resulting in the first Cr/PNP-based selective ethylene tetramerisation system displayed in Scheme 2.4.[20,21] An added advantage of the selective ethylene tetramerisation system shown in Scheme 2.4 is that it produces 1-hexene as the major byproduct (12 % liquid fraction selectivity).[20,21]

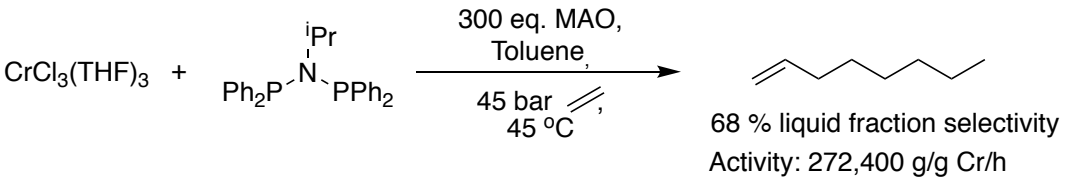

Scheme 2.4:Cr/PNP-based selective ethylene tetramerisation system patented by Sasol Technology Limited in 2004.[20,21]

The discovery of the selective ethylene tetramerisation system, illustrated in Scheme 2.4, was of great significance as it refuted the argument, made at the time, that ethylene tetramerisation was unlikely to occur *via* a similar metallacycle mechanism to that believed to be in operation for selective ethylene trimerisation (see section 2.1.3 for more discussion).[22-24] After conducting further research into the effect of process variables associated with the operation of the Cr/PNP-based selective ethylene tetramerisation system shown in Scheme 2.4, such as PNP ligand structure, catalysis temperature and concentration, workers at Sasol Technology Limited developed a Cr/PNP-based selective ethylene *tri*-/*tetra*-merisation process, which operated in a continuous tube reactor (Scheme 2.5).[25] The high activity of this Cr/PNP-based selective ethylene *tri*-/*tetra*merisation system, comparable to that of the Phillips-Mitsubishi selective ethylene trimerisation catalyst (Scheme 2.2), coupled with the high liquid fraction selectivity of 90 % to 1-hexene and 1-octene resulted in the commissioning of this system in the world's first ethylene tetramerisation plant by Sasol Technology.

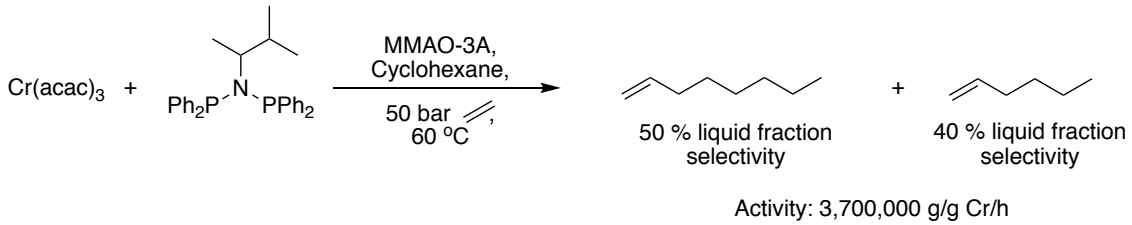

Scheme 2.5:Cr/PNP-based selective ethylene *tri*-/*tetra*-merisation system developed by Sasol Technology Limited in 2009.[25]

The work of Sasol Technology Limited[20,21,25] and BP Chemicals Limited[16,17] demonstrated that Cr/PNP-based catalyst systems can perform as highly active and selective ethylene *tri*-/*tetra*-merisation systems. This initiated a multitude of further academic and industrial research into the use of PNP ligands in selective ethylene *tri*-/*tetra*-merisation catalysis (see section 2.1.2.2.1). In addition to the plethora of research on Cr/PNP-based selective ethylene *tri*-/*tetra*-merisation systems, there is vast research disclosed in the open literature describing investigations into a diverse range of ligand scaffolds for use in Cr-based selective ethylene *tri*-/*tetra*-merisation.[1-8] The variety of different ligand scaffolds investigated in Cr-based selective ethylene *tri*-/*tetra*-merisation can be broadly split into two classes: aromatic ligands (such as pyrrole, maleimidyl, and cyclopentadienyl) and multidentate heteroatomic ligands (containing mixtures of O, P, N, and S donor atoms).[1-8] Since, ligand scaffolds containing phosphorus and nitrogen heteroatoms are the most ubiquitous out of the different ligand scaffolds studied for Cr-based selective ethylene *tri*-/*tetra*-merisation,[1-8] and due to these being the inspiration behind the PCN ligand scaffold investigated in this thesis (section 2.1.6), only Cr/P,N-ligand-based systems will be considered in further detail in the following section.

2.1.2. Cr/P,N-ligand-based selective ethylene *tri*-/*tetra*-merisation systems

2.1.2.1. Hemilabile nature of P,N-ligands

The term hemilabile was first introduced by Jeffery and Rauchfuss to describe ligands containing both soft and hard donor atoms.[26] Thus, P,N-ligands can potentially be considered as being hemilabile ligands due to them comprising electronically soft phosphorus atoms, which can exhibit both π-acceptor and σ-donor behaviour, as well as electronically hard nitrogen atoms, which only display σ-donor properties.[27] Due to the different electronic properties of the nitrogen and phosphorus atoms, the P,N-ligands can show different coordinative properties to a transition metal centre (*i.e.* hemilabile behaviour), which is important to consider due to the implications this has on catalysis (demonstrated by the hemilabile behaviour of PNP ligands bearing *ortho*-

OMe substituted P-aryl groups, discussed in section 2.1.2.2.1.1). In accordance with Pearson's "hard-soft-acid-base" theory[28] soft polarisable phosphorus atoms will coordinate strongly to large, soft late-transition metals while hard nitrogen atoms will bind strongly to harder early transition metal centres. Consequently, when a P,N-ligand is bound to a given metal centre one donor atom will coordinate more strongly than the other, allowing the weaker bound donor atom to display hemilabile behaviour by reversibly dissociating from the metal centre, thereby creating a vacant coordination site on the metal centre (Scheme 2.6).[27] By possessing the ability to create vacant coordination sites required in catalysis, at the same time as stabilising the reactive transition metal centre,[1] P,N-ligands offer the advantages of both mono- and bi-dentate ligands.

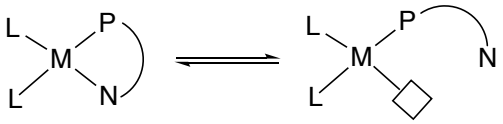

Scheme 2.6: Example of hemilabile behaviour of a P,N-ligand bound to a soft late-transition metal (M), where L represents an ancillary ligand and a vacant coordination site on the metal centre is illustrated by a square.

2.1.2.2. P,N-ligand systems employed in selective ethylene tri-/tetra-merisation systems

This section will review a range of different P,N-based ligands that generate selective ethylene *tri*-/*tetra*-merisation systems, when implemented in conjunction with a Cr source and activator. For the different Cr/P,N-based selective ethylene *tri*-/*tetra*-merisation systems discussed in this section, it was found that the activity and selectivity of the systems could be altered by varying the catalysis conditions (such as temperature, pressure, solvent, and activator) or modifying the substituents at the phosphorus and nitrogen positions of the P,N-ligands.[1-8] Since the work conducted in this thesis on Cr/PCN-based selective ethylene *tri*-/*tetra*-merisation systems examines correlations between the structure of the PCN ligands and performance of the catalysis systems, the structure-catalyst performance (in terms of activity and selectivity) relationships established in the literature Cr/P,N-ligand-based ethylene *tri*-/*tetra*-merisation systems will be the main focus of this section.

2.1.2.2.1. PNP-based ligand systems

Since the discovery of Cr/PNP-based selective ethylene *tri*-/*tetra*-merisation systems (previously detailed in sections 2.1.1.2 and 2.1.1.3), extensive academic and industrial research has been carried out into investigating the effects of varying the PNP ligand structure on the activity and selectivity of the ethylene oligomerisation systems.[1-8] As a

consequence of the research conducted on Cr/PNP-based selective ethylene *tri*-/*tetra*-merisation systems, two structural features of the PNP ligands have been found to impart the greatest influence on the ethylene *tri*-/*tetra*-merisation behavior of the Cr/PNP-based systems: the electronic and steric properties at the phosphorus and nitrogen substituents, which will each be discussed in turn in sections 2.1.2.2.1.1 and 2.1.2.2.1.2.[1-8] As a consequence of the studies into varying the PNP ligand structure, in addition to the catalysis conditions (*i.e.* solvent, temperature, and pressure), implemented in Cr/PNP-based ethylene oligomerisation catalysis a number of ethylene *tri*-/*tetra*-merisation systems with high activities and selectivities have been established in the literature.[1-8] By way of example, Table 2.1 outlines a selection of highly active and selective Cr/PNP-based ethylene *tri*-/*tetra*-merisation systems, including the original BP and Sasol systems in the first two entries, respectively, for comparison.

Table 2.1: A selection of active and selective Cr/PNP-based ethylene *tri*-/*tetra*-merisation systems, modified from Alferov *et al.*[8]

Catalyst precursor	Liquid fraction selectivity (wt %)		Activity (Kg/g Cr/h)	Polyethylene (wt %)	References
	1-C_6	1-C_8			
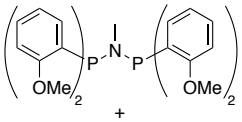 + $CrCl_3(THF)_3$	90	0	1033	0	16,17
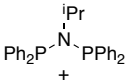 + $CrCl_3(THF)_3$	12	68	272	1	20,21
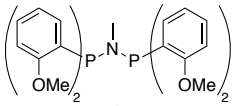 + $Cr(2\text{-}EH)_3$	84	9	7179	0.4	29
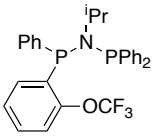 + $Cr(acac)_3$	32	52	12400	0.1	30
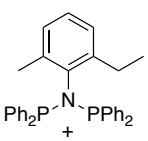 + $Cr(acac)_3$	48	40	3096	n.a.	31

2.1.2.2.1.1. Influence of steric and electronic properties of P-containing substituents of PNP ligands on Cr/PNP-based selective ethylene tri-/tetra-merisation

In a study by Blann *et al.* it was found that the selectivity of the Cr/PNP-based ethylene oligomerisation system towards *tri*- or *tetra*-merisation could be tuned *via* the steric bulk of the phosphorus substituents.[18] A series of PNP ligands possessing aryl-substituted phosphorus moieties were synthesised and tested in ethylene oligomerisation catalysis. It was observed that Cr/PNP-based systems with more sterically demanding diorganyl phosphorus groups were more selective to ethylene trimerisation than those with less bulky substituents at phosphorus (Table 2.2).

Table 2.2: Effect of steric bulk of P-aryl substituent of PNP ligand on liquid fraction selectivities to 1-hexene of Cr/PNP-based ethylene trimerisation systems, investigated by Blann *et al.*[18] Conditions of ethylene oligomerisation catalysis: 0.02 mmol $Cr(acac)_3$, 2 equiv. PNP ligand, 300 equiv. MAO, toluene, 45 bar ethylene, 45 ^{o}C.[18]

PNP ligand structure:	**R substituent** *(listed in order of increasing steric bulk)*	**Liquid fraction selectivity to 1-C_6 (wt %)**
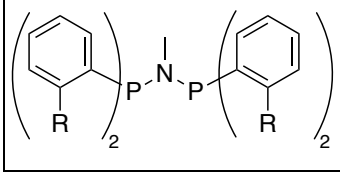	Me	85
	Et	90
	^{i}Pr	92

In addition to the steric demands imposed by substituents of the phosphorus centre of PNP ligands, their electronic character and coordination mode also impacted the performance of Cr/PNP-based selective ethylene trimerisation systems. For example, Cr/PNP-based systems utilising PNP ligands bearing *ortho*-OMe substituted P-aryl groups generally produce selective ethylene trimerisation systems with higher activities than those implementing PNP ligands without *ortho*-OMe substituted P-aryl groups; attributed to hemilabile behaviour of OMe groups (acting as pendant donors for Cr centre).[16,18,20,32] The hemilabile behaviour of PNP ligands containing *ortho*-OMe substituted P-aryl groups was confirmed in studies by Agapie *et al.* from the X-ray diffraction and ^{2}H NMR spectroscopic data of ligated Cr^{III} complexes of these ligands (an example of a Cr^{III}-PNP complex is given in Figure 2.1(a)).[33,34] The Cr^{III}-PNP complex shown in Figure 2.1(a) displays a κ^3(P,P,O) bonding mode with a relatively long Cr-O bond distance of 2.1562(15) Å (when compared to that of 1.939(2) Å of a Cr^{III} complex containing a bidentate P, O ligand,[35] shown in Figure 2.1(b)), which is indicative of a weak Cr-O interaction.[33] The weakness of the Cr-O bond is in accordance with the observed hemilabile nature of the Cr^{III}-PNP complex by variable-temperature ^{2}H NMR spectroscopy.[34] At low temperatures two peaks were detected for

OMe environments in the ^{2}H NMR spectra of the Cr^{III}-PNP complex, in an integration ratio of 1:3, corresponding to one coordinated OMe group and three uncoordinated OMe groups.[34] Upon increasing the temperature of the ^{2}H NMR spectroscopic measurement of the Cr^{III}-PNP complex, only one peak corresponding to an OMe environment remained, thereby evidencing a dynamic process involving ether exchange.

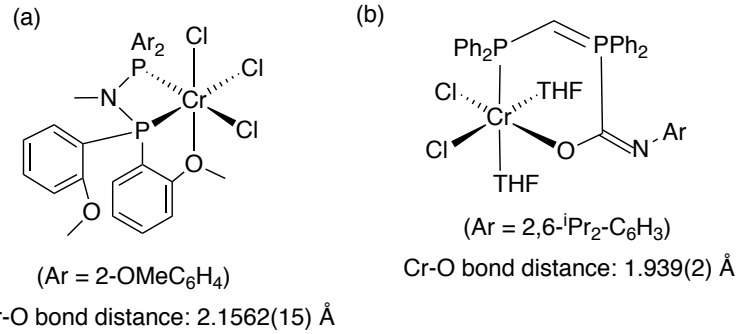

Figure 2.1: Comparison of Cr-O bond lengths of (a) Cr^{III}-PNP complex displaying pendant ether coordination and (b) Cr^{III}-P,O complex.[33,35]

Besides the presence of *ortho*-OMe substituted P-aryl groups affecting the activity of Cr/PNP-based selective ethylene trimerisation systems, the positions of the OMe groups were also found to be important in switching the selectivity from trimerisation to tetramerisation.[32] Overett *et al*. reported that changing the position of the P-aryl-OMe groups in the Cr-PNP complexes portrayed in Figure 2.2, from *ortho*- to *meta*- to *para*-resulted in a gradual increase in the amount of 1-octene formed at the expense of 1-hexene.[32]

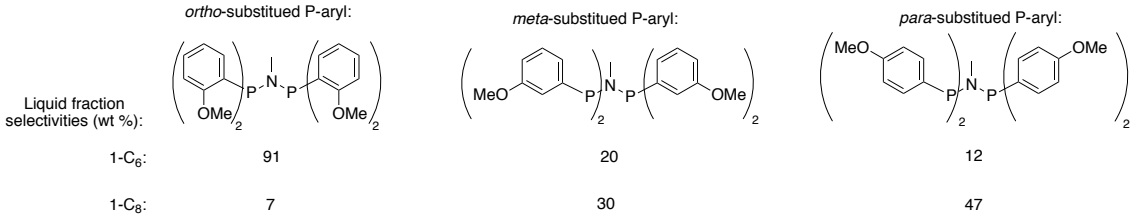

Figure 2.2: Effect of varying the position of the aryl OMe substituent on selectivity of Cr/PNP-based ethylene oligomerisation.[32] Ethylene oligomerisation catalysis conditions: 0.033 mmol $Cr(acac)_3$, 2 equiv. PNP ligand, 300 equiv. MAO, 100 mL toluene, 30 bar ethylene, 65 ^oC.[32]

2.1.2.2.1.2. Influence of steric and electronic properties of N donor motif of PNP ligands on Cr/PNP-based selective ethylene tri-/tetra-merisation

Numerous reports have shown that the steric bulk about the nitrogen substituent of PNP ligands affects both the activity and selectivity of Cr/PNP-based selective ethylene *tri*-/*tetra*-merisation systems.[20,36-40] It was observed in various studies on Cr/PNP-based selective ethylene *tri*-/*tetra*-merisation systems containing alkyl[20,36,37] or

meta-substituted aryl nitrogen groups[38,39] that increasing the steric bulk of these nitrogen substituents led to improvements in the catalytic activities. As a representative example of this trend, Figure 2.3 summarises the increase in activities of Cr/PNP-based selective ethylene tetramerisation systems observed by Kuhlmann *et al.*,[36] upon systematically increasing the steric bulk of the cycloalkyl-substituted N donor motifs.

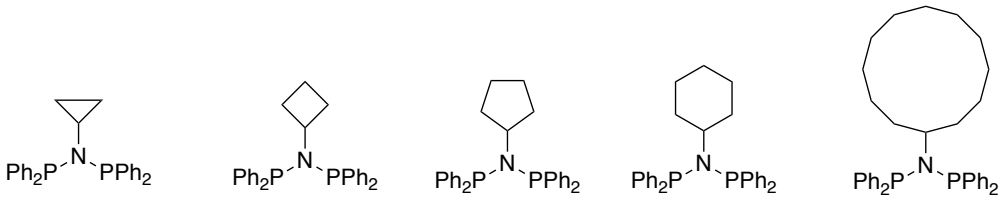

Activity (Kg/g Cr/h):	464	391	545	725	758

Figure 2.3: Effect of varying cycloalkyl ring size of nitrogen substituent on activity of Cr/PNP-based selective ethylene tetramerisation system.[36] Ethylene oligomerisation catalysis conditions: 100 mL methylcyclohexane, 60 ^{o}C, 45 barg ethylene, 5 µmol $Cr(acac)_3$, 7.5 µmol PNP ligand, 270 equiv. MMAO-3A.[36]

Interestingly, Killian *et al.*[40] and Jiang *et al.*[38] independently showed that as the steric bulk of *ortho*-substituted aryl nitrogen groups was increased, the activities of the Cr/PNP-based selective ethylene *tri*-/*tetra*-merisation systems were found to decrease. For example, progressively increasing the steric bulk of the *ortho*-aryl nitrogen substituents from hydrogen to *iso*-propyl led to an overall decrease in the activities of the Cr/PNP-based selective ethylene tetramerisation systems reported by Killian *et al.* (Figure 2.4).[40]

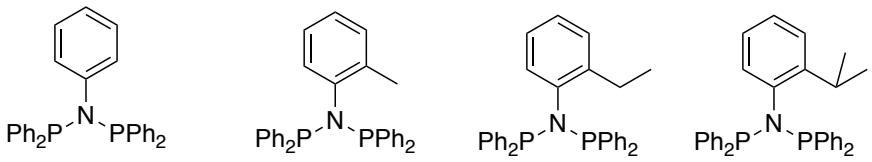

Activity (Kg/g Cr/h):	767	527	563	160
Liquid fraction selectivity to 1-C_6 (wt %):	9	15	17	29
Liquid fraction selectivity to 1-C_8 (wt %):	60	55	55	52

Figure 2.4: Effect of varying steric bulk of *ortho*-substituted aryl nitrogen groups on activity and selectivity of Cr/PNP-based selective ethylene tetramerisation system.[40] Ethylene oligomerisation catalysis conditions: 100 mL methylcyclohexane, 60 ^{o}C, 50 barg ethylene, 10 µmol $Cr(acac)_3$, 1 equiv. PNP ligand, 480 equiv. MMAO-3A.[40]

The steric properties of the aryl and alkyl substituents at the nitrogen of PNP ligands have also been observed to impact the selectivity of Cr/PNP-based ethylene *tri*-/*tetra*-merisation systems. Here, an increase in the total 1-hexene and 1-octene liquid

fraction selectivity is concomitant with an increase in the nitrogen steric bulk (an example shown previously in Figure 2.4).[20,36-38,40] The steric bulk of the nitrogen substituents of PNP ligands have also been found to be responsible for determining the degrees of ethylene *tri*- and/or *tetra*-merisation exhibited by the Cr/PNP-based ethylene oligomerisation systems. It has been disclosed in multiple studies that the 1-octene:1-hexene ratio (OTH) of Cr/PNP-based ethylene oligomerisation systems is decreased upon increasing the steric bulk of the *ortho*-aryl or alkyl nitrogen substituents (also exemplified by Figure 2.4),[36-38,40] and is increased as the steric bulk of the *meta*-aryl nitrogen substituents is raised.[38,39] The observed decrease in the OTH ratio upon an increase in the steric bulk of the *ortho*-aryl or alkyl nitrogen substituent is thought to be a direct consequence of the metallacycle mechanism believed to be in operation (discussed in further detail in section 2.1.3), with increased steric bulk on the catalyst argued to disfavour the formation of the metallacyclononane believed to be responsible for 1-octene formation.[36,37]

In addition to exploring the effect of the steric bulk of the nitrogen substituent of PNP ligands, many literature studies have also examined the effect of the electronic character of the nitrogen substituent on Cr/PNP-based selective ethylene *tri*-/*tetra*-merisation.[39-44] In work performed by Blann *et al.* it was reported that, while the basicity of the nitrogen affected the activity and selectivity of Cr/PNP-based selective ethylene tetramerisation systems (Figure 2.5), no conclusive trends could be drawn.[41] Additionally, the sterics of the nitrogen substituent of the PNP ligands were found to be most dominant in determining the selectivity of the system.[41]

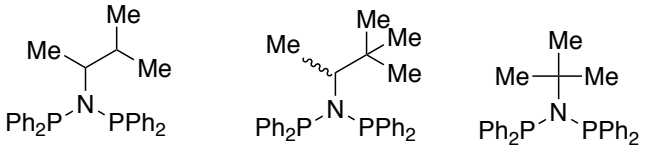

Activity (Kg/g Cr/h):	1920	1370	1550
Liquid fraction selectivity to 1-C_6 (wt %):	20	45	31
Liquid fraction selectivity to 1-C_8 (wt %):	66	41	58

Figure 2.5: Effect of nitrogen basicity on activity and selectivity of Cr/PNP-based selective ethylene tetramerisation systems.[41] Conditions of ethylene oligomerisation catalysis: 100 mL methylcyclohexane, 60 ^{o}C, 45 barg, 2.5 µmol $Cr(acac)_3$, 3 µmol PNP ligand, 300 equiv. MMAO-3A.[41]

The effect of changing the electron density of N-phenyl substituted PNP ligands on their performance in Cr/PNP-based ethylene tetramerisation was explored in a study by Killian *et al.*[40] In this work, the introduction of an electron-donating ^{t}Bu group in the *para* position resulted in a selective ethylene tetramerisation system with increased activity and reduced polymer formation (relative to that exhibited by the system bearing N-phenyl).[40] Conversely, the presence of an electron-withdrawing NO_2 group in the *para* position afforded an ethylene oligomerisation system with increased amounts of polymer and decreased selectivity towards 1-hexene and 1-octene (when compared to the N-phenyl system).[40] *Jiang et al.* similarly discovered an increase in the catalytic activity, in addition to the tetramerisation selectivity, of their Cr/PNP-based ethylene oligomerisation systems upon increasing the electron density of the N-phenyl substituents from 3,5-Cl_2-C_6H_3 to 3,5-Me_2-C_6H_3.[39]

Lastly, the effect of utilising PNP ligands with donor groups at the nitrogen position (such as OMe and SMe) has been considered in Cr/PNP-based selective ethylene *tri*-/*tetra*-merisation catalysis by multiple research groups, with the hope of exploiting the hemilabile behavior of the OMe and SMe donor groups to produce systems with increased catalytic activities (analogous to that observed for PNP systems possessing *ortho*-OMe substituted P-aryl groups, previously discussed in section 2.1.2.2.1.1).[42-44] Although it was found that Cr/PNP-based selective ethylene *tri*-/*tetra*-merisation systems containing pendant donor OMe and SMe groups at their nitrogen position generated systems with improved catalytic activities than those systems without pendant donor group-substituted nitrogen atoms, no concrete evidence of hemilabile behavior of the OMe and SMe groups was obtained.[42,43] In fact, molecular structures of Cr-PNP complexes bearing OMe and SMe donor groups at their nitrogen positions were obtained (chemical structures depicted in Figure 2.6) which illustrated bidentate P,P-coordination of the PNP ligands with the pendant donor groups remaining uncoordinated.[42,43] Nonetheless, it was noted by Suttil *et al.* that using TEA as an activator, in place of MAO, rendered Cr/PNP-based ethylene oligomerisation systems inactive. The difference in reactivity was hypothesised to be due to potential of TEA to coordinate to pendant N-donor group, thereby changing the reactivity of the active catalyst species.[44]

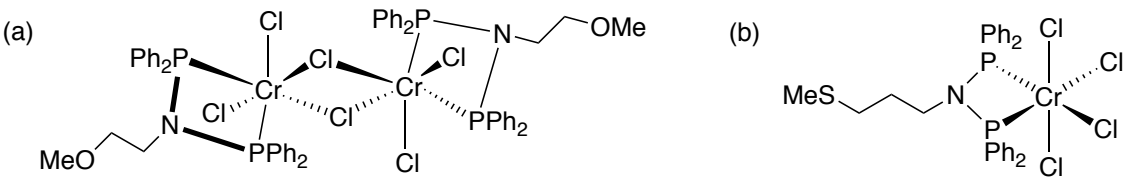

Figure 2.6: Cr-PNP complexes containing pendant donor-substituted nitrogen atoms.[42,43]

2.1.2.2.2. $P(C)_nN(C)_nP$-based ligand systems

Taking inspiration from the use of PNP ligands in Cr-based ethylene *tri-*/*tetra*-merisation, PNP ligands with carbon bridges connecting the P and N units (*i.e.* $P(C)_nN(C)_nP$ ligands where n=1 or 2) were tested in ethylene oligomerisation catalysis, in separate studies by Le Floch *et al*.[45] and McGuinness and Wasserchied *et al*.[46] In the study by Le Floch *et al*.,[45] Cr^{III} complexes containing PCNCP ligands, coordinated *via* the phosphorus atoms, generated ethylene *tri-*/*tetra*-merisation systems with high selectivities (with a number of systems exclusively forming hexene and octene with >97 % selectivity to the linear α-olefin content of these fractions) and modest activities up to 9783 g/g Cr/h, when activated by MAO (best performing system illustrated in Scheme 2.7)). Additionally, Le Floch *et al*. observed that the selectivity towards ethylene *tri-* or *tetra*-merisation shifted upon varying the steric bulk of the phosphine moiety, with decreasing steric bulk at the phosphorus position leading to an increase in the amount of tetramerisation *versus* trimerisation.[45] Both the activity and selectivity of the Cr/PCNCP-based ethylene *tri-*/*tetra*-merisation systems was also different if aryl or alkyl substituents were employed at the phosphorus substituents of the PCNCP ligands, with systems containing ligands bearing aryl phosphino groups displaying lower activities and selectivities towards ethylene trimerisation.[45]

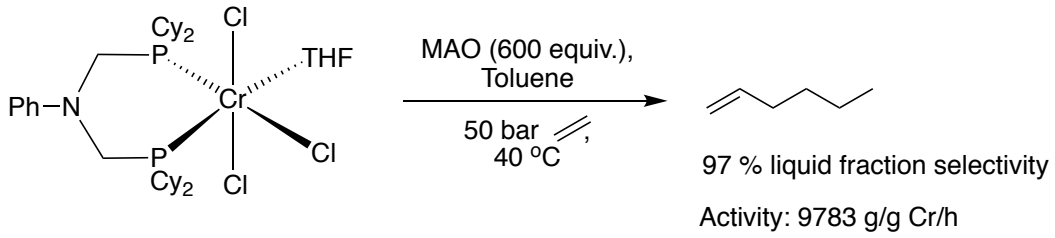

Scheme 2.7: Cr/PCNCP-based selective ethylene trimerisation system reported by Le Floch *et al.*[45]

The work by McGuinness and Wasserchied *et al*. explored the use of Cr complexes ligated by PCCN(H)CCP frameworks containing different phosphorus substituents (Ph, Cy or Et, Figure 2.7) in ethylene oligomerisation catalysis.[46,47] Systems consisting of PCCN(H)CCP ligands with sterically compact and basic phosphorus substituents (Ph or Et) yielded highly selective ethylene trimerisation systems (97 % liquid fraction selectivities to 1-hexene) with activities up to 17,300 g/g Cr/h.[46,47] The effect of changing the nitrogen substituent of the PCCN(H)CCP ligands was also considered by McGuinness and Wasserchied *et al*..[46] They found that substituting the N-H moiety for N-Benzyl or N-Me afforded Cr/PCCNCCP-based ethylene oligomerisation systems with decreased activities and selectivities; this led the authors to suggest that deprotonation of the N-H functionality occurs during catalyst formation.[46]

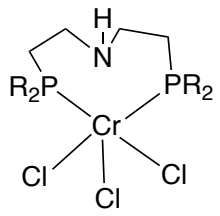

R = Ph, Cy or Et

Figure 2.7: Cr/PCCN(H)CCP complexes synthesised by Mc Guinness and Wasserchied *et al.*[46,47]

2.1.2.2.3. PNNP-based ligand system

The landmark study by Bollmann *et al.*, reporting the first Cr/PNP-based selective ethylene tetramerisation system (detailed beforehand in section 2.1.1.3) also explored the application of a PNNP ligand in ethylene oligomerisation catalysis.[20] The Cr/PNNP-based system investigated in ethylene oligomerisation catalysis, illustrated in Scheme 2.8, exhibits a total liquid fraction selectivity of 76 % to 1-hexene and 1-octene, with moderate activity.[20]

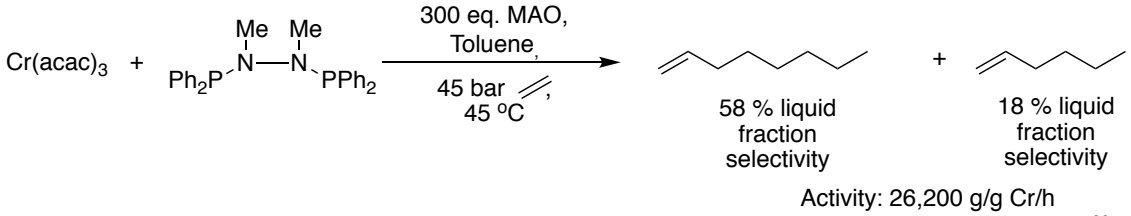

Scheme 2.8: Cr/PNNP-based selective tetramerisation system reported by Bollmann *et al.*[20]

2.1.2.2.4. PN(C)$_n$NP-based ligand systems

Gamboratta and Duchateau *et al.* published a study conveying the application of PNNP ligands containing carbon bridges between the nitrogen groups, *i.e.* PN(C)$_n$NP ligands (where n= 2 or 3).[48] This ligand motif was highly selective for ethylene *tri-*/*tetra*-merisation systems when implemented in conjunction with a Cr source and activator (some systems reported to solely produce 1-hexene and 1-octene with modest activities up to 88, 917 g/g Cr/h). [48] The effect of varying the substituents at nitrogen or phosphorus of the PN(C)$_n$NP ligands on the performance of the Cr/PN(C)$_n$NP-based ethylene oligomerisation systems was pursued with it being observed that more sterically demanding substituents at nitrogen or phosphorus led to a decrease in both the activity and selectivity of the systems.[48] Of greatest significance in this work by Gamboratta and Duchateau *et al.*[48] was the development of a highly selective Cr/PNCCCNP-based ethylene tetramerisation system, illustrated in Scheme 2.9, which displays 91 % selectivity towards 1-octene (much higher than that of the original Sasol Cr/PNP-based tetramerisation system previously detailed in section 2.1.1.3).

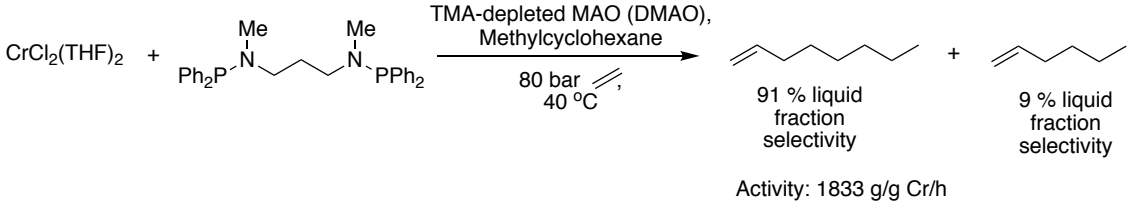

Scheme 2.9: Cr/PNCCCNP-based selective ethylene tetramerisation system reported by Gambarotta and Duchateau *et al.*[48]

2.1.2.2.5. PNPN-based ligand systems

The utilisation of PNPN(H) ligands in Cr-based selective ethylene trimerisation systems has been pursued in a number of studies published in collaborations between the Rosenthal group and Linde chemical company. These led to the announcement in 2015 by Linde chemical company of plans to commercialise a process based upon PNPN(H).[49] The main findings of the work by the Rosenthal group and Linde chemical company will be summarised in this section.[50-59] The first Cr/PNPN(H)-based selective ethylene trimerisation system reported by Rosenthal *et al.* is portrayed in Scheme 2.10.[50] This selective ethylene trimerisation system has various features that make it a potential candidate for use on an industrial scale, namely the exceptional purity of 1-hexene of >99 % in the hexene fraction, the low level of polyethylene production, and the use of cheap TEA activator (as opposed to the more commonly implemented, but more expensive MAO system).[50] It was also found in the work by Rosenthal *et al.* that the PNPN(H) ligand adopts a κ^2-P,P binding mode to Cr and that while the N-H group does not bind to Cr, it is essential in imparting ethylene trimerisation activity by undergoing deprotonation when reacted with TEA activator to produce an active catalyst species.[50]

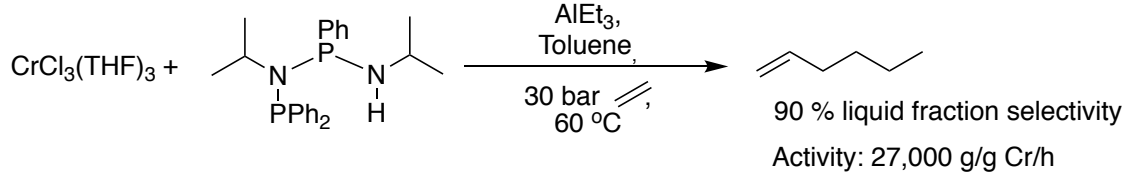

Scheme 2.10: Cr/PNPN(H)-based homogeneous selective ethylene trimerisation system reported by Rosenthal *et al.*[50]

Later work by Rosenthal *et al*. details a heterogeneous Cr/PNPN(H)-based selective ethylene trimerisation system (Scheme 2.11), which achieves a liquid fraction selectivity to 1-hexene of 82 %, comparable to that reported for the homogeneous system (Scheme 2.10).[51] Although, the activity of the homogeneous system far exceeds that of the heterogeneous system, the heterogeneous catalyst displays excellent stability from the absence of any catalyst deactivation in processes lasting over 40 hours.[51]

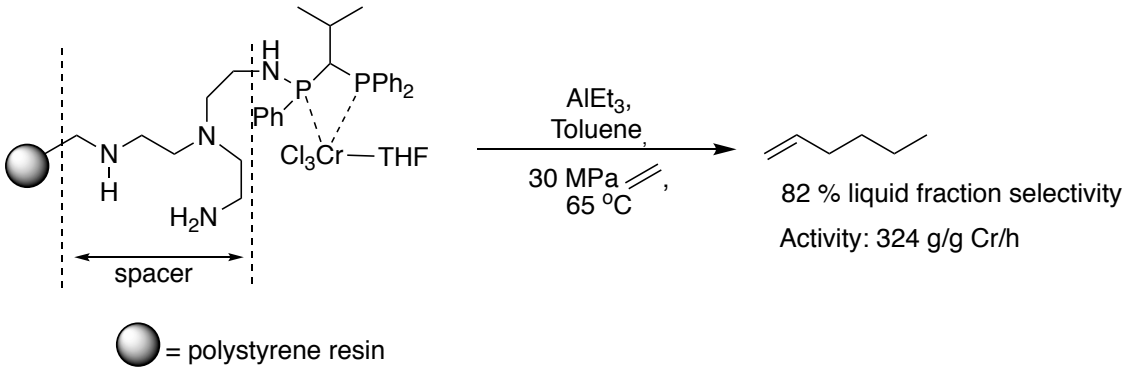

Scheme 2.11: Cr/PNPN(H)-based heterogeneous selective ethylene trimerisation system reported by Rosenthal *et al.*[51]

A number of publications have been released by Rosenthal *et al*. studying the coordination and metallation chemistry of PNPN(H) ligands,[52,53] kinetics of the Cr/PNPN(H)-based ethylene trimerisation systems,[54-56] and effects of varying the PNPN(H) ligand substituents on the performance of the Cr/PNPN(H)-based selective trimerisation systems.[57] To their surprise, Rosenthal *et al*.[57] observed that changes to the nitrogen substituents of the PNPN(H) ligands had little impact on the 1-hexene selectivity, catalytic activity and thermal stability of the Cr/PNPN(H)-based selective ethylene trimerisation systems; in contrast to the Cr/PNP-based selective ethylene *tri*-/*tetra*-merisation systems previously mentioned in section 2.1.2.2.1.2. Nevertheless, the nature of the phosphorus substituent on the PNPN(H) ligands was found to impact the efficiency of the Cr/PNPN(H)-based selective ethylene trimerisation systems, with systems containing PNPN(H) ligands bearing phenyl-substituted phosphorus atoms achieving the highest activities.[57]

In more recent work, Rosenthal *et al*. considered the use of PNPN ligands bearing an additional amine substituent at the initial phosphorus position (*i.e.* a NPNPN ligand framework) in ethylene oligomerisation catalysis.[58,59] The NPNPN ligands give rise to highly active and selective ethylene *tri*- and *tetra*-merisation systems, when used in combination with a Cr source and modified MMAO activator (MMAO-3A); a representative example is given in Scheme 2.12.[58] In contrast to the earlier work on Cr/PNPN(H)-based selective ethylene trimerisation systems that used TEA as activator,[50] it was found that an N-H functionality was not required on the NPNPN ligand scaffold to produce active catalytic systems.[58] Furthermore, the use of TEA activator in the NPNPN-Cr systems actually switched off ethylene oligomerisation catalysis (even for NPNPN ligands containing N-H functionalities).[58] Additionally, the effect of varying the nitrogen substituents of the NPNPN ligands on the performance of the Cr/NPNPN-based selective ethylene *tri*-/*tetra*-merisation systems was evaluated,

with it being observed that ligands containing a N-H functionality formed systems with greater selectivity towards 1-hexene formation, albeit it with lower activities and higher levels of polyethylene production.[58]

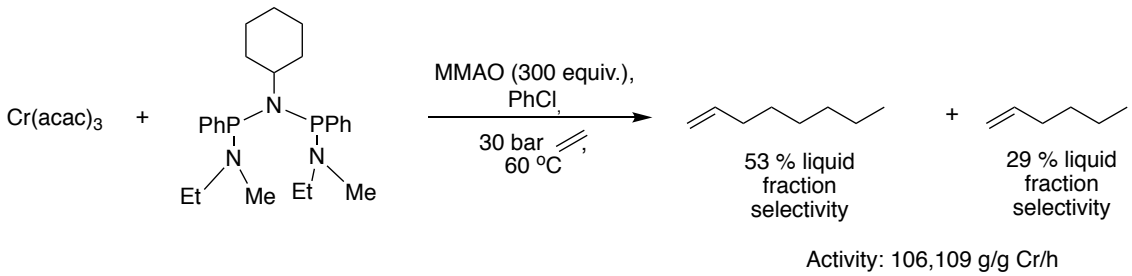

Scheme 2.12: Cr/NPNPN-based selective ethylene *tri-*/*tetra*-merisation system reported by Rosenthal *et al.*[58]

2.1.2.2.6. Anionic NPN-based ligand systems

In 2008, a series of publications by Gambarotta and Duchateau *et al.* reported the application of anionic NPN-based ligand systems in ethylene oligomerisation catalysis, in the presence of a Cr source and activator.[60-62] Interestingly, it was observed that the nature of the activator used largely determined if polymerisation (in the presence of $(^{i}BuAl)_2(\mu\text{-}O)$ as activator), non-selective oligomerisation (in presence of MAO as activator) or selective ethylene trimerisation (in presence of $Al^{i}Bu_3$ as activator) was achieved by the Cr/NPN-systems.[60-62] An example of a Cr/NPN-based selective ethylene trimerisation system, which exclusively produces close to 100 % 1-hexene with the only other byproduct being traces of polyethylene, is shown in Scheme 2.13.[60]

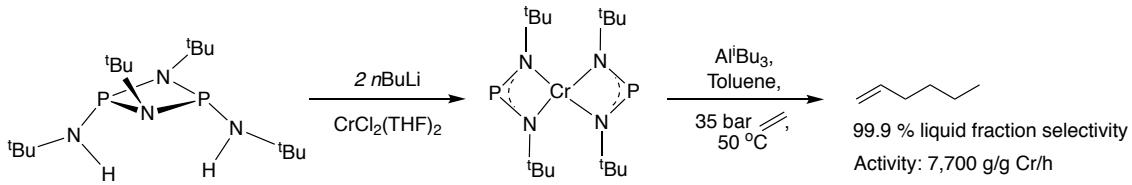

Scheme 2.13: Highly selective Cr/NPN-based selective ethylene trimerisation system, reported by Gambarotta and Duchateau *et al.*[60]

2.1.2.2.7. PNN-based ligand systems

A study by Duchateau *et al*. reported two Cr/PNN-based selective ethylene tetramerisation systems (portrayed in Figure 2.8), which possess moderate activities.[63] In a follow-up study, Duchateau and Gamboratta *et al.* further probed the potential of PNN ligands containing a pyridine moiety in Cr-based selective ethylene oligomerisation systems (Figure 2.9).[64]

(a)

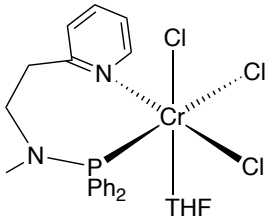

Liquid fraction selectivities to:
1- C_6 = 25 %
1-C_8 = 75 %

1.3 g polyethylene

Activity: 4506 g/g Cr/h

(b)

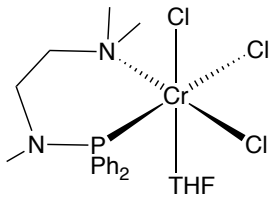

Liquid fraction selectivities to:
1- C_6 = 11 %
1-C_8 = 89 %

2.6 g polyethylene

Activity: 12,513 g/g Cr/h

Figure 2.8*:* Cr/PNN-based selective ethylene tetramerisation systems reported by Duchateau *et al.*[63] Ethylene oligomerisation catalysis conditions: DMAO (500 equiv.), 80 ^{o}C, 40 bar ethylene, toluene (for system (a)) or methylcyclohexane (for system (b)).[63]

(a)

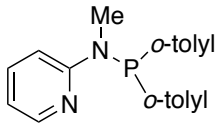

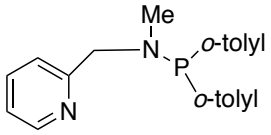

Liquid fraction selectivities to:
1- C_6 = 58 %
1-C_8 = 26 %

Polyethylene = 12 %

Activity: 7981 g/g Cr/h

Liquid fraction selectivities to:
1- C_6 = 56 %
1-C_8 = 20 %

Polyethylene = 48 %

Activity: 14,538 g/g Cr/h

(b)

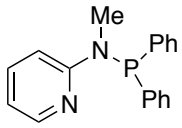

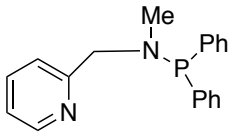

Liquid fraction selectivities to:
1- C_6 = 24 %
1-C_8 = 24 %

Polyethylene = 5 %

Activity: 22,269 g/g Cr/h

Liquid fraction selectivities to:
1- C_6 = 23 %
1-C_8 = 51 %

Polyethylene = 80 %

Activity: 4923 g/g Cr/h

(c)

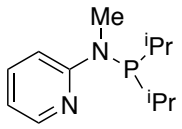

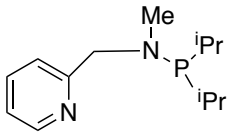

Liquid fraction selectivities to:
1- C_6 = 41 %
1-C_8 = 35 %

Polyethylene = 26 %

Activity: 9442 g/g Cr/h

Liquid fraction selectivities to:
1- C_6 = 71 %
1-C_8 = 27 %

Polyethylene = 12 %

Activity: 9615 g/g Cr/h

Figure 2.9: PNN ligands ligated to $CrCl_3(THF)_3$ and subsequently tested in ethylene oligomerisation catalysis, in a study by Duchateau and Gamboratta *et al.*[64] Ethylene oligomerisation catalysis conditions: 10 µmol [$CrCl_3(THF)(\kappa^2$-P,N-PNN)], 500 equiv. MAO, 60 °C, 30 bar ethylene, methylcyclohexane.[64]

From the systems portrayed in Figure 2.9, Duchateau and Gamboratta *et al.*[64] concluded that the P-Cr-N bite angles and the flexibility of the ligand played a crucial role in determining the catalytic performance of the Cr/PNN-based systems. On increasing the P-Cr-N bite angle and ligand flexibility, by the introduction of C spacer groups between the N groups of the PNN ligands bearing phenyl or *o*-tolyl phosphine groups, a dramatic reduction in the ethylene *tri*-/*tetra*-merisation selectivity was observed (evident from the systems depicted Figure 2.9(a) and (b)).[64] In contrast, on increasing the carbon bridge length between the nitrogen atoms of the PNN ligand containing the more basic ^{i}Pr phosphorus substituent (basicity relative to that of phenyl or *o*-tolyl phosphorus substituents), an increase in the ethylene *tri*-/*tetra*-merisation selectivity occurred (Figure 2.9(c)).[64]

2.1.2.2.8. N-pyrrolyldiphenylphosphine-based ligand system

In a study by Duchateau *et al.* considering the possibility of a series of compounds containing P-N bonds as ancillary ligands in Cr-based ethylene *tri*-/*tetra*-merisation systems, a highly selective ethylene *tri*-/*tetra*-merisation system utilising a N-pyrrolyldiphenylphosphine ligand was developed (Scheme 2.14).[65] The observed selectivity towards ethylene *tri*-/*tetra*-merisation of the Cr/N-pyrrolyldiphenylphosphine-based system is not unsurprising as Gambarotta *et al*.[66] reported that it may be possible for the P-N moiety of the N-pyrrolyldiphenylphosphine to break in selective ethylene oligomerisation systems. If breakage of the P-N moiety of the N-pyrrolyldiphenylphosphine does occur in the Cr/N-pyrrolyldiphenylphosphine-based system, then a system similar to the previously discussed Cr/pyrrole-based selective ethylene trimerisation systems is obtained (section 2.1.1.1).

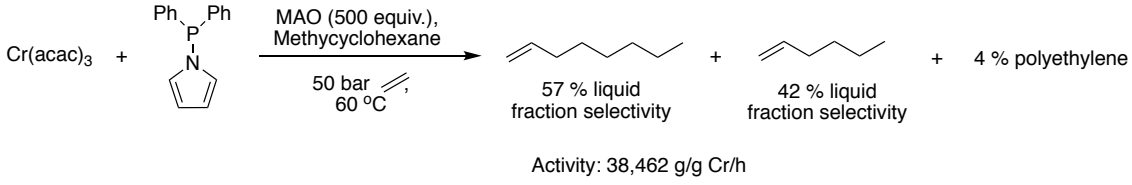

Scheme 2.14: Cr/N-pyrrolydiphenylphosphine-based selective ethylene *tri*-/*tetra*-merisation system reported by Duchateau *et al.*[65]

2.1.2.2.9. P-imine based ligand systems

The first selective ethylene trimerisation system employing a PN(imine)P-Cr complex, depicted in Scheme 2.15, was reported by Bluhm *et al.*[67] Although the Cr/PN(imine)P-based ethylene trimerisation system possesses a high liquid fraction selectivity of 97 % to 1-hexene and produces only 2 % polyethylene, it has a low activity of only 470 g/g Cr/h.

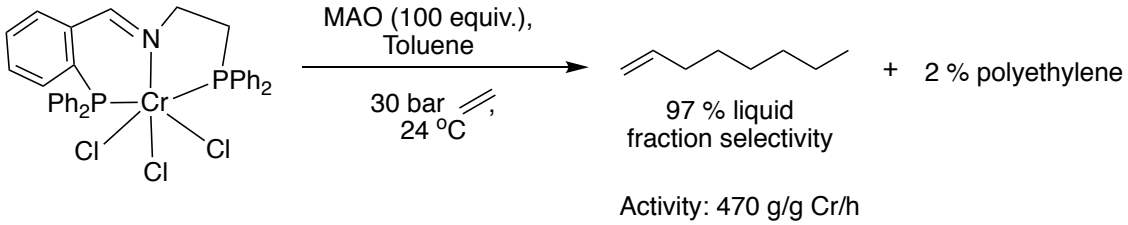

Scheme 2.15: Cr/PN(imine)P-based selective ethylene trimerisation system reported by Bluhm *et al.*[67]

The most notable examples of Cr/P-imine-based selective ethylene *tri*-/*tetra*-merisation system are those reported by workers from Chevron Phillips utilising N-phosphinoamidine ligands, bound to Cr in a bidentate fashion through the phosphorus and nitrogen atoms.[68,69] The significance of these systems is due to their ability to achieve high activities, in addition to high total liquid fraction selectivities to 1-hexene and 1-octene. The best-performing Cr/N-phosphinoamidine-based selective ethylene trimerisation system, illustrated in Scheme 2.16, has a 1-hexene selectivity and catalytic activity comparable to that of the Sasol Cr/PNP-based selective ethylene trimerisation system (section 2.1.1.2).[68] The selectivity of the Cr/N-phosphinoamidine-based systems could be switched from ethylene trimerisation to tetramerisation through modifications of the phosphorus substituents on the N-phosphinoamidine ligands; ligands with less bulky phosphine motifs demonstrating greater selectivity towards 1-octene formation.[68]

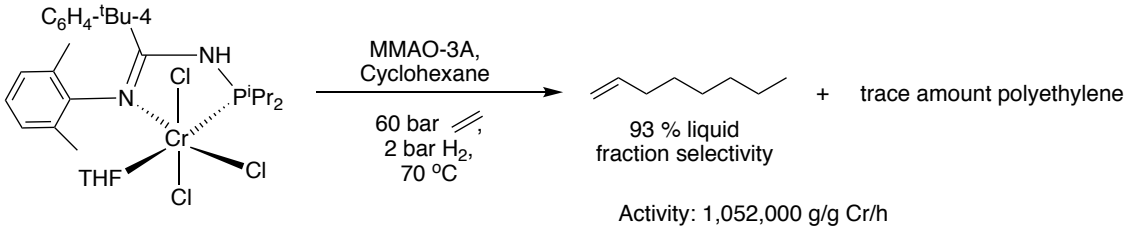

Scheme 2.16: Chevron Phillips Cr/N-phosphinoamidine-based selective ethylene trimerisation system.[68,69]

Interestingly, it was found that using an N-phosphinoamidine ligand which coordinated in a tridentate fashion to Cr, generating a [$CrCl_3(\kappa^3$-PNN)] complex, effectively shut down catalyst activity (Scheme 2.17).[68] The stark difference in reactivity between the systems using [$CrCl_3(\kappa^2$-P,N-PNN)(THF)] or [$CrCl_3(\kappa^3$-PNN)] complexes led the authors

to propose that bound THF is required at the chromium centre for the formation of active catalyst systems (the Lewis acidic activator, MMAO-3A, is believed to abstract THF from the chromium centre to generate an active catalyst bearing a vacant site for ethylene coordination).[68]

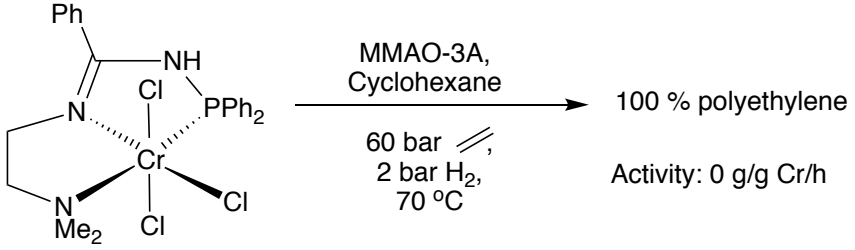

Scheme 2.17: Non-active ethylene polymerisation system generated by [$CrCl_3(\kappa^3$-PNN)] complex.[68]

2.1.2.2.10. Summary of P,N-ligands reviewed in Cr-based selective ethylene tri-/tetra-merisation systems

In summary, the studies reviewed of Cr/P,N-based selective ethylene *tri-*/*tetra*-merisation systems have demonstrated that various structural parameters of the P,N-donor ligands, such as steric bulk, pendant donor effect, basicity, and bite angle, can all influence the activity and selectivity of these systems. In most of the literature surrounding Cr/P,N-based selective ethylene *tri-*/*tetra*-merisation systems evaluated, the steric bulk at the nitrogen and/or phosphorus ligands provided a handle for tuning the selectivity towards trimerisation or tetramerisation, the latter being favoured by less bulky substituents. It has been reasoned that increasing the steric bulk of the P,N-ligands makes it more preferential for formation of the metallacycloheptane intermediate (believed to be responsible for the formation for 1-hexene; section 2.1.3.1) than the larger-sized metallacyclononane intermediate (believed to be responsible for the formation for 1-octene; section 2.1.3.2). Although most of the Cr/P,N-based selective ethylene *tri-*/*tetra*-merisation systems considered display high total liquid fraction selectivities to 1-hexene and 1-octene, accompanied by the formation of small amounts of polymer, only the Linde system employing an NPNPN ligand(section 2.1.2.2.5), and the Chevron Phillips system implementing a N-phosphinoamidine ligand(section 2.1.2.2.9), achieve activities as high as those reported for the ubiquitous Cr/PNP-based selective ethylene *tri-*/*tetra*-merisation systems (section 2.1.2.2.1). In addition, the majority of the Cr/P,N-based systems described in the literature are selective towards ethylene trimerisation, with only a few conveying high selectivities towards 1-octene formation. Therefore, the invention of novel efficient, selective ethylene tetramerisation catalysts is desirable, in addition to selective ethylene trimerisation catalysts (due to the ever increasing demand for 1-hexene and 1-octene). As such, research was conducted into the Cr/PCN-based

selective ethylene *tri*-/*tetra*-merisation system investigated in this thesis.[70,71] Prior to detailing the Cr/PCN-based selective ethylene *tri*-/*tetra*-merisation system explored in this thesis, it is important to consider other key features of homogeneous Cr-based ethylene *tri*-/*tetra*-merisation systems, aside from the ligand framework, which determine the activity and selectivity; specifically the mechanism, oxidation state of chromium, and role of activator.

2.1.3. Mechanism of Cr-based selective ethylene *tri*-/*tetra*-merisation systems

Although traditional olefin *olig*- and *poly*-merisation processes are known to proceed *via* the Cossee-Arlmann mechanism (previously considered in Chapter 1, section 1.2.1), it is unlikely that this mechanism can account for Cr-based selective ethylene oligomerisation processes.[1-8] Consequently, a different mechanistic pathway is widely accepted to be in operation for Cr-based selective ethylene *tri*-/*tetra*-merisation, namely a process involving chromacycles, termed the metallacyclic mechanism, in which the selectivity of the system (towards *tri*- or *tetra*-merisaton) is dictated by the ability of the catalyst to support the formation of metallacycles of certain sizes.[1-8] This section will review the different metallacycle mechanisms proposed to be in operation for selective ethylene *tri*-/*tetra*-merisation systems.

2.1.3.1. Metallacycle mechanism for selective ethylene trimerisation processes

The emergence of a metallacylic mechanism to explain selective ethylene trimerisation came from Manyik *et al.* in 1977 when they realized that the rate of 1-hexene formation, in their trimerisation system (detailed beforehand in section 2.1.1), was second order with respect to ethylene as opposed to first order (expected for a Cossee Arlmann mechanism).[10] The metallacyclic mechanism proposed by Manyik *et al.* is illustrated in Scheme 2.18 and proceeds *via* the coordination of two ethylene molecules to the chromium centre, generating a species which undergoes oxidative coupling to afford a metallacyclopentane.[10] A third ethylene molecule then coordinates to the metallacyclopentane, with β-H transfer then occuring to yield a chromium butenyl intermediate, from which 1-hexene is liberated by reductive elimination.[10]

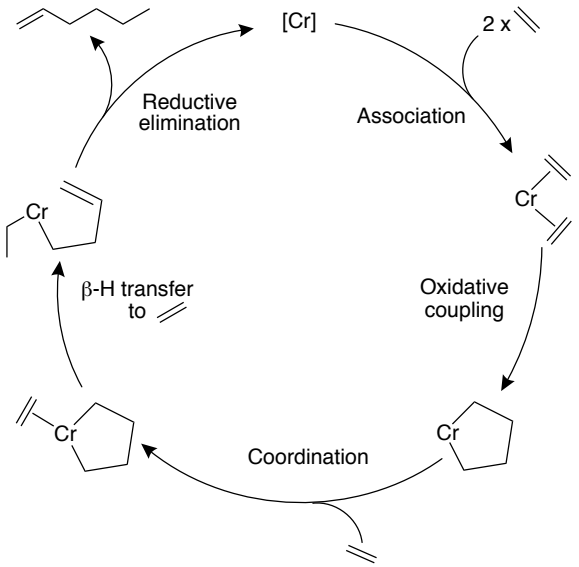

Scheme 2.18: Proposed metallacycle mechanism for 1-hexene formation, modified from Manyik *et al*.[10]

In 1989, Briggs[22] put forward a modified version (depicted in Scheme 2.19) of the metallacycle mechanism proposed by Manyik *et al.*,[10], in which ethylene insertion into the metallacyclopentane occurs to form a metallacycloheptane. β-Hydride elimination and subsequent reductive elimination from the metallacycloheptane is believed to lead to the production of 1-hexene and regeneration of the active catalytic species.[22] The formation of large amounts of 1-butene in the mechanism shown in Scheme 2.19 is believed to be deterred by the geometrical constraints of the metallacyclopentane, which are thought to limit interactions between its β-hydrogens and the metal centre, thereby preventing the elimination of 1-butene.[22] The catalytic cycle portrayed in Scheme 2.19 is the most widely accepted version of the metallacyclic mechanism for Cr-based selective ethylene trimerisation systems.

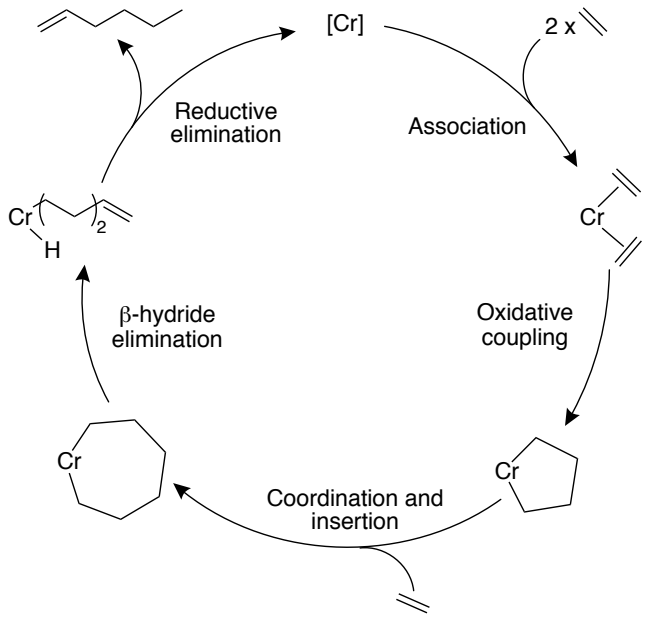

Scheme 2.19: Simplified version of the proposed metallacycle mechanism for selective ethylene trimerisation system, modified from Briggs.[22]

It was stipulated by Briggs[22] that the selectivity of the metallacycle mechanism (Scheme 2.19) towards 1-hexene formation is dependent upon two factors. The first is the difference in the rate of ethylene insertion into the metallacyclopentane intermediate *versus* the rate of decomposition of the metallacyclopentane intermediate; a faster rate of ethylene insertion leading to greater 1-hexene formation.[22] The second factor is the difference in the rates of further ethylene insertion into the metallacycloheptane intermediate *versus* the rate of β-hydride elimination from the metallacycloheptane intermediate; a faster rate of β-hydride elimination favouring 1-hexene formation.[22] The rates of ethylene insertion into the metallacyclopentane or metallacycloheptane intermediates, decomposition of the metallacyclopentane intermediate, and β-hydride elimination from the metallacycloheptane intermediate are dictated by the relative stabilities of the metallacyclopentane and metallacycloheptane intermediates.[22] Studies by Whitesides *et al.*[72,73] and Jolly *et al.*[74,75] on the thermal decomposition of metallacyclic platinum (in the former study) and chromium (in the latter study) complexes revealed that metallacyclopentane platinum or chromium complexes decompose at a slower rate than their metallacycloheptane analogues. Consequently, the metallacyclopentane complexes are more stable than their metallacycloheptane counterparts, and so can undergo ethylene insertion in the metallacycle mechanism described in Scheme 2.19.

Strong evidence for the proposed metallacycle mechanism for selective ethylene trimerisation was provided in a deuterium labelling study conducted by Bercaw and Labinger *et al.* in 2004.[33] In this investigation, a known selective ethylene trimerisation system employing a Cr-PNP complex (portrayed in Scheme 2.20) was tested in

ethylene oligomerisation utilising a feedstock comprising a 1:1 mixture of C_2H_4 and C_2D_4; GC-MS analysis was employed to determine the isotopic distribution of the hexene isotopologs produced.[33] It was reasoned that a metallacyclic mechanism would generate hexene isotopologs containing even numbers of deuterons, as in this mechanism the process of reductive elimination (shown in Scheme 2.19) means that the hexene formed would incorporate all of the deuterium atoms from the C_2D_4 monomer.[33] In contrast, if a Cossee-Arlmann mechanism is in operation then hexene isotopologs with odd number of deuterons would also be obtained, since in this process the hexene is liberated *via* β-hydride elimination (Chapter 1, section 1.2.1, Scheme 1.1) and so would leave behind the eliminated deuterium on the chromium centre.[33] The finding that only even-numbered hexene isotopologs were formed by the selective ethylene trimerisation system shown in Scheme 2.20 ruled out the possibility of a Cossee-Arlmann mechanism, and proved that this system operates by a metallacyclic mechanism.[33]

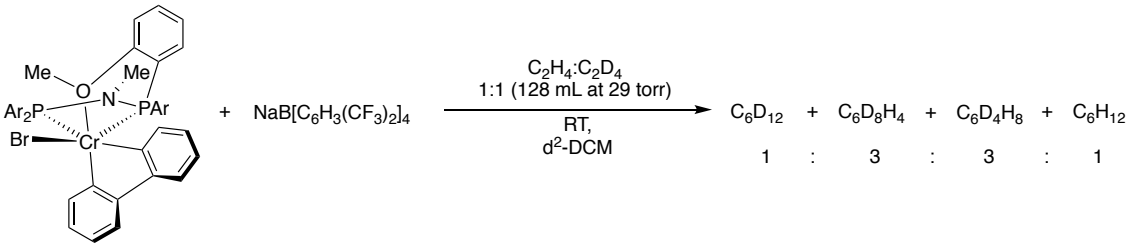

Scheme 2.20: Labelling study undertaken on Cr/PNP-based ethylene trimerisation system by Bercaw and Labinger *et al.*[33]

In a later publication, Bercaw and Labinger *et al.* performed a deuterium labeling study on a known ethylene oligomerisation catalyst (a Ni-based SHOP catalyst) and found that, as anticipated from the Cossee-Arlmann mechanism believed to be in operation, a broad distribution of both even- and odd-numbered hexene isotopologs were obtained.[76] Together, these results from the labeling studies by Bercaw and Labinger *et al.* have led to the wide acceptance that the majority of Cr-based selective ethylene trimerisation systems proceed by a metallacycle mechanism.[33,76]

2.1.3.2. Metallacycle mechanism for selective ethylene tetramerisation processes

In contrast to the case for trimerisation, a number of different metallacycle mechanisms have been speculated in the literature for different Cr-based ethylene tetramerisation systems, not least since there has been considerable debate over the exact nature of the metallacycle mechanism by which selective ethylene tetramerisation proceeds.[77] The first mechanism of Cr-based selective ethylene tetramerisation came from workers at Sasol Technology for their selective ethylene Cr/PNP-based tetramerisation system

(which has previously detailed in section Scheme 2.4).[78] Using a similar approach to that described in the previous section from the work of Bercaw and Labinger *et al*.,[33,76] researchers at Sasol Technology conducted a labelling study on the Cr/PNP-based tetramerisation system and found the exclusive formation of hexene isotopologs possessing even numbers of deuterons, leading them to propose the metallacycle mechanism portrayed in Scheme 2.21.[78] The relative stability of the different-sized metallacycle intermediates shown in Scheme 2.21 are thought to confer selectivity towards 1-hexene or 1-octene.[78] The mechanism conveyed in Scheme 2.21 implies that the metallacycloheptane intermediate is stable enough to enable insertion of an ethylene monomer,[78] contrary to earlier theoretical studies on tantalum-[23] and titanium-[24] based ethylene trimerisation systems.

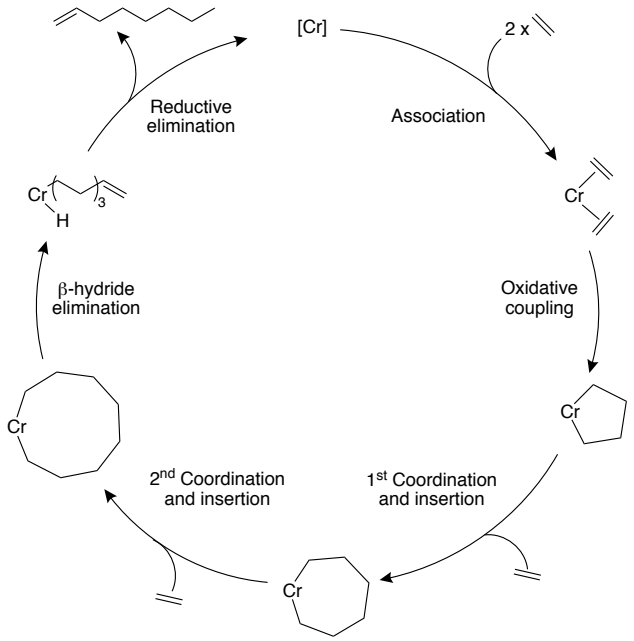

Scheme 2.21: Simplified version of the proposed metallacycle mechanism for Cr/PNP-based selective ethylene tetramerisation system, modified from Overett *et al.*[78]

Rosenthal and Müller *et al*.[79] proposed an alternative mechanism to that displayed in Scheme 2.21 for Cr-based selective ethylene tetramerisation, namely a bimetallic chromium-centred metallacycle mechanism. The mechanism proposed by Rosenthal and Müller *et al*. is described in Scheme 2.22 and speculates that 1-octene is formed *via* cooperative bimetallic reductive elimination from a species containing two chromacyclopentanes coupled to each other.[79] The inspiration for the mechanism shown in Scheme 2.22 came from the suggested mechanism for the Phillips and Union carbide CrO_3/SiO_2-based ethylene polymerisation system.[80,81] A combination of experimental and theoretical studies on the CrO_3/SiO_2-based ethylene polymerisation system suggested that this process is mediated by a binuclear chromium species.[80,81]

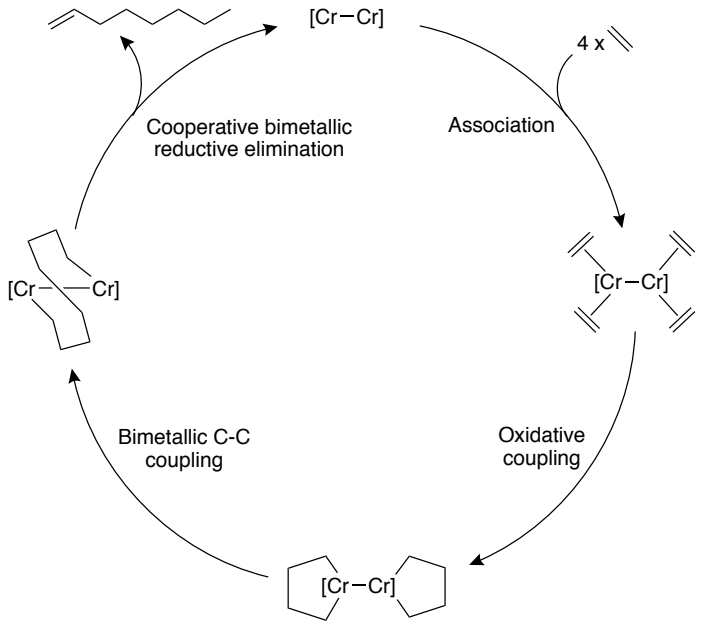

Scheme 2.22: Proposed bimetallic metallacyclic mechanism for ethylene tetramerisation, modified from Rosenthal and Müller *et al*.[79]

The possibility raised by Rosenthal and Müller *et al*.[79] that a bimetallic catalyst is in operation was addressed in a study by Theopold *et al*.[82] on a Cr-dinitrogen based selective ethylene trimerisation system. In this study, bimetallic Cr^{II} metallacycles were synthesised and found to generate non selective ethylene oligomerisation systems, indicating that these are not intermediates in the Cr-dinitrogen based selective ethylene trimerisation system.

In a recent combined experimental and theoretical study on the original Sasol Cr/PNP-based selective ethylene *tetra*-merisation system (system previously detailed in section 2.1.1.3), Britovsek and McGuinness *et al.*[83] have demonstrated that selective ethylene *tri*- and *tetra*-merisation is most likely to occur *via* a monometallic mechanism (similar to that proposed by workers at Sasol Technology,[78] Scheme 2.21). The work by

Britovsek and McGuinness *et al.*[83] suggests that 1-octene formation occurs *via* a *bis*(ethylene) chromacyclopentane intermediate (Scheme 2.23), possibly with additional involvement of a pathway involving a *mono*(ethylene) chromacycloheptane intermediate (as originally proposed by workers at Sasol Technology, Scheme 2.21[78]). The study by Britovsek and McGuinness *et al.*[83] also demonstrates that 1-hexene formation in the Cr/PNP-based system most likely occurs from a single route *via* a mono(ethylene) metallacyloheptane intermediate, as originally proposed by Briggs (section 2.1.3.1).[22]

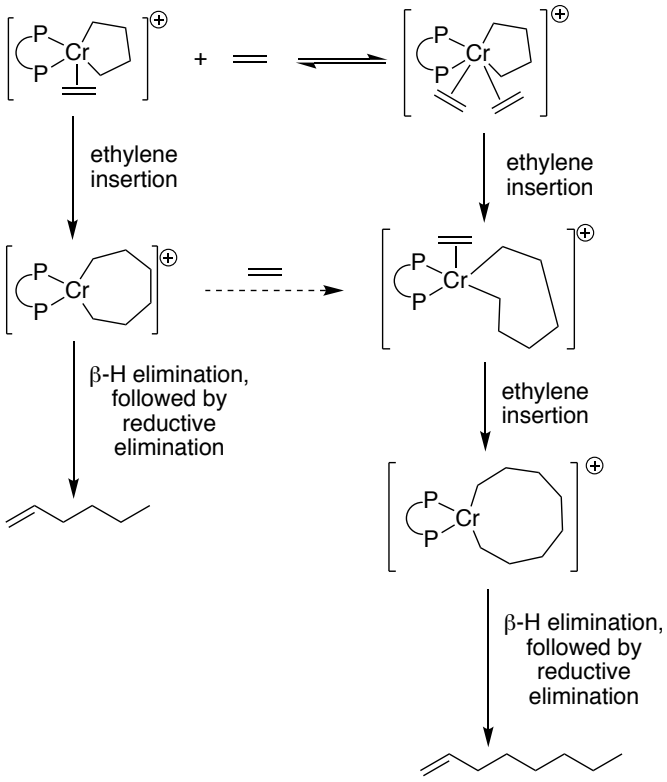

Scheme 2.23: Proposed mono- and bis-ethylene routes to 1-hexene and 1-octene by original Sasol Cr/PNP-based selective ethylene tetramerisation catalyst, modified from Britovsek and McGuinness *et al.*[83]

Britovsek and McGuinness *et al.* also undertook experimental and theoretical studies on Cr/PNP-based selective ethylene trimerisation systems, which led them to conclude that the selectivity of Cr/PNP-based selective *tri*-/*tetra*-merisation catalysts is dictated by competition between the *mono*- and *bis*-ethylene routes highlighted in Scheme 2.23.[84,85] The experimental observations that Cr/PNP-based selective ethylene oligomerisation systems display greater selectivity towards *tri*- *versus tetra*-merisation upon increasing the steric bulk of the phosphorous substituents, or using ligands bearing additional donor groups at their phosphorus positions, were rationalized in terms of these systems producing a more sterically-congested active species, which suppresses the pathways for 1-octene formation shown in Scheme 2.23.[84,85]

2.1.4. Oxidation state of Cr in selective ethylene *tri*-/*tetra*-merisation systems

A key feature of the metallacycle mechanisms widely believed to be in operation for Cr-based selective ethylene *tri*-/*tetra*-merisation processes is the accessibility of Cr^{n} and Cr^{n+2} oxidation states. This is inferred since the active catalytic species undergoes a two-electron redox process (by oxidative addition and reductive elimination steps). Consequently, much research has been focused on elucidating the oxidation states in operation for Cr-based selective ethylene *tri*-/*tetra*-merisation systems experimentally, which has resulted in speculation that these system operate *via* a Cr^{I}/Cr^{III} or Cr^{II}/Cr^{IV} redox couple.[1,4,5,8] The electronic nature of the ligand is believed to influence the exact nature of the Cr^{n}/Cr^{n+2} redox couple in operation in the ethylene *tri*-/*tetra*-merisation systems.[4,5,8]

The active catalyst species in Cr-based selective ethylene *tri*-/*tetra*-merisation systems are difficult to isolate, and difficult to analyse (due to their paramagnetism, which hinders the use of traditional NMR spectroscopic methods), something that makes deduction of their oxidation state challenging.[4] Furthermore, the oxidation state of chromium in the active catalyst species cannot always be inferred to be the same as that of the catalyst precursor (commonly Cr^{I}, Cr^{II}, or Cr^{III}) in the majority of Cr-based selective ethylene *tri*-/*tetra*-merisation systems, as these employ an activator (usually an alkyl aluminium reagent, section 2.1.5), which has the potential to alter the oxidation state of the catalyst precursor.[4] For example, Gamboratta and Duchateau *et al.* demonstrated that $AlMe_3$ was capable of reducing a Cr(III)-PNP complex, which generates a selective ethylene tetramerisation process in the presence of MAO activator, to a Cr^{II}-PNP complex (Scheme 2.24).[86] Since, the Cr^{II}-PNP complex also generated a selective ethylene tetramerisation system, in the presence of MAO, Gamboratta and Duchateau *et al.* inferred that reduction of the Cr^{III}-PNP complex to the Cr^{II}-PNP complex must be a step involved in the formation of the active catalytic species of the Cr/PNP-based selective ethylene tetramerisation system.[86]

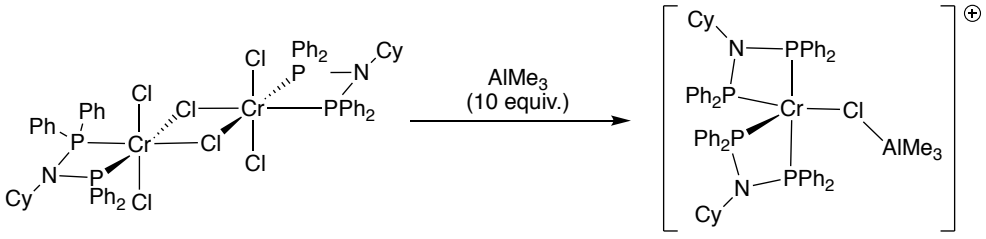

Scheme 2.24: $AlMe_3$-mediated reduction of Cr^{III}-PNP complex, observed by Gamboratta and Duchateau *et al.*[86]

The subsequent sections detail selected examples of literature studies implementing different analytic techniques for the elucidation of the chromium oxidation states of Cr/P,N-ligand-based selective ethylene *tri*-/*tetra*-merisation systems. Only Cr-based selective ethylene *tri*-/*tetra*-merisation systems utilising P,N-ligands will be considered as these ligands are the closest in electronic nature to the PCN ligands that have been investigated, subsequently, in this thesis for use in Cr-based selective ethylene *tri*-/*tetra*-merisation.

2.1.4.1. Cr^{I}/Cr^{III}-based systems

In a study by Bercaw and Labinger *et al.* electron paramagnetic resonance (EPR) spectroscopy was applied to monitor the reaction of MAO with the Cr^{III}-PNP complex portrayed in Figure 2.10.[87] The Cr^{III}-PNP complex, which generates a selective ethylene trimerisation system in the presence of MAO, was found by EPR spectroscopy to form multiple Cr^{III}-PNP species and an EPR silent Cr species as the major products, alongside a minor amount of a Cr^{I} complex.[87] Based on a series of studies, Bercaw and Labinger *et al.* found that the Cr^{III}-PNP and EPR silent Cr species were not involved in selective ethylene oligomerisation catalysis and so postulated that the observed Cr^{I} complex, although formed in minority, was most likely the active catalytic species.[87] Consequently, they inferred that a Cr^{I}/Cr^{III} redox couple is involved in the Cr/PNP-based selective ethylene trimerisation.

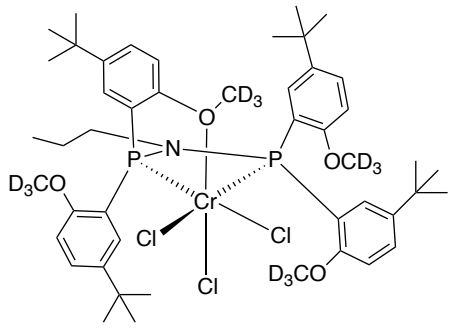

Figure 2.10: Cr^{III}-PNP selective ethylene trimerisation catalyst precursor, investigated by Bercaw and Labinger *et al.*[87]

In addition to experimental studies, computational investigations have also been found to be informative with regard to the possible oxidation state of chromium most likely present in Cr-based selective ethylene *tri*-/*tetra*-merisation systems. For example, a theoretical study by Britovsek and McGuinness *et al*.[88] on the original Sasol Cr/PNP-based selective ethylene tetramerisation catalyst (section 2.1.1.3) suggests that Cr^{I} and Cr^{III} are preferred oxidation states, both kinetically and thermodynamically, to Cr^{II} and Cr^{IV}.

2.1.4.2. Cr^{II}/Cr^{IV}-based system

A study by Brückner et al. applied *operando* EPR spectroscopy (*i.e.* spectroscopically probed species of interest under catalyst operating conditions) and *in situ* X-ray absorption spectroscopy (XAS) to a Cr/PNP-based selective ethylene tetramerisation system.[89] The results obtained by EPR spectroscopy and *in situ* XAS suggested that a $(PNP)Cr^{II}(CH_3)_2$ complex was the active catalytic species, having been formed *in situ* from $Cr(acac)_3$, PNP ligand and MMAO activator, leading the authors to propose that the ethylene tetramerisation proceeds *via* a metallacycle pathway involving a Cr^{II}/Cr^{IV} redox couple.[89] The observation that the activator reduces the chromium centre of the starting chromium species is in accordance with that observed in other Cr-based selective ethylene *tri-*/*tetra*-merisation systems utilising activators (Scheme 2.24).[4,86]

2.1.5. Role of activator in Cr-based selective ethylene *tri-*/*tetra*-merisation systems

The majority of Cr-based selective ethylene *tri-*/*tetra*-merisation systems utilise an aluminium-based activator (such as $AlMe_3$, $AlEt_3$, MAO, or MMAO) which reacts with the Cr-ligand catalyst precursor to form an active catalyst species.[1,4,5,8] The aluminium-based activators are believed to alkylate the chromium centre of the Cr-based selective ethylene oligomerisation systems and then subsequently act as a Lewis acid and abstract the alkyl group to generate a cationic chromium species which is thought to be the active catalyst species (Scheme 2.25).[5,90]

(a) Alkylation of metal centre:

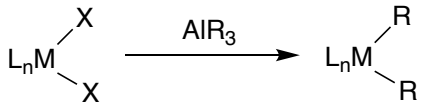

(b) Alkyl abstraction:

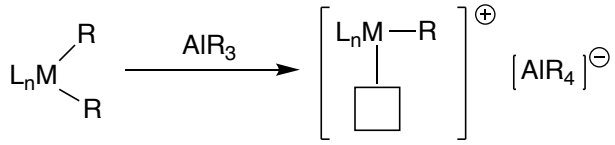

Scheme 2.25: Role of aluminium alkyl activator in generating a cationic metal-ligand species, where L represents a ligand, R and X refer to an alkyl group and halide, respectively, and a square corresponds to a vacant coordination site at the metal centre.

In addition to observing the formation of catalytically active cationic species, following the reaction of Cr-ligand complexes with alkyl aluminium activators in Cr-based selective ethylene *tri-*/*tetra*-merisation systems, studies have also found that the activator can act as an impurity scavenger[90] and/or reduce the Cr centre (as mentioned

previously in section 2.1.4).[4,86] Moreover, studies have shown that certain activators can have more diverse effects on PNP ligands, which are commonly used to support Cr-based ethylene *tri*-/*tetra*-merisation systems. For example, a study by Gamboratta *et al*.[66] revealed that $AlEt_3$ activator caused breakage of the P-N bonds of a Cr-PNP complex (Scheme 2.26(a)), whilst recent work by Agapie *et al.*[91] showed that chlorinated aluminium activators (such as $AlClMe_2$) isomerised PNP ligands to PPN ligands (Scheme 2.26(b)).

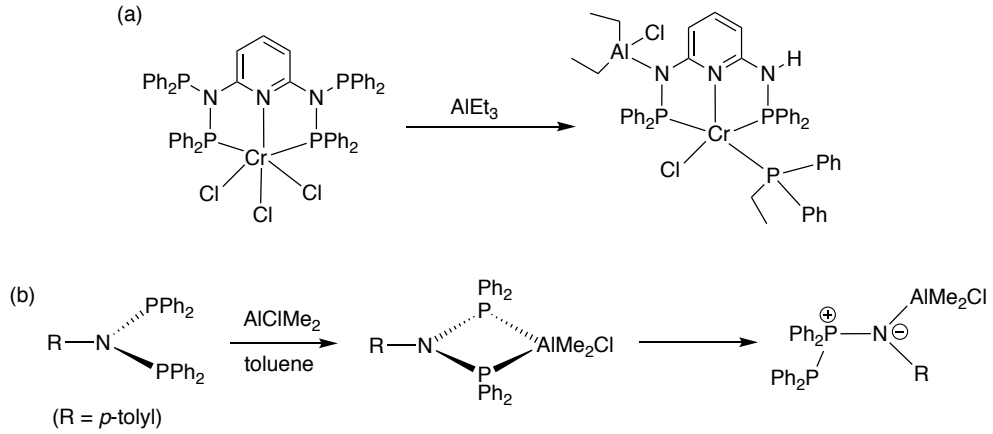

Scheme 2.26: Reactions between PNP ligands and aluminium alkyl activators: (a) breakage of P-N bond,[66] (b) isomerisation of PNP ligand to PPN ligand.[91]

Of the different aluminium activators implemented in Cr-based selective ethylene *tri*-/*tetra*-merisation systems described in the open literature, MAO or MMAO are the most commonly used as these generally give the most active and selective systems.[8] MAO is prepared by the controlled hydrolysis of $AlMe_3$ and has the general formula $[Al(CH_3)O]_n$.[90] The nature of the hydrated salt (*i.e.* H_2O source) and MAO synthetic reaction conditions used in the synthesis of MAO from $AlMe_3$ are known to influence the activity imparted to the resultant MAO-activated catalytic precursors, presumably as a consequence of differences in the structure of the MAO generated.[90] Although much research has focussed on deducing the structure of MAO, its precise structure is still a matter of wide debate with a number of different oligomeric structures being proposed in the literature (some examples of which are illustrated in Figure 2.11).[90,92] Of significance to note is a computational study on the interaction of various MAO structural models with chromacycloheptanes (well established intermediates in Cr-based selective ethylene *tri*-/*tetra*-merisation systems) by van Rensburg *et al.*, which found that a cage solution-state structure was energetically favourable for MAO.[93] Nevertheless, it is most likely that MAO exists in an equilibrium of interconverting structures in solution.[90,92] In addition to this fluxional behaviour of MAO, the participation of residual $AlMe_3$ in the equilibria of interconverting MAO oligomers,

further makes structural elucidation of MAO challenging, with the MAO itself acting as a reservoir for $AlMe_3$. [90,92]

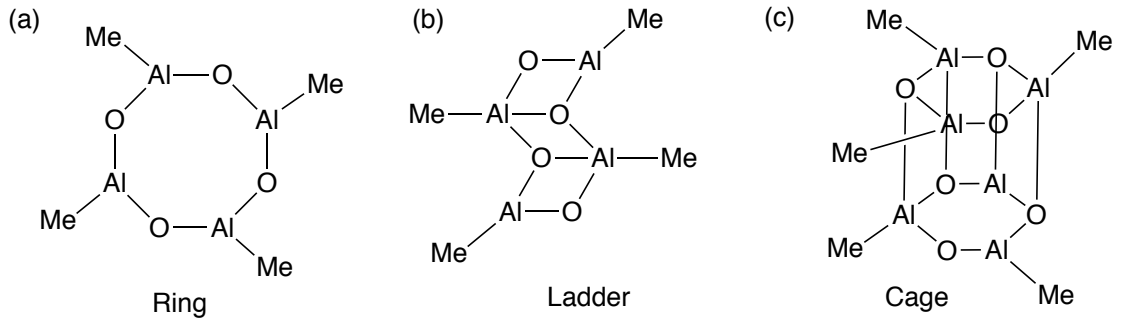

Figure 2.11: A selection of oligomeric structures proposed for MAO.[90,92]

The poor solubility of MAO in non-polar solvents, coupled with its poor shelf-life and limited stability at elevated temperatures, has led to the preferential implementation of modified versions of MAO (namely MMAO) in many selective ethylene *tri*-/*tetra*-merisation systems.[90,92] The presence of the bulky ^{i}Bu group in MMAO, which is afforded by the careful hydrolysis of a mixture of $AlMe_3$ and $Al^{i}Bu_3$, imparts its increased solubility in aliphatic solvents *versus* MAO, resulting in its better stability for storage.[90,92]

Due to the use of MAO or MMAO activators in Cr-based selective ethylene tri-/tetra-merisation systems typically being accompanied with several economic drawbacks, such as their high cost, difficulty in their handling on a large scale, and wasteful nature (since large excesses of these activators are generally utilised), many studies have focused on the development of selective and active Cr-based ethylene *tri*-/*tetra*-merisation systems implementing alternative activators to MAO/MMAO.[8] In this vein, a series of studies were conducted by workers at Sasol Technology Limited on evaluating the behaviour of a range of Cr-PNP complexes in ethylene oligomerisation, in the presence of different activators.[94,95] The first of these studies was by Overett *et al*.[94] and found that selective ethylene *tri*-/*tetra*-merisation systems were generated when stoichiometric amounts of trialkylaluminium activator and borate cocatalyst ($B(C_6F_5)_3$ or $[Ph_3C][B(C_6F_5)_3]$) were implemented. Due to the low Lewis acidity of trialkylaluminium activators, when compared to MAO,[96] a highly Lewis acidic borate cocatalyst was also implemented to increase the efficiency of alkyl abstraction in the generation of the active catalytic species (Scheme 2.25).[94] Although the selectivity for selected oligomer formation in the liquid fraction of these systems were comparable to systems utilising MAO as activator, they typically produced higher levels of polymer and exhibited much lower activities.[94] The catalysts in the Cr/PNP/AlR_3/borate systems

were also observed to rapidly deactivate, with the rate of deactivation being directly proportional to the amount of $AlEt_3$ utilised, something that led Overett et al. to suggest alkyl exchange of the borate cocatalyst with $AlEt_3$ as the source of catalyst deactivation. [94] Therefore, a study by McGuinness and Tooze *et al.* investigated the effect of using alternative cocatalysts to borate for the Cr/PNP/AlR_3 systems, with a highly active selective ethylene tetramerisation system being obtained when $[Ph_3C][Al\{OC(CF_3)_3\}_4]$ cocatalyst was implemented (Scheme 2.27).[95] The high stability and weakly coordinating nature of the aluminate anion ($[Al\{OC(CF_3)_3\}_4]^-$, Krossing's anion)[97] was believed to be responsible for the improved activity of the Cr/PNP/AlR_3/$[Ph_3C][Al\{OC(CF_3)_3\}_4]$ system, relative to that of the Cr/PNP/AlR_3/Borate system.[95]

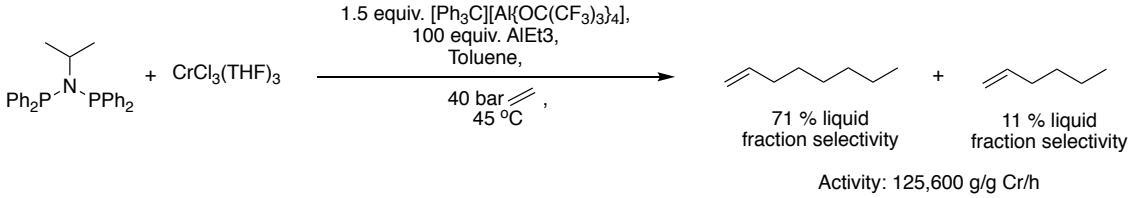

Scheme 2.27: Cr/PNP-based selective ethylene tetramerisation system utilising $AlEt_3$/aluminate activator, reported by McGuinness and Tooze *et al*.[95]

Lastly, it is important to note that while the majority of Cr-based selective ethylene *tri-*/*tetra*-merisation systems implement an activator, there are a limited number that operate activator-free (although these systems generally exhibit lower activities than those using an activator).[4,8] By way of example, Scheme 2.28 portrays a $Cr^{I}/^{II}$-NP ligand complex discovered by Gambarotta and Budzelaar *et al*. to catalyse ethylene almost exclusively to 1-hexene, albeit it with a low activity.[98] Computational calculations on this $Cr^{I}/^{II}$-NP selective ethylene trimerisation system suggested that the Cr^{I} centre was responsible for 1-hexene formation, whilst the Cr^{II} centre was responsible for 1-butene formation.[98]

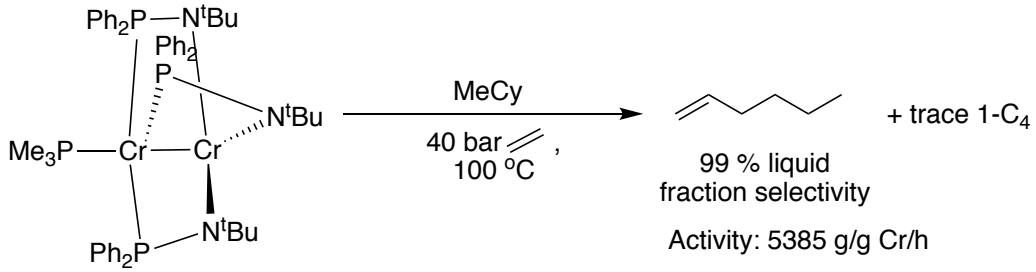

Scheme 2.28: $Cr^{I}/^{II}$-NP ligand based selective ethylene trimerisation system reported by Gambarotta and Budzelaar *et al*.[98]

2.1.6. Cr/PCN-based selective ethylene *tri*-/*tetra*-merisation system

Taking inspiration from the best-performing literature Cr/P,N-ligand-based selective ethylene *tri*-/*tetra*-merisation systems (in terms of activity and selectivity), *i.e.* Cr/PNP (section 2.1.2.2.1) and Chevron Phillips Cr/P-imine (section 2.1.2.2.9) systems, the idea of applying PCN ligands in Cr-based ethylene oligomerisation systems was developed in the Dyer group (Figure 2.12).[70]

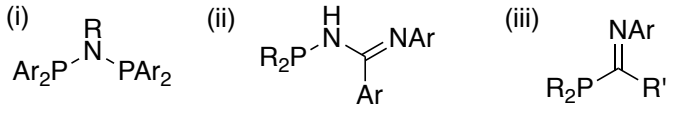

(R and R' = aryl or alkyl group)

Figure 2.12: Generalised structures of (i) PNP, (ii) P-imine, and (iii) PCN ligands.

The syntheses of iminophosphines with similar structures to that shown in Figure 2.12(iii) have been reported in multiple literature studies,[99-106] however their implementation in Cr-based selective ethylene *tri*-/*tetra*-merisation systems has yet only been reported by Dyer and Hanton *et al.*,[71] in 2015. By way of summary to the groundwork of the studies conducted in Chapters 2 and 3 of this thesis on Cr/PCN-based selective ethylene *tri*-/*tetra*-merisation systems, this section will briefly overview the best-performing Cr/PCN-based ethylene *tri*-/*tetra*-merisation systems (in terms of selectivity, activity and polymer level) developed by Dr. James Radcliffe and the coordination chemistry of PCN ligands with Cr^0 and Cr^{III}, before outlining the aims of Chapters 2 and 3 of this thesis.

2.1.6.1. Evaluation of best-performing Cr/PCN-based ethylene tri-/tetra-merisation systems

A library of 26 novel PCN compounds (bearing different nitrogen, imine carbon, and phosphorus substituents) was synthesised by Dr. James Radcliffe in the Dyer group and tested in ethylene oligomerisation catalysis, under a variety of different catalysis conditions (comparison of different catalysis conditions detailed in Chapter 3 of this thesis).[70] It was found that, depending on the substitution pattern of the PCN ligand implemented, Cr/PCN-based selective ethylene *tri*- and *tetra*-merisation systems displaying high selectivities and activities shown in Scheme 2.29, with varying polymer content (2 – 84 wt %), could be obtained under a set of optimised catalysis conditions (as illustrated in Scheme 2.29).[70,71]

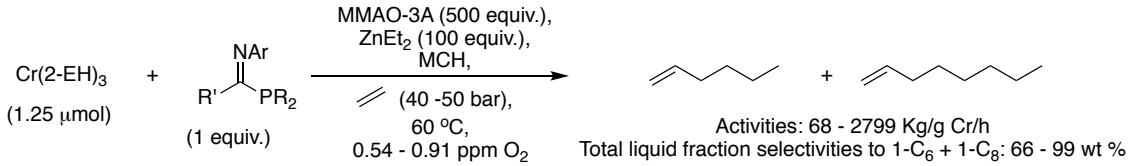

(R and R' = alkyl or aromatic group)

Scheme 2.29: Cr/PCN-based selective *tri-tetra*-merisation systems developed in the Dyer group.[70,71]

The structure-activity and structure-selectivity relationships established in the Cr-PCN based selective ethylene oligomerisation systems are detailed in Chapter 3. Nonetheless, the main observation was that PCN ligands possessing bulky substituents at both nitrogen and phosphorus produced the best-performing ethylene *tri*- and *tetra*-merisation systems (Figure 2.13), with no conclusive structure-activity or structure-selectivity relationships obtained on varying the imine carbon substituents.[70,71]

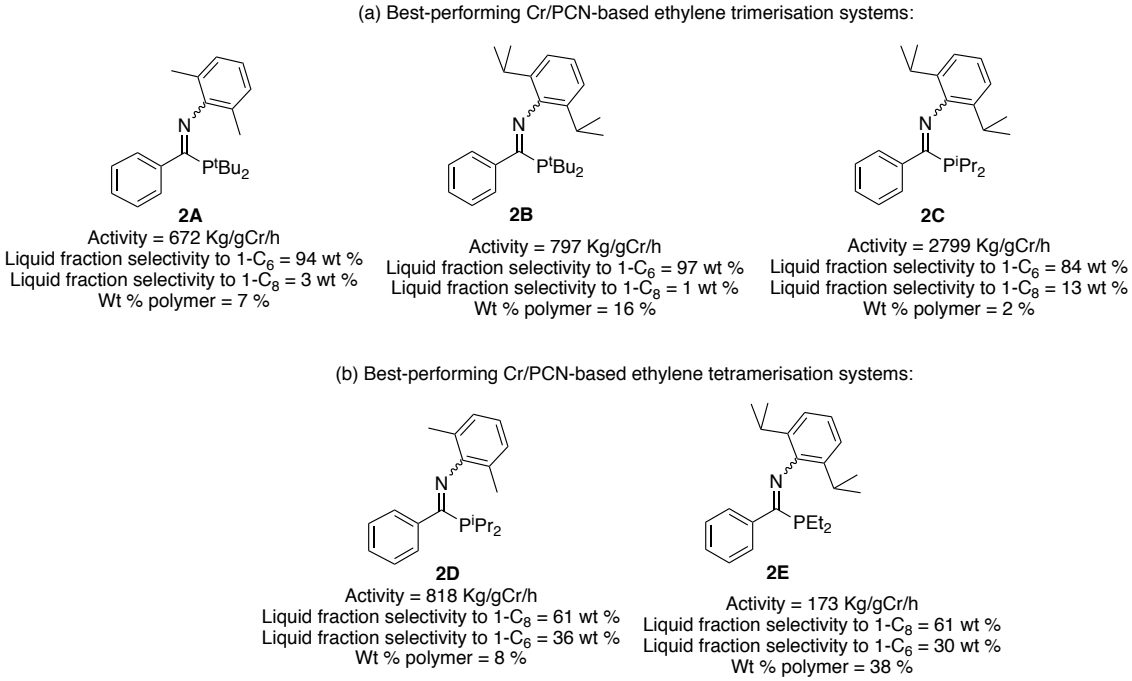

Figure 2.13: PCN ligands giving rise to the best-performing Cr/PCN-based selective ethylene *tri*- and *tetra*-merisation systems.[70,71] Conditions of ethylene oligomerisation catalysis: $Cr(2\text{-}EH)_3$ (1.25 μmol), 1 equiv. PCN ligand **2A** – **2E**, MMAO-3A (500 equiv.), $ZnEt_2$ (100 equiv.), MCH, C_2H_4 (40 - 50 bar), 60 °C, 0.63 - 0.89 ppm O_2.[70,71]

The best-performing Cr/PCN-based ethylene trimerisation systems shown in

Figure 2.13 are amongst the most selective (systems using ligands **2A** and **2B**) and active (system using ligand **2C**) known in the literature to-date (Table 2.3), albeit it with higher levels of polymer content. Conversely, the best-performing Cr/PCN-based ethylene tetramerisation systems shown in Figure 2.13 (systems using ligands **2D** and **2E**) exhibit lower activities, selectivities to 1-octene, and higher polymer content than a

selection of the best-performing ethylene tetramerisation systems reported in the literature thus far (Table 2.4).

Table 2.3: Activities, polymer formation percentages, and 1-hexene selectivities of a selection of best-performing literature ethylene trimerisation systems, modified from Alferov *et al.*[8]

Catalyst precursor	Liquid fraction selectivity to 1-C_6 (wt %)	Activity (Kg/g TM/h)	Polyethylene (wt %)	Reference
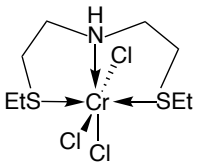	98	161	0.16	107
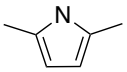 + $Cr(2\text{-}EH)_3$	95	3780	0.04	15
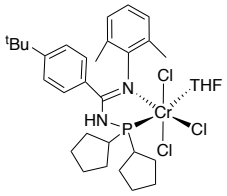	94	2142	0.07	108
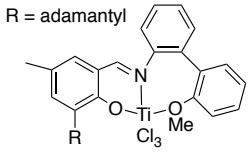	92	7140	0.40	109

Table 2.4: Activities, polymer formation percentages, and 1-octene selectivities of a selection of best-performing literature ethylene tetramerisation systems, modified from Alferov *et al.*[8]

Catalyst precursor	Liquid fraction selectivity to 1-C8 (wt %)	Activity (Kg/g Cr/h)	Polyethylene (wt %)	Reference
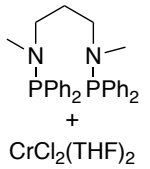	91	2	0	48
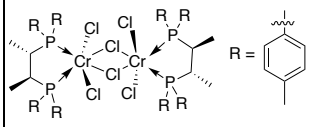	77	580	1.9	110
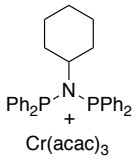	67	2147	0.8	36
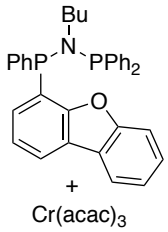	66	8000	0.2	30

2.1.6.2. Coordination chemistry of PCN ligands with Cr^0 and Cr^{III} complexes

2.1.6.2.1. Cr^{III}-PCN complexes

The coordination chemistry of PCN ligands **2F** – **2K** (Scheme 2.30) to $CrCl_3(THF)_3$ was investigated by Dr. James Radcliffe.[70] PCN ligands **2F** – **2G** (Scheme 2.30) and **2I – 2K** (Scheme 2.30) were found to exhibit κ^2-P,N bidentate binding modes to Cr^{III}, while ligand **2H** bound in a tridentate manner (κ^2-P,N,O), due to the presence of the pendant OMe donor group on its phenyl nitrogen (similar to Cr^{III}-PNP^{OMe} structures discussed previously in section 2.1.2.2.1.1).[70] In addition, molecular structures were obtained of Cr^{III}-PCN complexes **2L** and **2M** (Scheme 2.30), which revealed P-C-N angles of 103.89(15)° and 104.03(15),° respectively, which are comparable to P-N-P angles in Cr^{III}-PNP complexes (103 - 106°).[70] Consequently, from the similarities between the Cr^{III}-PCN and Cr^{III}-PNP complexes, it is not surprising that the best-performing Cr/PCN-based ethylene trimerisation systems exhibit comparable activities and

selectivities to the well-established Cr/PNP-based selective ethylene trimerisation systems.

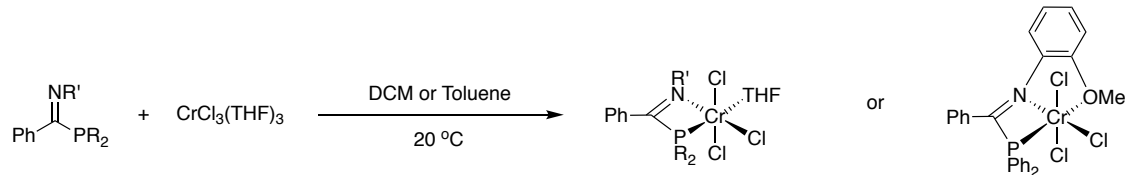

2F: R = Ph, R' = Ph,
2G: R = Ph, R' = 2-MeC_6H_4
2H: R = Ph, R' = 2-$OMeC_6H_4$
2I: R = ^{i}Pr, R' = 2-MeC_6H_4
2J: R = ^{i}Pr, R' = 2,6-MeC_6H_3
2K: R = ^{i}Pr, R' = 2,6-^{i}PrC_6H_3

2L: R = Ph, R' = Ph,
2M: R = Ph, R' = 2-MeC_6H_4
2O: R = ^{i}Pr, R' = 2-MeC_6H_4
2P: R = ^{i}Pr, R' = 2,6-MeC_6H_3
2Q: R = ^{i}Pr, R' = 2,6-^{i}PrC_6H_3

2N

Scheme 2.30: Cr^{III}-PCN complexes synthesised by Dr. James Radcliffe.[70]

2.1.6.2.2. Cr^0-PCN complexes

The PCN ligands **2R** and **2S** (Scheme 2.31) were reacted with $Cr(CO)_6$ and found to form Cr^0-PCN complexes displaying κ^2-P,N bidentate and κ^1-P monodentate binding modes, with the latter mode being favoured. The formation of both κ^2-P,N bidentate and κ^1-P monodentate Cr^0-PCN structures suggested hemilabile behaviour of the PCN ligands with Cr^0, which was proved upon the removal or addition of CO to an NMR tube reaction of PCN ligand **2X** (a representative PCN ligand, Scheme 2.32) with $Cr(CO)_6$.

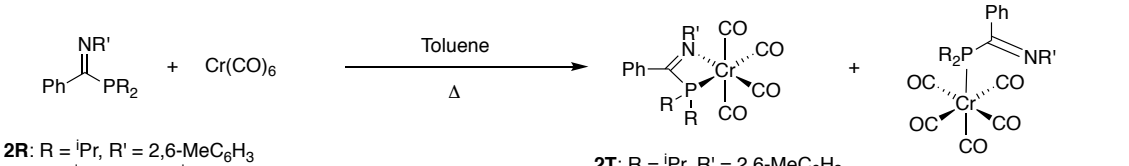

2R: R = ^{i}Pr, R' = 2,6-MeC_6H_3
2S: R = ^{i}Pr, R' = 2,6-^{i}PrC_6H_3

2T: R = ^{i}Pr, R' = 2,6-MeC_6H_3
2V: R = ^{i}Pr, R' = 2,6-^{i}PrC_6H_3

2U: R = ^{i}Pr, R' = 2,6-MeC_6H_3
2W: R = ^{i}Pr, R' = 2,6-^{i}PrC_6H_3

Scheme 2.31: Cr^0-PCN complexes synthesised by Dr. James Radcliffe.[70]

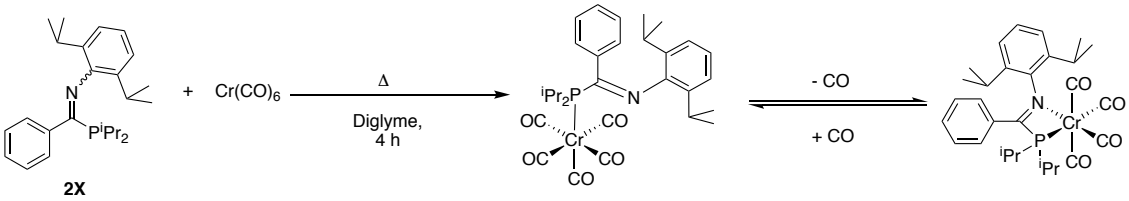

2X

Scheme 2.32: Reaction evidencing hemilabile behaviour of PCN ligand with Cr^0 complex.[70]

2.1.6.3. Aims of Chapters 2 and 3 of this thesis

The work in Chapters 2 and 3 of this thesis aims to build upon the previous work carried out by Dr. James Radcliffe in the Dyer group by:[70,71]

(a) synthesising a series of novel PCN ligands in order to further investigate the effects of varying the imine carbon and alkyl phosphorus substituents on the activity and selectivity in ethylene oligomerisation catalysis,

(b) completing the synthesis of a series of Cr^0-PCN complexes (incorporating complexes **2T** – **2W** (Scheme 2.31), originally synthesised by Dr. James Radcliffe) and carrying out oxidation reactions of these to obtain novel Cr^I-PCN complexes, which can then be evaluated as potential catalytic precursors in ethylene oligomerisation catalysis,

(c) completing the synthesis of the series of Cr^{III}-PCN complexes (including complexes **2O** – **2Q** (Scheme 2.30), originally synthesised by Dr. James Radcliffe) to further explore the coordination chemistry of PCN ligands to Cr^{III} complexes and obtain a full series of Cr^{III} -PCN complexes to compare in ethylene oligomerisation catalysis against their *in situ* generated equivalents.

The synthesis of the PCN ligands and Cr-PCN complexes will be detailed in this Chapter while their performance in ethylene oligomerisation catalysis will be discussed in Chapter 3.

2.2. Synthesis of PCN Ligands

A small library of 17 PCN ligands, **2.1** – **2.17** (Figure 2.14) was developed, with access *via* the route depicted in Scheme 2.33, previously developed in the Dyer group, with individual ligands being obtained in moderate yields varying between 50 – 78 %.[70,71] The modular synthetic approach used involves the synthesis of precursor imidoyl chlorides and trimethylsilylphosphines, which are then reacted in chlorobenzene to yield the desired PCN ligands.[70,71] The only by-product formed in the synthetic approach shown in Scheme 2.33 is TMSCl, which is easily separable from the product under reduced pressure.[70,71]

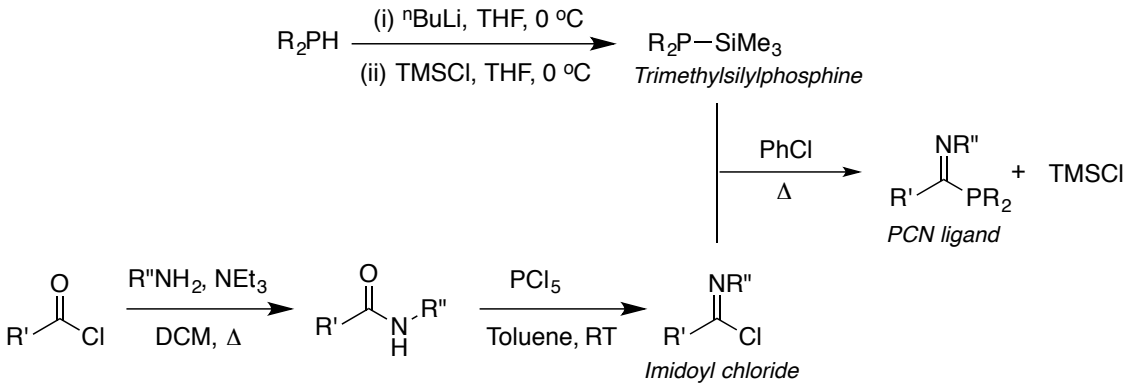

Scheme 2.33: Synthetic route to PCN ligands developed in the Dyer group, involving reactions between imidoyl chlorides and trimethylsilylphosphines in chlorobenzene.[70,71]

The nature of substituents at the phosphorus, carbon and nitrogen positions on the PCN ligands synthesised in this work, illustrated in Figure 2.14, were chosen based on

the results from previous investigations in the Dyer group, which demonstrated that PCN ligands encompassing alkyl substituents on the phosphorus atom and relatively bulky substituents on the nitrogen atom performed better in ethylene *tri-*/*tetra*-merisation catalysis.[70,71] Taking this into account, novel ligands **2.1** – **2.13** were designed with substituents at the phosphorus and nitrogen positions that met these requirements, but also broadened the range of steric and electronic properties that have previously been studied, in addition to exploring the effect of electronic properties of the imine carbon substituent on ethylene *tri-*/*tetra*-merisation catalysis. Ligands **2.14** – **2.17**, which have previously been synthesised in the Dyer group, were synthesised to act as precursors to Cr^0- and Cr^{III}-PCN complexes, which will be considered in section 2.4.

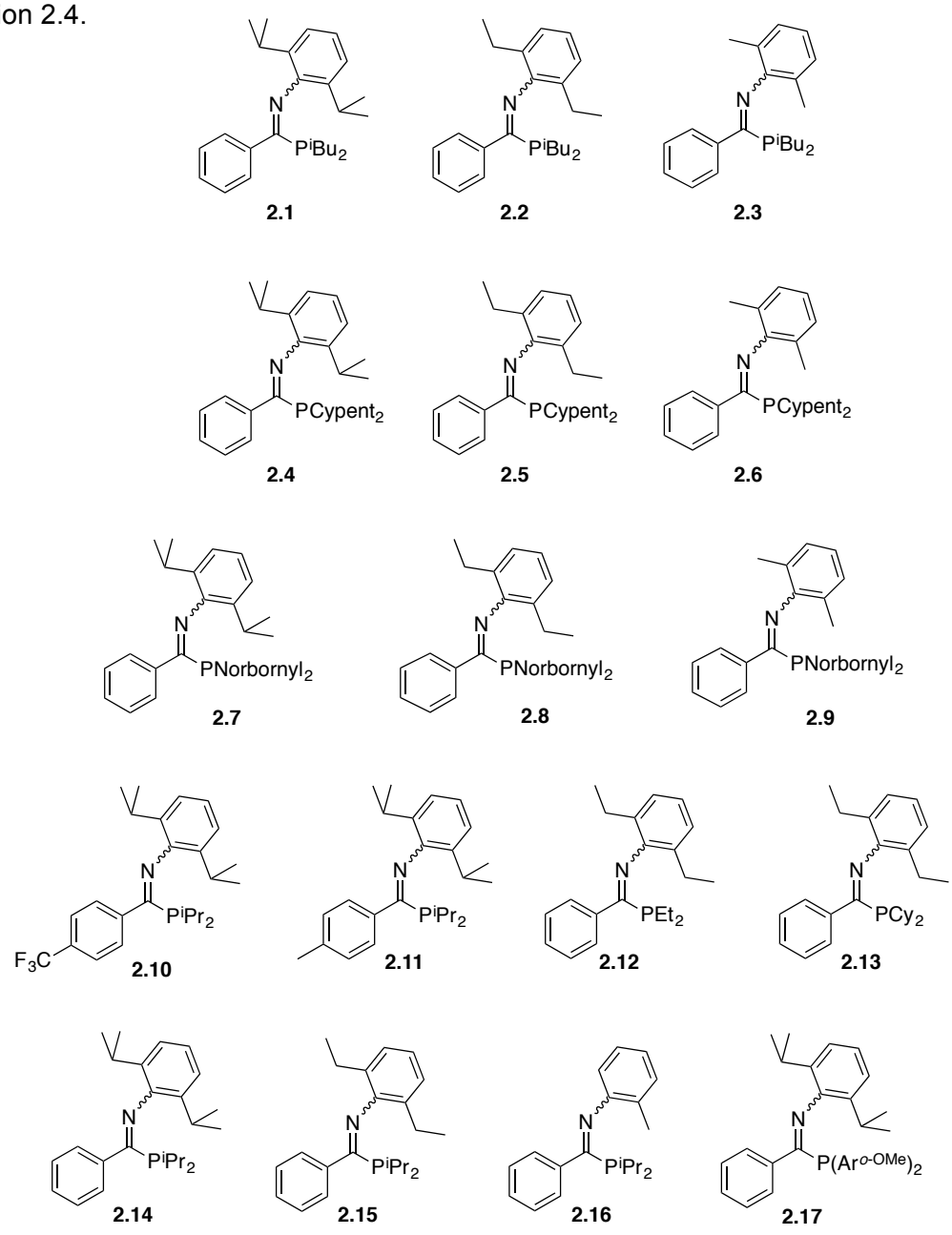

Figure 2.14: PCN ligands **2.1** - **2.17** synthesised in this thesis.

2.3. Characterisation of PCN Ligands

The PCN ligands synthesised in this thesis, **2.1** – **2.17** (Figure 2.14), have been fully characterised by elemental analysis, mass spectrometry, and NMR and IR spectroscopies. In agreement with the PCN ligands previously synthesised by Dr. James Radcliffe,[70] compounds **2.1** – **2.17** exhibit a characteristic doublet resonance in their ^{13}C NMR spectra in the chemical shift range of 174 – 181 ppm ($^{1}J_{PC}$ ranging between 15 – 27 Hz) corresponding to the imine carbons. In addition, ligands **2.1** – **2.17** also have a characteristic resonance attributed to their C=N-*C* ipso carbons, which lies in a chemical shift range of 147 – 151 ppm in their ^{13}C NMR spectra. Compounds **2.1** – **2.6** and **2.10** – **2.16** exhibit a single resonance in their solution-state ^{31}P{^{1}H} NMR spectra, indicating that these ligands exist as one conformer (*E* or *Z*, considered in further detail in section 2.3.2), whilst compound **2.17** exhibits two resonances (in a ratio of 1.0:0.22, attributed to *Z*:*E* conformers in previous work in the Dyer group).[70] In comparison, compounds **2.7** – **2.9** display three resonances in their solution-state ^{31}P{^{1}H} NMR spectra, suggestive of multiple isomers. A molecular structure of compound **2.8** was obtained, which enables understanding of the multiple resonances in the ^{31}P{^{1}H} NMR spectra of compounds **2.7** – **2.9**; discussed in section 2.3.1.

Analysis of ligands **2.1** – **2.17** by ASAP mass spectrometry reveals they undergo heterolytic cleavage across their imine C-PR_2 bond, as illustrated in Scheme 2.34. This results in the presence of two majority peaks in their mass spectra: the molecular ion and a peak resulting from fragment **2Y** shown in Scheme 2.34.

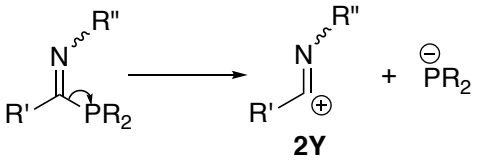

2Y

Scheme 2.34: Fragmentation of PCN ligands occurring in ASAP mass spectrometry *via* heterolytic cleavage along the imine C-PR_2 bond.

The following sections will discuss the molecular structure of compound **2.8** and properties of the PCN ligands (namely *E/Z* isomerisation, inference of their electronic properties (by analysis of their selenophosphine derivatives and C=N stretches of the PCN ligands in their IR spectra), and a consideration of their steric properties).

2.3.1. X-Ray crystallographic study of compound 2.8

The molecular structure of ligand **2.8** shows disorder about the norbornyl groups and isopropyl groups on the N substituent, revealing it to exist as a mixture of two *exo*

isomers, which co-crystallise, as illustrated in Figure 2.15. The *exo* isomers of ligand **2.8** are defined as having the bridgehead carbon (C7 and C7' in Figure 2.15) pointing in the same direction as the phosphorus atom. The *exo* isomers of ligand **2.8** differ in the position of the phosphorus atom on the norbornyl groups: 2-*exo* isomer (Figure 2.15 (i), in which the phosphorus atom is bonded to C2 and C2' of the norbornyl groups) or 3-*exo* isomer (Figure 2.15 (ii), in which the phosphorus atom is bonded to C3 and C3' of the norbornyl groups).

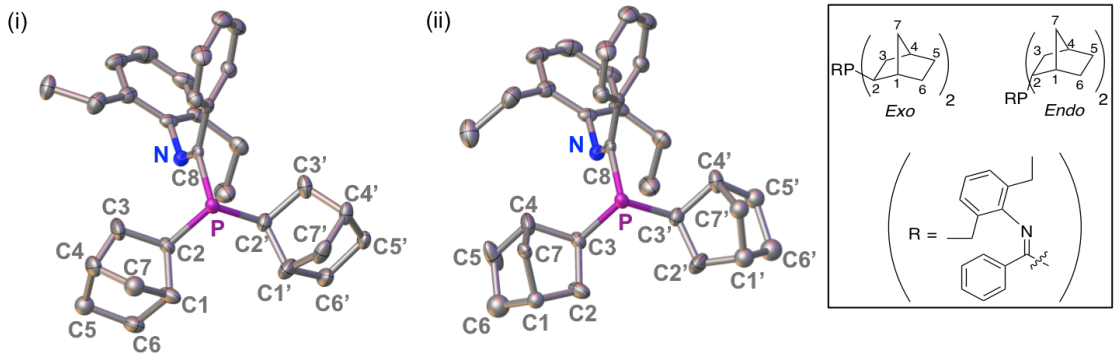

2-*exo* isomer of ligand **2.8** 3-*exo* isomer of ligand **2.8**

Figure 2.15: Molecular structures of ligand **2.8** found to exist as a mixture of (i) 2-*exo* and (ii) 3-*exo* isomers, which co-crystallised. Thermal ellipsoids are at the 50% probability level and H atoms have been omitted for clarity.

Table 2.5: Selected bond lengths and angles for 2-*exo* and 3-*exo* isomers of ligand **2.8**, refer to **Figure 2.15** for atom labels. Estimated standard deviations given in brackets.

Bond Lengths (Å)			**Bond Angles (°)**		
	2-*exo* isomer ligand **2.8**	3-*exo* isomer ligand **2.8**		2-*exo* isomer ligand **2.8**	3-*exo* isomer ligand **2.8**
N-C8	1.274(2)		P-C8-N	117.34(14)	
P-C8	1.878(19)		C2-P-C2'	102.91(9)	N/A
P-C2	1.841(2)	N/A	C3-P-C3'	N/A	102.91(9)
P-C2'	1.860(2)	N/A	C3-C2-C1	102.00(18)	111.0(2)
P-C3	N/A	1.841(2)	C2-C1-C6	101.1(2)	105.4(4)
P-C3'	N/A	1.860(2)	C1-C6-C5	106.3(3)	103.2(4)
C2-C1	1.556(3)	1.470(5)	C6-C5-C4	103.4(4)	109.5(4)
C1-C6	1.619(5)	1.521(7)	C5-C4-C3	113.4(4)	109.9(3)
C6-C5	1.552(7)	1.565(8)	C4-C3-C2	109.7(3)	102.00(18)
C5-C4	1.511(7)	1.484(5)	C4-C7-C1	99.3(3)	95.4(3)
C4-C3	1.384(5)	1.546(3)	C5-C4-C7	101.9(4)	94.4(3)
C3-C2	1.546(3)	1.556(3)	C3-C4-C7	96.1(3)	96.2(2)
C4-C7	1.528(7)	1.732(5)	C6-C1-C7	96.5(3)	101.2(4)
C7-C1	1.568(6)	1.523(6)	C2-C1-C7	96.7(3)	100.1(3)
C2'-C1'	1.538(3)	1.448(7)	C3'-C2'-C1'	101.99(18)	112.5(3)
C1'-C6'	1.649(4)	1.555(12)	C2'-C1'-C6'	102.3(2)	96.0(6)
C6'-C5'	1.558(6)	1.585(11)	C1'-C6'-C5'	103.8(3)	100.5(7)
C5'-C4'	1.505(6)	1.544(7)	C6'-C5'-C4'	103.7(3)	110.8(6)
C4'-C3'	1.459(4)	1.553(3)	C5'-C4'-C3'	108.2(3)	100.6(3)
C3'-C2'	1.553(3)	1.538(3)	C4'-C3'-C2'	107.4(2)	101.99(18)
C4'-C7'	1.521(5)	1.670(6)	C4'-C7'-C1'	99.6(3)	99.3(4)
C7'-C1'	1.507(5)	1.508(9)	C5'-C4'-C7'	102.0(4)	93.9(4)
			C3'-C4'-C7'	99.2(3)	98.2(3)
			C6'-C1'-C7'	97.6(3)	104.4(6)
			C2'-C1'-C7'	100.3(2)	101.1(5)

The majority of the C-C bond lengths in the norbornyl frangments of the two *exo* isomers of ligand **2.8** range between 1.51 and 1.59 Å (Table 2.5), which are similar to the corresponding distances reported for norbornyl and substituted norbornyl

derivatives in the literature (found to range between 1.51 – 1.58 Å).[111-113] The remainder of the C-C bond lengths in the norbornyl fragments of the 2-*exo and 3*-exo isomers of ligand **2.8** are however either significantly longer than that expected for a pure $C(sp^3)$-$C(sp^3)$ bond (1.54 Å),[114] or lie in the region between average pure $C(sp^3)$-$C(sp^3)$ (1.54 Å)[114] and pure $C(sp^2)$-$C(sp^2)$ (1.33 Å)[114] bond lengths. Lastly, as expected, the majority of the C-C-C bond angles of the 2-*exo and 3*-exo isomers of ligand **2.8** are smaller than that for a typical tetrahedral angle (109.5°),[114] with the bridgehead angles ranging between 95.4 – 99.6°, reflecting the strain present in the bicyclic motif.

The molecular structure of ligand **2.8** can be used to understand its solution-state $^{31}P\{^1H\}$ NMR spectrum, which exhibits three resonances at 17.1 ppm, 14.4 ppm, and 10.6 ppm present in a ratio of 25:51:24, respectively. From the molecular structure of ligand **2.8** four isomers can be drawn, depicted in Figure 2.16.

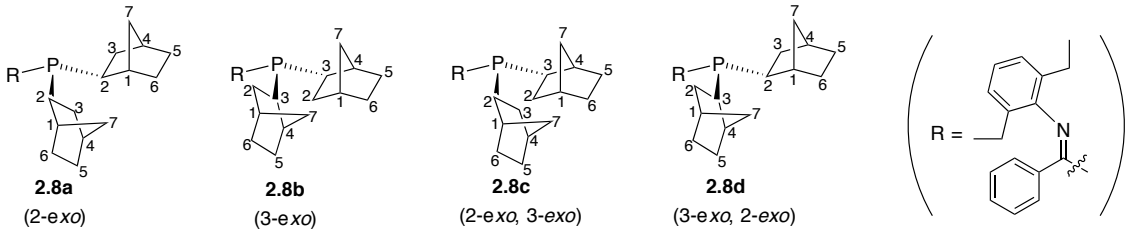

Figure 2.16: Isomers of ligand **2.8**.

The presence of the three resonances in the solution-state $^{31}P\{^1H\}$ NMR spectrum of ligand **2.8** therefore suggest that two of the isomers drawn in Figure 2.16 exhibit similar chemical shifts. It is postulated that of the four isomers in Figure 2.16, **2.8c** and **2.8d** are most likely to display similar chemical shifts, and hence it is proposed that, in the solution-state $^{31}P\{^1H\}$ NMR spectrum of ligand **2.8,** the resonance at 14.4 ppm corresponds to isomers **2.8c** and **2.8d**, while the resonances at 17.1 ppm and 10.6ppm are each attributed to isomers **2.8a** or **2.8b**.

The different isomers **2.8a** – **2.8d** are formed as a consequence of the starting materials used in the synthesis of ligand **2.8** {$TMSP(Norbornyl)_2$ and $HP(Norbornyl_2)$}[a] containing isomeric forms, evident from the presence of three resonances in their solution-state $^{31}P\{^1H\}$ NMR spectra (Table 2.6). Consequently, the $^{31}P\{^1H\}$ NMR spectra of ligands **2.7** and **2.9**, which also bare norbornyl substituents at phosphorus, display three resonances with chemical shifts and integration ratios comparable to

[a] The starting $ClP(Norbornyl)_2$ was obtained commercially from Strem as a mixture of isomers.

those observed for ligand **2.8** (Table 2.6), demonstrating that these ligands exist in isomeric forms analogous to **2.8a** – **2.8d**.

Table 2.6: Comparison of $^{31}P\{^{1}H\}$ NMR spectral data of ligands 2.7 – 2.9 and their starting precursors TMSPNorbornyl$_2$ and HPNorbornyl$_2$.[c]Ratios obtained by integration of the $^{31}P\{^{1}H\}$ NMR spectra.

	$^{31}P\{^{1}H\}$ NMR spectral data	
	δ_P (162 MHz, [a]in $CDCl_3$, [b]in C_6D_6)	Ratio[c]
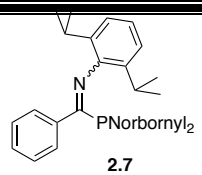 **2.7**	16.6, 13.6, 9.8[a]	21:51:28
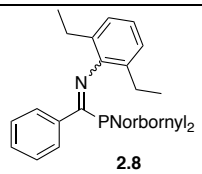 **2.8**	17.1, 14.4, 10.6[a]	25:51:24
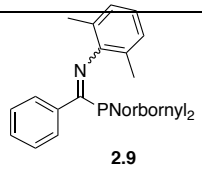 **2.9**	15.7, 13.5, 9.8[a]	28:50:22
TMSPNorbornyl$_2$	−56.2, −57.6, −61.4[b]	10:51:39
HPNorbornyl$_2$	−28.4, −33.9, −39.7[b]	26:51:23

2.3.2. *E/Z* isomerisation of PCN ligands

Depending on the substituents at phosphorus and nitrogen centres, this type of PCN ligands have been found to exist as *E* or *Z* conformers, which can interconvert, depending on the steric bulk of the substituents on the ligands.[70,104-106] The *E*/*Z* isomerisation of PCN ligands is important to consider due to the implications it has on their coordination chemistry, as it could be envisaged that a PCN ligand in the *Z* conformation may not bind to a metal centre *via* its nitrogen atom due to the incorrect orientation of its lone pair (Scheme 2.35).[70] Additionally, if the *Z* conformer of the PCN ligand bears a bulky nitrogen substituent, this may obstruct binding of its phosphorus atom to a metal centre. [70]

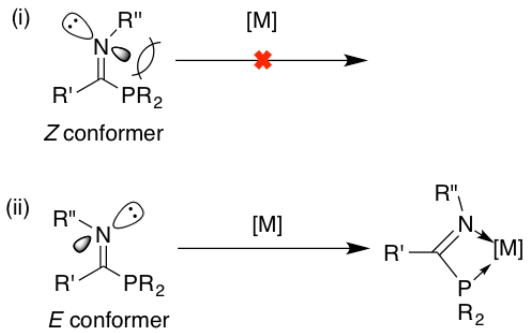

Scheme 2.35: Influence of *E*/*Z* isomerisation on coordination abilities of PCN ligands, where M represents a transition metal, and R-R" refer to alkyl or aromatic groups; adapted from Radcliffe.[70]

In previous work carried out in the Dyer group, it was found that alkyl P-substituted PCN ligands exhibit a single resonance in their solution-state ^{31}P NMR spectra, which was proposed to correspond to the *E* conformer, based on the results of computational studies (**Table 2.7**) which found the *E* conformers of a series of alkyl P-substituted PCN ligands to be lower in energy and therefore more stable than their *Z* counterparts.[70] In contrast, aryl P-substituted PCN ligands were found to display two resonances in their solution-state ^{31}P NMR spectra, corresponding to interconverting mixtures of *E* and *Z* isomers (confirmed by VT-NMR spectroscopic analysis), in agreement with literature studies.[70,104-106]

Table 2.7: Optimised C-N-C bond angles (Φ) and difference in energies of *E* and *Z* isomers for selected alkyl P-substituted PCN ligands, reported by Dr. James Radcliffe.[70]

PCN ligand	C-N-C bond angle, Φ (°)	Isomer	Favoured isomer	*E vs. Z* energy difference (kcal mol^{-1})
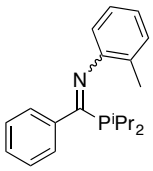	133 233 179	*Z* *E* T.S.	*E*	2.9
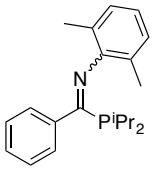	136 232 179	*Z* *E* T.S.	*E*	5.3
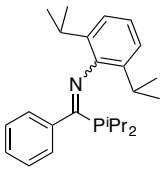	135 232 179	*Z* *E* T.S.	*E*	5.2

Of the PCN ligands synthesised in this thesis, crystals suitable for X-ray diffraction analysis were obtained of four ligands (**2.4**, **2.8** (discussed in previous section), **2.13**, and **2.17**), enabling insight into their solid-state conformations. X-Ray crystallographic analyses of alkyl P-substituted ligands **2.4**, **2.8** and **2.13** reveals they all exist as *E* conformers in the solid state (Figure 2.17 (i) – (iii)), consistent with their solution-state $^{31}P\{^{1}H\}$ NMR spectra, which exhibit single resonances. As mentioned in the previous section, the molecular structure of ligand **2.8** also shows that it contains two different *exo* isomers, of which only the 3-*exo* isomer is included in Figure 2.17. Additionally, aryl P-substituted ligand **2.17**, which displays two resonances in its solution-state $^{31}P\{^{1}H\}$ NMR spectra in a ratio of 1.0:0.22 (confirmed to correspond to separate *E* and *Z* isomers by VT-NMR spectroscopic analysis conducted in previous work in the Dyer group)[70] is also found to adopt an *E* conformation in the solid state (Figure 2.17 (iv)).

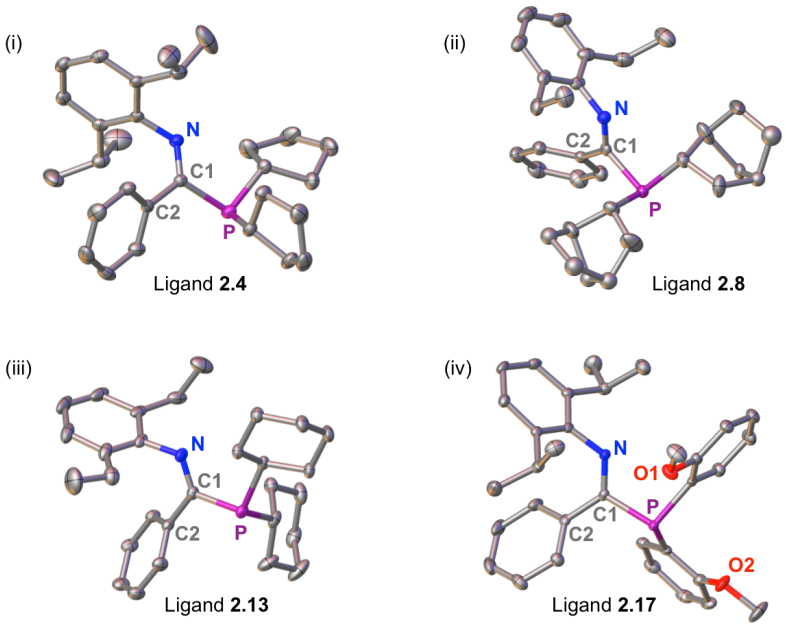

Figure 2.17: Molecular structures of ligands (i) **2.4**,[b] (ii) **2.8** (3-*exo* isomer), (iii) **2.13**,[c] and (iv) **2.17** with thermal ellipsoids at the 50% probability level; H atoms have been omitted for clarity.

Table 2.8: Selected bond lengths and angles for ligands **2.4**, **2.8**, **2.13**, and **2.17**; refer to **Figure 2.17** for atom labels. Estimated standard deviations given in brackets.

		Ligand **2.4**	Ligand **2.8**	Ligand **2.13**	Ligand **2.17**
Bond Lengths (Å)	**N-C1**	1.279(3)	1.274(2)	1.281(13)	1.278(18)
	P-C1	1.840(2)	1.878(19)	1.847(10)	1.849(14)
	C1-C2	1.497(3)	1.491(3)	1.495(13)	1.495(2)
Bond Angles (°)	**P-C1-N**	118.34(15)	117.34(14)	119.43(7)	116.13(11)

[b] The molecular structure of ligand **2.4** shows disorder about the isopropyl group on the N substituent.

[c] The molecular structure of ligand **2.13** shows disorder about the diethyl group on the N substituent.

The structural data presented in Table 2.8 show that ligands **2.4**, **2.8**, **2.13** and **2.17** all exhibit similar N-C1 and P-C1 bond lengths, with values close to that expected for a typical imine bond (1.28 Å),[114] and an average P-C bond (1.85 Å), respectively.[115] The C1-C2 bond lengths in ligands **2.4**, **2.8**, **2.13** and **2.17** are also similar with magnitudes falling in the region between values shown for average pure $C(sp^3)$-$C(sp^3)$ (1.54 Å)[114] and pure $C(sp^2)$-$C(sp^2)$ (1.33 Å)[114] bond lengths. Consequently, the C1-C2 bond lengths are indicative of partial double bond character, implying partial conjugation between the phenyl backbone and imine carbon. Finally, ligands **2.4**, **2.8**, **2.13** and **2.17** all display different P-C1-N angles, as expected from the different structural nature of their phosphorus and nitrogen substituents.

The finding that alkyl P-substituted ligands **2.4**, **2.8** and **2.13** exist as *E* conformers in the solid-state adds further weight to the suggestion made in previous work conducted in the Dyer group that alkyl P-substituted PCN ligands are likely to exist as *E* conformers.[70] Furthermore, from literature studies involving the syntheses of PCN compounds (such as that shown in **Table 2.9** and those displayed in Figure 2.18 on the next page) it can be inferred that the identity of the *E*/*Z* conformer may also be elucidated from the magnitude of the coupling between the *ipso* carbon of the substituent at nitrogen and the phosphorus centre, *i.e.* $|^3J_{PC}|$ in the $^{13}C\{^1H\}$ NMR spectrum.[104-106] For a series of aryl P-substituted PCN compounds synthesised by Slootweg and Lammertsma *et al*.[106] the $|^3J_{PC}|$ values are substantially lower for the *E* conformers *versus* the *Z* conformers (**Table 2.9**). The $|^3J_{PC}|$ of 8.0 Hz of aryl P-substituted PCN ligand **2.17** synthesised in this thesis, whose molecular structure shows it adopts an *E* conformation in the solid-state (Figure 2.17 (iv)), is in good agreement with the reported $|^3J_{PC}|$ of ~ 8 – 9 Hz for the *E* conformers of aryl P-substituted PCN compounds synthesised by Slootweg and Lammertsma *et al*.[106]

Table 2.9: Selected data for a series of aryl P-substituted PCN compounds synthesised in the literature; $^{13}C\{^1H\}$ NMR spectra measured in $CDCl_3$ at 125.78 MHz.[106]

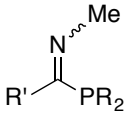 **1a -f**	**R**	**R'**	**Ratio of *E*:*Z* conformers**	**$\|^3J_{PC}\|$ (Hz)** *(Coupling between ipso-C of N substituent and P centre)*	
				***E* conformer**	***Z* conformer**
1a	Ph	Ph	71:29	8.2	33.6
1b	Ph	4-CH_3-C_6H_4	83:17	9.1	36.3
1c	Ph	4-CF_3-C_6H_4	45:55	8.2	32.7
1d	3-CF_3-C_6H_4	Ph	83:17	8.2	34.5
1e	3-CH_3-C_6H_4	Ph	68:32	9.1	33.6
1f	4-CH_3-C_6H_4	Ph	76:24	8.2	32.7

For alkyl P-substituted compounds synthesised by Slootweg and Lammertsma *et al*., examples given in Figure 2.18, the $|^3J_{PC}|$ values of the *E* conformers of these ligands are also lower than those of the *Z* conformers.[104,105] The PCN ligands **2.4** and **2.8** encompassing alkyl phosphorus substituents, synthesised in this thesis, whose molecular structures show them to exist as *E* conformers in the solid-state (Figure 2.17) have $|^3J_{PC}|$ values of 4.0 Hz and 3.5 Hz, respectively, similar to the $|^3J_{PC}|$ value of 2.7 Hz of literature compound **1g** (Figure 2.18, 100 % *E* conformer).[105] Additionally, the other alkyl P-substituted PCN ligands synthesised in this thesis, which exhibit doublets in their ^{13}C NMR spectra corresponding to the *ipso* carbons on the N-phenyl substituents (**2.1** – **2.3**, **2.5** – **2.7**, **2.9** – **2.11**, and **2.14** – **2.16**), have a range of $|^3J_{PC}|$ between 3.0 and 5.0 Hz, which are similar to the $|^3J_{PC}|$ of *E* conformers **1g**[105] and ligands **2.4** and **2.8**, suggesting that these ligands are also likely to exist as *E* conformers.

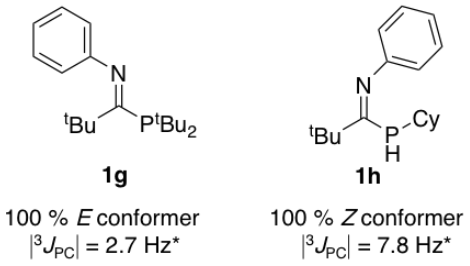

*$^3J_{PC}$ corresponds to coupling between *ipso* carbon of nitrogen substituent and phosphorus centre

Figure 2.18: Selected data for alkyl P-substituted PCN compounds synthesised in the literature, $^{13}C\{^1H\}$ NMR spectra measured in $CDCl_3$ at 125.78 MHz (for compound **1g**) and at 62.9 MHz (for compound **1h**).[104,105]

2.3.3. Analysis of selenophosphine derivatives of PCN ligands 2.1 - 2.17 by ^{31}P NMR spectroscopy

The electronic properties of phosphines can be assessed using the method reported by Allen *et al.,* which is based upon NMR spectroscopic analysis of phosphine selenides.[116,117] Due to ^{77}Se nucleus having a nuclear spin of ½ and a natural abundance of 7.5 %, the ^{31}P NMR spectroscopic resonance for a phosphine selenide compound has characteristic satellites resulting from a $^1J_{SeP}$ coupling.[116,117] Since the magnitude of the $^1J_{SeP}$ coupling constants can be regarded as being proportional to the degree of s-character of the phosphorus lone-pair of the parent phosphine, the $|^1J_{SeP}|$ is reflective of the Lewis basicity of the parent phosphine.[117] Therefore, a phosphine selenide exhibiting a large $^1J_{SeP}$ coupling is indicative of a parent phosphine that has a large degree of s-character and so is poorly σ-donating and weakly Lewis basic (*e.g.*

$SePF_2H$, $^1J_{SeP}$ = 1046 Hz),[118] with the converse applying for a phosphine selenide with a small $^1J_{SeP}$ coupling (*e.g.* $SePMe_3$, $^1J_{SeP}$ = 682 Hz).[119]

Consequently, in order to determine the Lewis basicity of the phosphorus(III) component of PCN ligands **2.1** – **2.17**, the synthesis of their selenide derivatives, which will be referred to as **2.1(Se)** – **2.17(Se)**, on an NMR-scale was undertaken. Compounds **2.1(Se)** – **2.17(Se)** were prepared *via* the reaction shown in Scheme 2.36, in which a mixture of the PCN ligand and excess elemental (grey) Se in $CDCl_3$ was sonicated for an hour, after which time 100% conversion to the selenide was observed to have occurred by ^{31}P NMR spectroscopic analysis. The $^{31}P\{^1H\}$ NMR chemical shifts and $^1J_{SeP}$ coupling constants of the resulting selenide derivatives of **2.1** - **2.17,** are listed in **Table 2.10**.

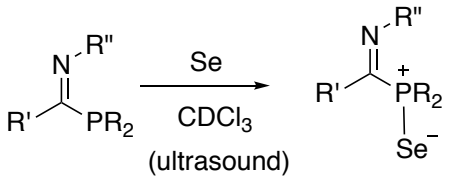

Scheme 2.36: Synthesis of selenides of PCN ligands **2.1(Se)** – **2.17(Se).**

Table 2.10: List of $^{31}P\{^1H\}$ NMR chemical shifts and $|^1J_{SeP}|$ of **2.1 (Se)** - **2.17 (Se)**, measured in $CDCl_3$ at 162 MHz.

Compound Number	Structural Formula of Compound	$\|^1J_{SeP}\|$ (Hz)	$^{31}P\{^1H\}$ δ (ppm)
2.1(Se)	$PhC(SeP^iBu_2)=N(2,6\text{-}^iPr_2C_6H_3)$	703	36.5
2.2(Se)	$PhC(SeP^iBu_2)=N(2,6\text{-}Et_2C_6H_3)$	701	36.2
2.3(Se)	$PhC(SeP^iBu_2)=N(2,6\text{-}Me_2C_6H_3)$	702	36.4
2.4(Se)	$PhC(SePCyPent_2)=N(2,6\text{-}^iPr_2C_6H_3)$	715	63.6
2.5(Se)	$PhC(SePCyPent_2)=N(2,6\text{-}Et_2C_6H_3)$	714	63.2
2.6(Se)	$PhC(SePCyPent_2)=N(2,6\text{-}Me_2C_6H_3)$	716	64.0
2.7(Se)	$PhC(SeP(Norbornyl)_2)=N(2,6\text{-}^iPr_2C_6H_3)$	721	58.7
		713	57.2
		724	56.7
2.8(Se)	$PhC(SeP(Norbornyl)_2)=N(2,6\text{-}Et_2C_6H_3)$	721	58.4
		725	56.9
		711	56.6
2.9(Se)	$PhC(SeP(Norbornyl)_2)=N(2,6\text{-}Me_2C_6H_3)$	721	58.2
		727	57.3
		713	56.9
2.10(Se)	$(p\text{-}CF_3\text{-}Ph)C(SeP^iPr_2)=N(2,6\text{-}^iPr_2C_6H_3)$	715	65.3
2.11(Se)	$(p\text{-}Me\text{-}Ph)C(SeP^iPr_2)=N(2,6\text{-}^iPr_2C_6H_3)$	709	64.1
2.12(Se)	$PhC(SePEt_2)=N(2,6\text{-}Et_2C_6H_3)$	701	42.9
2.13(Se)	$PhC(SePCy_2)=N(2,6\text{-}Et_2C_6H_3)$	706	55.8
2.14(Se)	$PhC(SeP^iPr_2)=N(2,6\text{-}^iPr_2C_6H_3)$	711	64.4
2.15(Se)	$PhC(SeP^iPr_2)=N(2,6\text{-}Et_2C_6H_3)$	709	64.0
2.16(Se)	$PhC(SeP^iPr_2)=N(2\text{-}MeC_6H_4)$	715	66.2
2.17(Se)	$PhC(SeP(2\text{-}(OMe)C_6H_4)_2)=N(2,6\text{-}^iPr_2C_6H_4)$	719	21.4

As expected, compounds **2.1(Se)** – **2.6(Se)** and **2.10(Se)** – **2.17(Se)** all give rise to one resonance in their $^{31}P\{^{1}H\}$ NMR spectra, which exhibits a pair of Se satellites (**Table 2.10**). Compounds **2.7(Se)** – **2.9(Se)** each display three resonances in their $^{31}P\{^{1}H\}$ NMR spectra, with each resonance showing coupling to a pair of Se satellites. The three resonances in the $^{31}P\{^{1}H\}$ NMR spectra of **2.7(Se)** – **2.9(Se)** are believed to correspond to isomers **(i)**-**(iv)** (Figure 2.19), for which it is reasonable to assume the same value of δ_P for isomers **(iii)** and **(iv)**, based on the previous discussion of the molecular structure of ligand **2.8** (section 2.3.1).

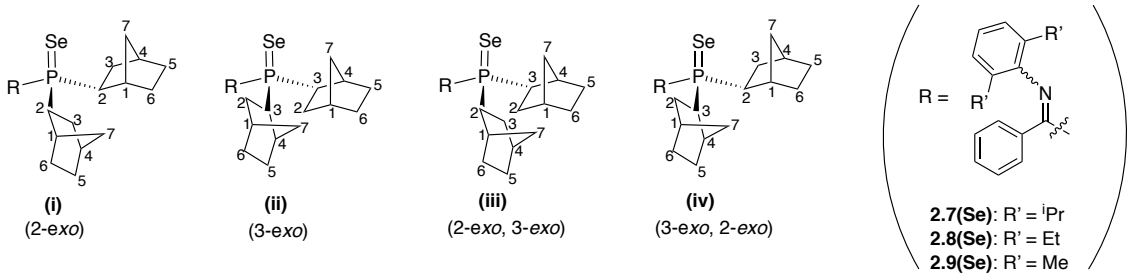

Figure 2.19: Proposed isomers of **2.7(Se)** – **2.9(Se)**.

Analysis of the $^{31}P\{^{1}H\}$ NMR spectroscopic data for compounds **2.1(Se)** – **2.17(Se)** (**Table 2.10**) reveals a narrow range of $^{1}J_{SeP}$ values, from 701 to 727 Hz, with their magnitudes being similar to those determined for PCN ligands that have been synthesised in previous work carried out in the Dyer group ($^{1}J_{SeP}$ ~ 701 – 750 Hz, Figure 2.20).[70] Additionally, on comparing the magnitudes of the $^{1}J_{SeP}$ coupling constants demonstrated by **2.1(Se)** – **2.17(Se)** to those of a selection of phosphine selenides reported in the literature (Table 2.11), it is apparent that $|^{1}J_{SeP}|$ of **2.1(Se)** – **2.17(Se)** are relatively small in magnitude, indicative of the phosphorus substituents on the parent PCN ligands possessing little s-character and therefore being relatively good σ donors (as would be expected for dialkyl-substituted phosphine derivatives).

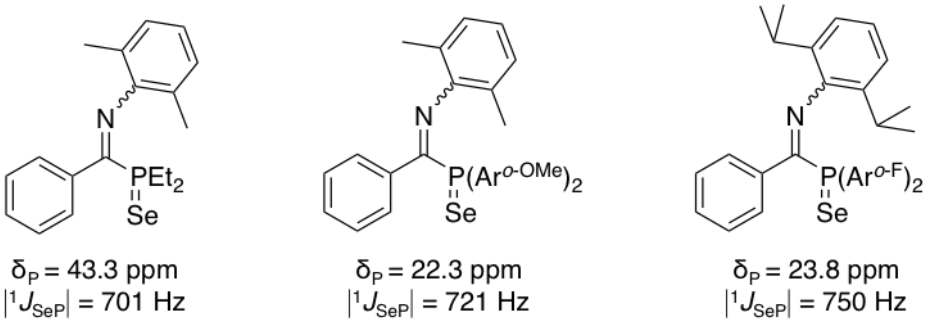

Figure 2.20: $^{31}P\{^{1}H\}$ spectral data of a selection of selenide derivatives of PCN ligands that have been synthesised in previous work conducted in the Dyer group ($^{31}P\{^{1}H\}$ spectra measured in $CDCl_3$ at 162 MHz).[70]

Table 2.11 $|^1J_{SeP}|$ of a selection of phosphine selenides reported in the literature; $^{31}P\{^1H\}$ NMR spectra recorded in $CDCl_3$ at 162 MHz.[119]

Se=PR_3, R=	$\|^1J_{SeP}\|$ (Hz)
Me[30]	682
Cy[31]	676
^{i}Pr[32]	688
Ph[31]	732
OPh[33]	1025

Upon closer examination of the $^1J_{SeP}$ values for compounds **2.1(Se)** – **2.17(Se)** (**Table 2.10**), trends can be established between the magnitudes of the $^1J_{SeP}$ coupling constants and the structural nature of the phosphorus or carbon substituents (which will be considered in further detail in sections 2.3.3.1 and 2.3.3.2, respectively). In comparison, variations at the nitrogen substituent across compounds **2.1(Se)** – **2.3(Se)**, **2.4(Se)** – **2.6(Se)**, and **2.7(Se)** – **2.9(Se)** reveals it has a negligible effect on the magnitude of the $^1J_{SeP}$ coupling constants, and hence no conclusive trends can be established in this case.

2.3.3.1. Relationship between the nature of the phosphorus substituents of 2.1(Se) - 2.17(Se) and the magnitude of their $^1J_{SeP}$ coupling constants

The compounds with the smallest $|^1J_{SeP}|$ out of those listed for **2.1(Se) – 2.17(Se)** in **Table 2.10**, are those that have either an ethyl (**2.12(Se)**) or isobutyl group (**2.1(Se)** – **2.3(Se)**) at the phosphorus atom, while the compounds bearing norbornyl groups (**2.7(Se)** – **2.9(Se)**) at the phosphorus atom exhibit the largest $|^1J_{SeP}|$. Consequently, in agreement with previous work carried out on PCN ligands in the Dyer group, a relationship between the steric bulk of the phosphine alkyl substituents and donor properties can be established.[70] The steric bulk of the phosphine substituents are known to impact the geometry the phosphine adopts, which in turn affects its degree of s-donor character.[120,121]

In order to understand which geometry is most favourable for a phosphine to adopt it is important to consider Walsh's rule, which states that "a molecule adopts the structure that best stabilises the HOMO, or the occupied molecular orbital that lies closest to the HOMO in cases where the HOMO is unperturbed by the structural change under consideration".[122] It is therefore important to apply the "Walsh Correlation Diagram Analysis" to the PR_3 fragment and consider the difference in molecular orbital energies of pyramidal and near-planar configurations of PR_3 species (Figure 2.21).

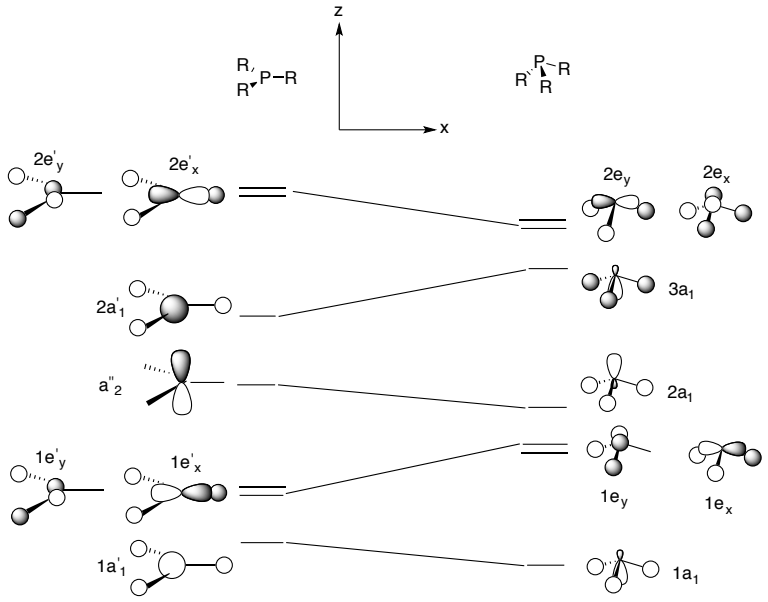

Figure 2.21: Relationship between the molecular orbitals of near planar (left) and pyramidal (right) PR_3 fragments, adapted from Gilheany.[120]

From the partial molecular orbital diagram in Figure 2.21 it would be expected that the pyramidal geometry is favoured for PR_3 compounds as the $2a_1$ HOMO is stabilised (relative to the more planar case). However, the presence of bulky substituents at the phosphorus centre causes steric repulsion that leads to a planarisation at phosphorus. Since the percentage s-character is greater in the planar arrangement, this is consistent with the greater $|^1J_{SeP}|$ measured for bulky phosphines (*e.g.* PCN ligands **2.7** – **2.9**).

2.3.3.2. Relationship between the nature of the carbon substituents of 2.1(Se) - 2.17(Se) and the magnitude of their $^1J_{SeP}$ coupling constants

On comparing the magnitudes of the $^1J_{SeP}$ coupling constants exhibited by compounds **2.10(Se)**, **2.11(Se)** and **2.14(Se)** (Figure 2.22), which encompass imine carbon substituents of similar steric bulk, it is apparent that as the electron-withdrawing nature of the imine carbon substituent increases (going right to left from **2.11(Se)** to **2.10(Se)** in Figure 2.22) the value of $|^1J_{SeP}|$ also increases, as expected. The increased electron-withdrawing nature of the imine carbon substituent of **2.10(Se)** (in comparison to those for **2.11(Se)** and **2.14(Se)**) increases the electron-withdrawing character at the phosphorus atom of **2.10(Se)**, resulting in a greater degree of s-character in the P=Se bond leading to an increase in the $^1J_{SeP}$ coupling constant, reflecting the weaker σ-donating ability of the phosphorus atom of **2.10** *versus* the phosphorus atoms of **2.11** and **2.14**.[117]

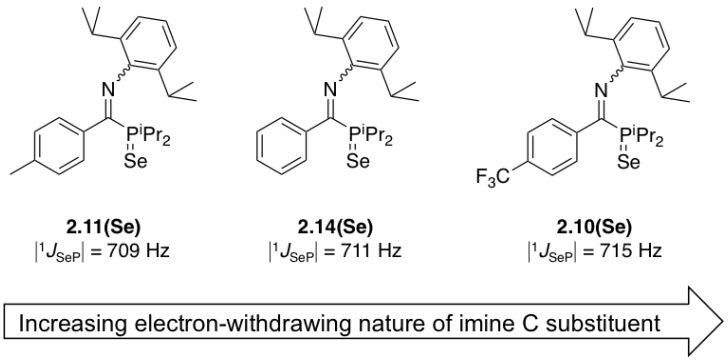

Figure 2.22: $|^1J_{SeP}|$ of compounds **2.10(Se)**, **2.11(Se)** and **2.10(Se)**; $^{31}P\{^1H\}$ NMR spectra recorded in $CDCl_3$ at 162 MHz.

2.3.4. Analysis of the IR spectra of PCN ligands, 2.1 – 2.17

The PCN ligands synthesised in this thesis, **2.1** – **2.17** (Figure 2.14), have been probed by IR spectroscopy in order to gain further insight into their electronic properties. Due to the complexity of data present in the IR spectra of **2.1** – **2.17,** only the C=N stretching frequencies will be considered; these are reported in Table 2.12, alongside the C=N stretching frequencies of their imidoyl chloride precursors. The C=N bonds of imines generally exhibit characteristic absorptions in their IR spectra at ~1600 cm^{-1}, with deviations correlating to the strength of the C=N bond.[123]

Table 2.12: IR spectroscopic data of C=N stretching frequencies for PCN ligands, **2.1** – **2.17**, and their imidoyl chloride precursors; measured neat using an ATR cell.

PCN Ligand	Structural Formula of PCN Ligand	$\nu_{C=N}$ of PCN ligand	$\nu_{C=N}$ of imidoyl chloride precursor to PCN ligand
2.1	PhC(P^{i}Bu$_2$)=N(2,6-^{i}Pr$_2$C$_6$H$_3$)	1587	1663
2.2	PhC(P^{i}Bu$_2$)=N(2,6-Et$_2$C$_6$H$_3$)	1587	1656
2.3	PhC(P^{i}Bu$_2$)=N(2,6-Me$_2$C$_6$H$_3$)	1589	1668
2.4	PhC(PCyPent$_2$)=N(2,6-^{i}Pr$_2$C$_6$H$_3$)	1596	1663
2.5	PhC(PCyPent$_2$)=N(2,6-Et$_2$C$_6$H$_3$)	1601	1656
2.6	PhC(PCyPent$_2$)=N(2,6-Me$_2$C$_6$H$_3$)	1587	1668
2.7	PhC(PNorbornyl$_2$)=N(2,6-^{i}Pr$_2$C$_6$H$_3$)	1610	1663
2.8	PhC(PNorbornyl$_2$)=N(2,6-Et$_2$C$_6$H$_3$)	1586	1656
2.9	PhC(PNorbornyl$_2$)=N(2,6-Me$_2$C$_6$H$_3$)	1586	1668
2.10	(*p*-CF$_3$-Ph)C(P^{i}Pr$_2$)=N(2,6-^{i}Pr$_2$C$_6$H$_3$)	1584	1660
2.11	(*p*-Me-Ph)C(P^{i}Pr$_2$)=N(2,6-^{i}Pr$_2$C$_6$H$_3$)	1583	1665
2.12	PhC(PEt$_2$)=N(2,6-Et$_2$C$_6$H$_3$)	1587	1656
2.13	PhC(PCy$_2$)=N(2,6-Et$_2$C$_6$H$_3$)	1584	1656
2.14	PhC(P^{i}Pr$_2$)=N(2,6-^{i}Pr$_2$C$_6$H$_3$)	1583	1663
2.15	PhC(P^{i}Pr$_2$)=N(2,6-Et$_2$C$_6$H$_3$)	1584	1656
2.16	PhC(P^{i}Pr$_2$)=N(2-MeC$_6$H$_4$)	1590	1661
2.17	PhC(P(2-(OMe)C$_6$H$_4$)$_2$)=N(2,6-^{i}Pr$_2$C$_6$H$_4$)	1584	1663

As is evident from the spectroscopic data presented in Table 2.12, ligands **2.1** – **2.17** display C=N absorption frequencies ranging from 1583 to 1610 cm^{-1}. The observed range of C=N stretches of **2.1** – **2.17** is similar to that reported for PCN ligands that have been synthesised in previous work conducted in the Dyer group (1549 – 1636 cm^{-1}, Figure 2.23).[70] Furthermore, comparing the C=N absorption frequencies of ligands **2.1** – **2.17** with those of their precursor imidoyl chlorides (Table 2.12) reveals that the C=N absorption stretches are at a lower frequency in ligands **2.1** – **2.17** (similar observation reported in previous work conducted in the Dyer group).[70] The lower C=N absorption frequencies of ligands **2.1** – **2.17** is suggestive of electron donation from their phosphorus lone pair (expected donating character from the low magnitude of $^1J_{SeP}$ coupling constants of their selenophosphine derivatives, section 2.3.3) to their C=N antibonding orbitals, as illustrated in Figure 2.24, resulting in a weakening of the C=N bond.

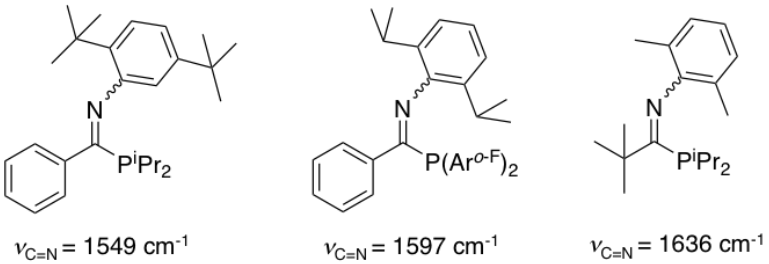

Figure 2.23: $\nu_{C=N}$ of a selection of PCN ligands, synthesised in previous work carried out in the Dyer group (IR spectra measured neat using an ATR cell).[70]

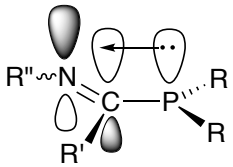

Figure 2.24: Illustration of the interaction between the phosphorus lone pair group and C=N antibonding orbitals of ligands **2.1** – **2.17**.

Additionally, from the range of C=N absorption frequencies found for ligands **2.1** – **2.13** (Table 2.12), it can be seen that compounds **2.5** and **2.7** exhibit the largest C=N absorption frequencies, 1601 and 1610 cm^{-1}, respectively. In this case, there is good correlation between the suggested weak donation of the phosphorus groups of compounds **2.5** and **2.7** from their relatively high C=N stretches and relatively large $^1J_{SeP}$ coupling constants of their selenides (714 Hz and 713 – 724 Hz, respectively, section 2.3.3). However, for the series of compounds **2.1** – **2.17** a linear correlation is not always observed between the magnitude of the $^1J_{SeP}$ coupling constants of their selenides and their C=N absorption frequencies, exemplified by the fact that compounds **2.2** and **2.9** have almost the same magnitude of C=N absorption frequencies (Table 2.12), despite their selenides displaying the smallest and largest

$^1J_{SeP}$ coupling constants, respectively, out of the series of selenides **2.1(Se)** – **2.17(Se)** (**Table 2.10**, section 2.3.3). Consequently, for ligands **2.1** – **2.17** it is apparent that other factors, in addition to the donating ability of their phosphorus lone pair, dictate their C=N bond strengths. Factors that would be expected to impact the C=N bond strength of ligands **2.1** – **2.17** are the nature of the substituents present on the carbon and nitrogen atoms of these compounds. However, from the data (Table 2.12) it is difficult to draw any trends between the nature of the nitrogen substituents on ligands **2.1** – **2.17** and their C=N bond strength. In addition, as can be seen from Figure 2.25, the C=N stretching frequencies displayed by PCN ligands **2.10**, **2.11**, and **2.14** is not affected by the electronic character of the imine C substituents.

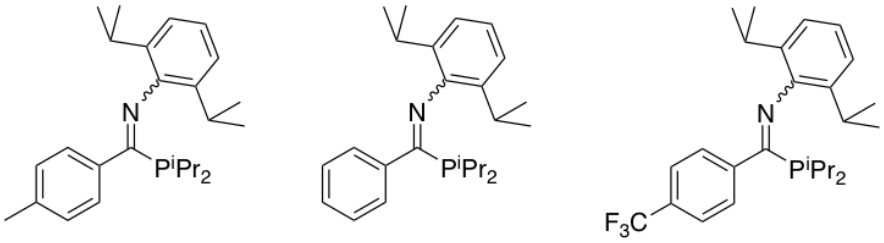

2.11 $\nu_{C=N}$ = 1583 cm^{-1} **2.14** $\nu_{C=N}$ = 1583 cm^{-1} **2.10** $\nu_{C=N}$ = 1584 cm^{-1}

Figure 2.25: $\nu_{C=N}$ of ligands **2.10**, **2.11**, and **2.14**; IR spectra recorded neat using an ATR cell.

2.3.5. Consideration of steric properties of PCN ligands

In addition to considering the electronic properties of PCN ligands (sections 2.3.3 and 2.3.4), the steric properties of the PCN ligands are also important to consider due to the finding, in previous work in the Dyer group, that more sterically demanding PCN ligands tend to furnish more active and selective ethylene *tri*-/*tetra*-merisation systems.[70] Two of the most popular methods of quantifying the steric bulk of ligands in the literature, illustrated in Figure 2.26, are the Tolman cone angle approach[124,125] and the percentage buried volume (%V_{bur}) approach.[126,127]

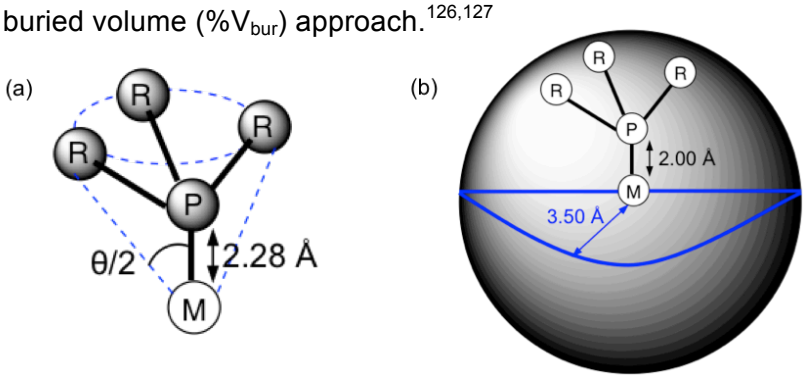

Figure 2.26: Comparison of popular methods used to determine the steric bulk of a tertiary phosphine (PR_3) (a) Tolman cone angle[125] or (b) %V_{bur}, using a fixed M-P bond distance of 2.00 Å and a sphere radius of 3.50 Å.[126] The circles in the illustrations represent the van der Waals radii of the substituents and M corresponds to a metal.

As depicted in Figure 2.26(a), the Tolman cone angle approach derives the steric bulk of a phosphine by using van der Waals radii and empirical bond length data of the phosphorus substituents to generate an imaginary cone in which the ligand sits, with the angle at the point of the cone corresponding to the Tolman cone angle (θ).[124,125] In contrast to the Tolman cone angle method, the $\%V_{bur}$ approach quantifies the steric bulk of ligands by using crystallographic or computational data of the specific ligand in order to determine the percentage of the total volume of a sphere (radius 3.50 Å) it occupies, measured at a fixed metal-ligand bond distance (Figure 2.26(b)).[126]

Determining the steric bulk of PCN ligands by the methods shown in Figure 2.26 is not straightforward due to (a) the observed different coordination modes adopted to the chromium centre and (b) the potential for *E*/*Z* isomerism to occur about the imine bonds (**Figure 2.27**), which impacts the conformations of the PCN ligands and hence their determined steric bulk. As a consequence of the difficulty in determining the most reliable structures of PCN ligands to accurately measure their steric bulk from, the steric bulk of the PCN ligands has not been measured in this thesis. Instead, relationships between PCN ligand steric bulk and ethylene *tri*-/*tetra*-merisation selectivity and activity in Chapter 3, have been established on the basis of expected steric bulk (in a similar manner to that done in the majority of literature studies).[1-8,70]

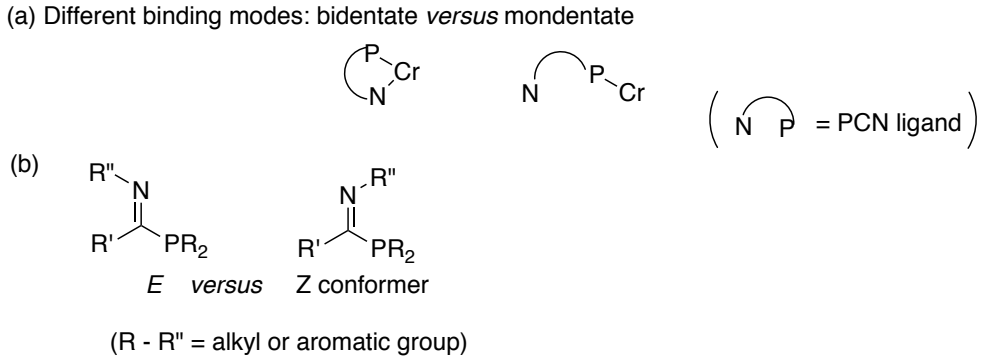

Figure 2.27: (a) Different binding modes of PCN ligands to Cr and (b) *E*/*Z* isomerism of PCN ligands**.**

In previous work done by Dr. James Radcliffe, the steric bulk of a series of PCN ligands, bearing different alkyl phosphorus groups, was quantified using the $\%V_{bur}$ approach, implementing the ligand conformation portrayed in Figure 2.28 (which was a computationally optimised structure).[70] The $\%V_{bur}$ values determined in this way are shown in Table 2.13, and based on these values the PCN ligands were listed in order of increasing steric bulk: **2Z** > **2AA**> **2AB** (with the order of **2AA** and **2AB** being reasoned in terms of their expected steric bulk).[70]

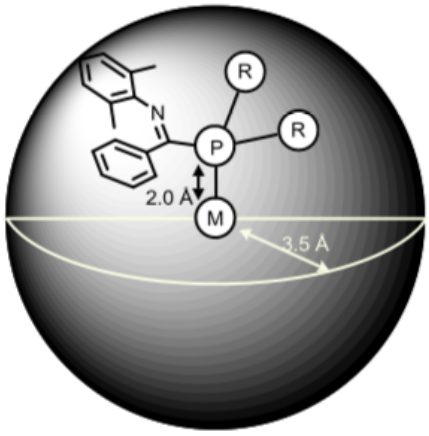

Figure 2.28: Schematic representation of $\%V_{bur}$ calculations conducted by Dr. James Radcliffe, where R refers to an alkyl group and M to a metal centre; copied from ref. 70.

Table 2.13: % Vbur determined from computational structures of a range of PCN ligands (**2Z** – **2AB**), and from the molecular structure of monodentate Cr^0-PCN complex **2AC**.[70]

PCN ligand	P-substituent	$\%V_{bur}$
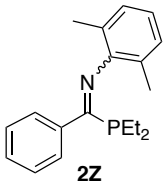 **2Z**	Et	34.5
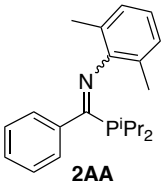 **2AA**	^{i}Pr	37.0
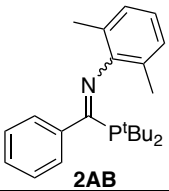 **2AB**	tBu	37.0
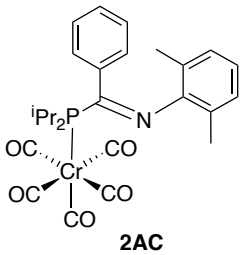 **2AC**	^{i}Pr	33.0

However, upon close examination of the data conveyed in Table 2.13 it may be argued that there is no difference in the $\%V_{bur}$ values for ligands **2Z, 2AA** and **2AB** (as the numerical differences in the $\%V_{bur}$ values are all within the ± 4 % error (obtained by comparison of $\%V_{bur}$ determined from computationally generated ligand **2AA** to that

determined from the molecular structure of monodentate Cr^0-PCN complex **2AC**). Therefore, the relationships between PCN ligand steric bulk and ethylene *tri-*/*tetra*-merisation selectivity and activity established in previous work in the Dyer group can be regarded as being done on the basis of the expected steric bulk of the PCN ligands.

2.4. Cr Coordination Chemistry of PCN Ligands

With the PCN ligands **2.1** – **2.17** (Figure 2.14) in hand, it was next important to investigate their coordination chemistry to Cr (metal of choice due to the vast majority of chromium-based selective ethylene *tri-*/*tetra*-merisation systems in the literature).[1-8] The coordination chemistry of PCN ligands to Cr^0, Cr^I, and Cr^{III} fragments was therefore investigated (each discussed in turn in the proceeding sections), in order to meet the aims previously outlined in Section 2.1.6.3, in addition to gaining an understanding into the nature of the potentially catalytically active species that may be present during ethylene oligomerisation catalysis and further insight into the electronic properties of the PCN ligands themselves.[128-130]

2.4.1. Coordination reactions of PCN Ligands with $Cr(CO)_6$

The syntheses of Cr^0-PCN complexes **2.22** – **2.25** (Figure 2.29) was undertaken in this thesis, to complete the series of Cr^0-PCN complexes shown in Figure 2.29 containing PCN ligands with different nitrogen substituents (of which complexes **2.18** – **2.21** were originally synthesised in previous work done in the Dyer group).[70] The series of Cr^0-PCN complexes **2.18** – **2.25** was chosen in order to obtain a series of Cr^0-PCN complexes analogous to the series of Cr^{III}-PCN complexes synthesised in previous work conducted in the Dyer group (Figure 2.30) to enable direct comparisons to be made between the properties of the series of complexes as a result of the nature of the chromium centre.[70]

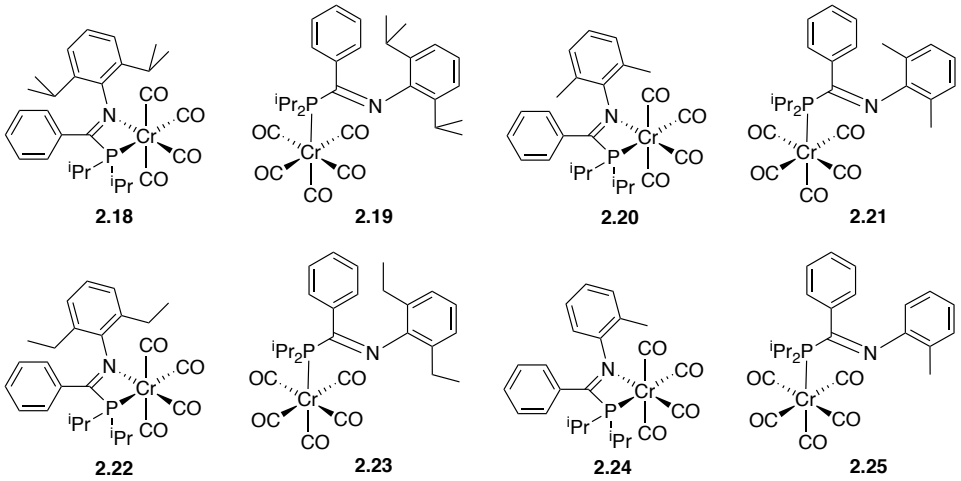

Figure 2.29: Small series of Cr^0-PCN complexes synthesised in this thesis (**2.18** – **2.19** and **2.22** – **2.25**) and previous work done in the Dyer group (**2.18** – **2.21**).[70]

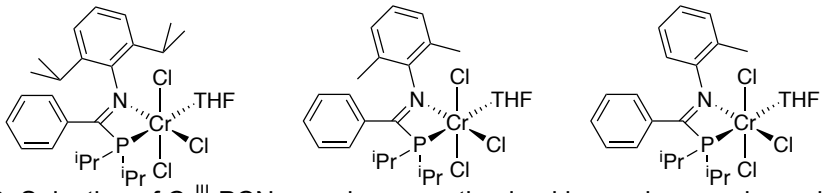

Figure 2.30: Selection of Cr^{III}-PCN complexes synthesised in previous work conducted in the Dyer group.[70]

2.4.1.1. Synthesis of Cr^0-PCN complexes

The synthesis of Cr^0-PCN complexes was initially attempted using a modified version of the method reported by Krishnamurthy *et al.* (Scheme 2.37),[131] which had proven successful in the original synthesis of complexes **2.18** – **2.21** in the previous work carried out on Cr^0-PCN complexes.[70] Complexes **2.18** and **2.19** were also successfully synthesised in this thesis *via* the route depicted in Scheme 2.37 and obtained in yields of 17 % and 37 %, respectively, after having been isolated, following separation based on their different solubilities in hexane (complex **2.19** was soluble in hexane, whereas complex **2.18** was insoluble in hexane).

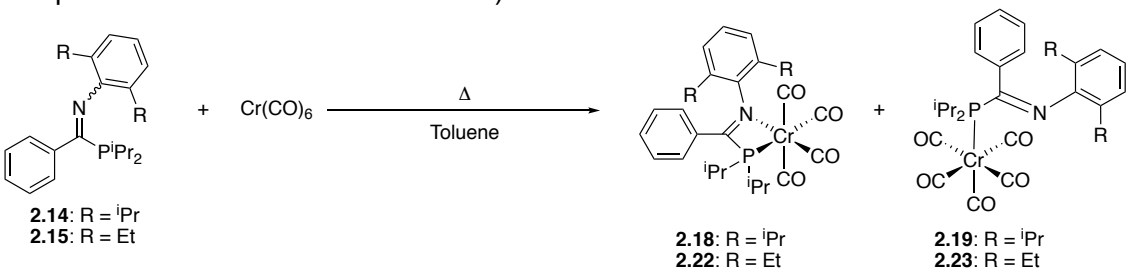

Scheme 2.37: Synthesis of **2.18** - **2.19** and **2.22** – **2.23** from the reaction between PCN ligands (**2.14** – **2.15**) and $Cr(CO)_6$ in toluene.

However, using the same synthetic approach to that outlined in Scheme 2.37 in order to prepare novel Cr^0-PCN complexes **2.22** and **2.23** proved difficult. A toluene solution of PCN ligand **2.15** and $Cr(CO)_6$ was heated at reflux for a total of 109 hours and reaction progress was monitored at various points during the reaction by $^{31}P\{^1H\}$ NMR spectroscopy (Table 2.14).

Table 2.14: $^{31}P\{^1H\}$ NMR spectroscopic data at various points of the reaction between **2.15** and $Cr(CO)_6$ in toluene (measured in C_6D_6 at 162 MHz). The resonances at 63.0 ppm and 85.1 ppm were attributed to complexes **2.22** and **2.23**, respectively, due to these resonances being at the expected chemical shifts for **2.22** and **2.23** (based on the chemical shifts of analogous complexes **2.18** and **2.19**: 63.3 and 83.1 ppm, respectively).

Reflux time (h)	Observed resonances (δ ^{31}P) in $^{31}P\{^1H\}$ NMR spectra
13	85.1 (10 %),[b] 63.0 (46 %),[a] 30.6 (1 %), 27.3 (43 %)[c]
17	85.1 (13 %),[b] 63.0 (45 %),[a] 30.6 (2 %), 27.3 (40 %)[c]
31	85.1 (5 %),[b] 63.0 (51 %),[a] 30.6 (11 %), 27.3 (33 %)[c]
54	108.9 (1 %), 85.1 (2 %),[b] 63.0 (38 %),[a] 47.5 (1 %), 30.6 (30 %), 27.3 (28 %)[c]
109	65.3 (2 %), 63.0 (12 %),[a] 30.6 (48 %), 27.3 (38 %)[c]
Assignment of resonances: complex **2.22**,[a] complex **2.23**,[b] ligand **2.15**[c]	

As can be seen from Table 2.14, the reaction between ligand **2.15** and $Cr(CO)_6$ proceeded relatively cleanly after heating at reflux for 31 hours with $^{31}P\{^1H\}$ NMR spectroscopic analysis of the crude reaction mixture revealing it to consist of 33% unreacted ligand **2.15**, 51% desired complex **2.22**, 5% desired complex **2.23** and 11% unknown impurities. However, further heating of the reaction did not encourage conversion of ligand **2.15** to the desired products (complexes **2.22** and **2.23**). Instead it was found to result in a depletion of complex **2.23**, a significant decrease in the amount of complex **2.22**, and an increase in the amounts of unreacted ligand **2.15** and unknown impurities. The observation that prolonged heating of the reaction between **2.15** and $Cr(CO)_6$ leads to decomposition of the desired products is not unexpected as the same was found by Boeré *et al.*[132] in their coordination reactions of phosphaamidines to $Cr(CO)_6$, following a similar synthetic route (Scheme 2.38).

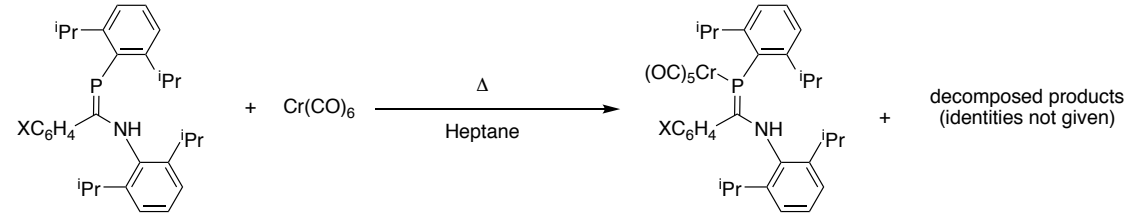

(X = Me or OMe)

Scheme 2.38: Synthesis of Cr^0-phosphaamidinecomplex, reported by Boeré *et al.*[132]

In an attempt to avoid prolonged heating of the reaction between PCN ligands and $Cr(CO)_6$, the synthesis of Cr^0-PCN ligands was instead pursued following the method reported by Grim *et al.* (Scheme 2.39),[133] in which the PCN ligand and $Cr(CO)_6$ were heated in diglyme as a reaction solvent (higher boiling point of 162 *versus* 111 °C of toluene should lead to faster rates of reaction and hence shorter heating times). Novel Cr^0-PCN complexes **2.22** – **2.25,** in addition to Cr^0-PCN complexes **2.18** – **2.19**, were successfully obtained *via* this route in moderate yields ($Cr(CO)_4(\kappa^2$-P,N-PCN): 9 – 15 % yield, $Cr(CO)_5(\kappa^1$-P-PCN): 40 – 47 % yield). The Cr^0-PCN complexes were again isolated following separation exploiting their different solubilities in hexane, ($Cr(CO)_4(\kappa^2$-P,N-PCN) complexes insoluble in hexane whilst $Cr(CO)_5(\kappa^1$-P-PCN) complexes soluble in hexane).

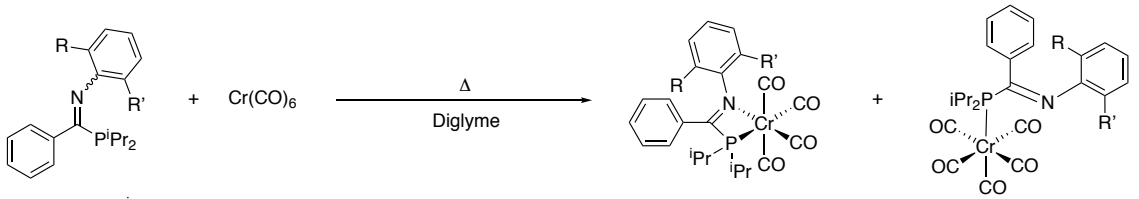

2.14: R = R' = ^{i}Pr
2.15: R = R' = Et
2.16: R = H, R' = Me

2.18: R = R' = ^{i}Pr
2.22: R = R' = Et
2.24: R = H, R' = Me

2.19: R = R' = ^{i}Pr
2.23: R = R' = Et
2.25: R = H, R' = Me

Scheme 2.39: Synthesis of complexes **2.18** – **2.19** and **2.22** – **2.25** from the reaction between PCN ligands (**2.14** – **2.16**) and $Cr(CO)_6$ in diglyme.

The diglyme solutions of the PCN ligands (**2.14** - **2.16**) and $Cr(CO)_6$ were heated at 160 °C until sublimation of unreacted $Cr(CO)_6$ was no longer observed, suggesting completion of the reaction. Although after this time (~ 1 hour), analysis of the crude reaction mixtures by $^{31}P\{^1H\}$ NMR spectroscopy revealed the reactions had only achieved 83 - 84 % conversion, the reactions were not heated any further in order to avoid decomposition of the target Cr^0-PCN complexes or the formation of any impurities which may introduce difficulties into the isolation of Cr^0-PCN complexes (as had been previously observed as a result of applying prolonged heating in the reaction between ligand **2.15** and $Cr(CO)_6$ in toluene, Table 2.14).

Close examination of the $Cr(CO)_5(\kappa^1$-P-PCN):$Cr(CO)_4(\kappa^2$-P,N-PCN) ratios present in the crude diglyme reaction mixtures of complexes **2.18** – **2.19**, and **2.22** – **2.25** (monitored by $^{31}P\{^1H\}$ NMR spectroscopy after 1 hour of heating at 160 °C) reveals an increase in these ratios upon an increase in the steric bulk of the nitrogen atoms on the PCN ligands bound to the Cr^0 centres (Table 2.15). The observed preference, for PCN ligands with bulky nitrogen substituents, of a κ^1-P monodentate binding mode to Cr^0 is as expected, due to the greater steric hindrance between the N and Cr atoms in κ^2-P, N bidentate Cr^0-PCN complexes.

Table 2.15: List of the $Cr(CO)_5$(PCN):$Cr(CO)_4$(PCN) ratios present in the crude diglyme reaction mixtures (after 1 hour of heating at 160 °C) of complexes **2.18 – 2.19,** and **2.22 – 2.25**, which have been derived from the integrations of the resonances present in the $^{31}P\{^1H\}$ NMR spectra (measured in C_6D_6 at 162 MHz) of the crude reaction mixtures of **2.18 – 2.19,** and **2.22 – 2.25**.

Structural Formula of PCN Ligand bound to Cr(0)	**$Cr(CO)_5(\kappa^1$-P-PCN):$Cr(CO)_4(\kappa^2$-P,N-PCN)ratios present in the crude reaction mixture after 1 hour of heating at 160 °C**
$PhC(P^iPr_2)=N(2\text{-}MeC_6H_4)$ (**2.16**)	1.6:1
$PhC(P^iPr_2)=N(2,6\text{-}Et_2C_6H_3)$ (**2.15**)	4.3:1
$PhC(P^iPr_2)=N(2,6\text{-}^iPr_2C_6H_3)$ (**2.14**)	5.5:1

In addition to being influenced by the steric bulk of the substituents at the N atoms of the precursor PCN ligands, the $Cr(CO)_5(\kappa^1$-P-PCN):$Cr(CO)_4(\kappa^2$-P,N-PCN) ratios are also influenced by the reaction conditions. For Cr^0-PCN complexes **2.18** and **2.19**, which have been synthesised under two different sets of reaction conditions (Scheme 2.40, Table 2.16), a longer heating time resulted in a lower **2.19**:**2.18** ratio. This observed temperature dependence on the ratio of **2.19**:**2.18** indicates that the $Cr(CO)_4(\kappa^2$-P,N-PCN) complex is the thermodynamic product, whilst the $Cr(CO)_5(\kappa^1$-P-PCN) complex is the kinetic product. The previous finding that prolonged heating, in

the reaction between ligand **2.15** and $Cr(CO)_6$ in toluene, led to the depletion of the $Cr(CO)_5(\kappa^1$-P-PCN) complex adds further weight to the idea that the $Cr(CO)_5(\kappa^1$-P-PCN) complex is the kinetic product.

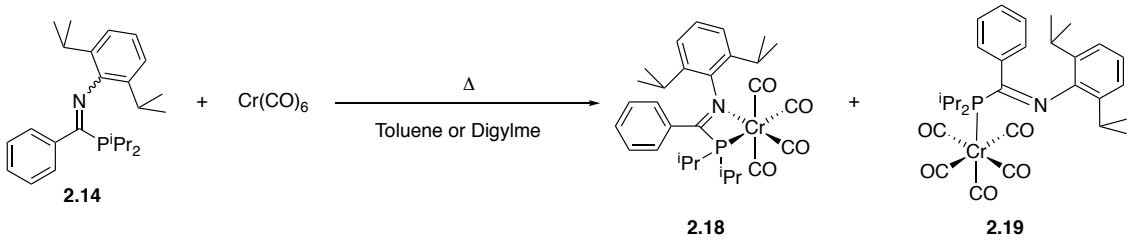

Scheme 2.40: Synthesis of complexes **2.18** and **2.19**.

Table 2.16: Conditions used in the syntheses of complexes **2.18** and **2.19** and comparison of **2.19**:**2.18** ratios present in the crude reaction mixtures after heating under different conditions.

Reaction solvent	Reflux time (h)	2.19:2.18 ratio present in the crude reaction mixture after heating
Toluene	21	1.4:1
Diglyme	1	5.5:1

2.4.1.2. Characterisation of Cr^0-PCN complexes

The identities of the Cr^0-PCN complexes synthesised in this thesis (Figure 2.29) have been confirmed by elemental and X-ray diffraction analysis, in addition to NMR and IR spectroscopies. Comparison of the IR spectra, as well as selected bond lengths and angles of the molecular structures of the Cr^0-PCN complexes, enables insight to be gained into the steric and electronic properties of the PCN ligands coordinated to the Cr^0 complexes, and will be discussed in the following sections.

2.4.1.2.1. Analysis of the IR spectra of Cr^0-PCN complexes 2.18-2.25

Due to the complexity of data of the IR spectra of Cr^0-PCN complexes **2.18** – **2.25,** only the C=N and CO stretching frequencies will be considered (Table 2.17). The $Cr(CO)_4(\kappa^2$-P,N-PCN) complexes display four carbonyl stretching bands, consistent with that expected for a bidentate complex with C_1 symmetry. The CO stretching frequencies for the $Cr(CO)_4(\kappa^2$-P,N-PCN) complexes are comparable to those of the $Cr(CO)_4(\kappa^2$-P,P-PNP) complexes synthesised by Bowen *et al*., which gave selective ethylene trimerisation systems when oxidised by $[N(4\text{-}C_6H_4Br)_4][B(C_6F_5)_4]$ in the presence of $AlEt_3$.[128] The similarity between the CO stretching frequencies of the $Cr(CO)_4(\kappa^2$-P,N-PCN) complexes and $Cr(CO)_4(\kappa^2$-P,P-PNP) complexes suggests that the precursor PCN ligands (to the $Cr(CO)_4(\kappa^2$-P,N-PCN) complexes) have similar coordinative properties to the PNP ligands synthesised by Bowen *et al*.[128] In addition, it is apparent from the IR data (Table 2.17) that as the substituent at N is changed in the series of $Cr(CO)_4(\kappa^2$-P,N-PCN) complexes there is little effect on the CO stretching

frequencies, suggesting that the N-substituents have similar electronic properties as expected.

Table 2.17: Selected IR stretches of complexes **2.18** – **2.25**; IR spectra recorded in DCM solution.

Selected IR stretches (cm^{-1})								
	$Cr(CO)_4(\kappa^2$-P,N-PCN) complex:				$Cr(CO)_5(\kappa^1$-P-PCN) complex:			
	2.18	**2.20**	**2.22**	**2.24**	**2.19**	**2.21**	**2.23**	**2.25**
ν_{CO}	1999. 1900, 1874, 1859	2000, 1899, 1874, 1858	2000, 1894, 1877, 1857	2002, 1901, 1880, 1857	2061, 1980, 1935	2060, 1980, 1934	2061, 1980, 1934	2060, 1981, 1936
$\nu_{C=N}$	1532	1536	1551	1538	1584	1587	1586	1591

In contrast to the $Cr(CO)_4(\kappa^2$-P,N-PCN) complexes, the $Cr(CO)_5(\kappa^1$-P-PCN) complexes have only three carbonyl stretching frequencies, which is in agreement with a monodentate complex with a C_{4v} point group. In addition, the carbonyl stretching bands of the $Cr(CO)_5(\kappa^1$-P-PCN) complexes are at higher frequencies to those of the analogous $Cr(CO)_4(\kappa^2$-P,N-PCN) complexes implying that the CO bonds are weaker in the bidentate Cr^0-PCN complexes than in their monodentate analogues, as expected from donation by both the Lewis basic P and N components of the ligands creating a more electron rich chromium centre.

On examining the imine stretching frequencies summarised in Table 2.17, it can be seen that the stretching frequencies of the $Cr(CO)_4(\kappa^2$-P,N-PCN) complexes are at lower wavenumbers than those of the $Cr(CO)_5(\kappa^1$-P-PCN) complexes (which themselves are similar to the imine stretching frequencies of the precursor PCN ligands: 1583 – 1590 cm^{-1}). The lower stretching frequencies of the imine bonds of the PCN ligands observed in the $Cr(CO)_4(\kappa^2$-P,N-PCN) complexes indicate that the imine group on the PCN ligands acts as a π acceptor by accepting electrons from chromium into its π^* antibonding orbitals (Figure 2.31), leading to a weakening of the C=N bond and lowering of the imine stretching frequency.

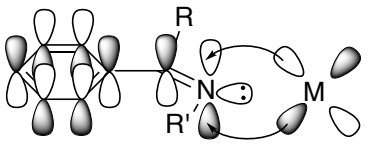

Figure 2.31: Interaction between the d orbitals on a metal centre (M) and π^* antibonding orbitals of a C=N group.

2.4.1.2.2. Analysis of the $^{13}C\{^1H\}$ spectra of Cr^0-PCN complexes 2.18-2.25

The $^{13}C\{^1H\}$ NMR spectra of the $Cr(CO)_5(\kappa^1$-P-PCN) complexes all exhibit two resonances in the CO region of the spectra, exemplified by the data shown in , indicative of two different CO environments in these complexes (CO *trans* to CO or CO trans to P, Figure 2.32(b)), as expected. In a similar manner, the $Cr(CO)_4(\kappa^2$-P,N-PCN) complexes all display at least three resonances in the CO region of their ^{13}C NMR spectra, which implies the presence of three different CO environments in these complexes (CO *trans* to CO, CO trans to P, or CO trans to N Figure 2.32(a)), as expected. The carbon chemical shifts corresponding to the *C*O trans P and *C*O trans CO are found to be higher in the $Cr(CO)_4(\kappa^2$-P,N-PCN) complexes than in their $Cr(CO)_5(\kappa^1$-P-PCN) analogues.

Table 2.18: List of CO and imine carbon chemical shifts, with couplings in Hertz in brackets ($^2J_{PC}$), observed in the ^{13}C NMR spectra (in $CDCl_3$ at 176 MHz or 151 MHz) of complexes **2.18 – 2.25**.

$^{13}C\{^1H\}$ NMR shifts (ppm)								
	$Cr(CO)_4(\kappa^2$-P,N-PCN) complex				$Cr(CO)_5(\kappa^1$-P-PCN) complex			
	2.18	**2.20**	**2.22**	**2.24**	**2.19**	**2.21**	**2.23**	**2.25**
***CO trans* P**	229.3 (12.0)	229.3 (12.0)	229.3	229.8 (12.0)	221.3 (5.0)	221.5 (5.0)	221.2 (5.0)	221.7 (5.0)
***CO trans* N**	225.5 (3.0)	225.4	225.4 (2.5)	225.8 (2.0)	N/A			
***CO trans* CO**	222.3 (13.0)	222.5 (12.0)	222.3 (12.5)	222.7 (11.0), 221.6 (10.5)	217.8 (12.5)	218.0 (13.0)	217.7 (12.5)	218.0 (13.0)
C=N	185.0 (18.0)	184.9 (18.0)	185.3	183.8 (18.5)	175.6 (28.5)	176.0 (30.0)	175.7 (29.0)	177.4 (33.5)

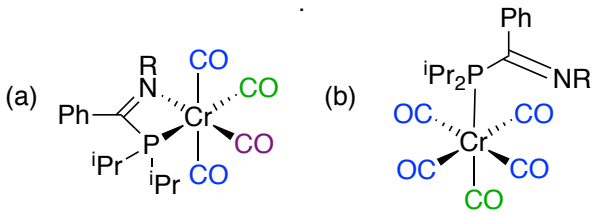

Figure 2.32: Illustration of different CO environments in (a) $Cr(CO)_4$(PCN) and (b) $Cr(CO)_5$(PCN) complexes, where R = aryl group.

In addition to the chemical shifts of the CO carbons of the Cr^0-PCN complexes, it is important to consider the chemical shifts of the imine C=N carbons of these complexes in order to gain insight into the electronic properties of the different substituents on the

N atoms of the PCN ligands. For both series of the $Cr(CO)_4(\kappa^2$-P,N-PCN) and $Cr(CO)_5(\kappa^1$-P-PCN) complexes changing the substituents on the N atoms of the PCN ligands has little impact on their imine carbon chemical shifts (), suggesting that the different N substituents have similar electronic character as might be expected.

On closer examination of the chemical shift data presented in it can be seen that the chemical shifts of the imine carbons of the $Cr(CO)_4(\kappa^2$-P,N-PCN) complexes are higher compared to that of their $Cr(CO)_5(\kappa^1$-P-PCN) analogues (which themselves have chemical shifts of similar magnitude to that of the imine carbons of the uncoordinated PCN ligands: 177.1 – 177.6 ppm), as would be expected from the involvement of both P and N atoms in σ-donation to the Cr centre of the bidentate Cr^0-PCN complexes.

2.4.1.2.3. Analysis of the $^{31}P\{^1H\}$ spectra of Cr(0)-PCN complexes 2.18-2.25

The $^{31}P\{^1H\}$ NMR spectra of complexes **2.18** – **2.25** exhibit a single resonance as expected (Table 2.19), which is observed at a higher frequency than those of the corresponding uncoordinated PCN ligands (δ_P: 26.9 – 27.7 ppm). In addition, the phosphorus signals for the bidentate Cr^0-κ^1-P-PCN complexes are at lower frequencies than those of their monodentate analogues. The observed difference in the chemical shift frequencies of the phosphorus signals of the uncoordinated PCN ligands and Cr^0-PCN complexes is believed to be caused by a combination of steric and electronic factors.

Table 2.19: $^{31}P\{^1H\}$ chemical shifts of complexes **2.18** – **2.25**; spectra measured in $CDCl_3$ at 243 MHz or 283 MHz.

$^{31}P\{^1H\}$ NMR shifts (ppm)							
$Cr(CO)_4(\kappa^2$-P,N-PCN) complex:				**$Cr(CO)_5(\kappa^1$-P-PCN) complex:**			
2.18	**2.20**	**2.22**	**2.24**	**2.19**	**2.21**	**2.23**	**2.25**
63.3	61.8	61.8	59.2	83.1	87.0	85.1	83.1

2.4.1.2.4. Analysis of the molecular structures of $Cr(CO)_4(\kappa^2$-P,N-PCN) complexes

The molecular structures of complexes **2.18**, **2.20**, **2.22**, and **2.24** (Figure 2.33; the molecular structures of complexes **2.18** and **2.20** were obtained by Dr. James Radcliffe in previous work and have been included here for comparison) show the *cis* bidentate bonding modes of the PCN ligands to Cr^0 centres.[70] The PCN ligands exist in *E* configurations about the imine bond in the bidentate Cr^0-κ^2-P,N-PCN complexes. The asymmetric unit of complex **2.20** reveals that it consists of two molecules of which one is ordered (shown in Figure 2.33) and the other is disordered (about the phenyl, dimethylphenyl and both isopropyl substituents). Since both molecules found in the asymmetric unit of complex **2.20** demonstrate the same metal coordination geometry,

the bond lengths and angles reported in Table 2.20 for complex **2.20** are the weighted average of those of its ordered and disordered molecules.

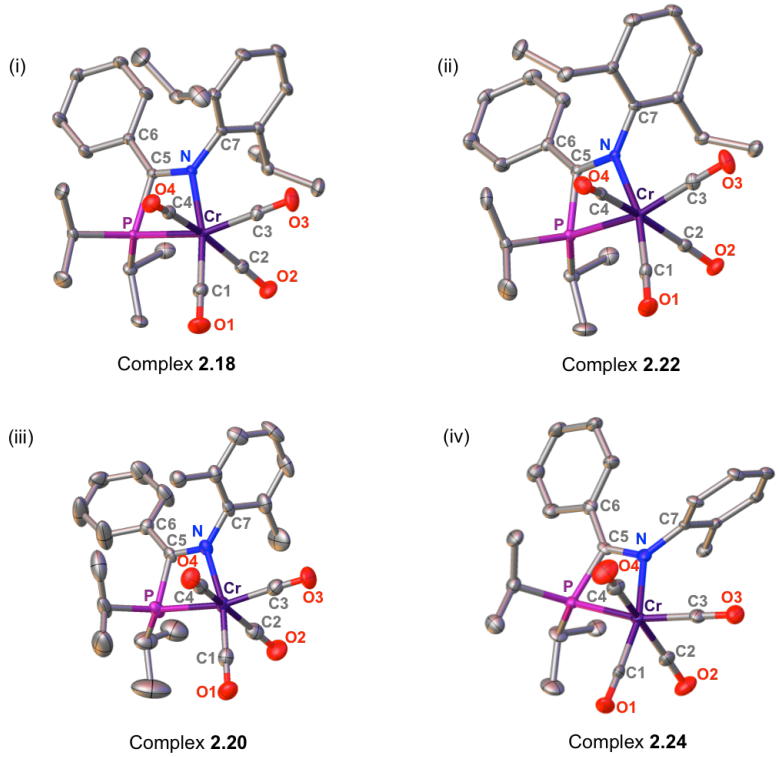

Figure 2.33: Molecular structures of $Cr(CO)_4(\kappa^2$-P,N-PCN) complexes (i) **2.18**, (ii) **2.22**, (iii) **2.20** (the ordered molecule in the asymmetric cell), and (iv) **2.24** (which displays disorder about its N substituent) with thermal ellipsoids at the 50% probability level; H atoms have been omitted for clarity.

Table 2.20: Selected bond lengths and angles for $Cr(CO)_4(\kappa^2$-P,N-PCN) complexes **2.18**, **2.22**, **2.20**, and **2.24**, refer to **Figure 2.33** for atom labels. Estimated standard deviations given in brackets. The bond lengths and angles reported for complex **2.20** are the weighted average of its ordered and disordered molecules found in the asymmetric cell

$Cr(CO)_4(\kappa^2$-P,N-PCN) complex		2.18	2.22	2.20	2.24
Bond Lengths (Å)	Cr-C1	1.8465(11)	1.8373(18)	1.83(8)	1.834(8)
	Cr-C2	1.8954(11)	1.8869(19)	1.876(8)	1.892(7)
	Cr-C3	1.8539(11)	1.8629(19)	1.843(8)	1.847(8)
	Cr-C4	1.8926(11)	1.8862(18)	1.892(8)	1.895(8)
	N-C5	1.3050(12)	1.298(2)	1.297(8)	1.292(9)
	C1-O1	1.1612(14)	1.156(2)	1.161(8)	1.162(8)
	C2-O2	1.1513(14)	1.150(2)	1.16(9)	1.150(7)
	C3-O3	1.1548 (14)	1.150(2)	1.153(9)	1.164(8)
	C4-O4	1.1507(14)	1.153(2)	1.154(9)	1.148(8)
	P-Cr	2.3829(3)	2.3761(5)	2.3938(19)	2.371(2)
	N-Cr	2.1425(8)	2.1446(14)	2.157(5)	2.127(6)
Bond Angles (°)	P-C5-N	100.47(7)	101.30(11)	103.0(4)	100.9(5)
	P-Cr-N	65.79(2)	65.80(4)	65.66(16)	65.67(16)
	Cr-P-C5	83.72(3)	83.69(5)	83.2(2)	83.5(2)
	Cr-N-C7	126.34(6)	127.29(10)	128.0(4)	129.1(17)

From the selected bond length and angle data in Table 2.20 it is evident that the bidentate Cr^0-κ^2-P,N-PCN complexes all adopt a distorted octahedral geometry around the chromium. The P-Cr-N angle deviates the greatest from the typical octahedral angle of 90°, with a value of ~66° across all bidentate Cr^0-κ^2-P,N-PCN complexes, most likely a result of the inherent constraints present in the chelate ring. Interestingly, the acute P-Cr-N bite angles of ~66° and P-C-N angles of 100.5 – 103.0° of the bidentate Cr^0-κ^2-P,N-PCN complexes are similar to the P-Cr-P bite angles of 66.6 – 68.4° and P-N-P angles of 99.9 – 106.5° reported in the literature for Cr^0-κ^2-P,P-PNP complexes of related Cr/PNP-based ethylene trimerisation and tetramerisation catalysts, *e.g.* $[Cr(CO)_4(\kappa^2\text{-P,P-Ph}_2PN(^iPr)PPh_2)]$ and $[Cr(CO)_4(\kappa^2\text{-P,P-Ar}_2PN(Me)PAr_2)]$ (where Ar = 2-C_6H_4(OMe).[128,134]

Additionally, the Cr-C bond lengths of the bidentate Cr^0-κ^2-P,N-PCN complexes are reflective of the *trans* influence of the different ligands, CO > P > N, hence Cr-$C_{trans\text{CO}}$ > Cr-$C_{trans\text{P}}$ > Cr-$C_{trans\text{N}}$.[135] The strongly electron-donating nature of the phosphine will also result in back donation from the Cr d-orbitals into the antibonding π^* orbital of the CO, shortening the Cr-C bond *trans* to P. The N=C bond lengths of the bidentate Cr^0-PCN complexes are longer than that expected for a typical imine bond (1.28 Å),[114] indicative of the π-acceptor nature of the imine bond, in agreement with the ν_{CN} stretches discussed previously in section 2.4.1.2.1. Finally, the Cr-N-C7 bond angle increases across the series of bidentate complexes (from **2.18** to **2.24**, Table 2.20) in line with a decrease in the steric bulk of the substituent at N.

2.4.1.2.5. Analysis of the molecular structures of $Cr(CO)_5(\kappa^1$-P-PCN) complexes

The PCN ligands are found to exhibit monodentate binding modes with an *E* configuration about the imine bonds in complexes **2.19**, **2,23**, **2.21** and **2.25** (Figure 2.34; the molecular structures of complexes **2.19** and **2.21** were obtained by Dr. James Radcliffe in previous work and have been included here for comparison[70]). The molecular structure of complex **2.25** reveals disorder about the whole molecule, therefore the bond lengths and angles reported in Table 2.21 for complex **2.25** are the weighted average of the two disordered parts of the molecule.

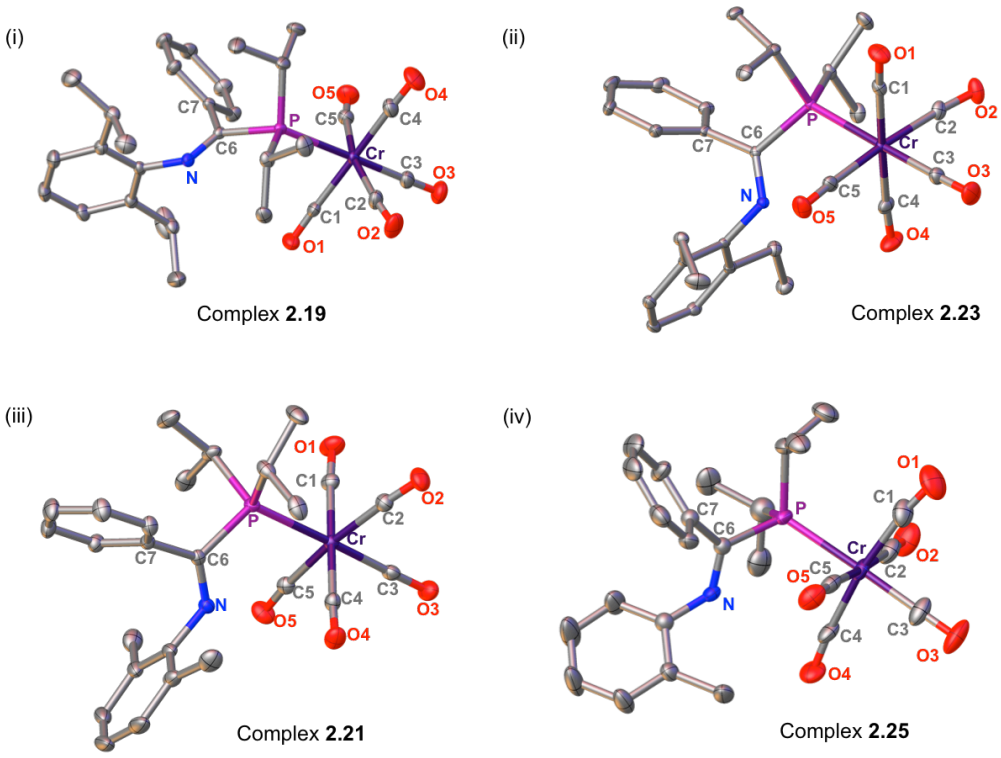

Figure 2.34: Molecular structures of $Cr(CO)_5(\kappa^1$-P-PCN) complexes (i) **2.19**, (ii) **2.23** (iii) **2.21**, and (iv) **2.25** (part 1 of the disordered molecule) with thermal ellipsoids at the 50% probability level; H atoms have been omitted for clarity.

Table 2.21: Selected bond lengths and angles for $Cr(CO)_5(\kappa^1$-P-PCN) complexes **2.19**, **2.23**, **2.21**, and **2.25**, refer to **Figure 2.34** for atom labels. Estimated standard deviations given in brackets. The bond lengths and angles reported for complex **2.25** are the weighted average of the two disordered parts of the molecule.

$Cr(CO)_5(\kappa^1$-P-PCN) complex		2.19	2.23	2.21	2.25
Bond Lengths (Å)	Cr-C1	1.9074(12)	1.8956(13)	1.8943(12)	1.882(8)
	Cr-C2	1.9003(12)	1.8935(14)	1.8884(12)	1.900(8)
	Cr-C3	1.8644(13)	1.8679(13)	1.8628(12)	1.854(7)
	Cr-C4	1.8953(13)	1.9043(14)	1.9097(12)	1.899(8)
	Cr-C5	1.9036(12)	1.9006(14)	1.9016(12)	1.887(5)
	N-C6	1.2768(13)	1.2760(14)	1.2768(14)	1.276(10)
	C1-O1	1.1415(15)	1.1417(16)	1.1404(15)	1.137(10)
	C2-O2	1.1458(15)	1.1432(16)	1.1475(15)	1.138(10)
	C3-O3	1.1478(16)	1.1439(16)	1.1461(15)	1.151(8)
	C4-O4	1.1436(17)	1.1430(17)	1.1382(15)	1.150(9)
	C5-O5	1.1440(15)	1.1392(17)	1.1416(15)	1.133(3)
	P-Cr	2.4431(3)	2.4073(4)	2.4103(3)	2.398(3)
Bond Angles (°)	P-C6-N	115.80(7)	115.57(8)	114.27(8)	112.8(6)
	Cr-P-C6	119.99(3)	115.08(4)	114.52(3)	114.03(11)

As was observed for the bidentate Cr^0-κ^2-P,N-PCN complexes, the monodentate Cr^0-κ^1-P-PCN complexes exhibit a disordered octahedral geometry around the chromium centre. As expected, the P-C-N angles of the monodentate Cr^0-κ^1-P-PCN complexes are bigger than the P-C-N angles of the analogous bidentate Cr^0-PCN complexes

(Table 2.20) and observed to decrease as the steric bulk of the substituent at N is increased (Table 2.21). In addition, the large Cr-P-C6 bond angles of 114 - 120° of the monodentate Cr^0-κ^1-P-PCN complexes, relative to the narrower analogous Cr-P-C5 angles of 83 - 84° of the bidentate complexes, are reflective of the strain imposed by the chelate ring in the bidentate Cr^0-κ^2-P,N-PCN complexes.

In agreement with the observation by IR spectroscopy that the monodentate Cr^0-κ^1-P-PCN complexes have stronger CO bonds than their bidentate counterparts (section 2.4.1.2.1), the monodentate Cr^0-κ^1-P-PCN complexes have shorter C-O bond lengths than those of their analogous bidentate complexes (C-O bond distances in Table 2.21 *vs.* Table 2.20) Consistent with the imine C=N stretches reported for the Cr^0-PCN complexes (section 2.4.1.2.1), the monodentate Cr^0-κ^1-P-PCN complexes have shorter C=N bond lengths (comparable to 1.28 Å, that expected for a typical imine bond)[114] than their bidentate counterparts, indicative of the absence of π-acceptance of the C=N bonds in the monodentate Cr^0-κ^1-P-PCN complexes. Finally, the Cr-C bond lengths of the monodentate Cr^0-κ^1-P-PCN complexes are also dictated by the *trans* influence of the ligands with the Cr-C bonds *trans* to CO being longer than the Cr-C bonds *trans* to P due to the weaker *trans* influence of the P ligand *versus* the CO ligand.[135]

2.4.1.2.6. *Comparison of the molecular structures of coordinated and uncoordinated PhC(P^iPr_2)=N(2-MeC_6H_4)*

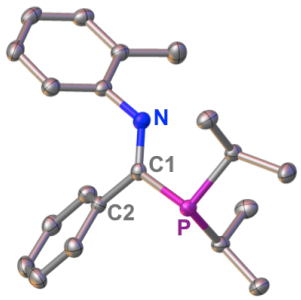

PhC(P^iPr_2)=N(2-MeC_6H_4)		
Bond Lengths (Å)	**N-C1**	1.2832(16)
	P-C1	1.8553(12)
	C1-C2	1.4936(17)
Bond Angles (°)	**P-C1-N**	118.41(9)

Figure 2.35: Molecular structure and selected bond lengths and angles of PhC(P^iPr_2)=N(2-MeC_6H_4) with thermal ellipsoids at the 50% probability level; H atoms have been omitted for clarity. Estimated standard deviations given in brackets.

Comparison of the bond lengths and angles of the molecular structure of the uncoordinated PCN ligand (PhC(P^iPr_2)=N(2-MeC_6H_4), Figure 2.35, obtained by Dr. James Radcliffe in previous work)[70] to the analogous bond lengths and angles of complexes **2.24** (Table 2.20) and **2.25** (Table 2.21), where the PCN ligand is coordinated in a κ^2-P,N and κ^1-P,N fashion to the Cr^0 centre, respectively, shows that coordination of the PCN ligand results in a decrease in the P-C-N angle. In addition,

the C=N bond distance is longer in the Cr^0-κ^2-P,N complex than in the uncoordinated PCN ligand, due to the C=N bond acting as a π-acceptor in the bidentate Cr^0 complex. The P-C and imine C-*ipso* phenyl C bond lengths are also found to vary upon coordination of the free ligand to Cr^0: both bonds increase in length as the PCN ligand binds to the Cr^0 centre in a κ^1-P,N manner and decrease in length upon κ^2-P,N coordination of the PCN ligand to the Cr^0 centre.

2.4.2. Coordination chemistry of PCN ligands with Cr^I

With the Cr^0-PCN complexes (**2.18** – **2.25**, Figure 2.29) in hand, attention next turned to conducting one-electron oxidation reactions of the Cr^0-PCN complexes in order to form the target Cr^I-PCN complexes (**2.26** – **2.33**), as illustrated in **Figure 2.36**. The synthesis of complexes **2.26** – **2.33** is desirable due to the potential of these complexes to act as catalytic precursors in ethylene oligomerisation catalysis, in a similar manner to the cations $[Cr(CO)_4(\kappa^2\text{-P,P-PNP})]^+$ and $[Cr(CO)_4(\kappa^2\text{-P,P-PCP})]^+$ reported in the literature, which were found to give selective ethylene *tri-*/*tetra*-merisation systems with modest activities upon activation with triethylaluminium.[128-130]

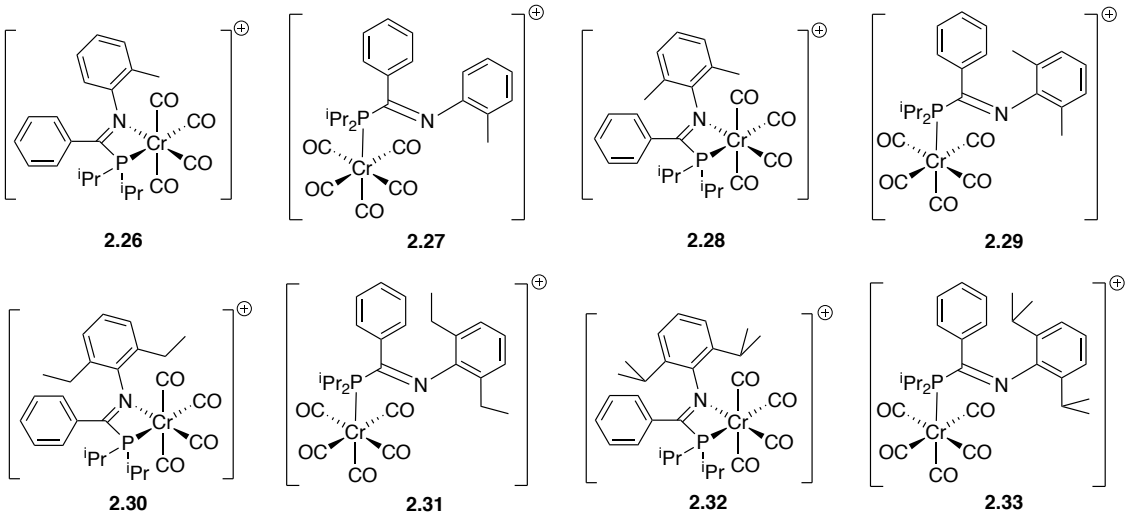

Figure 2.36: Target Cr^I-PCN complexes (**2.26** – **2.33**).

2.4.2.1. Synthesis and characterisation of Cr^I-PCN complexes 2.26 – 2.30 and 2.32

The Cr^I-PCN complexes, **2.26** – **2.30** and **2.32,** were synthesised *via* the route depicted in **Scheme 2.41**, in accordance with the literature procedure reported by Hanton *et al.*[129] for related systems. The Cr^0-PCN complexes were oxidised by $Ag[Al\{OC(CF_3)_3\}_4]$, as opposed to other Ag oxidising agents such as $AgBF_4$ or $AgPF_6$, based on the results described by Hanton *et al.,*[129] which showed that systems employing $[Cr(CO)_4(\kappa^2\text{-P,P-PNP})]^+$ and $AlEt_3$ were inactive towards ethylene *tri-*/*tetra*-

merisation in the presence of $[BF_4]^-$ or $[PF_6]^-$ anions. However, the same systems were active towards selective ethylene tetramerisation in the presence of the $[Al\{OC(CF_3)_3\}_4]^-$ anion. It was proposed that the stronger coordinating nature of the $[BF_4]^-$ and $[PF_6]^-$ anions, in comparison to the very weakly coordinating character of $[Al\{OC(CF_3)_3\}_4]^-$ resulted in the negative effects on ethylene *tri-*/*tetra*-merisation catalysis.[129]

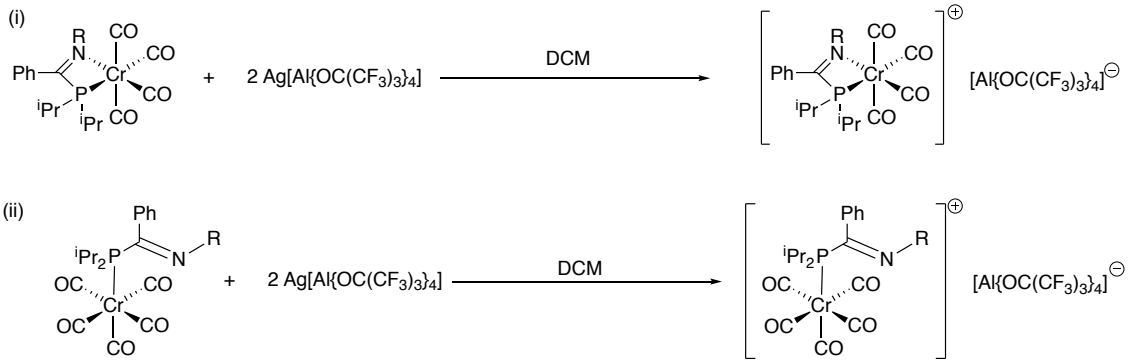

Scheme 2.41: Synthetic route employed to target (i) $[Cr(CO)_4(\kappa^2\text{-P,N-PCN})]^+$complexes and (ii) $[Cr(CO)_5(\kappa^1\text{-P-PCN})]^+$ complexes following literature procedure by Hanton *et al.*[129] for related systems.

Cr^I-PCN complexes **2.26** – **2.30** and **2.32** (**Figure 2.36**) were obtained in yields ranging from 31 – 83 %. The identities of the Cr^I-PCN complexes were confirmed by CHN, IR spectroscopy and mass spectrometry (for Cr^I-PCN complexes where sufficient material remained after testing in ethylene oligomerisation catalysis, which will be discussed in Chapter 3). Although, satisfactory elemental analyses were unable to be obtained of complex **2.32**, since its IR spectrum and mass spectrometry analysis yielded the expected results and there were no detectable impurities by ^1H or ^{31}P NMR (in the range of −450 to 300 ppm) spectroscopic analysis, it was reasoned that the complex had successfully been synthesised with deviation in the elemental analysis from the expected value possibly being due to the presence of trace amounts of residual silver salts as found for related complexes by Wass *et al*.[130] Despite multiple attempts to crystallise complexes **2.26** – **2.30** and **2.32**, which had been obtained as oily crude products, none proved successful. Crystallisation of complexes **2.26** – **2.30** and **2.32** was attempted in a number of different solvent mixtures (such as DCM/pentane, DCM/petroleum ether {40:60}, and toluene/petroleum ether {40:60}) and temperatures (ranging between 25 to –30 °C).

The IR spectra of complexes **2.26**, **2.28**, **2.30** and **2.32** revealed the presence of four CO stretching bands as shown in Table 2.22, which is in agreement with that expected for a $[Cr(CO)_4(\kappa^2\text{-P,N-PCN})]^+$ complex with C_1 symmetry, while the IR spectra of complexes **2.27** and **2.29** displayed three CO stretching frequencies, again as expected for a $[Cr(CO)_5(\kappa^1\text{-P-PCN})]$ cation with C_{4v} symmetry. The CO stretching

frequencies of the Cr^{I}-PCN complexes are similar to those reported in the literature for $[Cr(CO)_4(\kappa^2\text{-P,P-PNP})]^+$ species implying comparable coordinative properties of PCN ligands and PNP ligands.[128,129]

Table 2.22: Selected IR stretches of complexes **2.26** – **2.30** and **2.32**; IR spectra recorded in DCM solution.

Selected IR stretches (cm^{-1})						
	$[Cr(CO)_4(\kappa^2\text{-P,N-PCN})]^+$:				$[Cr(CO)_5(\kappa^1\text{-P-PCN})]^+$:	
	2.26	**2.28**	**2.30**	**2.32**	**2.27**	**2.29**
ν_{CO}	2092, 2054, 2038, 1967	2092, 2055, 2037, 1966	2104, 2053, 2031, 1950	2090, 2055, 2035, 1963	2092, 2038, 1968	2091, 2036, 1965

In addition, the CO stretching frequencies of the Cr^{I}-PCN complexes listed in Table 2.22 are at higher frequencies than those observed for their corresponding Cr^{0}-PCN precursors (Table 2.17), which is as expected on moving from a neutral to a positively charged species.[129] The CO stretching frequencies of the $[Cr(CO)_4(\kappa^2\text{-P,N-PCN})]$ and $[Cr(CO)_5(\kappa^1\text{-P-PCN})]$ cations are at similar wavenumbers suggesting that these complexes all have similar electronic properties and so, on simple electronic grounds, would be expected to display similar performance when tested in ethylene oligomerisation catalysis. Due to the complexity of the IR spectra of the Cr^{I}-PCN complexes in the region expected for C=N stretches, the imine stretching frequencies could not confidently be assigned.

In addition to analysis by IR spectroscopy, complexes **2.26** – **2.30** and **2.32** (**Figure 2.36**) were probed by ^{19}F NMR spectroscopy and found to display single resonances at approximately −76 ppm with peak half-height widths ranging between 6 - 26 Hz. It has been shown in the literature by Köhn *et al.*, that a broadening of the ^{19}F NMR signal of a fluorinated anion indicates interaction with a paramagnetic cation, with peak half-height widths in the region of 100 - 300 Hz indicating the presence of ion-pairing.[136] Since the peak half-height width of the $Ag[Al\{OC(CF_3)_3\}_4]$ oxidising reagent was determined to be 2.9 Hz by ^{19}F NMR spectroscopic analysis (376 MHz, CD_2Cl_2), it is clear that complexes **2.26** – **2.30** and **2.32** consist of a paramagnetic cation and is suggestive of the $[Al\{OC(CF_3)_3\}_4]$ anion being weakly coordinating in these systems.

Finally, the effective magnetic moments of complexes **2.26** – **2.30** and **2.32** were calculated *via* the Evans NMR spectroscopic method,[137] and found to be in the range between 1.71 – 1.96 μ_B. The values of the effective magnetic moments of complexes

2.26 – **2.30** and **2.32** are similar to the values of 1.78 – 1.83 μ_B of $[Cr(CO)_4(\kappa^2\text{-P,P-PNP})]^+$ species synthesised by Hanton *et al*.,[129] and comparable to the spin-only magnetic moment of 1.73 μ_B predicted for a low spin species with one unpaired electron, such as Cr^I.

2.4.2.2. Attempted synthesis and characterisation of Cr^I-PCN complex 2.31

The synthesis of complex **2.31** was attempted using the route shown in Scheme 2.42 and afforded a brown solid that was found by IR and NMR (^1H, ^{13}C, and $^{31}P\{^1H\}$) spectroscopies to consist of complex **2.31** along with other unknown products.

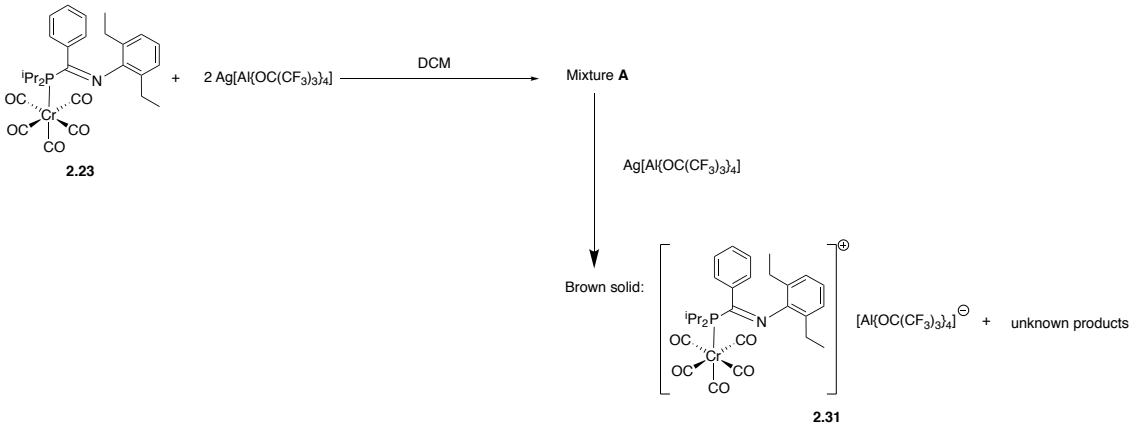

Scheme 2.42: Attempted synthesis of complex **2.31**.

The crude reaction mixture isolated from the reaction of complex **2.23** with 2 equivalents of $Ag[Al\{OC(CF_3)_3\}_4]$, mixture **A**, was analysed by IR spectroscopy, affording the spectrum displayed in Figure 2.37(a). The IR spectrum of mixture **A** contains two bands at 2035 and 2091 cm^{-1}, which are comparable to the CO stretching bands at 2038 and 2092 cm^{-1} generally observed for a $[Cr(CO)_5(\kappa^1\text{-P-PCN})]$ cationic species, such as complex **2.27** (Figure 2.37(b)). However, the IR spectrum of mixture **A** also exhibits two other bands at 1958 and 1979 cm^{-1}[d] (Figure 2.37(a)) in the region where the band at 1968 cm–$^{-1}$ is found for complex **2.27** (Figure 2.37(b)), in addition to a fourth band at 2074 cm.$^{-1}$ Since the band at 2074 cm^{-1} is not comparable to the bands found in the IR spectra of any of the Cr^I-PCN complexes (Table 2.22) or Cr^0-PCN complexes (Table 2.17) previously synthesised, it is attributed to an unknown CO-containing byproduct.

[d] A band at 1979 cm^{-1} is also present in the IR spectrum of the Cr^0-PCN precursor complex **2.23**.

(a)

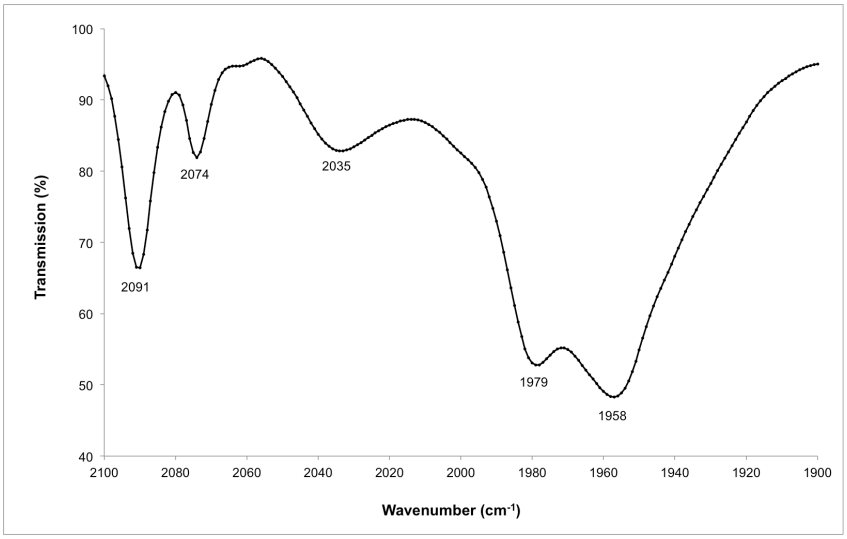

(b)

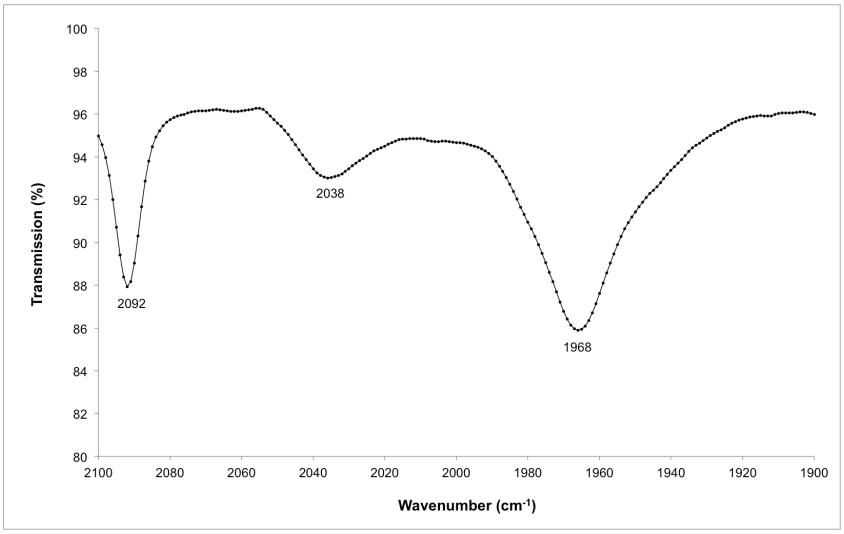

Figure 2.37: Comparison of the IR spectra (1900 – 2100 cm^{-1}, where CO bands for Cr^{I}-PCN complexes are expected) of (a) the filtrate of the crude reaction mixture between complex **2.23** and 2 equivalents of $Ag[Al\{OC(CF_3)_3\}_4]$ and (b) the cation $[Cr(CO)_5(\kappa^1\text{-P-PCN})]^+$ **2.27**. IR spectra measured in DCM.

Another equivalent of $Ag[Al\{OC(CF_3)_3\}_4]$ was added to mixture **A** and the resultant reaction mixture left to stir overnight, in order to investigate if any further reactions would occur. The crude reaction mixture obtained after the addition of a third equivalent of $Ag[Al\{OC(CF_3)_3\}_4]$, mixture **B**, was also subsequently analysed by IR spectroscopy (IR spectrum shown in Figure 2.38). In contrast to the IR spectrum of mixture **A** (Figure 2.37(a)), the IR spectrum of mixture **B** contains a band at 1965 cm^{-1}, while the band observed at 1958 cm^{-1} for mixture **A** is no longer present. The three bands found at 1965 cm, 2035 cm and 2091 cm^{-1} in the IR spectrum of mixture **B** are similar to the CO stretching frequencies expected for a $[Cr(CO)_5(\kappa^1\text{-P-PCN})]$ cation (Figure 2.37(b)), suggesting that mixture **B** contains the target complex **2.31,** in

addition to other unknown CO-containing by-products (that give rise to the bands at 1979 and 2075 cm^{-1}).

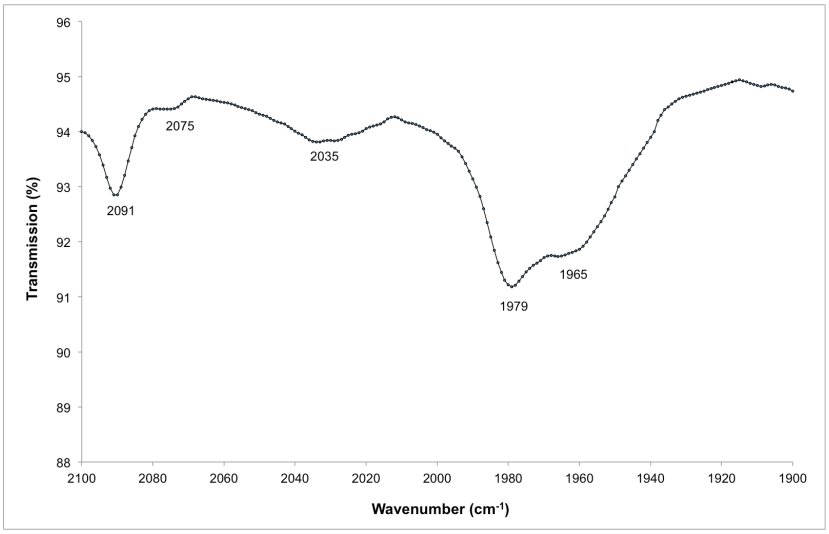

Figure 2.38: IR spectrum (1900 – 2100 cm^{-1}, where CO bands for Cr^{I}-PCN complexes are expected) of the filtrate of the crude reaction mixture between complex **2.23** and 3 equivalents of $Ag[Al\{OC(CF_3)_3\}_4]$.

Upon removing the volatile components of mixture **B**, a viscous red oil was obtained which failed to crystallise in a range of different solvent mixtures (such as DCM/pentane, DCM/petroleum ether {40:60}, and toluene/petroleum ether {40:60}). The viscous oil was therefore washed with various solvents (such as toluene, hexane and petroleum ether {40:60}) in an attempt to separate out the unwanted CO-containing by-products (observed by IR spectroscopy), before being left at −30 °C for 48 hours, after which point it solidified on scraping to generate a brown solid.

Analysis of this resulting brown solid by mass spectrometry confirmed the presence of the target complex **2.31**, with further support being added by the measured μ_{eff} value of 1.60 μ_B (comparable to the μ_{eff} values of 1.78 – 1.83 μ_B of the Cr^{I}-PCN complexes **2.26**– **2.30** and **2.32**) and the presence of a single resonance at −75.6 ppm in the ^{19}F NMR spectrum with a peak half-height width of 9.2 Hz implying the presence of a paramagnetic cation. However, analysis of the brown solid by NMR spectroscopy (^{1}H, $^{13}C\{^{1}H\}$ and $^{31}P\{^{1}H\}$) revealed that it also contained other products, in addition to the target complex **2.31**. The $^{31}P\{^{1}H\}$ spectrum of the brown solid contains five resonances: three doublets at 6.6 (J_{PP} = 53.6 Hz), 8.6 (J_{PP} = 33.8 Hz), and 9.7 ppm (J_{PP} = 54.0 Hz), in addition to two broad resonances at 86.5 and 89.2 ppm, all present in a ratio of 1:0.1:1:0.6:0.8, respectively. The doublets found at 6.6, 8.6, and 9.7 ppm arise from ^{31}P—^{31}P coupling, indicating that these correspond to species containing at least two phosphorus atoms in different chemical environments. Furthermore the

doublets in the $^{31}P\{^{1}H\}$ spectrum of the brown solid are multiplets in the ^{31}P ^{1}H-coupled NMR spectrum, which suggests that they most likely correspond to phosphorus atoms bearing ^{i}Pr groups. The ^{1}H and $^{13}C\{^{1}H\}$ NMR spectra of the brown solid are complex, exhibiting a multitude of resonances in the alkyl and aromatic regions. Unfortunately, due to the complexity of the ^{31}P, $^{13}C\{^{1}H\}$, and ^{1}H NMR spectroscopy data of the brown solid, and the inability to separate the different products in the brown solid, the identities of all of the products, except complex **2.31**, are unable to be elucidated.

2.4.2.3. Attempted synthesis and characterisation of Cr^{I}-PCN complex 2.33

The reaction between complex **2.19** and $Ag[Al\{OC(CF_3)_3\}_4]$ was carried out under the conditions depicted in Scheme 2.43. This reaction yielded a light brown solid that was found to consist of a mixture of products, of which one was the desired complex **2.33**, detectable and identifiable by mass spectrometry and NMR and IR spectroscopies.

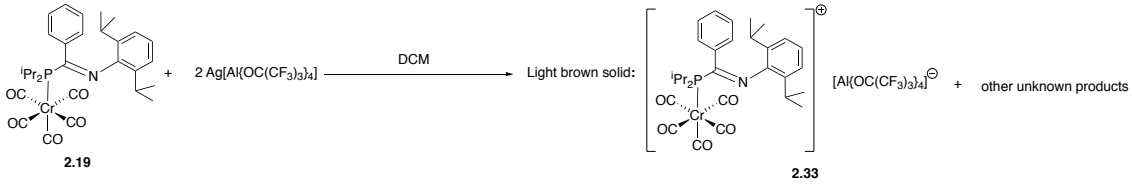

Scheme 2.43: Attempted synthesis of complex **2.33**.

The formation of complex **2.33** was further confirmed by the IR spectrum of the light brown solid, which gives rise to three CO stretches at 1963, 2036 and 2090 cm^{-1}, comparable to the CO stretches of the $[Cr(CO)_5(PCN)]$ cationic species synthesised previously (Table 2.22). The identity of complex **2.33** is further supported by mass spectrometry of the light brown solid, the determined μ_{eff} value of 1.68 μ_B (similar to the μ_{eff} values of 1.78 – 1.83 μ_B of the Cr^{I}-PCN complexes previously synthesised), and the broadening of the single resonance in its ^{19}F NMR spectrum (−75.5 ppm, $\nu_{½}$ = 25.7 Hz) relative to the resonance for $[Al\{OC(CF_3)_3\}_4]$ ($\nu_{½}$ = 2.9 Hz) indicating the presence of a paramagnetic cation (established as described above).

The presence of additional products was detected by $^{31}P\{^{1}H\}$, ^{1}H, and $^{13}C\{^{1}H\}$ NMR spectroscopic analysis of the light brown solid. The $^{31}P\{^{1}H\}$ NMR spectrum of the light brown solid displays six resonances: two mutually coupled doublets at 6.6 ppm(J_{PP} = 36.1 Hz) and 8.6 ppm (J_{PP} = 36.5 Hz) in addition to four singlets at 11.3, 27.4, 40.4, and 48.0 ppm, with all resonances present in a ratio of 1:1:0.2:0.03:0.1:0.2, respectively. The doublets at 6.6 and 8.6 ppm are also observed in the $^{31}P\{^{1}H\}$ NMR spectrum of the brown solid formed in the attempted synthesis of complex **2.31**

(section 2.4.2.2), although the doublet at 6.6 ppm is found to have a larger coupling constant of 53.6 Hz in the $^{31}P\{^{1}H\}$ NMR spectrum of the brown solid. The resonance at 27.4 ppm observed in the $^{31}P\{^{1}H\}$ NMR spectrum of the light brown solid corresponds to the precursor ligand **2.14**. The ^{1}H and $^{13}C\{^{1}H\}$ NMR spectra of the light brown solid exhibit multiple resonances in the alkyl and aromatic regions, similar to the ^{1}H and $^{13}C\{^{1}H\}$ NMR spectra of the brown solid formed in the attempted synthesis of complex **2.31** (section 2.4.2.2). The complexity of the ^{1}H, $^{13}C\{^{1}H\}$, and $^{31}P\{^{1}H\}$ NMR spectra of the light brown solid makes identifying the by-products difficult. Moreover, the by-products were found to have similar solubilities in a range of solvents (such as pentane, hexane, and petroleum ether (40:60)), hence preventing their separation by recrystallisation.

2.4.2.4. Reaction between ligand 2.14 and Ag[Al{OC(CF$_3$)$_3$}$_4$]

In an attempt to understand the nature of the by-products formed in the syntheses of complexes **2.31** and **2.33**, an NMR-scale reaction between PCN ligand **2.14** (the precursor ligand to complex **2.33**) and $Ag[Al\{OC(CF_3)_3\}_4]$ in a 1:1 ratio in CD_2Cl_2 was carried out. The reaction was allowed to proceed for 14 hours before being analysed by NMR spectroscopy, which indicated the formation of a mixture of products (which will be referred to as mixture **C**). The $^{31}P\{^{1}H\}$ NMR spectrum of mixture **C** exhibits four resonances: a mutually-coupled pair of doublets at 55.0 (J_{PP} = 35.1 Hz) and 58.0 ppm (J_{PP} = 35.1 Hz), in addition to two broad resonances at 86.4 and 90.3 ppm,[e] with these resonances present in relative ratios of 1:1:0.2:0.3. The two broad resonances at 86.4 ppm and 90.3 ppm are also observed in the $^{31}P\{^{1}H\}$ NMR spectrum of the brown solid (obtained in the attempted synthesis of complex **2.31**, section 2.4.2.2). The two doublets in the $^{31}P\{^{1}H\}$ NMR spectrum of mixture **C** correspond to species possessing more than one phosphorus atom, and are believed to arise from $P^{i}Pr_2$ environments as they demonstrate coupling to protons in the ^{31}P ^{1}H-coupled NMR spectrum. Interestingly, the coupling constants of the doublets in the $^{31}P\{^{1}H\}$ NMR spectrum of mixture **C** are similar in magnitude to (a) the coupling constant of the doublet observed at 8.6 ppm (J_{PP} = 33.8 Hz) in the $^{31}P\{^{1}H\}$ spectrum of the brown solid obtained in the attempted synthesis of complex **2.31** (section 2.4.2.2) and (b) the coupling constants of the doublets at 6.6 and 8.6 ppm ($J_{PP} \approx$ 36.5 Hz) in the $^{31}P\{^{1}H\}$ NMR spectrum of the light brown solid (obtained in the attempted synthesis of complex **2.33**, section 2.4.2.3).

[e] Difficult to elucidate multiplicities of resonances at 86.4 and 90.3 ppm due to their highly broadened nature.

The ^{1}H and $^{13}C\{^{1}H\}$ spectra of mixture **C** display a multitude of resonances in the alkyl and aromatic regions, of which some resonances are similar to those observed in the ^{1}H and $^{13}C\{^{1}H\}$ spectra of the brown solid obtained in the attempted synthesis of complex **2.31** (section 2.4.2.2) and light brown solid (obtained in the attempted synthesis of complex **2.33**, section 2.4.2.3). The ^{19}F spectrum of mixture **C** exhibits a single resonance at −75.7 ppm, which has a peak half-height width of 3.1 Hz, comparable to the peak half-height width of $Ag[Al\{OC(CF_3)_3\}_4]$, implying the presence of a diamagnetic cationic species, charge-balanced by $[Al\{OC(CF_3)_3\}_4]$. Additionally, the IR spectrum of mixture **C** has a C=N stretch at 1552 cm–^{1}, which is at a lower stretching frequency than the C=N band for the starting ligand **2.14** (1584 cm^{-1}), suggesting that the C=N bond of the C=N-containing product in mixture **C** is weaker than the C=N bond of ligand **2.14**. There are no amide stretches present in the IR spectrum of mixture **C** indicating that $Ag[Al\{OC(CF_3)_3\}_4]$ does not oxidise the C=N bond of ligand **2.14**.

Unfortunately, the identities of the products in mixture **C** could not be deduced from the IR and $^{31}P\{^{1}H\}$, ^{1}H and ^{13}C NMR spectra. However, the $^{31}P\{^{1}H\}$, ^{1}H and ^{13}C NMR spectra of mixture **C** illustrate that some of the by-products present in the attempted syntheses of complexes **2.31** and **2.33** are formed by a reaction between $Ag[Al\{OC(CF_3)_3\}_4]$ and the PCN moieties of the Cr^{0}-PCN complexes. The reaction of $Ag[Al\{OC(CF_3)_3\}_4]$ with PR_3 or NR_3 centres to form radical $PR_3^{+\bullet}$ or $NR_3^{+\bullet}$ species, respectively, is well documented in the literature.[138-141] The observance of products containing at least two phosphorus atoms in the attempted syntheses of complexes **2.31** and **2.33**, as well as in mixture **C**, suggests that the $Ag[Al\{OC(CF_3)_3\}_4]$ may have reacted at the P- and/or N-atoms of the PCN moiety to form radicals, which could then couple to generate products containing more than one phosphorus atom.

2.4.3. Coordination Chemistry of PCN Ligands with Cr^{III}

In addition to Cr^{I}-ligand complexes, Cr^{III}-ligand complexes have been shown in the literature to act as potential catalytic precursors for selective ethylene *tri-*/*tetra*-merisation making the synthesis of Cr^{III}-PCN complexes an area of interest.[5,45,67,68,110,64,142,143] As mentioned previously in section 2.1.6.2.1, a series of Cr^{III}-PCN complexes were synthesised in previous work conducted in the Dyer group (Scheme 2.30).[70] The synthesis of two target Cr^{III}-PCN complexes, **2.34** and **2.35** (Figure 2.39) have been attempted in this thesis. The synthesis of complex **2.34** is desirable in order to complete the series of Cr^{III}-PCN complexes previously described

in Scheme 2.30, which encompass diisopropyl substituents at the phosphorus atoms, phenyl groups at the imine carbon and phenyl substituents of differing steric bulk at the nitrogen positions, so that an analogous series to the Cr^0-PCN complexes (section 2.4.1) and Cr^I-PCN complexes (section 2.4.2) previously synthesised in this thesis could be obtained.

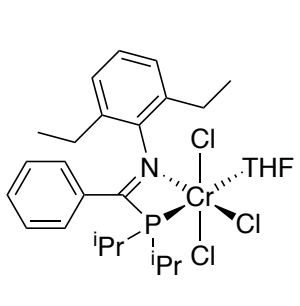

2.34

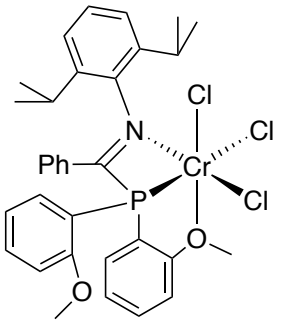

2.35

Figure 2.39: Target Cr^{III} PCN complexes **2.34** and **2.35**.

In addition, the synthesis of complex **2.35** is of interest in order to explore whether the OMe functionality on the phenyl phosphorus substituent acts a pendant donor to Cr (Figure 2.39). As previously mentioned in section 2.1.2.2.1.1 PNP ligands bearing *ortho*-OMe substituted P-aryl groups produced selective ethylene trimerisation systems, when implemented in conjunction with a Cr source and activator, with higher activities than those implementing PNP ligands without *ortho*-OMe substituted P-aryl groups. The high activity of the Cr/$PNP^{o\text{-}OMe}$-based selective ethylene trimerisation system was attributed to hemilabile behaviour of the OMe groups, which acted as pendant donors to the Cr centre.[16,18,20,32]

The syntheses of target complexes **2.34** and **2.35** were attempted following the literature procedure by Labinger and Bercaw *et al.*,[33] illustrated in Scheme 2.44. However, unfortunately, the target complexes **2.34** and **2.35** were unable to be successfully synthesised *via* this route (see sections 2.4.3.1 and 2.4.3.2).

(1.1 equiv.)

(R - R" = alkyl or aromatic group)

Scheme 2.44: Attempted synthesis route to Cr^{III}-PCN complexes, following modification of the method reported by Labinger and Bercaw *et al.*[33]

In contrast, the general synthetic route described in Scheme 2.44 proved effective for the syntheses of complexes **2.36** and **2.37** (Figure 2.40), which have also been

synthesised in previous work carried out in the Dyer group.[70] Complexes **2.36** and **2.37** were synthesised in this thesis with the intention of obtaining molecular structures of the complexes, so that the relationship between the P-Cr-N bite angles of the complexes and their 1-octene:1-hexene ratios could be studied. However, in spite of multiple attempts at crystallising complexes **2.36** and **2.37** from a variety of solvent mixtures (such as DCM/hexane, DCM/pentane and DCM/petroleum ether {40:60}) and attempts at crystallising the complexes in MeCN (with the aim of aiding crystallisation by substitution of the bound THF in complexes **2.36** and **2.37** by MeCN), suitable crystals for X-ray diffraction analysis were unable to be obtained.

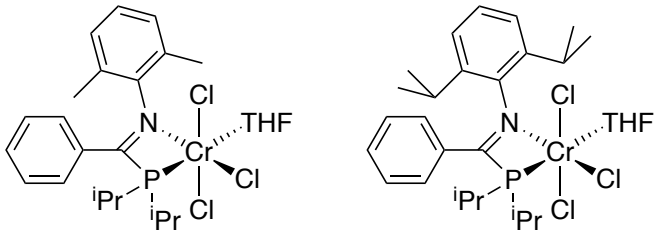

2.36 **2.37**

Figure 2.40: Cr^{III}-PCN complexes **2.36** and **2.37**.

The identities of complexes **2.36** and **2.37** were confirmed by elemental analysis and further supported by their experimentally-determined μ_{eff} values of 3.68 μ_B and 3.62 μ_B, respectively, which are in accordance with the expected spin-only magnetic moment of 3.87 μ_B for a species with three unpaired electrons, such as Cr^{III}. In addition, the C=N stretches of complexes **2.36** and **2.37** are at lower frequences (1552 cm^{-1}) than the C=N stretches of the corresponding PCN ligand precursors (1600 cm^{-1} of PCN ligand precursor to complex **2.36** and 1583 cm^{-1} of PCN ligand precursor to complex **2.37**), reflective of electron donation from the d-orbitals on the Cr centre of complexes **2.36** and **2.37** to the π^*-antibonding orbitals of the C=N groups of these complexes. Unfortunately, ASAP mass spectrometric analysis of complexes **2.36** and **2.37** proved inconclusive, as only fragments corresponding to the PCN ligand precursors of the complexes could be identified, possibly due to the low volatility of the Cr^{III}-PCN complexes.

2.4.3.1. Attempted synthesis of complex 2.34, $CrCl_3(THF)(PhC(P^iPr_2)=N(2,6\text{-}Et_2C_6H_3)$

The synthesis of complex **2.34** (Figure 2.39), under the conditions shown in Scheme 2.44 using PCN ligand **2.15** (Figure 2.14), was attempted multiple times. However, in all cases this was found to yield a green solid whose elemental analysis results did not match that expected for complex **2.34**. In accordance with that expected for complex **2.34**, ^1H and $^{31}P\{^1H\}$ NMR room temperature spectra of the green solid could not be

obtained and a μ_{eff} value of 3.60 μ_B was determined of the green solid. Additionally, the green solid exhibits a C=N stretch at 1552 cm^{-1} in its IR spectrum which is at a lower frequency than the C=N stretch of the precursor PCN ligand **2.15** (1584 cm^{-1}) and identical to the C=N stretches exhibited by Cr^{III}-PCN complexes **2.36** and **2.37**, suggesting electron donation from the d orbitals on the Cr centre of the green solid to the π^*-antibonding orbitals of the C=N group of the green solid. Although, the NMR and IR spectroscopic data from the green solid are as expected for complex **2.34,** there is insufficient evidence to conclusively state that the green solid is complex **2.34**. Consequently, attempts were undertaken to crystallise the green solid in different solvent systems (DCM/pentane, DCM/hexane and MeCN/Et_2O) at different temperatures (ranging from 25 to – 30 °C), to try and obtain a molecular structure from which its identity could be elucidated, but were to no avail.

2.4.3.2. Attempted synthesis of complex 2.35, $CrCl_3$(PhC(P(2-(OMe)C_6H_4)$_2$)=N(2,6-^{i}Pr$_2C_6H_3$)

The attempted synthesis of complex **2.35** (Figure 2.39) *via* the route illustrated in Scheme 2.44 using PCN ligand **2.17** (Figure 2.14), yielded a brown solid whose identity was unable to be elucidated by elemental analysis, NMR spectroscopy and IR spectroscopy. The elemental analysis results for the brown solid do not match with those expected for complex **2.35** (Figure 2.39) or structural variants of complex **2.35** containing different combinations of Cl and THF ligands as a result of different coordination modes of the PCN ligand (κ^2-P,N or κ^3-P,N,O). The $^{31}P\{^1H\}$ NMR spectrum of the brown solid exhibits three resonances, at –0.7, 24.4 and 70.5 ppm present in a ratio of 1:0.29:0.02, respectively, of which none correlate to the PCN ligand **2.17** indicating the presence of other diamagnetic P-containing species. In addition, the ^1H NMR spectrum of the brown solid exhibits significant broadening, something potentially indicating the presence of a paramagnetic species. This was confirmed by recording a ^1H NMR spectrum of the brown solid in a Young's NMR tube in CD_2Cl_2 containing an external capillary filled with CD_2Cl_2, and observing a shift in the NMR signal of the bulk CD_2Cl_2 solvent relative to the NMR signal of the external capillary filled with CD_2Cl_2 (a methodology akin to that used to determine magnetic moments *via* Evans' method) Finally, the IR spectrum of the brown solid displays two C=N stretches at 1552 and 1591 cm–^{1}, the former of which is at an identical frequency to the C=N stretch for Cr^{III}-PCN complexes **2.36** and **2.37**. From the analysis of the brown solid it is apparent that it consists of a mixture of products, of which one is paramagnetic.

2.5. Summary and Conclusions

In this chapter a series of PCN ligands, compounds **2.1** – **2.17**, have been synthesised with a variety of substituents on the N-, C- and P-atoms of the PCN ligands. Synthesis of the corresponding selenides of the PCN ligands, compounds **2.1(Se)** – **2.73(Se)**, revealed that the phosphorus atoms of the PCN ligands are relatively good σ-donors (based on the low magnitude of 701 – 727 Hz of the $|^1J_{SeP}|$ coupling constants of compounds **2.1(Se)** – **2.73(Se)**). In addition, it was found that the donor properties of the phosphorus atoms of the PCN ligands could be tuned *via* the steric bulk of the substituents on the phosphorus atoms or by the electronic nature of the imine carbon substituents of the PCN ligands; selenides of PCN ligands with bulkier phosphine substituents (such as norbornyl groups) or electron-withdrawing imine carbon substituents displayed larger $^1J_{SeP}$ coupling constants reflective of the weaker σ-donor character of their phosphorus groups. Analysis of the imine stretching frequencies of the C=N bonds of PCN ligands **2.1** – **2.17** by IR spectroscopy revealed them to be at lower frequencies than the imine stretching frequencies of the precursor imidoyl chlorides, thereby indicating conjugation between the phosphine and C=N bond.

The synthesis of a series of novel Cr^0-PCN complexes, **2.22** – **2.25**, was also synthesised in this chapter. It was found that the reactions of the PCN ligands and $Cr(CO)_6$ proceeded more efficiently in diglyme than toluene, as a result of the higher boiling point of diglyme, which prevented decomposition of the Cr^0-PCN complexes as a result of the shortened reaction times necessary. In addition, analysis of the crude reaction mixtures of the Cr^0-PCN complexes by $^{31}P\{^1H\}$ NMR spectroscopy revealed a correlation between the percentage of κ^1-P monodentate Cr^0-PCN complexes and κ^2-P, N bidentate Cr^0-PCN complexes and the steric bulk on the nitrogen atoms of the PCN ligands; as expected increasing the steric bulk on the nitrogen atom of the PCN ligand was found to increase the percentage of κ^1-P monodentate Cr^0-PCN complex present at the expense of κ^2-P,N bidentate coordination. It was also proposed, by comparison with the syntheses of Cr^0-PCN complexes **2.18** and **2.19** performed in toluene and diglyme, that the κ^2-P,N bidentate Cr^0-PCN complex is the thermodynamic product while the κ^1-P monodentate Cr^0-PCN complex is the kinetic product. Analysis of the monodentate and bidentate Cr^0-PCN complexes by IR spectroscopy and X-ray diffraction analysis revealed that the bidentate Cr^0-PCN complexes have weaker CO bonds, in comparison to their monodentate analogues, and that the C=N group acts as a π acceptor in the bidentate Cr^0-PCN complexes.

One-electron oxidation reactions of the Cr^0-PCN complexes with Ag[Al{OC-$(CF_3)_3$}$_4$], generating Cr^I-PCN complexes (**2.26** – **2.30** and **2.32**), were also successfully carried out in this chapter. However, the syntheses of Cr^I-PCN complexes **2.31** and **2.33** were accompanied by the formation of by-products, detectable by NMR spectroscopy, proposed to arise from reactions between Ag[Al{OC-$(CF_3)_3$}$_4$] and the phosphorus and nitrogen moities of the PCN moieties of the Cr^0-PCN precursor complexes to complexes **2.31** and **2.33**. A comparison of the carbonyl stretching frequencies of Cr^I-PCN complexes and their Cr^0-PCN complexes showed that the carbonyl bands of the latter appear at lower frequency, which is as expected upon moving from a charged to neutral species. In addition, the series of Cr^0-PCN complexes were found to have similar carbonyl stretching frequencies suggesting, on simple electronic grounds, that they should exhibit similar performance in ethylene oligomerisation catalysis.

Lastly, the synthesis of Cr^{III}-PCN complexes was attempted in this chapter. Cr^{III}-PCN complexes **2.36** and **2.37**, which have also been synthesised in previous work conducted in the Dyer group,[70] were successfully synthesised in this chapter. However, syntheses of the target Cr^{III}-PCN complexes **2.34** and **2.35** proved difficult with products being obtained whose identities could not be reliably deduced from CHN analysis, NMR or IR spectroscopic analysis.

The next step is to test the PCN ligands synthesised in this chapter in ethylene oligomerisation catalysis to investigate any trends present between the nature of the substituents present on the P-, N- and C-atoms of the PCN ligands and the performance of the PCN ligands in ethylene oligomerisation catalysis. In addition, the Cr^I-PCN complexes and Cr^{III}-PCN complexes synthesised in this chapter need to be tested in ethylene oligomerisation catalysis in order to probe their potential as catalytic precursors.

2.6. References

1 J. T. Dixon, M. J. Green, F. M. Hess and D. H. Morgan, *J. Organomet. Chem.*, 2004, **689**, 3641–3668.
2 D. F. Wass, *Dalt. Trans.*, 2007, 816–819.
3 P. W. N. M. van Leeuwen, N. D. Clément and M. J. L. Tschan, *Coord. Chem. Rev.*, 2011, **255**, 1499–1517.
4 T. Agapie, *Coord. Chem. Rev.*, 2011, **255**, 861–880.
5 D. S. McGuinness, *Chem. Rev.*, 2011, **111**, 2321–2341.
6 F. Zhu, L. Wang and H. Yu, *des monomers polym.*, 2011, **14**, 1–23.
7 G. P. Belov, *Pet. Chem.*, 2012, **52**, 139–154.
8 K. A. Alferov, G. P. Belov and Y. Meng, *Appl. Catal. A Gen.*, 2017, **542**, 71–124.
9 R. M. Manyik, W. E. Walker, T. P. Wilson,, US 3300458, Union Carbide

Corporation, 24 Jan 1967.
10 R. M. Manyik, W. E. Walker and T. P. Wilson, *J. Catal.*, 1977, **47**, 197–200.
11 W. K. Reagan, *Prepr.Am. Chem. Soc., Div. Pet. Chem.*, 1989, **34**, 583–588.
12 W. K. Reagan, EP 0417477, Phillips Petroleum Company, 20 March 1991.
13 W. K. Reagan, J. W. Freeman, B. K. Conroy, T. M. Pettijohn and E. A. Benham, EP 0608447, Phillips Petroleum Company, 3 August 1994.
14 J. W. Freeman, J. L. Buster and R. D. Knudsen, US 5856257, Phillips Petroleum Company, 5 Jan 1999.
15 Y. Araki, H. Nakamura, Y. Nanba and T. Okano, US 5856612, Mitsubishi Chemical Corporation, 5 Jan 1999.
16 A. Carter, S. A. Cohen, N. A. Cooley, A. Murphy, J. Scutt and D. F. Wass, *Chem. Commun.*, 2002, 858–859.
17 D. F. Wass, WO 02/04119, BP Chemicals Limited, 17 Jan 2002.
18 K. Blann, A. Bollmann, J. T. Dixon, F. M. Hess, E. Killian, H. Maumela, D. H. Morgan, A. Neveling, S. Otto and M. J. Overett, *Chem. Commun.*, 2005, **30**, 620–621.
19 K. Blann, A. Bollmann, J. T. Dixon, A. Neveling, D. H. Morgan, H. Maumela, E. Killian, F. M. Hess, S. Otto, L. Pepler, H. A. Mahomed and M. J. Overett, WO 2004/056477 A1, Sasol Technology Limited, 8 July 2004.
20 A. Bollmann, K. Blann, J. T. Dixon, F. M. Hess, E. Killian, H. Maumela, D. S. McGuinness, D. H. Morgan, A. Neveling, S. Otto, M. Overett, A. M. Z. Slawin, P. Wasserscheid and S. Kuhlmann, *J. Am. Chem. Soc.*, 2004, **126**, 14712–14713.
21 K. Blann, A. Bollmann, J. Dixon, A. Neveling, D. H. Morgan, H. Maumela, E. Killian, F. M. Hess, S. Otto, L. Pepler, H. A. Mahomed, and M. J. Overett,, WO 2004/056749A1, Sasol Technology Ltd, 8 July 2004.
22 J. R. Briggs, *J. Chem. Soc., Chem. Commun.*, 1989, 674–675.
23 Z. Yu and K. N. Houk, *Angew. Chem. Int. Ed.*, 2003, **42**, 808–811.
24 A. N. J. Blok, P. H. M. Budzelaar and A. W. Gal, *Organometallics*, 2003, **22**, 2564–2570.
25 S. Kuhlmann, C. Paetz, C. Hägele, K. Blann, R. Walsh, J. T. Dixon, J. Scholz, M. Haumann and P. Wasserscheid, *J. Catal.*, 2009, **262**, 83–91.
26 J. C. Jeffrey and T. B. Rauchfuss, *Inorg. Chem.*, 1979, **18**, 2658–2666.
27 P. Espinet and K. Soulantica, *Coord. Chem. Rev.*, 1999, **193-195**, 499–556.
28 R. G. Pearson, *J. Am. Chem. Soc.*, 1963, **85**, 3533–3539.
29 M. J. Hanton, D. M. Smith, W. F. Gabrielli and S. J. Evans, WO 2013/168103 A1, Sasol Technology Limited, 14 Nov 2013.
30 M. M. Mogorosi, M. C. Maumela and M. J. Overett, WO 2014/181248 A1, Sasol Technology Limited, 13 Nov 2014.
31 Y. H. Lee, S. P. Sa, E. J. Shin, K. S. Lee, J. Y. Park, S. K. Im and Y. K. Hong, EP 3118227 A1, LG Chem Limited, 18 Jan 2017.
32 M. J. Overett, K. Blann, A. Bollmann, J. T. Dixon, F. Hess, E. Killian, H. Maumela, D. H. Morgan, A. Neveling and S. Otto, *Chem. Commun.*, 2005, 622–624.
33 T. Agapie, S. J. Schofer, J. A. Labinger and J. E. Bercaw, *J. Am. Chem. Soc.*, 2004, **126**, 1304–1305.
34 T. Agapie, M. W. Day, L. M. Henling, J. A. Labinger and J. E. Bercaw, *Organometallics*, 2006, **25**, 2733–2742.
35 S. V. Kulangara, C. Mason, M. Juba, Y. Yang, I. Thapa, S. Gambarotta, I. Korobkov and R. Duchateau, *Organometallics*, 2012, **31**, 6438–6449.
36 S. Kuhlmann, K. Blann, A. Bollmann, J. Dixon, E. Killian, M. Maumela, H. Maumela, D. H. Morgan, M. Pretorius, N. Taccardi and P. Wasserscheid, *J. Catal.*, 2007, **245**, 279–284.
37 T. E. Stennett, T. W. Hey, L. T. Ball, S. R. Flynn, J. E. Radcliffe, C. L. McMullin, R. L. Wingad and D. F. Wass, *ChemCatChem*, 2013, **5**, 2946–2954.
38 T. Jiang, S. Zhang, X. Jiang, C. Yang, B. Niu and Y. Ning, *J. Mol. Catal. A-*

Chem., 2008, **279**, 90–93.
39 T. Jiang, H. Chen, C. Cao, G. Mao and Y. Ning, *Chin. Sci. Bull.*, 2010, **55**, 3750–3754.
40 E. Killian, K. Blann, A. Bollmann, J. T. Dixon, S. Kuhlmann, M. C. Maumela, H. Maumela, D. H. Morgan, P. Nongodlwana, M. J. Overett, M. Pretorius, K. Höfener and P. Wasserscheid, *J. Mol. Catal. A-Chem.*, 2007, **270**, 214–218.
41 K. Blann, A. Bollmann, H. de Bod, J. Dixon, E. Killian, P. Nongodlwana, M. Maumela, H. Maumela, A. E. McConnell, D. H. Morgan, M. J. Overett, M. Pretorius, S. Kuhlmann and P. Wasserscheid, *J. Catal.*, 2007, **249**, 244–249.
42 P. R. Elowe, C. McCann, P. G. Pringle, S. K. Spitzmesser and J. E. Bercaw, *Organometallics*, 2006, **25**, 5255–5260.
43 Z. Weng, S. Teo and T. S. Andy Hor, *Dalton Trans.*, 2007, 3493–3498.
44 J. A. Suttil, P. Wasserscheid, D. S. McGuinness, M. G. Gardiner and S. J. Evans, *Catal. Sci. Technol.*, 2014, **4**, 2574–2588.
45 C. Klemps, E. Payet, L. Magna, L. Saussine, X. F. Le Goff and P. Le Floch, *Chem. Eur. J.*, 2009, **15**, 8259–8268.
46 D. S. McGuinness, P. Wasserscheid, D. H. Morgan and J. T. Dixon, *Organometallics*, 2005, **24**, 552–556.
47 D. S. McGuinness, P. Wasserscheid, W. Keim, C. Hu, U. Englert, J. T. Dixon and C. Grove, *Chem. Commun.*, 2003, **49**, 334–335.
48 Y. Shaikh, K. Albahily, M. Sutcliffe, V. Fomitcheva, S. Gambarotta, I. Korobkov and R. Duchateau, *Angew. Chem. Int. Ed.*, 2012, **51**, 1366–1369.
49 C. Fliedel, A. Ghisolfi and P. Braunstein, *Chem. Rev.*, 2016, **116**, 9237–9304.
50 S. Peitz, N. Peulecke, B. R. Aluri, S. Hansen, B. H. Müller, A. Spannenberg, U. Rosenthal, M. H. Al-Hazmi, F. M. Mosa, A. Wöhl and W. Müller, *Eur. J. Inorg. Chem.*, 2010, **2010**, 1167–1171.
51 N. Peulecke, B. H. Müller, S. Peitz, B. R. Aluri, U. Rosenthal, A. Wöhl, W. Müller, M. H. Al-Hazmi and F. M. Mosa, *ChemCatChem*, 2010, **2**, 1079–1081.
52 B. Reddy Aluri, N. Peulecke, S. Peitz, A. Spannenberg, B. H. Müller, S. Schulz, H.-J. Drexler, D. Heller, M. H. Al-Hazmi, F. M. Mosa, A. Wöhl, W. Müller and U. Rosenthal, *Dalton Trans.*, 2010, **39**, 7911–7920.
53 S. Peitz, N. Peulecke, B. R. Aluri, B. H. Müller, A. Spannenberg, U. Rosenthal, M. H. Al-Hazmi, F. M. Mosa, A. Wöhl and W. Müller, *Organometallics*, 2010, **29**, 5263–5268.
54 W. Müller, A. Wöhl, S. Peitz, N. Peulecke, B. R. Aluri, B. H. Müller, D. Heller, U. Rosenthal, M. H. Al-Hazmi and F. M. Mosa, *ChemCatChem*, 2010, **2**, 1130–1142.
55 A. Wöhl, W. Müller, S. Peitz, N. Peulecke, B. R. Aluri, B. H. Müller, D. Heller, U. Rosenthal, M. H. Al-Hazmi and F. M. Mosa, *Chem. Eur. J.*, 2010, **16**, 7833–7842.
56 S. Heinig, A. Wöhl, W. Müller, M. H. Al-Hazmi, B. H. Müller, N. Peulecke and U. Rosenthal, *ChemCatChem*, 2013, **6**, 514–521.
57 S. Heinig, A. Wöhl, W. Müller, M. H. Al-Hazmi, B. H. Müller, N. Peulecke and U. Rosenthal, *ChemCatChem*, 2013, **5**, 3107–3113.
58 N. Peulecke, B. H. Müller, A. Spannenberg, M. Höhne, U. Rosenthal, A. Wöhl, W. Müller, A. Alqahtani and M. Al Hazmi, *Dalton Trans.*, 2016, **45**, 8869–8874.
59 M. H. Al-Hazmi, A. Alqahtani, U. Rosenthal, B. H. Muller, N. N. Peulecke, M. Harff, A. Wohl, A. Meiswinkle, H. Bolt, W. Muller, WO 2016/012948 A1, Sabic Global Technologies B.V. and Linde AG, 28 Jan 2016.
60 K. Albahily, E. Koç, D. Al-Baldawi, D. Savard, S. Gambarotta, T. J. Burchell and R. Duchateau, *Angew. Chem. Int. Ed.*, 2008, **47**, 5816–5819.
61 K. Albahily, D. Al-Baldawi, S. Gambarotta, R. Duchateau, E. Koç and T. J. Burchell, *Organometallics*, 2008, **27**, 5708–5711.
62 K. Albahily, D. Al-Baldawi, S. Gambarotta, E. Koç and R. Duchateau, *Organometallics*, 2008, **27**, 5943–5947.

63 Y. Shaikh, J. Gurnham, K. Albahily, S. Gambarotta and I. Korobkov, *Organometallics*, 2012, **31**, 7427–7433.
64 Y. Yang, J. Gurnham, B. Liu, R. Duchateau, S. Gambarotta and I. Korobkov, *Organometallics*, 2014, **33**, 5749–5757.
65 Y. Yang, Z. Liu, B. Liu and R. Duchateau, *ACS Catal.*, 2013, **3**, 2353–2361.
66 A. Alzamly, S. Gambarotta and I. Korobkov, *Organometallics*, 2014, **33**, 1602–1607.
67 M. E. Bluhm, O. Walter and M. Döring, *J. Organomet. Chem.*, 2005, **690**, 713–721.
68 O. L. Sydora, T. C. Jones, B. L. Small, A. J. Nett, A. A. Fischer and M. J. Carney, *ACS Catal.*, 2012, **2**, 2452–2455.
69 O. L. Sydora, M. J. Carney, B. L. Small, S. Hutshison and J. C. Gee, WO 2011/082192 A1, Chevron Phillips Comany LP. 7 July 2011, 2018.
70 J. E. Radcliffe, PhD Thesis, Durham University, 2015.
71 J. E. Radcliffe, A. S. Batsanov, D. M. Smith, J. A. Scott, P. W. Dyer and M. J. Hanton, *ACS Catal.*, 2015, **5**, 7095–7098.
72 J. X. McDermott, J. F. White and G. M. Whitesides, *J. Am. Chem. Soc.*, 1973, **95**, 4451–4452.
73 J. X. McDermott, J. F. White and G. M. Whitesides, *J. Am. Chem. Soc.*, 1976, **98**, 6521–6528.
74 P. W. Jolly, *Acc. Chem. Res.*, 1996, **29**, 544–551.
75 R. Emrich, O. Heinemann, P. W. Jolly, C. Krüger and G. P. J. Verhovnik, *Organometallics*, 1997, **16**, 1511–1513.
76 T. Agapie, J. A. Labinger and J. E. Bercaw, *J. Am. Chem. Soc.*, 2007, **129**, 14281–14295.
77 K. P. Bryliakov and E. P. Talsi, *Coord. Chem. Rev.*, 2012, **256**, 2994–3007.
78 M. J. Overett, K. Blann, A. Bollmann, J. T. Dixon, D. Haasbroek, E. Killian, H. Maumela, D. S. McGuinness and D. H. Morgan, *J. Am. Chem. Soc.*, 2005, **127**, 10723–10730.
79 S. Peitz, B. R. Aluri, N. Peulecke, B. H. Müller, A. Wöhl, W. Müller, M. H. Al-Hazmi, F. M. Mosa and U. Rosenthal, *Chem. Eur. J.*, 2010, **16**, 7670–7676.
80 B. Rebenstorf and R. Larsson, *J. Mol. Catal.*, 1981, **11**, 247–256.
81 Ø. Espelid and K. J. Børve, *J. Catal.*, 2002, **206**, 331–338.
82 W. H. Monillas, J. F. Young, G. P. A. Yap and K. H. Theopold, *Dalton Trans.*, 2013, **42**, 9198–9210.
83 G. J. P. Britovsek, D. S. McGuinness, T. S. Wierenga and C. T. Young, *ACS Catal.*, 2015, **5**, 4152–4166.
84 G. J. P. Britovsek and D. S. McGuinness, *Chem. Eur. J.*, 2016, **22**, 16891–16896.
85 G. J. P. Britovsek, D. S. McGuinness and A. K. Tomov, *Catal. Sci. Technol.*, 2016, **6**, 8234–8241.
86 A. Jabri, P. Crewdson, S. Gambarotta, I. Korobkov and R. Duchateau, *Organometallics*, 2006, **25**, 715–718.
87 L. H. Do, J. A. Labinger and J. E. Bercaw, *ACS Catal.*, 2013, **3**, 2582–2585.
88 D. S. McGuinness, B. Chan, G. J. P. Britovsek and B. F. Yates, *Aust. J. Chem.*, 2014, **67**, 1481–1490.
89 J. Rabeah, M. Bauer, W. Baumann, A. E. C. McConnell, W. F. Gabrielli, P. B. Webb, D. Selent and A. Brückner, *ACS Catal.*, 2013, **3**, 95–102.
90 E. Y.-X. Chen and T. J. Marks, *Chem. Rev.*, 2000, **100**, 1391–1434.
91 A. M. Lifschitz, N. A. Hirscher, H. B. Lee, J. A. Buss and T. Agapie, *Organometallics*, 2017, **36**, 1640–1648.
92 H. S. Zijlstra and S. Harder, *Eur. J. Inorg. Chem.*, 2015, **2015**, 19–43.
93 W. Janse van Rensburg, J.-A. van den Berg and P. J. Steynberg, *Organometallics*, 2007, **26**, 1000–1013.
94 D. S. McGuinness, M. Overett, R. P. Tooze, K. Blann, J. T. Dixon and A. M. Z.

Slawin, *Organometallics*, 2007, **26**, 1108–1111.
95 D. S. McGuinness, A. J. Rucklidge, R. P. Tooze and A. M. Z. Slawin, *Organometallics*, 2007, **26**, 2561–2569.
96 S. Pasynkiewicz, A. Boleslawski and A. Sadownik, *J. Organomet. Chem.*, 1976, **113**, 303–309.
97 I. Krossing, *Chem. Eur. J.*, 2001, **7**, 490–502.
98 I. Thapa, S. Gambarotta, I. Korobkov, M. Murugesu and P. Budzelaar, *Organometallics*, 2011, **31**, 486–494.
99 K. Issleib and O. Z. Low, *Anorg. Allg. Chem.*, 1966, **346**, 241–254.
100 K. Issleib, H. Schmidt and H. Meyer, *J. Organomet. Chem.*, 1978, **160**, 47–57.
101 I. Abdellah, E. Ibrahim and R. Farag, *Gazz. Chim. Italia.*, 1988, **118**, 141–143.
102 D. Walther, S. Liesicke, R. Fischer, H. Görls, J. Weston and A. Batista, *Eur. J. Inorg. Chem.*, 2003, **2003**, 4321–4331.
103 X. Li, H. Song and C. Cui, *Dalton Trans.*, 2009, **133**, 9728–3.
104 T. van Dijk, S. Burck, M. K. Rong, A. J. Rosenthal, M. Nieger, J. C. Slootweg and K. Lammertsma, *Angew. Chem. Int. Ed.*, 2014, **53**, 9068–9071.
105 T. van Dijk, S. Burck, A. J. Rosenthal, M. Nieger, A. W. Ehlers, J. C. Slootweg and K. Lammertsma, *Chem. Eur. J.*, 2015, **21**, 9328–9331.
106 M. K. Rong, K. van Duin, T. van Dijk, J. J. M. de Pater, B.-J. Deelman, M. Nieger, A. W. Ehlers, J. C. Slootweg and K. Lammertsma, *Organometallics*, 2017, **36**, 1079–1090.
107 D. S. McGuinness, P. Wasserscheid, W. Keim, D. Morgan, J. T. Dixon, A. Bollmann, H. Maumela, F. Hess and U. Englert, *J. Am. Chem. Soc.*, 2003, **125**, 5272–5273.
108 O. L. Sydora, M. Carney, B. L. Small, J. C. Gee and S. Hutchison, US 2014/0221645A1, Chevron Phillips Chemical Company, 7 August 2014.
109 Y. Suzuki, S. Kinoshita, A. Shibahara, S. Ishii, K. Kawamura, Y. Inoue and T. Fujita, *Organometallics*, 2010, **29**, 2394–2396.
110 S.-K. Kim, T.-J. Kim, J.-H. Chung, T.-K. Hahn, S.-S. Chae, H.-S. Lee, M. Cheong and S. O. Kang, *Organometallics*, 2010, **29**, 5805–5811.
111 M. G. Newton, N. S. Pantaleo, S. Kirbawy and N. L. Allinger, *J. Am. Chem. Soc.*, 1978, **10**, 2176–2180.
112 L. Doms, D. van Hemelrijk, W. Van de Mieroop, A. T. H. Lenstra and H. J. Geise, *Acta. Crystallogr. Sect. B Struct. Sci.*, 1985, **41**, 270–274.
113 S. V. Evans, C. Hwang and J. Trotter, *Acta. Crystallogr. Sect. C Cryst. Struct. Commun.*, 1988, **44**, 1457–1459.
114 M. B. Smith and J. March, *March's Advanced Organic Chemistry*, John Wiley & Sons, Inc., New Jersey, Sixth Edition, 2007.
115 J. E. Huheey, E. A. Keiter and R. L. Keiter, *Inorganic Chemistry*, HarperCollins College Publishers, USA, Fourth Edition, 1993.
116 D. W. Allen and B. F. Taylor, *J. Chem. Res. Synop.*, 1981, 220–221.
117 D. W. Allen and B. F. Taylor, *J. Chem. Soc. Dalt. Trans.*, 1982, 51–54.
118 W. McFarlane and D. S. Rycroft, *J. Chem. Soc. Dalt. Trans.*, 1973, 2162–2166.
119 R. García-Rodríguez and H. Liu, *J. Am. Chem. Soc.*, 2012, **134**, 1400–1403.
120 D. G. Gilheany, *Chem. Rev.*, 1994, **94**, 1339–1374.
121 D. G. Gilheany, *in The Chemistry of Organophosphorus Compounds, ed. F. R. Hartley*, John Wiley & Sons, England, vol. 1, 1990, ch. 2, pp. 19-23.
122 A. D. Walsh, *J. Chem. Soc.*, 1953, 2266–2288.
123 C. Sandorfy, *in The chemistry of the carbon-nitrogen double bond*, ed. S. Patai, John WIley & Sons Ltd, England, 1970, ch. 1, pp. 37-46.
124 C. A. Tolman, *J. Am. Chem. Soc.*, 1970, **92**, 2953–2956.
125 C. A. Tolman, *Chem. Rev.*, 1977, **77**, 313–348.
126 A. Poater, B. Cosenza, A. Correa, S. Giudice, F. Ragone, V. Scarano and L. Cavallo, *Eur. J. Inorg. Chem.*, 2009, **2009**, 1759–1766.
127 H. Clavier and S. P. Nolan, *Chem. Commun.*, 2010, **46**, 841–21.

128 L. E. Bowen, M. F. Haddow, A. G. Orpen and D. F. Wass, *Dalton Trans.*, 2007, **689**, 1160–1169.
129 A. J. Rucklidge, D. S. McGuinness, R. P. Tooze, A. M. Z. Slawin, J. D. A. Pelletier, M. J. Hanton and P. B. Webb, *Organometallics*, 2007, **26**, 2782–2787.
130 A. Dulai, H. de Bod, M. J. Hanton, D. M. Smith, S. Downing, S. M. Mansell and D. F. Wass, *Organometallics*, 2009, **28**, 4613–4616.
131 M. S. Balakrishna, T. K. Prakasha and S. S. Krishnamurthy, *J. Organomet. Chem.*, 1990, **390**, 203–216.
132 J. D. Masuda and R. T. Boeré, *Dalton Trans.*, 2016, **45**, 2102–2115.
133 S. O. Grim, W. L. Briggs, R. C. Barth, C. A. Tolman and J. P. Jesson, *Inorg. Chem.*, 1974, **13**, 1095–1100.
134 T. E. Stennett, M. F. Haddow and D. F. Wass, *Organometallics*, 2012, **31**, 6960–6965.
135 G. B. Kauffman, *J. Chem. Educ.*, 1977, **54**, 86–89.
136 R. D. Köhn, D. Smith, M. F. Mahon, M. Prinz, S. Mihan and G. Kociok-Köhn, *J. Organomet. Chem.*, 2003, **683**, 200–208.
137 D. F. Evans, *J. Chem. Soc.*, 1959, 2003–2005.
138 X. Wang, *in Organic Redox Systems: Synthesis, Properties, and Applications*, ed. T. Nishinaga, John Wiley & Sons, Inc, New Jersey, 2016, ch.18, pp.523-534.
139 X. Pan, X. Chen, T. Li, Y. Li and X. Wang, *J. Am. Chem. Soc.*, 2013, **135**, 3414–3417.
140 X. Pan, Y. Su, X. Chen, Y. Zhao, Y. Li, J. Zuo and X. Wang, *J. Am. Chem. Soc.*, 2013, **135**, 5561–5564.
141 X. Zheng, X. Wang, Y. Qiu, Y. Li, C. Zhou, Y. Sui, Y. Li, J. Ma and X. Wang, *J. Am. Chem. Soc.*, 2013, **135**, 14912–14915.
142 J. Zhang, X. Wang, X. Zhang, W. Wu, G. Zhang, S. Xu and M. Shi, *ACS Catal.*, 2013, **3**, 2311–2317.
143 R. Liu, K. Zhu, X. Zhong, J. Li, Z. Liu, S. Chen and H. Zhu, *Dalton Trans.*, 2016, **45**, 17020–17029.

Chapter 3:

Probing Performance of Phosphanyl Methanimine (PCN) Ligands and Preformed Cr-PCN Complexes in Selective Ethylene Oligomerisation Catalysis

3.1. Introduction

The synthesis and characterisation of a range of novel PCN ligands **2.1** – **2.13**, novel Cr^{I}-PCN complexes **2.26** - **2.30**, and Cr^{III}-PCN complexes **2.36** and **2.37** has been described in Chapter 2. In this Chapter, the behaviour of these compounds and complexes in ethylene oligomerisation catalysis will be evaluated, with particular emphasis placed on developing structure-activity and structure-selectivity relationships. This section will consider previous work conducted in the Dyer group on Cr/PCN-based selective ethylene *tri*-/*tetra*-merisation catalysis,[1,2] specifically the establishment of structure-activity/selectivity relationships (section 3.1.1) and optimal catalysis conditions (section 3.1.2).

3.1.1. Effect of varying PCN ligand structure on Cr/PCN-based ethylene oligomerisation catalysis

As mentioned in Chapter 2 section 2.1.6.1, during previous work conducted in the Dyer group it was found that the most active and selective Cr/PCN-based ethylene *tri*-/*tetra*-merisation catalytic systems were obtained by utilising PCN ligands with alkyl phosphorus and bulky nitrogen substituents.[1,2] It was also observed that the steric bulk of the substituents at the nitrogen and phosphorus donor centres dictated the 1-octene:1-hexene ratio (OTH), with bulkier substituents generating Cr-based ethylene oligomerisation systems exhibiting greater selectivity towards 1-hexene formation, at the expense of 1-octene formation (Figure 3.1 and Figure 3.2).[1,2] This observed relationship between the steric bulk of the PCN ligands and OTH ratios of the Cr-based ethylene oligomerisation systems is similar to that seen in a number of previously-reported Cr/P,N-ligand-based selective ethylene *tri*-/*tetra*-merisation systems (section 2.1.2.2, Chapter 2). For these published Cr/P,N-based selective ethylene *tri*-/*tetra*-merisation systems it is postulated that increased steric bulk of the P,N-ligands favours the formation of the metallacycloheptane intermediate (believed to be responsible for the formation of 1-hexene) *versus* the larger-sized metallacyclononane intermediate (thought to be responsible for the formation of 1-octene).

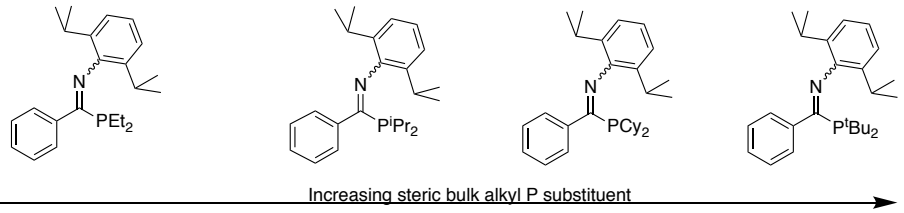

OTH:	2.0	1.5	0.1	0.0
Liquid fraction selectivity to 1-C_6 (wt %):	30	38	86	97
Liquid fraction selectivity to 1-C_8 (wt %):	61	58	12	1

Figure 3.1: Relationship between alkyl P steric bulk of PCN ligand and 1-octene:1-hexene (OTH) in Cr/PCN-based ethylene *tri*-/*tetra*-merisation systems studied in previous work in Dyer group.[1] Catalysis conditions: $Cr(acac)_3$(5 µmol), 1.2 equiv. PCN ligand, MMAO-3A (500 equiv.), 70 mL PhCl, C_2H_4 (40 bar), 60 °C, 0.6 ppm O_2.[1]

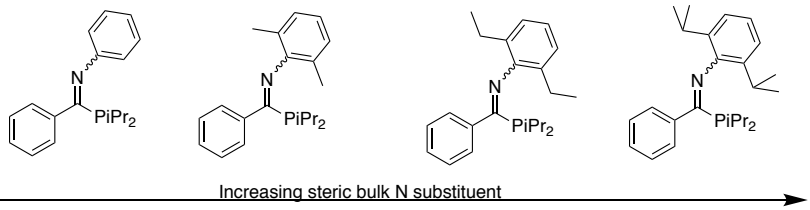

OTH:	6.0	2.9	1.9	0.3
Liquid fraction selectivity to 1-C_6 (wt %):	6	24	33	74
Liquid fraction selectivity to 1-C_8 (wt %):	36	69	63	25

Figure 3.2: Relationship between *ortho* aryl N steric bulk of PCN ligand and 1-octene:1-hexene (OTH) in Cr/PCN-based ethylene *tri*-/*tetra*-merisation systems studied in previous work in Dyer group.[1] Catalysis conditions: $Cr(acac)_3$ (5 µmol), 1.2 equiv. PCN ligand, MMAO-3A (500 equiv.), 70 mL PhCl, C_2H_4 (40 bar), 60 °C, 0.6 ppm O_2.[1]

Investigations into the use of PCN ligands bearing alkyl *versus* aryl phosphorus-substituted atoms in Cr-based ethylene oligomerisation, demonstrated that ligands with alkyl substituents at phosphorus afforded systems with higher activities and lower levels of polymer formation.[1,2] The electronic character of the *ortho* aryl phosphorus-substituted PCN ligands was also found to correlate with the levels of polymer produced and the activity of the Cr/PCN-based ethylene oligomerisation systems, with less donating aryl phosphino moieties giving rise to systems with lower activities, higher levels of polymer, and lower selectivity towards 1-hexene and 1-octene in the liquid fraction.[1]

The effect of varying the imine carbon substituents of the PCN ligands on the activity and selectivity of Cr/PCN-based ethylene oligomerisation systems was explored.[1] A

series of PCN ligands bearing ^{t}Bu or phenyl groups at their imine carbon were tested in ethylene oligomerisation catalysis, however no conclusive structure-activity or structure-selectivity trends were obtained (Figure 3.3).

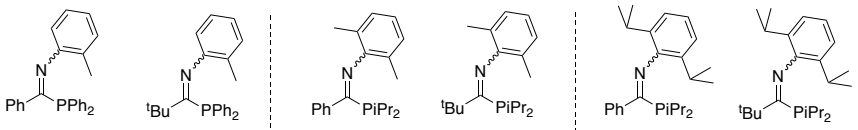

Activity (g/g Cr/h):	13,027	15,034	56,119	106,993	126,406	19,025
Liquid fraction selectivity to 1-C_6 (wt %):	46	37	24	47	74	84
Liquid fraction selectivity to 1-C_8 (wt %):	8	19	69	49	25	10
Wt % polyethylene:	59	58	34	34	30	80

Figure 3.3: Performance of PCN ligands containing ^{t}Bu or Ph substituents at the imine C in Cr-based ethylene oligomerisation catalysis, studied in previous work conducted in the Dyer group.[1] Catalysis conditions: $Cr(acac)_3$ (5 µmol), 1.2 equiv. PCN ligand, MMAO-3A (500 equiv.), 70 mL PhCl, C_2H_4 (40 bar), 60 °C, 0.6 ppm O_2.[1]

3.1.2. Effect of varying catalysis conditions on Cr/PCN-based ethylene oligomerisation catalysis

The effect of a variety of different catalytic test conditions (Cr source, temperature, pressure, solvent, activator, and activation protocol) used in the Cr/PCN-based ethylene oligomerisation catalysis runs was systematically studied in previous work carried out in the Dyer group.[1] These systematic studies resulted in the establishment of the optimal conditions illustrated in Scheme 3.1, for use in the Cr/PCN-based ethylene oligomerisation catalysis testing. The use of additives (oxygen and $ZnEt_2$) in the Cr/PCN-based ethylene *tri*-/*tetra*-merisation systems, developed in previous work in the Dyer group, is considered in further detail below.

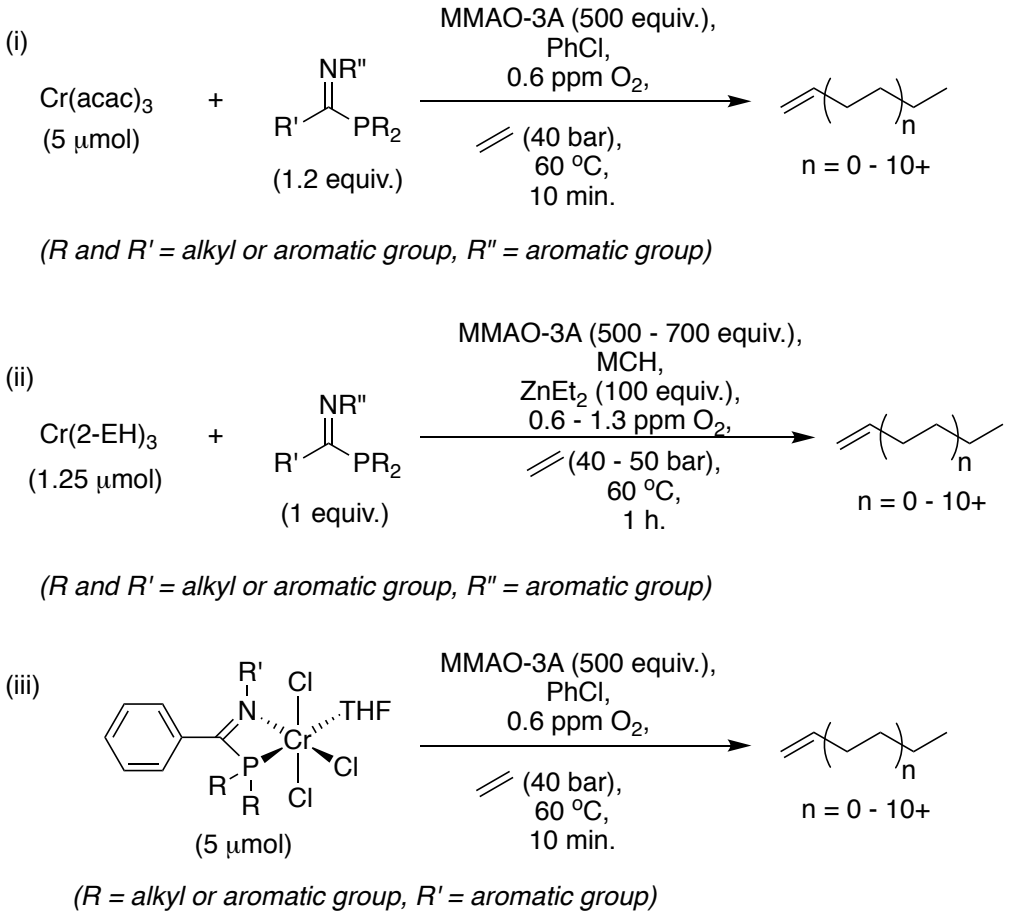

Scheme 3.1: Optimal ethylene oligomerisation catalysis conditions determined in previous work conducted in the Dyer group for (i) the initial screening of PCN ligands, (ii) larger-scale testing of PCN ligands under industrially relevant conditions, and (iii) initial screening of Cr^{III}-PCN preformed complexes.[1]

3.1.2.1. Effect of oxygen in Cr/PCN-based ethylene oligomerisation catalysis

In previous work conducted in the Dyer group,[1] it was observed that introducing low levels of oxygen into the Cr/PCN-based ethylene oligomerisation catalysis reactor impacted upon the activities and levels of polymer formation. The presence of a small amount of oxygen (0.6 – 1.3 ppm) generated systems with high activities and low levels of polymer formation.[1] This positive effect is similar to the observed effect of oxygen in other catalytic ethylene oligomerisation systems reported in a patent by Sasol Technology,[3] where using 0.1 – 1 ppm of oxygen generated catalytic packages with higher activities and lower amounts of polymer. To-date, no detailed mechanistic study of the effect played by oxygen on the Cr/PCN-based ethylene oligomerisation has been conducted, therefore it is not yet understood how the presence of oxygen in the Cr/PCN-based ethylene oligomerisation influences the activity and polymer formation of these systems.

3.1.2.2. Effect of $ZnEt_2$ in Cr/PCN-based ethylene oligomerisation catalysis

The effect of $ZnEt_2$ in reducing polymer formation with Cr-based *tri*-/*tetra*-merisation systems has been observed for a number of previously reported cases.[4] It is believed that $ZnEt_2$ limits the growth of long polymer chains in ethylene oligomerisation systems by acting as a chain transfer agent in a catalysed chain growth mechanism, where it receives the growing polymer chain from the active metal centre as illustrated in Scheme 3.2.[5] The zinc centre can then be freed up for more chain transfer reactions by undergoing chain termination to produce oligomers.[5]

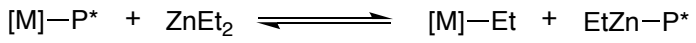

Scheme 3.2: Role of $ZnEt_2$ as a chain-transfer agent in selective ethylene oligomerisation, where M represents an active metal centre and P* represents a growing polymer chain, modified from van Meurs *et al.*[5]

In previous work conducted in the Dyer group, the addition of $ZnEt_2$ to Cr/PCN-based ethylene oligomerisation systems was observed to affect the levels of polymer formation and activities of the system.[1] It was found that, upon varying the amount of $ZnEt_2$ present in the larger-scale catalytic testing of the PCN ligands (Scheme 3.1 (ii)) between 0 and 400 equivalents (relative to Cr), the lowest levels of polymer formation and highest activities were obtained for Cr-PCN systems using 100 or 200 equivalents of $ZnEt_2$.[1]

3.2. Catalyst Testing Protocol for $Cr^{I}/^{III}$-PCN Based Ethylene Oligomerisation Systems Tested in this Thesis

The novel PCN ligands synthesised in Chapter 2 of this thesis were first screened in ethylene oligomerisation catalysis under the set of (previously established) conditions shown in Scheme 3.1(i). A selection of the best-performing PCN ligands from the screening runs were then tested on a larger scale under the industrially relevant conditions shown in Scheme 3.1(ii).

The Cr^{III}-PCN and Cr^{I}-PCN complexes described in Chapter 2 of this thesis were tested in ethylene oligomerisation catalysis using the conditions illustrated in Scheme 3.1(iii) with 150 equivalents of $AlEt_3$ (TEA) being used in the catalysis runs of the Cr^{I}-PCN complexes instead of 500 equivalents of MMAO-3A. TEA was used in place of MMAO-3A for the catalysis runs employing the Cr^{I}-PCN complexes since it has previously been reported that it is particularly effective in combination with Cr^{I}-PNP-based selective ethylene *tri*-/*tetra*-merisation systems, where it is proposed to remove

CO ligands from the Cr^{I}-PNP complexes, thereby generating vacant metal sites on the Cr^{I} centre for ethylene insertion.[6-9]

The catalytic testing of the PCN ligands, Cr^{III}-PCN and Cr^{I}-PCN complexes, whose syntheses were described in Chapter 2, has been carried out in collaboration with Dr. M. J. Hanton and Dr. D. M. Smith at Sasol Technology. All of the larger-scale catalysis runs have been performed by Dr. D. M. Smith. The initial screening of the PCN ligands and Cr-PCN complexes was carried out *via* semi-batch processes in a 250 mL steel autoclave, while the larger-scale testing of the PCN ligands was performed in a 1.2 L steel autoclave. For both the screening and larger-scale catalysis runs, the relevant autoclaves were filled with solvent prior to the addition of the activated catalyst solution, and then pressurised with ethylene (which had been entrained with 0.6 – 1.3 ppm O_2). The activated catalyst solutions were generated by adding the relevant activator to a Schlenk flask containing a solution of either the desired PCN ligand and chromium source or the preformed Cr-PCN complex, and stirring for a set amount of time.

Unfortunately, due to the time-consuming nature of the testing, a reproducibility study of the Cr/PCN-based ethylene oligomerisation catalysis runs conducted as part of the work for this thesis, could not be conducted, thereby preventing the generation of precise error bars for each run. However, comprehensive catalytic testing that has been carried out at Sasol Technology using the same equipment/test rig that has been used for the Cr-PCN catalysis runs described in this thesis has revealed that the equipment used for the Cr-PCN catalysis runs has an error of ±5 %. Therefore, it is assumed that the errors for the Cr-PCN catalysis runs reported in this Chapter will also be ±5 %. In addition, for the few Cr-PCN catalysis runs where a repeat run was able to be performed, the average of the results are reported in this Chapter (see Appendices, section 6.3 for full data tables of the Cr-PCN catalysis runs conducted). At this point, it should also be noted that the catalytic activities of all the systems tested and described in this Chapter will be reported in terms of Kg of all products formed per g of Cr per hour, unless otherwise stated.

3.3. Performance of PCN Ligands, 2.1 – 2.13, in Ethylene Oligomerisation Catalysis

As mentioned previously in section 3.2, the novel PCN ligands described in Chapter 2 of this thesis (ligands **2.1** – **2.13** of Figure 3.4) were initially screened in ethylene

oligomerisation catalysis before a selection of the best-performing ligands were tested under the larger-scale testing conditions. The results of the catalytic testing of ligands **2.1** – **2.13** under the different conditions will be discussed in sections 3.3.1 and 3.3.2.

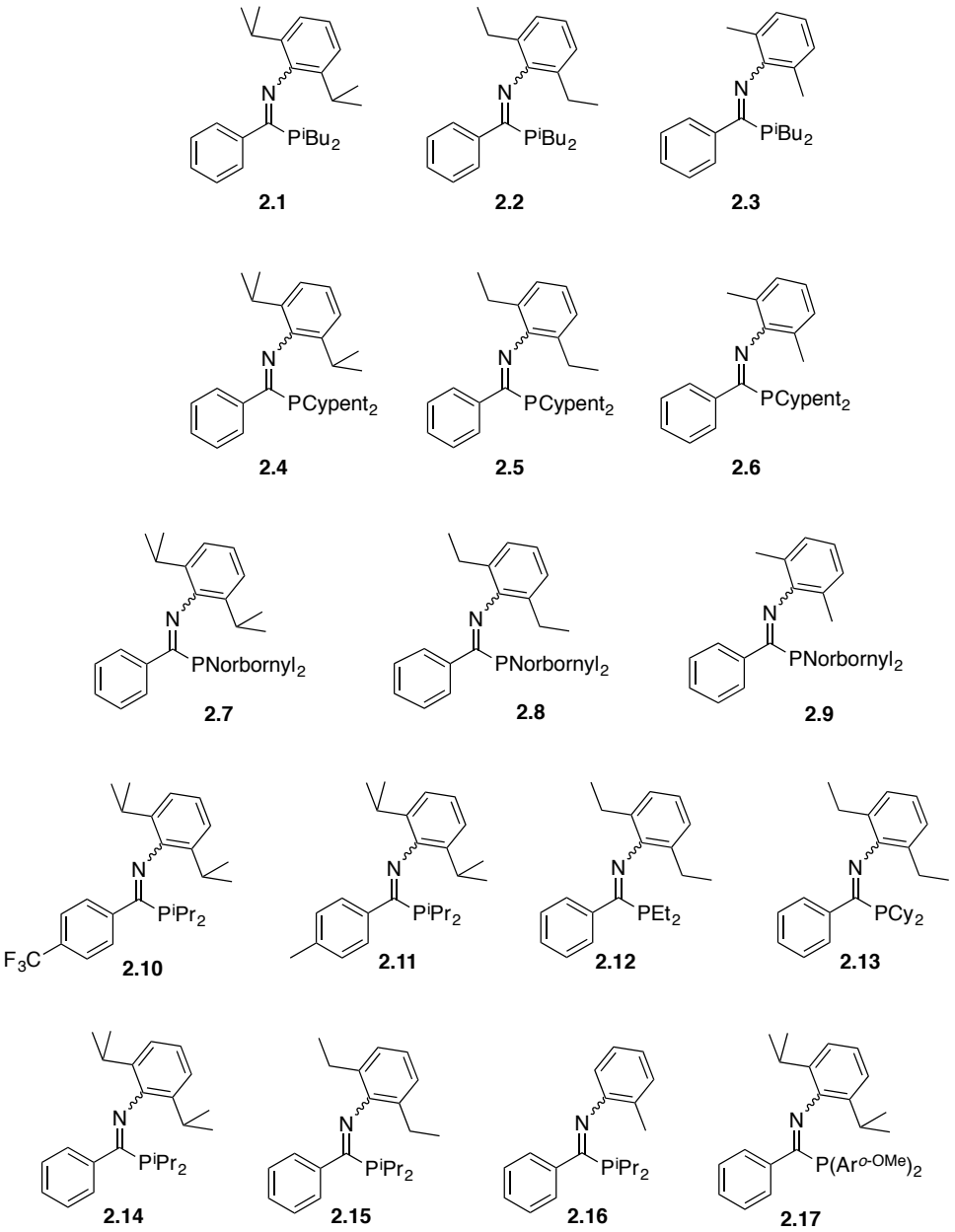

Figure 3.4: PCN ligands synthesised in Chapter 2 of this thesis, **2.1** – **2.17**.

3.3.1. Overview of screening results of ligands 2.1 – 2.13 in ethylene oligomerisation catalysis

The screening of PCN ligands **2.1** – **2.13** in ethylene oligomerisation catalysis revealed that, in combination with $Cr(acac)_3$ and MMAO-3A, these ligands give rise to systems exhibiting a range of activities (45 – 218 Kg/g Cr/h) and extents of polymer formation (5

– 64%), as illustrated in Graph 3.1. It should be noted that of the Cr/PCN-based ethylene oligomerisation systems utilising ligands **2.1** – **2.13**, a different batch of MMAO-3A was used for the systems employing ligands **2.10** and **2.11**, which may impact the activities and polymer levels achieved by these systems (see section 3.3.1.2.1).

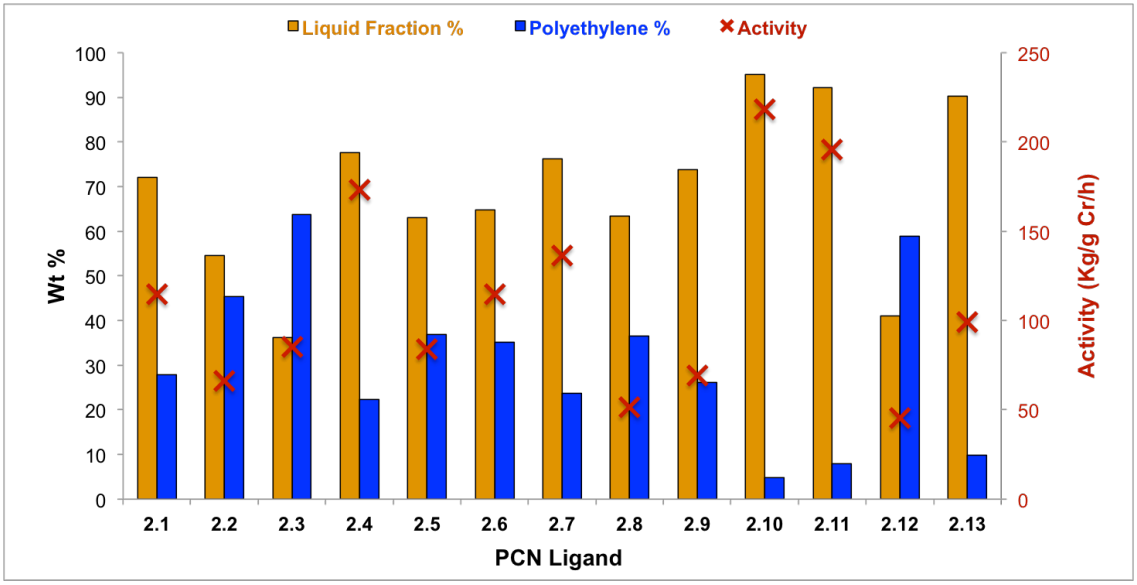

Graph 3.1: Catalytic activities and polymer/oligomer formation of Cr/PCN-based ethylene oligomerisation systems employing ligands **2.1** – **2.13**. Conditions of ethylene oligomerisation catalysis: 5 µmol $Cr(acac)_3$, 1.2 eq. PCN ligand, 500 eq. MMAO-3A, 0.6 ppm O_2, 60 ^{o}C, 40 bar ethylene, PhCl, 10 min.

On comparing the activities and extents of polymer formation of the Cr/PCN-based ethylene oligomerisation systems implementing ligands **2.1** – **2.13** to some of the most selective literature ethylene *tri*-/*tetra*-merisation catalytic systems listed in Chapter 2 (section 2.1.6.1, Tables 2.3 and 2.4) it is evident that the Cr-PCN ligand **2.1** - **2.13** systems exhibit significantly lower activities and higher levels of polymer formation. Nevertheless, it is apparent from the data described in Graph 3.2 that Cr/PCN-based selective ethylene *tri*-/*tetra*-merisation is achieved with ligands **2.1** – **2.13**, which all generate systems displaying total liquid fraction selectivities to 1-hexene and 1-octene greater than 60%.

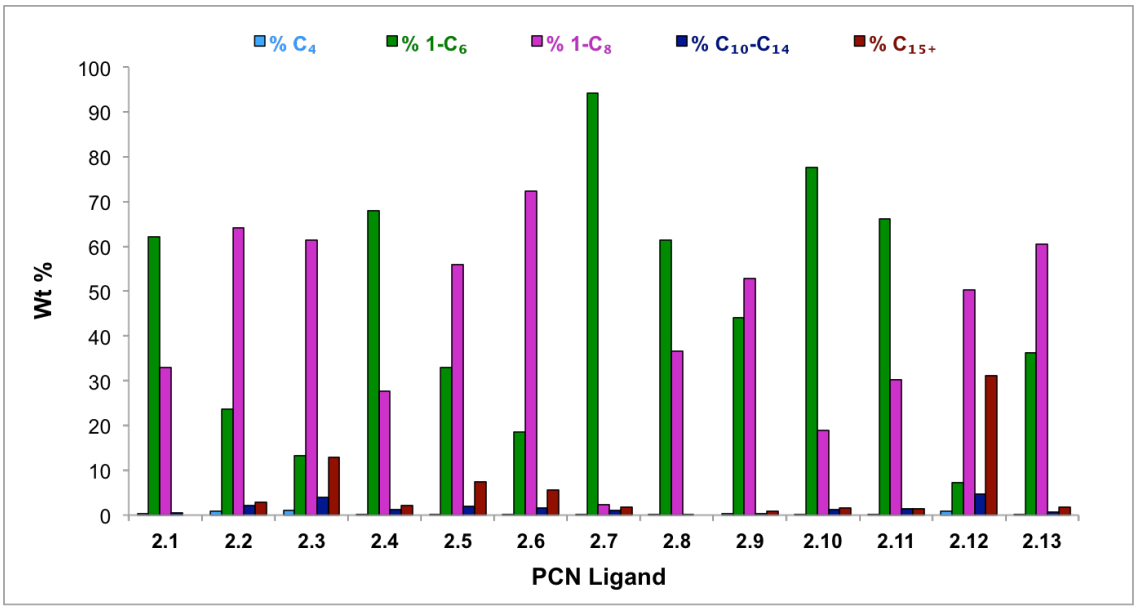

Graph 3.2: Liquid fraction selectivities of Cr/PCN-based ethylene oligomerisation systems employing ligands **2.1** – **2.13**. Conditions of ethylene oligomerisation catalysis: 5 µmol $Cr(acac)_3$, 1.2 eq. PCN ligand, 500 eq. MMAO-3A, 0.6 ppm O_2, 60 ^oC, 40 bar ethylene, PhCl, 10 min.

Notably, ligands **2.1**, **2.4**, **2.6** – **2.11**, and **2.13**, when used in conjunction with $Cr(acac)_3$ and MMAO-3A, result in highly selective ethylene *tri*-/*tetra*-merisation systems with total liquid fraction selectivities to 1-hexene and 1-octene ranging between 91 and 98%. These high selectivities rival those of 80 – 89% achieved using some of the best-performing PNP-based ethylene *tri*-/*tetra*-merisation systems described previously in the literature (shown in Table 2.1, Chapter 2 section 2.1.6.1). In addition, out of the PCN ligands tested in this thesis under the described screening conditions, ligand **2.7** generates the most selective ethylene trimerisation system (94% liquid fraction selectivity to 1-hexene), while ligand **2.6** generates the most selective ethylene tetramerisation system (72% liquid fraction selectivity to 1-octene), when employed in combination with MMAO-3A and $Cr(acac)_3$. The results of the screening runs of ligands **2.1** – **2.13** in ethylene oligomerisation catalysis (Graph 3.1 and Graph 3.2) demonstrate that the activity and selectivity engendered by these PCN ligands is influenced by the nature of substituents on their phosphorus, carbon and nitrogen atoms; these effects will be discussed in the next sections.

3.3.1.1. Investigating the effect of varying the phosphorus substituent of PCN ligands on their performance in ethylene oligomerisation catalysis

The performance of Cr/PCN-based ethylene oligomerisation catalysis mediated by ligands **2.2**, **2.5**, **2.8**, **2.12**, and **2.13** (Figure 3.4) have been compared in Graphs 3.3 and 3.4 in order to investigate the relationship between the nature of the alkyl

phosphorus substituent of these PCN ligands and the ligands behaviour in ethylene oligomerisation catalysis. Ligands **2.2**, **2.5**, **2.8**, **2.12**, and **2.13** all possess diethylphenyl substituents at their nitrogen atoms and phenyl substituents at their imine carbon atoms, with different alkyl phosphorus substituents (Et, ^{i}Bu, Cypent, Cy, and Norbornyl) of varying steric and electronic properties. The PCN ligands have been listed in order of decreasing phosphine donor ability in Graphs 3.3 and 3.4; an order that has been found to mirror the increasing steric bulk of the phosphine groups (Chapter 2, section 2.3.3). The phosphine donor abilities of the PCN ligands have been inferred from the magnitudes of the $^{1}J_{SeP}$ coupling constants of their corresponding selenides (Chapter 2, section 2.3.3).

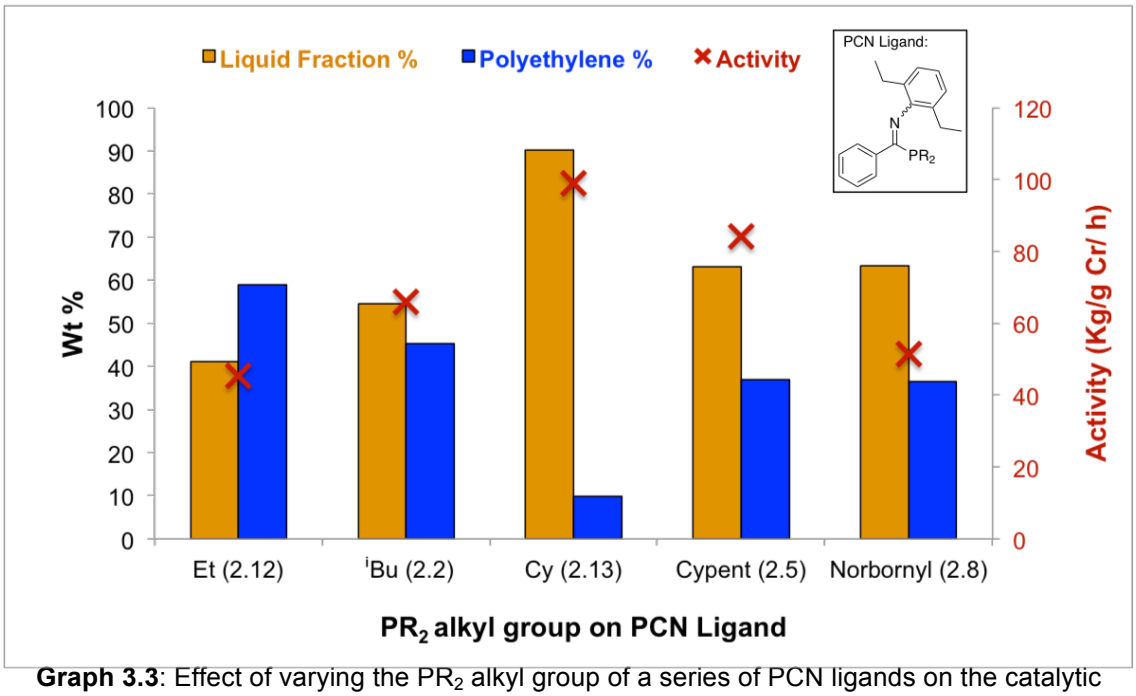

Graph 3.3: Effect of varying the PR_2 alkyl group of a series of PCN ligands on the catalytic activities and polymer/oligomer formation of the Cr/PCN-based ethylene oligomerisation systems. Conditions of ethylene oligomerisation catalysis: 5 µmol $Cr(acac)_3$, 1.2 eq. PCN ligand, 500 eq. MMAO-3A, 0.6 ppm O_2, 60 ^{o}C, 40 bar ethylene, PhCl, 10 min.

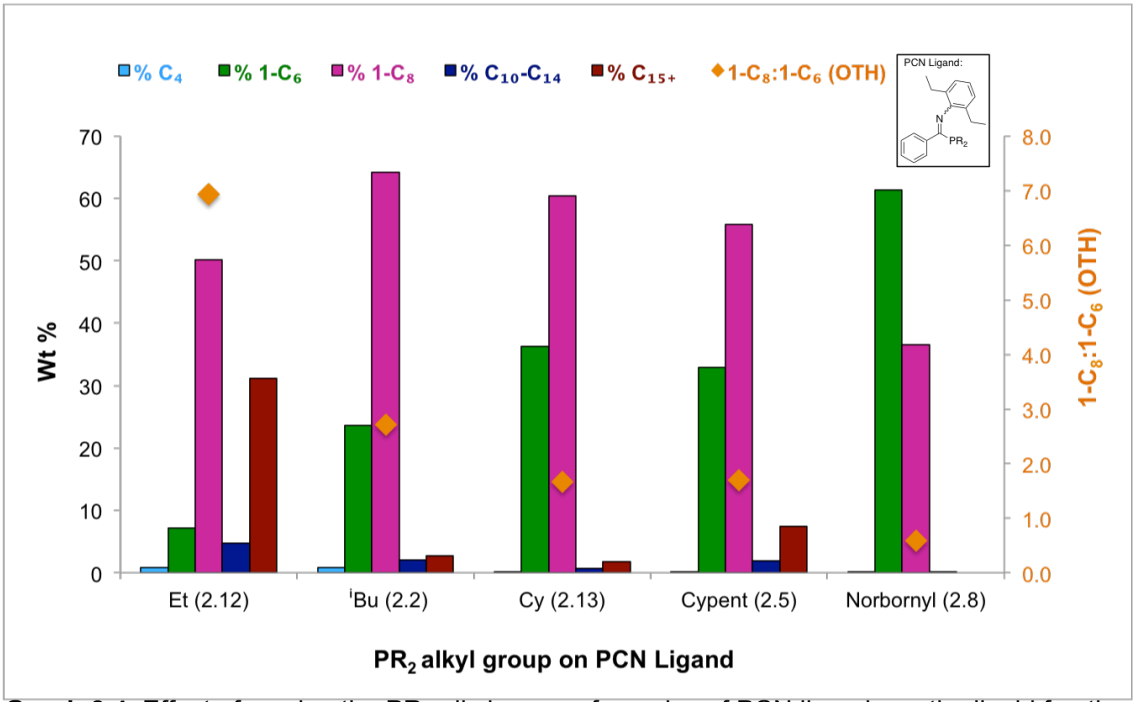

Graph 3.4: Effect of varying the PR_2 alkyl group of a series of PCN ligands on the liquid fraction selectivities of the Cr/PCN-based ethylene oligomerisation systems. Conditions of ethylene oligomerisation catalysis: 5 µmol $Cr(acac)_3$, 1.2 eq. PCN ligand, 500 eq. MMAO-3A, 0.6 ppm O_2, 60 ^{o}C, 40 bar ethylene, PhCl, 10 min.

From the results presented in Graph 3.3 it is apparent that as the phosphine donor ability of the PCN ligand is decreased, and the steric bulk of the phosphino moiety is increased from Et (ligand **2.12**) to Cy (ligand **2.13**), the activity of the Cr/PCN-based ethylene oligomerisation catalysis systems increases and the levels of polymer formation decrease. However, a further decrease in the phosphine donor ability of the PCN ligand, and increase in the steric bulk of the phosphine, from Cy (ligand **2.13**) to norbornyl (ligand **2.8**) has the converse effect. This decrease in activity and increase in degree of polymer formation of the Cr/PCN-based ethylene oligomerisation systems upon increasing the steric bulk of the substituents at phosphorus of the PCN ligands above a certain threshold was also observed in previous work conducted in the Dyer group.[1] In this prior work, the observed effects were reasoned to be due to the oligomerisation proceeding *via* a metallacyle mechanism (Scheme 3.3), whereby metallacycle expansion at the Cr centre becomes hindered as the steric bulk of the PCN ligand is increased above a certain threshold (Figure 3.5).

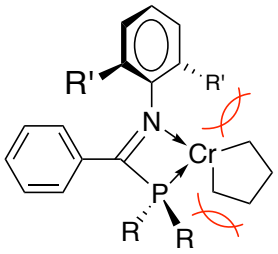

(R = alkyl or aromatic group, R' = alkyl group)

Figure 3.5: Schematic representation of the impact of steric bulk of the PCN ligand on a Cr-metallacycle, believed to be an intermediate in the Cr/PCN-based ethylene *tri*-/*tetra*-merisation systems; adapted from Radcliffe.[1]

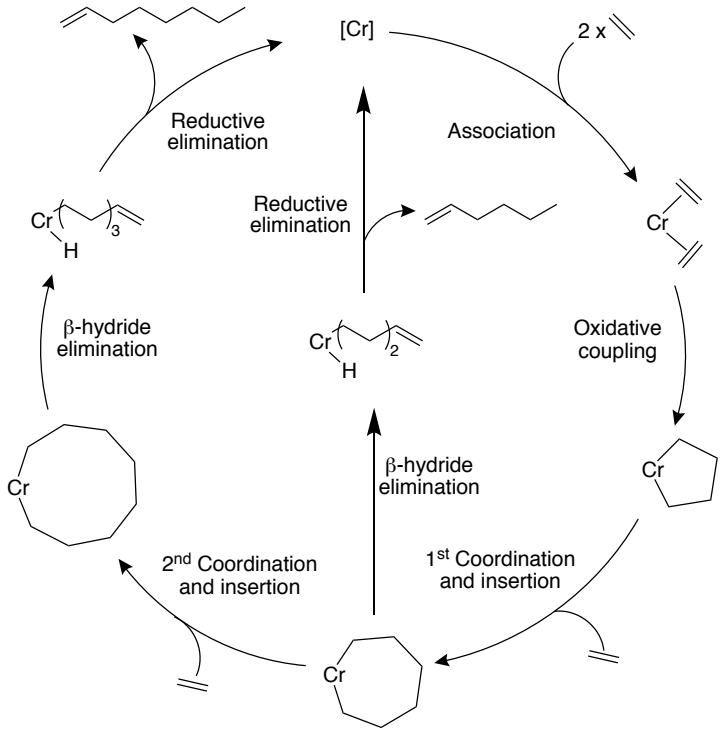

Scheme 3.3: Metallacycle mechanism believed to be in operation for ethylene *tri*-/*tetra*-merisation systems.[10,11]

The steric demands and donor abilities of the PCN ligand phosphorus substituents are also observed to affect the oligomer selectivities of the Cr/PCN-based ethylene oligomerisation catalysis systems. This is summarised in Graph 3.4 (on the previous page) where the data emphasise the trend that the OTH ratios decrease as the phosphine donor ability decreases, and the steric bulk of the phosphine increases from Et (ligand **2.12**) to norbornyl (ligand **2.8**).[12-15] A shift in the ethylene oligomerisation selectivity from tetramerisation to trimerisation upon an increase in the steric bulk of the phosphine substituent of the PCN ligand was also reported in previous work conducted in the Dyer group[1] and has been reported in numerous literature Cr/P,N-ligand based selective ethylene *tri*-/*tetra*-merisation systems.[12-15] In the literature Cr/P,N-ligand based selective ethylene oligomerisation systems, it is proposed that the

sterics of the ligands affect the stabilities of the metallacycloheptane and metallacyclononane intermediates which liberate 1-hexene and 1-octene, respectively (Scheme 3.3 on previous page).[12-15] Bulkier ligands are argued to retard the formation of the metallacyclononane, hence generating ethylene oligomerisation systems with increased selectivities towards ethylene trimerisation, with the converse argument applying for less bulky ligands.[12-15]

3.3.1.2. Investigating the effect of varying the imine carbon substituent of PCN ligands on their performance in ethylene oligomerisation catalysis

In order to explore the effect of the substitution pattern of the imine carbon of PCN ligands on their behaviour in Cr/PCN-based ethylene oligomerisation catalysis, the ligands illustrated in Figure 3.6 were tested under standard conditions. It is expected that ligands **2.10**, **2.11** and **2.14** (Figure 3.6) possess similar steric properties, so any differences seen in their performance in ethylene oligomerisation catalysis is assumed to be primarily an electronic effect. To explore this relationship, the electronic properties of the different aryl imine carbon substituents of the PCN ligands have been deduced from the magnitudes of the $^{1}J_{SeP}$ coupling constants of their corresponding selenides (previously discussed in Chapter 2, section 2.3.3), enabling these ligands to be listed in order of increasing electron withdrawing character of their aryl imine carbon substituents in Graphs 3.5 and 3.6.

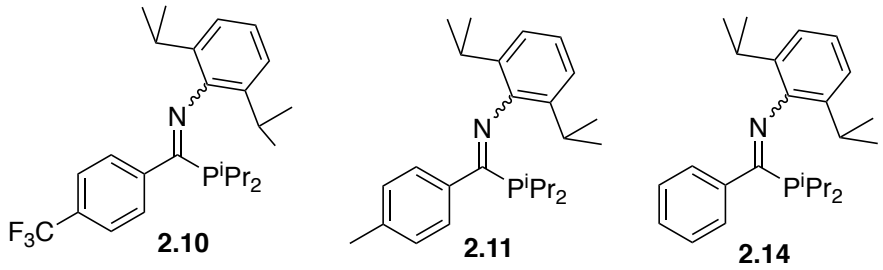

Figure 3.6: Series of PCN ligands (described in Chapter 2) with different imine carbon substituents.

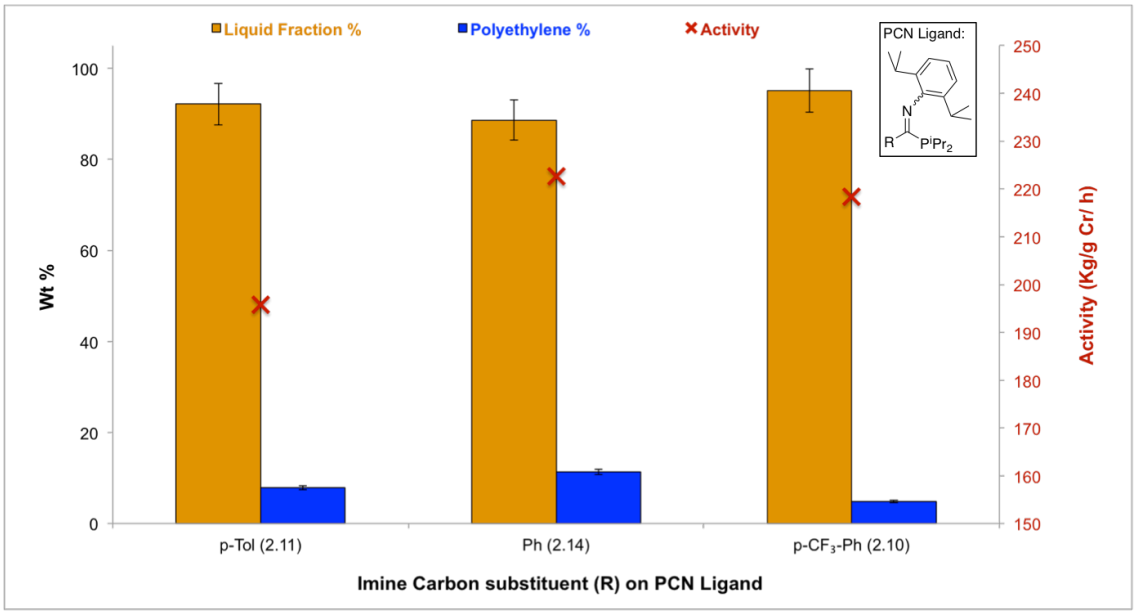

Graph 3.5: Effect of varying the imine carbon substituent of a series of PCN ligands on the catalytic activities and polymer/oligomer formation of the Cr/PCN-based ethylene oligomerisation systems. Conditions of ethylene oligomerisation catalysis: 5 µmol $Cr(acac)_3$, 1.2 eq. PCN ligand, 500 eq. MMAO-3A, 0.6 ppm O_2, 60 ^{o}C, 40 bar ethylene, PhCl, 10 min. Error bars (± 5 %) shown for Wt % liquid fraction and polyethylene.

The electronic character of the different aryl imine carbon substituents of the PCN ligands is observed to have no effect on the activity of the Cr/PCN-based ethylene oligomerisation catalysis (as the activities for systems employing ligands **2.10**, **2.11** and **2.14** are the same within the ±5% error, Graph 3.5). In contrast to the Cr/PCN ligand **2.14** ethylene oligomerisation system, systems utilising PCN ligands with electron donating (ligand **2.11**) or electron withdrawing (ligand **2.10**) imine carbon substituents give rise to lower levels of polymer formation (Graph 3.5). In addition to affecting the extent of polymer formation, varying the aryl imine carbon electronic character of PCN ligands **2.10, 2.11** and **2.14** also has a small effect on the product oligomer selectivity of the Cr/PCN-based ethylene oligomerisation systems (Graph 3.6). A decrease in the OTH ratio occurs as the electron withdrawing nature of the aryl imine carbon substituents is increased (Graph 3.6). The observation that utilising ligands containing electron donating substituents *versus* electron withdrawing substituents can be used to generate Cr-based ethylene oligomerisation systems with greater selectivities towards ethylene tetramerisation was also reported for Cr/PNP-based ethylene oligomerisation systems studied by Killian *et al.*[16] and Jiang *et al.*[17]

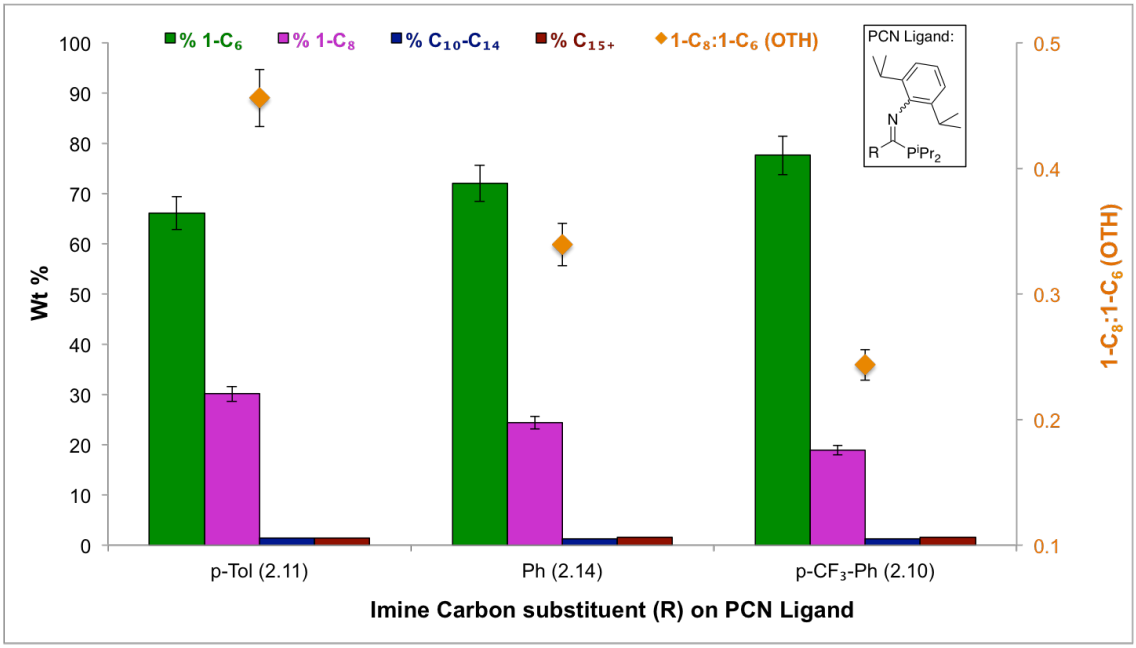

Graph 3.6: Effect of varying the imine carbon substituent of a series of PCN ligands on the liquid fraction selectivities of the Cr/PCN-based ethylene oligomerisation systems. Conditions of ethylene oligomerisation catalysis: 5 µmol $Cr(acac)_3$, 1.2 eq. PCN ligand, 500 eq. MMAO-3A, 0.6 ppm O_2, 60 °C, 40 bar ethylene, PhCl, 10 min. Error bars (± 5 %) shown for OTH ratios and Wt % of different oligomers.

3.3.1.2.1. Comparison of PCN ligands with aryl-substituted imine carbons versus alkyl substituted imine carbons in Cr/PCN-based ethylene oligomerisation catalysis

In order to compare the ethylene oligomerisation performance of PCN ligands bearing aryl-substituted imine carbons (**2.10**, **2.11** and **2.14**; synthesised and tested as part of work for this thesis) to those of PCN ligands possessing alkyl-substituted imine carbons (synthesised and tested in Cr/PCN-based ethylene oligomerisation in previous work conducted in the Dyer group),[1] the reproducibility of different batches of MMAO activator must be first considered. The set of catalytic runs utilising PCN ligands with alkyl-substituted imine carbons (conducted in previous work in the Dyer group)[1] used a different batch of MMAO-3A (referred to as batch 1) to the set of catalytic runs performed in this work with ligands encompassing aryl-substituted imine carbons (that used a batch of MMAO-3A that will be referred to as batch 2). In order to evaluate the effect of using batch 1 *versus* batch 2 of MMAO-3A in ethylene oligomerisation, catalytic runs utilising Cr/PCN ligand **2.14**/MMAO-3A batch 1 and Cr/PCN ligand **2.14**/MMAO-3A batch 2 were carried out. From the results of these two test runs (Graph 3.7) it can be seen that Cr/PCN ligand **2.14**/MMAO-3A batch 2 generates an ethylene oligomerisation system with a significantly higher activity and lower level of

polymer formation than that achieved with Cr/PCN ligand **2.14**/MMAO-3A batch 1. However, the batch of MMAO-3A implemented in Cr/PCN ligand **2.14**-based ethylene oligomerisation catalysis was found to have no impact on the liquid fraction selectivity (Graph 3.8). These effects directly related to the batch of aluminium activator being used, highlight a significant issue surrounding the use of such reagents on a commercial scale.

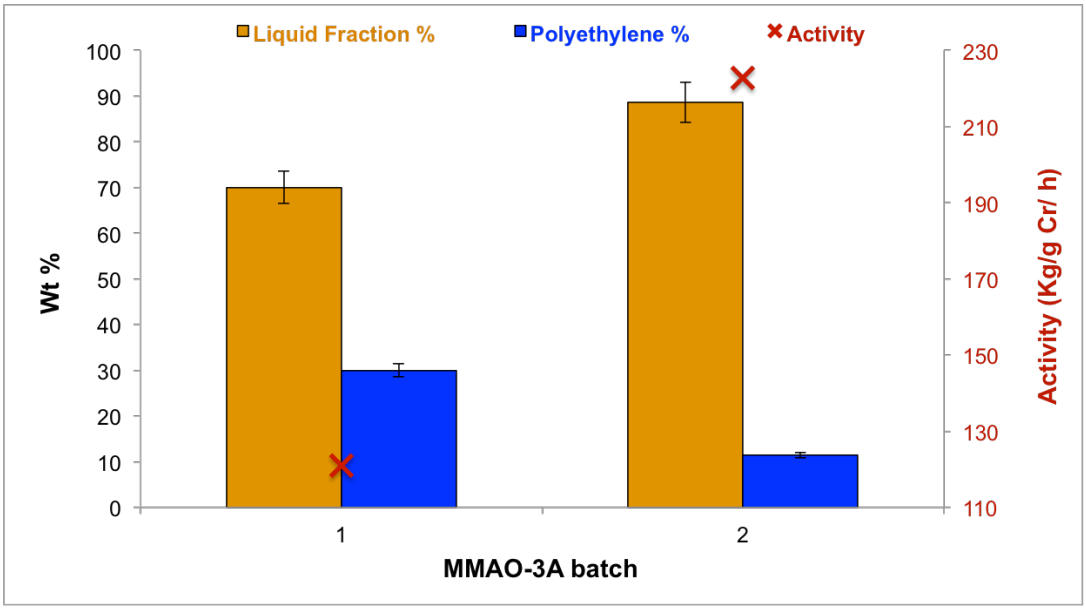

Graph 3.7: Effect of varying the batch of MMAO-3A on the catalytic activity and polymer/oligomer formation of Cr/PCN-based ethylene oligomerisation utilising ligand **2.14**. Conditions of ethylene oligomerisation catalysis: 5 µmol $Cr(acac)_3$, 1.2 eq. PCN ligand, 500 eq. MMAO-3A, 0.6 ppm O_2, 60 °C, 40 bar ethylene, PhCl, 10 min. Error bars (± 5 %) shown for Wt % liquid fraction and polyethylene.

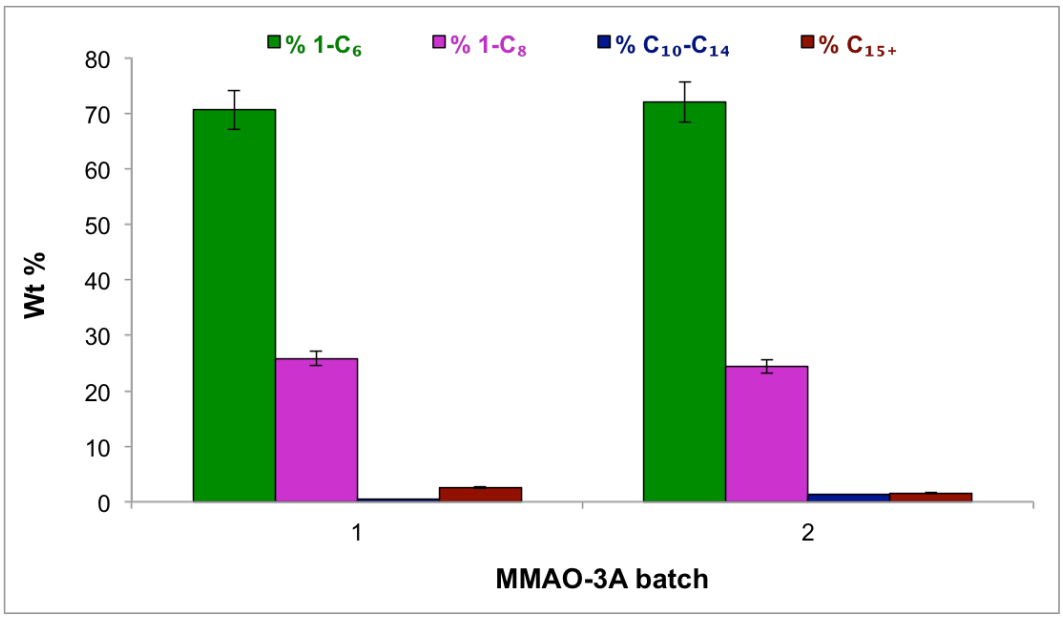

Graph 3.8: Effect of varying the batch of MMAO-3A on the liquid fraction selectivity of Cr/PCN-based ethylene oligomerisation utilising ligand **2.14**. Conditions of ethylene oligomerisation catalysis: 5 µmol $Cr(acac)_3$, 1.2 eq. PCN ligand, 500 eq. MMAO-3A, 0.6 ppm O_2, 60 °C, 40 bar ethylene, PhCl, 10 min. Error bars (± 5 %) shown for Wt % of different oligomers.

Since (for the tests undertaken here) the batch of MMAO-3A used in Cr/PCN-based ethylene oligomerisation catalysis has no impact on the liquid fraction selectivity, the variation in the liquid fraction selectivities of Cr/PCN-based systems utilising aryl or alkyl imine carbon substituents can reliably be compared (Graph 3.9). PCN ligands with aryl-substituted imine carbons give rise to systems with greater selectivity towards ethylene tetramerisation than their alkyl-substituted counterparts (Graph 3.9). This is similar to the finding from previous work carried out in the Dyer group, where the same trend was identified for related PCN ligands upon varying the nature of their phosphorus substituent (*i.e.* aryl or alkyl).[1]

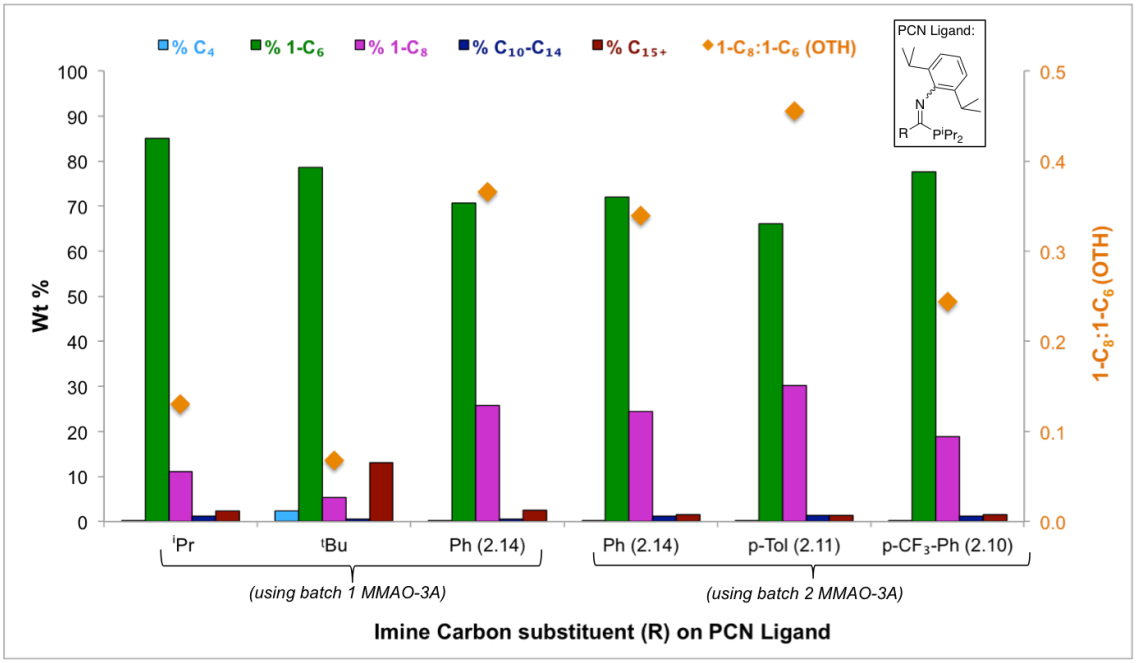

Graph 3.9: Effect of utilising alkyl *vs.* aryl imine carbon substituted PCN ligands upon the liquid fraction selectivities of Cr/PCN-based ethylene oligomerisation catalysis. Conditions of ethylene oligomerisation catalysis: 5 µmol $Cr(acac)_3$, 1.2 eq. PCN ligand, 500 eq. MMAO-3A, 0.6 ppm O_2, 60 °C, 40 bar ethylene, PhCl, 10 min.

3.3.1.3. Investigating the effect of varying the nitrogen substituent of PCN ligands on their performance in ethylene oligomerisation catalysis

An evaluation of the effect of the PCN nitrogen substituent on catalysis for three families of PCN ligands, which have different substituents at nitrogen within each family (ligands **2.1** – **2.3**, **2.4** – **2.6**, and **2.7** – **2.9** in Graphs 3.10 and 3.11) in ethylene oligomerisation catalysis has been carried out. The different nitrogen substituents explored within each family of PCN ligands are found to exhibit similar electronic properties (indirectly inferred from the magnitudes of the $^1J_{SeP}$ coupling constants of the corresponding PCN selenides, Chapter 2 section 2.3.3) and so have been listed in order of increasing steric bulk in Graphs 3.10 and 3.11.

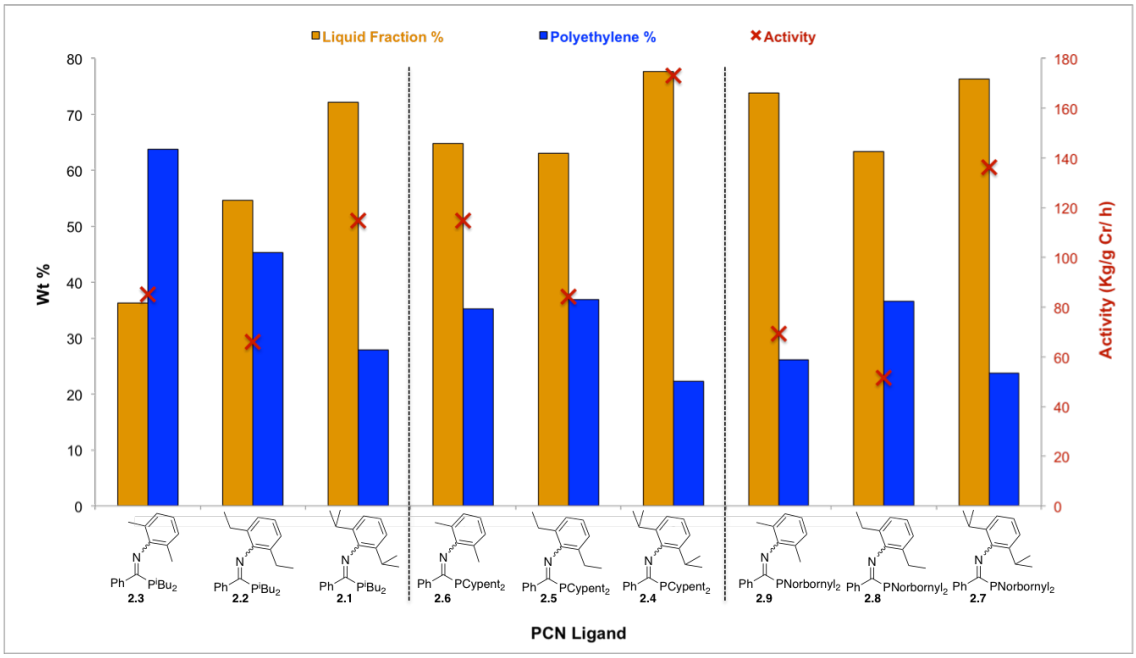

Graph 3.10: Effect of varying nitrogen substituent of PCN ligands upon the catalytic activities and polymer/oligomer formation of Cr/PCN-based ethylene oligomerisation catalysis. Conditions of ethylene oligomerisation catalysis: 5 μmol $Cr(acac)_3$, 1.2 eq. PCN ligand, 500 eq. MMAO-3A, 0.6 ppm O_2, 60 °C, 40 bar ethylene, PhCl, 10 min.

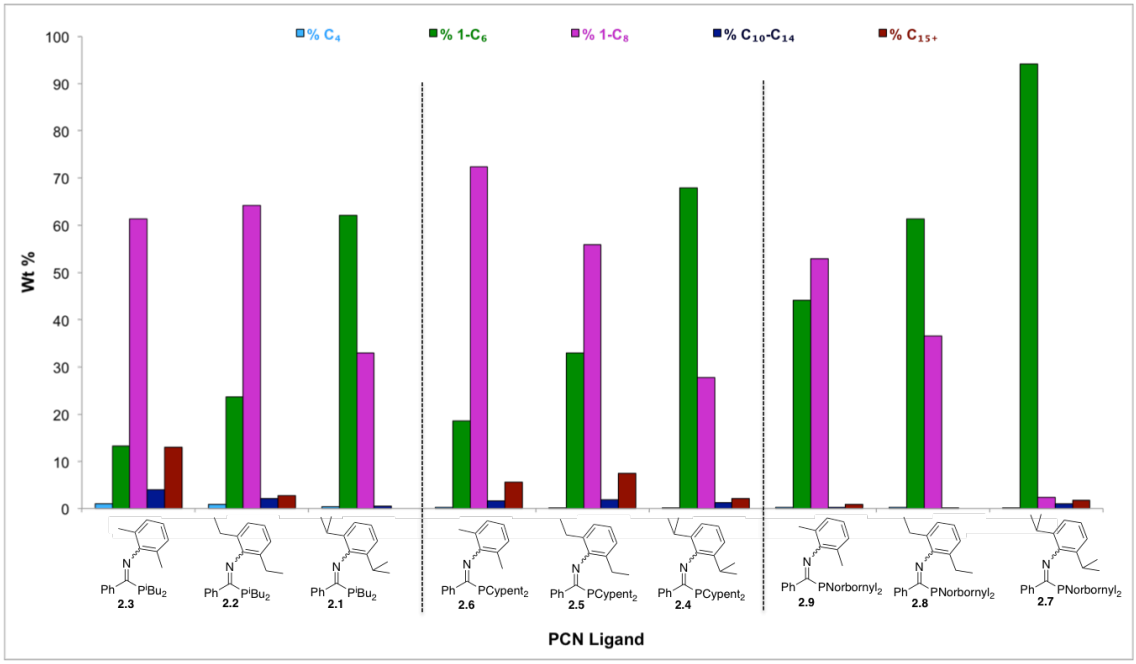

Graph 3.11: Effect of varying nitrogen substituent of PCN ligands upon the liquid fraction selectivities of Cr/PCN-based ethylene oligomerisation catalysis. Conditions of ethylene oligomerisation catalysis: 5 μmol $Cr(acac)_3$, 1.2 eq. PCN ligand, 500 eq. MMAO-3A, 0.6 ppm O_2, 60 °C, 40 bar ethylene, PhCl, 10 min.

In agreement with that observed for Cr/PCN-based ethylene oligomerisation systems tested in previous work in the Dyer group,[1] out of PCN ligands **2.1** – **2.9** those bearing the bulkiest nitrogen substituents (**2.1**, **2.4**, and **2.7**) produce ethylene oligomerisation systems with the highest activities and lowest levels of polymer formation.

Furthermore, the steric bulk of the substituents at the nitrogen centre of PCN ligands **2.1** – **2.9** affects the OTH, with ligands bearing bulkier nitrogen substituents furnishing ethylene oligomerisation systems with increased selectivity towards trimerisation (Graph 3.11). A switch in the ethylene oligomerisation behaviour from tetramerisation to trimerisation upon an increase in the steric bulk of the ligand nitrogen substituent was also reported in previous work performed in the Dyer group,[1] and described in a number of previously disclosed selective ethylene *tri*-/*tetra*-merisation systems.[16,18-22] The dependency of the OTH ratio on the steric bulk of the PCN ligand nitrogen substituent is believed to occur for the same reasons as discussed previously in section 3.3.1.1, where an analogous dependency of the OTH on the steric bulk of the PCN ligand phosphorus substituent was observed.

3.3.2. Optimisation of Cr/PCN-based ethylene oligomerisation catalysts systems

In an attempt to improve the activity and decrease the levels of polymer formation resulting from the use of Cr^{III}/PCN ligand combinations (ligands **2.1** – **2.13** of Figure 3.4) in ethylene oligomerisation catalysis, the ligands **2.1** – **2.7** were tested on a larger-scale under industrially applicable conditions (that will be referred to as conditions **B**, Scheme 3.1(ii)). PCN ligands **2.1** – **2.7** were chosen as they gave rise to Cr-based ethylene oligomerisation systems with high total liquid fraction selectivities for 1-hexene and 1-octene, when implemented under the screening conditions (referred to as conditions **A**, Scheme 3.1(i)). Comparison of the performance of ligands **2.1** – **2.7** under the ethylene oligomerisation conditions **A** (Graph 3.1) *versus* **B** (Graph 3.12) shows that significantly higher activities and decreased levels of polymer formation are obtained under catalysis conditions **B**. Notably, the total liquid fraction selectivities to 1-hexene and 1-octene are the same for ligands **2.1** – **2.7** using both test conditions **A** and **B** (Graph 3.2 *versus* Graph 3.13, respectively).

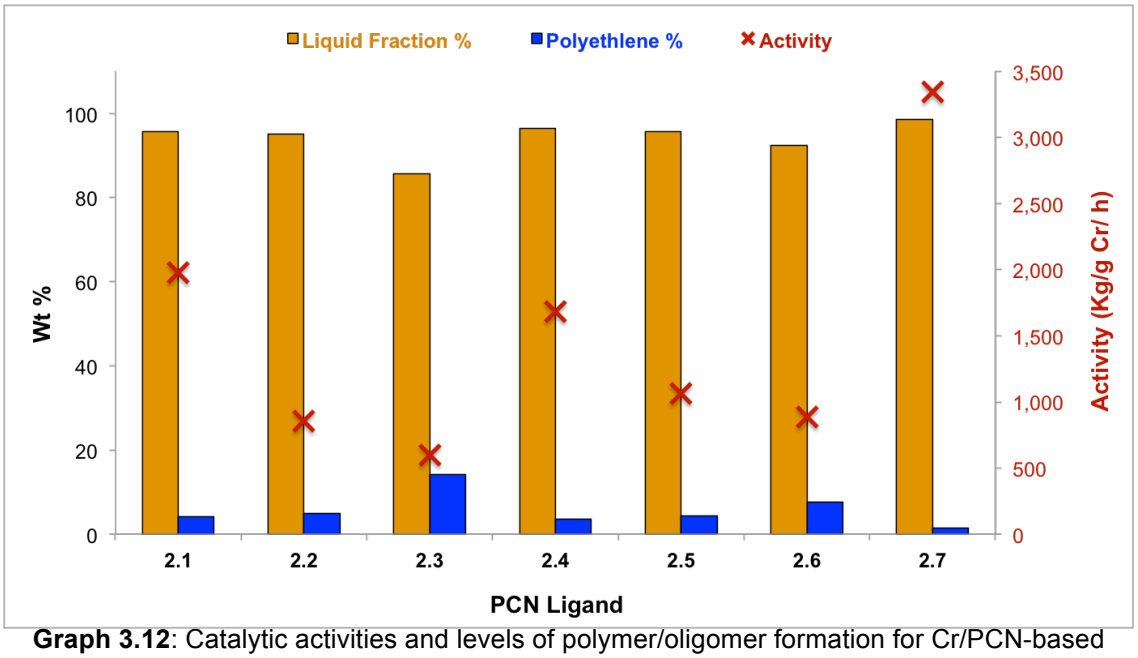

Graph 3.12: Catalytic activities and levels of polymer/oligomer formation for Cr/PCN-based ethylene oligomerisation catalysis mediated by ligands **2.1** – **2.7** under the optimised larger-scale testing conditions: 1.25 µmol $Cr(2\text{-}EH)_3$, 1.0 eq. PCN ligand, 700 eq. MMAO-3A, 0.91 – 1.26 ppm O_2, 100 eq. $ZnEt_2$, 60 °C, 45 bar ethylene, MCH, 1 h.

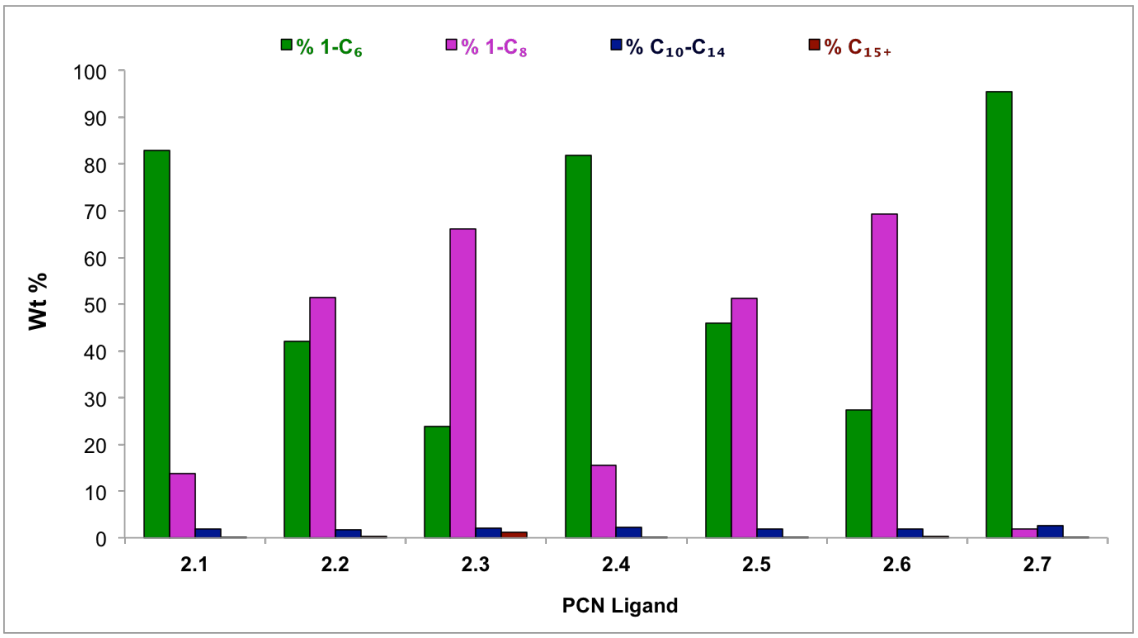

Graph 3.13: Liquid fraction selectivities of Cr/PCN-based ethylene oligomerisation catalysis mediated by ligands **2.1** – **2.7** under the optimised larger-scale testing conditions: 1.25 µmol $Cr(2\text{-}EH)_3$, 1.0 eq. PCN ligand, 700 eq. MMAO-3A, 0.91 – 1.26 ppm O_2, 100 eq. $ZnEt_2$, 60 °C, 45 bar ethylene, MCH, 1 h.

Of the PCN ligands tested under ethylene oligomerisation catalysis conditions **B** (Scheme 3.1(ii)), ligands **2.1**, **2.4** and **2.7** give rise to the best-performing ethylene *tri-*/*tetra*-merisation systems in terms of activity (1686 – 3346 Kg/g Cr/h) and total liquid fraction selectivities to 1-hexene and 1-octene (97%). The high activities and selectivities of these Cr/PCN-based systems are comparable to those of some of the

best-performing ethylene *tri-*/*tetra*-merisation systems described in the literature (Tables 2.3 and 2.4, Chapter 2 section 2.1.6.1), albeit with slightly higher levels of polymer formation (1 – 4%).

The Cr/PCN ligand **2.7**-based ethylene trimerisation system, generated under catalysis conditions **B,** is the best-performing ethylene trimerisation system out of those tested and reported in this Chapter and in previous work conducted in the Dyer group.[1] The activity of 3346 Kg/g Cr/h and liquid fraction selectivity to 1-hexene of 95% achieved using the Cr/PCN ligand **2.7** system are comparable to those achieved using the Mitsubishi Phillips system, which gives a reported activity of 3780 Kg/g Cr/h and 95% liquid fraction selectivity to 1-hexene.[23] However, a downside of the Cr/ligand **2.7**-based ethylene trimerisation system is the relatively high levels of polymer generated (1.4%) compared to some of the best literature selective ethylene trimerisation systems listed in Table 2.3 (Chapter 2, section 2.1.6.1). Polymer formation is an issue from an industrial perspective, not least because of increased risk of reactor fouling, but also from a resource efficiency stance.

In contrast to the results obtained using ligand **2.7**, testing ligand **2.6** under the same catalysis conditions **B** gives rise to the best performing Cr/PCN-based ethylene tetramerisation system of the systems tested in this work and previous work carried out in the Dyer group,[1] affording a similar liquid fraction 1-octene selectivity of 69% as those achieved using the Sasol Cr-PNP systems, typically 66 – 67%.[18,24] However, this Cr/PCN-**2.6** system exhibits a considerably lower activity (886 Kg/g Cr/h) and higher levels of polymer formation (8%) *versus* the literature Sasol Cr-PNP systems (Table 2.4, Chapter 2, section 2.1.6.1).[18,24]

3.4. Performance of Preformed Cr^{I}-PCN Complexes in Ethylene Oligomerisation Catalysis

The potential of the discrete Cr^{I}-PCN complexes, whose syntheses were described in Chapter 2 of this thesis (complexes **2.26** – **2.30**, Figure 3.7), as catalytic precursors in ethylene *tri-*/*tetra*-merisation was probed under the conditions described in section 3.2.

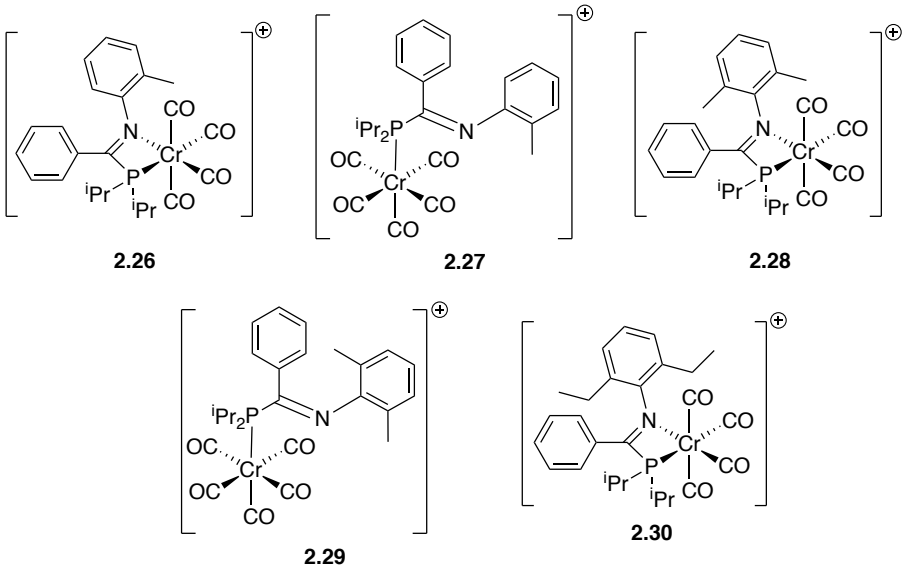

Figure 3.7: Cr^{I}-PCN complexes tested in ethylene oligomerisation catalysis.

Under the conditions described, the Cr^{I}-PCN complexes **2.26** – **2.30** perform as low activity ethylene oligomerisation systems (Graph 3.14), when used in conjuction with TEA. Moreover, they display little selectivity towards ethylene *tri*-/*tetra*-merisation with the system using complex **2.30** not forming any 1-hexene or 1-octene (Graph 3.15). Additionally, all of the catalysis tests employing the Cr^{I}-PCN complexes produce large amounts of polymer (24 – 57%), alongside C_4-C_{12} oligomers (Graph 3.15). Nevertheless, the ethylene oligomerisation systems utilising Cr^{I}-PCN complexes **2.27** – **2.29** achieve higher total liquid fraction selectivities to 1-hexene and 1-octene (62 – 78%) and lower or similar (in the case of the system employing complex **2.29**) levels of polymer formation than the ethylene oligomerisation systems mediated by Cr^{I}-PCP complexes in the literature,[25] albeit with lower activities. However, in comparison to the Cr^{I}-PNP based ethylene oligomerisation systems previously disclosed,[6,7] which achieve selective ethylene *tri*-/*tetra*-merisation with modest activities, the Cr^{I}-PCN based ethylene oligomerisation systems tested here perform poorly with lower activities, higher levels of polymer, and lower total liquid fraction selectivities to 1-hexene and 1-octene.

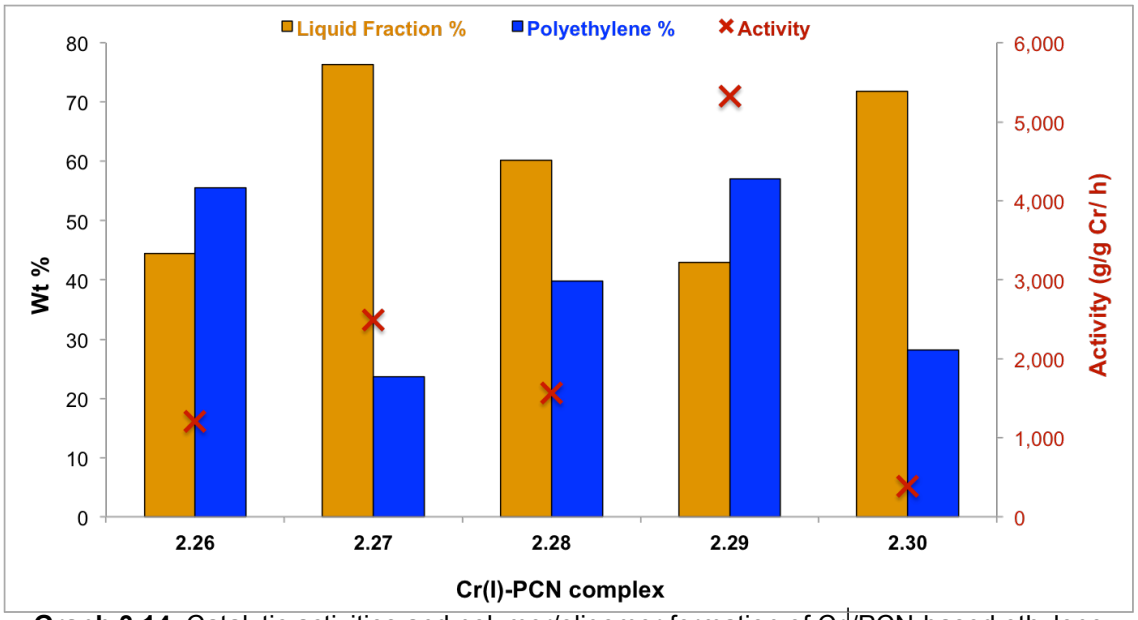

Graph 3.14: Catalytic activities and polymer/oligomer formation of Cr^{I}/PCN-based ethylene oligomerisation catalysis. Conditions of ethylene oligomerisation catalysis: 5 µmol Cr(I)-PCN complex **2.26** – **2.30**, 150 eq. TEA, 0.6 ppm O_2, 60 °C, 40 bar ethylene, PhCl, 10 min

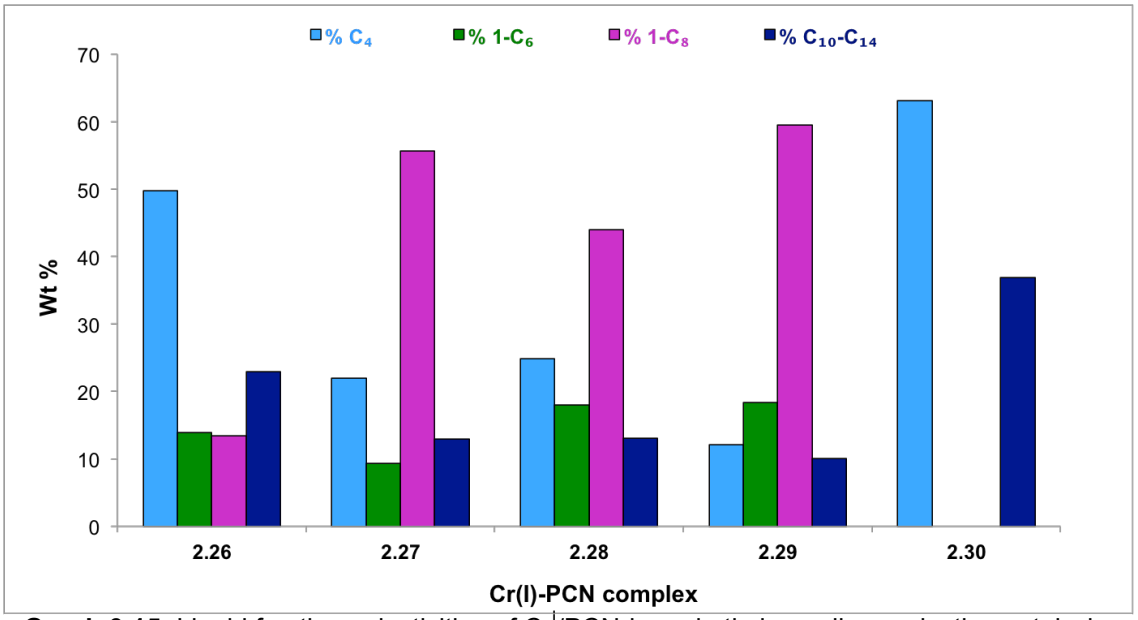

Graph 3.15: Liquid fraction selectivities of Cr^{I}/PCN-based ethylene oligomerisation catalysis. Conditions of ethylene oligomerisation catalysis: 5 µmol Cr^{I}-PCN complex **2.26** – **2.30**, 150 eq. TEA, 0.6 ppm O_2, 60 °C, 40 bar ethylene, PhCl, 10 min.

Since the different Cr^{I}-PCN complexes **2.26** – **2.30** have similar electronic properties (inferred from the CO stretches in their IR spectra, Chapter 2 section 2.4.2.1), the difference in the performance of the complexes in ethylene oligomerisation catalysis must be caused by another factor, possibly by the variation in the steric bulk of the Cr^{I}-PCN complexes. In addition, the ethylene oligomerisation behaviour of the Cr^{I}-κ^2-P,N-PCN complexes (*i.e.* complexes **2.26** and **2.28**) is different to that of the corresponding

Cr^{I}-κ^{1}-P-PCN complex (*i.e.* complexes **2.27** and **2.29**), suggesting that the different binding modes of the ligand (Figure 3.8) may remain in the active catalysts of these systems.

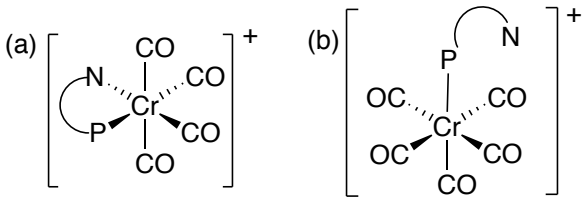

Figure 3.8: Different binding modes of PCN ligands in Cr^{I}-PCN complexes: (a) bidentate, (b) monodentate.

A comparison of the performance of the Cr^{I}-PCN complexes **2.26** – **2.30** with that of their corresponding Cr^{III}/PCN-based in ethylene oligomerisation catalysis (tested in previous work conducted in the Dyer group[1] and in section 3.5 using *in situ* or preformed Cr^{III}-PCN complexes) is presented in Table 3.1. The data in Table 3.1 demonstrate that the systems using Cr^{I}-PCN complexes exhibit the lowest activities and behave differently to their Cr^{III}-PCN counterparts. Since selective ethylene *tri-*/*tetra*-merisation systems could be obtained for some of the Cr^{III}-PCN catalyst systems displayed in Table 3.1, an investigation was undertaken into whether the difference in the catalysis conditions implemented for the Cr^{I} *vs*. Cr^{III} systems caused variations in the ethylene oligomerisation performance. Specifically, the effect of using 150 equiv. TEA in place of 500 equiv. MMAO-3A for Cr^{I} systems and the presence of CO in Cr^{I} systems was explored.

Table 3.1: Comparison of the ethylene oligomerisation behaviour of Cr^{I}-PCN complexes and their corresponding Cr^{III}/PCN-based systems (using *in situ* or preformed Cr^{III}-PCN complexes).

Cr/PCN ligand system	Activity (g/g Cr/h)	Wt % Polyethylene	Wt % 1-C_6 in liquid fraction	Wt % 1-C_8 in liquid fraction
Cr^{I}/**2.16** (complex **2.26**)[a]	1209	56	14	13
Cr(I)/**2.16** (complex **2.27**)[a]	2492	24	9	56
Cr^{III}/**2.16** (*in situ*-formed)[b]	7667	16	2	16
Cr^{III}/**2.16** (preformed)[b]	57,872	89	6	44
Cr^{I}/{PhC($P^{i}Pr_2$)=N(2,6-$Me_2C_6H_3$)} (complex **2.28**)[a]	1569	40	18	44
Cr^{I}/{PhC($P^{i}Pr_2$)=N(2,6-$Me_2C_6H_3$)} (complex **2.29**)[a]	5329	57	18	60
Cr^{III}/{PhC($P^{i}Pr_2$)=N(2,6-$Me_2C_6H_3$)} (*in situ*-formed)[b]	56,119	34	24	69
Cr^{III}/{PhC($P^{i}Pr_2$)=N(2,6-$Me_2C_6H_3$} (preformed)[a]	31,085	64	20	55
Cr^{I}/**2.15** (complex **2.30**)[a]	385	28	0	0
Cr^{I}/**2.15** (*in situ*-formed)[b]	113,613	55	34	60
Conditions of Cr/PCN-based ethylene oligomerisation catalysis: 5 µmol Cr^{I}-PCN complex or 5 µmol $Cr(acac)_3$ and 1.2 eq. PCN ligand or 5 µmol Cr^{III}-PCN complex, 500 eq. MMAO-3A or 150 eq. TEA (for Cr^{I}-PCN catalysis runs), 0.6 ppm O_2, 60 ^{o}C, 40 bar ethylene, PhCl, 10 min.				

Firstly, the effect of using MMAO-3A (500 equiv.) *versus* TEA (150 equiv.) as an activator in Cr^{I}/PCN-based ethylene oligomerisation mediated by Cr^{I}-PCN complex **2.30** was tested. It was found that MMAO-3A generated a system with a higher activity and lower level of polymer formation (Graph 3.16), suggesting that the lower activities and higher polymer levels of some of the Cr^{I}-PCN systems in comparison to their corresponding Cr^{III}-PCN systems may be due to use of MMAO-3A in the latter systems, compared to TEA in the former systems. However, using MMAO-3A for ethylene oligomerisation catalysis mediated by Cr^{I}-PCN complex **2.30** still yielded a system with no selectivity towards 1-hexene and 1-octene, indicating that another

[a] Catalysis testing carried out in this Chapter.
[b] Catalysis testing conducted in previous work carried out in Dyer group, included in this work for comparison.[1]

factor is responsible for the variation in the ethylene *tri-*/*tetra*-merisation behaviour of the Cr^{I}-PCN systems relative to the Cr^{III}-PCN systems.

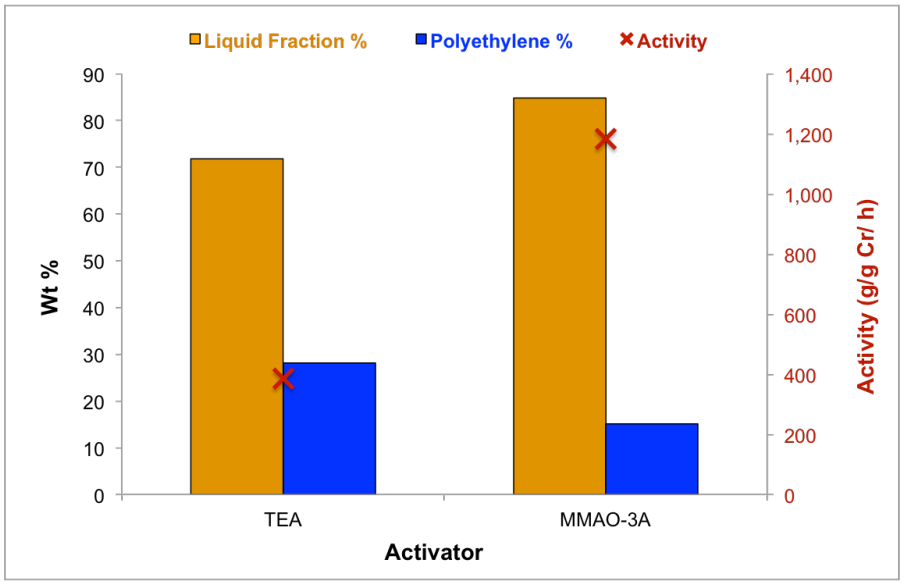

Graph 3.16: Effect of varying activator on catalytic activities and polymer/oligomer formation of Cr^{I}/PCN-based ethylene oligomerisation catalysis utilising complex **2.30**. Conditions of ethylene oligomerisation catalysis: 5 µmol Cr^{I}-PCN complex **2.30**, 150 eq. TEA or 500 eq. MMAO-3A, 0.6 ppm O_2, 60 °C, 40 bar ethylene, PhCl, 10 min.

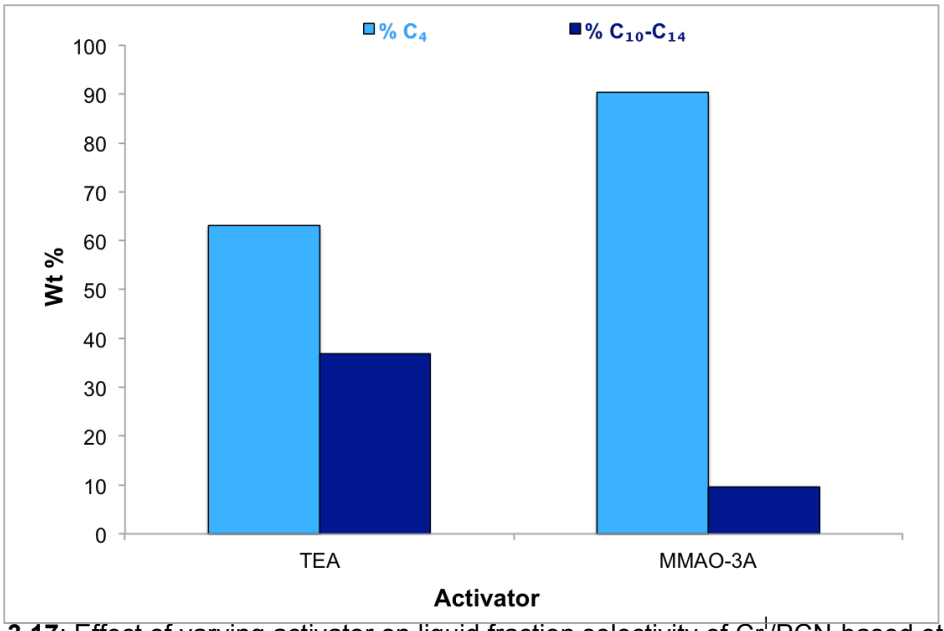

Graph 3.17: Effect of varying activator on liquid fraction selectivity of Cr^{I}/PCN-based ethylene oligomerisation catalysis utilising complex **2.30**. Conditions of ethylene oligomerisation catalysis: 5 µmol Cr^{I}-PCN complex **2.30**, 150 eq. TEA or 500 eq. MMAO-3A, 0.6 ppm O_2, 60 °C, 40 bar ethylene, PhCl, 10 min.

Secondly, since it is likely that CO is liberated from the Cr^{I}-PCN systems under the catalytic test conditions employed, it was important to test whether CO acts as a poison. Consequently, the Cr/PCN ligand **2.14** system (Figure 3.4) was screened in ethylene oligomerisation catalysis (Scheme 3.1 (i)) in (a) the absence of CO and (b)

the presence of 4 equiv. CO (relative to the PCN ligand, representative of the amount of CO present in the Cr^{I}-PCN systems utilising ligands **2.26**, **2.28**, and **2.30**). From the results summarised in Graphs 3.18 and 3.19 it is evident that introducing CO into the Cr/**2.14**-based ethylene oligomerisation system leads to a tenfold decrease in the activity and approximately 20% decrease in the total liquid fraction selectivity to 1-octene and 1-hexene. The negative impact of CO on the activity and oligomer selectivity of the Cr/PCN-based ethylene oligomerisation system mediated by ligand **2.14** demonstrates that CO is a potent poison in the Cr/PCN-based ethylene oligomerisation systems. Consequently, it is reasoned that CO poisoning is most likely responsible for the low activities and ethylene *tri*-/*tetra*-merisation selectivities of the Cr^{I}-PCN systems and the different behaviour of these systems *vs*. the Cr^{III}-PCN systems. It is proposed that CO acts by blocking coordination sites at the Cr centre of the active catalysts in these systems thus preventing ethylene coordination. In comparison to the Cr^{I}/PCN-based ethylene oligomerisation systems, the analogous Cr^{I}/PNP systems reported in the literature that also contain CO,[6,7] exhibit modest activities and selectivities towards ethylene *tri*-/*tetra*-merisation. This implies that the poisoning effect of CO is greater felt by the Cr^{I}-PCN systems than the literature Cr^{I}-PNP systems.

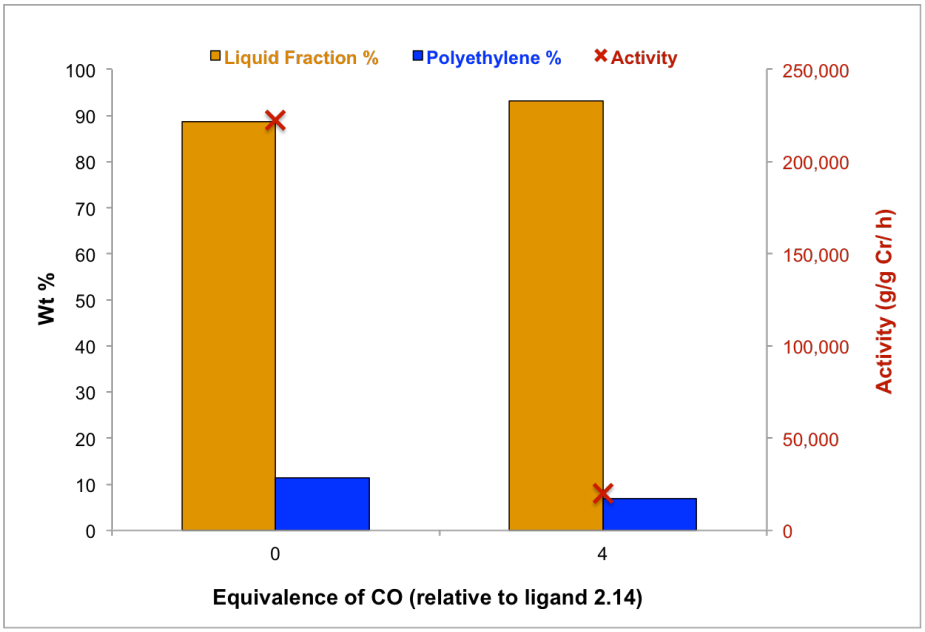

Graph 3.18: Effect of varying CO equivalence (relative to ligand **2.14**) on catalytic activities and polymer/oligomer formation of Cr/ligand **2.14** mediated ethylene oligomerisation catalysis. Conditions of ethylene oligomerisation catalysis: 5 µmol $Cr(acac)_3$, 1.2 eq. ligand **2.14**, 500 eq. MMAO-3A, 0.6 ppm O_2, 60 ^{o}C, 40 bar ethylene, PhCl, 10 min.

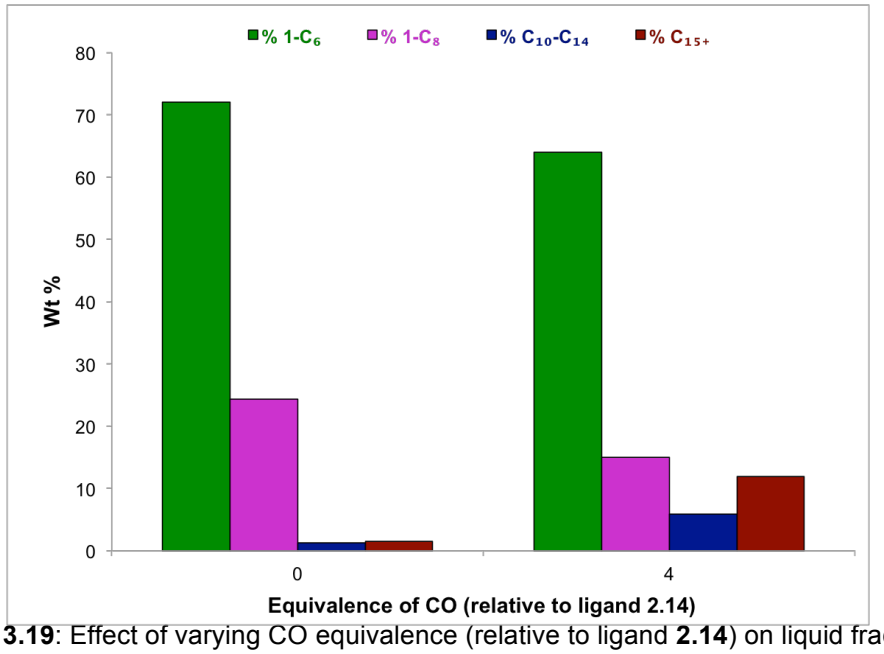

Graph 3.19: Effect of varying CO equivalence (relative to ligand **2.14**) on liquid fraction selectivity of Cr/ligand **2.14** mediated ethylene oligomerisation catalysis. Conditions of ethylene oligomerisation catalysis: 5 µmol $Cr(acac)_3$, 1.2 eq. ligand **2.14**, 500 eq. MMAO-3A, 0.6 ppm O_2, 60 °C, 40 bar ethylene, PhCl, 10 min.

3.5. Performance of Preformed Cr^{III}-PCN Complexes in Ethylene Oligomerisation Catalysis

The discrete Cr^{III}-PCN complexes **2.36** and **2.37** (Figure 3.9), described in Chapter 2 of this thesis, were tested in ethylene oligomerisation catalysis under the conditions detailed in Scheme 3.1(iii). Complexes **2.36** and **2.37** were found to give rise to ethylene oligomerisation systems with moderate activities, predominantly forming polymer (55 – 64%) and displaying little selectivity towards ethylene *tri*-/*tetra*-merisation (Graphs 3.20 and 3.21). The ethylene oligomerisation performance of complexes **2.36** and **2.37** is in line with that found for other preformed Cr^{III}-PCN complexes, tested in ethylene oligomerisation in previous work performed in the Dyer group,[1] which exhibited high levels of polymer formation (70 – 97%), moderate activities (14,589 – 57,872 g/g Cr/h), and negligible selectivity towards ethylene *tri*-/*tetra*-merisation (15 – 49% total liquid fraction selectivity to 1-C_6 + 1-C_8).

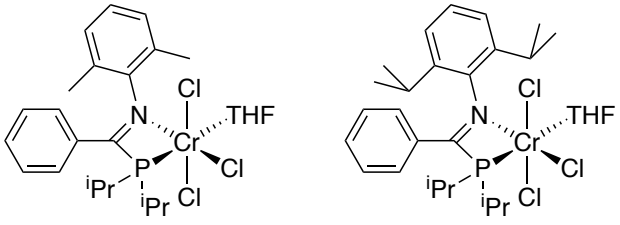

2.36 **2.37**

Figure 3.9: Cr^{III}-PCN complexes, **2.36** and **2.37**, tested in ethylene oligomerisation catalysis in this Chapter.

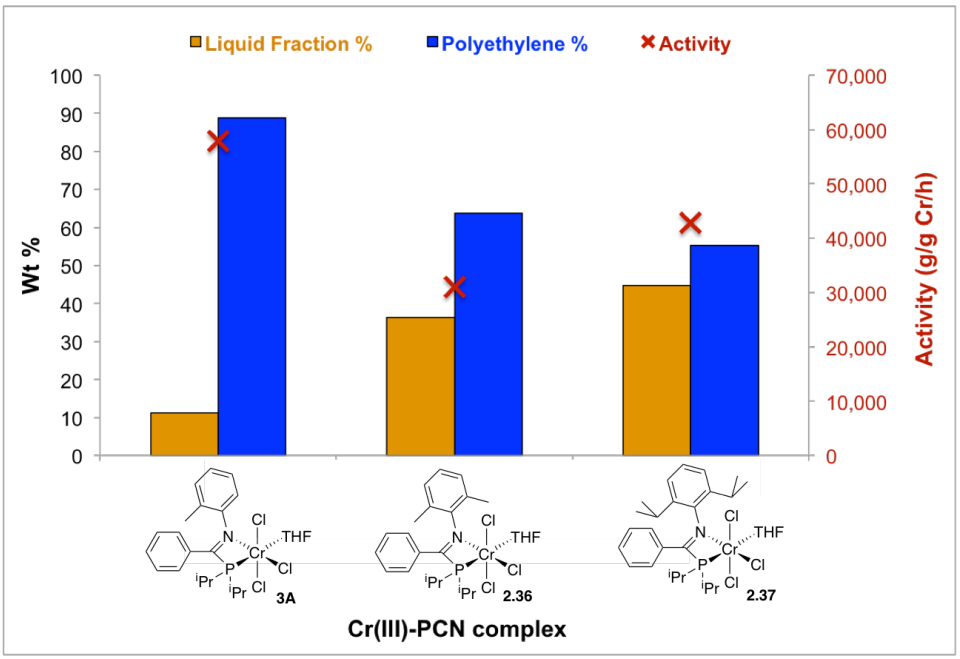

Graph 3.20: Catalytic activities and polymer/oligomer formation of Cr^{III}-PCN complexes[c] in ethylene oligomerisation. Conditions of ethylene oligomerisation catalysis: 5 µmol Cr(III)-PCN complex, 500 eq. MMAO-3A, 0.6 ppm O_2, 60 °C, 40 bar ethylene, PhCl, 10 min.

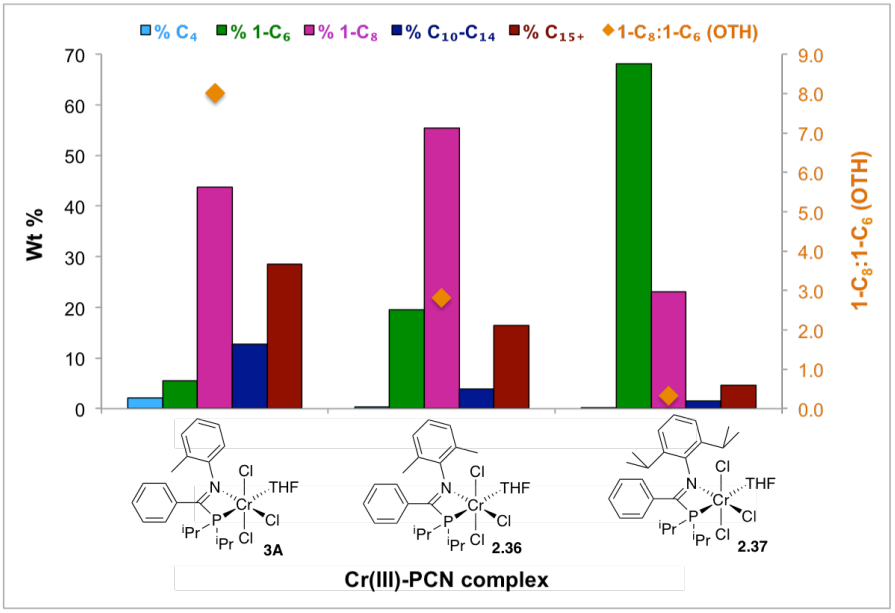

Graph 3.21: Liquid fraction selectivities of Cr^{III}-PCN complexes[c] in ethylene oligomerisation. Conditions of ethylene oligomerisation catalysis: 5 µmol Cr^{III}-PCN complex, 500 eq. MMAO-3A, 0.6 ppm O_2, 60 °C, 40 bar ethylene, PhCl, 10 min.

Additionally, on comparing the ethylene oligomerisation performance of complexes **2.36** and **2.37** to that of the Cr^{III}-PCN complex **3A**[c] shown in Graphs 3.20 and 3.21,

[c] Of the Cr^{III}-PCN complexes displayed in Graphs 3.20 and 3.21, only complexes **2.36** and **2.37** have been tested in ethylene oligomerisation catalysis in this thesis; the synthesis and testing of the Cr^{III}-PCN complex **3A** in ethylene oligomerisation was carried out in previous work conducted in the Dyer group and has been included in this work for comparison.[1]

which only differs in structure to complexes **2.36** and **2.37** by the nature of its N-substituent, trends can be seen between the performance of the complexes in catalysis and the steric bulk of their N-substituents. As the steric bulk of the substituents at nitrogen in the Cr^{III}-PCN complexes implemented in ethylene oligomerisation is increased, both the levels of polymer formation and OTH ratio are found to decrease. A decrease in OTH ratio with an increase in the N-steric bulk of the PCN ligand was also observed for the *in situ* generated Cr-PCN ethylene oligomerisation systems (section 3.3.1.3).

Further comparison of the ethylene oligomerisation performance of preformed Cr^{III}-PCN complexes **2.36** and **2.37** to that of their corresponding Cr-PCN complexes generated *in situ* (Graphs 3.22 and 3.23),[d] reveals that the catalysis mediated by the discrete complexes exhibits lower activities and higher levels of polymer formation than the catalysis using the *in situ* formed complexes. In order to obtain a more reliable comparison of the ethylene oligomerisation behaviour of preformed Cr^{III}-PCN complexes *vs.* their in-situ formed analogues, preformed and *in situ* formed Cr-PCN systems tested in ethylene oligomerisation catalysis in previous work conducted in the Dyer group[1] have also been included in Graphs 3.22 and 3.23.[d]

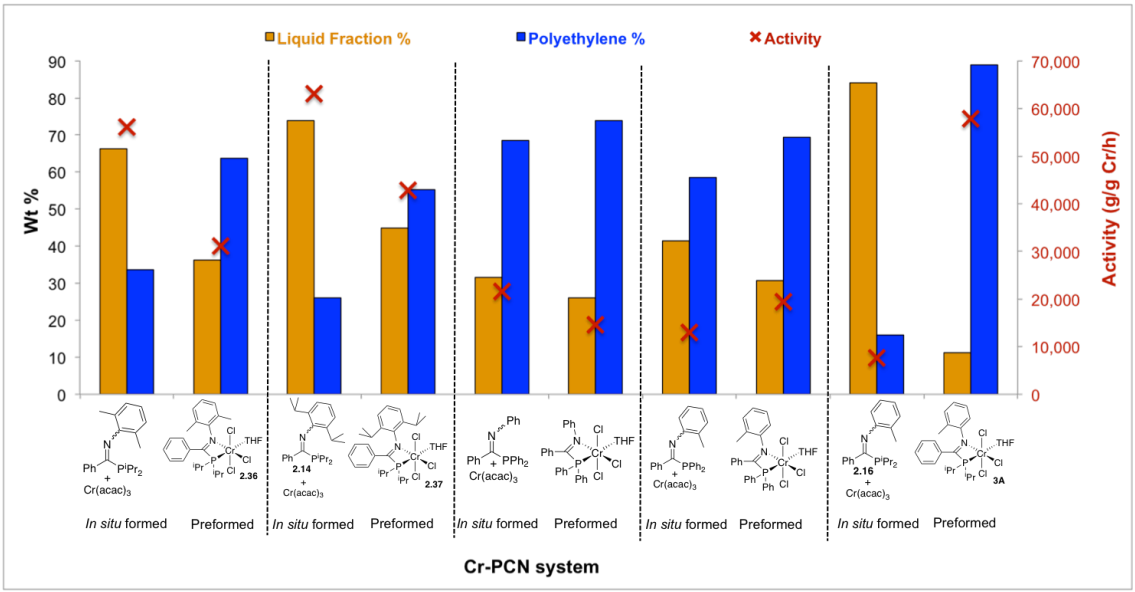

Graph 3.22*:* Comparison of catalytic activities and oligomer/polymer formation of Cr/PCN-based ethylene oligomerisation systems utilising *in situ* formed Cr-PCN complexes *vs.* preformed Cr^{III}-PCN complexes. Conditions of ethylene oligomerisation catalysis implementing 5 µmol $Cr(acac)_3$ and 1.2 eq. PCN ligand or 5 µmol Cr^{III}-PCN complex, 500 eq. MMAO-3A, 0.6 ppm O_2, 60 °C, 40 bar ethylene, PhCl, 10 min

[d] Of the data shown in Graphs 3.22 and 3.23, only ethylene oligomerisation catalysis using $Cr(acac)_3$ and ligand **2.14** or complexes **2.36** – **2.37** has been conducted in this work, all of the other data are from Cr/PCN-based ethylene oligomerisation catalysis performed in previous work conducted in the Dyer group and has been included in this work for comparison.[1]

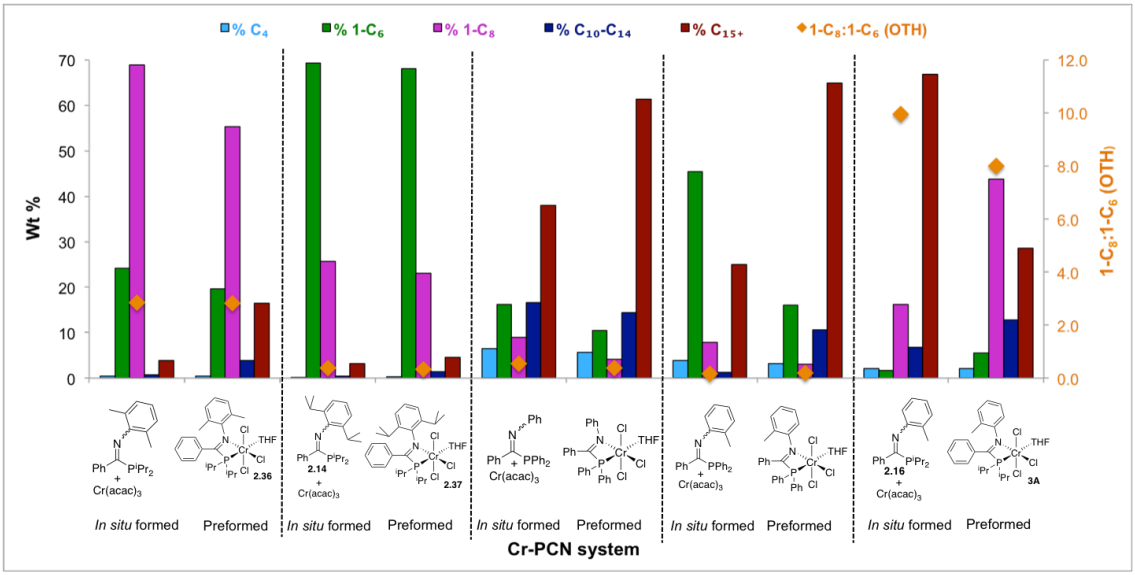

Graph 3.23: Comparison of liquid fraction selectivities of Cr/PCN-based ethylene oligomerisation systems utilising *in situ* formed Cr-PCN complexes *vs.* preformed Cr^{III}-PCN complexes. Conditions of ethylene oligomerisation catalysis implementing 5 µmol $Cr(acac)_3$ and 1.2 eq. PCN ligand or 5 µmol Cr^{III}-PCN complex, 500 eq. MMAO-3A, 0.6 ppm O_2, 60 ^{o}C, 40 bar ethylene, PhCl, 10 min

Overall, from the results shown in Graphs 3.22 and 3.23 it is clear that preformed Cr^{III}-PCN complexes behave differently in temrs of their catalytic ethylene oligomerisation performance compared to their *in situ*-formed analogues, with the majority of the systems utilising the *in situ* Cr-PCN complexes displaying better performance (*i.e.* higher activities, lower levels of polymer make, and higher total liquid fraction selectivities to 1-C_6 and 1-C_8). Notably, the nature of the Cr-ligand complex used (*i.e. in situ*-formed *vs*. preformed) is also found to affect the ethylene oligomerisation performance of a number of other systems disclosed in the literature,[19,26-32] where in some cases better ethylene oligomerisation systems are generated by the preformed Cr-ligand complexes (Figure 3.10)[19,26-28] whilst in others the *in situ* formed Cr-ligand complexes produce superior ethylene oligomerisation systems (Figure 3.11).[29-32]

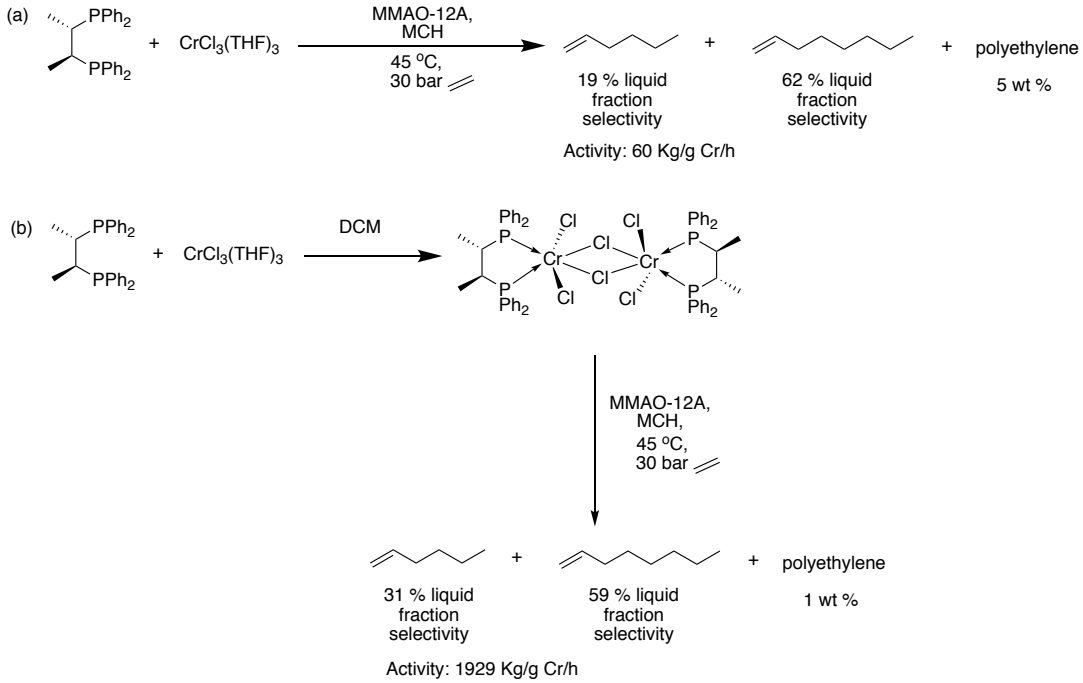

Figure 3.10: Comparison of using (a) *in situ versus* (b) preformed catalyst precursors in Cr-based ethylene *tri*-/*tetra*-merisation system reported by Cheong and Kang *et al.*[26]

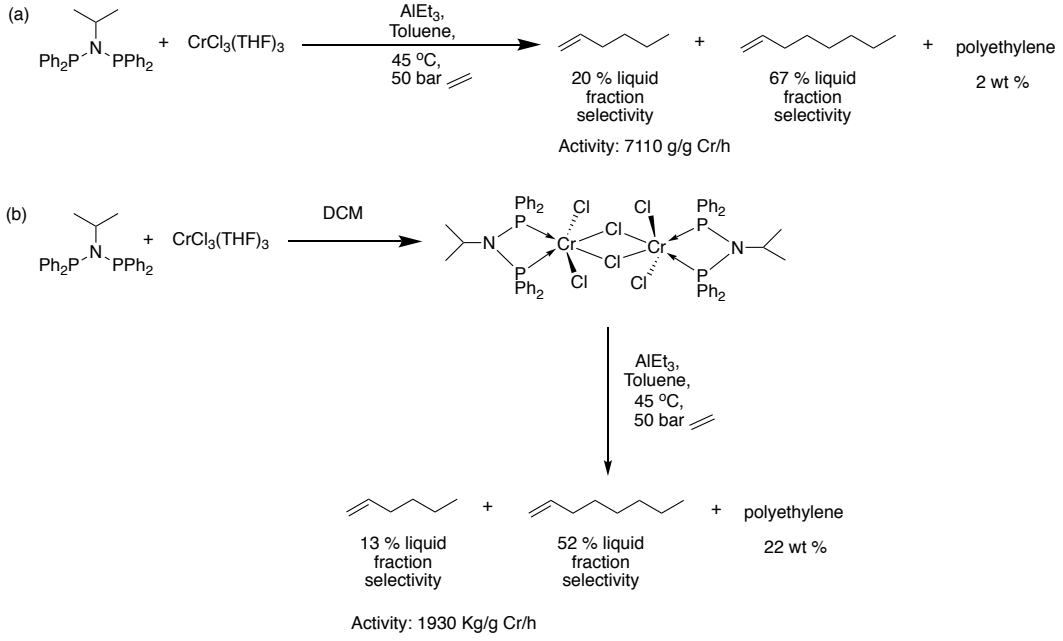

Figure 3.11: Comparison of using (a) *in situ versus* (b) preformed catalyst precursors in Cr-based ethylene *tri*-/*tetra*-merisation system reported by Overett *et al*.[30]

3.6. Summary and Conclusions

In this chapter the series of variously-substituted PCN ligands **2.1** – **2.13** were first tested in ethylene oligomerisation catalysis in order to establish their utility in combination with a source of Cr^{III} for ethylene *tri*-/*tetra*-merisation. Under the screening

conditions, Cr/PCN-based systems employing ligands **2.1**, **2.4**, **2.6** – **2.11** and **2.13** were found to give high total liquid fraction selectivities to 1-hexene and 1-octene (91 and 98%), comparable to some of the best-performing selective ethylene *tri*-/*tetra*-merisation systems described in the literature.[33-40] However, these systems also displayed lower activities and higher levels of polymer formation than those reported for the best literature systems.[33-40] Therefore, a selection of these new PCN ligands (**2.1** – **2.7**) were tested under optimised industrially-relevant conditions, something that led to improved activities and a decrease in the levels of polymer formed by the Cr/PCN-based ethylene oligomerisation systems, whilst maintaining their high total liquid fraction selectivities to 1-hexene and 1-octene. In particular, Cr/PCN-based ethylene oligomerisation systems using ligands **2.1**, **2.4** and **2.7** display activities (1686 – 3346 Kg/g Cr/h), levels of polymer formation (1 – 4%), and total liquid fraction selectivities to 1-hexene and 1-octene (97%), comparable to some of the best-performing selective ethylene *tri*-/*tetra*-merisation systems described in the literature.[33-40] Overall, out of the PCN ligands tested in this work and previous work in the Dyer group,[1] the Cr/ligand **2.7**-based catalytic system (Scheme 3.4(a)) is the best performing selective ethylene trimerisation system with an activity (3346 Kg/g Cr/h) and total liquid fraction selectivity to 1-hexene (95%) comparable to the Mitsubishi Phillips system,[4] albeit with a slightly higher level of polymer production (1.4%). In contrast, the Cr/ligand **2.6** variant (Scheme 3.4(b)) is the best-performing selective ethylene tetramerisation system, which achieves a similar selectivity to 1-octene (69%) as that given by the established Sasol Cr-PNP systems,[18,24] despite exhibiting a lower activity (886 Kg/g Cr/h) and higher levels of polymer formation (8%). Due to the high polymer formation exhibited by the best-performing Cr/PCN-based selective ethylene *tri*- and *tetra*-merisation systems, it is evident that further optimisation of the Cr-PCN systems is required in order to obtain industrially relevant systems.

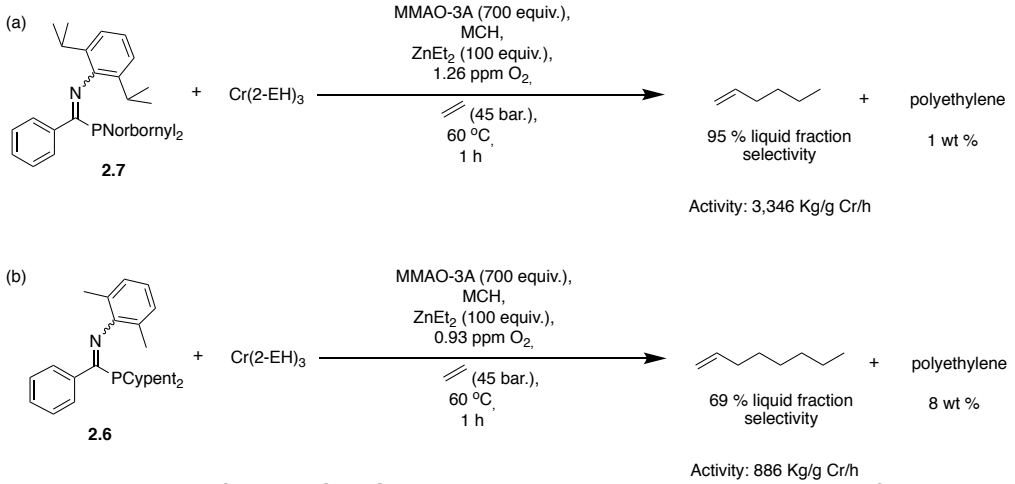

Scheme 3.4: Best-performing Cr/PCN-based systems developed in this work for (a) selective ethylene trimerisation (b) selective ethylene tetramerisation.

Further understanding of the structure-activity relationships of the Cr/PCN-based ethylene oligomerisation systems was also obtained. In agreement with previous work,[1,2] it was found that PCN ligands bearing bulky substituents at the phosphorus- and nitrogen-donor centres give rise to the best-performing ethylene oligomerisation systems, exhibiting high activities and low extents of polymer formation. In addition to finding that the steric bulk at the P and N positions of the PCN ligands could be used to tailor the OTH ratios of the Cr/PCN-based systems, it was also observed that manipulation of this ratio can also be achieved through modification of the electronic properties of the substituents at phosphorus and the imine carbon of the PCN ligands. Increasing the electron-withdrawing nature of the imine carbon substituents or phosphine substituents of the PCN ligands switched the selectivities of the Cr-based ethylene oligomerisation systems towards trimerisation. Additionally, the nature of the imine carbon substituents of the PCN ligands (alkyl *vs.* aryl) was also investigated. Utilising PCN ligands bearing aryl imine carbon substituents gives systems that display greater selectivities towards ethylene tetramerisation than their alkyl-substituted counterparts.

Finally, the performance of preformed Cr-PCN complexes in catalytic ethylene oligomerisation was evaluated. Cr^{I}-PCN complexes **2.26** – **2.30** were tested and found to behave poorly giving rise to low activities, high levels of polymer formation, and low selectivity towards 1-hexene and 1-octene; this contrasts to the selective ethylene *tri-*/*tetra*-merisation behaviour observed for Cr^{I}-PNP complexes.[6,7] The poor performance of complexes **2.26** – **2.30** in ethylene oligomerisation is proposed to be due to the presence of CO that acts as a potent poison in Cr/PCN-based ethylene oligomerisation catalyst systems blocking ethylene coordination at Cr. Cr^{III}-PCN complexes, **2.36** and **2.37**, were also tested for their ethylene oligomerisation behaviour and gave similar performance to that achieved using the preformed Cr^{III}-PCN complexes tested in previous work.[1] A comparison of the ethylene oligomerisation behaviour of the preformed Cr^{III}-PCN complexes, **2.36** and **2.37**, to that of their *in situ* formed analogues showed that systems utilising the preformed complexes exhibit lower activities, higher polymer levels, and lower total liquid fraction selectivities to 1-hexene and 1-octene.

3.7. Future Work and Outlook

In this Chapter, much work has been done in investigating the use of different PCN ligands and catalyst precursors of different oxidation states in Cr/PCN-based ethylene oligomerisation, with a thorough understanding being established. The biggest

challenge remains in reducing the level of polyethylene produced in the Cr/PCN-based selective ethylene *tri-*/*tetra*-merisation systems, which although reasonably low, is still not acceptable industrially. However, following preliminary attempts in this regard, it is unclear how this may be achieved. Additionally, the dependence of these Cr/PCN systems on low levels of oxygen is intriguing. Further work needs to be conducted here to explore this phenomenon, in particular looking at generating and isolating oxo-complexes of the Cr/PCN precursors and examining their role (if any) in catalysis. Alternatively, the redox chemistry of these systems needs to be investigated to probe changes occurring under catalytic conditions using chemical oxidants.

3.8. References

1 J. E. Radcliffe, PhD Thesis, Durham University, 2015.
2 J. E. Radcliffe, A. S. Batsanov, D. M. Smith, J. A. Scott, P. W. Dyer and M. J. Hanton, *ACS Catal.*, 2015, **5**, 7095–7098.
3 M. J. Hanton, D. M. Smith, W. F. Gabrielli and S. J. Evans, WO 2013/168103 A1, Sasol Technology Limited, 14 Nov 2013.
4 M. J. Hanton, D. M. Smith, W. F. Gabrielli and M. W. Kelly, WO 2011/048527 A1, Sasol Technology Limited, 28 April 2011.
5 M. van Meurs, G. J. P. Britovsek, V. C. Gibson and S. A. Cohen, *J. Am. Chem. Soc.*, 2005, **127**, 9913–9923.
6 A. J. Rucklidge, D. S. McGuinness, R. P. Tooze, A. M. Z. Slawin, J. D. A. Pelletier, M. J. Hanton and P. B. Webb, *Organometallics*, 2007, **26**, 2782–2787.
7 L. E. Bowen, M. F. Haddow, A. G. Orpen and D. F. Wass, *Dalton Trans.*, 2007, **689**, 1160–1169.
8 L. McDyre, E. Carter, K. J. Cavell, D. M. Murphy, J. A. Platts, K. Sampford, B. D. Ward, W. F. Gabrielli, M. J. Hanton and D. M. Smith, *Organometallics*, 2011, **30**, 4505–4508.
9 E. Carter, K. J. Cavell, W. F. Gabrielli, M. J. Hanton, A. J. Hallett, L. McDyre, J. A. Platts, D. M. Smith and D. M. Murphy, *Organometallics*, 2013, **32**, 1924–1931.
10 J. R. Briggs, *J. Chem. Soc., Chem. Commun.*, 1989, 674–675.
11 M. J. Overett, K. Blann, A. Bollmann, J. T. Dixon, D. Haasbroek, E. Killian, H. Maumela, D. S. McGuinness and D. H. Morgan, *J. Am. Chem. Soc.*, 2005, **127**, 10723–10730.
12 K. Blann, A. Bollmann, J. T. Dixon, F. M. Hess, E. Killian, H. Maumela, D. H. Morgan, A. Neveling, S. Otto and M. J. Overett, *Chem. Commun.*, 2005, **30**, 620–621.
13 M. J. Overett, K. Blann, A. Bollmann, J. T. Dixon, F. Hess, E. Killian, H. Maumela, D. H. Morgan, A. Neveling and S. Otto, *Chem. Commun.*, 2005, 622–624.
14 C. Klemps, E. Payet, L. Magna, L. Saussine, X. F. Le Goff and P. Le Floch, *Chem. Eur. J.*, 2009, **15**, 8259–8268.
15 O. L. Sydora, T. C. Jones, B. L. Small, A. J. Nett, A. A. Fischer and M. J. Carney, *ACS Catal.*, 2012, **2**, 2452–2455.
16 E. Killian, K. Blann, A. Bollmann, J. T. Dixon, S. Kuhlmann, M. C. Maumela, H. Maumela, D. H. Morgan, P. Nongodlwana, M. J. Overett, M. Pretorius, K. Höfener and P. Wasserscheid, *J. Mol. Catal. A-Chem.*, 2007, **270**, 214–218.
17 T. Jiang, H. Chen, C. Cao, G. Mao and Y. Ning, *Chin. Sci. Bull.*, 2010, **55**, 3750–3754.
18 S. Kuhlmann, K. Blann, A. Bollmann, J. Dixon, E. Killian, M. Maumela, H. Maumela, D. H. Morgan, M. Pretorius, N. Taccardi and P. Wasserscheid, *J.*

Catal., 2007, **245**, 279–284.
19 K. Blann, A. Bollmann, H. de Bod, J. Dixon, E. Killian, P. Nongodlwana, M. Maumela, H. Maumela, A. E. McConnell, D. H. Morgan, M. J. Overett, M. Pretorius, S. Kuhlmann and P. Wasserscheid, *J. Catal.*, 2007, **249**, 244–249.
20 T. Jiang, S. Zhang, X. Jiang, C. Yang, B. Niu and Y. Ning, *J. Mol. Catal. A-Chem.*, 2008, **279**, 90–93.
21 T. E. Stennett, T. W. Hey, L. T. Ball, S. R. Flynn, J. E. Radcliffe, C. L. McMullin, R. L. Wingad and D. F. Wass, *ChemCatChem*, 2013, **5**, 2946–2954.
22 J. A. Suttil, P. Wasserscheid, D. S. McGuinness, M. G. Gardiner and S. J. Evans, *Catal. Sci. Technol.*, 2014, **4**, 2574–2588.
23 Y. Araki, H. Nakamura, Y. Nanba and T. Okano, US 5856612, Mitsubishi Chemical Corporation, 5 Jan 1999.
24 M. C. Maumela, M. M. Mogorosi, M. S. Mokhadinyana, M. J. Overett, K. Blann and C. W. Holzapfel, WO 2014/181247 A1, Sasol Technology Limited, 13 November 2014.
25 A. Dulai, H. de Bod, M. J. Hanton, D. M. Smith, S. Downing, S. M. Mansell and D. F. Wass, *Organometallics*, 2009, **28**, 4613–4616.
26 S.-K. Kim, T.-J. Kim, J.-H. Chung, T.-K. Hahn, S.-S. Chae, H.-S. Lee, M. Cheong and S. O. Kang, *Organometallics*, 2010, **29**, 5805–5811.
27 M. J. Overett, K. Blann, A. Bollmann, R. de Villiers, J. T. Dixon, E. Killian, M. C. Maumela, H. Maumela, D. S. McGuinness, D. H. Morgan, A. Rucklidge and A. M. Z. Slawin, *J. Mol. Catal. A-Chem.*, 2008, **283**, 114–119.
28 O. L. Sydora, M. Carney, B. L. Small, J. C. Gee and S. Hutchison, US 8,680,003 B2, Chevron Phillips Chemical Company LP, 25 Mar 2014.
29 A. Bollmann, K. Blann, J. T. Dixon, F. M. Hess, E. Killian, H. Maumela, D. S. McGuinness, D. H. Morgan, A. Neveling, S. Otto, M. Overett, A. M. Z. Slawin, P. Wasserscheid and S. Kuhlmann, *J. Am. Chem. Soc.*, 2004, **126**, 14712–14713.
30 D. S. McGuinness, M. Overett, R. P. Tooze, K. Blann, J. T. Dixon and A. M. Z. Slawin, *Organometallics*, 2007, **26**, 1108–1111.
31 Z. Weng, S. Teo and T. S. Andy Hor, *Dalton Trans.*, 2007, 3493–3498.
32 A. Jabri, P. Crewdson, S. Gambarotta, I. Korobkov and R. Duchateau, *Organometallics*, 2006, **25**, 715–718.
33 J. T. Dixon, M. J. Green, F. M. Hess and D. H. Morgan, *J. Organomet. Chem.*, 2004, **689**, 3641–3668.
34 D. F. Wass, *Dalt. Trans.*, 2007, 816–819.
35 P. W. N. M. van Leeuwen, N. D. Clément and M. J. L. Tschan, *Coord. Chem. Rev.*, 2011, **255**, 1499–1517.
36 T. Agapie, *Coord. Chem. Rev.*, 2011, **255**, 861–880.
37 D. S. McGuinness, *Chem. Rev.*, 2011, **111**, 2321–2341.
38 F. Zhu, L. Wang and H. Yu, *des monomers polym.*, 2011, **14**, 1–23.
39 G. P. Belov, *Pet. Chem.*, 2012, **52**, 139–154.
40 K. A. Alferov, G. P. Belov and Y. Meng, *Appl. Catal. A Gen.*, 2017, **542**, 71–124.

Chapter 4:
Investigating the Catalytic Dimerisation of Linear α-olefins to Yield Linear α-olefins

4.1. Introduction

This Chapter is concerned with the catalytic dimerisation of linear α-olefins (LAOs) heavier than ethylene to their respective LAO dimers, by investigation of the selective LAO dimerisation catalysis system reported by Broene *et al*.[1] As mentioned previously in Chapter 1, selective LAO dimerisation catalysis is an important avenue of research due to its:

(a) potential for converting underexploited 1-propene and 1-butene, produced in large volumes in Fischer-Tropsch synthesis, to highly in-demand 1-hexene and 1-octene (for use as co-monomers in LDPE and HDPE manufacture);

(b) application in converting odd-numbered α-olefins (of limited use industrially) into even-numbered α-olefins.

The chapter starts with a brief literature review of homogeneous LAO selective dimerisation catalysis, considering the mechanistic details and evaluating selective LAO dimerisation catalysis systems reported in the literature. Subsequently, the chapter describes our work to better understand the Cp^*Co^I cation-based system reported by Broene *et al*.[1]

4.1.1. Mechanism of transition metal catalysed olefin dimerisation

This section reviews the two most commonly accepted mechanisms for transition metal catalysed olefin dimerisation and the factors controlling the processes' regioselectivity. It should be noted that although the mechanisms in this section have only been illustrated for ethylene dimerisation, the same mechanisms are believed to be operative in the catalytic dimerisation of heavier α-olefins (such as 1-propene and 1-butene).

4.1.1.1. The Cossee-Arlmann mechanism (step-wise addition)

The step-wise addition mechanism, first introduced by Cossee and Arlmann in 1964,[2,3] is widely believed to be in operation for the dimerisation, oligomerisation and polymerisation of olefins.[4,5] A simplified version of the Cossee-Arlmann mechanism for ethylene oligomerisation has previously been shown and described in Chapter 1 (section 1.2.1, Scheme 1.1). A more relevant version of the Cossee-Arlmann mechanism for ethylene dimerisation is shown in Scheme 4.1 (where the active species has been shown as a metal hydride species, but could also be a metal alkyl species (Chapter 1, section 1.2.1)).

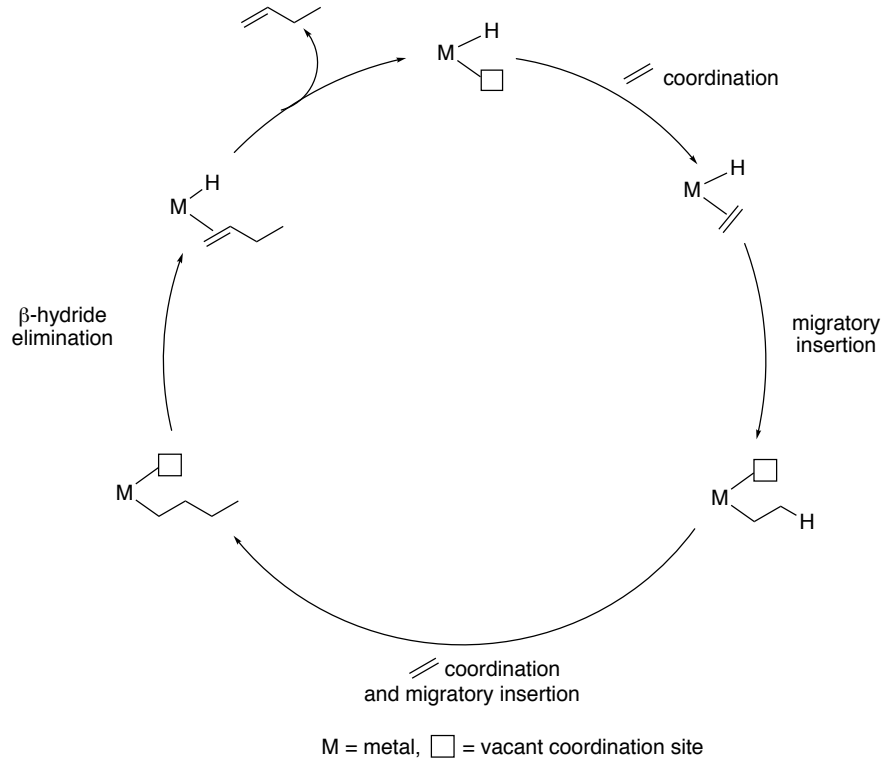

Scheme 4.1: Proposed Cossee-Arlmann mechanism for ethylene dimerisation, modified from Skupinska, 1991.[4]

The Cossee-Arlmann mechanism is selective towards olefin dimerisation, instead of oligomerisation or polymerisation, when the rate of chain termination (*via* β-hydride elimination, Scheme 4.1) is significantly greater than the rate of chain propagation (*via* consecutive olefin coordination and insertion, Scheme 4.1).[4] As mentioned previously in Chapter 1 (section 1.2.1), the relative rates of chain propagation and termination are dictated by the process conditions.

A key feature of the Cossee-Arlmann mechanism, which impacts the selectivity of the dimerisation processes towards the LAO dimer, is the process of chain walking (Scheme 4.2).[6] The process of chain-walking involves β-hydride elimination from a metal alkyl species and subsequent reinsertion of the alkene into the metal hydrogen bond, at a different position on the alkene, (Scheme 4.2: species **4A** (metal coordinated to the first carbon of the alkyl chain) is transformed into species **4B** (metal coordinated to second carbon of the alkyl chain) by process of chain-walking).[6,7] The implications of chain walking are significant, as the process shifts the orientation of the alkyl group coordinated to the metal centre, enabling the formation of linear and branched α-olefins.

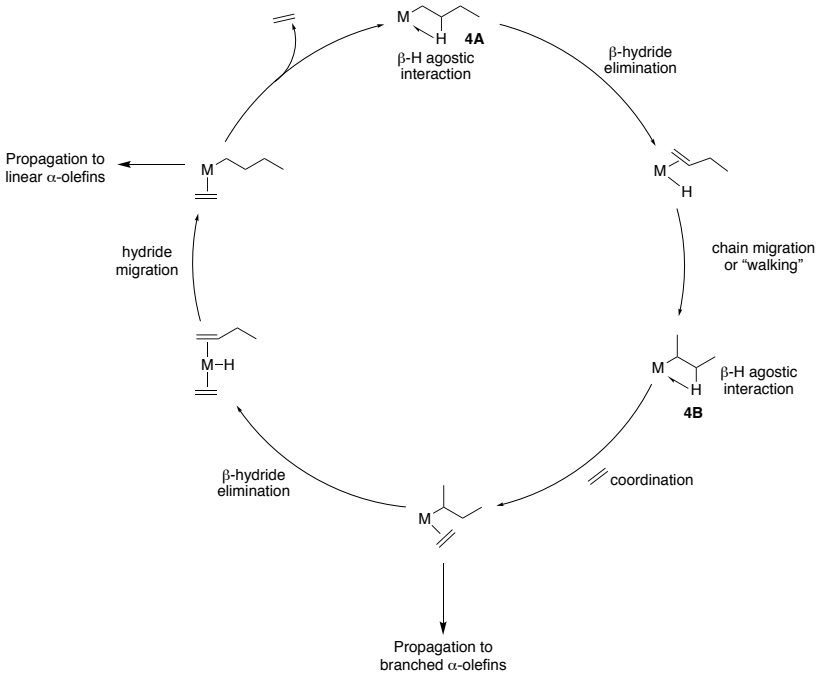

Scheme 4.2: Chain-walking process in operation during Cossee-Arlmann mechanism, modified from Hanton.[8]

4.1.1.2. The metallacycle mechanism

The metallacycle mechanism, which is well established to be in operation for selective ethylene *tri*-/*tetra*-merisation systems (Chapter 2, section 2.1.3), is also believed to be operative for LAO dimerisation systems (Scheme 4.3).[5,9] The selectivity of the metallacycle-mediated process towards LAO dimerisation is dictated by the relative stability of the metallacycloalkane species involved, specifically their disposition towards direct evolution to other species or their growth *via* ethylene insertion.[9] The stability of the metallacycloalkane species generally decreases as its size increases, hence metallacycle-mediated ethylene oligomerisation processes are typically more selective towards *tri*-/*tetra*-merisation than dimerisation.[9,10]

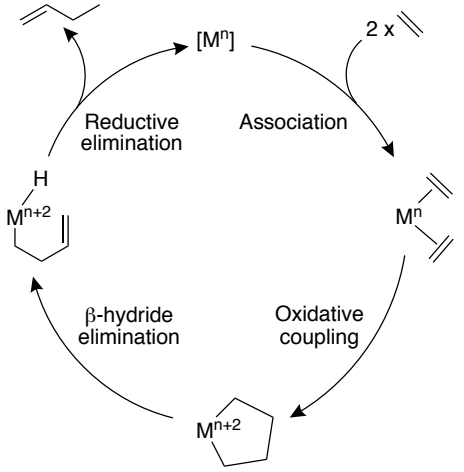

Scheme 4.3: Proposed metallacycle mechanism for ethylene dimerisation, modified from McGuinness *et al.*, where M represents a transition metal.[9]

Nevertheless the selectivity of metallacycle-mediated ethylene oligomerisation processes may be shifted towards LAO dimerisation by changing the steric and electronic demands about the metal centre of the catalyst. For example, a computational study on a ethylene trimerisation catalyst consisting of $Cr(EH)_3$, a dimethoxyethane (DME) ligand, and a partially-hydrolysed isobutyl aluminium oxide (PIBAO) activator, revealed that DME coordination led to ethylene dimerisation as a side reaction (Scheme 4.4).[11] It was postulated that both the weak electron-donating properties and steric bulk of DME caused the total energy barrier to metallacycloheptane formation (from which 1-hexene is obtained) to increase, resulting in the lower energy pathway that gives rise to formation of 1-butene.[11]

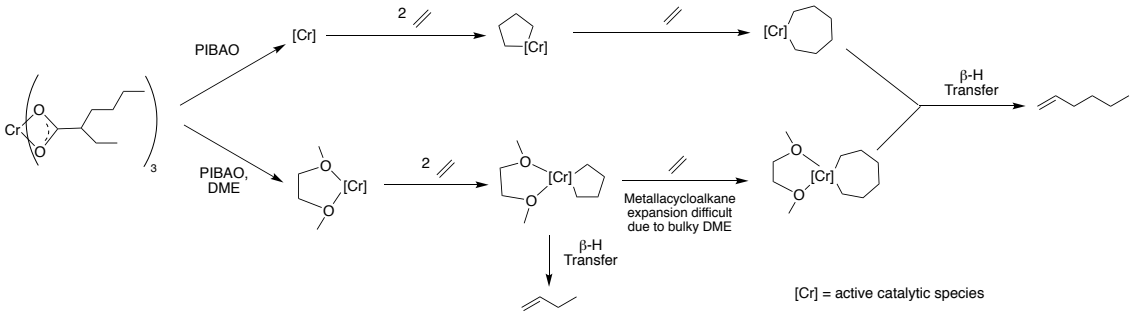

Scheme 4.4: Influence of DME on ethylene trimerisation catalysed by $Cr(EH)_3$ and PIBAO activator.[11]

4.1.1.3. Distinguishing between step-wise and metallacycle mechanisms

One of the most robust techniques employed for unambiguously elucidating the mechanism in operation in LAO oligomerisation processes (*i.e.* Cossee-Arlmann or metallacycle) is deuterium labelling studies. The deuterium labelling studies were originally developed by Bercaw and Labinger *et al*.[12] with a view to elucidating the mechanism for Cr/PNP-based selective ethylene trimerisation (Chapter 2, section 2.1.3.1). Since then, this approach has been implemented in mechanistic investigations of various dimerisation,[13,14] *tri*-/*tetra*-merisation (see Chapter 2, section 2.1.3.2 for an example),[15-18] and oligomerisation systems.[19-22]

In these deuterium labeling experiments the weight distribution of isotopomer oligomers, formed from transition metal-catalysed oligomerisation of a 1:1 mixture of the monomer and its deuterated analogue, respectively, are examined.[12] Isotopomers produced *via* a Cossee-Arlmann mechanism will contain either odd or even numbers of deuterons, since in this mechanism the isotopomer is released *via* β-H/D elimination leaving an eliminated proton or deuteron on the metal centre, resulting in H/D scrambling (Scheme 4.5).[12] In contrast, only isotopomers containing even numbers of deuterons will be formed in a metallacycle-mediated process; here, in this process

reductive elimination occurs after β-H/D elimination, hence H/D scrambling is absent (Scheme 4.6).[12]

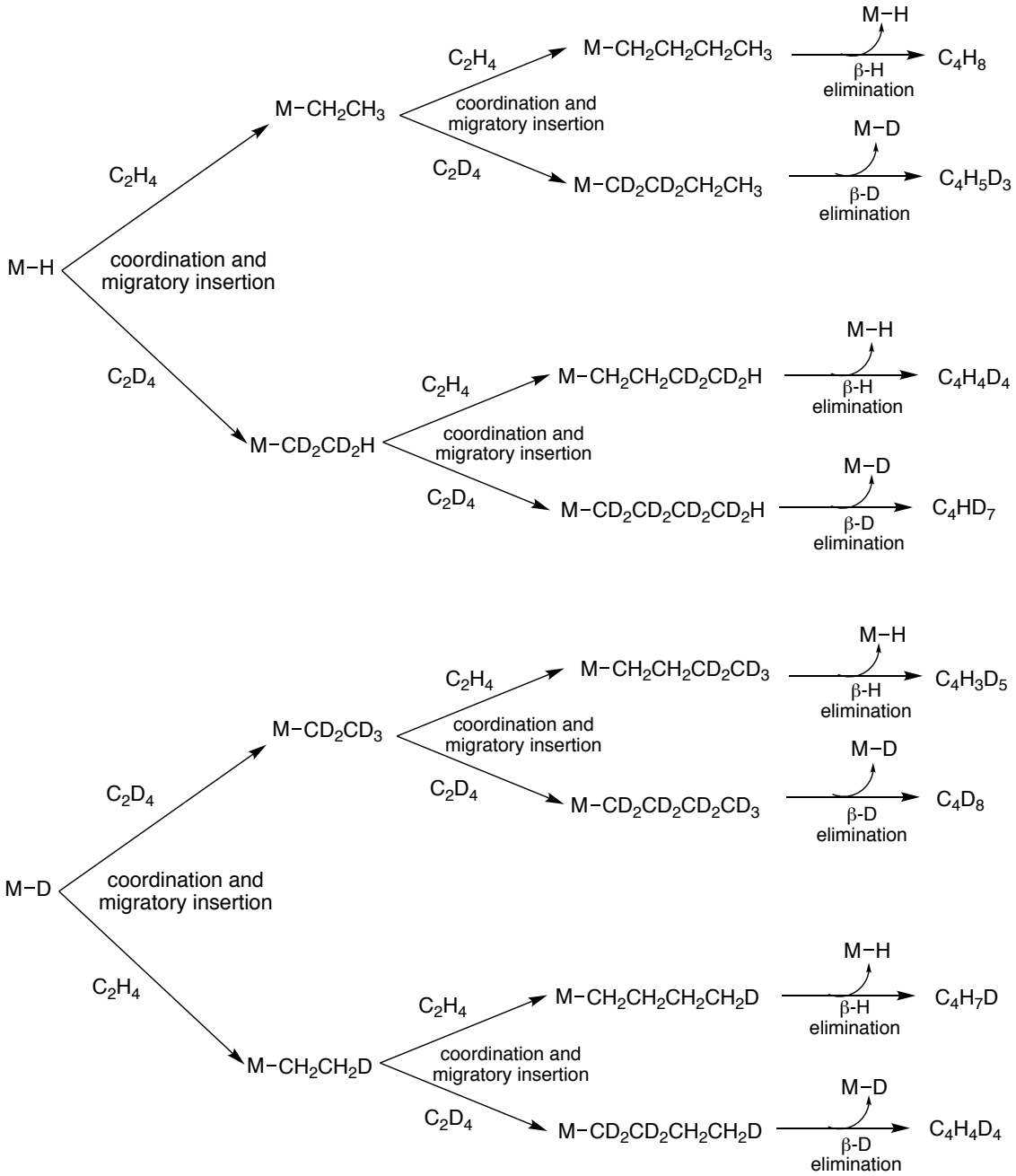

Scheme 4.5: Isotopomers expected from catalytic dimerisation of 1:1 mixture of C_2H_4:C_2D_4, proceeding *via* a Cossee-Arlmann-type mechanism (where M-H/D = catalytically active species and M= transition metal).[15]

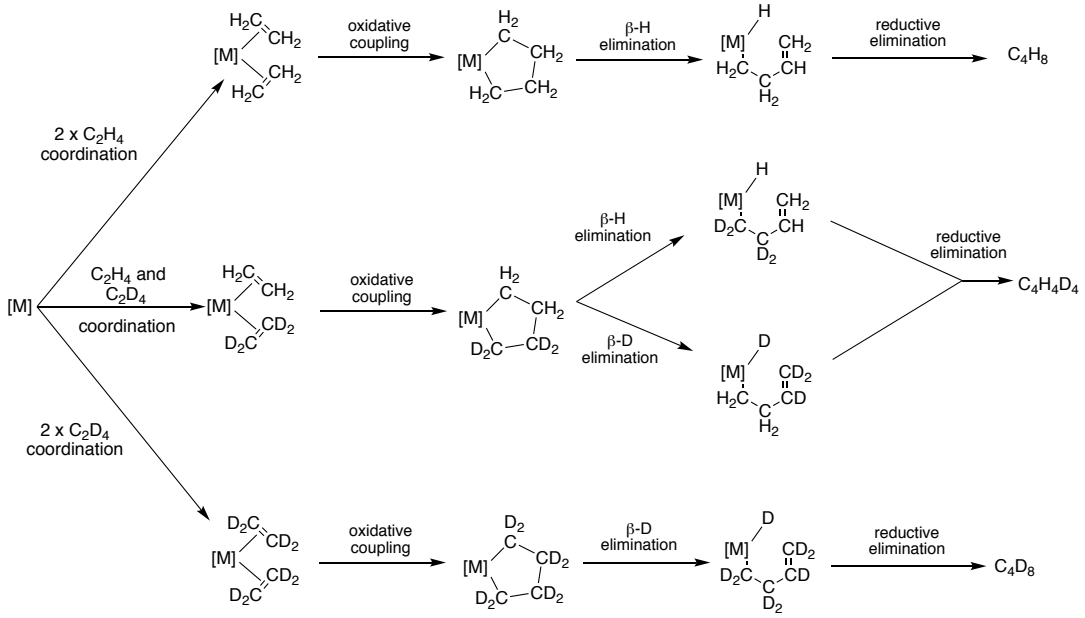

Scheme 4.6: Isotopomers expected from catalytic dimerisation of 1:1 mixture of C_2H_4:C_2D_4, proceeding *via* a metallacycle pathway.[15]

4.1.1.4. Regioselectivity of olefin dimerisation

The orientation with which two α-olefins combine (*i.e.* regioselectivity) in the Cossee-Arlmann or metallacycle mechanisms is important since it determines the linearity and position of the double bond of the resulting dimer. For an unsymmetrically-substituted α-olefin (*i.e.* any olefin heavier than ethylene) coordination to the catalytic metal centre can occur at either carbon atom of the double bond, resulting in the formation of different linear and branched dimer products (Scheme 4.7).[23,24] Although Scheme 4.7 demonstrates a catalytic dimerisation process proceeding *via* a Cossee-Arlmann mechanism, it should be noted that the same isomeric mixture of branched and internal olefins (see Scheme 4.7) would also be obtained in a dimerisation process mediated by a metallacycle mechanism as 1,2- and 2,1-insertions of the olefin substrates are also possible in this mechanism.

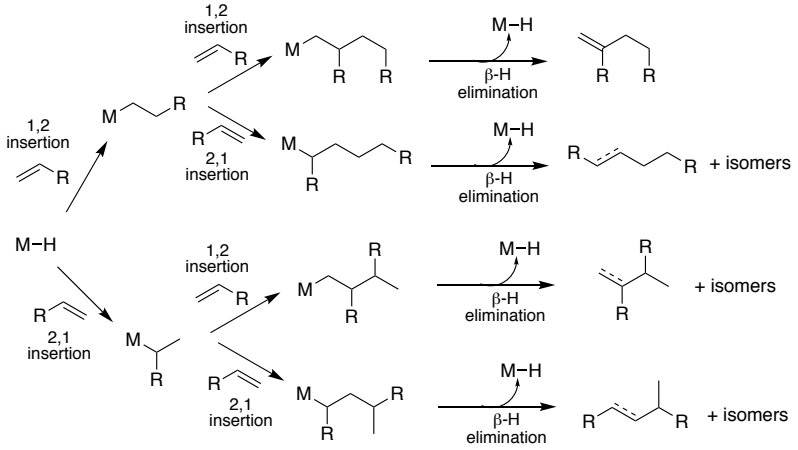

Scheme 4.7: Different reaction pathways in olefin dimerisation, proceeding *via* Cossee-Arlmann mechanism (M-H = catalytically active species, M = transition metal, R = alkyl group); modified from Forestière *et al.*[23]

It is demonstrated in Scheme 4.7 that branched dimers are the major products formed in catalytic dimerisation processes, with linear dimers only being obtained when a head-to-head insertion of the olefinic substrate occurs (*i.e.* the first olefin inserts in a 1,2-fashion and the second olefin undergoes a 2,1-insertion).[23,24] In addition, it is inherently the thermodynamically favoured internal linear olefin dimer that is formed in preference to the LAO dimer, which makes the synthesis of LAO dimers by catalytic dimerisation challenging.[23,24] Thus, to obtain the desired LAO dimer in a catalytic dimerisation process, a transition metal catalyst is required that encourages a head-to-head insertion and subsequent isomerisation of the linear internal olefin to the target LAO dimer.

4.1.2. Processes competing with dimerisation

It is important to consider other factors, in addition to regioselectivity, which affect the selectivity of a dimerisation catalyst in order to ensure that the desired LAO dimer product is maximised. The most common processes that may compete with, and therefore reduce, the selectivity of transition metal-catalysed dimerisation towards the LAO dimer are isomerisation to internal olefins and substrate-oligomer co-dimerisation;[23] each of these processes will be subsequently discussed in turn.

4.1.2.1.1. Isomerisation of LAO to internal olefin

Olefin isomerisation involves the migration of the olefinic double bond of the substrate along the carbon chain to form (usually) the thermodynamically more stable internal olefin.[25] This olefin isomerisation is not only detrimental as it reduces the selectivity towards the desired LAO dimer, but may also decrease the dimerisation conversion of the starting α-olefin as a result of its isomerisation to the internal olefin.

There are two mechanisms by which olefin isomerisation occurs, a hydride-mediated mechanism or an allyl-mediated mechanism.[25] The active site in the metal hydride-mediated mechanism of olefin isomerisation is identical to the catalytically-active species in metal hydride-mediated step-wise addition dimerisation (Scheme 4.1): a metal hydride species with a vacant site *cis* to the hydride.[25] This "hydride" pathway, illustrated in Scheme 4.8, proceeds *via* the coordination of an olefin at a vacant site on the metal hydride species, which is followed by migratory insertion, resulting in the formation of a secondary metal-alkyl intermediate.[25] β-Hydride elimination from the secondary metal-alkyl intermediate generates the isomerised internal olefin and regenerates the metal hydride species.[25] The disposition towards olefin isomerisation *via* the metal hydride-mediated mechanism is high due to the relative rates of olefin insertion into M-H bonds being 10^5 times faster than olefin insertion into M-C bonds.[24]

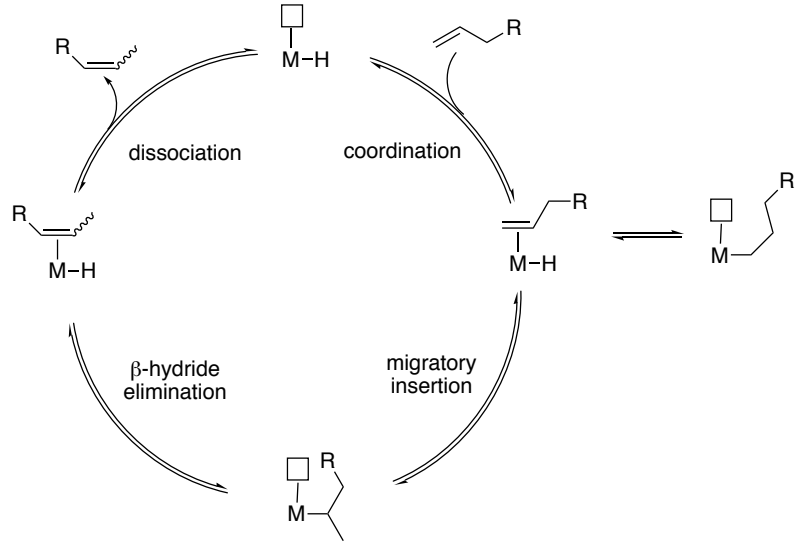

M= transition metal, R= alkyl group, □ = vacant coordination site

Scheme 4.8: Mechanism of metal hydride-mediated olefin isomerisation, modified from Crabtree.[25]

The second mechanism by which olefin isomerisation may occur is allyl-mediated and contains an active site comprising of a metal, which has two vacant sites *cis* to each other; identical to the active site found in metallacylic-based dimerisation (Scheme 4.3).[25] The allyl-mediated isomerisation pathway involves coordination of an olefin at one of the vacant sites on the metal, with the C-H bond at the activated allylic position of the olefin then undergoing oxidative addition to the metal, leading to the formation of an η^3-allyl intermediate and an M-H bond.[25] Finally, reductive elimination results in the formation of the isomerised internal olefin.[25]

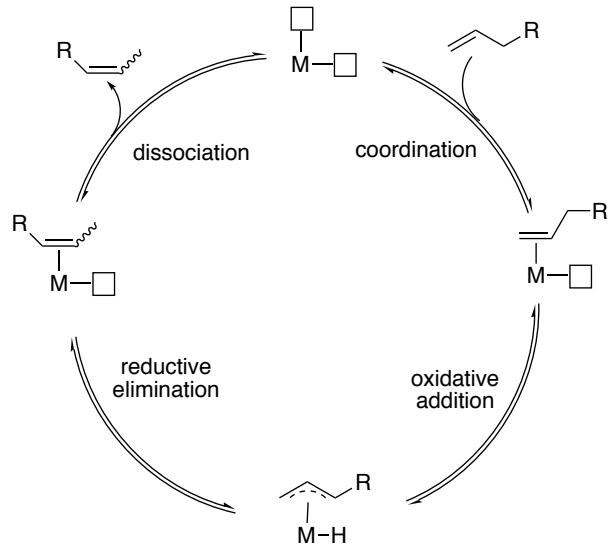

M= transition metal, R= alkyl group, □ = vacant coordination site

Scheme 4.9: Mechanism of allyl-mediated olefin isomerisation, modified from Crabtree.[25]

4.1.2.1.2. Substrate-oligomer co-dimerisation

In catalytic olefin dimerisation processes, the desired LAO dimer product formed may be consumed by re-entering the catalytic cycle and undergoing co-dimerisation with the olefinic substrate.[23,26] For example, in the Alphabutol process, a well-established commercial selective ethylene dimerisation process that utilises a titanium-based catalyst and $AlEt_3$ activator, the selective formation of 1-butene is accompanied by the formation of a small amount of hexene byproducts (which account for 5 – 8 % of the converted ethylene).[23,26] The observed formation of the hexene byproducts is believed to arise from the reactions portrayed in Scheme 4.17, whereby 1-butene that is formed undergoes co-dimerisation with ethylene, resulting in the formation of five different hexenes.[23,26]

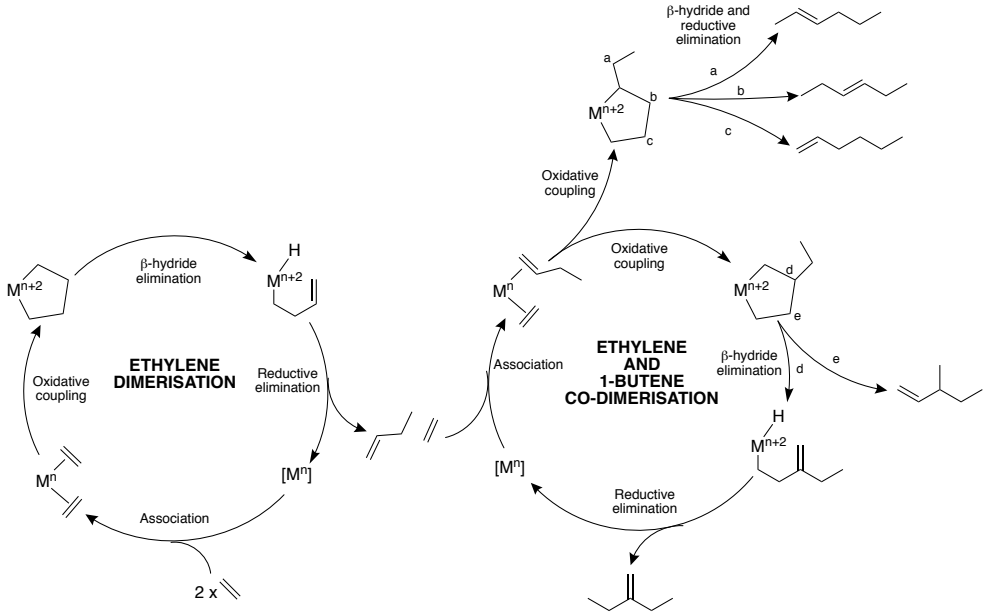

Scheme 4.10: Proposed example of 1-butene co-dimerisation with ethylene in a metallacycle-mediated ethylene dimerisation process, where M represents a transition metal, modified from Forestière *et al.*[23]

4.1.3. Literature LAO dimerisation systems

The development of catalytic olefin dimerisation processes is an area of significant academic and industrial interest due to these processes supplying higher olefins that are important building blocks for the chemical industry.[4,5,23,27] For example, olefin dimerisation can yield commercially valuable LAOs (see Chapter 1 section 1.1), linear internal olefins (utilised in the production of detergents) and branched dimeric products (implemented in production of fuel additives and synthetic oils).[4,5,23,27] Although the work in this Chapter is focused on the catalytic dimerisation of LAOs heavier than ethylene, it is important to note that there has been much research effort and success in the development of catalytic selective ethylene dimerisation processes for the production of the LAO dimer (1-butene); example shown in Scheme 4.11.[4,9,28]

However, there are significantly fewer literature studies on the development of catalyst systems capable of transforming LAOs heavier than ethylene to their respective LAO dimers, with only a handful of the systems reported producing linear olefins as the major products.[4,5,23] This observed disparity between the success in producing LAO dimers from ethylene *versus* heavier LAOs is most likely due to the greater propensity of heavier LAOs to participate in isomerisation reactions, as a result of their increased steric bulk (discussed in section 4.1.2.1.1).[4] For the purposes of this literature review, only α-olefin dimerisation systems utilising olefinic substrates heavier than ethylene and displaying selectivity towards LAO dimeric products will be considered, as this is where the interest of the work in this Chapter lies.

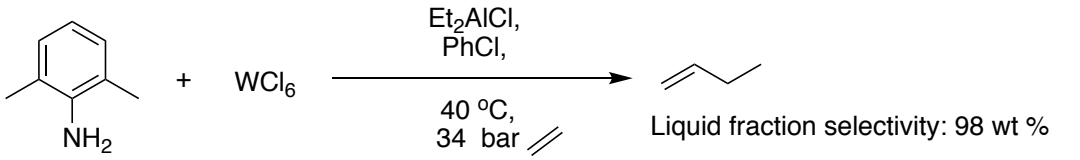

Scheme 4.11: Goodyear system for selective ethylene dimerisation to 1-butene.[29]

The LAO dimerisation systems (for olefinic substrates heavier than ethylene) exhibiting the greatest selectivity towards the linear dimeric products typically employ Ni, Co or Fe catalyst with ligands bearing nitrogen or oxygen donor atoms, in the presence of an activator. The role of the activator in the LAO catalytic dimerisation systems is identical to the role of activators discussed in catalytic ethylene *tri-*/*tetra*-merisation systems in Chapter 2, section 2.1.5. The following sections consider the Ni- and Co-/Fe-based LAO dimerisation systems.

4.1.3.1. Ni-based α-olefin dimerisation systems

One of the oldest reported Ni-based α-olefin dimerisation systems was described by Jones and Symes and employs $Ni(acac)_2$ with an $Et_2Al(OEt)$ activator at 40 °C.[30] This system is selective for the catalytic dimerisation of 1-propene, 1-butene and 1-hexene to their respective LAO dimers (62 -70 % liquid fraction selectivity towards LAO dimer product).[30] Due to the high linearity of the dimers formed by the $Ni(acac)_2/Et_2Al(OEt)$ catalytic system Jones and Symes proposed that the dimerisation catalysis occurred through a step-wise addition mechanism (Scheme 4.1), involving a Ni-H species.[30] Unfortunately, the $Ni(acac)_2/Et_2Al(OEt)$ catalytic system displays low activities (~5-10 g/g Ni/h) and significant isomerisation of the LAO olefinic substrate to internal olefins occurs.[30] For example, at 40 °C the rate of 1-hexene isomerisation to internal hexenes (2- and 3-hexene) was double that of the rate of the $Ni(acac)_2/Et_2Al(OEt)$-catalysed 1-hexene dimerisation process, causing an exponential decay of the dimerisation

activity.[30] da Rosa *et al.*[31] also investigated the use of the $Ni(acac)_2$-$Et_2Al(OEt)$ catalytic system for 1-butene, 1-hexene and 1-octene dimerisation and found similar results to those reported by Jones and Symes.[30] In the case of 1-butene dimerisation mediated by the $Ni(acac)_2$-$Et_2Al(OEt)$ initiator, da Rosa *et al.* observed 73 % selectivity towards dimerisation with > 98 % selectivity towards the formation of linear dimers, albeit with 43 % isomerisation of the 1-butene olefinic substrate.[31]

More recently, a novel nickel *bis*(amido) complex (shown in Scheme 4.12) was reported by Hey-Hawkins and Eisen *et al*. to dimerise selectively 1-hexene with a TON of 84,000 g/mol Ni/h, when used in conjuction with MAO activator.[32] Moreover, it was found to produce linear 1-dodecene as the major product (> 75%).[32] However, it was also observed that over time the 1-dodecene isomerised to a mixture of linear internal dodecenes.[32] In addition, the nickel *bis*(amido) complex/MMAO system (Scheme 4.12) was highly effective for the dimerisation of 1-propene, exhibiting the highest activity observed for propene oligomerisation at the time (50,000,000 g/ mol Ni/h).[32] Unfortunately, propene dimerisation catalysed by the *bis*(amido) complex (Scheme 4.12) was not selective towards 1-hexene, displaying only 59% selectivity towards linear hexenes (of which 75% was towards 1-hexene).[32]

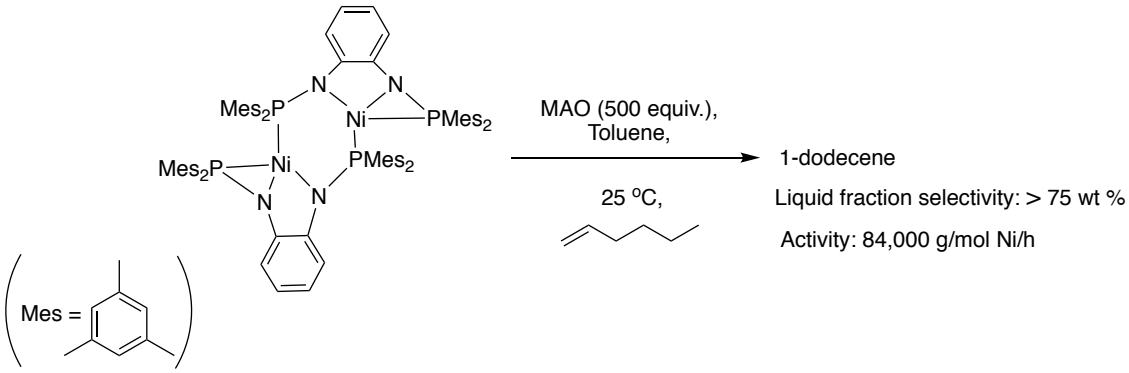

Scheme 4.12: Selective dimerisation of 1-hexene to 1-dodecene by a nickel *bis*(amido) complex activated with MAO (500 equiv.), reported by Hey-Hawkins and Eisen *et al*.[32]

4.1.3.2. Co- and Fe-based α-olefin dimerisation systems

There have been several reports in the literature that employ iron- and cobalt-based initiators to achieve the dimerisation of α-olefins to yield α-olefin dimeric products.[1,24,33,34] In the first of these reports by Small *et al.*, a series of *bis*(imino)pyridyl complexes of iron (**4C** – **4H**, Figure 4.1) were tested in 1-hexene dimerisation, at various temperatures (0 – 65 °C) using different activators (MMAO or TEA).[24] By varying systematically the substituents present on the *bis*(imino)pyridyl iron complexes (Figure 4.1), Small *et al.* obtained systems which exhibited high selectivity towards dimerisation (> 83 % dodecenes formation in liquid fraction), forming varying amounts

of linear internal dodecenes (29 – 81 % selectivity in dodecene fraction).[24] Interestingly, Small *et al.* observed that at lower temperatures, although the activity of the *bis*(imino)pyridyl iron-based hexene dimerisation system decreased, the selectivity towards linear dodecenes increased.[24] However, the *bis*(imino)pyridyl iron-based hexene dimerisation systems were still found not to produce any LAO dimer (1-dodecene).[24]

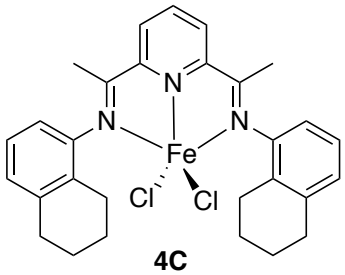

4C

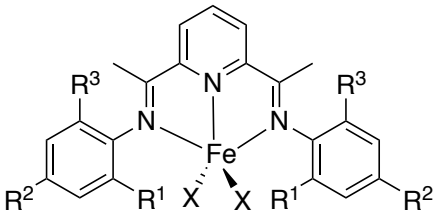

4D - 4H

4D: R^1 = Me, R^2 and R^3 = H, X = Cl
4E: R^1 = Et, R^2 and R^3 = H, X = Cl
4F: R^1 - R^3 = H, X = Br
4G: R^1 and R^2 = Me, R^3 = H, X = Cl
4H: R^1 = Me, R^2 = H, R^3 = Me, X = Cl

Figure 4.1: Series of *bis*(imino)pyridyl iron complexes tested in hexene dimerisation by Small *et al.*[24]

In a subsequent study, Small[33] extended the observed dimerisation chemistry of *bis*(imino)pyridyl iron complexes[24] to systems utilising cobalt *bis*(imino)pyridyl complexes. A series of cobalt *bis*(imino)pyridyl complexes (Figure 4.2) were tested in propene dimerisation, in the presence of MMAO activator at 30 ^{o}C, and found to exhibit mediocre dimer selectivity (45 – 76% liquid fraction selectivity) with exceptional selectivity towards linear dimeric products (> 99%).[33] The formation of dimers in the propene oligomerisation systems mediated by cobalt *bis*(imino)pyridyl complexes (Figure 4.2) was also accompanied by the formation of trimers and tetramers.[33]

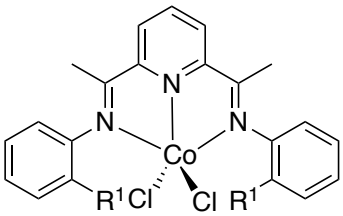

R^1 = H, Me, Et or ^{i}Pr

Figure 4.2: *Bis*(imino)pyridyl cobalt complexes tested in propene dimerisation by Small.[33]

The most notable feature of the Co-*bis*(imino)pyridyl-MMAO based propene dimerisation systems, was their high selectivity towards the LAO dimer in the hexene fraction, yielding between 10 – 59% 1-hexene (most selective system for 1-hexene

formation illustrated in Scheme 4.13).[33] The percentage of 1-hexene reported in the hexene fraction is significant as it is much higher than the expected yield of α-olefin in a thermodynamic equilibrium mixture of olefins (generally considered to be <5% α-olefin), formed *via* post-reaction isomerisation (by processes such as those considered previously in section 4.1.2.1.1).[33]

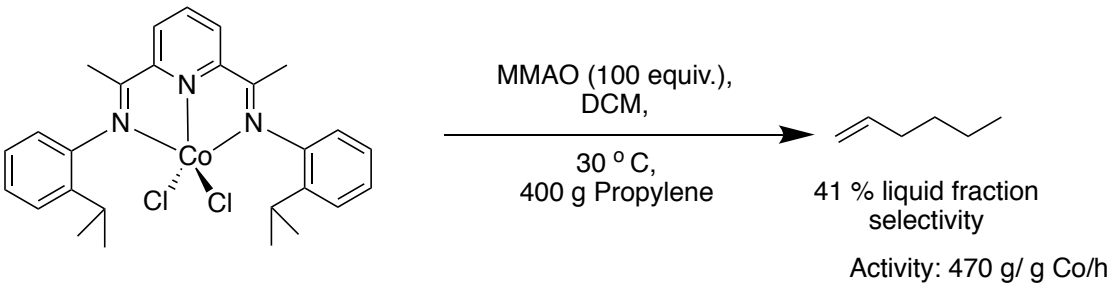

Scheme 4.13: Dimerisation system for the selective formation of 1-hexene, utilising a *bis*(imino)pyridyl cobalt complex and MMAO activator, reported by Small.[33]

In contrast to their application in propene dimerisation, in 1-butene dimerisation the cobalt *bis*(imino)pyridyl complexes were found to form only linear internal olefins and isomerisation of the 1-butene olefinic substrate occurred.[33] The performances of the *bis*(imino)pyridyl cobalt complexes in 1-butene dimerisation, in the presence of MMAO activator, were compared to that of the previously tested *bis*(imino)pyridyl iron complexes under analogous catalysis conditions.[24] This comparison revealed that the cobalt complexes generated systems with higher selectivity towards linear dimers (achieving 97%+ linearity in the dimeric products), but with lower activities and increased amounts of 1-butene isomerisation.[33] The product distributions obtained by Small *et al*.,[24,33] in the LAO dimerisation systems mediated by iron or cobalt *bis*(imino)pyridyl complexes led them to propose that step-wise mechanisms were in operation (Scheme 4.1). Small[33] postulated that the observed higher linearity of dimer products obtained in the Co- *versus* the Fe-catalysed systems was due to chain-transfer being dominant in the Co-systems, whereas propagation was preferential in the Fe-systems.

The olefin dimerisation behaviour of fluorinated versions of the iron and cobalt *bis*(imino)pyridyl complexes investigated by Small *et al*.,[24,33] were evaluated by Gibson *et al.*[34] The fluorinated iron and cobalt *bis*(imino)pyridyl complexes (Figure 4.3) were initially screened in propene oligomerisation, in the presence of MAO activator at 0 °C and 1 bar propene.[34] Surprisingly, Fe complexes **4I** and **4J** (Figure 4.3) afforded no products in propene oligomerisation;[34] in contrast to their non-fluorinated analogue (complex **4F**, Figure 4.1) observed to dimerise 1-hexene by Small *et al*.[24] Nevertheless, Co complexes **4K** and **4L** (Figure 4.3) formed oligomers (hexenes,

nonenes and dodecenes) in propene oligomerisation, conducted at 0 °C and 1 bar propene in the presence of MAO activator.[34]

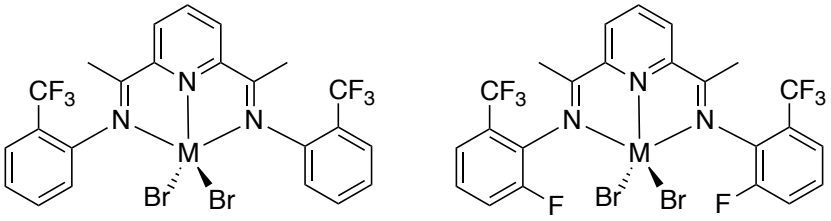

4I: M = Fe
4K: M = Co

4J: M = Fe
4L: M = Co

Figure 4.3: Fluorinated iron and cobalt *bis*(imino)pyridyl complexes tested in propene dimerisation by Gibson *et al.*[34]

Further investigation of the catalytic reaction conditions (catalyst loading and temperature) used in propene oligomerisation mediated by complex **4L** (Figure 4.3) resulted in systems with 72 - 88 % liquid fraction selectivity to hexenes (of which 57 – 91% was towards 1-hexene) and moderate activities (261 – 19,300 g/g Co/h). The best-performing propene dimerisation system utilising complex **4L** (in terms of activity and liquid fraction selectivity to 1-hexene) is illustrated in Scheme 4.14. In contrast, to the propene dimerisation systems generated by non-fluorinated cobalt *bis*(imino)pyridyl complexes investigated by Small (example shown previously in Scheme 4.13),[33] the propene dimerisation system produced by complex **4L** (Scheme 4.14) exhibits a higher activity and selectivity to 1-hexene in the liquid fraction. The higher liquid fraction selectivity towards 1-hexene obtained by complex **4L**, in the presence of MMAO, is a result of the decreased tendency towards post-reaction isomerisation relative to the system shown previously in Scheme 4.13.[33]

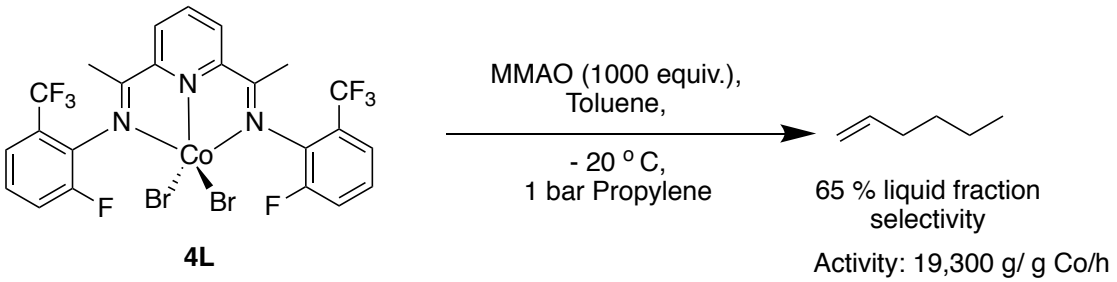

4L

Scheme 4.14: Selective propene dimerisation system reported by Gibson *et al.*[34]

Nevertheless, when complex **4L** (Scheme 4.14) was tested for the oligomerisation of higher α-olefins (1-butene and 1-hexene), only internal olefins were formed.[34] It was assumed by Gibson *et al.*[34] that, as was the case for the non-fluorinated versions of the cobalt *bis*(imino)pyridyl complexes, the fluorinated versions of the cobalt *bis*(imino)pyridyl complexes also mediated olefin dimerisation *via* a step-wise addition mechanism. The observed formation of trimers, in the propene dimerisation systems

mediated by fluorinated cobalt *bis*(imino)pyridyl complexes, were believed to occur from co-dimerisation of the 1-hexene product with propene, while tetramers were thought to form from hexene dimerisation.[34]

Lastly, a recent study by de Souza *et al*. also compared the use of fluorinated *versus* non-fluorinated cobalt *bis*(imino)pyridyl complexes (Scheme 4.15) in propene dimerisation, in the presence of MAO activator.[35] Similar to the study by Gibson *et al.,*[34] de Souza *et al*.[35] observed that the fluorinated Co catalyst precursor furnished propene dimerisation systems with increased activity and selectivity towards 1-hexene formation, in comparison to systems generated by the non-fluorinated Co catalyst precursor (Scheme 4.15). It was postulated by de Souza *et al*. that the higher activity of the fluorinated Co catalyst precursor was due to the Co centre being more electrophilic, thereby promoting coordination and insertion of propene.[35] In addition, comparison of the molecular structures of the fluorinated and non-fluorinated cobalt *bis*(imino)pyridyl complexes (Scheme 4.15) showed that the fluorinated complex possesses a slightly distorted square pyramidal base geometry around the Co centre. On this basis, de Souza *et al*. suggested that a head-to-head insertion of the propene dimers was more likely to occur in the system employing the fluorinated cobalt *bis*(imino)pyridyl catalyst precursor, resulting in the observed high 1-hexene selectivity.[35]

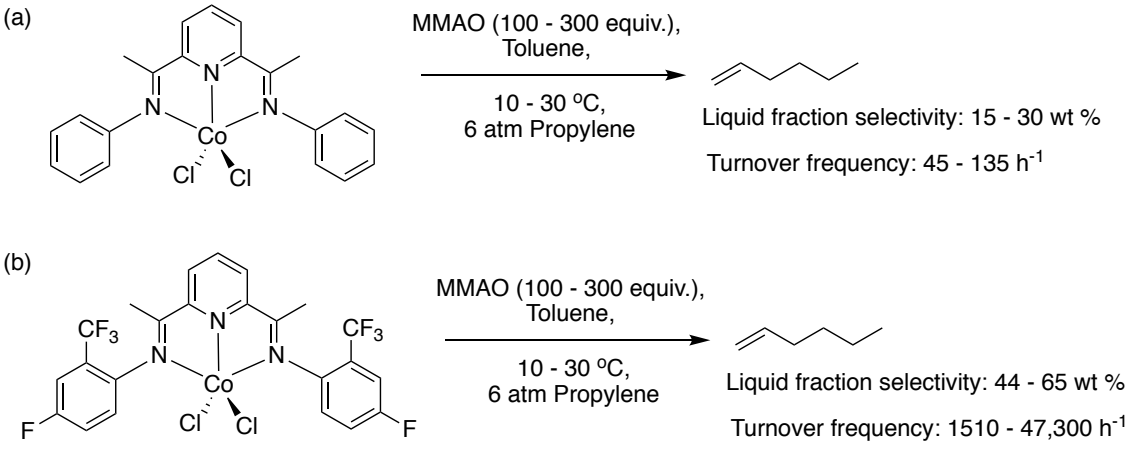

Scheme 4.15: Propene dimerisation systems implementing (a) non-fluorinated and (b) fluorinated cobalt *bis*(imino)pyridyl complexes, reported by de Souza *et al*.[35]

4.1.3.2.1. Broene selective LAO dimerisation system

The most revolutionary advancement in the application of cobalt-based catalyst precursors for α-olefin dimerisation systems was made by Broene *et al.,*[1] in 2005. In this paper it was shown that a catalytic system comprising [Cp*Co(η^2-C_2H_4)($P(OMe)_3$] and a deficit of Brookhart's acid ($HBAr_4^F$, {Ar^F=3,5-$(CF_3)_2C_6H_3$}, $HBAr_4^F$:Co =

0.82:1.00), was capable of dimerising 1-butene, 1-hexene, and 1-octene to their respective LAO dimers at a level above that expected from thermodynamic considerations. In the case of 1-hexene dimerisation, after 3.5 h it was observed that an unprecedented 14 % 1-dodecene had formed (alongside other C_{12} and C_{18} products illustrated in Scheme 4.16), and that after 12 h 25 % of the 1-dodecene had isomerised to internal olefins; similar reactivities for 1-butene and 1-octene dimerisation were reported.[1] The olefin dimerisation system reported by Broene *et al.*[1] is important due to it currently being the only literature system that can dimerise 1-butene, 1-hexene and 1-octene to their respective LAO dimers. Although 14% selectivity towards the LAO dimer, and TON of 7 (for dimer formation after 23 h) may seem low, the significance of this system should not be underestimated after taking into account the competing isomerisation processes in dimerisation systems and the inherent thermodynamic preference towards the formation of internal olefins (section 4.1.2.1.1).

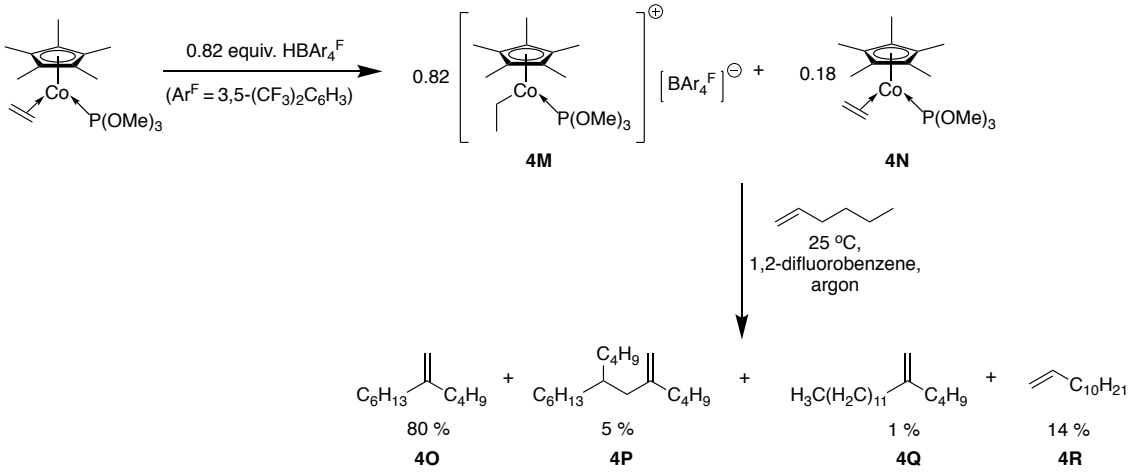

Scheme 4.16: Selective *di*- and *tri*-merisation of 1-hexene by [Cp*Co(η^2-C_2H_4)($P(OMe)_3$] activated with a deficit of Brookhart's acid.[1]

Broene *et al.* proposed that the 4:1 ratio of the activated cationic species (**4M**, Scheme 4.16) to the neutral species (**4N**, Scheme 4.16) was responsible for the observed selectivity towards 1-dodecene formation.[1] This suggestion was based on the fact that, in contrast, reactions undertaking employing [Cp*Co(η^2-C_2H_4)($P(OMe)_3$] and 1 equiv. of Brookhart's acid with 1-hexene did not form any 1-dodecene, instead yielding 66% **4O**, 7% **4P**, and 27% **4Q** (Scheme 4.16), *i.e.* olefin **4Q** is formed at the expense of 1-dodecene. Consequently, this supports the notion that a stepwise-addition mechanism (Scheme 4.17) is responsible for the formation of 1-dodecene catalysed by [Cp*Co(η^2-C_2H_4)($P(OMe)_3$] activated by a deficit of Brookhart's acid. Following one turnover of the mixture of **4M** and **4N** (Scheme 4.16), a mixture of **4S** and **4T** (Scheme 4.17) is formed. Complex **4T** then undergoes a 2,1-insertion of 1-hexene producing complex **4U** (Scheme 4.17), which is proposed to undergo isomerisation to generate the desired

cationic linear metal alkyl species (**4V** in Scheme 4.17), which is stabilised by a β-H agostic interaction.[1] Finally, proton exchange between species **4V** (Scheme 4.17) and **4S** (Scheme 4.17) may occur generating species **4W** and **4T** (Scheme 4.17). 1-Dodecene can then be liberated *via* exchange of 1-hexene with the coordinated 1-dodecene in species **4W** (Scheme 4.17), also producing species **4S** (Scheme 4.17) which can re-enter the catalytic cycle.[1]

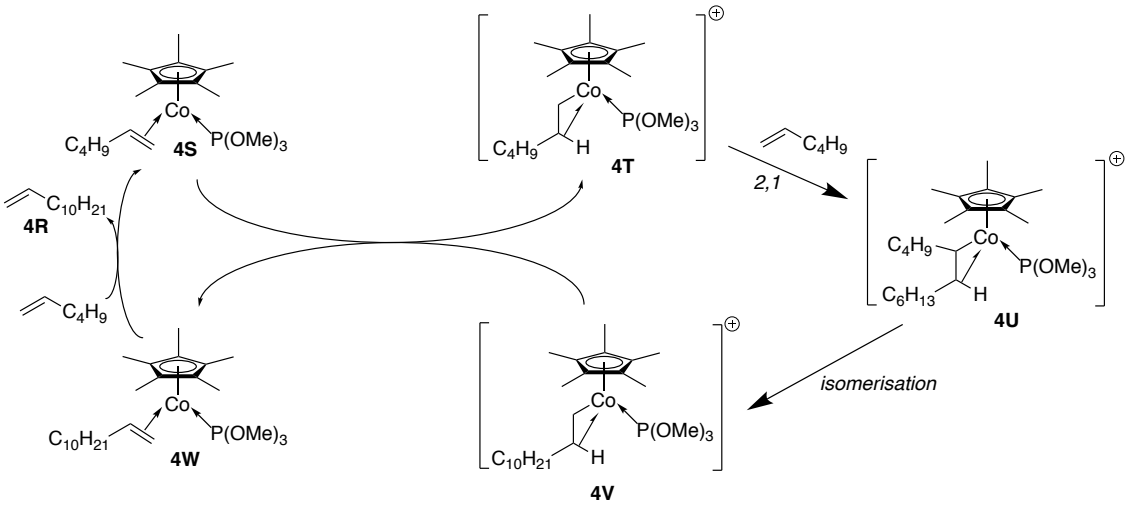

Scheme 4.17: Mechanism proposed by Broene *et al.*[1] for 1-dodecene formation from 1-hexene using [Cp*Co(η^2-C_2H_4)(P(OMe)$_3$] activated by a deficit of Brookhart's acid.

The proof for the role of an intermolecular agostic-H transfer between an agostic alkyl species and neutral alkene species (the proposed interaction between species **4V** and **4S** in Scheme 4.17) came from an NMR spectroscopic experiment conducted by Broene *et al.*[1] Here, treating the neutral propene complex with agostic ethyl species, as shown in Scheme 4.18, was found to give rise to an agostic propyl species and neutral ethene complex after 50 mins.

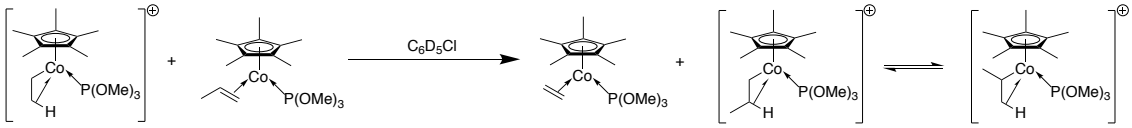

Scheme 4.18: Evidence of intermolecular exchange of an agostic hydrogen atom between a neutral alkene species and agostic alkyl species, modified from Broene *et al.*[1]

4.1.3.3. Summary of literature LAO dimerisation systems reviewed

Upon reviewing the literature systems capable of dimerising LAOs to their respective LAO dimers, it is evident that there are systems that demonstrate high activity and selectivity for 1-propene dimerisation to 1-hexene. For example, cobalt *bis*(imino)pyridyl complexes reported by Small are capable of generating propene dimerisation systems with moderate selectivity towards hexenes (45 – 76% liquid

fraction selectivity), producing 10 – 59% 1-hexene in the hexene fraction.[33] Propene dimerisation systems with improved activities and selectivities towards 1-hexene were obtained *via* implementation of fluorinated cobalt *bis*(imino)pyridyl complexes reported by Gibson *et al.*[34] The systems reported by Gibson *et al.* exhibit 72 - 88% liquid fraction selectivity to hexenes (of which 57 – 91% was towards 1-hexene) and moderate activities of 261 – 19, 300 g/g Co/h.[34] However, implementation of the cobalt *bis*(imino)pyridyl complexes reported by Small[33] and Gibson *et al.*[34] in 1-butene and 1-hexene oligomerisation reactions only yielded linear internal olefins instead of the desired LAO dimer product.

In terms of systems that have been reported in the literature that demonstrate potential for selective dimerisation of LAOs heavier than propylene to their respective LAO dimers, there are only two systems that stand out. The first system utilises a nickel *bis*(amido) complex, reported by Hey-Hawkins and Eisen *et al.*, which is active (84,000 g/mol Ni/h) and selective in dimerising 1-hexene to 1-dodecene (> 75 % liquid fraction selectivity).[32] The second system, developed by Broene *et al.*,[1] employs [Cp*Co(η^2-C_2H_4)($P(OMe)_3$] catalyst precursor and a deficit of Brookhart's acid activator to achieve dimerisation of a selection of LAOs (1-butene, 1-hexene and 1-octene) to their respective LAO dimers. However, industrial application of the catalytic system discovered by Broene *et al.* is not viable due to it only achieving 14 % liquid fraction selectivity to the LAO dimer product and displaying low TONs.[1]

4.1.4. Aims of Chapter 4

As is evident from the brief literature review on LAO dimerisation catalyst systems, the majority of systems inherently produce the thermodynamically favoured internal olefin products instead of the desired LAO dimeric products (especially in the case for dimerisation of olefinic substrates heavier than propene). Consequently, there is demand for research into the development of a catalytic dimerisation system capable of selectively producing LAO dimers from lower molecular weight LAOs (especially those substrates heavier than propene). Of the literature LAO dimerisation systems reviewed, the system by Broene *et al.* offers great potential to become an alternative strategy for the generation of higher LAO dimers (due to its capability of mediating dimerisation of a selection of LAOs heavier than propene to their respective LAO dimers).[1] However, much work is necessary to make Broene's system commercially viable, due to its low selectivity of towards the LAO dimer, 14%, and low TON of 7 (towards dimers after 23 h). Therefore, it is of interest to further investigate Broene's catalytic dimerisation system in order to gain insight into factors that affect its activity

and selectivity and subsequently to explore whether it is possible to develop a more active and selective version of this catalyst suitable for use on an industrial scale. To this end, the aims of the work in this Chapter are to:

(a) synthesise Broene's catalyst precursor and test in 1-butene and 1-hexene dimerisation catalysis, in order to obtain verification of the results reported by Broene *et al.*[1] and set an in-house benchmark comparison for other LAO catalytic dimerisation systems tested

(b) vary systematically a selection of catalysis conditions, implemented in 1-butene/1-hexene dimerisation mediated by Broene's catalyst precursor, to gain an understanding of the impact of different catalysis conditions on the selectivity and activity of the dimerisation system

(c) synthesise modified variants of Broene's catalyst precursor and subsequently test in 1-butene or 1-hexene dimerisation catalysis, to obtain insight into structure-activity and structure-selectivity relationships.

4.2. Synthesis of Broene's catalyst

4.2.1. Synthesis of Broene's cyclopentadienyl cobalt catalyst precursor

The synthesis of Broene's cyclopentadienyl cobalt catalyst precursor (**4.5**) was conducted *via* the five-step reaction sequence displayed in Scheme 4.19, following literature procedures (or modifications thereof in the case of complex **4.5**).[36-38] Complexes **4.1** – **4.5** were obtained in high yields (73 – 95%) and characterised by NMR and IR spectroscopies (complexes **4.1** – **4.3** only), and X-ray crystallography (complexes **4.4** and **4.5** only).

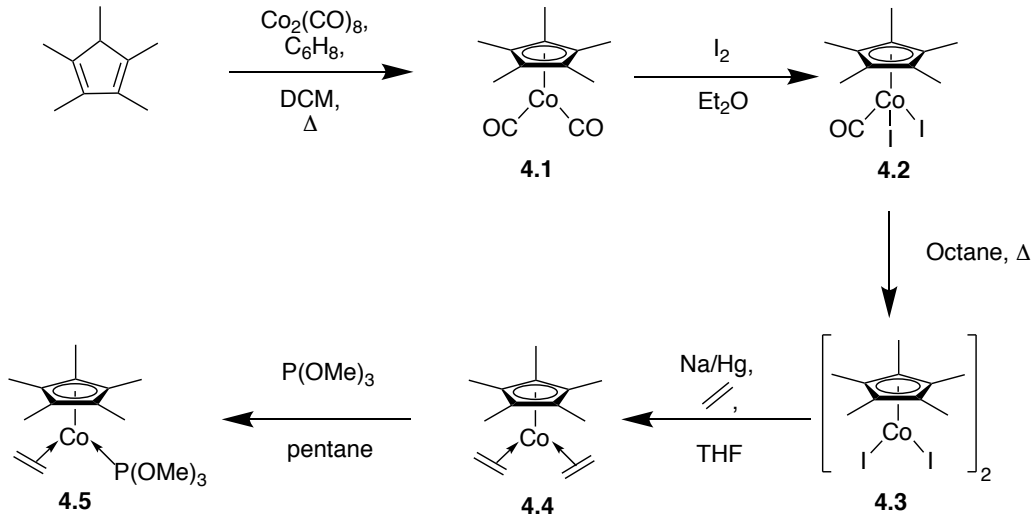

Scheme 4.19: Synthesis of Broene's cyclopentadienyl cobalt complex (**4.5**), based on literature procedures (or modification of literature procedures in the case of complex **4.5**).[36-38]

For the synthesis of complex **4.3**, it was found that it was vital to ensure that CO was effectively removed from the reaction medium in order to ensure complete conversion of complex **4.2**. Thus, the removal of CO was achieved by passing a slow flow of N_2 at atmospheric pressure across the top of the reflux condenser. The complete conversion of complex **4.2** to **4.3** is necessary for the synthesis of complex **4.4**, as the presence of minor quantities of complex **4.2** leads to the formation of [{Co(η-C_5Me_5)(μ-CO)}$_2$], which is difficult to separate from complex **4.4**.[36] At room temperature, the subsequent reaction of complex **4.4** with $P(OMe)_3$ was found to proceed slowly requiring 40 h for full conversion to complex **4.5**. In contrast, a reaction time of 3 h was obtained on heating the reaction mixture of $P(OMe)_3$ and complex **4.4** at 50 ^oC.

The ^1H and $^{13}C\{^1H\}$ NMR spectral data for complexes **4.1** – **4.5** and the IR spectroscopic data of complexes **4.1** – **4.3** match with those reported in the literature.[36,37,39-41] The $^{31}P\{^1H\}$ NMR spectrum of complex **4.5,** which has not previously been reported in the literature, exhibited a significantly broadened resonance at 175.4 ppm ($\nu_{½}$ = 675 Hz), which could only be observed with the application of line broadening (lb = 1.0 Hz). Line broadening (lb) is part of an exponential function, [W(*t*)-exp(-lb*t)*], by which the free induction decay (FID, the signal generated by NMR spectroscopy) may be multiplied in order to improve the signal to noise ratio (as the initial intensity of the FID is proportional to the signal to noise ratio).[42] However, the application of an exponential multiplication also causes an artificial rapid decay of the FID, and since line width is inversely proportional to the tranverse decay (T_2), broader lines result due to a shorter FID.[42] Consequently, the use of too much line broadening (which determines the steepness of the exponential multiplier) may not prove useful; an optimal signal to noise ratio is found when the lb factor used is equal to the peak width at half height.[42]

The broad nature of the phosphorus resonance in the $^{31}P\{^1H\}$ NMR spectrum of complex **4.5** is believed to be caused by the scalar (spin-spin) coupling between the ^{31}P nucleus (I = 1/2) and the quadrupolar ^{59}Co nucleus (I = 7/2).[43] In theory, coupling to a quadrupolar nucleus of spin I should give $2I$ + 1 lines, however if the relaxation of the quadrupolar nucleus (caused by interaction of its electric quadrupole moment with an electric field gradient) is rapid relative to the magnitude of the coupling then coupling between the two nuclei can be broadened or removed entirely.[43] In the case of complex **4.5**, rapid relaxation of the quadrupolar ^{59}Co nucleus would be expected as Co is in an asymmetric environment (*i.e*. not at the centre of tetrahedral or octahedral coordination environment where the symmetry dictates that the electric field gradient

should be zero, in principle, suppressing quadrupolar relaxation) and has a high quadrupole moment (0.38×10^{-28} m^2 relative to that of other quadrupolar nuclei, such as ^{11}B (I = 3/2): 4.1×10^{-30} m^2).[43] Other factors that have been reported to cause line broadening in NMR spectra include inhomogeneous samples, paramagnetic impurities or the occurrence of chemical exchange.[43] None of these, however, were observed (NMR sample for complex **4.5** was homogenous and no free $P(OMe)_3$ was detected in the $^{31}P\{^1H\}$ NMR spectrum) or expected (in the case of paramagnetic impurities) for complex **4.5**.

In addition to characterisation by NMR spectroscopy, complexes **4.4** and **4.5** were also characterised by X-ray crystallography. Crystals of complexes **4.4** and **4.5**, suitable for X-ray crystallographic studies, were obtained by recrystallisation from petroleum ether (b.p. 40 – 60 °C) at −78 °C. The molecular structures of complex **4.4** and **4.5** are shown in Figure 4.4; the molecular structure of complex **4.4** has been previously reported in the literature[44] (there is agreement between the bond lengths listed in Table 4.1 and the corresponding bond lengths in the literature); the structure of complex **4.5** has not been reported previously. The molecular structure of complex **4.5** reveals its two-legged piano stool geometry in which the η^5-Cp* ring deviates slightly from being symmetrically disposed with respect to the Co centre (evident from the unequal distances between Co and the ring C atoms on Cp*: 2.0693(16)-2.0980(16) Å). The plane of the Cp* ligand is at a distance of 1.696 Å from the Co metal in complex **4.5**. The C=C bond length of the coordinated ethylene in complex **4.5** (1.417(3) Å) is longer than that reported for free ethylene (1.339 Å),[45] reflecting the π-acceptor character of the ethylene ligand in **4.5**. In addition, the C=C bond length of 1.417(3) Å in complex **4.5** is longer than the average C=C bond length of the coordinated ethylene ligands in complex **4.4** (1.400(3) Å) indicating that the Co centre is more electron rich in complex **4.5** than in complex **4.4**, due to the greater σ-donor ability of the $P(OMe)_3$ ligand in complex **4.5** relative to the σ-donor ability of the ethylene ligand in complex **4.4**. This difference in donor character is further supported by the slightly shorter average Co-C(ethylene) bond length in complex **4.5** of 1.9977(18) Å compared to that of 2.0163(18) Å in complex **4.4**.

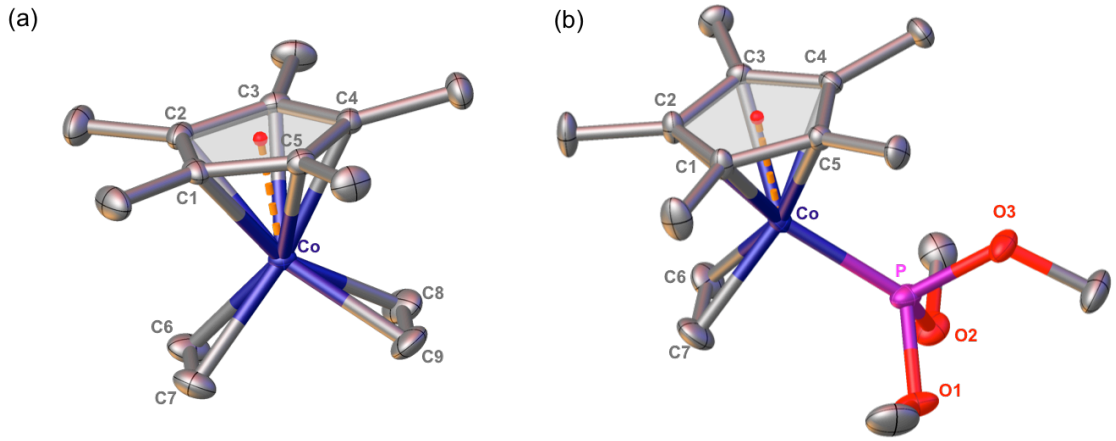

Figure 4.4: Molecular structures of complexes (a) **4.4** and (b) **4.5**, with thermal ellipsoids set at the 50% probability level; H atoms have been omitted for clarity. Computed centroids for Cp* rings shown in red with distances from centroid to Co centre represented by dashed orange lines.

Table 4.1: Selected bond lengths (Å) for complexes **4.4** and **4.5**, refer to **Figure 4.4** for atom labels. *Cent* used to represent computed centroid on Cp* rings. Estimated standard deviations given in brackets.

		Complex **4.4**	Complex **4.5**
Bond Lengths (Å)	Co-C1	2.1157(15)	2.0936(15)
	Co-C2	2.0966(15)	2.0693(16)
	Co-C3	2.0922(15)	2.0980(16)
	Co-C4	2.0738(15)	2.0850(14)
	Co-C5	2.1105(15)	2.0809(15)
	Co-*Cent*	1.713	1.696
	Co-C6	2.0239(18)	1.9994(17)
	Co-C7	2.0192(18)	1.9960(18)
	Co-C8	2.0147(18)	N/A
	Co-C9	2.0075(18)	N/A
	Co-P	N/A	2.0839(5)
	C6-C7	1.399(3)	1.417(3)
	C8-C9	1.401(3)	N/A

4.2.2. Synthesis of Broene's cyclopentadienyl cobalt catalyst

With complex **4.5** in hand, the next step was to synthesise Broene's cyclopentadienyl cobalt catalyst (complex **4.6**). To this end, complex **4.5** was activated with a deficit of Brookhart's acid, under the conditions reported by Brookhart *et al.* (Scheme 4.20), generating the agostic species **4.6**.[46] For note, an agostic species is defined by Brookhart and Green[47] as one that contains "a hydrogen atom which is covalently bonded simultaneously to both a carbon atom and to a transition metal atom," *i.e.* H_a in Scheme 4.20, resulting in the formation of a three-centre-two-electron bond. There is a plethora of examples of mononuclear transition-metal complexes possessing agostic ethyl groups in the literature.[7,38,47]

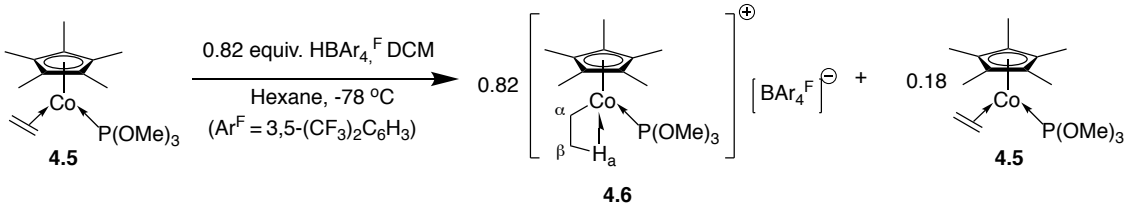

Scheme 4.20: Synthesis of Broene's cyclopentadienyl cobalt catalyst following literature procedure detailed by Brookhart *et al.*[46]

The identity of complex **4.6** was verified by CHN and ^{1}H NMR spectroscopic analyses (500 MHz, CD_2Cl_2, −90 °C). The ^{1}H NMR spectrum of the static structure of complex **4.6**, at −90 °C, matches that reported in the literature at −70 °C in CD_2Cl_2,[38,41,46,48] and displays features indicative of an agostic species: a low frequency shifted proton resonance at −12.18 to −12.45 ppm (corresponding to H_a in Scheme 4.20) and low $^{3}J_{PH}$ value of 11.2 Hz (corresponding to $P(OMe)_3$ protons).[38] The magnitude of the $^{3}J_{PH}$ coupling constant (11.2 Hz) is much lower than that reported for the related hydride species, $[Cp^*(P(OMe)_3)_2CoH]^+$,[49] of 80 Hz, and is similar in magnitude to J_{PH} couplings reported in other agostic species containing phosphine or phosphite ligands.[47,50] The analysis of complex **4.6** reported in the literature by ^{13}C NMR spectroscopy (CD_2Cl_2, −70 °C) also provides reliable evidence for the presence of the β-agostic C-H bond from the reduced $J_{C\beta\text{-}H\alpha}$ value of 61 Hz (caused by the reduced C-H bond order in the three-centre-two-electron bond), compared to that for a typical saturated sp^3 C-H bond where J_{CH} values of 120 – 130 Hz are normal and high-field shifted C_β at −9.2 ppm (Scheme 4.20).[38,47] In addition, the molecular structure of complex **4.6**, reported in the literature,[51] displays a small Co-C_α-C_β bond angle of 74.4(5)° and a short C_α-C_β bond length of 1.477(13) Å; these metric parameters provide further support for the agostic structure of complex **4.6** due to their consistency with those reported for related agostic complexes in the literature.[52-55] Dynamic NMR spectroscopic studies of complex **4.6** (in CD_2Cl_2 at temperatures above −50 °C) have also been reported previously. These demonstrated that at temperatures above −50 °C complex **4.6** exists as a dynamic equilibrium of three structural forms (terminal ethylene hydride, agostic, and unsaturated alkyl complex species as depicted in Scheme 4.21), which undergo three dynamic and essentially energetically degenerate processes shown in Scheme 4.22.[38,41]

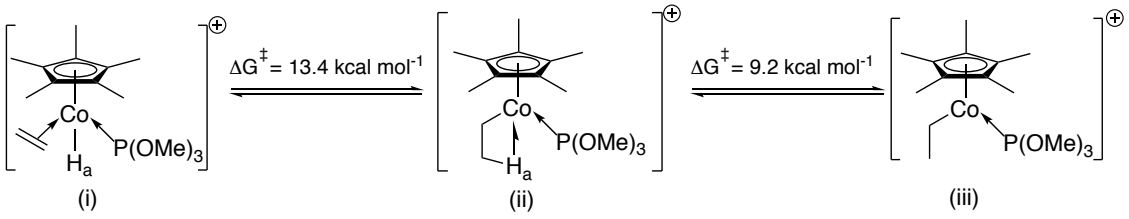

Scheme 4.21: Dynamic equilibrium of different structural forms of complex **4.6**: (i) terminal ethylene hydride species, (ii) agostic species, and (iii) unsaturated alkyl complex, modified from the work of Schmidt *et al.*, 1985.[41]

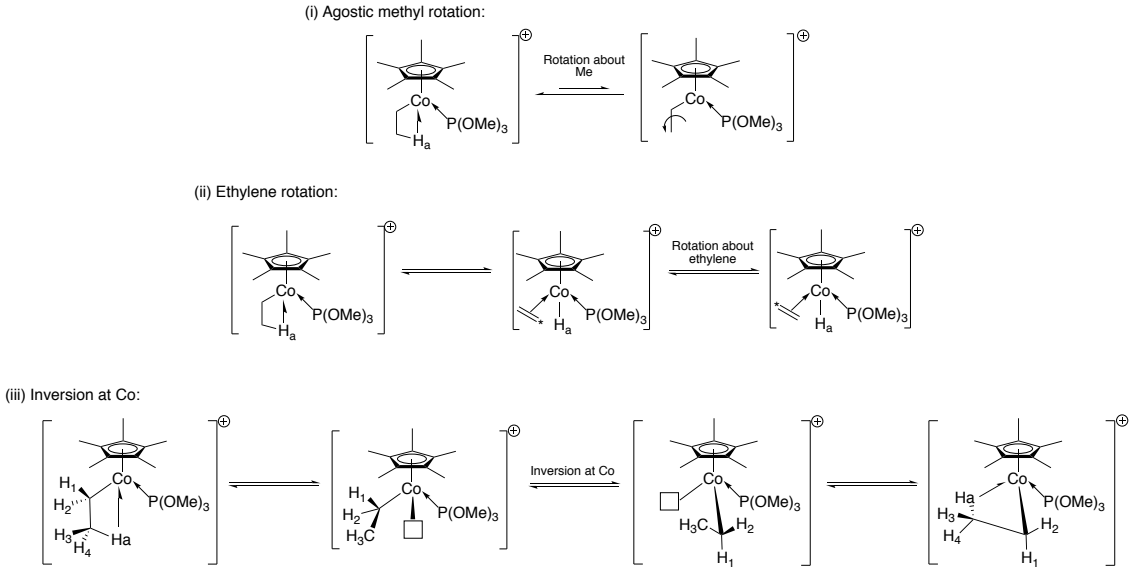

Scheme 4.22: Three dynamic degenerate processes exhibited by agostic complex **4.6**, modified from the work of Brookhart *et al.*, 1989.[38]

4.3. Investigating Complex 4.5/Brookhart's Acid Mediated 1-butene and 1-hexene Dimerisation Systems

4.3.1. Catalyst testing protocol

Broene's catalyst precursor (complex **4.5**) was tested in 1-butene and 1-hexene dimerisation. The 1-butene catalysis runs were conducted in collaboration with M. Hanton at Sasol Technology, while the 1-hexene catalysis runs were performed at Durham University. The ensuing parts of this section detail the conditions implemented in the 1-butene and 1-hexene dimerisation runs, as well as considering the reproducibility of the 1-butene and 1-hexene dimerisation runs.

4.3.1.1. Catalyst testing protocol adopted for 1-butene dimerisation mediated by complex 4.5

The 1-butene dimerisation catalysis runs were carried out in glass autoclaves under the conditions listed in Figure 4.5 (similar conditions to those employed by Broene *et*

al.[1] with the major differences being use of fluorobenzene {PhF} as solvent (as explained in section 4.3.3.1) and a longer reaction time due to the expected low TONs). The impact of varying the solvent, temperature, and activation method implemented in the 1-butene dimerisation runs was evaluated and will be discussed in section 4.3.3. The activities for all of the 1-butene dimerisation runs conducted in this work have been reported in terms of g of 1-C_4 converted to oligomers per g of Co per hour. It is important to note that for all of the 1-butene dimerisation runs carried out a small amount of isomerisation of the 1-butene to internal butenes was observed (~1 – 10%).

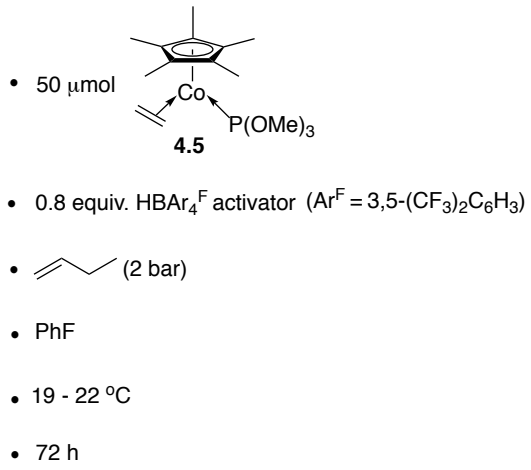

Figure 4.5: General conditions employed in 1-butene dimerisation catalysis testing mediated by **4.5**/Brookhart's acid.

In order to assess the reproducibility of the 1-butene dimerisation catalysis runs, a series of experiments was carried out under identical conditions (Figure 4.5; Table 4.2). The data summarised in Table 4.2 demonstrate good reproducibility for the 1-butene dimerisation runs with little overall variation between TONs, activities and liquid fraction selectivities. The relative standard deviations as a percentage of the mean (RSD %) were determined for the TONs, activities and liquid fraction selectivities and have been taken into consideration when making comparisons between data generated from the 1-butene dimerisation catalysis runs (sections 4.3.1.1 and 4.4.3, where, in most cases, repeat catalysis runs have not been undertaken).

Table 4.2: Reproducibility of 1-butene dimerisation mediated by complex **4.5**. [a] In units of mol 1-C_4 converted to oligomers (mol Co)$^{-1}$. [b] In units of g 1-C_4 converted to oligomers/g Co/h. [c] Wt % of liquid fraction; all catalysis runs only yielded liquid products. [d] LAO = linear α-olefin. [e] BO = branched olefin. [f] Methyl branched = 2-ethyl-1-hexene. [g] Dimethyl branched = 2-ethyl-3-methylpent-1-ene. [h] LIO = linear internal olefin. Catalysis conditions: 50 µmol $Cp^*Co(C_2H_4)(P(OMe)_3$, 0.8 eq. Brookhart's acid, 2 bar 1-C_4, PhF, 19 – 22 °C, 72h.

Run	TON[a]	Activity[b]	% C_8 (wt %)[c]				% branched C_{12} (wt %)[c]	% branched C_{16} (wt %)[c]
			LAO[d]	BO[e]				
				Methyl[f]	Dimethyl[g]	LIO[h]		
1	16.8	0.22	6	68	2	1	19	4
2	18.5	0.24	5	66	1	1	21	6
3	17.3	0.23	5	75	1	0	13	6
4	11.7	0.16	6	69	1	2	18	4
RSD %	16	15	9	5	35	71	17	20

4.3.1.2. Catalyst testing protocol adopted for 1-hexene dimerisation mediated by complex 4.5

The 1-hexene dimerisation catalysis runs were conducted in Schlenks using the general conditions shown in Figure 4.6. The general conditions illustrated in Figure 4.6 are identical to those reported by Broene *et al*.[1] for their complex **4.5**/Brookhart's acid mediated 1-hexene dimerisation systems, except for the use of PhF solvent (see section 4.3.3.1) and longer reaction time (due to anticipated low TONs). The performance of complex **4.5**/Brookhart's acid in 1-hexene dimerisation catalysis has been compared to that observed in 1-butene dimerisation (section 4.3.4.1). In addition, the influence of using *in situ versus* preformed catalyst precursor complex **4.5** in the 1-hexene catalysis runs was investigated (section 4.3.4.2). The activities of the 1-hexene dimerisation runs reported in this work are in terms of g of 1-C_6 converted to oligomers per g of Co per hour. It should also be noted that for all of the 1-hexene dimerisation runs carried out a small amount of isomerisation of the 1-hexene to internal hexenes occurred (~2 – 10 %).

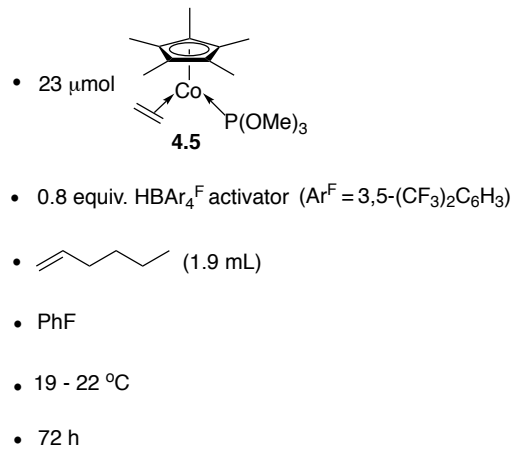

Figure 4.6: General conditions implemented in 1-hexene dimerisation catalysis testing mediated by **4.5**/Brookhart's acid.

In a similar manner to the 1-butene dimerisation catalysis runs, the reproducibility of the 1-hexene dimerisation catalysis tests was examined by performing a series of runs under identical conditions (Figure 4.6,). The results summarised in show good reproducibility with small overall variation between TONs, activities and liquid fraction selectivities. The relative standard deviations as a percentage of the mean (RSD %) have also been calculated for the TONs, activities and liquid fraction selectivities, so that these can be considered when comparing data generated from the 1-hexene dimerisation catalysis runs (sections 4.3.4.1 and 4.3.4.2, where, in most cases, repeat catalysis runs have not been undertaken).

Table 4.3: Reproducibility of 1-hexene dimerisation mediated by complex **4.5**. [a]In units of mol 1-C_6 converted to oligomers (mol Co)$^{-1}$. [b] In units of g 1-C_6 converted to oligomers/g Co/h [c] Wt % of liquid fraction; all catalysis runs only yielded liquid products. [d] LAO = linear α-olefin. [e] BO = branched olefin = 2-butyl-1-octene. Catalysis conditions: 23 µmol Cp*Co(C_2H_4)($P(OMe)_3$, 0.8 eq. Brookhart's acid, 1.9 mL 1-C_6, PhF, 19 – 22 ^oC, 72h.

Run	TON[a]	Activity[b]	% C_{12} (wt %)[c]		% branched C_{18} (wt %)[c]
			LAO[d]	BO[e]	
1	21.5	0.43	6	75	19
2	21.2	0.42	11	76	13
3	17.5	0.35	12	75	13
4	12.8	0.25	11	76	13
RSD %	19	20	23	1	18

4.3.2. Verification of LAO dimerisation catalysis results reported by Broene

Verification of the catalysis results obtained by Broene et al.[1] was obtained by testing Broene's cyclopentadienyl cobalt catalyst precursor (complex 4.5) in 1-butene dimerisation, under the conditions shown in Scheme 4.23 (i.e. those employed by Broene et al.[1] for 1-butene dimerisation catalysis mediated by complex **4.5**/Brookhart's acid with the main difference being the reaction time being extended in our work). This increased time period was used due to the expected low TON (reported by Broene et al.[1]) of the complex **4.5**/Brookhart's acid mediated 1-butene dimerisation system. The results shown in Scheme 4.23 confirm the finding by Broene et al.[1] that, when activated with a deficit of Brookhart's acid, complex **4.5** catalyses the LAO dimer (1-butene) to its respective LAO dimer (1-octene) with a low selectivity (6 %) and low TON (5.4 mol 1-C_4 converted to oligomers/ mol Co), in addition to forming other di-, tri-, and tetra-meric products.

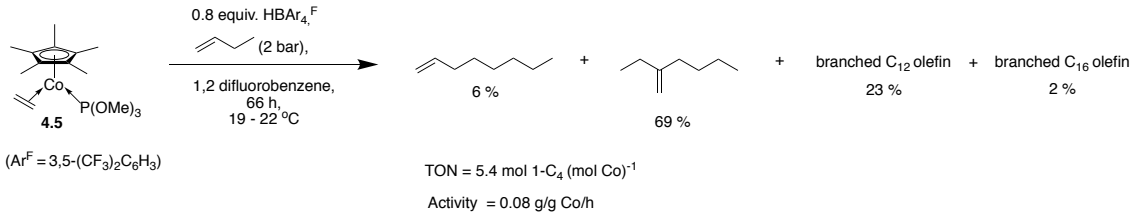

Scheme 4.23: Performance of complex **4.5** in 1-butene dimerisation, in the presence of Brookhart's acid activator, whereby the TON and activity are based on the conversion of 1-butene to oligomeric products.

4.3.3. Investigating effect of varying catalysis conditions in complex 4.5/Brookhart's acid mediated 1-butene dimerisation catalysis

4.3.3.1. Effect of varying solvent on 1-butene dimerisation with complex 4.5

In order to investigate the impact of using alternative solvents to 1,2-difluorobenzene (implemented in the literature study by Broene *et al.*[1] in complex **4.5**/Brookhart's acid mediated LAO dimerisation), a series of 1-butene dimerisation catalytic runs were conducted in a range of different solvents, as listed in Table 4.4, under the reaction conditions described in Scheme 4.23. From the results in Table 4.4, in which the different solvents are listed in order of their dielectric constant, it can be seen that in some instances the nature of the solvent impacts the TON, activities and liquid fraction selectivities of the 1-butene dimerisation systems (*e.g.* using 1,3-$(CF_3)_2$-C_6F_{10} *vs*. 1,2-F_2-C_6H_4). However, there is no correlation observed between solvent polarity and performance of complex **4.5** in 1-butene dimerisation.

Table 4.4: Impact of solvent on catalytic 1-butene dimerisation mediated by complex **4.5**/Brookhart's acid.[a] From ref. 56.[b] In units of mol 1-C_4 converted to oligomers (mol Co)$^{-1}$. [c] In units of g 1-C_4 converted to oligomers/g Co/h. [d] Wt % of liquid fraction; all catalysis runs only yielded liquid products.[e] LAO = linear α-olefin. [f] BOs = branched olefins (2-ethyl-1-hexene (≥ 98 %) and 2-ethyl-3-methylpent-1-ene (≤ 2 %). [g] LIO = linear internal olefin. [h] Average of repeat runs reported previously in Table 4.2. Catalysis conditions: 50 μmol Cp*Co(C_2H_4)($P(OMe)_3$, 0.8 eq. Brookhart's acid, 2 bar 1-C_4, 19 – 22 °C, 66-72h.

Solvent	Dielectric constant[a]	TON[b]	Activity[c]	% C_8 (wt %)[d]			% branched C_{12} (wt %)[d]	% branched C_{16} (wt %)[d]
				LAO[e]	BOs[f]	LIO[g]		
1,3-$(CF_3)_2$-C_6F_{10}	1.9	18.0	0.24	2	64	1	25	8
PhMe	2.4	0	0	0	0	0	0	0
1,3-F_2-C_6H_4	5.2	9.7	0.14	8	71	0	21	0
PhF[h]	5.6	16.1	0.21	5	71	1	18	5
1,2-F_2-C_6H_4	14.3	5.4	0.08	6	69	0	23	2

The lack of catalysis observed in the catalytic run using toluene as a solvent (Table 4.4) is not surprising as the activated catalyst species (complex **4.6**) is insoluble in

toluene. Although, using unoptimised reaction conditions, the other solvents employed (with the exception of toluene) produced 1-butene dimerisation systems with higher TONs and activities than the system using 1,2-difluorobenzene, none of the systems tested can be regarded as being efficient. However, based on the results summarised in Table 4.4, PhF was implemented as the solvent for all subsequent 1-butene dimerisation and 1-hexene dimerisation catalysis tests as this combination demonstrated both the greatest selectivity towards the LAO dimer and greatest activity (same activity as 1,3-$(CF_3)_2$-C_6F_{10} within error) out of those tested (Table 4.4).

4.3.3.2. Effect of varying temperature on 1-butene dimerisation mediated by complex 4.5

The effect of temperature on 1-butene dimerisation mediated by complex **4.5** was evaluated by conducting two catalysis runs that were allowed to exotherm to different temperatures (see Table 4.5), under the general conditions depicted in Figure 4.5. It was found that allowing the catalysis run to exotherm to 33 ^oC had no effect on the liquid fraction selectivities, however halved the TON and activity, relative to that of the analogous catalysis run whose temperature was controlled (run 1, Table 4.5). This observation is suggestive that low temperature reactions are more favoured for 1-butene dimerisation when using pro-initiator complex **4.5** and Brookhart's acid activator. Lower temperatures were not investigated in complex **4.5**-mediated 1-butene dimerisation as these conditions would not be practical on an industrial scale.

Table 4.5: Impact of temperature on the performance of complex **4.5** mediated 1-butene dimerisation. [a] In units of mol 1-C_4 converted to oligomers (mol Co)$^{-1}$. [b] In units of g 1-C_4 converted to oligomers/g Co/h. [c] Wt % of liquid fraction; all catalysis runs only yielded liquid products. [d] LAO = linear α-olefin. [e] BO = branched olefins (2-ethyl-1-hexene (≥ 97 %)and 2-ethyl-3-methylpent-1-ene (≤ 3 %). [f] LIO= linear internal olefin. [g] Average of repeat runs reported previously in Table 4.2. Catalysis conditions: 50 μmol Cp*Co(C_2H_4)($P(OMe)_3$, 0.8 eq. Brookhart's acid, 2 bar 1-C_4, PhF, 72h.

Run	Exotherm temperature (^oC)	TON [a]	Activity [b]	% C_8 (wt %) [c]			% branched C_{12} (wt %) [c]	% branched C_{16} (wt %) [c]
				LAO [d]	BOs [e]	LIO [f]		
1 [g]	22	16.1	0.21	5	71	1	18	5
2	33	7.8	0.10	6	71	1	18	4

4.3.3.3. Effect of activation method on 1-butene dimerisation with complex 4.5

The effect of varying the activation method for complex **4.5** in 1-butene dimerisation was explored by carrying out three catalysis runs, each using different activation methods (runs 1 – 3, Table 4.6) to that typically employed (run 4, Table 4.6). The absence of any 1- butene *di*- and *oligo*-merisation in the system solely employing complex **4.5** without any activator (run 1, Table 4.6) demonstrates that complex **4.5** is

unreactive towards 1-butene di-/oligo-merisation catalysis. In addition, the similar performances of runs 3 and 4 (Table 4.6) show that complex **4.6** is indeed the active catalyst in the 1-butene dimerisation system using complex **4.5**, activated by 0.8 equiv. Brookhart's acid. A comparison of the performances achieved in runs 3 and 4 to that of run 2 (which only uses the active catalyst complex **4.6**, Table 4.6) adds further weight to the observation by Broene *et al.*[1] that a mixture of the active catalyst complex **4.6** and neutral catalyst precursor complex **4.5** is required to catalyse dimerisation of the LAO dimer towards its LAO dimer. Furthermore, the lower TONs determined for the catalysis runs employing 4:1 ratios of complex **4.6**: **4.5** (runs 3 and 4, Table 4.6) compared to that from the run solely using complex **4.6** (run 2, Table 4.6) suggest that the rate of exchange between complexes **4.5** and **4.6** is faster than 1-butene consumption.

Table 4.6: Impact of activation method on the performance of complex **4.5** mediated 1-butene dimerisation. [a] In units of mol 1-C_4 converted to oligomers (mol Co)$^{-1}$. [b] In units of g 1-C_4 converted to oligomers/g Co/h. [c] Wt % of liquid fraction; all catalysis runs only yielded liquid products. [d] LAO = linear α-olefin. [e] BO = branched olefins (2-ethyl-1-hexene (≥ 98 %)and 2-ethyl-3-methylpent-1-ene (≤ 2 %). [f] LIO= linear internal olefin.[g]Branched LAO. Catalysis conditions: 2 bar 1-C_4, PhF, 19 – 22 ^{o}C and (a) 50 µmol Cp*Co(C_2H_4)($P(OMe)_3$ (complex **4.5**) for Runs 1 and 4, (b) 50 µmol [Cp*Co(C_2H_5)($P(OMe)_3$] [B{1,3-(CF_3)$_2$-C_6H_3}$_4$] (complex **4.6**) for Run 2, or (c) 40 µmol complex **4.6** and 10 µmol complex **4.5** for Run 3.

Run	Activation method	Run time (h)	TON[a]	Activity[b]	% C_8 (wt %)[c]			% C_{12}[g] (wt %)[c]	% C_{16}[g] (wt %)[c]
					LAO[d]	BOs[e]	LIO[f]		
1	Complex **4.5**, without Brookhart's acid activator	72	0	0	0	0	0	0	0
2	Complex **4.6** only	44	59.2	1.28	0	65	1	25	9
3	Complexes **4.6** and **4.5** only (in 4:1 ratio, respectively)	40	11.8	0.28	2	63	2	24	9
4	Complex **4.5** and 0.8 eq. Brookhart's acid activator	44	14.9	0.32	4	67	2	20	7

4.3.4. Investigating effect of varying catalysis conditions in complex 4.5/Brookhart's acid mediated 1-hexene dimerisation catalysis

4.3.4.1. Comparison of 1-butene and 1-hexene dimerisation mediated by complex 4.5

Broene *et al.*[1] stated that complex **4.5** performed similarly in 1-hexene and 1-butene dimerisation systems, in the presence of 0.82 equiv. Brookhart's acid activator, however reported no data evidencing this statement. Therefore, complex **4.5** was tested in 1-hexene dimerisation in work carried out as a part of this thesis, under analogous conditions to those implemented for complex **4.5** mediated 1-butene dimerisation systems tested in section 4.3.3 (Figure 4.5). Upon comparing the 1-hexene and 1-butene dimerisation systems generated by complex **4.5**/Brookhart's acid (Table 4.7), it is evident that there are no differences in the TONs and activities (same within error), or liquid fraction selectivities to branched dimer and branched trimer products. However, application of complex **4.5**/Brookhart's acid in 1-hexene dimerisation generated twice as much LAO dimer than that formed in 1-butene dimerisation, with the latter process instead forming branched tetramers. The increased tendency of the 1-butene dimerisation system utilising complex **4.5**/Brookhart's acid to form tetramers may be rationalised in terms of the lower steric bulk of 1-butene *versus* 1-hexene.

Table 4.7: Comparison of performance of complex **4.5** in 1-butene and 1-hexene dimerisation. [a]In units of mol LAO monomer converted to oligomers (mol Co)$^{-1}$. [b] In units of g LAO monomer converted to oligomers/g Co/h. [c]Wt % of liquid fraction; all catalysis runs only yielded liquid products. [d] LAO = linear α-olefin. [e] BO = branched olefin. [f] LIO = linear internal olefin. [g] Average of repeat runs reported previously in Table 4.2. Catalysis conditions: 50 μmol Cp*Co(C_2H_4)($P(OMe)_3$, 0.8 eq. Brookhart's acid, 2 bar 1-C_4 or 15.3 mL 1-C_6, PhF, 72 h, 19 – 22 ^oC.

Run	Starting LAO monomer	TON[a]	Activity[b]	% dimer (wt %)[c]			% branched trimer (wt %)[c]	% branched tetramer (wt %)[c]
				LAO[d]	BO[e]	LIO[f]		
1[g]	1-C_4	16.1	0.21	5	71	1	18	5
2	1-C_6	10.0	0.20	9	72	0	19	0

4.3.4.2. Comparison of using in situ versus preformed complex 4.5 in 1-hexene dimerisation

The effect of using *in situ versus* preformed complex **4.5** in 1-hexene dimerisation was evaluated by conducting two catalysis runs (runs 1 and 2) under the conditions listed in Table 4.8. As expected, the results presented in Table 4.8 show that there is no

change to the TON, activity or liquid fraction selectivity of 1-hexene dimerisation if *in-situ* or preformed complex **4.5** is implemented in 1-hexene dimerisation. In addition, Cp*Co(C_2H_4)$_2$ (**4.4**) was tested in 1-hexene dimerisation in the presence of Brookhart's acid activator (run 3, Table 4.8) in order to test whether the observed 1-hexene *di-*/*tri-*merisation in run 2 (Table 4.8) was brought about by the presence of any unreacted complex **4.4**. The results from run 3 (Table 4.8) demonstrate that complex **4.4** displays negligible catalytic activity and exclusively forms linear internal dodecenes in 1-hexene dimerisation, in the presence of Brookhart's acid activator.

Table 4.8: Comparison of using *in-situ versus* preformed complex 4.5 in 1-hexene dimerisation. [a]In units of mol 1-C_6 converted to oligomers (mol Co)$^{-1}$. [b] In units of g 1-C_6 converted to oligomers/g Co/h. [c]Wt % of liquid fraction; all catalysis runs only yielded liquid products. [d] LAO = linear α-olefin. [e] BO = branched olefin = 2-butyl-1-octene. [f] LIO = linear internal olefin. [g]Average of repeat runs reported previously in Table 4.2. Catalysis conditions: 23 µmol Cp*Co(C_2H_4)(P(OMe)$_3$ (complex **4.5**) or Cp*Co(C_2H_4)$_2$ (complex **4.4**), 1.9 mL 1-C_6, 19 – 22 ^{o}C, PhF, 0.80 equiv. Brookhart's acid.

Run	Catalyst precursor	TON[a]	Activity[b]	% C_{12} (wt %)[c]			% branched C_{18} (wt %)[c]
				LAO[d]	BO[e]	LIO[f]	
1[g]	Preformed complex **4.5**	18.3	0.36	10	76	0	14
2	Cp*Co(C_2H_4)$_2$ and P(OMe)$_3$ (*in situ*)	14.8	0.29	8	76	0	16
3	Cp*Co(C_2H_4)$_2$	0.60	0.01	0	0	100	0

4.4. Attempted Synthesis and Catalytic Testing of Modified Variants of Broene's Cyclopentadienyl Cobalt Catalyst Precursor

Following a broad-brush evaluation of the impact of a range of catalysis test conditions on the activity and selectivity of Broene's cyclopentadienyl cobalt LAO dimerisation catalyst, which gave a baseline performance reference, little/no improvement in catalytic performance has been achieved. Consequently, with a view to developing a catalyst system for α-olefin to α-olefin dimerisation with enhanced catalytic activity and selectivity, attention then turned towards synthesising modified versions of Broene's cyclopentadienyl cobalt catalyst precursor. In particular, efforts were initially focussed on the impact of the steric and electronic properties of the ligands on selectivity and activity. To this end, the structure of Broene's cyclopentadienyl catalyst precursor was broken down into its constituent fragments and represented as (L_2X)CoL(C_2H_4), where Cp* is formally regarded as an L_2X ligand and P(OMe)$_3$ as an L ligand. The following

sections will discuss attempts undertaken as a part of this thesis to synthesise modified variants of Broene's catalyst precursor with different L_2X and L ligands, in addition to the synthesis of a constrained geometry cyclopentadienyl cobalt complex.

4.4.1. Attempts at synthesising modified variants of Broene's cyclopentadienyl cobalt catalyst precursor encompassing different L_2X ligands

From the proposed mechanism of 1-hexene *di*- and *tri*-merisation mediated by Broene's cyclopentadienyl cobalt catalyst (Scheme 4.24) it is evident that a fine balance of steric and electronic demands at the Co centre are required for the formation of 1-dodecene (species **4R** in Scheme 4.24).[1] It can be reasoned that the steric bulk about the Co centre (imposed by the Cp* and $P(OMe)_3$ moieties) is responsible for dictating an initial 1,2-insertion of the first 1-hexene molecule, followed by a 2,1-insertion of the second 1-hexene molecule. Following 2,1-insertion of the second 1-hexene molecule, the steric bulk at the Co centre can also be argued to promote isomerisation to the sterically favoured linear complex (**4V** in Scheme 4.24) from which 1-dodecene is then liberated by intermolecular proton exchange. In addition to the impact of the steric bulk at the Co centre on the formation of species **4V** (Scheme 4.24), the electronic properties associated with the Co centre are also important in determining the stability of species **4V**. Species **4V** (Scheme 4.24) is stabilised by a β-H agostic interaction, which arises due to the electron deficiency of the Co centre (16 VE).

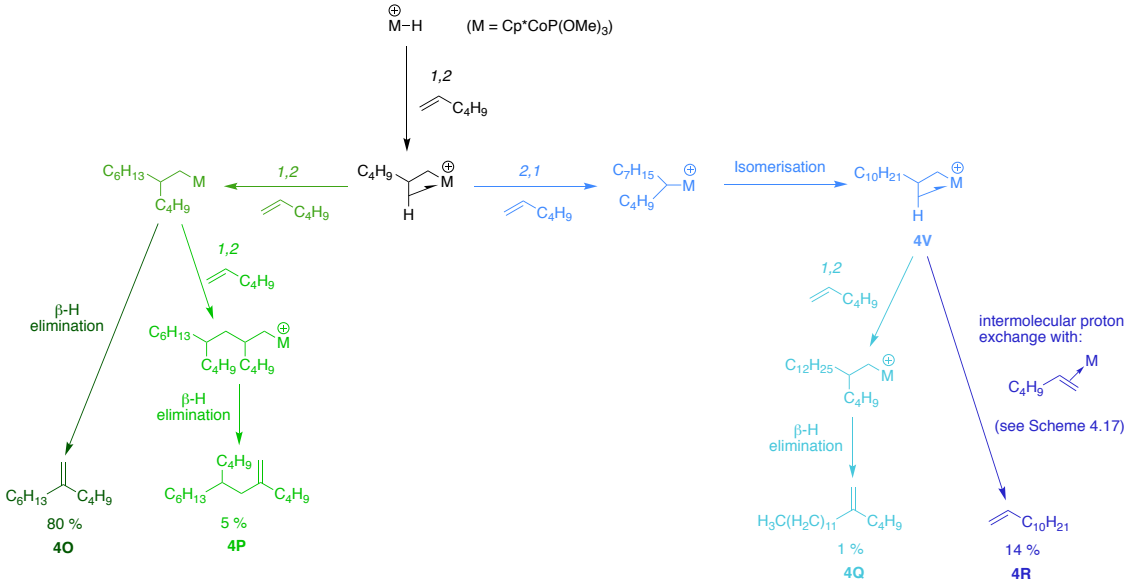

Scheme 4.24: Proposed mechanism of 1-hexene *di*- and *tri*-merisation mediated by [Cp*Co(η^2-C_2H_4)$(P(OMe)_3$] activated with a deficit of Brookhart's acid.[1]

Taking into consideration these steric and electronic factors, the effect of replacing the Cp* motif with bulkier L_2X ligands, such as indenyl and fluorenyl ligands was pursued (Figure 4.7). It was hoped that catalysts bearing these bulkier indenyl and fluorenyl moieties, in comparison to Cp*, would promote initial 1,2-insertion of the first hexene molecule and encourage isomerisation following 2,1-insertion of the second hexene molecule in 1-hexene dimerisation (Scheme 4.24). In addition, it is postulated that catalysts encompassing bulkier indenyl and fluorenyl ligands, compared to Cp*, should prevent the insertion of a third hexene molecule and so result in a catalytic system displaying greater selectivity towards 1-hexene dimerisation. Furthermore, the less electron donating nature of indenyl and fluorenyl, relative to Cp*,[57] also makes them attractive L_2X ligand variants to explore as this should also encourage production of species **4V** (Scheme 4.24) by stabilising its β-H agostic interaction.

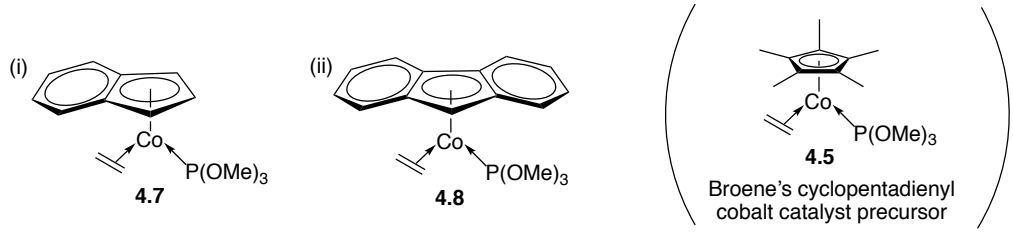

Figure 4.7: Target variants of Broene's cyclopentadienyl cobalt catalyst precursor with (i) indenyl (**4.7**) and (ii) fluorenyl (**4.8**) L_2X ligands in place of Cp*.

In addition to their different electron donating properties, indenyl and fluorenyl ligands are amenable to ring slippage η^5-M to η^3-M (illustrated in Scheme 4.25) in contrast to their cyclopentadienyl analogues.[58,59] It was hoped that this ability to undergo ring slippage would afford the η^5-indenyl and η^5-fluorenyl complexes increased reactivity in thermal ligand exchange reactions.[58,59] For example, the rates of the substitution reaction between $(L_2X)Mn(CO)_3$ and P(*n*-Bu)$_3$ to form $(L_2X)Mn(CO)_2P(n\text{-Bu})_3$ at ~140 °C in decalin vary with the nature of L_2X: L_2X = Cp, rate = 0 $M^{-1}\,s^{-1}$; L_2X = indenyl, rate = 1.34×10^{-4} $M^{-1}\,s^{-1}$; L_2X = fluorenyl, rate = 3.30×10^{-2} $M^{-1}\,s^{-1}$. [60,61] The greater disposition of indenyl and fluorenyl ligands towards ring slippage has been attributed to their better ability to stabilise the η^3-allyl intermediates, which are formed in the ligand exchange reactions, *via* aromatisation of the benzene rings of the indenyl and fluorenyl moeities. [58,59,61] Consequently, complexes containing fluorenyl ligands are the most reactive due to delocalisation of the π electrons over three aromatic rings.[58,59,61] The greater "coordination flexibility" of indenyl and fluorenyl ligands, compared to their cyclopentadienyl analogues, therefore makes transition metal complexes containing these ligands interesting to investigate in dimerisation catalysis as it provides them with

the potential to adapt as a function of the electronic and steric demands during the dimerisation catalytic cycle.

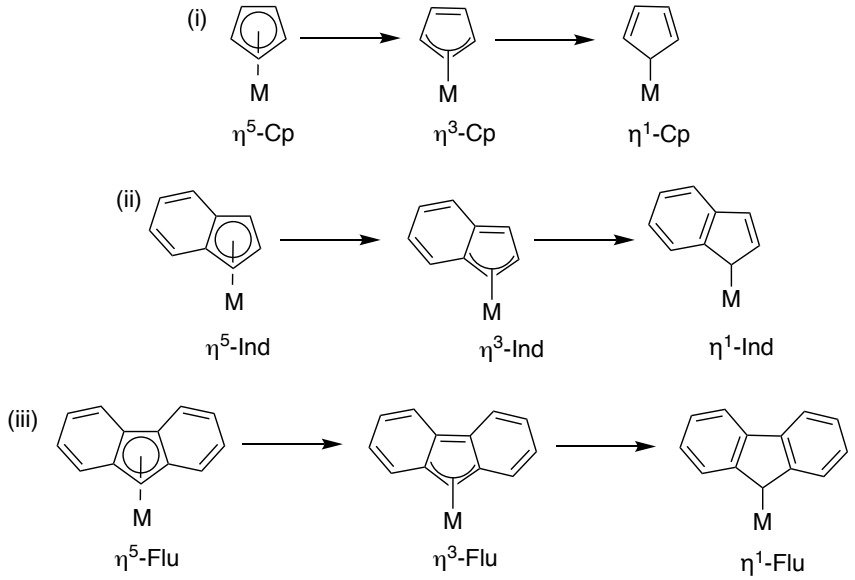

Scheme 4.25: Ring slippage displayed by (i) η^5-Cp, (ii) η^5-indenyl, and (iii) η^5-fluorenyl complexes, where M represents a transition metal.[58,59]

The following sections outline the different synthetic strategies used with a view to preparing the target complexes **4.7** and **4.8** (Figure 4.7).

4.4.1.1. Attempted syntheses of indenyl and fluorenyl cobalt dicarbonyl complexes

The synthesis of indenyl and fluorenyl variants of Broene's cyclopentadienyl cobalt catalyst precursor (complex **4.5**) *via* modifications of the synthetic route implemented for the synthesis of complex **4.5** seemed the obvious first starting point (Scheme 4.26). Unfortunately, the first synthesis step in Scheme 4.26 proved troublesome, thereby preventing attempts of the preceding reactions to complexes **4.7** and **4.8**.

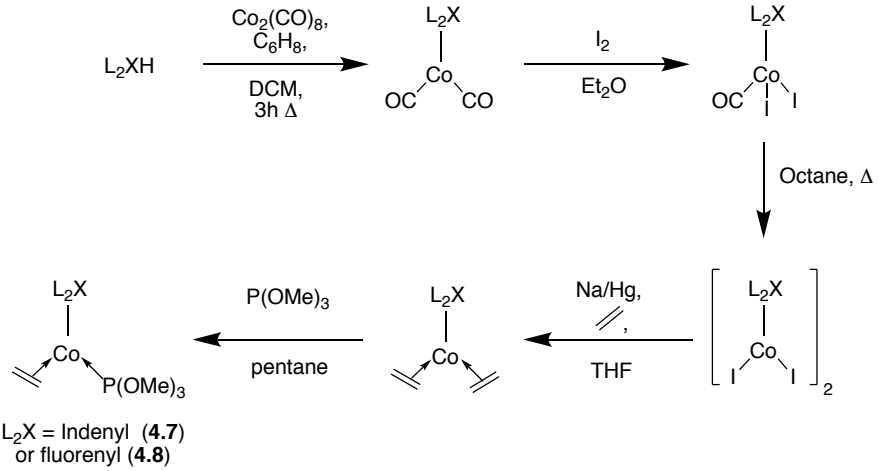

Scheme 4.26: Target synthetic routes to indenyl and fluorenyl variants of Broene's cyclopentadienyl cobalt catalyst precursor, by analogy with literature work related to the synthesis of $Cp^*Co(C_2H_4)(P(OMe)_3$.[36-38]

The reaction between indene and $Co_2(CO)_8$ in the presence of 1,3-cyclohexadiene and DCM (Scheme 4.27), afforded a mixture of $Co_4(CO)_{12}$ and $[Co(\eta^4\text{-}C_6H_8)(CO)(\mu\text{-}CO)]_2$ (**4.9**); identities of these products were elucidated by NMR spectroscopic, IR spectroscopic and mass spectrometric analyses.

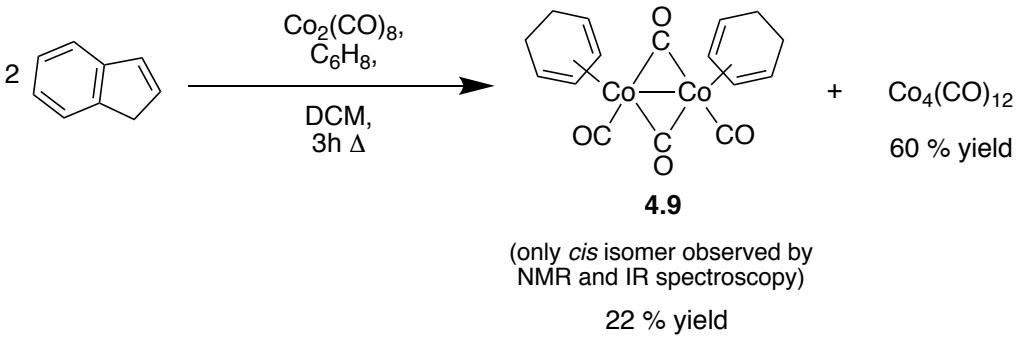

Scheme 4.27: Reaction between indene, $Co_2(CO)_8$, and 1,3-cyclohexadiene (C_6H_8).

Using a similar experimental methodology to that shown in Scheme 4.27, the synthesis of (Flu)$Co(CO)_2$ was also attempted by C. Brodie in the Dyer group (Scheme 4.28).[62] However, the reaction shown in Scheme 4.28 only yielded $Co_4(CO)_{12}$ and the dimeric η^4-cyclohexadiene complex **4.9**, in addition to unreacted fluorene starting material (identities of each of these products being confirmed by NMR and IR spectroscopic and mass spectrometric analyses).[62a]

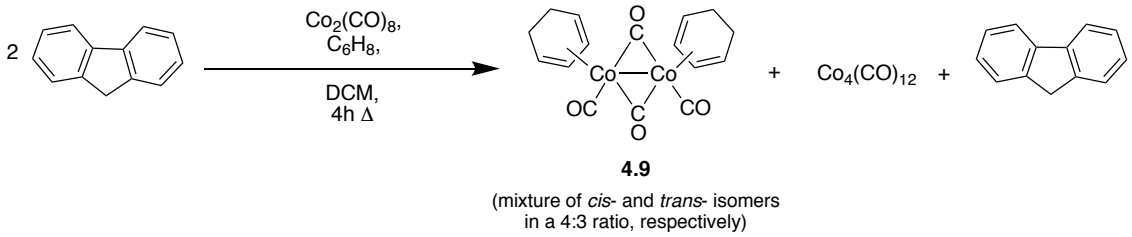

Scheme 4.28: Reaction between fluorene, $Co_2(CO)_8$, and 1,3-cyclohexadiene, conducted by C. Brodie in the Dyer group.[62]

With hindsight, the undesired formation of $Co_4(CO)_{12}$ and cyclohexadiene complex **4.9** as the major products in the reactions between $Co_2(CO)_8$ and 1,3-cyclohexadiene with indene or fluorene is not surprising. Firstly, the thermal decomposition of $Co_2(CO)_8$ to $Co_4(CO)_{12}$ is documented in the literature.[63] Additionally, Winkhaus and Wilkinson reported the formation of the cyclohexadiene complex **4.9** by the reaction between $Co_2(CO)_8$ and 1,3-cyclohexadiene (Scheme 4.29), and found that longer reaction times and higher temperatures led to partial decomposition of complex **4.9** and formation of $Co_4(CO)_{12}$ and metallic Co.[64,65]

[a] The mixture of products was not separated and hence the actual yields of the individual products could not be determined.

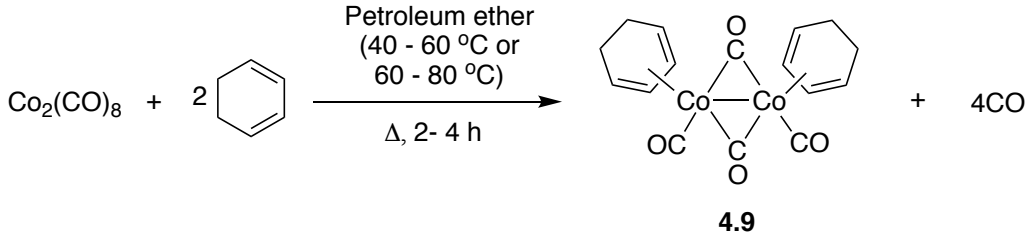

Scheme 4.29: Synthesis of $[Co(\eta^4\text{-}C_6H_8)(CO)(\mu\text{-}CO)]_2$ reported by Winkhaus and Wilkinson.[64,65]

With the above observations in mind, it is therefore proposed that in the reactions between $Co_2(CO)_8$, 1,3-cyclohexadiene and indene or fluorene, the formation of $Co_4(CO)_{12}$ and cyclohexadiene complex **4.9** occurs *via* the reactions outlined in Scheme 4.30.

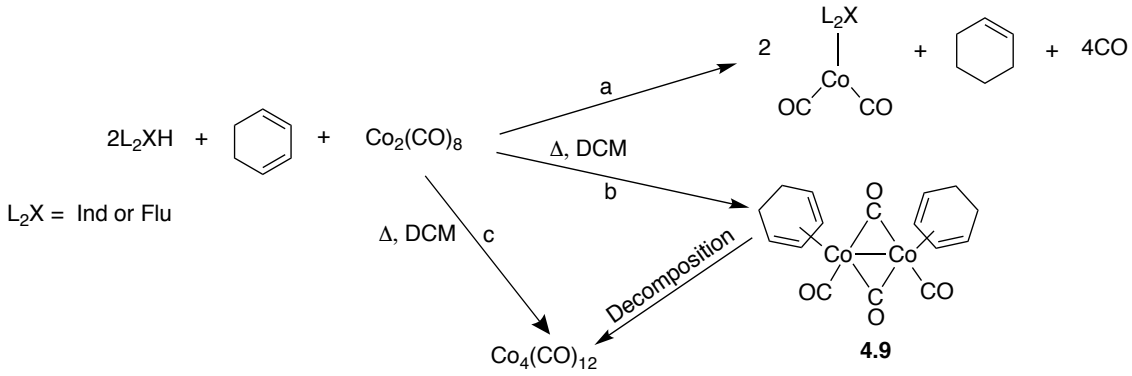

Scheme 4.30: Competing reactions in synthesis of target $(L_2X)Co(CO)_2$ complexes.

Although $IndCo(CO)_2$ or $(Flu)Co(CO)_2$ failed to be obtained in reactions between $Co_2(CO)_8$ and 1,3-cyclohexadiene with indene or fluorine under the conditions shown in Schemes 4.27 and 4.28, the analogous reaction with pentamethylcyclopentadiene resulted in a 81% yield of the desired product $Cp^*Co(CO)_2$ (section 4.2.1). The difference in reactivity between pentamethylcyclopentadiene, indene, and fluorene with $Co_2(CO)_8$ and 1,3-cyclohexadiene is attributed to differences in sterics and electronics of these different L_2X ligands, in particular the differing extents of aromatic stabilisation. For the synthesis of $(L_2X)Co(CO)_2$ *via* the reaction between L_2XH ligands, $Co_2(CO)_8$ and 1,3-cyclohexadiene (Scheme 4.30), the L_2XH ligands must undergo deprotonation – and hence reactivity may be affected by the ease with which deprotonation takes place. However, a comparison of the pK_a values of indene, fluorene, and Cp*H reveals that the latter is the least acidic out of the trio (pK_a values: 20.1 {indene}, 22.6 {fluorene}, 26.1 {Cp*H}),[66] suggesting that another factor than the different acidities of the L_2X ligands is responsible for the observed differences in the reaction illustrated in Scheme 4.30 with different L_2X ligands. The success of formation of $(L_2X)Co(CO)_2$ by

the reaction depicted in Scheme 4.30 can also be argued to be dependent upon the strength of the L_2XH ligands as reducing agents for 1,3-cyclohexadiene. The strength of L_2XH as reducing agents can be inferred from their oxidation potentials, E_{ox} (reported in units of V *vs* SCE): indene = 1.71,[67] fluorene = 1.58,[68] Cp*H = 0.87.[69] These data show that fluorene and indene are poorer reducing agents than Cp*H. Therefore, it can be reasoned that the observed differences in reactivity of Cp*H, indene and fluorene, under the conditions shown in Scheme 4.30, are likely to be due to their different reduction potentials. Finally, the increased steric bulk of the indenyl and fluorenyl ligands, compared to Cp*H, may also be responsible for the observed difficulty in forming $IndCo(CO)_2$ and $(Flu)Co(CO)_2$ by the reaction shown in Scheme 4.30. Due to the unsuccessful synthesis of indenyl and fluorenyl cobalt dicarbonyl complexes by the route shown in Scheme 4.30, the synthesis of target complexes **4.7** and **4.8** (Figure 4.7) by a different route to that displayed in Scheme 4.26, which avoids the use of $Co_2(CO)_8$ starting material (due to its propensity to thermally decompose to $Co_4(CO)_{12}$), was subsequently pursued.

4.4.1.2. Attempted syntheses of indenyl and fluorenyl cobalt halide complexes

The synthesis of indenyl and fluorenyl cobalt halide complexes, as precursors to target complexes **4.7** and **4.8,** was subsequently attempted by the route shown in Scheme 4.31. A salt metathesis strategy was chosen in this context due to the ample precedence of related Cp* cobalt halide complexes being prepared in such a fashion in the literature.[70-73]

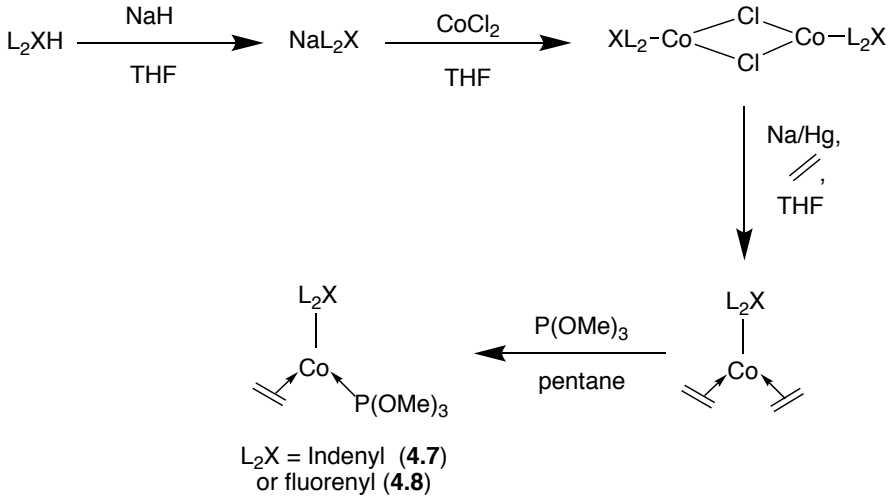

Scheme 4.31: Proposed synthetic route to target complexes **4.7** and **4.8** starting from indenyl and fluorenyl cobalt halide complexes.

The synthesis of fluorenyl cobalt chloride was first attempted by reacting pre-prepared sodium fluorenide with $CoCl_2$ under similar conditions to those used in the literature for

the synthesis of pentamethylcyclopentadienyl cobalt chloride (Scheme 4.32).[72] However, this reaction was found to form bifluorene (**4.10**) and a black solid (believed to be Co metal based on its appearance and insolubility in a range of organic solvents), instead of the desired fluorenyl cobalt chloride. In addition unreacted starting materials, namely fluorene and the previously reported $nCo_2Cl_4(THF)_4$ (**4.11**),[b] were also recovered in the reaction between sodium fluorenide with $CoCl_2$.

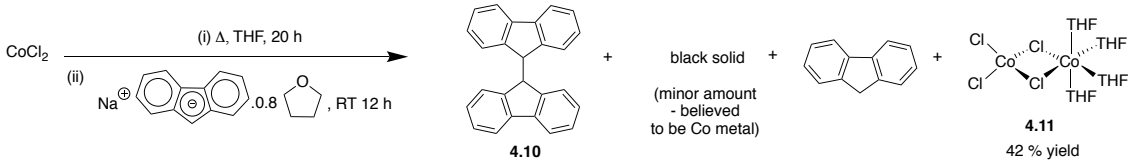

Scheme 4.32: Reaction of sodium fluorenide with $CoCl_2$.

The formation of bifluorene was confirmed by ^1H NMR spectroscopy, which revealed its existence alongside fluorene, in a ratio of 1:0.8, respectively. The production of bifluorene *via* the reaction shown in Scheme 4.32 is in agreement with the experiments conducted by Al-Afyouni *et al.* who demonstrated that salt metathesis reactions of lithium fluorenide with $CoCl_2$ or CoI_2 generated mixtures of bifluorene and fluorine.[75] The formation of bifluorene in the salt metathesis reactions performed by Al-Afyouni *et al.* was proposed to be a result of radical coupling as illustrated in Scheme 4.33 (evidence of this being obtained from radical trapping experiments).[75] Al-Afyouni *et al.* also stated that an alternative mechanism for the formation of bifluorene could be the formation of Flu_2Co, which then undergoes reductive coupling generating Co^0 and bifluorene, however discounted this mechanism due to the stability of related *bis*(indenyl) cobalt complexes.[75] Due to the observed formation of Co metal under the conditions shown in Scheme 4.32, it is believed that under these conditions the formation of bifluorene may occur from reductive coupling of Flu_2Co, as well as by the mechanism shown in Scheme 4.33.

[b] The formation of complex **4.11** was confirmed by X-ray crystallography (with the data being obtained matching those for $CoCl_2(THF)_4$ reported in the literature)[74] and mass spectrometry.

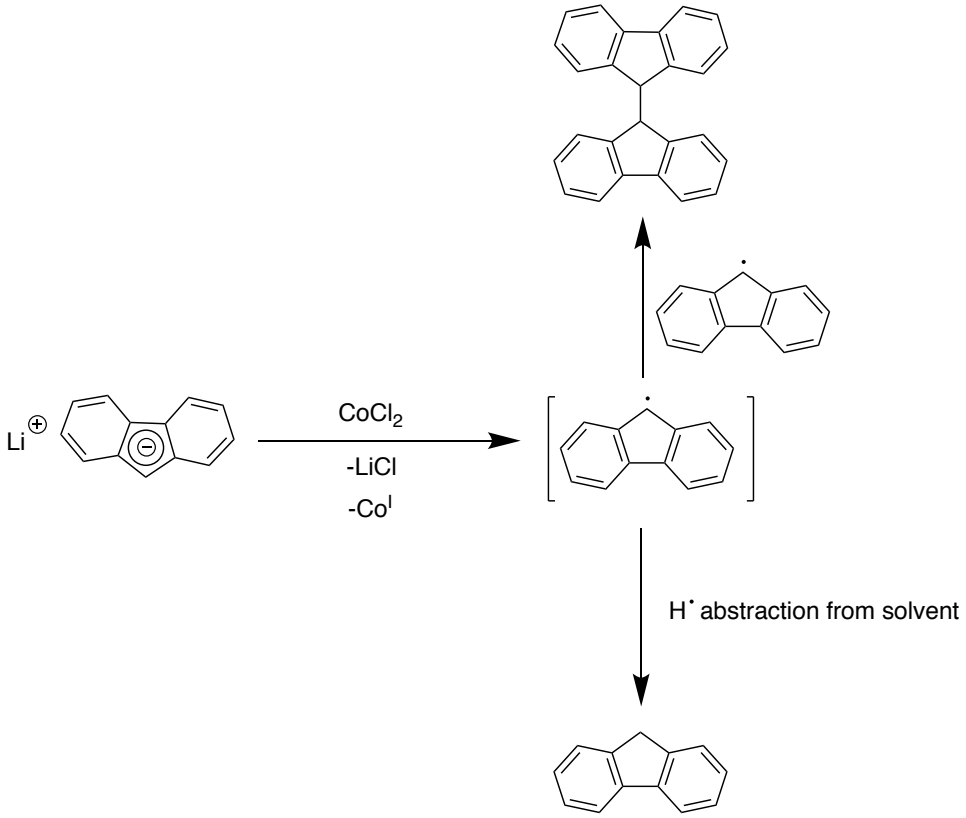

Scheme 4.33: Proposed formation of bifluorene in salt metathesis reactions, adapted from Al-Afyouni *et al.*[75]

Following the failure of the reaction between sodium fluorenide and $CoCl_2$ to yield the desired (fluorenyl)cobalt chloride, analogous reactions with sodium indenide were conducted to compare how these would fair. The reactions between pre-formed sodium indenide and cobalt chloride, under analogous conditions implemented in the literature for the synthesis of pentamethylcyclopentadienyl cobalt chloride (Scheme 4.34),[70-73,76] also did not form the desired (indenyl)cobalt chloride and instead afforded complexes **4.12**, **4.13**, and a black solid (believed to be Co). The structure of complex **4.12** was confirmed by mass spectrometry and X-ray crystallography (which was in agreement with the molecular structure previously reported in the literature).[77]

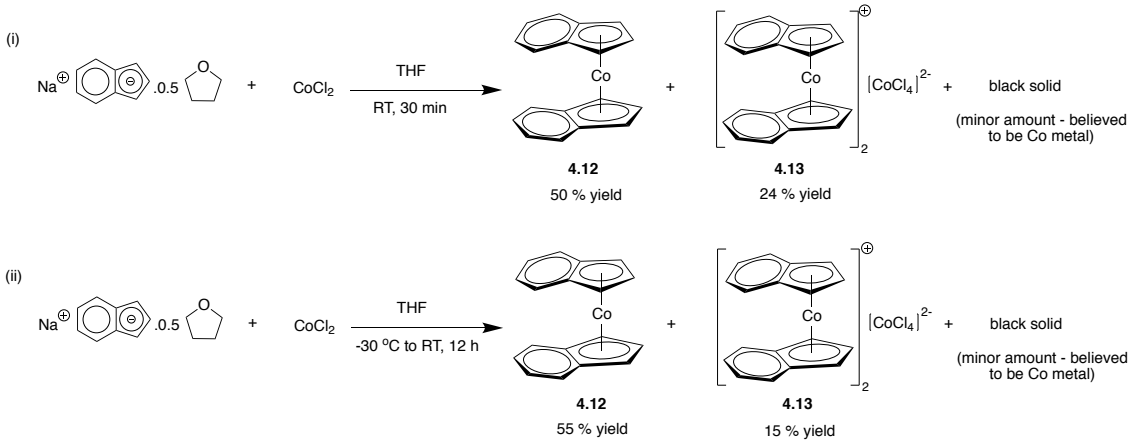

Scheme 4.34: Reactions between sodium indenyl and $CoCl_2$ at (i) room temperature and (ii) −30 °C.

In addition to mass spectrometry and X-ray crystallography, NMR spectroscopy was also implemented to verify the structure of complex **4.13**. The choice of NMR solvent used for the analysis of complex **4.13** was found to be important, with well-defined proton spectra only being obtained in D_2O, with samples dissolved in deuterated DCM, THF, and acetone all giving rise to spectra with broad, uninterpretable resonances. Crystals of complex **4.13**, suitable for an X-ray crystallography study, were obtained by recrystallisation of the reaction mixture from THF at −30 °C**.** A discussion of the molecular structure of complex **4.13**, which has previously not been reported in the literature, is given in the Appendices, section 6.2.1.

In order to investigate if the source of cobalt halide affected the reactivity of the salt metathesis reactions with sodium indenide, the reaction between cobalt diiodide and sodium indenide was conducted under the conditions shown in Scheme 4.35. Similar to the reactions between sodium indenide and cobalt chloride (Scheme 4.34), the comparable reaction with cobalt iodide yielded Co metal and the cationic indenyl metallocene (complex **4.14**). However, the formation of the neutral indenyl metallocene species (complex **4.12**, Scheme 4.34) was not observed (Scheme 4.35).

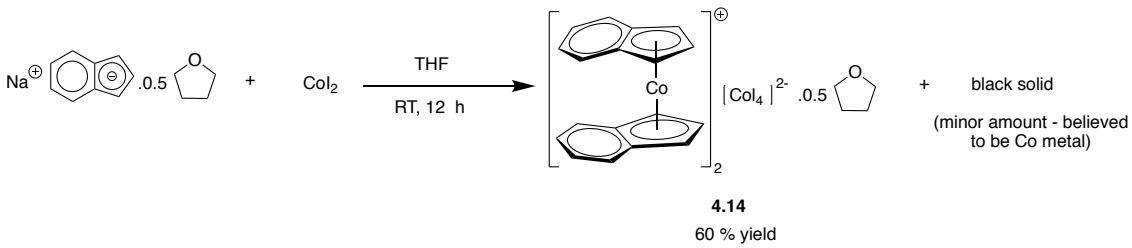

Scheme 4.35: Reaction between sodium indenide and cobalt iodide.

The identity of complex **4.14** was verified by NMR spectroscopy, mass spectrometry, and X-ray crystallography. Crystals suitable for X-ray crystallography were obtained by

recrystallisation from THF at −30 °C**.** A discussion of the molecular structure of complex **4.14**, which has previously not been reported in the literature, is given in the Appendices, section 6.2.1.

The formation of Co metal and complexes **4.12** – **4.14** in the reactions shown in Scheme 4.34 and Scheme 4.35 suggest that the desired (indenyl)cobalt chloride species may have been produced, but subsequently underwent decomposition to afford complexes **4.12** – **4.14** under the reaction conditions employed. This suggestion is based on the literature reports by Roe *et al.*[78] and Chakraborty *et al.*[79] in which the decomposition of heteroleptic cyclopentadienyl metal halides $[CpM(\mu\text{-}X)]_2$ into homoleptic MX_2 and neutral or cationic Cp_2M species is observed. Nevertheless, stable heteroleptic complexes of the form $[CpM(\mu\text{-}X)]_2$ have been obtained using bulkier ligands such as Cp*, which are rationalised to provide substantial kinetic stabilisation.[37–40,42] Since the indenyl ligand is arguably more sterically demanding than cyclopentadienyl, the observed decomposition that occurs on reaction between sodium indenide and cobalt dichloride (Scheme 4.34) are unlikely to result from unfavourable steric interactions. Indeed, Roe *et al.* reported that the choice of reaction solvent can significantly influence the rates of decomposition of $[CpM(\mu\text{-}X)]_2$ species, with degradation only occurring in polar, coordinating solvents (such as THF).[78] Since THF was used for the reactions between sodium indenide and CoX_2 (X= Cl or I, Scheme 4.34 and Scheme 4.35), it is believed that this choice of solvent medium contributed to the observed decomposition of the desired (indenyl)cobalt chloride complexes. Therefore, it is of interest to investigate the reactions between sodium indenide and cobalt halides in non-polar solvents (such as DCM) to see if the desired indenyl cobalt chloride species can be obtained. Unfortunately, time restrictions prevented the attempt of such reactions as part of work towards this thesis.

4.4.1.3. Attempted synthesis of $IndCo(C_2H_4)(P(OMe)_3)$ from Ind_2Co

The undesired formation of complex **4.12** in the salt metathesis reactions between $CoCl_2$ and sodium indenide (Scheme 4.34) inspired an attempt into the synthesis of $IndCo(C_2H_4)(P(OMe)_3)$ (complex **4.7**) by the route depicted in Scheme 4.36. The transformation of cobaltocene (Cp_2Co), **4.12**, into $CpCo(C_2H_4)_2$ is well documented in the literature, and so it is hoped that under the same conditions (Scheme 4.36) Ind_2Co could also react in this way to form $IndCo(C_2H_4)_2$. [80-82]

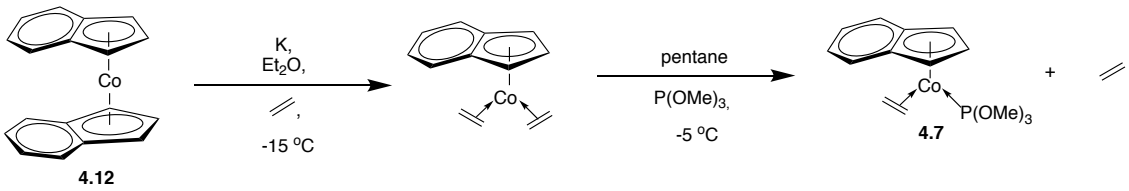

Scheme 4.36: Proposed synthetic route to complex **4.7** starting from complex **4.12**.

On attempting the potassium reduction of complex **4.12** under an atmosphere of ethylene (Scheme 4.36), a red solution was obtained, which was separated by filteration from unreacted potassium. This red solution, believed to be $IndCo(C_2H_4)_2$,[c] was reacted with $P(OMe)_3$ over a period of 15 h. Subsequent extraction of the reaction mixture with pentane and analysis of the products by NMR spectroscopy (^1H, $^{13}C\{^1H\}$, and $^{31}P\{^1H\}$), revealed the presence of a mixture of species with multiple, different $P(OMe)_3$ and indenyl environments. Unfortunately, all attempts to separate and isolate products by recrystallisation (hexane, −30 °C) led to the formation of a black solution, something believed to be a result of decomposition yielding a suspension of finely divided cobalt. All further attempts to prepare complexes of this nature were stopped.

4.4.2. Synthesis of modified version of Broene's cyclopentadienyl cobalt catalyst precursor with different L donor ligands

The successful dimerisation of LAOs (C_4, C_6, and C_8) to their respective LAO dimers by Broene's cyclopentadienyl cobalt catalyst may, in part, be attributed to the electronic properties of the phosphite moiety, $P(OMe)_3$, employed. Phosphites are strong π-acceptors.[84] We propose that this π-acidic character is important, reducing the electron density at the Co centre, thereby preventing β-H elimination of the metal alkyl complex (complex **4V** in Scheme 4.17). This, in turn, prevents the formation of internal olefinic products (favoured on thermodynamic grounds) *via* isomerisation.

Therefore, in order to test whether the validity of this supposition that a π-acidic ligand on Broene's cyclopentadienyl cobalt catalyst favours selectivity towards the LAO dimer, the synthesis of the analogous $[Cp^*Co(C_2H_4)(P(pyrrolyl)_3]$ complex (**4.15**) was undertaken. The reported "exceptional π-acceptor character" of $P(pyrrolyl)_3$ makes it an attractive alternative two-electron L donor ligand to $P(OMe)_3$.[85] The π-acceptor character of $P(pyrrolyl)_3$ was inferred from a comparison of the molecular structures of a series of $RhCl(CO)L_2$ complexes (L = phosphine, phosphite, or $P(pyrrolyl)_3$), which

[c] Due to the reported instability of $IndCo(C_2H_4)_2$ at temperatures higher than 0 °C, the reaction intermediate could not be isolated and characterised in order to confirm its identity as being $IndCo(C_2H_4)_2$.[83]

revealed shorter Rh-P distances and longer Rh-C distances when L= $P(pyrrolyl)_3$.[85] Further demonstration of the "exceptional π-acceptor character" of $P(pyrrolyl)_3$ came from their reactivity with $[PPN][Rh(CO)_4]$, where the stepwise displacement of CO with $P(pyrrolyl)_3$ was observed, generating the series of $[PPN][Rh(CO)_{4-x},\{P(pyrrolyl)_3\}_x]$ (x = 1 - 4) complexes.[85]

The synthesis of $[Cp^*Co(C_2H_4)(P(pyrrolyl)_3]$ (**4.15**) was conducted under the conditions shown in Scheme 4.37 with complex **4.15** being obtained in 70 % isolated yield. The identity of complex **4.15** was verified by ^1H, $^{13}C\{^1H\}$, and $^{31}P\{^1H\}$ NMR spectroscopies. The resonance in the $^{31}P\{^1H\}$ NMR spectrum of complex **4.15** at 133.1 ppm is very broad ($\nu_{½}$ = 287 Hz), as would be expected from the scalar coupling between the quadrupolar Co nucleus and the P nucleus (as previously discussed in section 4.2.1).

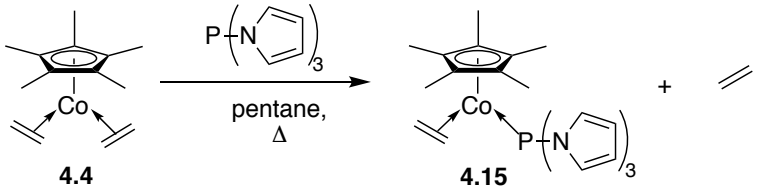

Scheme 4.37: Synthesis of $[Cp^*Co(C_2H_4)(P(pyrrolyl)_3]$ (**4.15**).

A molecular structure of complex **4.15** was obtained by recrystallizing the crude reaction product from petroleum ether (b.p. 40 – 60 °C) at −78 °C. The molecular structure of complex **4.15,** which has not previously been reported in the literature, is shown in Figure 4.8 alongside selected bond lengths.[d] Similar to the molecular structure of complex **4.5** (Figure 4.4), the cobalt centre of **4.15** also exhibits a two-legged piano stool geometry in which the Cp* ring deviates slightly from being symmetrically disposed with respect to the Co centre (evident from the unequal distances between Co and the ring C atoms on Cp*: 2.078(2) - 2.128(2) Å). The plane of the Cp* ligand is at a distance of 1.719 Å from the Co atom in complex **4.15**. As expected, the C–C bond distance of the coordinated ethylene ligand in complex **4.15** (1.415(4) Å) is longer than that reported for a pure $C(sp^2)$-$C(sp^2)$ (1.33 Å) bond,[86] indicative of the π-acceptor character of the ethylene ligand. Although the C=C bond length in complex **4.15** is the same (within error) as the C=C bond length in complex

[d] The unit cell for complex **4.15** contains two molecules, one of which exhibits disorder about the whole structure (present in 6%). Since, both molecules have similar bond angles and lengths, only the molecular structure and bond lengths and angles of the ordered molecule (present in majority, 94%) are reported here.

4.5 (Table 4.1), the shorter Co-P distance of 2.0693(7) Å in complex **4.15** *vs.* the Co-P distance of 2.0839(5) Å in complex **4.5** is indicative of the greater π-acceptor character of P(pyrrolyl)$_3$ relative to P(OMe)$_3$. Further evidence for the π-acceptor character of P(pyrrolyl)$_3$ in complex **4.15** comes from the longer average P-N bond length of 1.732(2) Å in complex **4.15**, compared to the P-N bond length of 1.70 Å of the uncoordinated P(pyrrolyl)$_3$ ligand.[87]

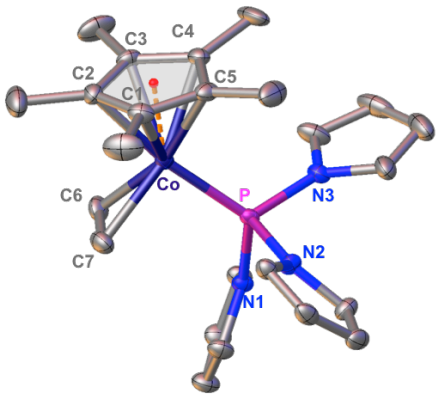

Bond lengths (Å)	
Co-C1	2.108(2)
Co-C2	2.078(2)
Co-C3	2.102(2)
Co-C4	2.128(2)
Co-C5	2.101(2)
Co-Cent	1.719
Co-C6	2.005(2)
Co-C7	2.010(2)
Co-P	2.0693(7)
C6-C7	1.415(4)
P-N1	1.7435(19)
P-N2	1.7154(19)
P-N3	1.739(2)

Figure 4.8: Molecular structure and selected bond lengths of complex **4.15**, with thermal ellipsoids set at the 50 % probability level; H atoms have been omitted for clarity. Computed centroid (Cent) for Cp ring shown in red with distance from centroid to Co centre represented by dashed orange line. Estimated standard deviations given in brackets.

4.4.2.1. Performance of complex 4.15 in 1-hexene dimerisation

The performance of complex **4.15** in 1-hexene dimerisation, under comparable conditions to those used for Broene's P(OMe)$_3$ cobalt catalyst precursor (complex **4.5**), was tested (Table 4.9). From these data it is apparent that complex **4.15** shows no selectivity towards the desired LAO dimer in 1-hexene dimerisation, when activated with 0.8 eq. Brookhart's acid, despite the strong π-acidic character of P(pyrrolyl)$_3$. Instead, the catalytic system generated using complex **4.15** is selective towards 1-hexene trimerisation, albeit with an extremely low TON and activity (Table 4.9). The increased trimerisation selectivity of complex **4.15** in 1-hexene dimerisation *versus* complex **4.5** is surprising due to the greater steric bulk of P(pyrrolyl)$_3$ *versus* P(OMe)$_3$ (145^o cone angle for the former phosphine compared to 107^o for the latter). [85,88] The results in Table 4.9 also show that the use of *in situ versus* preformed catalyst precursor **4.15** produces 1-hexene trimerisation systems with essentially identical TONs, activities and liquid fraction product selectivities. The identical 1-hexene catalysis results observed here for using *in situ versus* preformed catalyst precursor

4.15, coupled with those previously observed in section 4.3.4.2 using *in situ*/preformed catalyst precursor **4.5**, show that screening of different "L" ligands in 1-hexene dimerisation catalysis can be efficiently conducted using Cp*Co(C_2H_4), making the relevant Cp*Co(C_2H_4)L catalyst precursor *in situ*.

Table 4.9: Comparison of the performances of complexes **4.5** and **4.15** in 1-hexene dimerisation. [a] In units of mol 1-C_6 converted to oligomers (mol Co)$^{-1}$. [b] In units of g 1-C_6 converted to oligomers/g Co/h. [c] Wt % of liquid fraction; all catalysis runs only yielded liquid products. [d] LAO = linear α-olefin. [e] BO = branched olefin = 2-butyl-1-octene. [f] LIO = linear internal olefin. Catalysis conditions for runs 1 and 3: 23 μmol Cp*Co(C_2H_4)(P(OMe)$_3$) (**4.5**) or [Cp*Co(C_2H_4)(P(pyrrolyl)$_3$] (complex **4.15**), 1.9 mL 1-C_6, 19 – 22 ^{o}C, PhF, 0.80 equiv. Brookhart's acid. Catalysis conditions for run 2: 168 μmol Cp*Co(C_2H_4)$_2$, 13.8 mL 1-C_6, 19 – 22 ^{o}C, PhF, 0.80 equiv. Brookhart's acid.

Run	Catalyst precursor	TON[a]	Activity[b]	% C_{12} (wt %)[c]			% branched C_{18} (wt %)[c]
				LAO[d]	BO[e]	LIO[f]	
1	Preformed complex **4.15**	0.9	0.02	0	0	29	71
2	*In situ* formed complex **4.15** (from Cp*Co(C_2H_4)$_2$ and P(pyrrolyl)$_3$)	0.7	0.01	0	0	35	65
3	Preformed complex **4.5**	18.3	0.36	10	76	0	14

4.4.3. Synthesis of constrained geometry cyclopentadienyl cobalt complex

The poor TON achieved using Broene's cyclopentadienyl cobalt catalyst (TON for dimers: 7 after 23 h)[1] may be attributed to poor catalyst stability. It was therefore hypothesized that analogous structures to Broene's cyclopentadienyl cobalt catalyst in which the L_2X and L ligands are linked by an ethylene bridge, resulting in the formation of constrained geometry-type complexes (CGC, Figure 4.9), could perform better in LAO dimerisation catalysis. The tether motif is expected to impart greater stability to the CGC complexes by preventing dissociation of the L ligand through exploitation of the chelate effect.

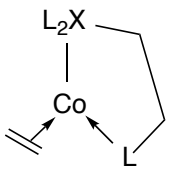

Figure 4.9: Proposed structure of constrained geometry complexes.

To this end, initial work was conducted at Sasol (by B. Core) in which a series of CGC Co halide complexes with different L donor ligands were synthesised and tested in ethylene oligomerisation catalysis (Scheme 4.38, Table 4.10).[89] Of the CGC Co halide complexes tested in ethylene oligomerisation catalysis (Scheme 4.38, Table 4.10), the best selectivity towards LAO dimerisation was obtained with (Cp*^NMe$_2$)CoI$_2$. [89]

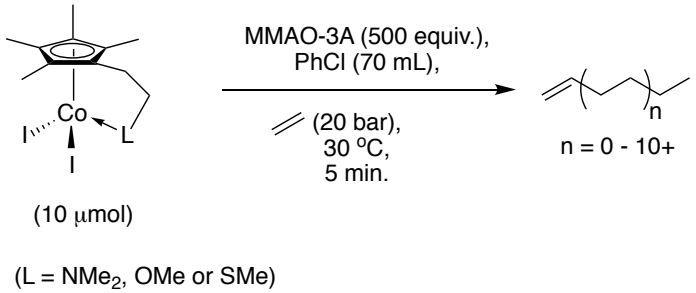

Scheme 4.38: Catalysis testing conditions of CGC Co halide complexes in ethylene oligomerisation, conducted by B. Core and M. Hanton.[89]

Table 4.10: Performance of CGC Co halide complexes in ethylene oligomerisation, under the conditions shown in **Scheme 4.38**.[89]

Catalyst precursor	Activity (mol =)(mol Co)$^{-1}$h^{-1}	C_4 {1-C_4} (wt %)	C_6 {1-C_6} (wt %)	C_{8+} (wt %)
(Cp*^NMe$_2$)CoI$_2$	14,126	97.7 {80.7}	2.3	0
(Cp*^OMe)CoI$_2$	96,530	97.4 {5.1}	2.4 {1.5}	0.2
(Cp*^SMe)CoI$_2$	36,160	96 {8.5}	3.8 {3.5}	0.2

Building on the promising results demonstrated by (Cp*^NMe$_2$)CoI$_2$, the *bis*(ethylene) complex **4.16** (a known literature complex) was synthesised from previously-prepared (Cp*^NMe$_2$)CoI$_2$, under the conditions shown in Scheme 4.39. The structure of complex **4.16** was confirmed by ^{1}H and ^{13}C{^{1}H} NMR analysis, which matched with that reported in the literature. [90,91]

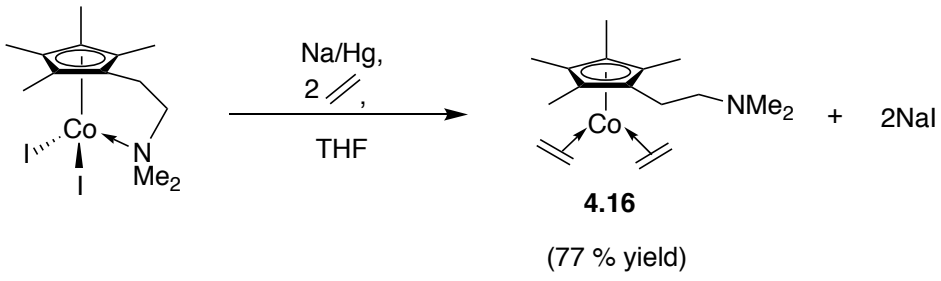

Scheme 4.39: Synthesis of complex **4.16**.

Complex **4.16** was subsequently tested in 1-butene dimerisation (Table 4.11) and found to give rise to a system displaying negligible catalysis and with no selectivity

towards the desired LAO dimer. The low TON and activity of complex **4.16** in 1-butene dimerisation, relative to the TON and activity displayed by complex **4.5** under analogous conditions (Table 4.11) is suggestive that the active catalytic species formed in the system using complex **4.16** is less stable than complex **4.6** (the active species generated from complex **4.5**). Based on the structure of the active catalyst species generated in the system implementing complex **4.5**, it is reasonable to assume that the active catalytic species produced in the system using complex **4.16** has the structure shown in Figure 4.10(a) (complex **4.16a**, *i.e.* a constrained geometry complex). The observed low TON and activity of complex **4.16** in 1-butene dimerisation is suggestive of complex **4.16a** (Figure 4.10(a)) exhibiting low stability under the conditions implemented in dimerisation; contrary to the hypothesis that the presence of the tether group should impart stability to the catalyst. In a study by Daugulis *et al.*[92] it was reported that a related CGC complex (Figure 4.10 (b)) to complex **4.16a** (Figure 4.10 (a)) decomposed at room temperature, both in the solid and solution-state, adding further weight to the idea that complex **4.16a** (Figure 4.10 (a)) is responsible for the observed low TON and activity of complex **4.16** in 1-butene dimerisation.

Table 4.11: Comparison of the performance of complex **4.16** in 1-butene dimerisation to that of complex **4.5**. [a] In units of mol 1-C_4 converted to oligomers (mol Co)$^{-1}$. [b] In units of g 1-C_4 converted to oligomers/g Co/h. [c]Wt % of liquid fraction; all catalysis runs only yielded liquid products. [d] LAO = linear α-olefin. [e] BO = branched olefin. [f] LIO = linear internal olefin. Catalysis conditions: 50 μmol $Cp^*Co(C_2H_4)(P(OMe)_3$ (complex **4.5**) or 50 μmol $Cp^*CH_2CH_2NMe_2Co(C_2H_4)_2$, PhF, 19 – 22 °C, 0.8 equiv. Brookhart's acid, 2 bar 1-C_4, 19 – 22 °C, 40 - 44 h.

Run	Catalyst precursor	TON[a]	Activity[b]	% C_8 (wt %)[c]			% branched C_{12} (wt %)[c]	% branched C_{16} (wt %)[c]
				LAO[d]	BO[e]	LIO[f]		
1	Complex **4.16**	0.3	0.01	0	31	69	0	0
2	Complex **4.5**	14.9	0.32	4	67	2	20	7

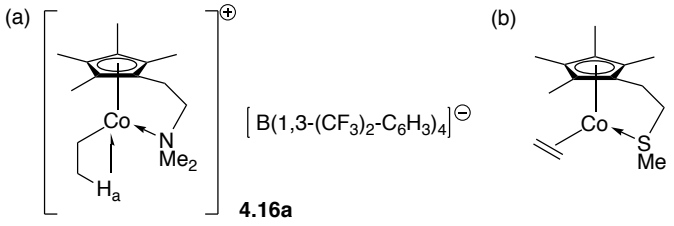

Figure 4.10: (a)Complex **4.16a**: proposed active catalytic species in 1-hexene trimerisation system produced by complex **4.16** and Brookhart's acid and (b) unstable CGC complex reported by Dauglis *et al*.[92]

4.5. Summary and Conclusions

In this Chapter, Broene's cyclopentadienyl cobalt catalyst precursor (complex **4.5**) and activated catalyst species (complex **4.6**) were successfully synthesised.[1] Complex **4.5** was tested in 1-butene dimerisation and verification of the catalysis results of complex **4.5** reported by Broene *et al.*,[1] for dimerisation was achieved. In addition, the effect of varying solvent and temperature in 1-butene dimerisation mediated by complex **4.5** was investigated**.** Of the solvents tested, PhF gave the best performing catalysis system. Reaction temperature was also shown to play a role, with temperatures above room temperature having a detrimental effect on the system's TON. Complex **4.5** was also tested in 1-hexene dimerisation with similar TONs and activities to those observed for 1-butene dimerisation. Complex **4.5** displayed a greater liquid fraction selectivity towards the LAO in 1-hexene *vs.* 1-butene dimerisation. A comparison of using *in situ vs.* preformed catalyst precursors (namely complex **4.5** or **4.15**) in 1-hexene dimerisation was evaluated, with it being found that systems with identical TONs, activities and liquid fractions were obtained regardless of the manner in which the catalyst precursor is obtained. This finding is significant as it means future investigations into varying the L-donor ligand of Broene's catalyst precursor ($Cp^*CoC_2H_4\{L\}$) can be quickly conducted by screening different L-donor ligands in 1-hexene dimerisation tests using *in situ* generated catalyst precursors (*i.e.* from $Cp^*Co(C_2H_4)_2$ and the relevant L ligand).

The syntheses of (fluorenyl)- and (indenyl)-cobalt carbonyl complexes and (fluorenyl)- and (indenyl)-cobalt halide complexes were attempted, with the desired end goal of transforming these complexes to indenyl and fluorenyl variants of complex **4.5**. The attempted syntheses of (fluorenyl)- and (indenyl)-cobalt carbonyl complexes, by reactions of the L_2X ligands with $Co_2(CO)_8$ and 1,3-cyclohexadiene, yielded $Co_4(CO)_{12}$ and $[Co(\eta^4\text{-}C_6H_8)(CO)(\mu\text{-}CO)]_2$ (**4.9**). $Co_4(CO)_{12}$ is believed to be formed from the thermal decomposition of the $Co_2(CO)_8$ starting material or *via* complex **4.9**, itself formed from the binding of 1,3-cyclohexadiene to $Co_2(CO)_8$ instead of indene or fluorene. The attempted synthesis of (fluorenyl)cobalt chloride *via* a salt metathesis reaction between sodium fluorenide and $CoCl_2$ afforded bifluorene, in addition to $Co_2Cl_4(THF)_4$ and unreacted fluorene; the course of this reaction is proposed to occur *via* radical coupling (Scheme 4.33) or reductive coupling of cobaltocene. In contrast to the salt metathesis reaction between $CoCl_2$ and sodium fluorenide, salt metathesis reactions between sodium indenide and CoX_2 (X = Cl, I) generated decomposition products of the desired indenyl cobalt halide complexes {Ind_2Co, $[Ind_2Co]_2[CoCl_4]$, and

$[Ind_2Co]_2[CoI_4]\cdot 0.5$ THF}, which are proposed to be formed due to use of THF solvent in these reactions. Finally, the synthesis of $IndCo(C_2H_4)(P(OMe)_3$ was attempted by reduction of Ind_2Co in the presence of ethylene, and subsequent reaction with $P(OMe)_3$; this yielded a red solid that NMR spectroscopy (^1H, $^{13}C\{^1H\}$, and $^{31}P\{^1H\}$) revealed to consist of a mixture of products (containing indenyl and $P(OMe)_3$ moeities); unfortunately, attempts to separate this mixture of products by recrystallisation led to the decomposition of the products.

The synthesis of $Cp^*Co(C_2H_4)(P(pyrrolyl)_3)$ (**4.15**) was conducted and its performance in 1-hexene dimerisation evaluated, in order to assess the effect of substituting the $P(OMe)_3$ ligand in complex **4.5** by the more π-accepting $P(pyrrolyl)_3$ framework. Under comparable catalysis conditions to those implemented for complex **4.5** in 1-hexene dimerisation, complex **4.15** gave rise to a selective hexene trimerisation system and failed to produce any of the desired LAO dimer. The observed difference in the performances of complexes **4.15** and **4.5** in 1-hexene dimerisation is surprising, based on the more pi-accepting and bulkier $P(pyrrolyl)_3$ framework in complex **4.15** compared to that of $P(OMe)_3$ in complex **4.5**.

Lastly, the complex $Cp^*CH_2CH_2NMe_2Co(C_2H_4)_2$ (**4.16**) was synthesised and its performance in 1-hexene dimerisation evaluated. Disappointingly, however, following activation with 0.8 equiv. Brookhart's acid, complex **4.16** generated a system with an extremely low TON (0.3) and a selectivity towards trimerisation, with none of the desired LAO dimer being detected. It is postulated that the observed low TON of the complex **4.16**/Brookhart's acid-mediated hexene trimerisation system is due to the low stability of the active catalyst precursor, hence it would be interesting to react complex **4.16** with a deficit of Brookhart's acid to gain insight into the structure of the catalytically active species.

4.6. Future work and outlook

Although knowledge has been obtained from the work reported in this Chapter, primarily concerning the impact of solvent, temperature and different activation methods in 1-butene and 1-hexene dimerisation catalysis mediated by Broene's catalyst precursor, a lot more work remains to be done to try and establish an optimal set of catalysis conditions and indeed catalyst precursor. With this aim in mind, it would be of significant interest to investigate the following:

- The effect of varying the activator used (normally Brookhart's acid) in the 1-butene and 1-hexene dimerisation systems employing Broene's catalyst precursor. In particular, exploring the use of MMAO activator, due to the high activities of other literature dimerisation systems discussed in section 4.1.3 employing it. Alternatively, the use of activators bearing different counter anions (such as $[B(C_6F_5)_4]$ and $[Al\{OC(CF_3)_3\}_4]$) to that of Brookhart's acid $[B\{3,5\text{-}(CF_3)_2C_6H_3\}_4]$ is appealing, in order to gain insight into the role played by the $[B\{3,5\text{-}(CF_3)_2C_6H_3\}_4]$ anion in the LAO dimerisation systems.
- Varying the ratio of Co:activator implemented in the LAO dimerisation systems mediated by the complex $Cp^*Co(C_2H_4)(P\{OMe\}_3)$ (**4.5**) in order to assess the optimum ratio for high activity and selectivity towards the LAO dimer.
- Screening different L-donor ligands (such as phosphines bearing different steric and electronic properties, *e.g.* PMe_3, PEt_3, P^iPr_3) in LAO dimerisation catalysis, generating the catalyst precursor *in situ* (*i.e.* from $Cp^*Co(C_2H_4)_2$ and relevant L-donor ligand).

In addition to work focused on improving the activity and selectivity of the LAO dimerisation system mediated by complex **4.5**, there is further scope for the synthesis of modified variants of complex **4.5** as use for catalyst precursors. As has already been mentioned in section 4.4.1.2, it would be interesting to conduct salt metathesis reactions of Co halides with sodium indenide in non-polar solvents in order to see if the desired indenyl cobalt halide complexes can be obtained, which can subsequently be reacted to form the target indenyl variant of complex **4.5**. In addition to investigating the nature of the solvent implemented in these salt metathesis reactions, it would also be informative to look at the nature of the Co source (*i.e.* use a non-halide Co source such as $Co(OAc)_2$ or $Co(acac)_2$) to see how this impacts reactivity. Alternatively, the formation of fluorenyl and indenyl variants of complex **4.5** could be attempted by the route shown in Scheme 4.40; the first step of which has been reported to be successful for $IndCo(CO)_2$ by Jablonski *et al.*[93]

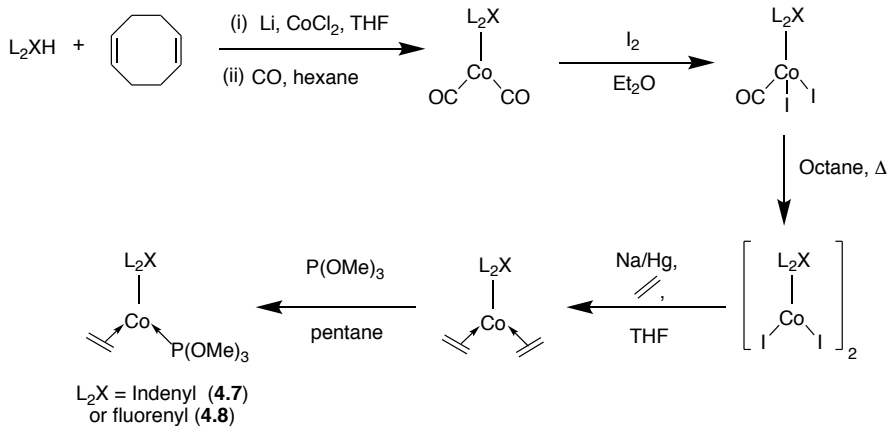

Scheme 4.40: Proposed synthesis route to complexes **4.7** and **4.8**.[36-38,93]

Lastly, the potential application of CGC-type complexes in selective LAO dimerisation systems should not be ruled out based on the disappointing results obtained for the use of complex **4.16** in 1-hexene dimerisation in section 4.4.3. Here, the synthesis and LAO dimerisation catalysis testing of a range of different CGC complexes bearing different L_2X ligands and different L-donor atoms could be attempted (Figure 4.11).

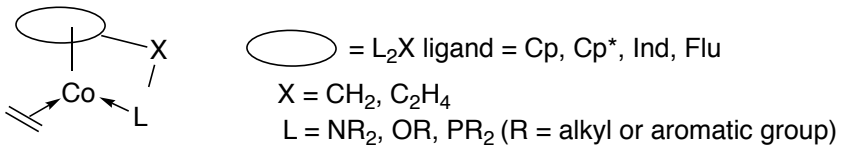

Figure 4.11: Interesting CGC catalyst precursors to investigate in LAO dimerisation catalysis.

4.7. References

1 R. D. Broene, M. Brookhart, W. M. Lamanna and A. F. Volpe, *J. Am. Chem. Soc.*, 2005, **127**, 17194–17195.
2 P. Cossee, *J. Catal.*, 1964, **3**, 80–88.
3 E. J. Arlman and P. Cossee, *J. Catal.*, 1964, **3**, 99–104.
4 J. Skupinska, *Chem. Rev.*, 1991, **91**, 613–648.
5 S. M. Pillai, M. Ravindranathan and S. Sivaram, *Chem. Rev.*, 1986, **86**, 353–399.
6 S. D. Ittel, K. L. Johnson and M. Brookhart, *Chem. Rev.*, 2000, **100**, 1169–1204.
7 M. Brookhart, M. L. H. Green and G. Parkin, *Proc. Natl. Acad. Sci.*, 2007, **104**, 6908–6914.
8 M. J. Hanton, PhD Thesis, University of Leicester, 2002.
9 D. S. McGuinness, *Chem. Rev.*, 2011, **111**, 2321–2341.
10 F. Zheng, A. Sivaramakrishna and J. R. Moss, *Coord. Chem. Rev.*, 2007, **251**, 2056–2071.
11 Y. Qi, Q. Dong, L. Zhong, Z. Liu, P. Qiu, R. Cheng, X. He, J. Vanderbilt and B. Liu, *Organometallics*, 2010, **29**, 1588–1602.
12 T. Agapie, S. J. Schofer, J. A. Labinger and J. E. Bercaw, *J. Am. Chem. Soc.*, 2004, **126**, 1304–1305.
13 J. A. Suttil and D. S. McGuinness, *Organometallics*, 2012, **31**, 7004–7010.
14 E. D. Metzger, R. J. Comito, C. H. Hendon and M. Dincă, *J. Am. Chem. Soc.*, 2017, **139**, 757–762.
15 T. Agapie, J. A. Labinger and J. E. Bercaw, *J. Am. Chem. Soc.*, 2007, **129**, 14281–14295.

16 M. J. Overett, K. Blann, A. Bollmann, J. T. Dixon, D. Haasbroek, E. Killian, H. Maumela, D. S. McGuinness and D. H. Morgan, *J. Am. Chem. Soc.*, 2005, **127**, 10723–10730.
17 J. A. Suttil, D. S. McGuinness and S. J. Evans, *Dalton Trans.*, 2010, **39**, 5278–8.
18 J. A. Suttil, D. S. McGuinness, M. Pichler, M. G. Gardiner, D. H. Morgan and S. J. Evans, *Dalton Trans.*, 2012, **41**, 6625–10.
19 A. K. Tomov, J. J. Chirinos, D. J. Jones, R. J. Long and V. C. Gibson, *J. Am. Chem. Soc.*, 2005, **127**, 10166–10167.
20 A. K. Tomov, J. J. Chirinos, R. J. Long, V. C. Gibson and M. R. J. Elsegood, *J. Am. Chem. Soc.*, 2006, **128**, 7704–7705.
21 D. S. McGuinness, J. A. Suttil, M. G. Gardiner and N. W. Davies, *Organometallics*, 2008, **27**, 4238–4247.
22 A. K. Tomov, V. C. Gibson, G. J. P. Britovsek, R. J. Long, M. van Meurs, D. J. Jones, K. P. Tellmann and J. J. Chirinos, *Organometallics*, 2009, **28**, 7033–7040.
23 A. Forestière, H. Olivier-Bourbigou and L. Saussine, *Oil Gas Sci. Technol. - Rev. IFP*, 2009, **64**, 649–667.
24 B. L. Small and A. J. Marcucci, Organometallics, 2001, **20**, 5738–5744.
25 R. H. Crabtree, The Organometallic Chemistry of the Transition Metals, John WIley & Sons, Inc, New Jersey, Fifth., 2001.
26 Industrial Applications of Homogenous Catalysis, ed. A. Morteux and F. Petit, D. Riedel Publishing Company, Holland, 1988.
27 Applied Homogeneous Catalysis with Organometallic compounds, ed. B. Cornils and W. A. Hermann, Volume 1, Wiley-VCH, Weinheim, 2002.
28 A. M. Al-Jarallah, J. A. Anabtawi, M. A. B. Siddiqui and A. M. Aitani, *Catal. Today*, 1992, **14**, 1–124.
29 L. G. Wideman, US 3,813,453, Goodyear Tyre and Rubber Company, 28 May 1974.
30 J. R. Jones and T. J. Symes, *J. Chem. Soc., C*, 1971, 1124–1130.
31 R. G. da Rosa, M. O. de Souza and R. F. de Souza, *J. Mol. Catal. A*-Chem, 1997, **120**, 55–62.
32 F. Majoumo-Mbe, P. Lonnecke, V. Volkis, M. Sharma, M. S. Eisen and E. Hey-Hawkins, *J. Organomet. Chem.*, 2008, **693**, 2603–2609.
33 B. L.Small, *Organometallics*, 2003, **22**, 3178–3183.
34 K. P. Tellmann, V. C. Gibson, A. J. P. White and D. J. Williams, *Organometallics*, 2005, **24**, 280–286.
35 A. P. R. Ehlert, E. M. Carvalho, D. Thiele, C. Favero, I. Vicente, K. Bernardo-Gusmão, R. Stieler, R. F. de Souza and M. O. de Souza, *Catal. Today*, 2017, **296**, 272–276.
36 S. Frith and J. L. Spencer, *Inorg. Synth.*, 1990, **28**, 273–280.
37 R. G. Beevor, S. Frith and J. L. Spencer, *J. Organomet. Chem.*, 1981, **221**, C25–C27.
38 M. Brookhart, D. M. Lincoln, A. F. Volpe and G. F. Schmidt, *Organometallics*, 1989, **8**, 1212–1218.
39 I. R. Lyatifov, G. M. Jafarov, V. N. Babin, P. V. Petrovskii and V. D. Zagorevskii, *J. Organomet. Chem.*, 1989, **368**, 223–230.
40 B. Sun, T. Yoshino, S. Matsunaga and M. Kanai, *Adv. Synth. Catal.*, 2014, **356**, 1491–1495.
41 G. F. Schmidt and M. Brookhart, *J. Am. Chem. Soc.*, 1985, **107**, 1443–1444.
42 Basic Practical NMR Concepts: A Guide for the Modern Laboratory, https://www2.chemistry.msu.edu/facilities/nmr/handouts/DH%20NMR%20Basics.pdf, (last accessed December 2017)
43 T. D. W. Claridge, *High-Resolution NMR Techniques in Organic Chemistry*, Elsevier, Netherlands, Third Edition, 2015.
44 C. D. Ramful, K. N. Robertson and K. E. O. Ylijoki, *Acta Crystallogr. Sect. E Crystallogr. Commun.*, 2016, **72**, 1301–1304.

45 L. E. Sutton, *Tables of Interatomic Distances and Configuration in Molecules and Ions*, ed. The Chemical Society, London, 1958.
46 M. Brookhart, B. Grant and A. F. Volpe, *Organometallics*, 1992, **11**, 3920–3922.
47 M. Brookhart and M. L. H. Green, *J. Organomet. Chem.*, 1983, **250**, 395–408.
48 M. Brookhart, A. F. Volpe, D. M. Lincoln, I. T. Horvath and J. M. Millar, *J. Am. Chem. Soc.*, 1990, **112**, 5634–5636.
49 A. F. Volpe, PhD Thesis, University of North Carolina, 1991.
50 M. Brookhart, M. L. H. Green and L.-L. Wong, in *Progress in Inorganic Chemistry*, ed. S. J. Lippard, John Wiley & Sons, 1988, vol. 36, chap. 1, pp. 1–124.
51 M. D. Doherty, B. Grant, P. S. White and M. Brookhart, *Organometallics*, 2007, **26**, 5950–5960.
52 R. B. Cracknell, A. G. Orpen and J. L. Spencer, *J. Chem. Soc., Chem. Commun.*, 1984, 326–328.
53 N. Carr, B. J. Dunne, A. G. Orpen and J. L. Spencer, *J. Chem. Soc., Chem. Commun.*, 1988, 926–928.
54 F. M. Conroy-Lewis, L. Mole, A. D. Redhouse, S. A. Litster and J. L. Spencer, *J. Chem. Soc., Chem. Commun.*, 1991, **36**, 1601–1603.
55 N. Carr, L. Mole, A. G. Orpen and J. L. Spencer, *J. Chem. Soc., Dalton Trans.*, 1992, **36**, 2653–2662.
56 C. Laurence, P. Nicolet, M. T. Dalati, J.-L. M. Abboud and R. Notario, *J. Phys. Chem.*, 1994, **98**, 5807–5816.
57 M. F. Ryan, A. R. Siedle, M. J. Burk and D. E. Richardson, *Organometallics*, 1992, **11**, 4231–4237.
58 J. M. O'Connor and C. P. Casey, *Chem. Rev.*, 1987, **87**, 307–318.
59 I. A. Lobanova and V. I. Zdanovich, *Russ. Chem. Rev.*, 1988, **57**, 967–980.
60 R. J. Angelici and W. Loewen, *Inorg. Chem.*, 1967, **6**, 682–686.
61 L. N. Ji, M. E. Rerek and F. Basolo, *Organometallics*, 1984, **3**, 740–745.
62 C. Brodie, First year PhD Report, Durham University, 2017.
63 F. P. Pruchnik, *Organometallic Chemistry of the Transition Elements*, Plenum Press, New York and London, 1990.
64 G. Winkhaus and G. Wilkinson, *J. Chem. Soc.*, 1961, 602–604.
65 G. Wilkinson, US 3,141,031, Ethyl Corporation, 14 July 1964.
66 F. G. Bordwell and M. J. Bausch, *J. Am. Chem. Soc.*, 1983, **105**, 6188–6189.
67 C. Huo, X. Jia, W. Zhang, L. Yang, J. Lü and Z.-L. Liu, *Synlett*, 2004, 251–254.
68 M. E. Walther, J. Grilj, D. Hanss, E. Vauthey and O. S. Wenger, *Eur. J. Inorg. Chem.*, 2010, **2010**, 4843–4850.
69 M. Schmittel and H. von Seggern, *Angew. Chemie.*, 1991, **103**, 981–983.
70 U. Kolle, F. Khouzami and B. Fuss, *Angew. Chem. Int. Ed. Engl.*, 1982, **21**, 131–132.
71 U. Kolle and B. Fuss, *Chem. Ber.*, 1984, **117**, 743–752.
72 U. Kolle, B. Fuss, M. Belting and E. Raabe, *Organometallics*, 1986, **5**, 980–987.
73 F. Baumann, E. Dormann, Y. Ehleiter, W. Kaim, J. Karcher, M. Kelemen, R. Krammer, D. Saurenz, D. Stalke, C. Wachter, G. Wolmershauser and S. H, *J. Organomet. Chem.*, 1999, **587**, 267–283.
74 D. Stinghen, A. L. Rudiger, S. O. K. Giese, G. G. Nunes, J. F. Soares and D. L. Hughes, *Acta. Crystallogr. C.*, 2017, **73**, 104–114.
75 M. H. Al-Afyouni, T. A. Huang, F. Hung-Low and C. A. Bradley, *Tetrahedron Lett.,* 2011, **52**, 3261–3265.
76 U. Kolle, F. Khouzami and B. Fuss, *Angew. Chem. Int. Ed. Engl.*, 1982, **21**, 230–240.
77 S. A. Westcott, A. K. Kakkar, G. Stringer, N. J. Taylor and T. B. Marder, *J. Organomet. Chem.*, 1990, **394**, 777–794.
78 D. M. Roe and P. M. Maitlis, *J. Chem. Soc. A Inorg., Phys. Theor.*, 1971, 3173–3175.
79 U. Chakraborty, M. Modl, B. Mühldorf, M. Bodensteiner, S. Demeshko, N. J. C.

van Velzen, M. Scheer, S. Harder and R. Wolf, *Inorg. Chem.*, 2016, **55**, 3065–3074.
80 V. K. Jonas, E. Deffense and D. Habermann, *Angew. Chem. Suppl.*, 1983, 1005–1006.
81 J. A. Hamilton, T. Pugh, A. L. Johnson, A. J. Kingsley and S. P. Richards, *Inorg. Chem.*, 2016, **55**, 7141–7151.
82 M. Hapke, N. Weding and A. Spannenberg, *Organometallics*, 2010, **29**, 4298–4304.
83 K. Jonas, *Angew. Chem. Int. Ed. Engl.*, 1984, **24**, 295–311.
84 A. Gual, C. Godard, V. Fuente and S. Castillon, *in Phosphorus(III) Ligands in Homogeneous Catalysis: Design and Synthesis*, ed. P. C. J. Kramer and P. W. N. M. Van Leeuwen, John Wiley & Sons Ltd, Sussex, 2012, pp. 81-82.
85 K. G. Moloy and J. L. Petersen, *J. Am. Chem. Soc.*, 1995, **117**, 7696–7710.
86 M. B. Smith and J. March, *March's Advanced Organic Chemistry*, John Wiley & Sons, Inc., New Jersey, Sixth Edition, 2007.
87 J. L. Atwood, A. H. Cowley, W. E. Hunter and S. K. Mehrotra, *Inorg. Chem.*, 1982, **21**, 1354–1356.
88 C. A. Tolman, *Chem. Rev.*, 1977, **77**, 313–348.
89 B. A. Core and M. Hanton, Sasol internal report, 2009.
90 P. Jutzi, M. Kristen, J. Dahlhaus, B. Neumann and H. Stammler, *Organometallics*, 1993, **12**, 2980–2985.
91 S. Holle and P. W. Jolly, *J. Organomet. Chem.*, 2000, **605**, 157–167.
92 O. Daugulis, M. Brookhart and P. S. White, *Organometallics*, 2003, **22**, 4699–4704.
93 C. Jablonski, Z. Zhou and N. Bridson, *J. Organomet. Chem.*, 1992, **429**, 379–389.

Chapter 5:
Experimental

5.1. General Considerations

COSHH assessments were carried out prior to all experimental work. All experiments were conducted in an efficient fume-hood with a laboratory coat, safety spectacles and appropriate gloves being worn at all times during experimental work. In accordance with the departmental health and safety policy, solvents were disposed of in the appropriate waste solvent container.

Unless stated otherwise, all experiments were performed under ambient laboratory lighting with oven-dried glassware under an atmosphere of dry oxygen-free nitrogen using standard Schlenk and cannula techniques, or in a Saffron Scientific oxygen-free nitrogen-filled glovebox. All NMR-scale reactions were carried out in NMR tubes fitted with J. Young's tap valves. The solvents, toluene, DCM, THF, hexane, Et_2O, MeCN, and petroleum ether (40:60) were dried and purified using an Innovative Technologies SPS facility and degassed prior to use by freeze-pump-thaw cycles. Diglyme, pentane, and octane were dried over CaH_2 before being distilled and degassed by freeze-pump-thaw cycles. Chlorobenzene and fluorobenzene were dried over P_2O_5 prior to distillation and degassing by freeze-pump-thaw cycles. Solvents for NMR spectroscopy (C_6D_6, d_2-DCM, d_8-THF, $CDCl_3$, D_2O) were purchased from Apollo or Goss Scientific and, with the exception of D_2O, dried over CaH_2 (C_6D_6, d_2-DCM, d_8-THF) or P_2O_5 ($CDCl_3$), distilled, and degassed prior to use.

$CrCl_3(THF)_3$ was synthesised by Dr. James Radcliffe following literature methods and its purity validated by IR spectroscopy and elemental analysis.[1] $Ag[Al\{OC(CF_3)_3\}_4]$ was obtained from Sasol Technology UK Ltd. All other reagents were purchased from Sigma Aldrich, Alfa Aesar or Strem. Where appropriate, liquid reagents were dried, distilled and degassed prior to use while gases were passed through a drying column ($CaCO_3/P_2O_5$).

Solution-phase NMR spectra were collected on a Varian Mercury 400, Varian Inova 500, Varian VNMRS-600, Varian VNMRS-700 or a Bruker Advance 400 spectrometer at temperatures of 298 K unless otherwise stated. Variable temperature NMR spectroscopic experiments were carried out by Dr. A. Kenwright, Dr. J. A. Aguilar Malavia, Mrs. C. F. Heffernan and Ms. R. Belda-Vidal. All chemical shifts were referenced with respect to the ^{13}C shift of the solvent (for ^{13}C NMR), residual protio impurities in the deuterated solvent (for ^{1}H NMR), to an external aqueous standard of 85% H_3PO_4 (for ^{31}P NMR), to external $CFCl_3$ (for ^{19}F NMR) or to an external standard

of 15 % $BF_3.OEt_2$ (for ^{11}B NMR). Solvent proton shifts (ppm): $CDCl_3$, 7.26 (s); C_6D_6, 7.16 (s); CD_2Cl_2, 5.32 (t); $(CD_2)_4O$, 1.73 (s), 3.58 (s); D_2O, 4.79 (s). Solvent carbon shifts (ppm): $CDCl_3$, 77.2 (t); C_6D_6, 128.1 (t); CD_2Cl_2, 54.0 (quin); $(CD_2)_4O$, 25.6 (quin), 67.6 (quin). Where necessary, ^1H and ^{13}C NMR spectra were assigned with the aid of 2D COSY, HSQC and HMBC spectroscopic experiments. All spectra are reported with chemical shifts in ppm and coupling constants in Hz. Where appropriate, the progress of reactions have been monitored by solution state ^{31}P and $^{31}P\{^1H\}$ NMR spectroscopy with relative ratios of phosphorus-containing species being evaluated from the integration of corresponding resonances in the $^{31}P\{^1H\}$ NMR spectra.

Mass spectra were recorded by the Durham University Mass Spectrometry Service; ASAP: Waters LCT Premier XE mass spectrometer equipped with an ASAP ionisation source, ESI: Waters TQD equipped with Acquity UPLC and an electrospray ion source, and are reported as *m*/*z*. Infrared spectra were collected on a Perkin Elmer Frontier ATR-FT-IR spectrophotometer using a Golden Gate ATR cell to record solid state IR spectra or a solution cell with KBr windows to record solution state IR spectra. Due to the complexity of the IR spectroscopic data obtained for the phosphanyl methanimine (PCN) ligands synthesised in this thesis, only their C=N stretching frequencies are reported. Elemental analyses were carried out by Stephen Boyer of London Metropolitan University. Single crystal X-ray analyses were conducted by Dr. A. Batsanov and Dr. D. Yufit of the Durham University X-ray crystallography service. DSC analysis of polyethylene was carried out by Mr. W. D. Carswell of Durham University using a TA instrument DSC Q1000.

GC-FID analyses were performed on a PerkinElmer Clarus 400 or an Agilent Technologies 6890N GC system, both equipped with a PONA (50 m × 0.20 mm × 0.50 μm) column. GC-MS analyses were performed on (a) a Shimadzu QP2010-Ultra equipped with a Rxi-5Sil MS column (10 m × 0.15 mm × 0.15 μm) or (b) an Agilent Technologies 6890N GC system equipped with PONA (50 m × 0.20 mm × 0.50 μm) column, coupled to an Agilent Technologies 5973N MSD Mass Spectrometric instrument equipped with EI source. Hydrogenative GC-FID analyses were performed using an Agilent Technologies 6890N GC System equipped with an inlet liner packed with hydrogenating catalyst (Pt on Chromosorb W at 200 °C) and a PONA column (50 m × 0.20 mm × 0.50 μm).

5.2. Chapter 2 Experimental

5.2.1. Synthesis of imidoyl chlorides

The synthesis of imidoyl chlorides was carried out following a two-step procedure modified from Budzelaar *et al.*[2] An example for the synthesis of N-(2,6-diisopropylphenyl)-4-methylbenzimidoyl chloride is detailed below. The imidoyl chlorides listed in **Table 5.1** were synthesised in the same way using the relevant acyl chloride and aniline precursors, with their identities being verified by ^{1}H and ^{13}C{^{1}H} NMR spectroscopy which gave data matching with that reported in the literature.

(i) Synthesis of N-(2,6-diisopropylphenyl)-4-methylbenzamide

Triethylamine (6.82 g, 67.4 mmol) and 2,6-diisopropylaniline (12.0 g, 67.7 mmol) were added to a three-necked round bottom flask containing DCM (160 mL), fitted with a condenser and dropping funnel. A solution of *p*-toluoyl chloride (10.5 g, 67.9 mmol) in DCM (40 mL) was then added dropwise to the amine solution. After the addition was complete, the reaction mixture was heated at reflux for 1 hour. The solution was then cooled and washed with distilled water (3 × 50 mL). The organic fraction was dried over magnesium sulphate, isolated by filtration and the solvent removed *in vacuo*. The resulting white solid product was washed with cold diethyl ether and dried under vacuum to yield the target compound as a white crystalline solid (15.3 g, 77 % yield). The identity of the product was validated by ^{1}H and ^{13}C{^{1}H} NMR spectroscopy, which gave data matching those previously reported in the literature.[3]

^{1}H NMR (700 MHz, $CDCl_3$) δ: 7.82 (d, $^{3}J_{HH}$ = 7.8 Hz, 2H, C-*o*-C_6H_4), 7.34 (t, $^{3}J_{HH}$ = 7.7 Hz, 2H, N-*p*-C_6H_3/N*H*), 7.30 (d, $^{3}J_{HH}$ = 7.8 Hz, 2H, C-*m*-C_6H_4), 7.22 (d, $^{3}J_{HH}$ = 7.8 Hz, 2H, N-*m*-C_6H_3), 3.14 (hept, $^{3}J_{HH}$ = 6.9 Hz, 2H, N-C_6H_3(C*H*$(CH_3)_2)_2$), 2.44 (s, 3H, C-C_6H_4(CH_3)), 1.21 (d, $^{3}J_{HH}$ = 6.9 Hz, 12H, N-C_6H_3(CH(C$H_3)_2)_2$).

^{13}C{^{1}H} NMR (176 MHz, $CDCl_3$) δ: 167.0 (*C*ONH), 146.6 (N-*o*-C_6H_3), 142.4 (C-*p*-C_6H_4), 131.9 (C-*i*-C_6H_4), 131.4 (N-*i*-C_6H_3), 129.6 (C-*m*-C_6H_4), 128.5 (N-*p*-C_6H_3), 127.4 (C-*o*-C_6H_4), 123.7 (N-*m*-C_6H_3), 29.1 (N-C_6H_3(*C*H$(CH_3)_2)_2$), 23.8 (N-C_6H_3(CH(*C*$H_3)_2)_2$), 21.7 (C-C_6H_4(*C*H_3)).

IR (ATR)**:** ν_{NH} = 3345 cm^{-1}, $\nu_{C=O}$ = 1644 cm^{-1}.

(ii) Synthesis of N-(2,6-diisopropylphenyl)-4-methylbenzimidoyl chloride

A slurry of N-(2,6-diisopropylphenyl)-4-methylbenzamide (14 g, 47.4 mmol) in toluene (125 mL) was prepared in a two-necked round bottom flask. Small portions of solid PCl_5 (9.9 g, 47.5 mmol) were then added to the slurry with vigorous stirring. During the addition of PCl_5, HCl gas was evolved (which was trapped by bubbling through water) and the slurry dissolved resulting in the formation of a clear yellow solution. Upon completion of the addition of PCl_5, the resulting solution was stirred overnight. The volatile components were then removed *in vacuo* leaving behind a crude yellow oil, which was subsequently purified *via* Kugelrohr vacuum distillation (0.15 mbar, 140 °C) yielding the final product as a clear yellow oil that solidified upon scraping (12.0 g, 81 % yield). The identity of the product was verified by ^{1}H and $^{13}C\{^{1}H\}$ NMR spectroscopy, which had data in agreement with those previously reported in the literature.[3]

^{1}H NMR (700 MHz, $CDCl_3$) δ: 8.11 (d, $^{3}J_{HH}$ = 8.2 Hz, 2H, C-*o*-C_6H_4), 7.31 (d, $^{3}J_{HH}$ = 8.0 Hz, 2H, C-*m*-C_6H_4), 7.19 – 7.17 (m, 3H, N-*m*/*p*-C_6H_3), 2.82 (hept, $^{3}J_{HH}$ = 6.9 Hz, 2H, N-$C_6H_3(CH(CH_3)_2)_2$), 2.46 (s, 3H, C-$C_6H_4(CH_3)$), 1.22 (d, $^{3}J_{HH}$ = 7.0 Hz, 6H, N-$C_6H_3(CH(CH_3)_2)_2$),1.16 (d, $^{3}J_{HH}$ = 7.0 Hz, 6H, N-$C_6H_3(CH(CH_3)_2)_2$).

$^{13}C\{^{1}H\}$ NMR (176 MHz, $CDCl_3$) δ: 146.3 (*C*=N), 144.1 (N-*i*-C_6H_3), 143.6 (C-*i*-C_6H_4), 142.9 (C-*p*-C_6H_4), 137.0 (N-*o*-C_6H_3), 129.6 (C-*o*-C_6H_4), 129.4 (C-*m*-C_6H_4), 124.9 (N-*p*-C_6H_3), 123.2 (N-*m*-C_6H_3), 28.8 (N-$C_6H_3(CH(CH_3)_2)_2$), 23.5 (N-C_6H_3 $(CH(CH_3)_2)_2$), 23.0 (N-$C_6H_3(CH(CH_3)_2)_2$), 21.7 (C-$C_6H_4(CH_3)$).

IR (ATR)**:** $\nu_{C=N}$ = 1665 cm^{-1}.

Table 5.1: Properties of imidoyl chlorides synthesised in this work and in previous work conducted in the Dyer group.[1]

Compound	*p*-CF_3-C_6H_4(Cl)C=N(2,6-$^iPr_2C_6H_3$)[4]	Ph(Cl)C=N(2,6-$^iPr_2C_6H_3$)[5]	Ph(Cl)C=N(2,6-$Et_2C_6H_3$)[6]	Ph(Cl)C=N(2,6-$Me_2C_6H_3$)[6]	Ph(Cl)C=N(2-MeC_6H_4)[7]
	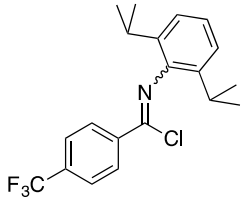	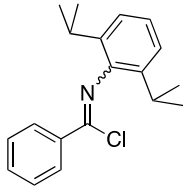	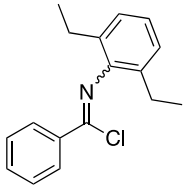	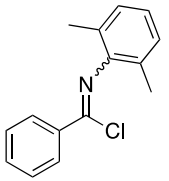	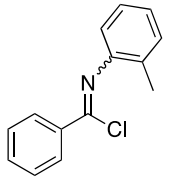
Conditions used for purification	Recrystallisation from hexane	Kugelrohr vacuum distillation: 165 – 167 °C, 0.45 mbar	Kugelrohr vacuum distillation: 145 – 146 °C, 1 mbar	Kugelrohr vacuum distillation: 143 – 147 °C, 1 mbar	Kugelrohr vacuum distillation: 135 °C, 1 mbar
Yield (%)	70	90[a]	85[a]	90[a]	87[a]
Product appearance	Pale yellow crystalline solid	Yellow crystalline solid	Pale yellow oil	Pale yellow oil	Yellow oil
$\nu_{C=N}$ (cm^{-1})[b]	1660	1663	1656	1668	1661

[a] Synthesised by Dr. James Radcliffe.[1]
[b] IR spectra measured neat using an ATR cell.

5.2.2. Synthesis of trimethylsilylphosphines

5.2.2.1. Synthesis of trimethylsilyl-(dicyclopentyl)-phosphine

The synthesis of trimethylsilyl-(dicyclopentyl)-phosphine was carried out in accordance with the literature procedure described by Fritz *et al*.[8] A pre-weighed two-necked round bottom flask was charged with dicyclopentylphosphine (10 wt. % solution in hexanes, 3.12 g, 18.3 mmol) and THF (15 mL). After cooling the phosphine solution to 0 °C, a solution of ^{n}BuLi (2.5 M solution in hexanes, 9.5 mL, 23.8 mmol) in THF (15 mL) was added dropwise to the round bottom flask, at 0 °C, upon which the colourless phosphine solution turned orange. Upon completion of addition, the phosphine solution was allowed to warm to room temperature and subsequently stirred at room temperature for an hour. The solution was then cooled back to 0 °C and TMSCl (3.3 mL, 26.0 mmol) was added dropwise, at 0 °C, resulting in the immediate formation of a white precipitate and a colourless solution. The crude reaction mixture was then allowed to reach room temperature before the solvent was removed under vacuum,[c] producing a solid residue. The organic product was extracted from the lithium salt by washing with pentane (3 × 10 mL), before removing the pentane under vacuum[c] to isolate the product as a colourless oil (4.27 g, 96 % yield).

^{1}H NMR (700 MHz, C_6D_6) δ: 2.04 - 1.93 (m, 2H, P(C_5H_9)$_2$), 1.92 - 1.79 (m, 4H, P(C_5H_9)$_2$), 1.68 - 1.55 (m, 4H, P(C_5H_9)$_2$), 1.53 - 1.33 (m, 8H, P(C_5H_9)$_2$), 0.20 (d, *J* = 3.9 Hz, 9H, Si(CH_3)$_3$).

^{13}C{^{1}H} NMR (176 MHz, C_6D_6) δ: 34.5 (d, J_{PC} = 12.5 Hz, P(C_5H_9)$_2$), 33.6 (d, J_{PC} = 16.5 Hz, P(C_5H_9)$_2$), 32.5 (d, J_{PC} = 16.0 Hz, P(C_5H_9)$_2$), 26.6 (d, J_{PC} = 6.5 Hz, P(C_5H_9)$_2$), 26.4 (d, J_{PC} = 8.0 Hz, P(C_5H_9)$_2$), 0.3 (d, *J* = 10.0 Hz, Si(CH_3)$_3$).

^{31}P{^{1}H} NMR (162 MHz, C_6D_6) δ: −64.6.

^{29}Si NMR (139 MHz, C_6D_6) δ: −0.7 (d,$^{1}J_{PSi}$ = 26.5 Hz).

MS (ASAP^{+}) *m*/*z*: 259.2 ([MOH]$^{+}$), 243.2 ([MH]$^{+}$).

[c] The product was only kept under vacuum for a minimum period of time due to its high volatility.

5.2.2.2. Synthesis of trimethylsilyl-(dicyclohexyl)-phosphine

Trimethylsilyl-(dicyclohexyl)-phosphine was synthesised following the same procedure described in section 5.2.2.1 using dicyclohexylphosphine (10 wt. % solution in hexanes, 3.47 g, 17.5 mmol), ^{n}BuLi (2.5 M solution in hexanes, 8.9 mL, 22.3 mmol) and TMSCl (3.1 mL, 24.4 mmol). The product was obtained as a colourless oil (3.45 g, 73 % yield). (calc.: $C_{15}H_{31}PSi$ C, 66.42; H, 11.40; N, 0.00. Found: C, 66.61; H, 11.55; N, 0.00).

^{1}H NMR (700 MHz, C_6D_6) δ 1.98 – 1.83 (m, 6H, P(C_6H_{11})$_2$), 1.75 – 1.56 (m, 6H, P(C_6H_{11})$_2$), 1.46 – 1.30 (m, 4H, P(C_6H_{11})$_2$), 1.29 – 1.08 (m, 6H, P(C_6H_{11})$_2$), 0.25 (d, J = 3.8 Hz, 9H, Si(CH_3)$_3$).

^{13}C{^{1}H} NMR (176 MHz, C_6D_6) δ 33.8 (d, J_{PC} = 10.5 Hz, P(C_6H_{11})$_2$), 33.3 (d, J_{PC} = 12.5 Hz, P(C_6H_{11})$_2$), 31.6 (d, J_{PC} = 16.5 Hz, P(C_6H_{11})$_2$), 28.1 (dd, J = 14.5, 9.5 Hz, P(C_6H_{11})$_2$), 26.8 (P(C_6H_{11})$_2$), 1.3 (d, J = 11.0 Hz, Si(CH_3)$_3$).

^{31}P{^{1}H} NMR (283 MHz, C_6D_6) δ −53.3.

^{29}Si NMR (139 MHz, C_6D_6) δ −1.1 (d,$^{1}J_{PSi}$ = 29.6 Hz).

MS (ASAP^{+}) *m*/*z*: 287.4 ([MOH]$^{+}$), 271.4 ([MH]$^{+}$).

5.2.2.3. Synthesis of trimethylsilyl-(dinorbornyl)-phosphine

Trimethylsilyl-(dinorbornyl)-phosphine was synthesised following the same procedure described in section 5.2.2.1 using di-2-norbornylphosphine (10 wt. % solution in hexanes, 3.20 g, 14.4 mmol), ^{n}BuLi (2.5 M solution in hexanes, 7.5 mL, 18.8 mmol) and TMSCl (2.6 mL, 20.5 mmol). The product was obtained as a colourless oil (3.06 g, 72 % yield). Elemental analysis was carried out on the product, however due to its highly air sensitive and oily nature inconclusive results were obtained. (calc.: $C_{17}H_{31}PSi$ C, 69.33; H, 10.61; N, 0.00. Found: C, 68.43; H, 10.83; N, 0.00).

^{1}H NMR (700 MHz, C_6D_6) δ 2.37 (t, $^{3}J_{HH}$ = 4.7 Hz, 1H, P(C_7H_{11})$_2$), 2.28 (t, $^{3}J_{HH}$ = 4.9 Hz, 1H, P(C_7H_{11})$_2$), 2.24 - 2.18 (m, 1H, P(C_7H_{11})$_2$), 2.17 - 2.11 (m, 1H, P(C_7H_{11})$_2$), 1.88 – 1.76 (m, 3H, P(C_7H_{11})$_2$), 1.75 – 1.62 (m, 2H, P(C_7H_{11})$_2$), 1.59 – 1.30 (m, 7H, P(C_7H_{11})$_2$), 1.23 – 1.16 (m, 2H, P(C_7H_{11})$_2$), 1.15 – 1.05 (m, 4H, P(C_7H_{11})$_2$), 0.25 – 0.23 (m, 2H, Si(CH_3)$_3$), 0.21 (d, J = 3.4 Hz, 4H, Si(CH_3)$_3$), 0.19 (d, J = 3.2 Hz, 3H, Si(CH_3)$_3$).

$^{13}C\{^1H\}$ NMR (176 MHz, C_6D_6) δ 42.9 (dd, *J* = 11.5, 3.5 Hz, P(C_7H_{11})$_2$), 42.5 (dd, *J* = 12.5, 3.5 Hz, P(C_7H_{11})$_2$), 40.2 (d, J_{PC} = 7.5 Hz, P(C_7H_{11})$_2$), 40.0 (d, J_{PC} = 8.5 Hz, P(C_7H_{11})$_2$), 38.5 (d, J_{PC} = 12.5 Hz, P(C_7H_{11})$_2$), 38.3 (d, J_{PC} = 12.5 Hz, P(C_7H_{11})$_2$), 38.2 (dd, *J* = 11.5, 2.0 Hz, P(C_7H_{11})$_2$), 37.6 (dd, *J* = 21.0, 2.5 Hz, P(C_7H_{11})$_2$), 37.3 (dd, *J* = 5.5, 2.5 Hz, P(C_7H_{11})$_2$), 37.2 – 37.1 (m, P(C_7H_{11})$_2$), 36.9 (d, J_{PC} = 19.0 Hz, P(C_7H_{11})$_2$), 36.2 (dd, *J* = 19.0, 3.5 Hz, P(C_7H_{11})$_2$), 35.6 (dd, *J* = 19.0, 7.0 Hz, P(C_7H_{11})$_2$), 32.5 – 32.4 (m, P(C_7H_{11})$_2$), 31.9 (d, J_{PC} = 5.0 Hz, P(C_7H_{11})$_2$), 29.8 – 29.6 (m, P(C_7H_{11})$_2$), 29.3 (d, J_{PC} = 3.5 Hz, P(C_7H_{11})$_2$), 0.8 (dd, *J* = 9.0, 3.5 Hz, Si(CH$_3$)$_3$), 0.6 (d, *J* = 9.5 Hz, Si(CH$_3$)$_3$).

$^{31}P\{^1H\}$ NMR (162 MHz, C_6D_6) δ –56.2, –57.6, –61.4.[d]

^{29}Si NMR (139 MHz, C_6D_6) δ 0.6 (d,$^1J_{PSi}$ = 26.6 Hz), –0.3 (d,$^1J_{PSi}$ = 27.0 Hz), –0.7 (d,$^1J_{PSi}$ = 27.6 Hz).[e]

MS (ASAP$^+$) *m*/*z*: 311.2 ([MOH]$^+$), 295.2 ([MH]$^+$).

5.2.2.4. Synthesis of trimethylsilyl-(diisobutyl)-phosphine

Trimethylsilyl-(diisobutyl)-phosphine was synthesised following the same procedure described in section 5.2.2.1 using diisobutylphosphine (10 wt. % solution in hexanes, 1.07 g, 7.31 mmol), ^{n}BuLi (2.5 M solution in hexanes, 3.8 mL, 9.5 mmol) and TMSCl (1.3 mL, 10.2 mmol). The product was obtained as a colourless oil (1.28 g, 80 % yield) with its identity being verified by ^1H, $^{13}C\{^1H\}$ and $^{31}P\{^1H\}$ NMR spectroscopy which gave data matching that previously reported in the literature.[9]

^1H NMR (700 MHz, C_6D_6) δ 1.69 (dh, *J* = 14.0, 7.0 Hz, 2H, P-(CH$_2$CH(CH$_3$)$_2$)$_2$), 1.46 – 1.40 (m, 2H, P-(CH_2CH(CH$_3$)$_2$)$_2$), 1.39 – 1.32 (m, 2H, P-(CH_2CH(CH$_3$)$_2$)$_2$), 1.10 – 1.00 (m, 12 H, P-(CH$_2$CH(CH_3)$_2$)$_2$), 0.17 – 0.09 (m, 9H, Si(CH_3)$_3$).

[d] Three resonances at –56.2, –57.6, and –61.4 ppm present in relative ratio 10:51:39, respectively (ratio derived by integration of the peaks in $^{31}P\{^1H\}$ NMR spectrum) believed to correspond to the three exo isomers of TMSPNorbornyl$_2$, as discussed in Chapter 2 section 2.3.1.

[e] Three sets of doublets at 0.6, –0.3, and –0.7 ppm present in relative ratio 37:50:13, respectively (ratio derived by integration of the peaks in ^{29}Si NMR spectrum) proposed to correspond to the three exo isomers of TMSPNorbornyl$_2$, as discussed in Chapter 2 section 2.3.2.

$^{13}C\{^{1}H\}$ NMR (176 MHz, C_6D_6) δ 33.4 (d, $^{1}J_{PC}$ = 16.5 Hz, P-($CH_2CH(CH_3)_2)_2$), 28.9 (d, $^{2}J_{PC}$ = 15.5 Hz, P-($CH_2CH(CH_3)_2)_2$), 24.6 (d, $^{3}J_{PC}$ = 8.5 Hz, P-($CH_2CH(CH_3)_2)_2$), 23.9 (d, $^{3}J_{PC}$ = 10.0 Hz, P-($CH_2CH(CH_3)_2)_2$), −2.1 (d, *J* = 11.0 Hz, $Si(CH_3)_3$).

$^{31}P\{^{1}H\}$ NMR (162 MHz, C_6D_6) δ −113.7.

^{29}Si NMR (139 MHz, C_6D_6) δ 2.2 (d,$^{1}J_{PSi}$ = 18.4 Hz).

MS (ASAP^{+}) *m*/*z*: 235.2 ($[MOH]^{+}$), 219.2 ($[MH]^{+}$).

5.2.2.5. Synthesis of trimethylsilyl-(diisopropyl)-phosphine

Trimethylsilyl-(diisopropyl)-phosphine was synthesised following the same procedure described in section 5.2.2.1 using diisopropylphosphine (10 wt. % solution in hexanes, 3.20 g, 27.1 mmol), ^{n}BuLi (2.5 M solution in hexanes, 14.1 mL, 35.3 mmol) and TMSCl (4.8 mL, 37.8 mmol). The product was obtained as a colourless oil (3.60 g, 90 % yield) with its identity validated by ^{1}H, $^{13}C\{^{1}H\}$ and $^{31}P\{^{1}H\}$ NMR spectroscopy which had data in agreement with that previously reported in the literature.[10]

^{1}H NMR (700 MHz, C_6D_6) δ 1.99 (hd, *J* = 7.1, 3.3 Hz, 2H, P-($CH(CH_3)_2)_2$), 1.14 (ddd, *J* = 22.6, 12.7, 7.1 Hz, 12H, P-($CH(CH_3)_2)_2$), 0.21 (d, *J* = 3.8 Hz, 9H, $Si(CH_3)_3$).

$^{13}C\{^{1}H\}$ NMR (176 MHz, C_6D_6) δ 23.1 (d, $^{2}J_{PC}$ = 12.0 Hz, P-($CH(CH_3)_2)_2$), 22.9 (d, $^{2}J_{PC}$ = 13.5 Hz, P-($CH(CH_3)_2)_2$), 21.3 (d, $^{1}J_{PC}$ = 16.0 Hz, P-($CH(CH_3)_2)_2$), 1.0 (d, *J* = 11.0 Hz, $Si(CH_3)_3$).

$^{31}P\{^{1}H\}$ NMR (283 MHz, C_6D_6) δ −44.5.

^{29}Si NMR (139 MHz, C_6D_6) δ −1.3 (d,$^{1}J_{PSi}$ = 30.8 Hz).

5.2.2.6. Synthesis of trimethylsilyl-(diethyl)-phosphine

Trimethylsilyl-(diethyl)-phosphine was synthesised following the same procedure described in section 5.2.2.1 using diethylphosphine (10 wt. % solution in hexanes, 1.82 g, 20.2 mmol), ^{n}BuLi (2.5 M solution in hexanes, 10.5 mL, 26.3 mmol) and TMSCl (3.6 mL, 28.4 mmol). The product was obtained as a colourless oil (1.64 g, 50 % yield)[f] with

[f] Low yield thought to be due to loss of product when solvent removed under vacuum due to high volatility of $TMSPEt_2$ (b.p. = 71 – 72 °C).

its identity being verified by ^{1}H and $^{31}P\{^{1}H\}$ NMR spectroscopy which gave data matching that previously reported in the literature.[11]

^{1}H NMR (400 MHz, C_6D_6) δ 1.41 (q, $^{3}J_{HH}$ = 7.9 Hz, 4H, P-(CH_2CH$_3$)$_2$), 1.11 (dt, *J* = 15.2, 7.6 Hz, 6H, P-(CH$_2$CH_3)$_2$), 0.11 (d, *J* = 3.9 Hz, 9H, Si(CH_3)$_3$).

$^{31}P\{^{1}H\}$ NMR (162 MHz, C_6D_6) δ −87.9.

5.2.2.7. Synthesis of trimethylsilyl-bis(ortho-methoxyphenyl)-phosphine

Trimethylsilyl-*bis*(*ortho*-methoxyphenyl)phosphine was synthesised following an analogous procedure to that described in section 5.2.2.1 using *bis*(*ortho*-methoxyphenyl)phosphine[g] (1.00 g, 4.1 mmol), ^{n}BuLi (2.5 M solution in hexanes, 2.5 mL, 6.3 mmol) and TMSCl (0.9 mL, 7.1 mmol). The product was obtained as a white solid (1.02 g, 78 % yield) with its identity validated by ^{1}H, $^{13}C\{^{1}H\}$, $^{31}P\{^{1}H\}$ and ^{29}Si NMR spectroscopy which had data in agreement with that previously reported by Dr. James Radcliffe.[1]

^{1}H NMR (700 MHz, C_6D_6) δ 7.46 – 7.40 (m, 2H, *p*-(C$_6H_4$)$_2$), 7.10 (ddd, *J* = 8.2, 7.3, 1.8 Hz, 2H, *o*-(C$_6H_4$)$_2$), 6.78 (tt, *J* = 7.4, 1.1 Hz, 2H, *m*-(C$_6H_4$)$_2$), 6.52 (dd, *J* = 8.2, 2.8, 1.1 Hz, 2H, *m*-(C$_6H_4$)$_2$), 3.27 (s, 6H, (OCH_3)$_2$), 0.25 (d, *J* = 5.0 Hz, 9H, Si(CH_3)$_3$).

$^{13}C\{^{1}H\}$ NMR (176 MHz, C_6D_6) δ 160.5 (d, $^{2}J_{PC}$ = 6.5 Hz, *o*-(OMe-*C*$_6$H$_4$)$_2$), 136.3 (d, $^{4}J_{PC}$ = 20.5 Hz, *p*-(*C*$_6$H$_4$)$_2$), 129.2 (*o*-(*C*$_6$H$_4$)$_2$), 124.9 (d, $^{1}J_{PC}$ = 19.5 Hz, *i*-(*C*$_6$H$_4$)$_2$), 121.2 (d, $^{3}J_{PC}$ = 7.5 Hz, *m*-(*C*$_6$H$_4$)$_2$), 110.0 (*m*-(*C*$_6$H$_4$)$_2$), 54.5 ((O*C*H$_3$)$_2$) 0.4 (d, *J* = 12.5 Hz, Si(*C*H$_3$)$_3$).

$^{31}P\{^{1}H\}$ NMR (283 MHz, C_6D_6) δ −72.3.

^{29}Si NMR (139 MHz, C_6D_6) δ 2.1 (d,$^{1}J_{PSi}$ = 19.2 Hz).

[g] Synthesised by Dr. James Radcliffe.[1]

5.2.3. Synthesis of 1-phosphanyl methanimine (PCN) ligands

5.2.3.1. Synthesis of PhC(P^{i}Bu$_2$)=N(2,6-^{i}Pr$_2$C$_6$H$_3$) (2.1)

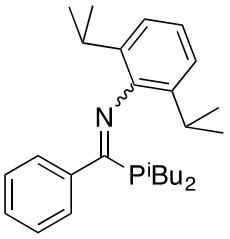

The synthesis of ligand **2.1** was conducted following the method developed by Dr. James Radcliffe.[1] A solution of N-(2,6-diisopropylphenyl)benzimidoyl chloride (1.30 g, 4.34 mmol) in chlorobenzene (15 mL) was added dropwise to a 2-necked round bottom flask which contained a solution of trimethylsilyl-(diisobutyl)-phosphine (0.95 g, 4.35 mmol) in chlorobenzene (15 mL). The reaction mixture was then heated at reflux for 18 hours, during which time the solution turned yellow. The solution was subsequently left to cool to room temperature before the volatile components were removed under vacuum. The resulting crude product was distilled under vacuum (130 °C, 0.1 mbar) to yield the final product as a yellow oil (0.96 g, 54 % yield). (calc.:$C_{27}H_{40}NP$ C, 79.17; H, 9.84; N, 3.42. Found: C, 79.02; H, 9.94; N, 3.49).

^{1}H NMR (700 MHz, $CDCl_3$) δ 7.23 - 7.14 (m, 5H, C-*o*/*m*/*p*-C_6H_5), 6.98 - 6.95 (m, 2H, N-*m*-C_6H_3), 6.93 (dd, *J* = 8.7, 6.3 Hz, 1H, N-*p*-C_6H_3), 2.80 (hept, $^3J_{HH}$ = 7.5 Hz, 2H, N-C_6H_3(C*H*$(CH_3)_2)_2$), 1.96 - 1.84 (m, 2H, P-(C*H*$_2$CH$(CH_3)_2)_2$), 1.81 - 1.66 (m, 2H, P-(CH_2C*H*$(CH_3)_2)_2$), 1.43 - 1.36 (m, 2H, P-(C*H*$_2$CH$(CH_3)_2)_2$), 1.13 (d, $^3J_{HH}$ = 6.8 Hz, 6H, N-C_6H_3(CH(C*H*$_3)_2)_2$), 0.98 (dd, *J* = 10.7, 6.7 Hz, 12H, P-(CH_2CH(C*H*$_3)_2)_2$), 0.89 (d, $^3J_{HH}$ = 7.0 Hz, 6H, N-C_6H_3(CH(C*H*$_3)_2)_2$).

^{13}C{^{1}H} NMR (176 MHz, $CDCl_3$) δ 179.7 (d, $^1J_{PC}$ = 15.0 Hz, *C*=N), 147.3 (d, $^3J_{PC}$ = 5.0 Hz, N-*i*-C_6H_3), 135.6 (d, $^4J_{PC}$ = 2.0 Hz, N-*o*-C_6H_3), 129.6 (C-*i*-C_6H_5), 128.9 (C-*o*/*m*/*p*-C_6H_5), 128.1 (C-*o*/*m*/*p*-C_6H_5), 127.7 (d, J_{PC} = 10.0 Hz, C-*o*/*m*/*p*-C_6H_5), 123.1 (N-*p*-C_6H_3), 122.8 (N-*m*-C_6H_3), 36.5 (d, $^1J_{PC}$ = 11.5 Hz, P-(*C*H$_2$CH$(CH_3)_2)_2$), 28.3 (N-C_6H_3 (*C*H$(CH_3)_2)_2$), 27.1 (d, $^2J_{PC}$ = 15.0 Hz, P-(CH_2*C*H$(CH_3)_2)_2$), 24.2 (N-C_6H_3(CH(*C*H$_3)_2)_2$), 24.1 (d, $^3J_{PC}$ = 9.5 Hz, P-(CH_2CH(*C*H$_3)_2)_2$), 22.0 (N-C_6H_3(CH(*C*H$_3)_2)_2$).

^{31}P{^{1}H} NMR (162 MHz, $CDCl_3$) δ −14.9.

MS (ASAP$^+$) *m*/*z*: 410.3 ([MH]$^+$), 366.2 ([M−^{i}Pr]$^+$), 264.2 ([M−P^{i}Bu$_2$]$^+$).

IR (ATR)**:** $\nu_{C=N}$ = 1587 cm^{-1}.

5.2.3.2. Synthesis of PhC(P^{i}Bu$_2$)=N(2,6-Et$_2$C$_6$H$_3$) (2.2)

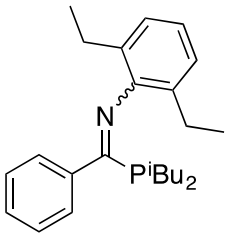

Ligand **2.2** was synthesised by an analogous procedure to that described for ligand **2.1**, using trimethylsilyl-(diisobutyl)-phosphine (0.95 g, 4.35 mmol) and *N*-(2,6-diethylphenyl)benzimidoyl chloride (1.18 g, 4.34 mmol). Vacuum distillation (140 °C, 0.1 mbar) yielded the product as a yellow oil (0.98 g, 60 % yield). (calc.: $C_{25}H_{36}NP$ C, 78.70; H, 9.51; N, 3.67. Found: C, 78.90; H, 9.62; N, 3.73).

^{1}H NMR (600 MHz, $CDCl_3$) δ 7.26 - 7.12 (m, 5H, C-*o*/*m*/*p*-C_6H_5), 6.98 - 6.91 (m, 2H, N-*m*-C_6H_3), 6.90 - 6.85 (m, 1H, N-*p*-C_6H_3), 2.45 (dq, *J* = 15.0, 7.5 Hz, 2H, N-$C_6H_3(CH_2CH_3)_2$), 2.31 - 2.14 (m, 2H, N-$C_6H_3(CH_2CH_3)_2$), 1.95 - 1.85 (m, 2H, P-$(CH_2CH(CH_3)_2)_2$), 1.81 - 1.67 (m, 2H, P-$(CH_2CH(CH_3)_2)_2$), 1.48 – 1.36 (m, 2H, P-$(CH_2CH(CH_3)_2)_2$), 1.11 (t, $^3J_{HH}$ = 7.5 Hz, 6H, N-$C_6H_3(CH_2CH_3)_2$), 1.05 - 0.92 (m, 12H, P-$(CH_2CH(CH_3)_2)_2$).

^{13}C{^{1}H} NMR (151 MHz, $CDCl_3$) δ 180.2 (d, $^1J_{PC}$= 16.0 Hz, *C*=N), 148.7 (d, $^3J_{PC}$= 3.5 Hz, N-*i*-C_6H_3), 138.7 (d, $^2J_{PC}$ = 25.5 Hz, C-*i*-C_6H_5), 131.1 (N-*o*-C_6H_3), 129.0 (C-*o*/*m*/*p*-C_6H_5), 128.0 (C-*o*/*m*/*p*-C_6H_5), 127.2 (d, J_{PC} = 9.5 Hz, C-*o*/*m*/*p*-C_6H_5), 125.7 (N-*m*-C_6H_3), 122.8 (N-*p*-C_6H_3), 36.6 (d, $^1J_{PC}$ = 11.5 Hz, P-$(CH_2CH(CH_3)_2)_2$), 27.0 (d, $^2J_{PC}$ = 15.0 Hz, P-$(CH_2CH(CH_3)_2)_2$), 24.7 (N-$C_6H_3(CH_2CH_3)_2$), 24.2 (d, $^3J_{PC}$ = 9.0 Hz, P-$(CH_2CH(CH_3)_2)_2$), 24.1 (d, $^3J_{PC}$ = 9.5 Hz, P-$(CH_2CH(CH_3)_2)_2$), 13.8 (N-$C_6H_3(CH_2CH_3)_2$).

^{31}P{^{1}H} NMR (162 MHz, $CDCl_3$) δ −14.5.

MS (ASAP$^+$) *m*/*z*: 382.3 ($[MH]^+$), 352.2 ($M-Et]^+$), 236.2 ($[M-P^iBu_2]^+$).

IR (ATR)**:** $\nu_{C=N}$ = 1587 cm^{-1}.

5.2.3.3. Synthesis of PhC(P^{i}Bu$_2$)=N(2,6-Me$_2$C$_6$H$_3$) (2.3)

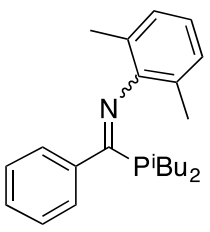

Ligand **2.3** was synthesised by an analogous procedure to that described for ligand **2.1** using trimethylsilyl-(diisobutyl)-phosphine (0.95 g, 4.35 mmol) and *N*-(2,6- dimethylphenyl)benzimidoyl chloride (1.06 g, 4.35 mmol). Vacuum distillation (140 - 145 °C, 0.1 mbar) afforded the product as a yellow oil (0.97 g, 63 % yield). (calc.: $C_{23}H_{32}NP$ C, 78.15; H, 9.13; N, 3.96. Found: C, 78.33; H, 9.25; N, 4.01).

^{1}H NMR (700 MHz, $CDCl_3$) δ 7.24 – 7.14 (m, 5H, C-*o*/*m*/*p*-C_6H_5), 6.88 (d, $^{3}J_{HH}$ = 7.4 Hz, 2H, N-*m*-C_6H_3), 6.77 (t, $^{3}J_{HH}$ = 7.5 Hz, 1H, N-*p*-C_6H_3), 1.99 (s, 6H, N-$C_6H_3(CH_3)_2$), 1.95 – 1.87 (m, 2H, P-(CH_2CH(CH_3)$_2$)$_2$), 1.79 – 1.70 (m, 2H, P-(CH_2CH(CH_3)$_2$)$_2$), 1.46 – 1.39 (m, 2H, P-(CH_2CH(CH_3)$_2$ $_2$), 1.05 – 0.93 (m, 12H, P-(CH_2CH(CH_3)$_2$)$_2$).

^{13}C{^{1}H} NMR (176 MHz, $CDCl_3$) δ 180.8 (d, $^{1}J_{PC}$= 16.5 Hz, *C*=N), 149.8 (d, $^{3}J_{PC}$= 4.5 Hz, N-*i*-C_6H_3), 139.1 (d, $^{2}J_{PC}$ = 26.0 Hz, C-*i*-C_6H_5), 129.0 (C-*o*/*m*/*p*-C_6H_5), 128.1 (C-*o*/*m*/*p*-C_6H_5), 127.8 (N-*m*-C_6H_3),127.0 (d, *J* = 9.0 Hz, C-*o*/*m*/*p*-C_6H_5), 125.6 (N-*o*-C_6H_3), 122.5 (N-*p*-C_6H_3), 39.1 (P-(CH_2CH(CH_3)$_2$)$_2$), 36.4 (d, $^{1}J_{PC}$ = 12.0 Hz, P-(CH_2CH(CH_3)$_2$)$_2$), 30.7 (P-(CH_2CH(CH_3)$_2$)$_2$), 27.0 (d, $^{2}J_{PC}$ = 14.5 Hz, P-(CH_2CH(CH_3)$_2$)$_2$), 24.4 – 23.9 (m, P-(CH_2CH(CH_3)$_2$)$_2$), 18.5 (N-$C_6H_3(CH_3)_2$).

^{31}P{^{1}H} NMR (162 MHz, $CDCl_3$) δ −14.6.

MS (ASAP^{+}) *m*/*z*: 354.2 ([MH]$^{+}$), 208.1 ([M−P^{i}Bu$_2$]$^{+}$).

IR (ATR)**:** $\nu_{C=N}$ = 1589 cm^{-1}.

5.2.3.4. Synthesis of PhC(PCypent$_2$)=N(2,6-^{i}Pr$_2$C$_6$H$_3$) (2.4)

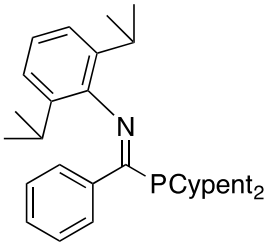

Ligand **2.4** was synthesised by an analogous procedure to that described for ligand **2.1** using trimethylsilyl-(dicyclopentyl)-phosphine (0.95 g, 3.92 mmol) and *N*-(2,6-diisopropylphenyl)benzimidoyl chloride (1.18 g, 3.94 mmol). Kugelrohr vacuum distillation (168 °C, 0.1 mbar) afforded the crude product as a yellow oil which crystallised over a period of two weeks at −30 °C to yield the pure product as yellow crystals suitable for an X-ray crystallographic study (1.10 g, 65 % yield). (calc.: $C_{29}H_{40}NP$ C, 80.33; H, 9.30; N, 3.23. Found: C, 80.23; H, 9.41; N, 3.05). See Appendices, section 6.2 for X-ray crystallographic data.

^{1}H NMR (700 MHz, $CDCl_3$) δ 7.30 - 7.23 (m, 2H, C-*o*-C_6H_5), 7.21 - 7.11 (m, 3H, C-*m*/*p*-C_6H_5), 6.99 - 6.89 (m, 3H, N-*m*/*p*-C_6H_3), 2.83 (hept, $^{3}J_{HH}$ = 6.9 Hz, 2H, N-C_6H_3(C*H*(CH_3)$_2$)$_2$), 2.32 – 2.24 (m, 2H, C*H* on P(C_5H_9)$_2$), 2.01 - 1.91 (m, 2H, P(C_5H_9)$_2$), 1.89 - 1.79 (m, 2H, P(C_5H_9)$_2$), 1.68 - 1.38 (m, 12H, P(C_5H_9)$_2$), 1.13 (d, $^{3}J_{HH}$ = 6.8 Hz, 6H, N-C_6H_3(CH(CH_3)$_2$)$_2$), 0.86 (d, $^{3}J_{HH}$ = 6.9 Hz, 6H, N-C_6H_3(CH(CH_3)$_2$)$_2$).

$^{13}C\{^{1}H\}$ NMR (176 MHz, $CDCl_3$) δ 178.2 (d, $^{1}J_{PC}$ = 18.0 Hz, *C*=N), 147.4 (d, $^{3}J_{PC}$ = 4.0 Hz, N-*i*-C_6H_3), 139.4 (d, $^{2}J_{PC}$ = 27.0 Hz, C-*i*-C_6H_5), 135.4 (d, $^{4}J_{PC}$ = 1.5 Hz, N-*o*-C_6H_3), 128.9 (d, J_{PC}= 1.0 Hz, C-*o*/*m*/*p*-C_6H_5), 128.3 (d, J_{PC} = 10.5 Hz, C-*o*/*m*/*p*-C_6H_5), 127.9 (d, J_{PC}= 1.0 Hz, C-*o*/*m*/*p*-C_6H_5), 123.1 (N-*m*/*p*-C_6H_3), 122.9 (N-*m*/*p*-C_6H_3), 35.1 (d, $^{1}J_{PC}$ = 11.0 Hz, *C*H on P(C_5H_9)$_2$), 31.4 (d, J_{PC} = 13.0 Hz, P(C_5H_9)$_2$), 30.1 (d, J_{PC} = 13.0 Hz, P(C_5H_9)$_2$), 28.4 (N-C_6H_3(*C*H(CH_3)$_2$)$_2$), 26.7 (d, J_{PC} = 7.0 Hz, P(C_5H_9)$_2$), 26.3 (d, J_{PC} = 7.0 Hz, P(C_5H_9)$_2$), 24.4 (N-C_6H_3(CH(*C*H_3)$_2$)$_2$), 22.1 (N-C_6H_3(CH(*C*H_3)$_2$)$_2$).

$^{31}P\{^{1}H\}$ NMR (162 MHz, $CDCl_3$) δ 17.1.

MS (ASAP$^+$) *m*/*z*: 434.3 ([MH]$^+$), 390.2 ([M–^{i}Pr]$^+$), 264.2 ([M–PCypent$_2$]$^+$).

IR (ATR)**:** $\nu_{C=N}$ = 1596 cm^{-1}.

5.2.3.5. Synthesis of PhC(PCypent$_2$)=N(2,6-Et$_2$C$_6$H$_3$) (2.5)

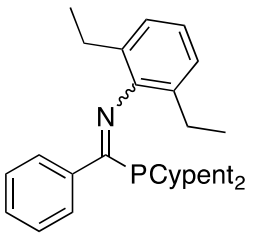

Ligand **2.5** was synthesised by an analogous procedure to that used for ligand **2.1** using trimethylsilyl-(dicyclopentyl)-phosphine (1.00 g, 4.13 mmol) and *N*-(2,6-diethylphenyl)benzimidoyl chloride (1.12 g, 4.12 mmol). Kugelrohr vacuum distillation (163 °C, 0.1 mbar) afforded the final product as a yellow oil which solidified upon scraping (1.14 g, 68 % yield). (calc.: $C_{27}H_{36}NP$ C, 79.96; H, 8.95; N, 3.45. Found: C, 79.86; H, 9.08; N, 3.51).

^{1}H NMR (600 MHz, $CDCl_3$) δ 7.28 - 7.22 (m, 2H, C-*o*-C_6H_5), 7.21 - 7.17 (m, 1H, C-*p*-C_6H_5), 7.16 - 7.13 (m, 2H, C-*m*-C_6H_5), 6.95 - 6.91 (m, 2H, N-*m*-C_6H_3), 6.87 (dd, *J* = 8.4, 6.6 Hz, 1H, N-*p*-C_6H_3), 2.47 (dq, *J* = 15.0, 7.5 Hz, 2H, N-C_6H_3(CH_2CH_3)$_2$), 2.30 - 2.24 (m, 2H, C*H* on P(C_5H_9)$_2$), 2.23 - 2.16 (m, 2H, N-C_6H_3(CH_2CH_3)$_2$), 2.04 – 1.93 (m, 2H, P(C_5H_9)$_2$), 1.87 – 1.77 (m, 2H, P(C_5H_9)$_2$), 1.66 - 1.35 (m, 12H, P(C_5H_9)$_2$), 1.09 (t, $^{3}J_{HH}$ = 7.5 Hz, 6H, N-C_6H_3(CH_2CH_3)$_2$).

$^{13}C\{^{1}H\}$ NMR (176 MHz, $CDCl_3$) δ 178.6 (d, $^{1}J_{PC}$ = 18.5 Hz, *C*=N), 148.9 (d, $^{3}J_{PC}$ = 3.5 Hz, N-*i*-C_6H_3), 139.8 (d, $^{2}J_{PC}$ = 26.0 Hz, C-*i*-C_6H_5), 130.9 (d, $^{4}J_{PC}$ = 1.5 Hz, N-o-C_6H_3), 129.0 (C-*p*-C_6H_5), 127.9 (C-*m*-C_6H_5), 127.8 (d, $^{3}J_{PC}$ = 10.0 Hz, C-*o*-C_6H_5), 125.5 (N-m-C_6H_3), 122.8 (N-*p*-C_6H_3), 34.9 (d, $^{1}J_{PC}$ = 11.5 Hz, *C*H on P(C_5H_9)$_2$), 31.5 (d, J_{PC} = 13.5 Hz, P(C_5H_9)$_2$), 30.0 (d, J_{PC} = 12.5 Hz, P(C_5H_9)$_2$), 26.6 (d, J_{PC} = 7.0 Hz, P(C_5H_9)$_2$), 26.2 (d, J_{PC} = 7.0 Hz, P(C_5H_9)$_2$), 24.6 (N-C_6H_3(*C*H_2CH_3)$_2$), 13.8 ((N-C_6H_3(CH_2*C*H_3)$_2$).

$^{31}P\{^{1}H\}$ NMR (243 MHz, $CDCl_3$) δ 17.1.

MS (ASAP$^+$) *m*/*z*: 406.3 ($[MH]^+$), 376.2 ($[M–Et]^+$), 236.2 ($[M–PCyPent_2]^+$).

IR (ATR)**:** $\nu_{C=N}$ = 1601 cm^{-1}.

5.2.3.6. Synthesis of PhC(PCypent$_2$)=N(2,6-Me$_2$C$_6$H$_3$) (2.6)

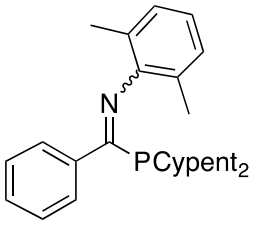

Ligand **2.6** was synthesised by an analogous procedure to that used for ligand **2.1** using trimethylsilyl-(dicyclopentyl)-phosphine (1.00 g, 4.13 mmol) and *N*-(2,6-dimethylphenyl)benzimidoyl chloride (1.01 g, 4.14 mmol). Kugelrohr vacuum distillation (157 °C, 0.1 mbar) yielded the final product as a yellow oil which solidified over 2 days at -30 °C (1.01 g, 65 % yield). (calc.: $C_{25}H_{32}NP$ C, 79.54; H, 8.54; N, 3.71. Found: C, 79.36; H, 8.64; N, 3.53).

^{1}H NMR (600 MHz, $CDCl_3$) δ 7.27 – 7.22 (m, 2H, C-*o*-C_6H_5), 7.21 – 7.19 (m, 1H, C-*p*-C_6H_5), 7.18 – 7.13 (m, 2H, C-*m*-C_6H_5), 6.87 (d, $^{3}J_{HH}$ = 7.4 Hz, 2H, N-*m*-C_6H_3), 6.77 (t, $^{3}J_{HH}$ = 7.4 Hz, 1H, N-*p*-C_6H_3), 2.34 – 2.23 (m, 2H, C*H* on $P(C_5H_9)_2$), 2.00 (s, 6H, N-$C_6H_3(CH_3)_2$), 1.89 – 1.78 (m, 2H, $P(C_5H_9)_2$), 1.67 – 1.26 (m, 12H, $P(C_5H_9)_2$), 0.96 (t, *J* = 7.5 Hz, 1H, $P(C_5H_9)_2$), 0.91 (t, *J* = 6.8 Hz, 1H, $P(C_5H_9)_2$).

$^{13}C\{^{1}H\}$ NMR (151 MHz, $CDCl_3$) δ 178.9 (d, $^{1}J_{PC}$ = 19.0 Hz, *C*=N), 150.1 (d, $^{3}J_{PC}$ = 4.0 Hz, N-*i*-C_6H_3), 140.3 (d, $^{2}J_{PC}$ = 27.0 Hz, C-*i*-C_6H_5), 129.1 (d, $^{5}J_{PC}$ = 1.0 Hz, C-*p*-C_6H_5), 127.9 (C-*m*-C_6H_5), 127.8 (N-m-C_6H_3), 127.6 (d, $^{3}J_{PC}$ = 10.0 Hz, C-*o*-C_6H_5), 125.3 (d, $^{4}J_{PC}$ = 1.5 Hz, N-o-C_6H_3), 122.5 (N-*p*-C_6H_3), 34.8 (d, $^{1}J_{PC}$ = 11.5 Hz, *C*H on $P(C_5H_9)_2$), 31.4 (d, J_{PC} = 13.5 Hz, $P(C_5H_9)_2$), 30.7 ($P(C_5H_9)_2$), 30.0 (d, J_{PC} = 13.0 Hz, $P(C_5H_9)_2$), 29.1 ($P(C_5H_9)_2$), 26.6 (d, J_{PC} = 7.0 Hz, $P(C_5H_9)_2$), 26.2 (d, J_{PC} = 7.0 Hz, $P(C_5H_9)_2$), 18.8 (N-$C_6H_3(CH_3)_2$), 14.2 ($P(C_5H_9)_2$), 11.3 $P(C_5H_9)_2$).

$^{31}P\{^{1}H\}$ NMR (243 MHz, $CDCl_3$) δ 16.5.

MS (ASAP$^+$) *m*/*z*: 378.2 ($[MH]^+$), 208.1 ($[M–PCyPent_2]^+$).

IR (ATR)**:** $\nu_{C=N}$ = 1587 cm^{-1}.

5.2.3.7. Synthesis of PhC(PNorbornyl$_2$)=N(2,6-^{i}Pr$_2$C$_6$H$_3$) (2.7)

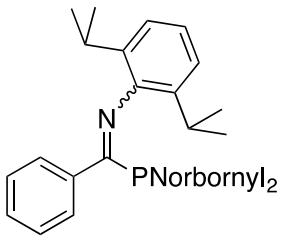

Ligand **2.7** was synthesised by an analogous procedure to that described for ligand **2.1** using trimethylsilyl-(dinorbornyl)-phosphine (0.93 g, 3.16 mmol) and *N*-(2,6-diisopropylphenyl)benzimidoyl chloride (0.95 g, 3.17 mmol). Kugelrohr vacuum distillation (200 °C, 0.1 mbar) afforded the final product as a yellow oil that solidified upon scraping (0.98 g, 64 % yield). (calc.: $C_{33}H_{44}NP$ C, 81.61; H, 9.13; N, 2.88. Found: C, 81.68; H, 9.05; N, 2.96).

^{1}H NMR (600 MHz, $CDCl_3$) δ 7.35 – 7.24 (m, 2H, C-*o*-C_6H_5), 7.21 – 7.12 (m, 3H, C-*m*/*p*-C_6H_5), 7.02 – 6.92 (m, 3H, N-*m*/*p*-C_6H_3), 2.86 – 2.75 (m, 2H, N-C_6H_3(C*H*$(CH_3)_2)_2$), 2.42 – 2.25 (m, 2H, P($C_7H_{11})_2$), 2.24 – 2.07 (m, 3H, P($C_7H_{11})_2$), 2.05 – 1.99 (m, 1H, P($C_7H_{11})_2$), 1.74 – 1.34 (m, 11H, P($C_7H_{11})_2$), 1.30 – 1.07 (m, 11H, N-C_6H_3(CH(C$H_3)_2)_2$/ P($C_7H_{11})_2$), 0.87 – 0.77 (m, 6H, N-C_6H_3(CH(C$H_3)_2)_2$).

^{13}C{^{1}H} NMR (151 MHz, $CDCl_3$) δ 177.9 (d, $^1J_{PC}$ = 22.5 Hz, *C*=N), 177.4 (d, $^1J_{PC}$ = 21.5 Hz, *C*=N), 177.1 (d, $^1J_{PC}$ = 20.0 Hz, *C*=N), 147.5 (d, $^3J_{PC}$ = 3.0 Hz, N-*i*-C_6H_3), 147.4 (d, $^3J_{PC}$ = 3.5 Hz, N-*i*-C_6H_3), 147.3 (d, $^3J_{PC}$ = 3.5 Hz, N-*i*-C_6H_3), 140.0 (dd, J_{PC} = 28.0, 4.5 Hz, C-*i*-C_6H_5), 135.2 (N-*o*-C_6H_3), 135.1 (N-*o*-C_6H_3), 135.0 (N-*o*-C_6H_3), 129.1 – 128.7 (m, C-*o*/*m*/*p*-C_6H_5), 127.9 – 127.8 (m, C-*o*/*m*/*p*-C_6H_5), 123.2 – 122.9 (m, N-*m*/*p*-C_6H_3), 40.8 (P($C_7H_{11})_2$), 40.7 (P($C_7H_{11})_2$), 40.7 (P($C_7H_{11})_2$), 40.3 – 39.8 (m, (P($C_7H_{11})_2$), 39.5 (dd, J_{PC} = 13.5, 5.0 Hz, (P($C_7H_{11})_2$), 37.7 (d, J_{PC} = 2.5 Hz, P($C_7H_{11})_2$), 37.6 (d, J_{PC} = 3.0 Hz, P($C_7H_{11})_2$), 37.3 – 37.1 (m, P($C_7H_{11})_2$), 37.1 (d, J_{PC} = 2.0 Hz, P($C_7H_{11})_2$), 36.9 (P($C_7H_{11})_2$), 36.9 (P($C_7H_{11})_2$), 36.8(P($C_7H_{11})_2$), 35.9 (d, J_{PC} = 11.5 Hz, P($C_7H_{11})_2$), 35.3 (d, J_{PC} = 10.5 Hz, P($C_7H_{11})_2$), 32.2 (dd, J_{PC} = 17.5, 7.0 Hz, P($C_7H_{11})_2$), 29.3 (d, J_{PC} = 2.5 Hz, P($C_7H_{11})_2$), 28.9 (d, J_{PC} = 15.5 Hz, P($C_7H_{11})_2$), 28.2 (dd, J_{PC} = 8.0, 2.0 Hz, N-C_6H_3(*C*H$(CH_3)_2)_2$), 24.7 – 24.2 (m, N-C_6H_3(CH(*C*$H_3)_2)_2$), 22.2 (dd, J_{PC} = 16.5, 7.5 Hz, N-C_6H_3(CH(*C*$H_3)_2)_2$).[h]

^{31}P{^{1}H} NMR (162 MHz, $CDCl_3$) δ 16.6, 13.6, 9.8.[i]

[h] Presence of multiple resonances believed to arise from three *exo* isomers of ligand **2.7** (see Chapter 2, section 2.3.1).

[i] Three resonances at 16.6, 13.6, and 9.8 ppm present in relative ratio 21:51:28, respectively (ratio derived by integration of the peaks in ^{31}P{^{1}H} NMR spectrum), proposed to correspond to the three *exo* isomers of ligand **2.7** (as discussed in Chapter 2, section 2.3.1).

MS (ASAP$^+$) *m*/*z*: 486.3 ([MH]$^+$), 442.3 (M–^{i}Pr]$^+$). 264.2 ([M–PNorbornyl$_2$]$^+$).

IR (ATR)**:** $\nu_{C=N}$ = 1610 cm^{-1}.

5.2.3.8. Synthesis of PhC(PNorbornyl$_2$)=N(2,6-Et$_2$C$_6$H$_3$) (2.8)

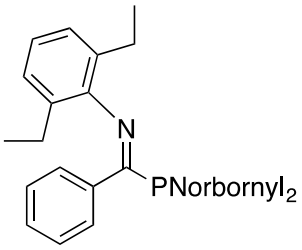

Ligand **2.8** was synthesised by an analogous procedure to that described for ligand **2.1** using trimethylsilyl-(dinorbornyl)-phosphine (1.12 g, 3.80 mmol) and *N*-(2,6-diethylphenyl)benzimidoyl chloride (1.03 g, 3.79 mmol). Kugelrohr vacuum distillation (196 °C, 0.05 mbar) afforded the crude product as a yellow oil which crystallised over a period of two weeks at −30 °C to yield the pure product as yellow block-shaped crystals suitable for an X-ray crystallographic study (1.17 g, 68% yield). (calc.: $C_{31}H_{40}NP$ C, 81.36; H, 8.81; N, 3.06. Found: C, 81.59; H, 8.99; N, 3.19). See Appendices, section 6.2 for X-ray crystallographic data.

^{1}H NMR (700 MHz, $CDCl_3$) δ 7.35 – 7.23 (m, 2H, C-*o*-C_6H_5), 7.22 – 7.11 (m, 3H, C-*m*/*p*-C_6H_5), 7.00 – 6.87 (m, 3H, N-*m*/*p*-C_6H_3), 2.55 – 1.97 (m, 10H, N-$C_6H_3(CH_2CH_3)_2$/ $P(C_7H_{11})_2$), 1.76 – 1.38 (m, 10H, $P(C_7H_{11})_2$), 1.32 – 0.98 (m, 12H, N-$C_6H_3(CH_2CH_3)_2$/ $P(C_7H_{11})_2$).

^{13}C{^{1}H} NMR (176 MHz, $CDCl_3$) δ 177.9 (d, $^1J_{PC}$ = 26.5 Hz, *C*=N), 148.8 (d, $^3J_{PC}$ = 3.5 Hz, N-*i*-C_6H_3), 140.3 (d, $^2J_{PC}$ = 28.0 Hz, C-*i*-C_6H_5), 131.0 – 130.4 (m, N-*o*-C_6H_3), 129.2 – 128.8 (m, C-*m*/*p*-C_6H_5), 128.5 – 128.1 (m, C-*o*-C_6H_5), 127.8 (d, J_{PC} = 7.0 Hz, C-*m*/*p*-C_6H_5), 125.7 – 125.5 (m, N-*m*/*p*-C_6H_3), 122.9 (N-*m*/*p*-C_6H_3), 40.8 (d, J_{PC} = 10.0 Hz, $P(C_7H_{11})_2$), 40.2 (d, J_{PC} = 15.0 Hz, $P(C_7H_{11})_2$), 40.0 (d, J_{PC} = 12.0 Hz, $P(C_7H_{11})_2$), 39.8 (d, J_{PC} = 15.0 Hz, $P(C_7H_{11})_2$), 39.6 (d, J_{PC} = 15.5 Hz, $P(C_7H_{11})_2$), 39.4 (d, J_{PC} = 15.0 Hz, $P(C_7H_{11})_2$), 37.8 ($P(C_7H_{11})_2$), 37.6 $P(C_7H_{11})_2$), 37.4 – 36.9 (m, $P(C_7H_{11})_2$), 36.0 (d, J_{PC} = 11.0 Hz, $P(C_7H_{11})_2$), 35.4 (d, J_{PC} = 9.5 Hz, $P(C_7H_{11})_2$), 32.1 (td, J_{PC} = 15.0, 14.0, 6.5 Hz, $P(C_7H_{11})_2$), 29.4 – 28.6 (m, $P(C_7H_{11})_2$), 24.5 (dd, J_{PC} = 22.5, 14.5 Hz, N-$C_6H_3(CH_2CH_3)_2$), 13.9 (N-$C_6H_3(CH_2CH_3)_2$), 13.9 (N-$C_6H_3(CH_2CH_3)_2$).[j]

[j] Presence of multiple resonances due to three *exo* isomers of ligand **2.8**, see Chapter 2, section 2.3.1.

$^{31}P\{^{1}H\}$ NMR (162 MHz, $CDCl_3$) δ 17.1, 14.4, 10.6.[k]

MS (ASAP$^+$) *m*/*z*: 458.3 ($[MH]^+$), 428.3 ($M-Et]^+$). 236.2 ($[M-PNorbornyl_2]^+$).

IR (ATR)**:** $\nu_{C=N}$ = 1586 cm^{-1}.

5.2.3.9. Synthesis of PhC(PNorbornyl$_2$)=N(2,6-Me$_2$C$_6$H$_3$) (2.9)

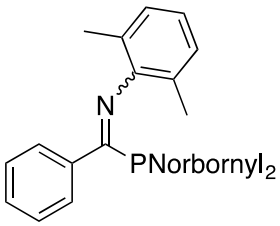

Ligand **2.9** was synthesised by an analogous procedure to that described for ligand **2.1** using trimethylsilyl-(dinorbornyl)-phosphine (1.21 g, 4.11 mmol) and *N*-(2,6-dimethylphenyl)benzimidoyl chloride (1.00 g, 4.10 mmol). Kugelrohr vacuum distillation (180 °C, 0.08 mbar) yielded the final product as a yellow oil, which solidified upon scraping (1.24 g, 70% yield). (calc.: $C_{29}H_{36}NP$ C, 81.08; H, 8.45; N, 3.26. Found: C, 80.98; H, 8.56; N, 3.39).

^{1}H NMR (700 MHz, $CDCl_3$) δ 7.36 – 7.12 (m, 5H, C-*o*/*m*/*p*-C_6H_5), 6.96 – 6.86 (m, 2H, N-*m*-C_6H_3), 6.84 – 6.76 (m, 1H, N-*p*-C_6H_3), 2.45 – 2.20 (m, 4H, $P(C_7H_{11})_2$), 2.17 – 1.90 (m, 8H, N-$C_6H_3(CH_3)_2$/ $P(C_7H_{11})_2$), 1.74 – 1.41 (m, 10H, $P(C_7H_{11})_2$), 1.34 – 1.09 (m, 6H, $P(C_7H_{11})_2$).

$^{13}C\{^{1}H\}$ NMR (176 MHz, $CDCl_3$) δ 177.9 (dd, J_{PC} = 21.0, 15.5 Hz, *C*=N), 150.1 (d, $^3J_{PC}$ = 3.5 Hz, N-*i*-C_6H_3), 141.0 – 140.4 (m, C-*i*-C_6H_5), 129.2 – 128.9 (m, C-*o*/*m*/*p*-C_6H_5), 128.1 – 127.8 (m, C-*o*/*m*/*p*-C_6H_5/, N-*m*-C_6H_3), 125.7 – 124.7 (m, N-*o*-C_6H_3), 122.5 (N-*p*-C_6H_3), 40.8 (d, J_{PC} = 9.5 Hz, $P(C_7H_{11})_2$), 40.3 (d, J_{PC} = 15.5 Hz, $P(C_7H_{11})_2$), 39.8 (dd, J_{PC} = 17.5, 14.0 Hz, $P(C_7H_{11})_2$), 39.5 (d, J_{PC} = 13.0 Hz, $P(C_7H_{11})_2$), 39.3 (d, J_{PC} = 15.5 Hz, $P(C_7H_{11})_2$), 37.6 (dd, J_{PC} = 9.0, 2.5 Hz, $P(C_7H_{11})_2$), 37.4 – 36.9 (m, $P(C_7H_{11})_2$), 36.0 (d, J_{PC} = 10.5 Hz, $P(C_7H_{11})_2$), 35.2 (d, J_{PC} = 10.0 Hz, $P(C_7H_{11})_2$), 32.1 (dt, J_{PC} = 26.5, 6.5 Hz, $P(C_7H_{11})_2$), 29.2 (d, J_{PC} = 5.5 Hz, $P(C_7H_{11})_2$), 28.9 (d, J_{PC} = 8.5 Hz, $P(C_7H_{11})_2$), 18.8 (dd, J_{PC} = 14.5, 9.5 Hz, N-$C_6H_3(CH_3)_2$).[l]

[k] Three resonances at 17.1, 14.4, and 10.6 ppm present in relative ratio 25:51.24, respectively (ratio derived by integration of the peaks in $^{31}P\{^{1}H\}$ NMR spectrum), corresponding to the three exo isomers of ligand **2.8** (as discussed in Chapter 2, section 2.3.1).

[l] Presence of multiple resonances due to three *exo* isomers of ligand **2.8**, see Chapter 2, section 2.3.1.

$^{31}P\{^{1}H\}$ NMR (162 MHz, $CDCl_3$) δ 15.7, 13.5, 9.8.[m]

MS (ASAP$^+$) *m*/*z*: 430.0 ($[MH]^+$), 208.0 ($[M–PNorbornyl_2]^+$).

IR (ATR)**:** $\nu_{C=N}$ = 1586 cm^{-1}.

5.2.3.10. Synthesis of (p-CF_3-Ph)C(P^iPr_2)=N(2,6-^{i}$Pr_2C_6H_3$) (2.10)

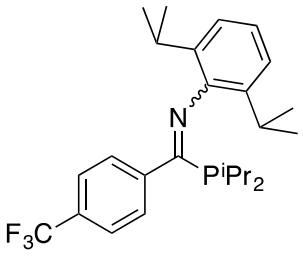

Ligand **2.10** was synthesised by an analogous procedure to that described for ligand **2.1** using trimethylsilyl-(diisopropyl)-phosphine (0.98 g, 5.15 mmol) and *N*-(2,6-diisopropylphenyl)-4-(trifluoromethyl)benzimidoyl chloride (1.89 g, 5.14 mmol). Kugelrohr vacuum distillation (113 °C, 0.1 mbar) afforded the final product as yellow oil that solidified on scraping (1.43 g, 62 % yield). (calc.: $C_{26}H_{35}F_3NP$ C, 69.47; H, 7.85; N, 3.12. Found: C, 69.38; H, 7.78; N, 3.26).

^{1}H NMR (700 MHz, $CDCl_3$) δ 7.47 – 7.43 (m, 2H, C-*m*-C_6H_4), 7.40 – 7.35 (m, 2H, C-*o*-C_6H_4), 7.00 - 6.93 (m, 3H, N-*m*/*p*-C_6H_3), 2.81 (hept, $^3J_{HH}$ = 6.4 Hz, 2H, N-$C_6H_3(CH(CH_3)_2)_2$), 2.27 – 2.19 (m, 2H, P($CH(CH_3)_2)_2$), 1.32 - 1.17 (m, 6H, P($CH(CH_3)_2)_2$), 1.13 (d, $^3J_{HH}$ = 6.8 Hz, 6H, N-$C_6H_3(CH(CH_3)_2)_2$), 1.08 - 0.94 (m, 6H, P($CH(CH_3)_2)_2$), 0.88 (d, $^3J_{HH}$ = 7.0 Hz, 6H, N-$C_6H_3(CH(CH_3)_2)_2$).

$^{13}C\{^{1}H\}$ NMR (176 MHz, $CDCl_3$) δ 175.9 (d, $^1J_{PC}$ = 22.0 Hz, *C*=N), 146.7 (d, $^3J_{PC}$ = 3.5 Hz, N-*i*-C_6H_3), 142.8 (d, $^2J_{PC}$ = 26.5 Hz, C-*i*-C_6H_4), 135.2 (d, $^4J_{PC}$ = 2.0 Hz, N-*o*-C_6H_3), 130.6 (q, $^2J_{FC}$ = 32.5 Hz, C-*p*-C_6H_4), 128.3 (d, $^3J_{PC}$ = 10.5 Hz, C-*o*-C_6H_4), 124.8 (q, $^3J_{FC}$ = 3.5 Hz, C-*m*-C_6H_4), 123.5 (N-*m*/*p*-C_6H_3), 122.9 (N-*m*/*p*-C_6H_3), 28.3 (N-$C_6H_3(CH(CH_3)_2)_2$), 24.3 (N-$C_6H_3(CH(CH_3)_2)_2$), 22.8 (d, $^1J_{PC}$ = 12.5 Hz, P($CH(CH_3)_2)_2$), 21.9 (N-$C_6H_3(CH(CH_3)_2)_2$), 20.6 (d, $^2J_{PC}$ = 12.0 Hz, P($CH(CH_3)_2)_2$), 19.4 (d, $^2J_{PC}$ = 11.0 Hz, P($CH(CH_3)_2)_2$). The quaternary carbon corresponding to CF_3 was not observed in the $^{13}C\{^{1}H\}$ NMR spectrum due to the long relaxation times associated with quaternary carbon centres.

$^{31}P\{^{1}H\}$ NMR (283 MHz, $CDCl_3$) δ 29.5.

[m] Three resonances at 15.7, 13.5, and 9.8 ppm present in relative ratio 28:50:22, respectively (ratio derived by integration of the peaks in $^{31}P\{^{1}H\}$ NMR spectrum), believed to correspond to the three *exo* isomers of ligand **2.9** (as discussed in Chapter 2, section 2.3.1).

^{19}F NMR (376 MHz, $CDCl_3$) δ −62.8.

MS (ASAP$^+$) *m*/*z*: 450.0 ([MH]$^+$), 406.0 ([M−^{i}Pr]$^+$), 332.0 ([M−P^{i}Pr$_2$]$^+$).

IR (ATR)**:** $\nu_{C=N}$ = 1584 cm^{-1}, ν_{CF} = 1323 cm^{-1}.

5.2.3.11. Synthesis of (p-Me-Ph)C(P^{i}Pr$_2$)=N(2,6-^{i}Pr$_2$C$_6$H$_3$) (2.11)

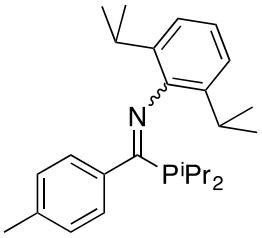

Ligand **2.11** was synthesised by an analogous procedure to that described for ligand **2.1** using trimethylsilyl-(diisopropyl)-phosphine (0.97 g, 5.10 mmol) and *N*-(2,6-diisopropylphenyl)-4-(methyl)benzimidoyl chloride (1.60 g, 5.10 mmol). Kugelrohr vacuum distillation (140 °C, 0.15 mbar) yielded the final product as a yellow oil that solidified on leaving at − 30 °C for a period of weeks (1.37 g, 68 % yield). (calc.: $C_{26}H_{38}NP$ C, 78.95; H, 9.68; N, 3.54. Found: C, 78.81; H, 9.53; N, 3.64).

^{1}H NMR (700 MHz, $CDCl_3$) δ 7.22 – 7.19 (m, 1H, N-*p*-C_6H_3), 7.18 – 7.15 (m, 2H, C-*o*-C_6H_4), 7.01 – 6.93 (m, 4H, C-*m*-C_6H_4/ N-*m*-C_6H_3), 2.92 – 2.85 (m, 2H, N-C_6H_3(C*H*(CH$_3$)$_2$)$_2$), 2.28 – 2.20 (m, 5H, C-C_6H_4(C*H*$_3$)/ P(C*H*(CH$_3$)$_2$)$_2$), 1.27 – 1.20 (m, 6H, P(CH(C*H*$_3$)$_2$)$_2$), 1.15 (d, $^3J_{HH}$ = 6.9 Hz, 6H, N-C_6H_3(CH(C*H*$_3$)$_2$)$_2$), 1.07 – 1.00 (m, 6H, P(CH(C*H*$_3$)$_2$)$_2$), 0.89 (d, $^3J_{HH}$ = 7.0 Hz, 6H, N-C_6H_3(CH(C*H*$_3$)$_2$)$_2$).[n]

^{13}C{^{1}H} NMR (176 MHz, $CDCl_3$) δ 176. 9 (d, $^1J_{PC}$ = 19.5 Hz, *C*=N), 147.8 (d, $^3J_{PC}$ = 4.0 Hz, N-*i*-C_6H_3), 139.0 (d, $^5J_{PC}$ = 1.0 Hz, C-*p*-C_6H_4), 137.0 (d, $^2J_{PC}$ = 2.0 Hz, C-*i*-C_6H_4), 135.5 (d, $^4J_{PC}$ = 1.5 Hz, N-*o*-C_6H_3), 128.6 (d, J_{PC} = 1.5 Hz, C-*m*-C_6H_4/ N-*m*-C_6H_3), 128.2 (d, $^3J_{PC}$ = 10.5 Hz, C-*o*-C_6H_4), 123.2 (N-*p*-C_6H_3), 122.9 (C-*m*-C_6H_4/ N-*m*-C_6H_3), 28.4 (N-C_6H_3(*C*H(CH$_3$)$_2$)$_2$), 24.4 (N-C_6H_3(CH(*C*H$_3$)$_2$)$_2$), 23.0 (d, $^1J_{PC}$ = 12.0 Hz, P(*C*H(CH$_3$)$_2$)$_2$), 22.2 (N-C_6H_3(CH(*C*H$_3$)$_2$)$_2$), 21.4 (C-C_6H_4(*C*H$_3$)), 20.7 (d, $^2J_{PC}$ = 11.5 Hz, P(CH(*C*H$_3$)$_2$)$_2$), 19.6 (d, $^2J_{PC}$ = 11.0 Hz, P(CH(*C*H$_3$)$_2$)$_2$).[m]

^{31}P{^{1}H} NMR (243 MHz, $CDCl_3$) δ 26.7.

MS (ASAP$^+$) *m*/*z*: 396.0 ([MH]$^+$), 352.0 ([M−^{i}Pr]$^+$), 278.0 ([M−P^{i}Pr$_2$]$^+$).

IR (ATR)**:** $\nu_{C=N}$ = 1583 cm^{-1}.

[n] ^{1}H and ^{13}C{^{1}H} NMR spectra of the product revealed the presence of imidoyl chloride starting material (~ 15 %). It is thought that the imidoyl chloride starting material and ligand **2.11** have similar boiling points causing them to be difficult to separate *via* distillation.

5.2.3.12. Synthesis of PhC(PEt$_2$)=N(2,6-Et$_2$C$_6$H$_3$) (2.12)

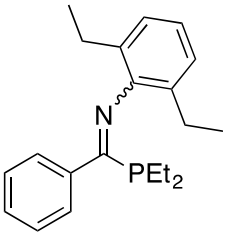

Ligand **2.12** was synthesised by an analogous procedure to that described for ligand **2.1** using trimethylsilyl-(diethyl)-phosphine (0.93 g, 5.73 mmol) and *N*-(2,6-diethylphenyl)benzimidoyl chloride (1.56 g, 5.74 mmol). Kugelrohr vacuum distillation (120 °C, 0.1 mbar) yielded the final product as a yellow oil, which solidified upon scraping (1.45 g, 78% yield). (calc.: $C_{21}H_{28}NP$ C, 77.51; H, 8.67; N, 4.30. Found: C, 77.55; H, 8.52; N, 4.40).

^{1}H NMR (700 MHz, $CDCl_3$) δ 7.28 - 7.12 (m, 5H, C-*o*/*m*/*p*-C_6H_5), 6.94 (d, $^3J_{HH}$ = 7.5 Hz, 2H, N-*m*-C_6H_3), 6.89 (t, $^3J_{HH}$ = 7.5 Hz, 1H, N-*p*-C_6H_3), 2.53 – 2.43 (m, 2H, N-$C_6H_3(CH_2CH_3)_2$), 2.30 - 2.14 (m, 2H, N-$C_6H_3(CH_2CH_3)_2$), 1.95 - 1.75 (m, 2H, $P(CH_2CH_3)_2$), 1.69 - 1.54 (m, 2H, $P(CH_2CH_3)_2$), 1.21 - 0.95 (m, 12H, $P(CH_2CH_3)_2$/ N-$C_6H_3(CH_2CH_3)_2$).

^{13}C{^{1}H} NMR (151 MHz, $CDCl_3$) δ 179.2 (d, $^1J_{PC}$ = 16.0 Hz, *C*=N), 148.7 (N-*i*-C_6H_3), 132.3 (d, $^2J_{PC}$ = 14.0 Hz, C-*i*-C_6H_5), 131.1 (d, $^4J_{PC}$ = 2.0 Hz, N-*o*-C_6H_3), 129.0 (d, J_{PC} = 1.0 Hz, C-*o*/*m*/*p*-C_6H_5), 128.1 (C-*o*/*m*/*p*-C_6H_5), 127.0 (d, J_{PC} = 9.0 Hz, C-*o*/*m*/*p*-C_6H_5), 125.6 (N-*m*-C_6H_3), 122.9 (N-*p*-C_6H_3), 24.8 (N-$C_6H_3(CH_2CH_3)_2$), 16.3 (d, $^1J_{PC}$ = 11.0 Hz, $P(CH_2CH_3)_2$), 13.6 (N-$C_6H_3(CH_2CH_3)_2$), 10.2 (d, $^2J_{PC}$ = 10.5 Hz, $P(CH_2CH_3)_2$).

^{31}P{^{1}H} NMR (162 MHz, $CDCl_3$) δ 3.0.

MS (ASAP$^+$) *m*/*z*: 326.2 ($[MH]^+$), 296.2 ($[M–Et]^+$), 236.2 ($[M–PEt_2]^+$).

IR (ATR)**:** $\nu_{C=N}$ = 1587 cm^{-1}.

5.2.3.13. Synthesis of PhC(PCy$_2$)=N(2,6-Et$_2$C$_6$H$_3$) (2.13)

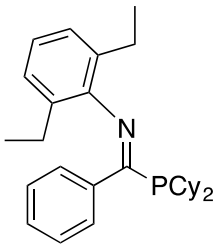

Ligand **2.13** was synthesised by an analogous procedure to that described for ligand **2.1** using trimethylsilyl-(dicyclohexyl)-phosphine (0.96 g, 3.55 mmol) and *N*-(2,6-diethylphenyl)benzimidoyl chloride (0.97 g, 3.57 mmol). The resulting crude product was recrystallised from hot hexane to yield the final product as yellow platelets, which were suitable for X-ray diffraction (1.08 g, 70 % yield). (calc.: $C_{29}H_{40}NP$ C, 80.33; H, 9.30; N, 3.23. Found: C, 80.24; H, 9.41; N, 3.35). See Appendices, section 6.2 for X-ray crystallographic data.

^{1}H NMR (700 MHz, $CDCl_3$) δ 7.27 – 7.22 (m, 2H, C-*o*-C_6H_5), 7.21 – 7.18 (m, 1H, C-*p*-C_6H_5), 7.17 – 7.14 (m, 2H, C-*m*-C_6H_5), 6.97 – 6.93 (m, 2H, N-*m*-C_6H_3), 6.92 – 6.87 (m, 1H, N-*p*-C_6H_3), 2.56 – 2.45 (m, 2H, N-$C_6H_3(CH_2CH_3)_2$), 2.28 – 2.17 (m, 2H, N-$C_6H_3(CH_2CH_3)_2$), 2.12 – 1.98 (m, 4H, $P(C_6H_{11})_2$), 1.83 – 1.68 (m, 6H, $P(C_6H_{11})_2$), 1.66 (d, *J* = 13.2 Hz, 2H, $P(C_6H_{11})_2$), 1.38 – 1.21 (m, 6H, $P(C_6H_{11})_2$), 1.18 – 1.07 (m, 8H, $P(C_6H_{11})_2$/ N-$C_6H_3(CH_2CH_3)_2$), 1.05 – 0.95 (m, 2H, $P(C_6H_{11})_2$).

^{13}C{^{1}H} NMR (176 MHz, $CDCl_3$) δ 177.4 (d, $^{1}J_{PC}$ = 19.5 Hz, *C*=N), 149.0 (N-*i*-C_6H_3), 140.2 (d, $^{2}J_{PC}$ = 26.0 Hz, C-*i*-C_6H_5), 131.1 (N-*o*-C_6H_3), 129.0 (C-*p*-C_6H_5), 127.8 (C-*m*-C_6H_5), 127.8 (d, $^{3}J_{PC}$ = 10.0 Hz, C-*o*-C_6H_5), 125.5 (N-*m*-C_6H_3), 122.8 (N-*p*-C_6H_3), 32.9 (d, J_{PC} = 12.5 Hz, $P(C_6H_{11})_2$), 31.1 ($P(C_6H_{11})_2$), 29.6 ($P(C_6H_{11})_2$), 27.6 (d, $P(C_6H_{11})_2$), 26.6 ($P(C_6H_{11})_2$), 24.8 (N-$C_6H_3(CH_2CH_3)_2$), 13.9 (N-$C_6H_3(CH_2CH_3)_2$).

^{31}P{^{1}H} NMR (283 MHz, $CDCl_3$) δ 19.4.

MS (ASAP^{+}) *m*/*z*: 434.0 ($[MH]^+$), 404.0 ($[M–Et]^+$), 236.0 ($[M–PCy_2]^+$).

IR (ATR)**:** $\nu_{C=N}$ = 1584 cm^{-1}.

5.2.3.14. Synthesis of PhC(P^{i}Pr$_2$)=N(2,6-^{i}Pr$_2$C$_6$H$_3$) (2.14)

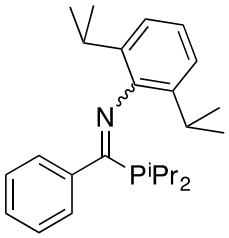

Ligand **2.14** was synthesised by an analogous procedure to that described for ligand **2.1** using trimethylsilyl-(diisopropyl)-phosphine (1.20 g, 6.30 mmol) and *N*-(2,6-diisopropylphenyl)benzimidoyl chloride (1.89 g, 6.30 mmol). Kugelrohr vacuum distillation (132 °C, 0.2 mbar) yielded the final product as a yellow oil which solidified upon scraping (1.49 g, 62% yield). The identity of the product was validated by ^{1}H, ^{13}C and ^{31}P{^{1}H} NMR spectroscopy which gave data in agreement with those previously reported by Dr. James Radcliffe.[1] (calc.: $C_{25}H_{36}NP$ C, 78.70; H, 9.51; N, 3.67. Found: C, 78.39; H, 9.67; N, 3.71).

^{1}H NMR (700 MHz, $CDCl_3$) δ 7.28 – 7.24 (m, 2H, C-*o*-C_6H_5), 7.20 – 7.14 (m, 3H, C-*m*/*p*-C_6H_5), 6.98 – 6.95 (m, 2H, N-*m*-C_6H_3), 6.95 – 6.91 (m, 1H, N-*p*-C_6H_3), 2.90 – 2.83 (m, 2H, N-$C_6H_3(CH(CH_3)_2)_2$), 2.23 (heptd, *J* = 7.1, 3.0 Hz, 2H, $P(CH(CH_3)_2)_2$), 1.21 (dd, *J* = 15.9, 6.8 Hz, 6H, $P(CH(CH_3)_2)_2$), 1.13 (d, $^{3}J_{HH}$ = 6.8 Hz, 6H, N-$C_6H_3(CH(CH_3)_2)_2$), 1.01 (dd, *J* = 12.7, 7.3 Hz, 6H, $P(CH(CH_3)_2)_2$), 0.87 (d, $^{3}J_{HH}$ = 7.0 Hz, 6H, N-$C_6H_3(CH(CH_3)_2)_2$).

$^{13}C\{^{1}H\}$ NMR (176 MHz, $CDCl_3$) δ 177.1 (d, $^{1}J_{PC}$ = 20.0 Hz, *C*=N), 147.5 (d, $^{3}J_{PC}$ = 3.5 Hz, N-*i*-C_6H_3), 139.7 (d, $^{2}J_{PC}$ = 26.0 Hz, C-*i*-C_6H_5), 135.5 (d, $^{4}J_{PC}$ = 1.5 Hz, N-*o*-C_6H_3), 129.0 (d, J_{PC} = 1.0 Hz, C-*m*/*p*-C_6H_5), 128.2 (d, $^{3}J_{PC}$ = 10.5 Hz, C-*o*-C_6H_5), 128.0 (d, J_{PC} = 1.5 Hz, C-*m*/*p*-C_6H_5), 123.2 (N-*p*-C_6H_3), 122.9 (N-*m*-C_6H_3), 28.4 (N-$C_6H_3(CH(CH_3)_2)_2$), 24.5 (N-$C_6H_3(CH(CH_3)_2)_2$), 23.0 (d, $^{1}J_{PC}$ = 12.0 Hz, P($CH(CH_3)_2)_2$), 22.2 (N-$C_6H_3(CH(CH_3)_2)_2$), 20.7 (d, $^{2}J_{PC}$ = 11.5 Hz, P($CH(CH_3)_2)_2$), 19.6 (d, $^{2}J_{PC}$ = 11.0 Hz, P($CH(CH_3)_2)_2$).

$^{31}P\{^{1}H\}$ NMR (283 MHz, $CDCl_3$) δ 27.6.

MS (ASAP^{+}) *m*/*z*: 382.3 ($[MH]^+$), 338.2 ($[M-{}^{i}Pr]^+$), 264.2 ($[M-P^{i}Pr_2]^+$).

IR (ATR)**:** $\nu_{C=N}$ = 1583 cm^{-1}.

5.2.3.15. Synthesis of PhC(P^{i}Pr$_2$)=N(2,6-Et$_2$C$_6$H$_3$) (2.15)

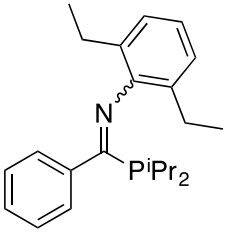

Ligand **2.15** was synthesised by an analogous procedure to that used for ligand **2.1** using trimethylsilyl-(diisopropyl)-phosphine (1.18 g, 6.20 mmol) and *N*-(2,6-diethyphenyl)benzimidoyl chloride (1.68 g, 6.18 mmol). Kugelrohr vacuum distillation (120 °C, 0.1 mbar) yielded the final product as a yellow oil, which solidified upon scraping (1.64 g, 75% yield). The identity of the product was verified by ^{1}H, ^{13}C and $^{31}P\{^{1}H\}$ NMR spectroscopy, which gave data matching that previously reported by Dr. James Radcliffe.[1] (calc.: $C_{23}H_{32}NP$ C, 78.15; H, 9.13; N, 3.96. Found: C, 77.97; H, 9.26; N, 4.03).

^{1}H NMR (700 MHz, $CDCl_3$) δ 7.25 - 7.22 (m, 2H, C-*o*-C_6H_5), 7.21 - 7.17 (m, 1H, C-*p*-C_6H_5), 7.17 - 7.12 (m, 2H, C-*m*-C_6H_5), 6.95 - 6.92 (m, 2H, N-*m*-C_6H_3), 6.90 - 6.86 (m, 1H, N-*p*-C_6H_3), 2.57 – 2.45 (m, 2H, N-$C_6H_3(CH_2CH_3)_2$), 2.29 – 2.13 (m, 4H, N-$C_6H_3(CH_2CH_3)_2$/ P($CH(CH_3)_2)_2$), 1.28 – 1.19 (m, 6H, P($CH(CH_3)_2)_2$), 1.11 (t, $^{3}J_{HH}$ = 7.5 Hz, 6H, N-$C_6H_3(CH_2CH_3)_2$), 1.00 (dd, *J* = 12.5, 7.5 Hz, 6H, P($CH(CH_3)_2)_2$).

$^{13}C\{^{1}H\}$ NMR (176 MHz, $CDCl_3$) δ 177.6 (d, $^{1}J_{PC}$ = 22.0 Hz, *C*=N), 148.9 (d, $^{3}J_{PC}$ = 4.0 Hz, N-*i*-C_6H_3), 140.1 (d, $^{2}J_{PC}$ = 26.0 Hz, C-*i*-C_6H_5), 131.0 (N-*o*-C_6H_3), 129.1 (C-*p*-C_6H_5), 128.0 (d, $^{4}J_{PC}$ = 1.0 Hz, C-*m*-C_6H_5), 127.7 (d, $^{3}J_{PC}$ = 10.0 Hz, C-*o*-C_6H_5), 125.5 (N-*m*-C_6H_3), 122.9 (N-*p*-C_6H_3), 24.7 (N-$C_6H_3(CH_2CH_3)_2$), 22.9 (d, $^{1}J_{PC}$ = 12.5 Hz,

P(*C*H(CH$_3$)$_2$)$_2$), 20.9 (d, $^2J_{PC}$ = 12.0 Hz, P(CH(*C*H$_3$)$_2$)$_2$), 19.5 (d, $^2J_{PC}$ = 10.5 Hz, P(CH(*C*H$_3$)$_2$)$_2$), 13.9 (N-C$_6$H$_3$(CH$_2$*C*H$_3$)$_2$).

^{31}P{^{1}H} NMR (162 MHz, $CDCl_3$) δ 27.7.

MS (ASAP$^+$) *m*/*z*: 354.2 ([MH]$^+$), 236.2 ([M–P^{i}Pr$_2$]$^+$).

IR (ATR)**:** $\nu_{C=N}$ = 1584 cm^{-1}.

5.2.3.16. Synthesis of PhC(P^{i}Pr$_2$)=N(2-MeC$_6$H$_4$) (2.16)

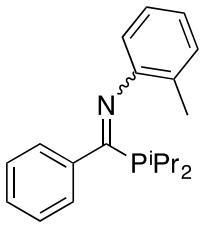

Ligand **2.16** was synthesised by an analogous procedure to that described for ligand **2.1** using trimethylsilyl-(diisopropyl)-phosphine (1.00 g, 5.25 mmol) and *N*-*o*-tolylbenzimidoyl chloride (1.21 g, 5.27 mmol). Kugelrohr vacuum distillation (114 °C, 0.08 mbar) yielded the final product as a yellow oil, which solidified upon scraping (0.98 g, 60 % yield). The identity of the product was validated by ^{1}H, ^{13}C and ^{31}P{^{1}H} NMR spectroscopy, which gave data in agreement with those previously reported by Dr. James Radcliffe.[1] (calc.: $C_{20}H_{26}NP$ C, 77.14; H, 8.42; N, 4.50. Found: C, 77.16; H, 8.54; N, 4.58).

^{1}H NMR (700 MHz, $CDCl_3$) δ 7.24 – 7.15 (m, 5H, C-*o*/*m*/*p*-C$_6$*H*$_5$), 7.10 – 7.05 (m, 1H, N-*o*-C$_6$*H*$_4$), 6.90 – 6.86 (m, 1H, N-*m*-C$_6$*H*$_4$), 6.85 – 6.79 (m, 1H, N-*m*-C$_6$*H*$_4$), 6.29 – 6.24 (m, 1H, N-*p*-C$_6$*H*$_4$), 2.25 – 2.18 (m, 5H, N-C$_6$H$_4$(C*H*$_3$)/ P(C*H*(CH$_3$)$_2$)$_2$), 1.21 (dd, *J* = 13.4, 7.0 Hz, 6H, P(CH(C*H*$_3$)$_2$)$_2$), 1.00 (dd, *J* = 12.7, 7.3 Hz, 6H, P(CH(C*H*$_3$)$_2$)$_2$).

^{13}C{^{1}H} NMR (176 MHz, $CDCl_3$) δ 177.7 (d, $^1J_{PC}$ = 21.5 Hz, *C*=N), 151.2 (d, $^3J_{PC}$ = 3.5 Hz, N-*i*-*C*$_6$H$_4$), 139.9 (d, $^2J_{PC}$ = 26.0 Hz, C-*i*-*C*$_6$H$_5$), 130.2 (N-*o*-*C*$_6$H$_4$), 128.9 (C-*o*/*m*/*p*-*C*$_6$H$_5$), 128.3 (N-*o*-*C*$_6$H$_4$(CH$_3$)), 128.3 (C-*o*/*m*/*p*-*C*$_6$H$_5$), 128.1 (C-*o*/*m*/*p*-*C*$_6$H$_5$), 126.2 (N-*m*-*C*$_6$H$_4$), 123.0 (N-*m*-*C*$_6$H$_4$), 119.0 (N-*p*-*C*$_6$H$_4$), 22.7 (d, $^1J_{PC}$ = 12.5 Hz, P(*C*H(CH$_3$)$_2$)$_2$), 20.5 (d, $^2J_{PC}$ = 12.0 Hz, P(CH(*C*H$_3$)$_2$)$_2$), 19.3 (d, $^2J_{PC}$ = 11.0 Hz, P(CH(*C*H$_3$)$_2$)$_2$), 18.5 (N-C$_6$H$_4$(*C*H$_3$)).

^{31}P{^{1}H} NMR (283 MHz, $CDCl_3$) δ 27.1.

IR (ATR)**:** $\nu_{C=N}$ = 1590 cm^{-1}.

5.2.3.17. Synthesis of PhC(P(2-(OMe)C$_6$H$_4$)$_2$)=N(2,6-^{i}Pr$_2$C$_6$H$_4$) (2.17)

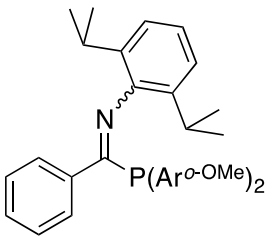

Ligand **2.17** was synthesised by an analogous procedure to that described for ligand **2.1** using trimethylsilyl-*bis*(*ortho*-methoxyphenyl)-phosphine (0.67 g, 2.10 mmol) and *N*-(2,6-diisopropylphenyl)benzimidoyl chloride (0.63 g, 2.10 mmol). The resulting crude product was recrystallised from hot hexane to yield the final product as a yellow block-shaped crystals, which were suitable for X-ray diffraction (0.53 g, 50 % yield). In addition to X-ray diffraction analysis, the identity of the product was further confirmed by ^{1}H, ^{13}C and ^{31}P{^{1}H} NMR spectroscopy which gave data matching that previously reported by Dr. James Radcliffe.[1] (calc.: $C_{33}H_{36}NO_2P$ C, 77.77; H, 7.12; N, 2.75. Found: C, 77.50; H, 7.07; N, 2.66). See Appendices, section 6.2 for X-ray crystallographic data.

^{1}H NMR (700 MHz, $CDCl_3$, 50 °C) δ 7.39 – 7.33 (m, 2H, P-*o*/*m*/*p*-(C$_6$*H*$_4$)$_2$), 7.29 – 7.24 (m, 2H, C-*o*/*m*-C$_6$*H*$_5$), 7.22 – 7.16 (m, 2H, P-*o*/*m*/*p*-(C$_6$*H*$_4$)$_2$), 7.09 – 7.03 (m, 3H, P-*o*/*m*/*p*-(C$_6$*H*$_4$)$_2$/ C-*p*-C$_6$*H*$_5$), 6.94 – 6.89 (m, 3H, N-*m*/*p*-C$_6$*H*$_3$), 6.83 (t, *J* = 7.0 Hz, 2H, C-*o*/*m*-C$_6$*H*$_5$), 6.79 – 6.74 (m, 2H, P-*o*/*m*/*p*-(C$_6$*H*$_4$)$_2$), 3.76 – 3.70 (m, 6H, P-(C$_6$H$_4$(OC*H*$_3$))$_2$), 2.85 (hept, $^3J_{HH}$ = 7.0 Hz, 2H, N-C$_6$H$_3$(C*H*(CH$_3$)$_2$)$_2$), 0.92 (d, $^3J_{HH}$ = 7.0 Hz, 6H, N-C$_6$H$_3$(CH(C*H*$_3$)$_2$)$_2$), 0.90 (d, $^3J_{HH}$ = 7.0 Hz, 6H, N-C$_6$H$_3$(CH(C*H*$_3$)$_2$)$_2$).

^{13}C NMR (151 MHz, $CDCl_3$, 50 °C) δ 174.4 (*C*=N), 161.9 (P-*o*-(*C*$_6$H$_4$(OCH$_3$))$_2$), 147.5 (d, $^3J_{PC}$ = 8.0 Hz, N-*i*-*C*$_6$H$_3$), 138.4 (P-*i*-(*C*$_6$H$_4$)$_2$), 135.5 (N-*o*-*C*$_6$H$_3$), 135.3 (C-*i*-*C*$_6$H$_5$), 130.8 (C-*o*/*m*-*C*$_6$H$_5$), 128.7 (P-*o*/*m*/*p*-(*C*$_6$H$_4$)$_2$), 128.1 (P-*o*/*m*/*p*-(*C*$_6$H$_4$)$_2$), 127.6 (C-*p*-*C*$_6$H$_5$), 123.0 (N-*p*-*C*$_6$H$_3$), 122.6 (N-*m*-*C*$_6$H$_3$), 120.9 (C-*o*/*m*-*C*$_6$H$_5$), 110.3 (P-*o*/*m*/*p*-(*C*$_6$H$_4$)$_2$), 55.6 (P-(C$_6$H$_4$(O*C*H$_3$))$_2$), 28.2 (N-C$_6$H$_3$(*C*H(CH$_3$)$_2$)$_2$), 23.8 (N-C$_6$H$_3$(CH(*C*H$_3$)$_2$)$_2$), 22.4 (N-C$_6$H$_3$(CH(*C*H$_3$)$_2$)$_2$).

^{31}P{^{1}H} NMR (283 MHz, $CDCl_3$) δ −12.1, −24.7.[o]

MS (ASAP$^+$) *m*/*z*: 510.2 ([MH]$^+$), 264.2 ([M−P(2-(OMe)C$_6$H$_4$)$_2$]$^+$).

IR (ATR)**:** $\nu_{C=N}$ = 1584 cm^{-1}.

[o] Two resonances at −12.1 and −24.7 ppm present in relative ratio 1:0.22, respectively (ratio derived by integration of the peaks in ^{31}P{^{1}H} NMR spectrum), due to presence of imine *E* and *Z* isomers in solution.[1]

5.2.4. Synthesis of selenide derivatives of PCN ligands 2.1 – 2.17

An excess of selenium powder (15 mg) was added to a Young's tap NMR tube, which contained a sample of a PCN ligand (**2.1** - **2.17**, 20 mg) in 0.7 mL $CDCl_3$. The reaction mixture was sonicated for at least an hour, after which time the reactions had gone to 100 % conversion. The products, **2.1(Se)** - **2.17(Se)**, were analysed by $^{31}P\{^1H\}$ NMR spectroscopy; the resulting data are presented in Chapter 2, section 2.3.3, Table 2.10.

5.2.5. Synthesis of Cr^0-PCN complexes

5.2.5.1. Synthesis of $Cr(CO)_4(PhC(P^iPr_2)=N(2,6\text{-}^iPr_2C_6H_3))$ (2.18) and $Cr(CO)_5(PhC(P^iPr_2)=N(2,6\text{-}^iPr_2C_6H_3))$ (2.19)

(a) Using a modification of the method reported by Krishnamurthy *et al*.[12]

PCN ligand **2.14** (0.47 g, 1.23 mmol) and $Cr(CO)_6$ (0.33 g, 1.50 mmol) were added to a two-necked round bottom flask, equipped with a reflux condenser. Toluene (40 mL) was added to the round bottom flask before the resultant yellow solution was heated at reflux for 21 hours, during which time the solution turned purple. The solution was subsequently allowed to cool to room temperature and found to consist of a mixture of 4 phosphorus-containing products by $^{31}P\{^1H\}$ NMR spectroscopy (162 MHz, C_6D_6): 83.2 ppm (55 %, corresponding to **2.19**[1]), 64.3 ppm (39 %, corresponding to **2.18**[1]), 47.6 ppm (2 %) and 27.1 ppm (4 %, corresponding to **2.14**). Following filtration, the solvent was removed from the filtrate under vacuum to leave a purple residue. Hexane (20 mL) was added to the purple residue and the mixture filtered to yield a purple solid and yellow solution.

*Isolation of $Cr(CO)_4(PhC(P^iPr_2)=N(2,6\text{-}^iPr_2C_6H_3))$ (**2.18**)*

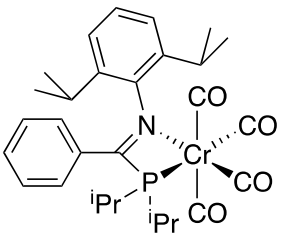

The purple solid (from the hexane filtration) was dissolved in the minimum amount of DCM before being layered with hexane, and subsequently left at –30 °C overnight yielding purple crystals of **2.18**. This process was repeated with the purple filtrate to yield more batches of **2.18** (0.11 g, 17 % yield). The identity of **2.18** was verified by ^1H, $^{13}C\{^1H\}$, and $^{31}P\{^1H\}$ NMR spectroscopy, in addition to IR spectroscopy; the data were all in agreement with those previously reported by Dr. James Radcliffe.[1]

^1H NMR (700 MHz, $CDCl_3$) δ 7.34 (t, $^3J_{HH}$ = 7.4 Hz, 1H, C-*p*-C_6H_5), 7.25 – 7.22 (m, 1H, N-*p*-C_6H_3), 7.22 – 7.19 (m, 2H, C-*m*-C_6H_5), 7.19 – 7.15 (m, 2H, N-*m*-C_6H_3), 6.92 (d, *J* = 8.0 Hz, 2H, C-*o*-C_6H_5), 3.15 (hept, $^3J_{HH}$ = 7.0 Hz, 2H, N-C_6H_3(C*H*(CH_3)$_2$)$_2$), 2.81 – 2.67

(m, 2H, P(C*H*(CH_3)$_2$)$_2$), 1.49 (dd, *J* = 18.5 Hz, 6.8 Hz, 6H, P(CH(C*H*$_3$)$_2$)$_2$), 1.41 (d, $^3J_{HH}$ = 6.5 Hz, 6H, N-C_6H_3(CH(C*H*$_3$)$_2$)$_2$), 1.39 – 1.33 (m, 6H, P(CH(C*H*$_3$)$_2$)$_2$), 0.81 (d, $^3J_{HH}$ = 6.9 Hz, 6H, N-C_6H_3(CH(C*H*$_3$)$_2$)$_2$).

^{13}C{^{1}H} NMR (176 MHz, $CDCl_3$) δ 229.3 (d, $^2J_{PC}$ = 12.0 Hz, *trans*-PCr(*C*O)), 225.5 (d, $^2J_{PC}$ = 3.0 Hz, *trans*-NCr(*C*O)), 222.3 (d, $^2J_{PC}$ = 13 .0 Hz, *trans*-Cr(*C*O)), 185.0 (d, $^1J_{PC}$ = 18.0 Hz, *C*=N), 147.3 (d, $^3J_{PC}$ = 24.0 Hz, N-*i*-*C*$_6$H$_3$), 136.2 (N-*o*-*C*$_6$H$_3$), 133.3 (d, $^2J_{PC}$ = 5.0 Hz, C-*i*-*C*$_6$H$_5$), 132.3 (C-*p*-*C*$_6$H$_5$), 129.1 (C-*m*-*C*$_6$H$_5$), 128.9 (C-*o*-*C*$_6$H$_5$), 127.2 (N-*p*-*C*$_6$H$_3$), 125.0 (N-*m*-*C*$_6$H$_3$), 30.2 (d, $^1J_{PC}$ = 9.0 Hz, P(*C*H(CH_3)$_2$)$_2$), 28.4 (N-C_6H_3(*C*H(CH_3)$_2$)$_2$), 25.0 (N-C_6H_3(CH(*C*H$_3$)$_2$)$_2$), 23.9 (N-C_6H_3(CH(*C*H$_3$)$_2$)$_2$), 20.5 (d, $^2J_{PC}$ = 12.0 Hz, P(CH(*C*H$_3$)$_2$)$_2$), 19.5 (d, $^2J_{PC}$ = 2.0 Hz, P(CH(*C*H$_3$)$_2$)$_2$).

^{31}P{^{1}H} NMR (283 MHz, $CDCl_3$) δ 63.3.

IR (CH_2Cl_2)**:** $\nu_{C=O}$ = 1999 cm^{-1}, 1900 cm^{-1}, 1874 cm^{-1}, 1859 cm^{-1}.

$\nu_{C=N}$ = 1532 cm^{-1}.

*Isolation of Cr(CO)$_5$(PhC(P^{i}Pr$_2$)=N(2,6-^{i}Pr$_2$C$_6$H$_3$)) (**2.19**)*

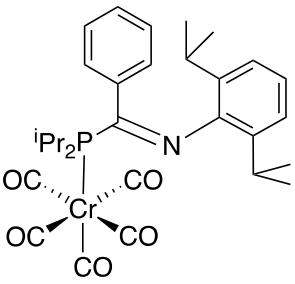

The yellow solution (from the hexane filtration) was concentrated under vacuum and stored at – 30 °C overnight, yielding yellow crystals of **2.19**. This process was repeated with the yellow filtrate to yield more batches of **2.19** (0.25 g, 37 % yield). The identity of **2.19** was validated by ^{1}H, ^{13}C, and ^{31}P{^{1}H} NMR spectroscopy, in addition to IR spectroscopy, which were all similar to those previously reported by Dr. James Radcliffe.[1]

^{1}H NMR (700 MHz, $CDCl_3$) δ 7.23 – 7.17 (m, 3H, C-*m*/*p*-C_6H_5), 7.08 (dd, *J* = 7.4, 2.1 Hz, 2H, C-*o*-C_6H_5), 6.96 – 6.88 (m, 3H, N-*m*/*p*-C_6H_3), 2.89 (hept, $^3J_{HH}$ = 6.9 Hz, 2H, N-C_6H_3(C*H*(CH_3)$_2$)$_2$), 2.66 – 2.57 (m, 2H, P(C*H*(CH_3)$_2$)$_2$), 1.35 – 1.27 (m, 12H, P(CH(C*H*$_3$)$_2$)$_2$), 1.11 (d, $^3J_{HH}$= 6.8 Hz, 6H, N-C_6H_3(CH(C*H*$_3$)$_2$)$_2$), 1.06 (d, *J* = 6.9 Hz, 6H, N-C_6H_3(CH(C*H*$_3$)$_2$)$_2$).

^{13}C{^{1}H} NMR (176 MHz, $CDCl_3$) δ 221.3 (d, $^2J_{PC}$ = 5.0 Hz, *trans*-PCr(*C*O)), 217.8 (d, $^2J_{PC}$ = 12.5 Hz, *trans*-Cr(*C*O)), 175.6 (d, $^1J_{PC}$ = 28.5 Hz, *C*=N), 145.8 (d, $^3J_{PC}$ = 15.5 Hz, N-*i*-*C*$_6$H$_3$), 137.6 (d, $^2J_{PC}$ = 21.0 Hz, C-*i*-*C*$_6$H$_5$), 135.3 (N-*o*-*C*$_6$H$_3$), 129.2 (C-*p*-*C*$_6$H$_5$), 128.1 (C-*m*-*C*$_6$H$_5$), 127.0 (d, $^3J_{PC}$ = 1.5 Hz, C-*o*-*C*$_6$H$_5$), 124.5 (N-*p*-*C*$_6$H$_3$), 122.9 (N-*m*-

C_6H_3), 28.6 (N-C_6H_3($CH(CH_3)_2$)$_2$), 28.4 (d, $^1J_{PC}$ = 16.0 Hz, P($CH(CH_3)_2$)$_2$), 25.2 (N-C_6H_3(CH(CH_3)$_2$)$_2$), 22.0 (N-C_6H_3(CH(CH_3)$_2$)$_2$), 19.2 (P(CH(CH_3)$_2$)$_2$), 18.3 (d, $^2J_{PC}$ = 3.5 Hz, P(CH(CH_3)$_2$)$_2$),).

$^{31}P\{^1H\}$ NMR (283 MHz, $CDCl_3$) δ 83.1.

IR (CH_2Cl_2)**:** $\nu_{C=O}$ = 2061 cm^{-1}, 1980 cm^{-1}, 1935 cm^{-1}.
$\nu_{C=N}$ = 1584 cm^{-1}.

(b) Using a modification of the method reported by Grim *et al*.[13]
A Schlenk was charged with PCN ligand **2.14** (0.24 g, 0.63 mmol), $Cr(CO)_6$ (0.17 g, 0.77 mmol) and diglyme (20 mL). The resultant yellow solution was heated to 160 °C, and then kept at 160 °C for 1 hour, after which time the solution turned purple and sublimation of $Cr(CO)_6$ was no longer observed. The solution was subsequently allowed to cool to room temperature and analysed by $^{31}P\{^1H\}$ NMR spectroscopy (162 MHz, C_6D_6) which revealed the solution to consist of a mixture of four phosphorus-containing products: 84.0 ppm (71 %, corresponding to **2.19**[1]), 63.6 ppm (13 %, corresponding to **2.18**[1]), 51.9 ppm (3 %), and 27.4 ppm (13 %, corresponding to **2.14**). The solution was then filtered and the solvent removed from the filtrate under vacuum to leave a purple residue, which was worked up in the same way as described previously in section (a) to yield **2.18** (0.03 g, 9 % yield) and **2.19** (0.17 g, 47 % yield).

5.2.5.2. Synthesis of $Cr(CO)_4(PhC(P^iPr_2)=N(2,6\text{-}Me_2C_6H_3))$ (2.20) and $Cr(CO)_5(PhC(P^iPr_2)=N(2,6\text{-}Me_2C_6H_3))$ (2.21)[p]

A flask was charged with $Cr(CO)_6$ (0.402 g, 1.8 mmol), PCN ligand $PhC(P^iPr_2)=N(2,6\text{-}Me_2C_6H_3)$ (0.495 g, 1.5 mmol), and toluene (40 mL). The mixture was heated to reflux for 24 hours after which time the solution was cooled to 0 °C and filtered, giving a purple solution. The solvent was removed *in vacuo* to leave a purple residue.

5.2.5.2.1. Isolation of $Cr(CO)_4(PhC(P^iPr_2)=N(2,6\text{-}Me_2C_6H_3))$ (2.20)

The majority of the purple solid was dissolved in hot hexane and the solution filtered and left to slowly cool. The remaining purple solid was separately dissolved in hot hexane and slowly cooled. Purple crystals formed in both flasks, and these were isolated by filtration and combined to

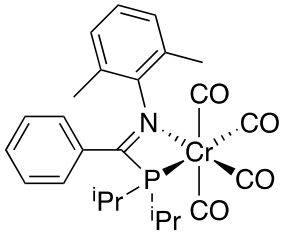

[p] Synthesised by Dr. James Radcliffe.[1]

yield the first product, the bidentate complex **2.20** (47 mg, 6 % yield). Successful elemental analysis data of the complex could not be obtained (calc.: $C_{25}H_{28}CrNO_4P$ C, 61.35; H, 5.77; N, 2.86. Found: C, 46.63; H, 3.90; N, 1.95). Mass spectrometry was attempted, but yielded inconclusive results. The identity of complex **2.20** was confirmed by NMR spectroscopic and X-ray crystallographic analyses. See Appendices, section 6.2 for X-ray crystallographic data.

^{1}H NMR (700 MHz, $CDCl_3$) δ 7.35 (t, $^3J_{HH}$ = 6.9 Hz, 1H, C-*p*-C_6H_5), 7.27 – 7.22 (m, 2H, C-*m*-C_6H_5), 7.01 (s, 3H, N-*m/p*-C_6H_3), 6.95 (d, *J* = 7.6 Hz, 2H, C-*o*-C_6H_5), 2.75 – 2.67 (m, 2H, P(C*H*$(CH_3)_2)_2$), 2.27 (s, 6H, N-$C_6H_3(CH_3)_2$), 1.51 – 1.39 (m, 12H, P(CH(C*H*$_3)_2)_2$).

^{13}C{^{1}H} NMR (176 MHz, $CDCl_3$) δ 229.3 (d, $^2J_{PC}$ = 12.0 Hz, *trans*-PCr(*C*O)), 225.4 (*trans*-NCr(*C*O)), 222.5 (d, $^2J_{PC}$ = 12.0 Hz, *trans*-Cr(*C*O)), 184.9 (d, $^1J_{PC}$ = 18.0 Hz, *C*=N), 149.4 (d, $^3J_{PC}$ = 23.0 Hz, N-*i*-C_6H_3), 134.1 (d, $^2J_{PC}$ = 4.0 Hz, C-*i*-C_6H_5), 131.8 (C-*p*-C_6H_5), 129.4 (C-*m*-C_6H_5), 129.2 (N-*m*-C_6H_3), 127.2 (C-*o*-C_6H_5), 126.2 (N-*p*-C_6H_3), 125.9 (N-*o*-C_6H_3), 28.9 (d, $^1J_{PC}$ = 9.0 Hz, P(*C*H$(CH_3)_2)_2$), 20.0 (P(CH(*C*H$_3)_2)_2$), 19.2 (N-C_6H_3(*C*H$_3)_2$).

^{31}P{^{1}H} NMR (283 MHz, $CDCl_3$) δ 61.8.

IR (CH_2Cl_2)**:** $\nu_{C=O}$ = 2000 cm^{-1}, 1899 cm^{-1}, 1874 cm^{-1}, 1858 cm^{-1}.
$\nu_{C=N}$ = 1536 cm^{-1}.

5.2.5.2.2. Isolation of Cr(CO)$_5$(PhC(P^{i}Pr$_2$)=N(2,6-Me$_2$C$_6$H$_3$)) (2.21)

The solution isolated from the first hexane washing was heated and concentrated under vacuum before being left to slowly cool. After 16 hours large yellow crystals had formed which were suitable for X-ray diffraction (0.337 g, 43 % yield). Analysis showed this yellow product to be complex **2.21**. (calc.: $C_{26}H_{28}CrNO_5P$ C, 60.35; H, 5.45; N, 2.71. Found: C, 60.21; H, 5.50; N, 2.80). See Appendices, section 6.2 for X-ray crystallographic data.

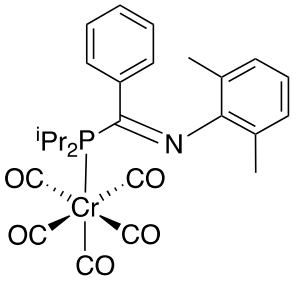

^{1}H NMR (600 MHz, $CDCl_3$) δ 7.25 – 7.20 (m, 3H, C-*m/p*-C_6H_5), 7.12 – 7.07 (m, 2H, C-*o*-C_6H_5), 6.85 – 6.80 (m, 2H, N-*m*-C_6H_3), 6.78 – 6.72 (m, 1H, N-*p*-C_6H_3), 2.60 (heptd,

$^{2}J_{PH}$ = 14.0 Hz, $^{3}J_{HH}$ = 7.0 Hz, 2H, P(C*H*(CH_3)$_2$)$_2$), 2.13 (s, 6H, N-C_6H_3(C*H*$_3$)$_2$), 1.37 (dd, $^{3}J_{PH}$ = 16.0 Hz, $^{3}J_{HH}$ = 7.0 Hz, 6H, P(CH(C*H*$_3$)$_2$)$_2$), 1.23 (dd, $^{3}J_{PH}$ = 14.0 Hz, 7.0 Hz, $^{3}J_{HH}$ = 6H, P(CH(C*H*$_3$)$_2$)$_2$).

^{13}C{^{1}H} NMR (151 MHz, $CDCl_3$) δ 221.5 (d, $^{2}J_{PC}$ = 5.0 Hz, *trans*-PCr(*C*O)), 218.0 (d, $^{2}J_{PC}$ = 13.0 Hz, *trans*-Cr(*C*O)), 176.0 (d, $^{1}J_{PC}$ = 30.0 Hz, *C*=N), 149.2 (d, $^{3}J_{PC}$ = 17.0 Hz, N-*i*-C_6H_3), 138.3 (d, $^{2}J_{PC}$ = 17.0 Hz, C-*i*-C_6H_5), 129.3 (C-*p*-C_6H_5), 128.3 (C-*m*-C_6H_5), 128.1 (N-*m*-C_6H_3), 126.1 (C-*o*-C_6H_5), 124.8 (N-*o*-C_6H_3), 123.7 (N-*p*-C_6H_3), 27.9 (d, $^{1}J_{PC}$ = 15.0 Hz, P(*C*H(CH_3)$_2$)$_2$), 19.7 (N-C_6H_3(*C*H_3)$_2$), 19.0 (P(CH(*C*H_3)$_2$)$_2$), 18.2 (d, $^{2}J_{PC}$ = 4.0 Hz, P(CH(*C*H_3)$_2$)$_2$).

^{31}P{^{1}H} NMR (243 MHz, $CDCl_3$) δ 87.0.

MS (ASAP^{+}) *m*/*z*: 518.1 ([MH]$^{+}$), 489.1 ([M-CO]$^{+}$), 326.2 ([MH-Cr(CO)$_5$)]$^{+}$), 208.1 ([M-Cr(CO)$_5$(P^{i}Pr$_2$)]$^{+}$).

IR (CH_2Cl_2)**:** $\nu_{C=O}$ = 2060 cm^{-1}, 1980 cm^{-1}, 1934 cm^{-1}.
$\nu_{C=N}$ = 1587 cm^{-1}.

5.2.5.3. Synthesis of Cr(CO)$_4$(PhC(P^{i}Pr$_2$)=N(2,6-Et$_2$C$_6$H$_3$)) (2.22) and Cr(CO)$_5$(PhC(P^{i}Pr$_2$)=N(2,6-Et$_2$C$_6$H$_3$)) (2.23)

(a) Attempted synthesis using a modification of the method reported by Krishnamurthy *et al*.[12]

PCN ligand **2.15** (0.30 g, 0.85 mmol) and $Cr(CO)_6$ (0.22 g, 1.00 mmol) were added to a two-necked round bottom flask, equipped with a reflux condenser. Toluene (25 mL) was added to the round bottom flask before the resultant yellow solution was heated at reflux for a total of 109 hours. The progress of the reaction was monitored by ^{31}P{^{1}H} NMR spectroscopy at various points during reflux (Chapter 2, section 2.4.1.1, Table 2.14). Since it was found that prolonged reflux times led to increased decomposition of the desired products (**2.22** and **2.23**), the reaction was abandoned after 109 hours of reflux.

(b) Synthesis using a modification of the method reported by Grim *et al*.[13]

$Cr(CO)_6$ (0.23 g, 1.05 mmol) and ligand **2.15** (0.31 g, 0.88 mmol) were added to a Schlenk, along with diglyme (25 mL). The reaction solution was heated to 160 °C, and

then kept at 160 °C for 1 hour, after which time the colour of the solution changed from yellow to purple and sublimation of $Cr(CO)_6$ had ceased. The solution was subsequently allowed to cool to room temperature and analysed by $^{31}P\{^1H\}$ NMR spectroscopy (162 MHz, C_6D_6), which revealed the solution to consist of a mixture of three phosphorus-containing products: 86.4 ppm (68 %, corresponding to **2.23**), 62.2 ppm (16 %, corresponding to **2.22**), and 27.7 ppm (16 %, corresponding to **2.15**). After filtering the solution, the solvent of the filtrate was removed under vacuum leaving behind a purple residue. Hexane (20 mL) was added to the purple residue and the mixture filtered generating a purple solid and yellow solution.

*Isolation of $Cr(CO)_4(PhC(P^iPr_2)=N(2,6\text{-}Et_2C_6H_3))$ (**2.22**)*

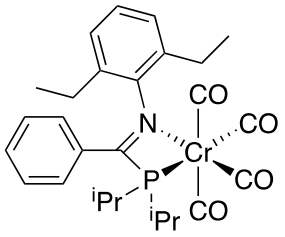

The purple solid (from the hexane filtration) was dissolved in the minimum amount of DCM and layered with hexane. After 16 hours at – 30 °C purple crystals of **2.22** were formed which were suitable for X-ray diffraction and isolated by filtration. The process was repeated with the remaining purple filtrate to generate a second batch of **2.22** (0.07 g, 15 % yield). There was insufficient material left of **2.22** for CHN analysis and mass spectrometry to be carried out (after complex **2.22** had been characterised by X-ray diffraction, NMR spectroscopy, and IR spectroscopy and used in the synthesis of **2.30**. See Appendices, section 6.2 for X-ray crystallographic data.

^{1}H NMR (600 MHz, $CDCl_3$) δ 7.33 (t, $^3J_{HH}$ = 7.4 Hz, 1H, C-*p*-C_6H_5), 7.24 -7.20 (m, 2H, C-*o*-C_6H_5), 7.19 - 7.13 (m, 1H, N-*p*-C_6H_3), 7.12 - 7.08 (m, 2H, N-*m*-C_6H_3), 6.97 - 6.90 (m, 2H, C-*m*-C_6H_5), 2.85 (dq, ^3J = 15.1, 7.6 Hz, 2H, N-$C_6H_3(CH_2CH_3)_2$), 2.77 - 2.63 (m, 2H, P($CH(CH_3)_2)_2$), 2.39 (dq, J = 14.8, 7.4 Hz, 2H, N-$C_6H_3(CH_2CH_3)_2$), 1.62 - 1.19 (m, 12H, P($CH(CH_3)_2)_2$), 1.17 (t, $^3J_{HH}$ = 7.5 Hz, 6H, N-$C_6H_3(CH_2CH_3)_2$).

^{13}C{^{1}H} NMR (151 MHz, $CDCl_3$) δ 229.3 (*trans*-PCr(*C*O)), 225.4 (d, $^2J_{PC}$ = 2.5 Hz, *trans*-NCr(*C*O)), 222.3 (d, $^2J_{PC}$ = 12.5 Hz, *trans*-Cr(*C*O)), 185.3 (*C*=N), 148.5 (N-*i*-C_6H_3), 133.8 (C-*i*-C_6H_5), 131.8 (C-*p*-C_6H_5), 131.2 (N-*o*-C_6H_3), 129.2 (C-*o*-C_6H_5), 127.7 (C-*m*-C_6H_5), 126.5 (N-*p*-C_6H_3), 126.4 (N-*m*-C_6H_3), 29.2 (d, $^1J_{PC}$ = 9.0 Hz, P(*C*H$(CH_3)_2)_2$), 23.9 (N-$C_6H_3(CH_2CH_3)_2$), 20.2 (d, $^2J_{PC}$ = 10.0 Hz, P($CH(CH_3)_2)_2$), 20.0 (d, $^2J_{PC}$ = 3.0 Hz, PCH($CH_3)_2$), 14.2 (N-$C_6H_3(CH_2CH_3)_2$).

^{31}P{^{1}H} NMR (243 MHz, $CDCl_3$) δ 61.8.

IR (CH_2Cl_2)**:** $\nu_{C=O}$ = 2000 cm^{-1}, 1894 cm^{-1}, 1877 cm^{-1}, 1857 cm^{-1}.

$\nu_{C=N}$ = 1551 cm^{-1}.

*Isolation of $Cr(CO)_5(PhC(P^iPr_2)=N(2,6\text{-}Et_2C_6H_3))$ (**2.23**)*

The yellow solution (from the hexane filtration) was concentrated and cooled to – 30 °C for 16 hours, after which time yellow crystals of **2.23** (0.20 g, 42 % yield) were obtained which were suitable for X-ray crystal diffraction. (calc.: $C_{28}H_{32}CrNO_5P$ C, 61.65; H, 5.91; N, 2.57. Found: C, 61.76; H, 5.84; N, 2.70). See Appendices, section 6.2 for X-ray crystallographic data.

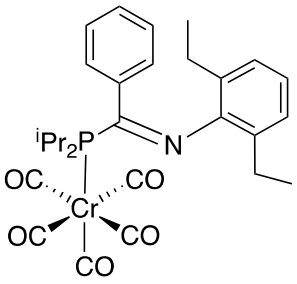

^{1}H NMR (700 MHz, $CDCl_3$) δ 7.23 - 7.14 (m, 3H, C-*m*/*p*-C_6H_5), 7.10 - 7.01 (m, 2H, C-*o*-C_6H_5), 6.92 - 6.88 (m, 2H, N-*m*-C_6H_3), 6.88 - 6.84 (m, 1H, N-*p*-C_6H_3), 2.58 (ddq, *J* = 32.8, 15.0, 7.3 Hz, 4H, N-$C_6H_3(CH_2CH_3)_2$/ $P(CH(CH_3)_2)_2$), 2.29 (dq, *J* = 15.0, 7.5 Hz, 2H, N-$C_6H_3(CH_2CH_3)_2$), 1.32 (dd, *J* = 15.4, 7.2 Hz, 6H, $P(CH(CH_3)_2)_2$),1.27 (dd, *J* = 14.0, 6.9 Hz, 6H, $P(CH(CH_3)_2)_2$), 1.16 (t, $^3J_{HH}$ = 7.5 Hz, 6H, N-$C_6H_3(CH_2CH_3)_2$).

^{13}C{^{1}H} NMR (176 MHz, $CDCl_3$) δ 221.2 (d, $^2J_{PC}$ = 5.0 Hz, *trans*-PCr(*C*O)), 217.7 (d, $^2J_{PC}$ = 12.5 Hz, *trans*-Cr(*C*O)), 175.7 (d, $^1J_{PC}$ = 29.0 Hz, *C*=N), 147.5 (d, $^3J_{PC}$ = 16.0 Hz, N-*i*-C_6H_3), 137.9 (d, $^2J_{PC}$ = 19.0 Hz, C-*i*-C_6H_5), 130.2 (N-*o*-C_6H_3), 129.0 (C-*m*-C_6H_5), 128.0 (C-*p*-C_6H_5), 126.1 (C-*o*-C_6H_5), 125.1 (N-*m*-C_6H_3), 123.8 (N-*p*-C_6H_3), 28.0 (d, $^1J_{PC}$ = 16.0 Hz, $P(CH(CH_3)_2)_2$), 24.7 (N-$C_6H_3(CH_2CH_3)_2$), 18.9 (N-$C_6H_3(CH_2CH_3)_2$), 18.1 (d, $^2J_{PC}$ = 3.5 Hz, $P(CH(CH_3)_2)_2$), 14.0 (N-$C_6H_3(CH_2CH_3)_2$).

^{31}P{^{1}H} NMR (243 MHz, $CDCl_3$) δ 85.1.

MS (ASAP$^+$) *m*/*z*: 545.4 ($[M]^+$), 518.2 ($[MH\text{-}CO]^+$), 354.3 ($[MH\text{-}Cr(CO)_5]^+$), 236.2($[M\text{-}Cr(CO)_5(P^iPr_2)]^+$).

IR (CH_2Cl_2)**:** $\nu_{C=O}$ = 2061 cm^{-1}, 1980 cm^{-1}, 1934 cm^{-1}.

$\nu_{C=N}$ = 1586 cm^{-1}.

5.2.5.4. Synthesis of $Cr(CO)_4(PhC(P^iPr_2)=N(2\text{-}MeC_6H_4))$ (2.24) and $Cr(CO)_5(PhC(P^iPr_2)=N(2\text{-}MeC_6H_4))$ (2.25)

Following a modification of the literature procedure by Grim *et al*.,[13] a Schlenk was charged with ligand **2.16** (0.47 g, 1.51 mmol), $Cr(CO)_6$ (0.40 g, 1.82 mmol) and diglyme (40 mL). The resultant yellow solution was heated to 160 °C for 1 hour, and then kept at 160 °C for 1 hour, after which time the solution turned purple and sublimation of $Cr(CO)_6$ was no longer observed. The solution was subsequently allowed to cool to room temperature before being analysed by $^{31}P\{^1H\}$ NMR spectroscopy (162 MHz, C_6D_6), which revealed the solution to consist of a mixture of six phosphorus-containing products: 96.5 ppm (1 %), 85.6 ppm (1 %), 84.0 ppm (51 %, corresponding to **2.25**), 59.5 ppm (32 %, corresponding to **2.24**), 51.1 ppm (2 %), and 26.9 ppm (13 %, corresponding to **2.16**). The solution was then filtered and the solvent subsequently removed from the filtrate under vacuum to leave a purple residue. Hexane (20 mL) was added to the purple residue and the mixture filtered generating a purple solid and yellow solution.

5.2.5.4.1. Isolation of $Cr(CO)_4(PhC(P^iPr_2)=N(2\text{-}MeC_6H_4))$ (2.24)

The purple solid (from the hexane filtration) was dissolved in the minimum amount of DCM and layered with hexane. After 16 hours at – 30 °C purple crystals of **2.24** were formed (0.10 g, 14 % yield), which were suitable for X-ray diffraction and isolated by filtration. (calc.: $C_{24}H_{26}CrNO_4P$ C, 60.63; H, 5.51; N, 2.95. Found: C, 60.70; H, 5.45; N, 3.03). See Appendices, section 6.2 for X-ray crystallographic data.

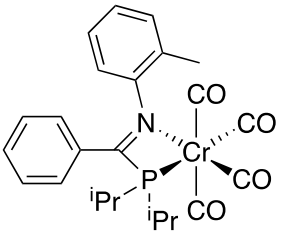

^{1}H NMR (700 MHz, $CDCl_3$) δ 7.31 (t, $^3J_{HH}$ = 7.5 Hz, 1H, N-C_6H_4), 7.25 - 7.19 (m, 3H, C-*m*-C_6H_5/ N-C_6H_4), 7.10 - 7.03 (m, 2H, C-*o*-C_6H_5), 7.00 (d, $^3J_{HH}$ = 7.7 Hz, 1H, C-*p*-C_6H_5), 6.93 (d, $^3J_{HH}$ = 7.5 Hz, 2H, N-C_6H_4), 2.87 - 2.70 (m, 1H, P(C*H*$(CH_3)_2)_2$), 2.62 - 2.48 (m, 1H, P(C*H*$(CH_3)_2)_2$), 2.03 (s, 3H, N-C_6H_4(C*H*$_3$)), 1.52 (dd, *J* = 15.7, 7.0 Hz, 3H, P(CH(C*H*$_3)_2)_2$), 1.43 (dd, *J*= 18.1 Hz, 6.8 Hz, 3H, P(CH(C*H*$_3)_2)_2$), 1.39 - 1.28 (m, 6H, P(CH(C*H*$_3)_2)_2$).

^{13}C{^{1}H} NMR (176 MHz, $CDCl_3$) δ 229.8 (d, $^2J_{PC}$ = 12.0 Hz, *trans*-PCr(*C*O)), 225.8 (d, $^2J_{PC}$ = 2.0 Hz, *trans*-NCr(*C*O)), 222.7 (d, $^2J_{PC}$ = 11.0 Hz, *trans*-Cr(*C*O)), 221.6 (d, $^2J_{PC}$ = 10.5 Hz, *trans*-Cr(*C*O)), 183.8 (d, $^1J_{PC}$ = 18.5 Hz, *C*=N), 150.5 (d, $^3J_{PC}$ = 24.0 Hz, N-*i*-C_6H_4), 134.2 (d, $^2J_{PC}$ = 4.0 Hz, C-*i*-C_6H_5), 131.3 (N-C_6H_4), 129.2 (C-*m*-C_6H_5), 127.6 (N-

C_6H_4), 127.2 (N-C_6H_4), 126.7 (C-*o*-C_6H_5), 125.3 (N-*o*-$C_6H_4(CH_3)$), 121.1 (C-*p*-C_6H_5), 29.0 (d, $^1J_{PC}$ = 9.5 Hz, P($CH(CH_3)_2)_2$), 27.4 (d, $^1J_{PC}$ = 8.0 Hz, P($CH(CH_3)_2)_2$), 20.1 (P(CH($CH_3)_2)_2$), 20.0 (d, $^2J_{PC}$ = 11.5 Hz, P(CH($CH_3)_2)_2$), 19.7 (P(CH($CH_3)_2)_2$), 19.6 (P(CH($CH_3)_2)_2$), 18.4 (N-$C_6H_4(CH_3)$).

$^{31}P\{^1H\}$ NMR 283 MHz, $CDCl_3$) δ 59.2.

MS (ASAP$^+$) *m*/*z*: 448.2 ([MH-CO]$^+$), 311.2 ([M-Cr$(CO)_4$)]$^+$), 195.1 ([M-Cr$(CO)_4(P^iPr_2)]^+$).

IR (CH_2Cl_2)**:** $\nu_{C=O}$ = 2002 cm^{-1}, 1901 cm^{-1}, 1880 cm^{-1}, 1857 cm^{-1}.
$\nu_{C=N}$ = 1538 cm^{-1}.

5.2.5.4.2. Isolation of Cr(CO)$_5$(PhC(P^{i}Pr$_2$)=N(2-MeC$_6$H$_4$)) (2.25)

The yellow solution (from the hexane filtration) was concentrated and cooled to – 30 °C for 16 hours, after which time yellow crystals of **2.25** (0.30 g, 40 % yield) were obtained which were suitable for X-ray crystal diffraction. (calc.: $C_{25}H_{26}CrNO_5P$ C, 59.64; H, 5.21; N, 2.78. Found: C, 59.80; H, 5.12; N, 2.87). See Appendices, section 6.2 for X-ray crystallographic data.

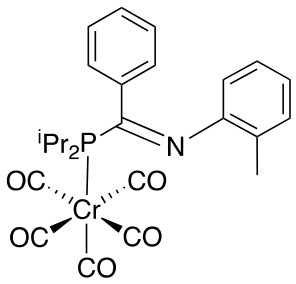

^1H NMR (700 MHz, $CDCl_3$) δ 7.25 - 7.19 (m, 3H, C-*m*/*p*-C_6H_5), 7.10 – 7.06 (m, 2H, C-*o*-C_6H_5), 7.02 (d, $^3J_{HH}$ = 7.3 Hz, 1H, N-C_6H_4), 6.84 (dtd, *J* = 25.6, 7.5, 1.3 Hz, 2H, N-C_6H_4), 6.28 (d, $^3J_{HH}$ = 8.0 Hz, 1H, N-C_6H_4), 2.57 (dp, *J* = 14.4, 7.3 Hz, 2H, P($CH(CH_3)_2)_2$), 2.24 (s, 3H, N-$C_6H_4(CH_3)$), 1.36 (dd, *J* = 15.1, 7.1 Hz, 6H, P(CH($CH_3)_2)_2$), 1.20 (dd, *J* = 14.2, 6.9 Hz, 6H, P(CH($CH_3)_2)_2$).

$^{13}C\{^1H\}$ NMR (176 MHz, $CDCl_3$) δ 221.7 (d, $^2J_{PC}$ = 5.0 Hz, *trans*-PCr(*C*O)), 218.0 (d, $^2J_{PC}$ = 13.0 Hz, *trans*-Cr(*C*O)), 177.4 (d, $^1J_{PC}$ = 33.5 Hz, *C*=N), 149.5 (d, $^3J_{PC}$ = 18.0 Hz, N-*i*-C_6H_4), 137.5 (d, $^2J_{PC}$ = 17.0 Hz, C-*i*-C_6H_5), 130.4 (N-C_6H_4), 128.9 (C-*m*/*p*-C_6H_5), 128.5 (C-*m*/*p*-C_6H_5), 127.9 (N-*o*-$C_6H_4(CH_3)$), 127.0 (d, $^3J_{PC}$ = 1.5 Hz, C-*o*-C_6H_5), 125.9 (N-C_6H_4), 124.3 (N-C_6H_4), 119.1 (N-C_6H_4), 27.9 (d, $^1J_{PC}$ = 16.0 Hz, P($CH(CH_3)_2)_2$), 19.2 (P(CH($CH_3)_2)_2$), 19.0 (N-$C_6H_4(CH_3)$), 18.6 (d, $^2J_{PC}$ = 3.0 Hz, (P(CH($CH_3)_2)_2$).

$^{31}P\{^1H\}$ NMR (283 MHz, $CDCl_3$) δ 83.1.

MS (ASAP$^+$) *m*/*z*: 503.2 ([M]$^+$), 311.2 ([M-Cr(CO)$_5$)]$^+$), 195.1([M-Cr(CO)$_5$(P^{i}Pr$_2$)]$^+$).

IR (CH_2Cl_2)**:** $\nu_{C=O}$ = 2060 cm^{-1}, 1981 cm^{-1}, 1936 cm^{-1}.

$\nu_{C=N}$ = 1591 cm^{-1}.

5.2.6. Synthesis of Cr^I-PCN complexes[q]

5.2.6.1. Synthesis of [Cr(CO)$_4$(Ph(P^{i}Pr$_2$)C=N(2-MeC$_6$H$_4$))][Al{OC(CF$_3$)$_3$}$_4$] (2.26)

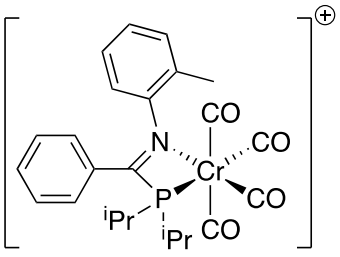

The synthesis of **2.26** was carried out following the literature procedure reported by Hanton *et al*.[14] A solution of Ag[Al{OC(CF$_3$)$_3$}$_4$] (0.06 g, 0.06 mmol) in DCM (5 mL) was added dropwise to a solution of complex **2.24** (0.03 g, 0.06 mmol) in DCM (5 mL). The reaction solution was stirred for an hour at room temperature, in which time it turned dark purple, before a second equivalent of Ag[Al{OC(CF$_3$)$_3$}$_4$] (0.06 g, 0.06 mmol) in DCM (5 mL) was added dropwise to the reaction mixture. After stirring overnight at room temperature, the reaction mixture was filtered away from decomposed Ag[Al{OC(CF$_3$)$_3$}$_4$]. Analysis of the filtrate by IR spectroscopy revealed absence of starting material **2.24**, indicating completion of the reaction, therefore the volatile components of the filtrate were removed under vacuum to yield an oily orange residue, which was washed with petroleum ether (40:60, 3 × 5 mL) and dried *in vacuo*. After leaving at −30 °C for 48 hours, the oily orange residue solidified on scraping to yield **2.26** as a light brown solid (0.06 g, 69 % yield). (calc.: $C_{40}H_{26}AlCrF_{36}NO_8P$ C, 33.30; H 1.82; N, 0.97. Found: C, 33.17; H, 1.98; N, 0.86). There was insufficient material left of **2.26** after characterising it by NMR and IR spectroscopy, and testing it in ethylene oligomerisation catalysis, for mass spectrometry to be carried out.

μ_{eff} = 1.71 μ_B.

^{19}F NMR (376 MHz, CD_2Cl_2) δ −75.6 ($\nu_{½}$ = 10.0 Hz).

IR (CH_2Cl_2)**:** $\nu_{C=O}$ = 2092 cm^{-1}, 2054 cm^{-1}, 2038 cm^{-1}, 1967 cm^{-1}.

[q] Due to the light sensitive nature of Ag[Al{OC(CF$_3$)$_3$}$_4$] these syntheses were carried out in Schlenks covered in foil.

5.2.6.2. Synthesis of [Cr(CO)$_5$(Ph(P^{i}Pr$_2$)C=N(2-MeC$_6$H$_4$))][Al{OC(CF$_3$)$_3$}$_4$] (2.27)

Complex **2.27** was synthesised in an analogous manner to complex **2.26** using complex **2.25** (0.07 g, 0.14 mmol) and Ag[Al{OC(CF$_3$)$_3$}$_4$] (0.30 g, 0.28 mmol). The product was obtained as a brick red solid (0.17 g, 83 % yield). (calc.: $C_{41}H_{26}AlCrF_{36}NO_9P$ C, 33.49; H 1.78; N, 0.95. Found: C, 33.22; H, 1.60; N, 0.91).

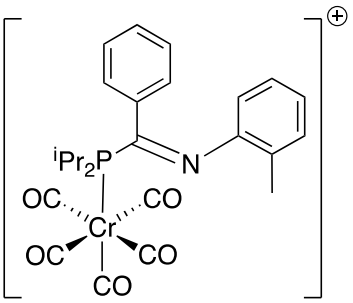

μ_{eff} = 1.71 μ_B.

^{19}F NMR (376 MHz, CD_2Cl_2) δ −75.2 ($\nu_{½}$ = 26.1 Hz).

IR (CH_2Cl_2)**:** $\nu_{C=O}$ = 2092 cm^{-1}, 2038 cm^{-1}, 1968 cm^{-1}.

MS (ASAP$^+$) *m*/*z*: 966.1 ([Al{OC(CF$_3$)$_3$}$_4$]$^-$), 503.2 ([M]$^+$), 311.2 ([M-Cr(CO)$_5$)]$^+$), 195.1 ([M-Cr(CO)$_5$(P^{i}Pr$_2$)]$^+$).

5.2.6.3. Synthesis of [Cr(CO)$_4$(Ph(P^{i}Pr$_2$)C=N(2,6-Me$_2$C$_6$H$_3$))][Al{OC(CF$_3$)$_3$}$_4$] (2.28)

The synthesis of complex **2.28** was conducted in an analogous manner to that described for complex **2.26** using complex **2.20** (0.03 g, 0.06 mmol) and Ag[Al{OC(CF$_3$)$_3$}$_4$] (0.13 g, 0.12 mmol). The product was obtained as a red solid (0.05 g, 57 % yield). (calc.: $C_{41}H_{28}AlCrF_{36}NO_8P$ C, 33.81; H 1.94; N, 0.96. F ound: C, 33.69; H, 2.04; N, 1.02). There was insufficient material left of **2.28** after characterising it by NMR and IR spectroscopy, and testing it in ethylene oligomerisation catalysis, for mass spectrometry to be carried out.

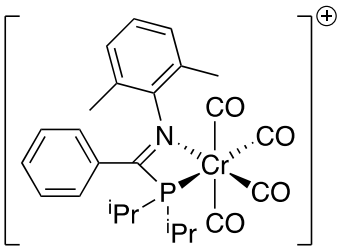

μ_{eff} = 1.80 μ_B.

^{19}F NMR (376 MHz, CD_2Cl_2) δ −75.7 ($\nu_{½}$ = 8.7 Hz).

IR (CH_2Cl_2)**:** $\nu_{C=O}$ = 2092 cm^{-1}, 2055 cm^{-1}, 2037 cm^{-1}, 1966 cm^{-1}.

5.2.6.4. Synthesis of [Cr(CO)$_5$(Ph(P^{i}Pr$_2$)C=N(2,6-Me$_2$C$_6$H$_3$))][Al{OC(CF$_3$)$_3$}$_4$] (2.29)

Complex **2.29** was synthesised in a similar manner to complex **2.26** using Ag[Al{OC(CF$_3$)$_3$}$_4$] (0.42 g, 0.40 mmol) and complex **2.21** (0.10 g, 0.19 mmol). The product was obtained as a dark red solid (0.17 g, 60 % yield). (calc.: $C_{42}H_{28}AlCrF_{36}NO_9P$ C, 33.98; H 1.90; N, 0.94. Found: C, 33.84; H, 1.99; N, 1.00).

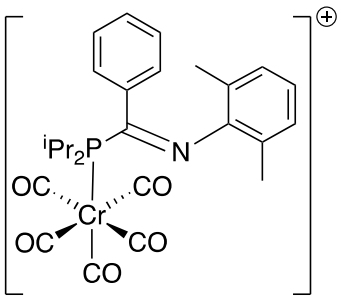

μ_{eff} = 1.95 μ_B.

^{19}F NMR (376 MHz, CD_2Cl_2) δ – 75.7 ($\nu_{½}$ = 6.8 Hz).

IR (CH_2Cl_2)**:** $\nu_{C=O}$ = 2091 cm^{-1}, 2036 cm^{-1}, 1965 cm^{-1}.

MS (ASAP$^+$) *m*/*z*: 966.1 ([Al{OC(CF$_3$)$_3$}$_4$]$^-$), 517.2 ([M]$^+$), 326.2 ([M-Cr(CO)$_5$)]$^+$), 208.1 ([M-Cr(CO)$_5$(P^{i}Pr$_2$)]$^+$).

5.2.6.5. Synthesis of [Cr(CO)$_4$(Ph(P^{i}Pr$_2$)C=N(2,6-Et$_2$C$_6$H$_3$))][Al{OC(CF$_3$)$_3$}$_4$] (2.30)

The synthesis of complex **2.30** was achieved *via* the same procedure as described for complex **2.26** using complex **2.22** (0.05 g, 0.10 mmol) and Ag[Al{OC(CF$_3$)$_3$}$_4$] (0.21 g, 0.20 mmol). The product was obtained as a red solid (0.06 g, 40 % yield). (calc.: $C_{43}H_{32}AlCrF_{36}NO_8P$ C, 34.79; H 2.17; N, 0.94. Found: C, 34.92; H, 2.06; N, 0.76). There was insufficient material left of **2.30** after characterising it by NMR and IR spectroscopy, and testing it in ethylene oligomerisation catalysis, for mass spectrometry to be carried out.

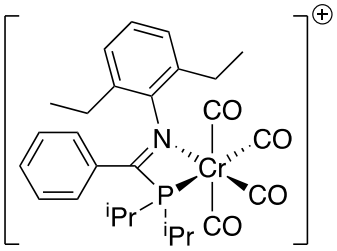

μ_{eff} = 1.86 μ_B.

^{19}F NMR (376 MHz, CD_2Cl_2) δ – 75.7 ($\nu_{½}$ = 7.6 Hz).

IR (CH_2Cl_2)**:** $\nu_{C=O}$ = 2104 cm^{-1}, 2053 cm^{-1}, 2031 cm^{-1}, 1950 cm^{-1}.

5.2.6.6. Synthesis of [Cr(CO)$_5$(Ph(P^{i}Pr$_2$)C=N(2,6-Et$_2$C$_6$H$_3$))][Al{OC(CF$_3$)$_3$}$_4$] (2.31)

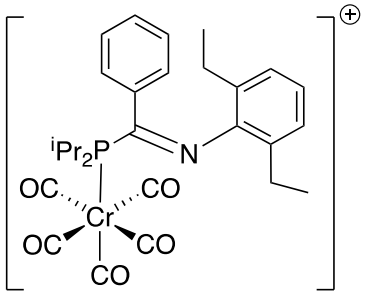

The synthesis of complex **2.31** was conducted *via* an analogous procedure to that implemented for complex **2.26** using Ag[Al{OC(CF$_3$)$_3$}$_4$] (0.28 g, 0.26 mmol) and complex **2.23** (0.07 g, 0.13 mmol). After the crude reaction mixture had been stirred overnight, it was filtered and the filtrate analysed by IR spectroscopy which revealed the presence of five bands in the region 1900 – 2100 cm^{-1} (characteristic for CO stretching frequencies): 1958 cm^{-1}, 1979 cm^{-1}, 2035 cm^{-1}, 2074 cm^{-1}, and 2091 cm^{-1}. A third equivalent of Ag[Al{OC(CF$_3$)$_3$}$_4$] (0.14 g, 0.13 mmol) was added to the crude reaction mixture and the resultant mixture left to stir overnight. The mixture was subsequently filtered and IR spectroscopy of the resulting filtrate showed the presence of five bands in the region 1900 – 2100 cm^{-1}: 1965 cm^{-1}, 1979 cm^{-1}, 2035 cm^{-1}, 2075 cm^{-1}, and 2091 cm^{-1}. The volatile components of the filtrate were then removed under vacuum to generate a viscous red oil. The red oil was then washed with petroleum ether (40:60), toluene and hexane and the insoluble components of the washings were dried under vacuum before being left at −30 °C for 48 hours, after which time the oil solidified upon scraping to yield a brown solid (0.038 g). Analysis of the brown solid by IR and NMR spectroscopy revealed it to consist of a mixture of products, of which one was the desired product **2.31** (confirmed by mass spectrometry). Due to the complexity of the ^{1}H (CD_2Cl_2, 600 MHz) and ^{13}C{^{1}H} NMR spectra (CD_2Cl_2, 151 MHz) of the mixture of products, the peaks have not been reported.

Characterisation for complex **2.31**:

μ_{eff} = 1.60 μ_B.

^{19}F NMR (376 MHz, CD_2Cl_2) δ – 75.6 ($\nu_{½}$ = 9.2 Hz).

IR (CH_2Cl_2)**:** $\nu_{C=O}$ = 2091 cm^{-1}, 2035 cm^{-1}, 1965 cm^{-1}.

MS (ASAP$^+$) *m*/*z*: 966.1 ([Al{OC(CF$_3$)$_3$}$_4$]$^-$), 545.2 ([M]$^+$), 355.1 ([MH-Cr(CO)$_5$)]$^+$), 236.2 ([M-Cr(CO)$_5$(P^{i}Pr$_2$)]$^+$).

Characterisation of byproducts:

$^{31}P\{^{1}H\}$ NMR (243 MHz, CD_2Cl_2) δ 89.2 (br, $\nu_{½}$ = 182.2 Hz, 24 %), 86.5 (br, $\nu_{½}$ = 163.1 Hz, 17 %), 9.7 (d, J_{PP} = 54.0 Hz, 28 %), 8.6 (d, J_{PP} = 33.8 Hz, 2 %), 6.6 (d, J_{PP} = 53.6 Hz, 29 %).

IR (CH_2Cl_2)**:** $\nu_{C=O}$ = 2075 cm^{-1}, 1979 cm^{-1}.

5.2.6.7. Synthesis of [Cr(CO)$_4$(Ph(P^{i}Pr$_2$)C=N(2,6-^{i}Pr$_2$C$_6$H$_3$))][Al{OC(CF$_3$)$_3$}$_4$] (2.32)

Complex **2.32** was synthesised in an analogous manner to complex **2.26** using complex **2.18** (0.08 g, 0.15 mmol) and Ag[Al{$OC(CF_3)_3$}$_4$] (0.32 g, 0.30 mmol). The product was obtained as a light brown solid (0.07 g, 31 %). Satisfactory elemental analysis of the product could not be obtained, possibly due to the presence of trace amounts of residual silver salts. (calc.: $C_{45}H_{36}AlCrF_{36}NO_8P$ C, 35.73; H 2.40; N, 0.93. Found: C, 26.49; H, 1.92; N, 0.50).

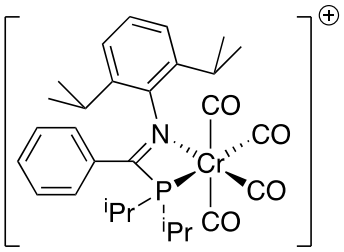

μ_{eff} = 1.96 μ_B.

^{19}F NMR (376 MHz, CD_2Cl_2) δ – 75.7 ($\nu_{½}$ = 6.0 Hz).

IR (CH_2Cl_2)**:** $\nu_{C=O}$ = 2090 cm^{-1}, 2055 cm^{-1}, 2035 cm^{-1},1963 cm^{-1}.

MS (ASAP$^+$) *m*/*z*: 966.1 ([Al{$OC(CF_3)_3$}$_4$]$^-$), 546.2 ([MH]$^+$), 381.3 ([M-Cr(CO)$_4$)]$^+$), 264.2 ([M-Cr(CO)$_4$(P^{i}Pr$_2$)]$^+$).

5.2.6.8. Synthesis of [Cr(CO)$_5$(Ph(P^{i}Pr$_2$)C=N(2,6-^{i}Pr$_2$C$_6$H$_3$))][Al{OC(CF$_3$)$_3$}$_4$] (2.33)

The synthesis of **2.33** was achieved *via* the same procedure as that implemented for complex **2.26** using Ag[Al{$OC(CF_3)_3$}$_4$] (0.38 g, 0.36 mmol) and complex **2.19** (0.10 g, 0.17 mmol). The product was obtained as a light brown solid (0.115 g) which was found by elemental analysis, IR and NMR spectroscopy, and mass spectrometry to consist of complex **2.33** and

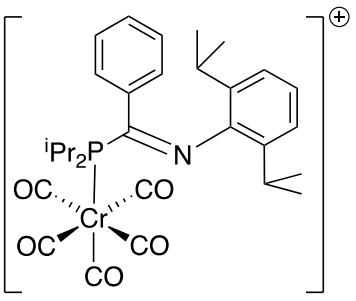

other unknown byproducts. (calc.: $C_{46}H_{36}AlCrF_{36}NO_9P$ C, 35.86; H 2.36; N, 0.91. Found: C, 32.42; H, 2.46; N, 1.10).

μ_{eff} = 1.68 μ_B.

^{19}F NMR (376 MHz, CD_2Cl_2) δ – 75.5 ($\nu_{½}$ = 25.7 Hz).

^{31}P{^{1}H} NMR (243 MHz, CD_2Cl_2) δ 48.0 (7 %), 40.4 (3 %), 27.4 (1 %), 11.3 (7 %), 8.6 (d, J_{PP} = 36.5 Hz, 40 %), 6.6 (d, J_{PP} = 36.1 Hz, 42 %).

IR (CH_2Cl_2)**:** $\nu_{C=O}$ = 2090 cm^{-1}, 2036 cm^{-1}, 1963 cm^{-1}.

MS (ASAP$^+$) *m*/*z*: 966.1 ([Al{OC(CF_3)$_3$}$_4$]$^-$), 573.2 ([M]$^+$), 381.3 ([M-Cr(CO)$_5$)]$^+$), 264.2 ([M-Cr(CO)$_4$(P^iPr_2)]$^+$).

5.2.7. Reaction of PCN ligand 2.14 with Ag[Al{OC(CF_3)$_3$}$_4$]

A Young's tap NMR tube was charged with ligand **2.14** (0.01 g, 0.03 mmol), Ag[Al{OC(CF_3)$_3$}$_4$] (0.03 g, 0.03 mmol), and CD_2Cl_2 (0.7 mL). The NMR tube was covered in foil and left in the dark for 14 hours, after which time it was analysed by NMR and IR spectroscopy and found to consist of a mixture of products. Due to the complexity of the ^{1}H and ^{13}C{^{1}H} NMR spectra of the mixture of unknown products, the peaks have not been reported.

^{19}F NMR (376 MHz, CD_2Cl_2) δ – 75.7 ($\nu_{½}$ = 3.1 Hz).

^{31}P{^{1}H} NMR (162 MHz, CD_2Cl_2) δ 90.3 (13 %), 86.4 (9 %), 58.0 (d, J_{PP} = 35.1 Hz, 39 %), 55.0 (d, J_{PP} = 35.1 Hz, 39 %).

IR (CH_2Cl_2)**:** $\nu_{C=N}$ = 1552 cm^{-1}.

5.2.8. Synthesis of Cr^{III}-PCN complexes

5.2.8.1. Attempted synthesis of $CrCl_3(THF)(PhC(P^iPr_2)=N(2,6\text{-}Et_2C_6H_3))$ (2.34)

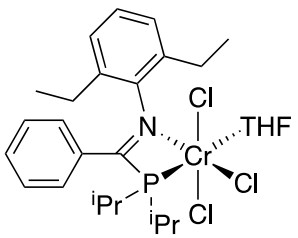

The synthesis of complex **2.34** was attempted using the method reported by Agapie *et al.*[15] A solution of ligand **2.15** (0.14 g, 0.40 mmol) in DCM (5 mL) was added dropwise to a solution of $CrCl_3(THF)_3$ (0.13 g, 0.35 mmol) in DCM (5 mL), resulting in the immediate formation of a green solution. The reaction solution was allowed to stir overnight before being filtered to remove any precipitate. The volatile components of the filtrate were subsequently removed *in vacuo* to yield a green residue, which was triturated three times with hexane (3 × 10 mL). The resulting green solid was isolated by filtration and dried under vacuum (0.11 g). Although IR and NMR spectroscopic data of the green solid imply the desired product is present, CHN analysis suggests otherwise (calc: $C_{27}H_{40}Cl_3CrNOP$ C, 55.54; H, 6.90; N, 2.40. Found: C 52.79; H, 7.73; N, 2.34).

μ_{eff} = 3.60 μ_B *(calculated using RMM of expected product)*.

IR (CH_2Cl_2)**:** $\nu_{C=N}$ = 1552 cm^{-1}.

MS (ASAP$^+$) *m*/*z*: 354.2 ($[M-CrCl_3(THF)]^+$), 236.2 ($[M-P^iPr_2CrCl_3(THF)]^+$).

5.2.8.2. Attempted synthesis of $CrCl_3(PhC(P(2\text{-}(OMe)C_6H_4)_2)=N(2,6\text{-}^iPr_2C_6H_3)$ (2.35)

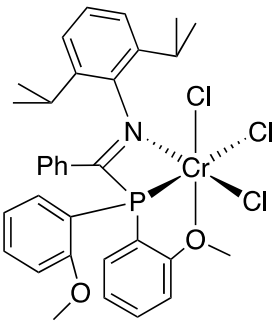

The synthesis of complex **2.35** was attempted *via* the same procedure described for the synthesis attempt of complex **2.34**, using ligand **2.17** (0.20 g, 0.39 mmol) and $CrCl_3(THF)_3$ (0.13 g, 0.35 mmol). The final product was obtained as a brown solid (0.08 g) which was found by CHN analysis and $^{31}P\{^1H\}$ NMR spectroscopic analysis to not be the desired product. (calc: $C_{33}H_{36}Cl_3CrNO_2P$ C, 59.34; H, 5.43; N, 2.10. Found: C 50.50; H, 4.84; N, 1.93). Due to the broadened nature of the ^1H NMR spectrum, the peaks present in the ^1H NMR spectrum have not been reported.

$^{31}P\{^1H\}$ NMR (243 MHz, CD_2Cl_2) δ 70.5 (2 %), 24.4 (br, $\nu_{½}$ = 49.8 Hz, 22 %), –0.7 (br, $\nu_{½}$ = 156.6 Hz, 76 %).

IR (CH_2Cl_2)**:** $\nu_{C=N}$ = 1591 cm^{-1},1552 cm^{-1}.

MS (ASAP$^+$) *m*/*z*: 510.2 ([M−$CrCl_3$]$^+$), 236.2 ([M– P(2-(OMe)C_6H_4)$_2$$CrCl_3$]$^+$).

5.2.8.3. Synthesis of $CrCl_3$(THF)(PhC(P^{i}Pr$_2$)=N(2,6-$Me_2C_6H_3$) (2.36)

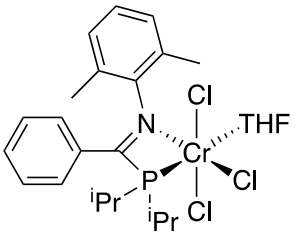

Complex **2.36** was synthesised in an analogous manner to that described for the attempted synthesis of complex **2.34** using PCN ligand PhC(P^{i}Pr$_2$)=N(2,6-$Me_2C_6H_3$)[r] (0.20 g, 0.61 mmol) and $CrCl_3(THF)_3$ (0.21 g, 0.56 mmol). The final product was obtained as a green solid (0.22 g, 71 %). (calc.:$C_{25}H_{36}Cl_3CrNOP$ C, 54.02; H, 6.53; N, 2.52. Found: C, 53.91; H, 6.66; N, 2.67). Mass spectrometry analysis of the product afforded inconclusive results, thought to be due to the lack of volatility of the product.

μ_{eff} = 3.68 μ_B.

IR (CH_2Cl_2)**:** $\nu_{C=N}$ = 1552 cm^{-1}.

MS (ASAP$^+$) *m*/*z*: 326.2 ([M−$CrCl_3$(THF)]$^+$), 208.1 ([M–P^iPr_2CrCl_3(THF)]$^+$).

5.2.8.4. Synthesis of $CrCl_3$(THF)(PhC(P^{i}Pr$_2$)=N(2,6-^{i}$Pr_2C_6H_3$) (2.37)

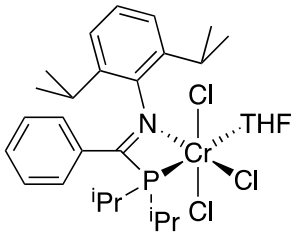

The synthesis of complex **2.37** was conducted *via* the method detailed for the attempted synthesis of complex **2.34** using ligand **2.14** (0.50 g, 1.31 mmol) and $CrCl_3(THF)_3$ (0.46 g, 1.23 mmol). The final product was obtained as a green solid (0.56 g, 74 % yield). (calc.:$C_{29}H_{44}Cl_3CrNOP$ C, 56.91; H, 7.25; N, 2.29. Found: C, 56.81; H, 7.06; N, 2.25). Mass spectrometry analysis of the product afforded inconclusive results, thought to be due to the lack of volatility of the product.

μ_{eff} = 3.62 μ_B.

IR (CH_2Cl_2)**:** $\nu_{C=N}$ = 1552 cm^{-1}.

[r] Synthesised by Dr. James Radcliffe.[1]

MS (ASAP$^+$) *m*/*z*: 382.3 ([M−$CrCl_3$(THF)]$^+$), 338.3 ([M–^{i}Pr $CrCl_3$(THF)]$^+$), 264.2 ([M–$P^iPr_2CrCl_3$(THF)]$^+$).

5.2.9. Evans' NMR spectroscopic method for the determination of effective magnetic moments

The effective magnetic moments of the paramagnetic species synthesised in Chapter 2 were determined using Equations **5.1** – **5.4**. The mass magnetic susceptibilities, χ_g, were obtained *via* the Evans' NMR spectroscopic method.[16] 0.5 mL of a standard solution of the sample (20 mg in 2 mL DCM) was transferred into a Young's tap NMR tube which contained a sealed capillary filled with CD_2Cl_2. The DCM was then removed from the Young's tap NMR tube under vacuum and CD_2Cl_2 (0.5 mL) was added to the NMR tube. A ^{1}H NMR spectrum (400 MHz) was recorded of the sample and Δv (Equation 5.4) obtained.

$$\mu_{eff} = \sqrt{\frac{3k\chi_m T}{N_A}} = 2.828\sqrt{\chi_m T}$$

Equation 5.1: Equation for determining the effective magnetic moment (μ_{eff}) where k = Boltzmann constant, χ_m = molar magnetic susceptibility, T = temperature (K), and N_A = Avogadro constant.[17]

$$\chi_m = \chi_{m(uncorrected)} - diamagnetic\ contibution$$

Equation 5.2: Equation for determining molar magnetic susceptibility (χ_m) where $\chi_{m(uncorrected)}$ = uncorrected molar magnetic susceptibility.[16,18,19]

$$\chi_{m(uncorrected)} = \chi_g \times RMM$$

Equation 5.3: Equation for determining the uncorrected molar magnetic susceptibility ($\chi_{m(uncorrected)}$) where χ_g= mass magnetic susceptibility and RMM = relative molecular mass of paramagnetic species.[16,18,19]

$$\chi_g = \frac{\Delta_v}{sFvc} + \chi_o$$

Equation 5.4: Equation for determining the mass magnetic susceptibility (χ_g) where Δv = frequency difference (Hz) in ^{1}H NMR spectrum of paramagnetic species between residual solvent resonance for the bulk solvent and the standard present in the sealed capillary, sF = shape factor (equal to 4π/3 for a cylindrical sample in a superconducting NMR spectrometer), v = spectrometer frequency (Hz), c = concentration of sample in NMR tube, and χ_o = mass susceptibility of solvent (=−0.549 e^{-6} cm^3 g^{-1} for CD_2Cl_2).[16,18-20]

5.3. Chapter 3 Experimental

5.3.1. Cr/PCN-based ethylene oligomerisation catalysis testing protocol

The screening catalytic tests were performed in a 250 mL steel autoclave, while the larger-scale optimised catalytic runs were carried out in a stainless steel 1.2 L autoclave; both autoclaves contained a customised gas-entraining mechanical stirrer, internal cooling coil (tap water) and fluidised jacket (connected to a Huber 405w thermostatic bath). The same procedure was implemented for the screening catalytic tests and larger-scale catalytic runs. The relevant rigorously-cleaned autoclave was first heated at 130 °C under vacuum for an hour, before being cooled to the reaction temperature and back-filled with 10 bar ethylene. The autoclave was then vented to 0 barg, *via* a septa, in order to purge the inlet valve prior to the addition of the relevant solvent. Following addition of the solvent, the pre-activated catalyst solution (prepared *via* the addition of a MMAO or TEA stock solution to a solution of the preformed or *in-situ* formed Cr-PCN complex) was transferred to the autoclave *via* syringe. Ethylene was then re-introduced into the autoclave and its pressure was kept constant throughout the reaction by the use of a mass-flow meter (Siemens Sitrans F C Massflo system (Mass 6000-Mass 2100)), which continually added in ethylene as necessary. A stable reaction temperature was maintained by applying heating and cooling. As soon as ethylene uptake or the set reaction time had ceased, the gas supply was closed and the reactor cooled to 5 °C. The reactor was then cautiously vented and a portion of the vent gas was streamed directly to a GC-FID instrument that was equipped with a gas-sampling loop. 1000 µL of nonane (GC internal standard) and 10% HCl (aq) were added to the reactor contents, before a sample of the organic phase was extracted for GC-FID analysis. Any solid formed was collected and washed with 10% HCl (aq), EtOH, and acetone before being left to dry overnight and its weight recorded. DSC analysis of the solid samples was also performed (section 5.3.2).

Stock solutions of the catalyst precursors and catalytic additives were made up in the relevant solvent to the desired concentration. The ethylene (grade 4.5, sourced from BOC) had been passed through alumina and oxygen scrubbing columns and entrained with 0.6 – 1.3 ppm O_2 before being used. A GPR-1200 oxygen meter from Advanced Instruments Inc., which had been calibrated with 10 ppm O_2 stock gas, was used to measure the ethylene gas stream in order to monitor its O_2 level.

5.3.2. DSC analysis of polyethylene produced in Cr/PCN-based ethylene oligomerisation catalysis tests

DSC analyses of a selection of polyethylene samples, obtained in the Cr/PCN-based catalysis runs, were performed on a TA instruments DSC Q1000. The protocol implemented for DSC analysis of the polyethylene samples was identical to that implemented in previous work carried out in the Dyer group,[1] which was based on methods reported by Cavallo and Basset *et al.*[21] The polymer samples were first heated at a rate of 10 °C/min from room temperature to 200 °C, and then cooled to 50 °C at a rate of 10 °C/min. This cycle was repeated and the data from the second heating cycle were used to determine the melting point and % crystallisation of the polymer samples.

The polyethylene samples analysed exhibited a range of melting points (119.4 – 132.5 °C) and degrees of crystallinity (5 – 18 %). The low crystallinities of the polyethylene samples suggest that the polymers are highly branched, something not consistent with the high melting points, which are indicative of high density polyethylene (HDPE).[22] It is believed that the observed inconsistencies between the melting points and degrees of crystallinity of the polyethylene samples are due to the method by which the degrees of crystallinity have been obtained. The degrees of crystallinity of the polyethylene samples have been calculated using Equation 5.5, where H_f is the heat of fusion of the polymer (determined from the integration of the melting endotherm shown in Figure 5.1) and H_{std} is the heat of fusion of perfectly crystalline polyethylene (reported to be 293.0 J g^{-1} in the literature).[21,23,24] The curve for the melting endotherm (an example illustrated in Figure 5.1) is not well-defined and so determining its integration boundaries, which impact the value of H_f (Equation 5.5) determined, is based upon human judgement. Therefore, it is believed that the values of H_f obtained for the polyethylene samples may be unreliable, causing the observed discrepancies between the melting points and degrees of crystallinity of the polymer samples. Unfortunately, due to the insolubility of the polyethylene samples other analytical techniques, such as NMR and gel permeation chromatography (GPC), could not be pursued in order to gain further understanding of their structural and physical properties.

$$\%crystallinity = \frac{\Delta H_f}{\Delta H_{std}}$$

Equation 5.5: Equation for determining the degree of crystallinity for a sample of polyethylene, where H_f is the heat of fusion of the polymer and H_{std} = 293.0 J g^{-1} the heat of fusion of perfectly crystalline polyethylene.[21,23,24]

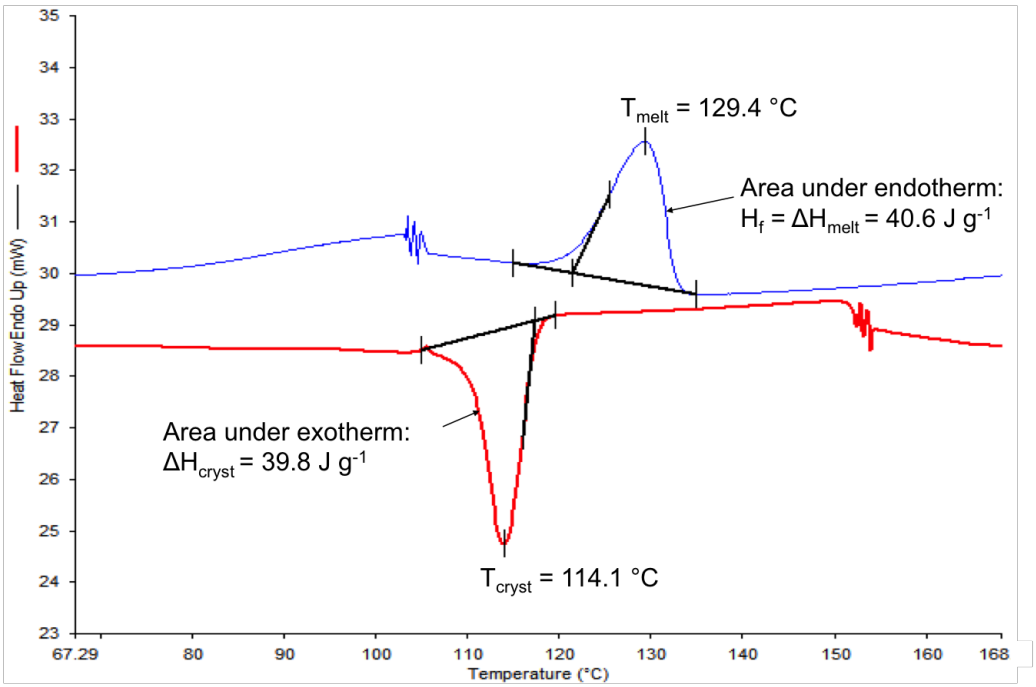

Figure 5.1: Thermogram of polyethylene characterised by DSC analysis, where T_m= melting temperature, H_{melt} = enthalpy of melting, T_{cryst}= crystallisation temperature, and H_{cryst} = enthalpy of crystallisation. The sample of polyethylene analysed was produced in Cr/PCN-based ethylene oligomerisation utilising Cr^{I}-PCN complex **2.27**. Conditions of ethylene oligomerisation catalysis: 5 µmol Cr^{I}-PCN complex **2.27**, 150 eq. TEA, 0.66 ppm O_2, 60 °C, 40 bar ethylene, PhCl, 10 min.

5.4. Chapter 4 Experimental

5.4.1. Synthesis of [(η^5-pentamethylcyclopentadienyl)(η^2-ethene) trimethyl phosphite cobalt(I)] (4.5)

5.4.1.1. Synthesis of dicarbonyl-(η^5-pentamethylcyclopentadienyl)cobalt(I) (4.1)

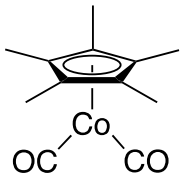

Complex **4.1** was synthesised in accordance with the literature procedure described by Frith and Spencer.[25] A two-necked round bottom flask, fitted with a reflux condenser was charged with $Co_2(CO)_8$ (13.0 g, 38.0 mmol), which was dissolved in DCM (120 mL). The flask was then charged with pentamethylcyclopentadiene (6.6 mL, 42.1 mmol) and 1,3-cyclohexadiene (5.4 mL, 56.7 mmol), and the resultant reaction mixture heated at reflux for 1 h. The mixture was then allowed to cool to room temperature, before a further portion of pentamethylcyclopentadiene (6.6 mL, 42.1 mmol) was added and the mixture then heated again at reflux for a further 2 h. The mixture was then left to reach room temperature before the volatile components were removed *in vacuo*, yielding complex **4.1** as red-brown crystals (15.4 g, 81 %). Complex **4.1** was characterised by ^{1}H NMR, ^{13}C{^{1}H} NMR, and IR spectroscopic analyses; the resulting are in agreement

with those reported in the literature.[25,26] (calc.:$C_{12}H_{15}CoO_2$ C, 57.61; H, 6.04. Found: C, 57.74; H, 6.15).

^{1}H NMR (400 MHz, CD_2Cl_2) δ 1.90 (s, 15H, $C_5(CH_3)_5$).

^{13}C{^{1}H} NMR (101 MHz, CD_2Cl_2) δ 209.1 (*C*O), 97.5 ($C_5(CH_3)_5$), 10.9 ($C_5(CH_3)_5$).

IR (CH_2Cl_2)**:** $\nu_{C=O}$ = 1999 cm^{-1}, 1935 cm^{-1}.

5.4.1.2. Synthesis of carbonyldiiodo-(η^5-pentamethylcyclopentadienyl) cobalt(III) (4.2)

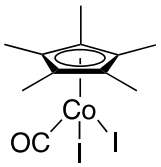

The synthesis of complex **4.2** was achieved following the literature procedure reported by Frith and Spencer.[25] An ethereal solution (250 mL) of iodine (7.90 g, 31.1 mmol) was added dropwise to a stirred ethereal solution (70 mL) of complex **4.1** (7.50 g, 30.0 mmol). The evolution of CO gas was observed from the reaction mixture over a 15 h period. Subsequently, the solvent was subsequently removed under vacuum to yield a black solid, which was recrystallised from DCM at −20 °C to give complex **4.2** as black crystals (13.6 g, 95 % yield). The ^{1}H NMR, ^{13}C{^{1}H} NMR, and IR spectroscopic analyses of complex **4.2** all match with those reported in the literature.[25,27]

^{1}H NMR (400 MHz, $CDCl_3$) δ 2.23 (s, 15H, $C_5(CH_3)_5$).

^{13}C{^{1}H} NMR (101 MHz, $CDCl_3$) δ 101.2 ($C_5(CH_3)_5$), 11.6 ($C_5(CH_3)_5$).

IR (CH_2Cl_2)**:** $\nu_{C=O}$ = 2052 cm^{-1}.

5.4.1.3. Synthesis of di-μ-iodo-bis[iodo(η^5-pentamethylcyclopentadienyl) cobalt(III)] (4.3)

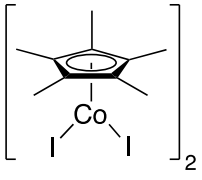

Complex **4.3** was prepared following the literature procedure described by Frith and Spencer with slight modifications.[25] A two-necked round bottom flask, equipped with a nitrogen inlet and reflux condenser (the outlet of which was connected to a mineral oil bubbler *via* a T-piece), was charged with complex **4.2** (13.4 g, 28.2 mmol) and octane (200 mL) and subsequently heated at reflux for 16 h under a slow N_2 purge (to encourage loss of CO). The solution was then left to reach room temperature before the solvent was removed *in vacuo* to yield a dark-green solid that was extracted *via*

Soxhlet extraction in DCM (200 mL) for 48 hours. Recrystallisation of the DCM solution at −20 °C yielded complex **4.3** as dark-green crystals (11.6 g, 92 %). The ^{1}H NMR spectrum of complex **4.3** is in agreement with that reported in the literature; the $^{13}C\{^{1}H\}$ NMR spectroscopic analysis of complex **4.3** has not been reported previously.[25] In addition, complex **4.3** was also analysed by IR spectroscopy to further confirm full consumption of the starting complex **4.2**.

^{1}H NMR (400 MHz, $CDCl_3$) δ 1.83 (s, 15H, $C_5(CH_3)_5$).

$^{13}C\{^{1}H\}$ NMR (101 MHz, $CDCl_3$) δ 91.3 ($C_5(CH_3)_5$), 12.0 ($C_5(CH_3)_5$).

IR (CH_2Cl_2)**:** absence of CO bands.

5.4.1.4. Synthesis of bis(η^2-ethene)(η^5-pentamethylcyclopentadienyl)cobalt(I) (4.4)

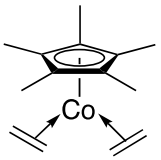

The synthesis of complex **4.4** was conducted in accordance with the literature procedure described by Beevor *et al*.[28] A 1 % Na/Hg amalgam was first prepared by cautiously adding Na sand (2.8 g, 121.8 mmol) to Hg (270.6 g, 1349 mmol) in a nitrogen-filled glovebox. A solution of complex **4.3** (10.0 g, 11.2 mmol) in THF (150 mL) was then added dropwise to the amalgam, under an atmosphere of ethylene in a Schlenk. The resultant reaction mixture was stirred under an atmosphere of ethylene for 1 h, during which time it changed colour from dark-green to orange-brown. The reaction mixture was then filtered from the amalgam and the filtrate evaporated to dryness *in vacuo* to yield an orange residue and a white solid (sodium iodide). The orange residue was extracted into petroleum ether (b.p. 40 – 60 °C) with subsequent recrystallisation at −78 °C (in petroleum ether), affording complex **4.4** (4.15 g, 74 %) as orange crystals that were suitable for an X-ray crystallographic study. See Appendices, section 6.2 for X-ray crystallographic data, which matches with that reported for $Cp^*Co(C_2H_4)_2$ in the literature.[29] The ^{1}H and $^{13}C\{^{1}H\}$ NMR analyses of complex **4.4** match those reported in the literature.[28] (calc.:$C_{14}H_{23}Co$ C, 67.19; H, 9.26. Found: C, 67.08; H, 9.13).

^{1}H NMR (400 MHz, C_6D_6) δ 1.77 – 1.66 (m (AA'BB'), 4H, $(C_2H_4)_2$), 1.42 (s, 15H, $C_5(CH_3)_5$), 1.05 – 0.96 (m (AA'BB'), 4H, $(C_2H_4)_2$)

$^{13}C\{^{1}H\}$ NMR (101 MHz, C_6D_6) δ 92.4 ($C_5(CH_3)_5$), 45.2 (C_2H_4), 9.2 ($C_5(CH_3)_5$).

5.4.1.5. Synthesis of trimethylphosphite(η²-ethene)-(η⁵-pentamethylcyclopentadienyl)cobalt(I) (4.5)

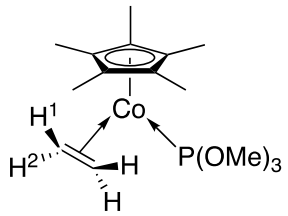

Complex **4.5** was prepared following modifications of the literature procedure reported by Brookhart *et al*.[30] Neat $P(OMe)_3$ (0.7 mL, 5.93 mmol) was added to a solution of complex **4.4** (1.48 g, 5.91 mmol) in pentane (80 mL) and left to stir for 40 h, after which time ^1H NMR spectroscopic analysis of the reaction mixture confirmed the reaction had gone to completion. The reaction mixture was then filtered and the filtrate evaporated to dryness under vacuum to yield an orange residue. The orange residue was recrystallised from petroleum ether (b.p. 40 – 60 °C) at −78 °C, generating orange crystals of complex **4.5** (1.50 g, 73 %), which were suitable for an X-ray crystallographic study. See Appendices, section 6.2 for X-ray crystallographic data. In addition to X-ray analysis, the identity of complex **4.5** was verified by CHN and NMR spectroscopic analysis (^1H, $^{13}C\{^1H\}$, and $^{31}P\{^1H\}$). The ^1H and $^{13}C\{^1H\}$ NMR spectroscopic data for complex **4.5** match those reported in the literature; the $^{31}P\{^1H\}$ NMR spectral analysis of complex **4.5** has not been reported previously.[31] (calc.:$C_{15}H_{28}CoO_3P$ C, 52.03; H, 8.15. Found: C, 51.85; H, 8.26).

^1H NMR (700 MHz, C_6D_6) δ 3.27 (d, $^3J_{PH}$ = 11.4 Hz, 9H, $P(OCH_3)_3$), 1.73 (s, 15H, $C_5(CH_3)_5$), 1.63 – 1.58 (m (AA'BB'), 2H, H^1), 1.38 – 1.33 (m (AA'BB'), 2H, H^2).

$^{13}C\{^1H\}$ NMR (176 MHz, C_6D_6) δ 91.1 (d, $^2J_{PC}$= 3.0 Hz, $C_5(CH_3)_5$), 49.6 ($P(OCH_3)_3$), 31.8 (d, $^2J_{PC}$= 6.5 Hz, C_2H_4), 9.9 ($C_5(CH_3)_5$).

$^{31}P\{^1H\}$ NMR (283 MHz, C_6D_6) δ 175.4 (vbr, $\nu_{½}$ = 675.2 Hz).

5.4.1.5.1. Repeat of synthesis of complex 4.5, on an NMR-scale

A Young's tap NMR tube was charged with complex **4.4** (0.02 g, 0.08 mmol), neat $P(OMe)_3$ (0.01 mL, 0.08 mmol) and C_6D_6 (0.7 mL), and heated at 50 °C for 3 h. After 3 h of heating, NMR spectroscopic analysis ($^{31}P\{^1H\}$ and $\{^1H\}$: both identical to those reported in section 5.4.1.5) confirmed complete conversion to complex **4.5** had occurred.

5.4.2. Synthesis of Brookhart's acid, $[H(Et_2O)_2][(3,5\text{-}(CF_3)_2C_6H_3)_4B]$

Brookhart's acid was synthesised following a modification of the literature procedure reported by Brookhart *et al*.[32] A solution of $NaBAr_4^F$ (Ar_4^F = 3,5-$(CF_3)_2C_6H_3$, 2.06 g, 2.32

mmol) in diethyl ether (50 mL) was left to stand over 4Å molecular sieves for 15 h to remove residual water. The $NaBAr_4^F$ solution was then filtered away from the molecular sieves and cooled to −78 °C. A solution of HCl in Et_2O (2 M, 2.4 mL, 4.8 mmol) was added dropwise to the $NaBAr_4^F$ solution, at −78 °C, resulting in the immediate formation of a white precipitate. The reaction mixture was then left to stir for 1 h at −78 °C, before being filtered at −78 °C to remove the sodium chloride (white precipitate). The white precipitate was washed with Et_2O (3 × 20 mL) at −78 °C, and the Et_2O washings combined with the filtrate of the reaction mixture. The resultant solution was then concentrated *in vacuo* and left to crystallise at −78 °C over several days to generate the final product as white crystals (1.76 g, 75 %). The ^1H and $^{13}C\{^1H\}$ NMR spectroscopic data of the final product are in agreement with those reported in the literature (^{19}F and ^{11}B NMR spectroscopic analyses have not previously been reported in the literature).[32] (calc.:$C_{40}H_{33}O_2BF_{24}$ C, 47.45; H, 3.29. Found: C, 47.45; H, 3.39).

^1H NMR (400 MHz, CD_2Cl_2) δ 14.44 (vbr, $\nu_{½}$ = 966.1 Hz, 1H, *H*$(Et_2O)_2$), 7.72 (br, $\nu_{½}$ = 10.4 Hz, 8H, B-*o*-C_6H_3), 7.58 (br, $\nu_{½}$ = 4.3 Hz, 4H, B-*p*-C_6H_3), 3.96 (q, $^3J_{HH}$ = 7.2 Hz, 8H, CH_2CH_3), 1.36 (t, $^3J_{HH}$ = 7.2 Hz, 12H, CH_2CH_3).

$^{13}C\{^1H\}$ NMR (101 MHz, CD_2Cl_2) δ 162.3 (dd, *J* = 100.0, 50.0 Hz, B-*i*-C_6H_3), 135.4 (B-*o*-C_6H_3), 129.5 (q, $^2J_{FC}$ = 32.5 Hz, B-*m*-C_6H_3), 126.4 – 126.6 (m, CF_3), 118.1 (dt, J=8.1, 3.9 Hz, B-*p*-C_6H_3), 69.8 (CH_2CH_3), 14.3 (CH_2CH_3).

^{19}F NMR (376 MHz, CD_2Cl_2) δ – 62.9.

^{11}B NMR (128 MHz, CD_2Cl_2) δ – 6.6.

5.4.3. Synthesis of [Cp*Co(P(OMe)$_3$)(C$_2$H$_5$)][(3,5-(CF$_3$)$_2$C$_6$H$_3$)$_4$B] (4.6)

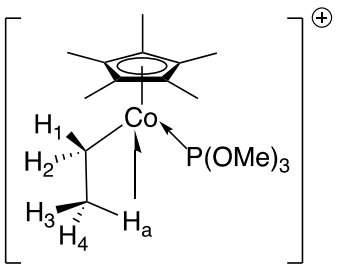

The synthesis of complex **4.6** was carried out in accordance with the literature procedure described by Brookhart *et al.*[32] Complex **4.5** (0.18 g, 0.52 mmol) and Brookhart's acid (0.47 g, 0.46 mmol) were added to a Schlenk, which was subsequently charged with DCM (2 mL). The resultant red solution was stirred at room temperature for 1 min to enable dissolution of the reactants, before being cooled to −78 °C. Hexane (10 mL) was then slowly added to the red solution, at −78 °C, over a

period of 2 h resulting in the precipitation of complex **4.6**. The mixture was then filtered at −78 °C yielding a red solid and orange filtrate. The red solid was washed with hexane (2 × 10 mL) and subsequently dried under vacuum yielding complex **4.6** as a brick-red solid (0.45 g, 80 %). The solvent was removed from the orange filtrate to afford a brick red-solid (0.05 g), which was found by NMR spectroscopic analysis (^{1}H, ^{13}C{^{1}H}, and ^{31}P{^{1}H}) to be unreacted complex **4.5**. The variable-temperature ^{1}H NMR spectrum of complex **4.6** matches with that reported in the literature.[30-33] (calc.:$C_{47}H_{41}O_3BCoF_{24}P$ C, 46.63; H, 3.41. Found: C, 46.67; H, 3.32).

^{1}H NMR (500 MHz, CD_2Cl_2, −90 °C) δ 7.72 (br, $\nu_{½}$ = 11.6 Hz, 8H, B-*o*-C_6H_3), 7.53 (br, $\nu_{½}$ = 7.8 Hz, 4H, B-*p*-C_6H_3), 3.47 (d, $^{3}J_{PH}$ = 11.2 Hz, 9H, P(OCH_3)$_3$), 2.41 (s, 1H, $H_{1/2}$), 2.00 – 1.76 (m, 1H, $H_{1/2}$), 1.57 (s, 15H, C_5(CH_3)$_5$), −0.27 – −0.43 (m, 1H, $H_{3/4}$), −0.44 – −0.61 (m, 1H, $H_{3/4}$), −12.18 – −12.45 (m, 1H, H_a).

^{31}P{^{1}H} NMR (400 MHz, CD_2Cl_2, 25 °C) δ 145.6 (vbr, $\nu_{½}$ = 332.5 Hz).

5.4.4. Attempted synthesis of IndCo(CO)$_2$

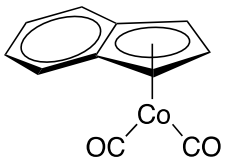

The synthesis of IndCo(CO)$_2$ was attempted *via* a modification of the literature procedure described by Frith and Spencer for the synthesis of complex **4.1**.[23] A two-necked round bottom flask, fitted with a reflux condenser, was charged with $Co_2(CO)_8$ (4.05 g, 11.8 mmol) and DCM (40 mL). Indene (1.6 mL, 13.7 mmol) and 1,3-cyclohexadiene (1.7 mL, 17.8 mmol) were subsequently added to the round bottom flask before the resultant reaction mixture was heated at reflux for 1 h. The mixture was then left to cool to room temperature, before a further portion of indene (1.5 mL, 12.9 mmol) was added and the mixture heated again at reflux for a further 2 h, resulting in the formation of an orange precipitate. The orange precipitate was isolated by filtration and found by NMR, mass spectrometry and IR spectroscopic analysis to be [Co(η^4-C_6H_8)(CO)(μ-CO)]$_2$ (**4.9**, 1.01 g, 22 %). The volatile components of the filtrate were removed *in vacuo* to yield a black solid which was recrystallised from DCM at −30 °C, generating black crystals that were suitable for an X-ray crystallographic study and found to be $Co_4(CO)_{12}$ (2.02 g, 60 %).

Analysis for complex **4.9**:

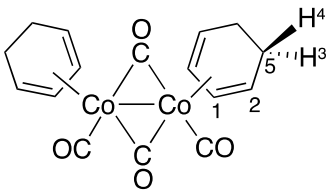

^{1}H NMR (400 MHz, C_6D_6) δ 4.41 (br, $\nu_{½}$ = 19.8 Hz, 1H, *H*^{1}), 3.66 (br, $\nu_{½}$ = 22.7 Hz, 1H, *H*^{2}), 1.65 (br, $\nu_{½}$ = 36.1 Hz, 1H, *H*^{3}), 1.15 (br, $\nu_{½}$ = 33.8 Hz, 1H, *H*^{4}).

^{13}C{^{1}H} NMR (176 MHz, C_6D_6) δ 92.0 (*C*^{1}), 79.0 (*C*^{2}), 23.6 (*C*^{5}).

IR (Nujol mull on KBr)**:** $\nu_{C=O}$ = 2010 and 1980 cm^{-1} (terminal CO), 1780 cm^{-1} (bridging CO).

MS (ASAP^{+}) *m*/*z*: 391.3 ([MH]$^{+}$).

Analysis for $Co_4(CO)_{12}$:

IR (CH_2Cl_2)**:** $\nu_{C=O}$ = 2065 and 2055 cm^{-1} (terminal CO), 1860 cm^{-1} (bridging CO).

MS (ASAP^{+}) *m*/*z*: 572.0 ([M]$^{+}$).

5.4.5. Attempted synthesis of FluCo(CO)$_2$[s]

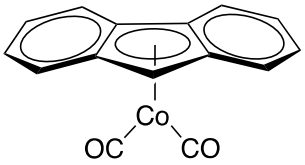

The synthesis of $FluCo(CO)_2$ was attempted *via* a modification of the literature procedure described by Frith and Spencer for the synthesis of complex **4.1**.[23] $Co_2(CO)_8$ (2.00 g, 5.85 mmol) was added to a two-necked round bottom flask, fitted with a reflux condenser, and dissolved in DCM (30 mL). The flask was then charged with an ethereal solution (10 mL) of fluorene (1.33 g, 8.0 mmol), and 1,3-cyclohexadiene (0.8 mL, 8.40 mmol). The resultant reaction mixture was heated at reflux for 2 h. The mixture was then allowed to cool to room temperature, before the addition of a further ethereal solution (10 mL) of fluorene (1.33 g, 8.0 mmol) and subsequent heating at reflux for a further 2 h. The mixture was then left to reach room temperature before the volatile components were removed *in vacuo*, yielding a light brown powder (4.55 g). Characterisation of this light brown powder by ^{1}H NMR, ^{13}C{^{1}H} NMR, and IR spectroscopies revealed it to consist of a mixture of complex **4.9**, unreacted fluorene and $Co_4(CO)_{12}$.[t]

[s] Synthesis carried out by C. Brodie in Dyer group.[34]

[t] The mixture was not separated meaning the yields of the individual products cannot be calculated.

Analysis of the mixture of complex **4.9**, fluorene and $Co_4(CO)_{12}$:
The ^{1}H NMR spectrum shows the mixture to contain 54 % unreacted fluorene and 46 % complex **4.9** (as a mixture of *cis*- and *trans*- isomers in a 4:3 ratio, respectively).

***cis*-4.9:**

^{1}H NMR (400 MHz, CD_2Cl_2) δ 5.54 (br s, 1H, *H*^{1}), 4.17 (br s, 1H, *H*^{2}), 2.00 (br s, 1H, *H*^{3}), 1.52 (br s 1H, *H*^{4}).

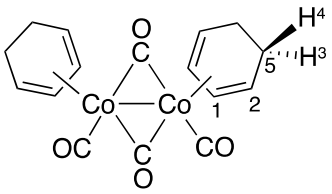

^{13}C NMR (176 MHz, CD_2Cl_2) δ 96.0 (*C*^{1}), 79.8 (*C*^{2}), 23.7 (*C*^{5}).

***trans*-4.9:**

^{1}H NMR 400 MHz, CD_2Cl_2) δ 4.90 (br s, 1H, *H*^{1}), 3.80 (br s, 1H, *H*^{2}), 1.93 (br s, 1H, *H*^{3}), 1.54 (br s 1H, *H*^{4}).

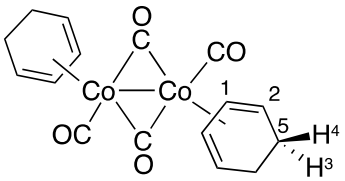

^{13}C NMR (176 MHz, CD_2Cl_2) δ 92.7 (*C*^{1}), 80.0 (*C*^{2}), 24.3 (*C*^{5}).

***cis*-/*trans*-4.9:**

MS (ASAP$^+$) *m*/*z*: 391.3 ([MH]$^+$).

fluorene:

^{1}H NMR (400 MHz, CD_2Cl_2) δ 7.81 (d, $^3J_{HH}$ = 6.4 Hz, 2H, *H*^{2}), 7.57 (d, $^3J_{HH}$ = 6.0 Hz, 2H, *H*^{5}), 7.38 (s, 2H, *H*^{3}), 7.31 (s, 2H, *H*^{4}), 3.92 (s, 2H, *H*^{1}).

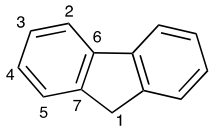

^{13}C{^{1}H} NMR (176 MHz, CD_2Cl_2) δ 143.9 (s, *C*^{6}), 142.2 (s, *C*^{7}) 127.3 (s, *C*^{4}), 127.2 (s, *C*^{3}), 125.6 (s, *C*^{5}), 120.3 (s, *C*^{2}), 37.5 (s, *C*^{1})

$Co_4(CO)_{12}$:

^{13}C{^{1}H} NMR (176 MHz, CD_2Cl_2) δ 211.5 (br s, *C*O).

MS (ASAP$^+$) *m*/*z*: 572.0 ([M]$^+$).

Mixture of *cis*-/*trans*-4.9 and $Co_4(CO)_{12}$

IR (Nujol mull on KBr)**:** $\nu_{C=O}$ = 2072, 2054, 2028 and 2008 cm^{-1}(terminal CO), 1865 and 1841 cm^{-1} (bridging CO).

5.4.6. Synthesis of sodium indenide, $NaC_9H_7.0.5THF$

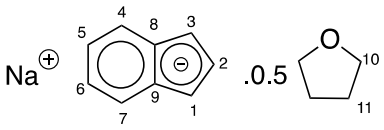

The synthesis of sodium indenide was conducted in accordance with the literature procedure reported by Green and Hughes.[35] A solution of indene (30.0 mL, 257 mmol) in THF (200 mL), at 0 °C, was added dropwise to a solution of sodium hydride (10.0 g, 417 mmol) in THF (100 mL), at 0 °C. The addition was undertaken over 1 h, during which time hydrogen was evolved and the mixture became mustard yellow in colour. The mixture was then stirred at room temperature for 18 h. Following filtration of the mixture to remove excess unreacted sodium hydride, the solvent was removed under vacuum to yield a light brown solid. The light brown solid was washed with petroleum ether (3 × 20 mL) and dried under vacuum to afford the final product as a light brown solid (31.3 g, 66 %). The identity and stoichiometry of the final product were confirmed by NMR spectroscopy (^{1}H and ^{13}C{^{1}H}), which were in agreement with those detailed in the literature.[36,37]

^{1}H NMR (700 MHz, d_8-THF) δ: 7.32 (dd, *J* = 6.0, 3.1 Hz, 2H, $H^{4/7}$), 6.61 (t, $^3J_{HH}$ = 3.3 Hz, 1H, H^2), 6.41 (dd, *J* = 6.1, 3.0 Hz, 2H, $H^{5/6}$), 5.94 (d, $^3J_{HH}$ = 3.4 Hz, 2H, $H^{1/3}$), 3.63 – 3.59 (m, 2H, H^{10}), 1.81 – 1.75 (m, 2H, H^{11}).[u]

^{13}C{^{1}H} NMR (176 MHz, d_8-THF) δ: 129.5 ($C^{8/9}$), 119.4 ($C^{4/7}$), 116.7 (C^2), 113.5 ($C^{5/6}$), 92.3 ($C^{1/3}$), 68.3 (C^{10}), 26.4 (C^{11}).[v]

5.4.7. Synthesis of sodium fluorenide, $NaC_{13}H_9.0.8THF$

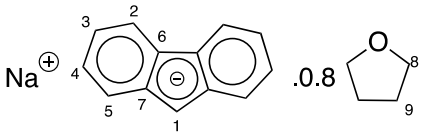

Sodium fluorenide was prepared following a modification of the literature procedure reported by Dinnebier *et al*.[38] A two-necked round bottom flask, fitted with a reflux condenser, was charged with sodium hydride (2.13 g, 88.8 mmol) and THF (20 mL). A solution of fluorene (15.9 g, 95.7 mmol) in THF (80 mL) was then added dropwise to the round bottom flask, and the resultant solution heated at reflux for 12 h (during which time hydrogen was evolved and the solution changed colour from yellow to orange). Once the solution attained room temperature it was concentrated *in vacuo* and subsequently layered with hexane before being left at −30 °C for 12 h, after which time yellow crystals had formed. The yellow crystals were

[u] NMR spectra also show the presence of indene (~7 %: determined from the relative integration of the resonances corresponding to indene to those corresponding to sodium indenide in the ^{1}H NMR spectrum).

isolated by filtration and washed with hexane (3 × 40 mL) to afford the final product as a yellow solid (18.9 g, 70 %). The identity and stoichiometry of the final product were confirmed by NMR spectroscopy (^{1}H and ^{13}C{^{1}H}), which were in agreement with those detailed in the literature.[38]

^{1}H NMR (700 MHz, d_8-THF) δ: 8.00 (d, $^{3}J_{HH}$ = 7.7 Hz, 2H, *H*^{2}), 7.41 (d, $^{3}J_{HH}$ = 8.0 Hz, 2H, *H*^{5}), 6.89 (t, $^{3}J_{HH}$ = 7.2 Hz, 2H, *H*^{4}), 6.54 (t, $^{3}J_{HH}$ = 7.1 Hz, 2H, *H*^{3}), 6.03 (s, 1H, *H*^{1}), 3.64 – 3.60 (m, 3H, *H*^{8}), 1.80 – 1.76 (m, 3H, *H*^{9}).[v]

^{13}C{^{1}H} NMR (176 MHz, d_8-THF) δ: 136.6 (*C*^{7}), 127.5 (*C*^{6}), 120.6 (*C*^{4}), 120.0 (*C*^{2}), 117.0 (*C*^{5}), 110.1 (*C*^{3}), 80.6 (*C*^{1}), 68.3 (*C*^{8}), 26.4 (*C*^{9}).[u]

5.4.8. Reaction of sodium fluorenide with $CoCl_2$

The reaction was conducted following modifications of the literature procedure reported by Kölle *et al*.[39] A two-necked round bottom flask, fitted with a reflux condenser, was charged with $CoCl_2$ (1.36 g, 10.5 mmol) and THF (30 mL) and subsequently heated at reflux for 20 h. A solution of sodium fluorenide (3.14 g, 10.3 mmol) in THF (80 mL) was then added dropwise to the round bottom flask, which was at room temperature, and the resultant green suspension left to stir for 12 h at room temperature. The green suspension was then filtered to afford a black solid (0.40 g)[w] and green filtrate. The volatile components of the green filtrate were removed *in vacuo* generating a green solid. The addition of toluene (50 mL) to the green solid afforded a blue solid and yellow solution, which were isolated by filtration. The blue solid was dissolved in THF and left at −30 °C for 12 h, after which time blue crystals of $Co_2Cl_4(THF)_4$ (**4.11**) had formed which were isolated by filtration (1.22 g, 42 %) and characterised by X-ray crystallography (giving bond lengths and angles matching those reported for $Co_2Cl_4(THF)_4$ in the literature)[40] and mass spectrometry. The solvent of the yellow solution was removed *in vacuo* generating a yellow solid (1.52 g) which was found by ^{1}H NMR spectroscopy to consist of a mixture of bifluorene (**4.10**) and fluorene in a 1:0.8 ratio, respectively.[41,42]

[v] NMR spectra also show the presence of fluorene (~35 %: determined from the relative integration of the resonances corresponding to fluorene to those corresponding to sodium fluorenide in the ^{1}H NMR spectrum).

[w] This black solid is believed to be Co metal due to its appearance and insolubility in a range of organic solvents (including THF, DCM, MeCN, pentane, toluene).

*Analysis of complex **4.11**:*

Despite a number of attempts, successful elemental analysis data of the complex could not be obtained (calc.: $Co_2Cl_4C_{16}H_{32}O_4$ C, 35.06; H, 5.88. Found: C, 24.50; H, 4.69).

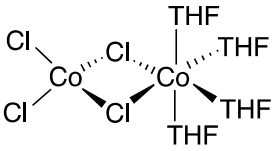

MS (ASAP$^+$) *m*/*z*: 548.2 ([M]$^+$), 347.1 ([M−$CoCl_4$]$^+$), 200.0 ([M−$Co(THF)_4$]$^+$).

*Analysis of mixture of fluorene and bifluorene (**4.10**):*

^{1}H NMR (700 MHz, $CDCl_3$) δ: 7.80 (d, $^3J_{HH}$ = 7.6, 1.7H, H^9), 7.66 (d, $^3J_{HH}$ = 7.5 Hz, 4H, H^2), 7.56 (d, $^3J_{HH}$ = 7.5, 1.7H, H^{12}), 7.41 – 7.36 (t, $^3J_{HH}$ = 7.4, 1.7H, H^{10}), 7.31 (td, J^3J_{HH} = 7.4, 1.2 Hz, 1.7H, H^{11}), 7.28 (s, 4H, H^5), 7.10 (s, 4H, H^3), 6.96 (s, 4H, H^4), 4.85 (s, 2H, H^1), 3.91 (s, 1.6H, H^8).

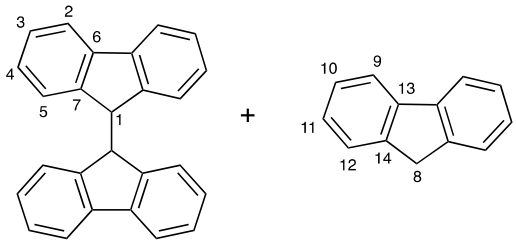

^{13}C{^{1}H} NMR (176 MHz, $CDCl_3$) δ: 144.8 (C^7), 143.4 (C^{14}), 141.9 (C^{13}), 141.7 (C^6), 127.4 (C^5), 126.9 (C^3/C^{11}),[x] 126.8 (C^{10}), 125.2 (C^{12}), 124.2 (C^4), 120.0 (C^9), 119.8 (C^2), 50.0 (C^1), 37.1 (C^8).

5.4.9. Reaction of sodium indenide with $CoCl_2$

5.4.9.1. Addition at room temperature

The reaction was conducted following modifications of the literature procedure reported by Kölle *et al*.[39] A solution of sodium indenide (1.07 g, 5.76 mmol) in THF (20 mL) was added dropwise to a suspension of $CoCl_2$ (0.75 g, 5.78 mmol) in THF (30 mL) at room temperature. The resultant mixture was left to stir for 30 min before being filtered to yield a black solid (0.21 g)[y] and dark red filtrate. The volatile components of the dark red filtrate were removed *in vacuo*, leaving behind a dark red residue. The addition of hexane (50 mL) to the dark red residue generated a dark green solid and dark red solution, which were separated by filtration. The dark red solution was concentrated *in vacuo* and left at −30 °C for 12 h, after which time black crystals of Ind_2Co (**4.12**) had formed which were isolated by filtration (0.83 g, 50 %) and characterised by X-ray crystallography (giving bond lengths and angles matching those reported for Ind_2Co in the literature)[43] and mass spectrometry. The dark green solid was dissolved in THF

[x] Two overlapping resonances observed in NMR spectrum.
[y] This black solid is believed to be Co metal due to its appearance and insolubility in a range of organic solvents (including THF, DCM, MeCN, pentane, toluene).

and left at −30 °C for 12 h, after which time dark green crystals had formed which were isolated by filtration (0.36 g, 24 %). Characterisation of the dark green crystals by X-ray crystallography, NMR spectroscopy and mass spectrometry revealed them to be $[Ind_2Co]_2[CoCl_4]$(**4.13**). See Appendices, section 6.2 for X-ray crystallographic data.

*Analysis of complex **4.12**:*

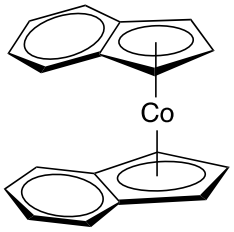

MS (ASAP$^+$) *m*/*z*: 290.0 ($[MH]^+$), 174.1 ($[M-C_9H_7]^+$), 115.1 ($[C_9H_7]^+$).

*Analysis of complex **4.13**:*

^{1}H NMR (600 MHz, D_2O) δ: 7.43 (s, 2H, $H^{4/7}$), 6.73 (s, 2H, $H^{5/6}$), 6.02 (s, 2H, $H^{1/3}$), 5.60 (s, 1H, H^2).

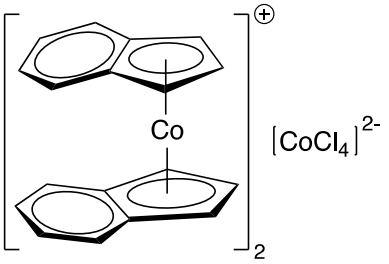

^{13}C{^{1}H} NMR (151 MHz, D_2O) δ: 130.0 ($C^{4/7}$), 121.8 ($C^{5/6}$), 97.3 ($C^{8/9}$), 81.7 (C^2), 75.6 ($C^{1/3}$).

MS (ASAP$^+$) *m*/*z*: 289.1 ($[M]^+$), 201.1 ($[CoCl_4]^{2-}$), 174.1 ($[M-C_9H_7]^+$), 115.1 ($[C_9H_7]^+$).

5.4.9.2. Addition at −30 °C

The reaction was carried out in accordance with modifications of literature procedures.[44-47] A solution of sodium indenide (2.50 g, 13.5 mmol) in THF (30 mL), at −30 °C, was added dropwise to a cooled (−30 °C) suspension of $CoCl_2$ (1.75 g, 13.5 mmol) in THF (30 mL). The resultant mixture was left to stir for 12 h, during which time it was left to attain room temperature. Filtration of the mixture afforded a black solid (0.68 g)[z] and red filtrate. The red filtrate was treated in the same way as described previously in section 5.4.9.1, yielding Ind_2Co (**4.12**, 2.15 g, 55 %) and $[Ind_2Co]_2[CoCl_4]$ (**4.13**, 0.52 g, 15 %). The identities of complexes **4.12** and **4.13** were verified by NMR spectroscopy and mass spectrometry, giving data identical to that previously detailed in section 5.4.9.1.

5.4.10. Reaction of sodium indenide with CoI_2

The reaction was conducted following modifications of the literature procedure reported by Kölle *et al*.[39] A solution of sodium indenide (1.33 g, 7.16 mmol) in THF (30 mL) was

[z] This black solid is believed to be Co metal due to its appearance and insolubility in a range of organic solvents (including THF, DCM, MeCN, pentane, toluene).

added dropwise to a solution of CoI_2 (2.23 g, 7.13 mmol) in THF (30 mL). The resultant mixture was stirred at room temperature for 12 h, before being filtered to yield a black solid (0.24 g)[aa] and brown filtrate. The solvent of the brown filtrate was removed under vacuum to afford a brown solid, which was found to be insoluble in hexane. Recrystallisation of the brown solid in THF (30 mL) at −30 °C afforded brown crystals of $[Ind_2Co]_2[CoI_4].0.5THF$ (**4.14**) (1.65 g, 60 %) which were characterised by X-ray crystallography (See Appendices, section 6.2 for X-ray crystallographic data), NMR and mass spectrometry.

*Analysis of complex **4.14**:*

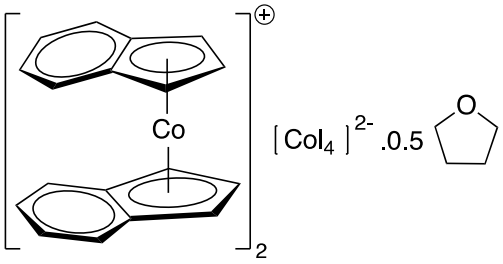

^{1}H NMR (600 MHz, D_2O) δ: 7.27 (d, $^3J_{HH}$ = 7.3 Hz, 2H, $H^{4/7}$), 6.59 (d, $^3J_{HH}$ = 8.3 Hz, 2H, $H^{5/6}$), 5.89 (s, 2H, $H^{1/3}$), 5.46 (s, 1H, H^2), 3.52 (s, 2H, H^{10}), 1.65 (s, 2H, H^{11}).

^{13}C {^{1}H} NMR (151 MHz, D_2O) δ: 130.0 ($C^{4/7}$), 121.7 ($C^{5/6}$), 97.1 ($C^{8/9}$), 81.8 (C^2), 75.6 ($C^{1/3}$), 67.8 (C^{10}), 25.0 (C^{11}).

MS (ASAP$^+$) *m*/*z*: 567.2 ($[CoI_4]^{2-}$), 289.1 ($[M]^+$), 174.1 ($[M-C_9H_7]^+$), 115.1 ($[C_9H_7]^+$).

5.4.11. Synthesis of Ind_2Co (4.12)

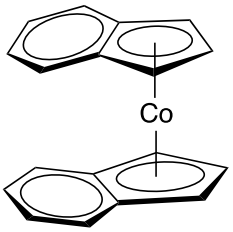

The reaction was conducted following modifications of a literature procedure.[48] A solution of sodium indenide (3.20 g, 17.2 mmol) in THF (30 mL) was added dropwise to a suspension of $CoCl_2$ (1.12 g, 8.63 mmol) in THF (30 mL) at −30 °C. The resultant dark red solution was allowed to attain room temperature and subsequently stirred at room temperature for 12 h. The solvent of the solution was then removed *in vacuo* to yield complex **4.12** as a black solid (1.87 g, 75 %). (calc.: $CoC_{18}H_{14}$ C, 74.75; H, 4.88. Found: C, 74.60; H, 4.79).

MS (ASAP$^+$) *m*/*z*: 290.0 ($[MH]^+$), 174.1 ($[M-C_9H_7]^+$), 115.1 ($[C_9H_7]^+$).

[aa] This black solid is believed to be Co metal due to its appearance and insolubility in a range of organic solvents (including THF, DCM, MeCN, pentane, toluene).

5.4.12. Attempted synthesis of [(η^5-indenyl)(η^2-ethene) trimethyl phosphite cobalt(I)] (4.7)

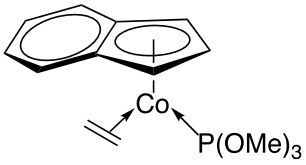

The reaction was conducted following modifications of literature procedures.[30,49,50] A solution of complex **4.12** (1.20 g, 4.15 mmol) in Et_2O (60 mL) was added dropwise to a solution of activated potassium (0.20 g, 5.12 mmol)[bb] in Et_2O (30 mL) at −15 °C,[cc] under an atmosphere of ethylene. The resultant dark red mixture was sealed under an atmosphere of ethylene and stirred at −15 °C for 21 h. The dark red mixture was subsequently filtered from unreacted potassium. Et_2O was slowly removed from the dark red filtrate under vacuum, at −10 °C, affording a black solid. Hexane (50 mL) was added to the black solid, at −10 °C, followed by neat $P(OMe)_3$ (0.5 mL, 4.23 mmol). The resultant dark red solution was stirred at −5 °C for 15 h. The solution was then left to attain room temperature before the volatile components were removed *in vacuo* generating a dark red solid. Pentane was added to the dark red solid and subsequent filtration afforded a brown solid (which showed no peaks in ^1H, $^{13}C\{^1H\}$ or ^{31}P NMR spectroscopy (C_6D_6)) and a red filtrate (which showed a mixture of products containing peaks characteristic of indenyl and $P(OMe)_3$ in ^1H, ^{13}C and ^{31}P NMR spectra (C_6D_6)). The solvent was removed from the red filtrate and the subsequent red residue was dissolved in the minimum amount of hexane and left to crystallise at −30 °C. However, after 48 h at −30 °C decomposition of the red hexane solution had occurred resulting in the formation of a black solution.

NMR analysis of the red pentane filtrate:

Due to the complexity of the ^1H (C_6D_6, 700 MHz) and $^{13}C\{^1H\}$ NMR spectra (C_6D_6, 176 MHz) of the mixture of products, the peaks have not been reported.

$^{31}P\{^1H\}$ NMR (283 MHz, C_6D_6) δ 171 – 180 ppm (overlapping broad peaks).

5.4.13. Synthesis of tris(1-pyrrolyl)phosphane

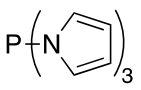

tris(1-Pyrrolyl)phosphane was prepared following the literature procedure described by Beller *et al*.[51] Phosphorus trichloride (8 mL, 91.7 mmol) was slowly added to a cooled solution (0 °C) of triethylamine (38.4 mL, 276 mmol) in THF (150 mL). Pyrrole (19.1 mL, 275 mmol) was subsequently added dropwise to the reaction mixture at 0 °C, resulting in the immediate formation of a white precipitate. The resultant mixture was then left to warm to room temperature and subsequently

[bb] The potassium was activated by heating in heptane.
[cc] A cryostat thermostatically-controlled bath was used to maintain the cold temperatures used throughout the experiment.

stirred at room temperature for 1 h, before being heated at reflux for 20 h. Following reflux, the reaction mixture was left to attain room temperature before being filtered. After removing the volatile components of the filtrate *in vacuo*, the crude white solid obtained was recrystallised from hot hexane to yield the final product as colourless crystals (14.7 g, 70 %). The ^{31}P {^{1}H}, ^{1}H and ^{13}C NMR spectroscopic data of the final product are in agreement with that reported in the literature.[51] (calc.:$C_{12}H_{12}N_3P$ C, 62.88; H, 5.28; N, 18.33. Found: C, 62.75; H, 5.19; N, 18.16).

^{1}H NMR (400 MHz, $CDCl_3$) δ 6.80 (dt, *J* = 4.2, 2.1 Hz, 6H, C*H*), 6.38 (t, *J* = 2.1 Hz, 6H, C*H*).

$^{13}C\{^{1}H\}$ NMR (101 MHz, $CDCl_3$) δ 122.9 (d, J_{PC} = 14.5 Hz, *C*H), 113.2 (d, J_{PC} = 4.5 Hz, *C*H).

$^{31}P\{^{1}H\}$ NMR (162 MHz, $CDCl_3$) δ 78.8.

5.4.14. Synthesis of tris(1-pyrrolyl)phosphane(η²-ethene)-(η⁵-penta methylcyclopentadienyl)cobalt(I) (4.15)

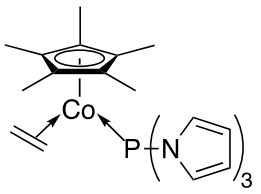

A solution of *tris*(1-pyrrolyl)phosphane (0.14 g, 0.61 mmol) in pentane (10 mL) was added dropwise to a solution of complex **4.4** (0.15 g, 0.60 mmol) in pentane (10 mL), and the resultant red solution heated at reflux for 3 h. The reaction mixture was then allowed to reach temperature before being filtered. The volatile components of the filtrate were subsequently removed under vacuum, yielding a maroon residue that was recrystallised from petroleum ether (b.p. 40 – 60 °C) at −78 °C, generating maroon crystals of complex **4.15** (0.19 g, 70 %), which were suitable for an X-ray crystallographic study. See Appendices, section 6.2 for X-ray crystallographic data. (calc.:$C_{24}H_{31}CoPN_3$ C, 63.85; H, 6.92; N, 9.31. Found: C, 63.72; H, 7.06; N, 9.20).

^{1}H NMR (700 MHz, C_6D_6) δ 6.97 – 6.88 (m, 6H, $P(NC_4H_4)_3$), 6.24 – 6.18 (m, 6H, $P(NC_4H_4)_3$), 1.43 – 1.36 (m (overlapping resonances), 19 H, $C_2H_4/C_5(CH_3)_5$).

$^{13}C\{^{1}H\}$ NMR (176 MHz, C_6D_6) δ 124.5 (d, J_{PC}= 6.5 Hz, $P(NC_4H_4)_3$), 111.3 (d, J_{PC}= 5.5 Hz, $P(NC_4H_4)_3$), 93.5 (d, $^{2}J_{PC}$= 3.0 Hz, $C_5(CH_3)_5$), 36.1 (d, $^{2}J_{PC}$= 3.0 Hz, C_2H_4), 9.5 ($C_5(CH_3)_5$).

$^{31}P\{^{1}H\}$ NMR (283 MHz, C_6D_6) δ 133.1 (vbr, $\nu_{½}$ = 287.1 Hz).

5.4.15. Synthesis of [(η^5-1-(2-(*N*,*N*-dimethylamino)ethyl)-2,3,4,5-tetramethyl-cyclopentadienyl)*bis*(η^2-ethene)cobalt(I)] (4.16)

5.4.15.1. Synthesis of 1-(2-Dimethylaminoethyl)-2,3,4,5-tetramethylcyclopent adiene[dd]

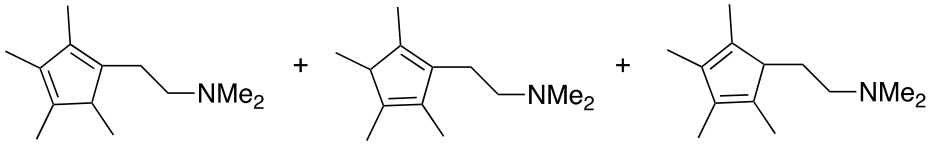

1-(2-Dimethylaminoethyl)-2,3,4,5-tetramethylcyclopentadiene was prepared in accordance with the literature procedure detailed by Jutzi *et al.*[53] 2-Bromo-2-butene (101 mL, 997 mmol) was added dropwise to a stirred ethereal suspension (500 mL) of lithium (13.9 g, 2003 mmol), and the resultant mixture heated at reflux for 15 h. Methyl-3-dimethylaminopropionate (71.5 mL, 500 mmol) was then added dropwise to the reaction mixture, at 0 °C, and the resultant mixture was heated at reflux overnight. A saturated solution of NH_4Cl (3 × 50 mL) was then added to the reaction mixture and the resultant suspension was poured onto more NH_4Cl solution (200 mL) and left for 1h, during which time the solution changed colour from green to orange and a precipitate gradually formed. The mixture was then filtered and the organic layer of the filtrate extracted with Et_2O (3 × 60 mL). The Et_2O fractions were combined and dried over $MgSO_4$. Following filtration from $MgSO_4$, *p*-toluenesulfonic acid (118.9 g, 630 mmol) was added to the filtrate and the subsequent solution heated at reflux for 15 h. A saturated Na_2CO_3 solution (400 mL) was then added to the reaction mixture in order to neutralise it, and the organic layer subsequently extracted with Et_2O (3 × 50 mL). The organic fractions were combined, dried over $MgSO_4$, and filtered. The solvent of the filtrate was then removed under vacuum, leaving behind yellow oil that was purified by distillation (60 °C, 3 mbar) to yield the final product as a pale green oil (45.7 g, 47 %). (calc.:$C_{13}H_{23}N$ C, 80.76; H, 11.99; N, 7.25. Found: C, 80.88; H, 11.89; N, 7.12). The ^1H NMR spectrum of the final product is in agreement with that reported in the literature.[53]

[dd] Synthesis conducted by B.A. Core (Sasol placement student).[52]

^{1}H NMR (400 MHz, $CDCl_3$) δ 2.42 – 2.65 (m, 1H, C*H*), 2.21 – 2.37 (m, 2H, CH_2NMe_2), 2.15 - 2.26 (3s, 6H, N(CH_3)$_2$), 1.74 – 1.81 (m, 11H, =CCH_3/CH_2NMe_2), 0.98 – 0.99 (m, 3H, =CCH_3)

5.4.15.2. Synthesis of 1-(2-Dimethylaminoethyl)-2,3,4,5-tetramethylcyclopentadiene cobalt(III) diiodide[ee]

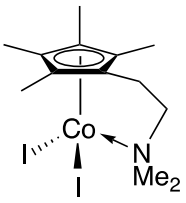

The synthesis of 1-(2-dimethylaminoethyl)-2,3,4,5-tetramethylcyclopentadiene cobalt(III) diiodide was carried out following a modification of the literature procedure described by Jutzi *et al*.[54] A solution of 1-(2-dimethylaminoethyl)-2,3,4,5-tetramethylcyclopentadiene (0.50 g, 2.59 mmol) in DCM (50 mL) was added dropwise to a solution of $Co_2(CO)_8$ (0.86 g, 2.51 mmol) in DCM (100 mL). 1,3-Cyclohexadiene (0.5 mL, 5.25 mmol) was then added dropwise to the reaction mixture and the mixture left to stir at room temperature overnight. The volatile components of the reaction were subsequently removed *in vacuo*, yielding a red solid residue. A solution of iodine (1.27 g, 5.00 mmol) in DCM (100 mL) was then added dropwise to the red residue, at 0 °C, and the reaction mixture left to stir at room temperature for 4 h. Following removal of the volatile components of the reaction mixture under vacuum, the crude product was recrystallised from DCM and layered with cyclohexane, generating the final product as a dark green powder (1.00 g, 80 %). The ^{1}H NMR spectrum of the final product is in agreement with that reported in the literature.[54] (calc.:$C_{13}H_{22}NCoI_2$ C, 30.91; H, 4.39; N, 2.77. Found: C, 30.94; H, 4.21; N, 2.61).

^{1}H NMR (400 MHz, $CDCl_3$) δ 3.81 (t, $^3J_{HH}$ = 6.4 Hz, 2H, CH_2), 2.44 (s, 6H, N(CH_3)$_2$), 2.16 – 2.22 (m, 8H, CH_2 and CH_3), 1.63 (s, 6H, CH_3).

[ee] Synthesis conducted by B.A. Core (Sasol placement student).[52]

5.4.15.3. Synthesis of [(η⁵-1-(2-(N,N-dimethylamino)ethyl)-2,3,4,5-tetramethyl-cyclopentadienyl)bis(η²-ethene)cobalt(I)] (4.16)

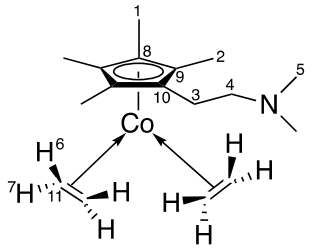

Complex **4.16** was prepared in accordance with the literature procedure reported by Jutzi *et al*.[54] A 1 % Na/Hg amalgam was prepared by cautiously adding Na sand (0.68 g, 29.6 mmol) to Hg (67.2 g, 335 mmol) in a nitrogen-filled glovebox. A solution of 1-(2-dimethylaminoethyl)-2,3,4,5-tetramethylcyclopentadiene cobalt(III) diiodide (1.00 g, 1.98 mmol) in THF (60 mL) was then added dropwise to the amalgam, under an atmosphere of ethylene. The resultant reaction mixture was stirred under an atmosphere of ethylene for 2 h, during which time it changed colour from dark-green to brown. The reaction mixture was then filtered away from the amalgam and the solvent of the filtrate removed *in vacuo* to yield a brown residue that was extracted in hexane. Following removal of the hexane *in vacuo* complex **4.16** was obtained as a brown oil (0.47 g, 77 %). The ^{1}H and ^{13}C{^{1}H} NMR spectra for complex **4.16** are in agreement with those reported in the literature.[54,55] (calc.:$C_{17}H_{30}CoN$ C, 66.43; H, 9.84; N, 4.56. Found: C, 66.68; H, 9.74; N, 4.66).

^{1}H NMR (700 MHz, C_6D_6) δ 2.44 – 2.39 (m, 2H, *H*^{3}), 2.28 – 2.20 (m, 2H, *H*^{4}), 2.12 (s, 6H, *H*^{5}), 1.81 – 1.69 (m, 4H, *H*$^{6/7}$), 1.47 (s, 6H, *H*^{1}), 1.40 (s, 6H, *H*^{2}), 1.06 – 0.95 (m, 4H, *H*$^{6/7}$).

^{13}C{^{1}H} NMR (176 MHz, C_6D_6) δ 95.2 (*C*^{10}), 93.1 (*C*^{8}), 92.1 (*C*^{9}), 60.4 (*C*^{4}), 45.6 (*C*^{5}), 45.1 (*C*^{11}), 24.1 (*C*^{3}), 9.4 (*C*^{1}), 9.0 (*C*^{2}).

5.4.16. 1-Butene dimerisation catalysis testing protocol

The catalysis runs were carried out in a glass 250 mL autoclave, fitted with a gas-entraining mechanical stirrer and internal cooling coil (tap water). The rigorously-cleaned autoclave was placed under vacuum for 30 minutes, before being back-filled with 1-butene (1.4 barg). The autoclave was then vented to 0 bar, *via* a septa, in order to purge the inlet valve prior to the addition of the relevant standard solutions. The autoclave was then placed in a water bath (to maintain a temperature of 19-22 °C during catalysis) and refilled with 1-butene (1.4 barg). Standard solutions of the relevant catalyst precursor and activator were subsequently added to the autoclave, which resulted in a decrease in the pressure of 1-butene. The autoclave was then filled with more 1-butene (so that the total pressure of 1-butene was 2 bar), and stirred at room temperature for the necessary reaction time. Once the set reaction time had ceased, excess 1-butene was vented and 1000 µL of nonane, 20 mL distilled water,

and 5 mL heptane (to bring the density of the organic phase to < 1) were added. A sample of the organic phase was subsequently taken for GC-FID analysis.

Stock solutions of the catalyst precursors and Brookhart's acid were made up in the relevant solvent to the desired concentration. The 1-butene (grade 2.0, sourced from BOC) had been passed through alumina and BOT scrubbing columns before being used.

5.4.17. 1-Hexene dimerisation catalysis testing protocol

The catalysis runs were carried out in Schlenks (containing stirrer bars), which were placed in water baths for the duration of the catalysis (to maintain a temperature of 19 – 22 °C), under an atmosphere of nitrogen. A standard solution of the relevant catalyst precursor in PhF was first added to the Schlenk, before the relevant volume of 1-hexene and standard solution of Brookhart's acid in PhF were added. The Schlenk was then sealed under nitrogen and left to stir for the desired reaction time. Once the set reaction time had ceased, 1000 µL of nonane, 20 mL distilled water, and 5 mL heptane (to bring the density of the organic phase to < 1) were added. A sample of the organic phase was subsequently taken for GC-FID analysis.

Stock solutions of the catalyst precursors and Brookhart's acid were made up in the relevant solvent to the desired concentration. The 1-hexene had been dried over Na wire, distilled, degassed and its water content determined to be 5 ppm by Karl Fischer Titration prior to use. The fluorobenzene had been dried over P_2O_5, distilled, degassed and its water content determined to be 5 ppm by Karl Fischer Titration prior to use.

5.5. References

1 J. E. Radcliffe, PhD Thesis, Durham University, 2015.
2 P. H. M. Budzelaar, A. B. van Oort and A. G. Orpen, *Eur. J. Inorg. Chem.*, 1998, **1998**, 1485–1494.
3 R. T. Boeré, V. Klassen and G. Wolmershäuser, *J. Chem. Soc., Dalton Trans.*, 1998, 4147–4154.
4 D. Tian, J. Jiang, H. Hu, J. Zhang and C. Cui, *J. Am. Chem. Soc.*, 2012, **134**, 14666–14669.
5 C. A. Nijhuis, E. Jellema, T. J. J. Sciarone, A. Meetsma, P. H. M. Budzelaar and B. Hessen, *Eur. J. Inorg. Chem.*, 2005, **2005**, 2089–2099.
6 M. L. Rosenberg, E. Langseth, A. Krivokapic, N. S. Gupta and M. Tilset, *New J. Chem.*, 2011, **35**, 2306–2313.
7 S. Chen, X. Zhang, H. Ma, Y. Lu, Z. Zhang, H. Li, Z. Lu, N. Cui and Y. Hu, *J. Organomet. Chem.*, 2005, **690**, 4184–4191.
8 G. Fritz and G. Poppenburg, *Angew. Chemie.*, 1960, **72**, 208–208.
9 P. Ramírez-López, A. Ros, B. Estepa, R. Fernández, B. Fiser, E. Gómez-Bengoa and J. M. Lassaletta, *ACS Catal.*, 2016, **6**, 3955–3964.

10 M. El Mkadmi, M. Lazraq, A. Kerbal, J. Escudie, C. Couret and H. Ranaivonjatovo, *Phosphorus, Sulfur Silicon Relat. Elem.*, 1998, **134**, 151–169.
11 J. P. van Linthoudt, E. V. van den Berghe and G. P. van der Kelen, *Spectrochim. Acta A*, 1980, **36**, 17–21.
12 M. S. Balakrishna, T. K. Prakasha and S. S. Krishnamurthy, *J. Organomet. Chem.*, 1990, **390**, 203–216.
13 S. O. Grim, W. L. Briggs, R. C. Barth, C. A. Tolman and J. P. Jesson, *Inorg. Chem.*, 1974, **13**, 1095–1100.
14 A. J. Rucklidge, D. S. McGuinness, R. P. Tooze, A. M. Z. Slawin, J. D. A. Pelletier, M. J. Hanton and P. B. Webb, *Organometallics*, 2007, **26**, 2782–2787.
15 T. Agapie, S. J. Schofer, J. A. Labinger and J. E. Bercaw, *J. Am. Chem. Soc.*, 2004, **126**, 1304–1305.
16 D. F. Evans, *J. Chem. Soc.*, 1959, 2003–2005.
17 C. E. Housecroft and E. C. Constable, *Chemistry*, Pearson Education Limited, England, Third Edition, 2006.
18 E. M. Schubert, *J. Chem. Educ.*, 1992, **69**, 62–62.
19 C. Piguet, *J. Chem. Educ.*, 1997, **74**, 815–816.
20 G. D. Jones, C. McFarland, T. J. Anderson and D. A. Vicic, *Chem. Commun.*, 2005, **42**, 4211–4213.
21 Y. Chen, R. Credendino, E. Callens, M. Atiqullah, M. A. Al-Harthi, L. Cavallo and J. M. Basset, *ACS Catal.*, 2013, **3**, 1360–1364.
22 F. J. Karol, *Chemtech*, 1983, **13**, 222–228.
23 F. A. Quinn Jr. and L. Mandelkern, *J. Am. Chem. Soc.*, 1958, **80**, 3178–3182.
24 M. Atiqullah, M. S. Winston, J. E. Bercaw, I. Hussain, A. Fazal, M. A. Al-Harthi, A. H. M. Emwas, M. J. Khan and A. Hossaen, *Polym. Degrad. Stab.*, 2012, **97**, 1164–1177.
25 S. Frith and J. L. Spencer, *Inorg. Synth.*, 1990, **28**, 273–280.
26 I. R. Lyatifov, G. M. Jafarov, V. N. Babin, P. V. Petrovskii and V. D. Zagorevskii, *J. Organomet. Chem.*, 1989, **368**, 223–230.
27 B. Sun, T. Yoshino, S. Matsunaga and M. Kanai, *Adv. Synth. Catal.*, 2014, **356**, 1491–1495.
28 R. G. Beevor, S. Frith and J. L. Spencer, *J. Organomet. Chem.*, 1981, **221**, C25–C27.
29 C. D. Ramful, K. N. Robertson and K. E. O. Ylijoki, *Acta Crystallogr. Sect. E Crystallogr. Commun.*, 2016, **72**, 1301–1304.
30 M. Brookhart, D. M. Lincoln, A. F. Volpe and G. F. Schmidt, *Organometallics*, 1989, **8**, 1212–1218.
31 G. F. Schmidt and M. Brookhart, *J. Am. Chem. Soc.*, 1985, **107**, 1443–1444.
32 M. Brookhart, B. Grant and A. F. Volpe, *Organometallics*, 1992, **11**, 3920–3922.
33 M. Brookhart, A. F. Volpe, D. M. Lincoln, I. T. Horvath and J. M. Millar, *J. Am. Chem. Soc.*, 1990, **112**, 5634–5636.
34 C. Brodie, First year PhD Report, Durham University, 2017.
35 M. L. H. Green and A. K. Hughes, *J. Chem. Soc. Dalt. Trans.*, 1992, 527–536.
36 T. Schaefer and W. G. Schneider, *Can. J. Chem.*, 1963, **41**, 966–982.
37 B. Eliasson, D. Johnels, S. Wold and U. Edlund, *Acta Chem. Scand.*, 1982, **36B**, 155–164.
38 R. E. Dinnebier, S. Neander, U. Behrens and F. Olbrich, *Organometallics*, 1999, **18**, 2915–2918.
39 U. Kolle, B. Fuss, M. Belting and E. Raabe, *Organometallics*, 1986, **5**, 980–987.
40 D. Stinghen, A. L. Rudiger, S. O. K. Giese, G. G. Nunes, J. F. Soares and D. L. Hughes, *Acta. Crystallogr. C.*, 2017, **73**, 104–114.
41 S. K. Sahoo, *Tetrahedron Lett.*, 2016, **57**, 3476–3480.
42 S. K. Talapatra, S. Chakrabarti, A. K. Malik and B. Talapatra, *Tetrahedron*, 1990, **46**, 6047–6052.
43 S. A. Westcott, A. K. Kakkar, G. Stringer, N. J. Taylor and T. B. Marder, *J.*

Organomet. Chem., 1990, **394**, 777–794.
44 U. Kolle, F. Khouzami and B. Fuss, *Angew. Chem. Int. Ed. Engl.*, 1982, **21**, 131–132.
45 U. Kolle, F. Khouzami and B. Fuss, *Angew. Chem. Int. Ed. Engl.*, 1982, **21**, 230–240.
46 U. Kolle and B. Fuss, *Chem. Ber.*, 1984, **117**, 743–752.
47 F. Baumann, E. Dormann, Y. Ehleiter, W. Kaim, J. Karcher, M. Kelemen, R. Krammer, D. Saurenz, D. Stalke, C. Wachter, G. Wolmershauser and S. H, *J. Organomet. Chem.*, 1999, **587**, 267–283.
48 K. Wang, Y. Yujie, L. Wang and D. Wang, CN101693211(B), Nutrichem Lab Co Ltd, 10 April 2013.
49 V. K. Jonas, E. Deffense and D. Habermann, *Angew. Chem. Suppl.*, 1983, 1005–1006.
50 J. A. Hamilton, T. Pugh, A. L. Johnson, A. J. Kingsley and S. P. Richards, *Inorg. Chem.*, 2016, **55**, 7141–7151.
51 R. Jackstell, H. Klein, M. Beller, K. Wiese and D. Rottger, *Eur. J. Inorg. Chem.*, 2001, **2001**, 3871–3877.
52 B. A. Core and M. Hanton, Sasol internal report, 2009.
53 P. Jutzi and O. Daugulis, *Synthesis*, 1993, 684–686.
54 P. Jutzi, M. Kristen, J. Dahlhaus, B. Neumann and H. Stammler, *Organometallics*, 1993, **12**, 2980–2985.
55 S. Holle and P. W. Jolly, *J. Organomet. Chem.*, 2000, **605**, 157–167.

Chapter 6:

Appendices

6.1. List of Compound/Complex Numbers for Chapters 2 – 4

6.1.1. Chapters 2 and 3

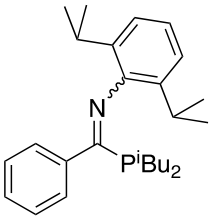

2.1

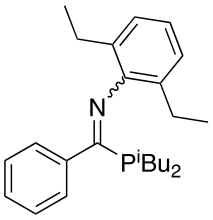

2.2

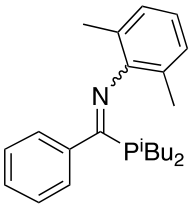

2.3

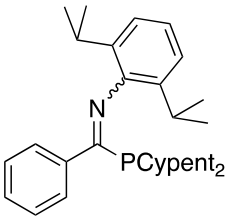

2.4

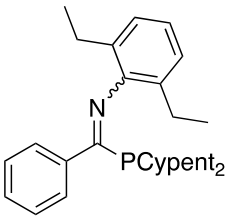

2.5

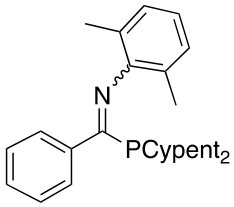

2.6

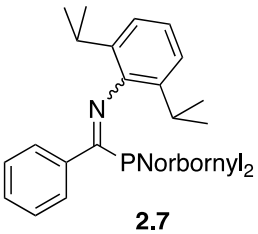

2.7

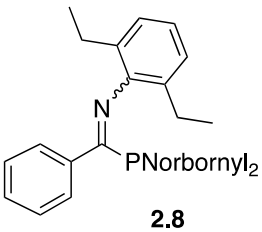

2.8

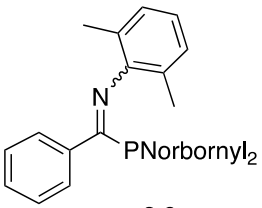

2.9

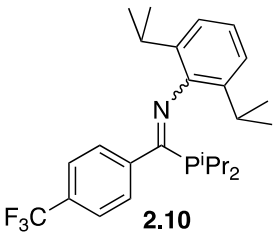

2.10

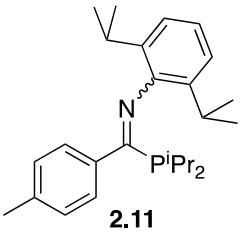

2.11

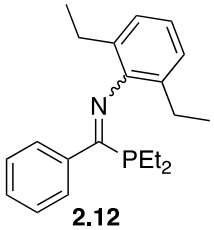

2.12

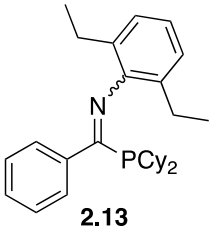

2.13

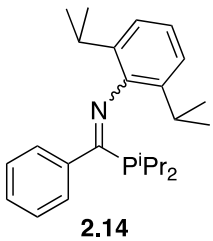

2.14

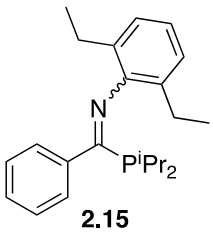

2.15

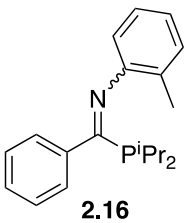

2.16

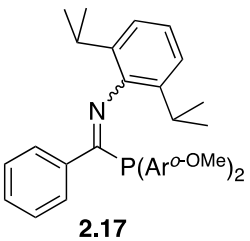

2.17

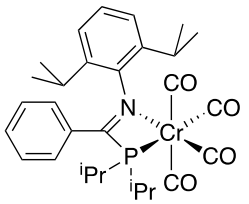

2.18

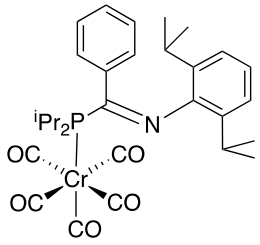

2.19

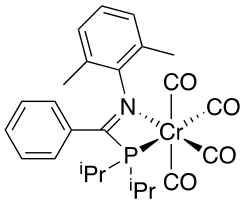

2.20

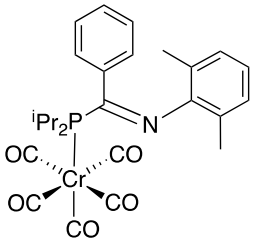

2.21

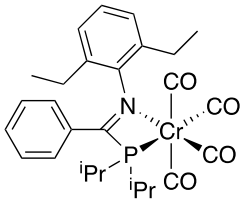

2.22

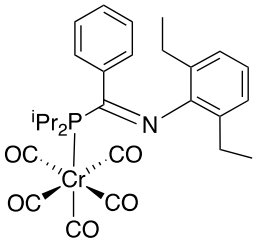

2.23

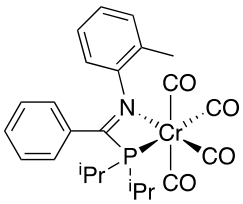

2.24

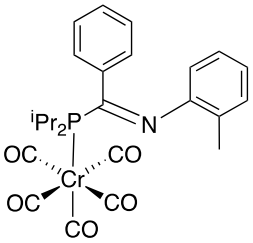

2.25

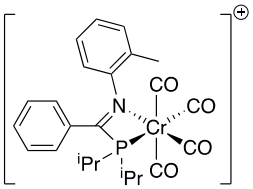

2.26

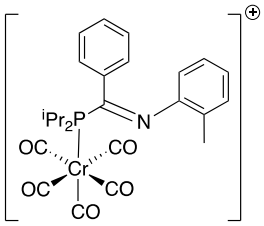

2.27

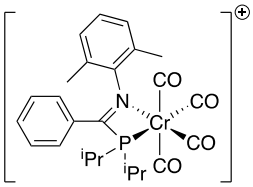

2.28

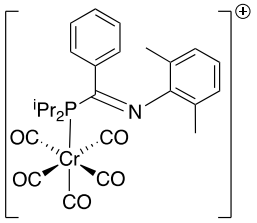

2.29

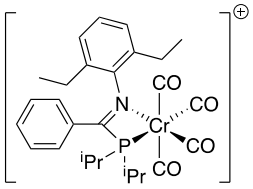

2.30

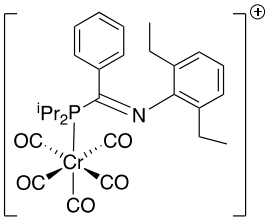

2.31

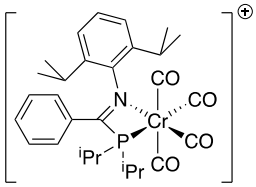

2.32

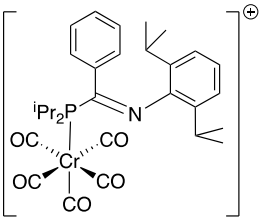

2.33

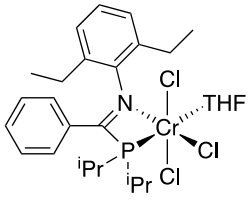

2.34

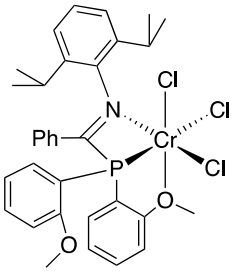

2.35

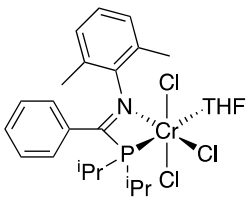

2.36

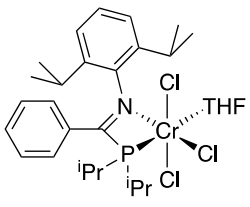

2.37

6.1.2. Chapter 4

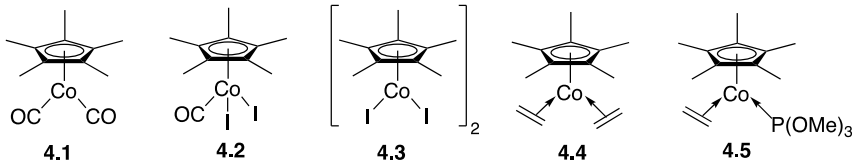

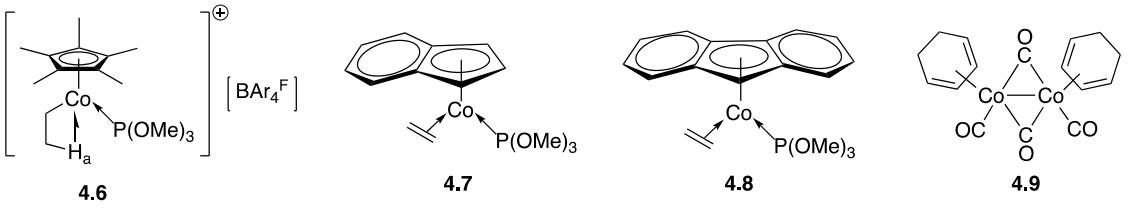

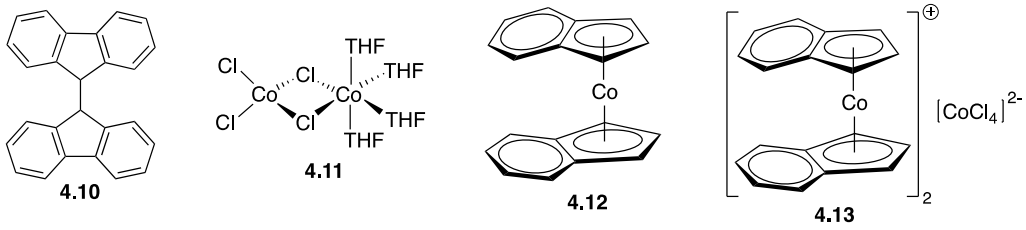

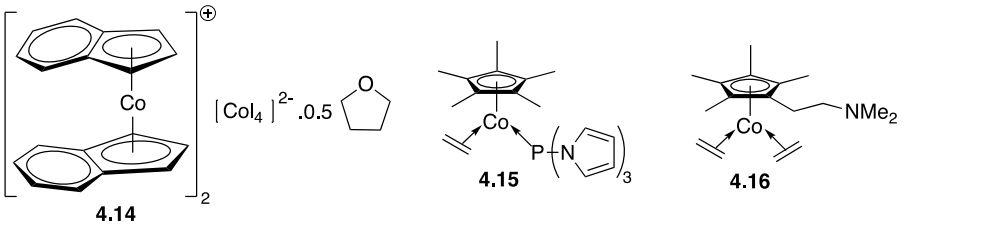

6.2. Crystallographic Data

X-Ray crystallographic analyses were performed by Dr. Andrei S. Batsanov or Dr. D. Yufit (Department of Chemistry, Durham University). A Bruker SMART 6000 CCD or Bruker D8 Venture diffractometer was used to carry out single crystal X-ray diffraction experiments. All samples were cooled to 120 K using a Cryostream open-flow N_2 cryostat, before applying the radiation source of graphite-monochromated Mo-K_α (λ = 0.71073 Å). All data were processed using Olex2, implementing direct methods (SHELXS 2013/1 software) to solve the structures and full-matrix least squares (SHELXL 2014/7 software) to refine the structures.[1-3] Anisotropic displacement parameters were used to refine non-hydrogen atoms, with H atoms “riding” in idealised positions. Full crystallographic data, including (.cif) files, can be found on the CD accompanying this thesis.

PCN Ligand	2.4	2.8	2.13	2.17	PhC(P^iPr_2)=N(2-MeC_6H_4)[a]
Identifier code	17srv099	17srv100	16srv196	16srv415	13srv133
Empirical formula	$C_{29}H_{40}NP$	$C_{31}H_{40}NP$	$C_{29}H_{40}NP$	$C_{33}H_{36}NO_2P$	$C_{20}H_{26}NP$
Formula weight	433.59	456.91	433.59	509.60	311.39
Temperature/K	120	120	120	120	120
Crystal system	triclinic	monoclinic	monoclinic	monoclinic	monoclinic
Space group	P-1	$P2_1/n$	C2/c	C2/c	C2/c
a/Å	9.8903(4)	9.9442(5)	32.3814(16)	28.3297(15)	11.8903(6)
b/Å	10.4102(4)	18.5767(10)	9.9343(5)	9.6873(5)	11.5015(4)
c/Å	13.5982(6)	13.9807(7)	16.8024(8)	20.5364(11)	27.0719(12)
α/°	72.5074(17)	90	90	90	90
β/°	76.3831(17)	93.291(2)	109.0854(18)	95.027(2)	101.613(11)
γ/°	81.3850(17)	90	90	90	90
Volume/$Å^3$	1293.07(9)	2578.4(2)	5108.0(4)	5614.3(5)	3626.5(3)
Z	2	4	8	8	8
$\rho_{calc}g/cm^3$	1.114	1.177	1.128	1.206	1.141
μ/mm^{-1}	0.122	0.126	0.123	0.128	0.149
F(000)	472.0	990.0	1888.0	2176.0	1344.0
Crystal size/ mm^3	0.479 × 0.372 × 0.308	0.196 × 0.18 × 0.137	0.4 × 0.337 × 0.113	0.26 × 0.24 × 0.08	0.2 × 0.1 × 0.05
2θ range for data collection/°	4.252 to 54.998	4.386 to 49.998	4.31 to 66.558	4.446 to 57.998	3.072 to 59.99
Index ranges	–12 ≤ h ≤ 12, –13 ≤ k ≤ 13, –17 ≤ l ≤ 17	–11 ≤ h ≤ 11, –22 ≤ k ≤ 22, –16 ≤ l ≤ 16	–49 ≤ h ≤ 49, –15 ≤ k ≤ 15, –25 ≤ l ≤ 25	–38 ≤ h ≤ 38, –13 ≤ k ≤ 13, –28 ≤ l ≤ 28	–16 ≤ h ≤ 16, –16 ≤ k ≤ 16, –38 ≤ l ≤ 38
Reflections collected	23758	40261	66242	42196	24930
Independent reflections	5937 [R_{int} = 0.0393, R_{sigma} = 0.0415]	4533 [R_{int} = 0.0453, R_{sigma} = 0.0253]	9819 [R_{int} = 0.0456, R_{sigma} = 0.0366]	7458 [R_{int} = 0.0558, R_{sigma} = 0.0459]	5305 [R_{int} = 0.0568]
Data/restraints/ parameters	5937/6/291	4533/265/342	9819/253/295	7458/0/340	5305/0/209
Goodness-of-fit on F^2	1.082	1.034	1.022	1.017	1.007
Final R indexes [I>=2σ (I)]	R_1 = 0.0612, wR_2 = 0.1402	R_1 = 0.0479, wR_2 = 0.1126	R_1 = 0.0460, wR_2 = 0.1104	R_1 = 0.0488, wR_2 = 0.1048	R_1 = 0.0401, wR_2 = 0.0986
Final R indexes [all data]	R_1 = 0.0805, wR_2 = 0.1499	R_1 = 0.0600, wR_2 = 0.1195	R_1 = 0.0704, wR_2 = 0.1222	R_1 = 0.0728, wR_2 = 0.1138	R_1 = 0.0608, wR_2 = 0.1059
Largest diff. peak/hole / e $Å^{-3}$	0.72/–0.40	0.51/–0.38	0.46/–0.28	0.38/–0.35	0.41/–0.20

[a] Crystal structure reported by Dr. James Radcliffe and included for comparison.[4]

Cr^0-PCN complex	**2.18**[b]	**2.20**[b]	**2.22**	**2.24**
Identifier code	14srv241	14srv261	16srv429	16srv165
Empirical formula	$C_{29}H_{36}CrNO_4P$	$C_{25}H_{28}CrNO_4P$	$C_{27}H_{32}CrNO_4P$	$C_{24}H_{26}CrNO_4P$
Formula weight	545.56	489.45	517.50	475.43
Temperature/K	120	120	120	120
Crystal system	monoclinic	orthorhombic	monoclinic	orthorhombic
Space group	$P2_1/n$	$P2_12_12_1$	$P2_1/n$	$Pna2_1$
a/Å	11.79138(14)	10.0194(8)	10.0043(4)	24.155(3)
b/Å	14.69577(18)	14.8755(12)	16.5682(7)	8.6024(11)
c/Å	16.3394(2)	33.308(2)	15.9969(7)	11.3369(14)
α/°	90	90	90	90
β/°	94.4771(11)	90	101.0610(15)	90
γ/°	90	90	90	90
Volume/Å^3	2822.70(6)	4964.3(7)	2602.28(19)	2355.7(5)
Z	4	8	4	4
ρ_{calc}g/cm^3	1.284	1.310	1.321	1.341
μ/mm^{-1}	0.495	0.555	0.533	0.583
F(000)	1152.0	2048.0	1088.0	992.0
Crystal size/ mm^3	0.6323 × 0.4741 × 0.3061	0.22 × 0.2 × 0.03	0.14 × 0.04 × 0.03	0.416 × 0.049 × 0.025
2θ range for data collection/°	3.732 to 64.944	3.672 to 50	4.452 to 59.998	4.928 to 50.13
Index ranges	–17 ≤ h ≤ 16, –22 ≤ k ≤ 21, –24 ≤ l ≤ 23	–11 ≤ h ≤ 11, –17 ≤ k ≤ 17, –39 ≤ l ≤ 39	–14 ≤ h ≤ 14, –23 ≤ k ≤ 23, –22 ≤ l ≤ 22	–28 ≤ h ≤ 28, –10 ≤ k ≤ 10, –13 ≤ l ≤ 13
Reflections collected	53488	41354	57704	27899
Independent reflections	9401 [R_{int} = 0.0318, R_{sigma} = 0.0209]	8695 [R_{int} = 0.0876, R_{sigma} = 0.0701]	7587 [R_{int} = 0.0758, R_{sigma} = 0.0530]	4169 [R_{int} = 0.1430, R_{sigma} = 0.1104]
Data/restraints/ parameters	9401/0/341	8695/6/573	7587/0/313	4169/269/302
Goodness-of-fit on F^2	1.032	1.017	1.027	1.011
Final R indexes [I>=2σ (I)]	R_1 = 0.0310, wR_2 = 0.0815	R_1 = 0.0525, wR_2 = 0.1132	R_1 = 0.0439, wR_2 = 0.0847	R_1 = 0.0521, wR_2 = 0.0921
Final R indexes [all data]	R_1 = 0.0367, wR_2 = 0.0853	R_1 = 0.0788, wR_2 = 0.1269	R_1 = 0.0723, wR_2 = 0.0935	R_1 = 0.1007, wR_2 = 0.1070
Largest diff. peak/hole / e Å^{-3}	0.45/–0.35	0.66/–0.39	0.41/–0.51	0.31/–0.39
Flack parameter	-	0.026(14)	-	0.01(3)

[b] Crystal structure reported by Dr. James Radcliffe and included for comparison.[4]

Cr^0-PCN complex	**2.19**[c]	**2.21**[c]	**2.23**	**2.25**
Identifier code	14srv239	14srv262	17srv117	17srv116
Empirical formula	$C_{30}H_{36}CrNO_5P$	$C_{26}H_{28}CrNO_5P$	$C_{28}H_{32}CrNO_5P$	$C_{25}H_{26}CrNO_5P$
Formula weight	573.57	517.46	545.51	503.44
Temperature/K	120	120.0	120	120
Crystal system	monoclinic	monoclinic	triclinic	monoclinic
Space group	$P2_1/n$	$P2_1/c$	P-1	$P2_1/n$
a/Å	10.12630(15)	8.49510(14)	8.4305(6)	12.1686(17)
b/Å	23.3526(4)	15.4117(3)	8.8639(6	10.4728(14)
c/Å	12.62634(19)	19.9673(4)	19.3128(13)	19.556(3)
α/°	90	90	93.502(3)	90
β/°	98.4258(14)	99.7804(17)	97.825(3)	95.549(5)
γ/°	90	90	107.992(3)	90
Volume/Å^3	2953.58(8)	2576.20(8)	1351.66(16)	2480.5(6)
Z	4	4	2	4
ρ_{calc}g/cm^3	1.290	1.334	1.340	1.348
μ/mm^{-1}	0.479	0.542	0.520	0.561
F(000)	1208.0	1080.0	572.0	1048.0
Crystal size/ mm^3	0.642 × 0.4515 × 0.2662	0.4286 × 0.2752 × 0.2119	0.373 × 0.323 × 0.248	0.154 × 0.148 × 0.108
2θ range for data collection/°	4.424 to 64.696	4.14 to 64.674	4.284 to 66.282	4.13 to 55.154
Index ranges	–14 ≤ h ≤ 14, –34 ≤ k ≤ 35, –18 ≤ l ≤ 17	–12 ≤ h ≤ 12, –21 ≤ k ≤ 21, –29 ≤ l ≤ 29	–12 ≤ h ≤ 12, –13 ≤ k ≤ 13, –29 ≤ l ≤ 29	–15 ≤ h ≤ 15, –13 ≤ k ≤ 13, –25 ≤ l ≤ 25
Reflections collected	46323	48933	34983	46634
Independent reflections	9651 [R_{int} = 0.0348, R_{sigma} = 0.0212]	8600 [R_{int} = 0.0427, R_{sigma} = 0.0260]	10283 [R_{int} = 0.0343, R_{sigma} = 0.0423]	5735 [R_{int} = 0.0492, R_{sigma} = 0.0312]
Data/restraints/ parameters	9651/0/359	8600/0/319	10283/0/337	5735/432/430
Goodness-of-fit on F^2	1.070	1.044	1.027	1.083
Final R indexes [I>=2σ (I)]	R_1 = 0.0335, wR_2 = 0.0878	R_1 = 0.0321, wR_2 = 0.0819	R_1 = 0.0377, wR_2 = 0.0822	R_1 = 0.0623, wR_2 = 0.1361
Final R indexes [all data]	R_1 = 0.0372, wR_2 = 0.0901	R_1 = 0.0394, wR_2 = 0.0863	R_1 = 0.0565, wR_2 = 0.0886	R_1 = 0.0788, wR_2 = 0.1438
Largest diff. peak/hole / e Å^{-3}	0.53/–0.44	0.41/–0.45	0.51/–0.57	0.93/–0.66

[c] Crystal structure reported by Dr. James Radcliffe and included for comparison.[4]

Complex	**4.4**[d]	**4.5**	**4.11**[e]	**4.13**
Identifier code	16srv351	16srv331	17srv004	16srv365
Empirical formula	$C_{14}H_{23}Co$	$C_{16}H_{28}CoO_3P$	$C_{16}H_{32}Cl_4Co_2O_4$	$C_{36}H_{28}Co_3Cl_4$
Formula weight	250.25	358.28	548.07	779.22
Temperature/K	120	120	120	120
Crystal system	monoclinic	monoclinic	monoclinic	triclinic
Space group	$P2_1/n$	I2/a	$P2_1/c$	P-1
a/Å	6.6658(4)	14.6201(10)	14.6977(6)	10.4819(6)
b/Å	14.2665(8)	8.3668(5)	9.6191(4)	13.1833(8)
c/Å	13.5183(8)	27.796(2)	16.1184(6)	13.6277(7)
α/°	90	90	90	91.672(2)
β/°	90.259(2)	92.115(2)	93.8332(16)	93.529(2)
γ/°	90	90	90	102.151(2)
Volume/Å^3	1285.55(13)	3397.8(4)	2273.70(16)	1835.76(18)
Z	4	8	4	2
ρ_{calc}g/cm^3	1.293	1.401	1.601	1.670
μ/mm^{-1}	1.302	1.111	1.947	1.671
F(000)	536.0	1520.0	1128.0	946.0
Crystal size/ mm^3	0.236 × 0.158 × 0.051	0.347 × 0.2 × 0.09	0.307 × 0.177 × 0.097	0.74 × 0.119 × 0.094
2θ range for data collection/°	4.15 to 66.392	5.084 to 65.152	5.064 to 60.196	5.15 to 60.066
Index ranges	–10 ≤ h ≤ 10, –21 ≤ k ≤ 21, –20 ≤ l ≤ 20	–22 ≤ h ≤ 22, –12 ≤ k ≤ 12, –42 ≤ l ≤ 42	–20 ≤ h ≤ 19, –13 ≤ k ≤ 13, –22 ≤ l ≤ 22	–14 ≤ h ≤ 14, –18 ≤ k ≤ 18, –18 ≤ l ≤ 19
Reflections collected	30893	44472	34001	27425
Independent reflections	4908 [R_{int} = 0.0529, R_{sigma} = 0.0439]	6187 [R_{int} = 0.0604, R_{sigma} = 0.0445]	6691 [R_{int} = 0.0509, R_{sigma} = 0.0441]	10682 [R_{int} = 0.0828, R_{sigma} = 0.1082]
Data/restraints/ parameters	4908/0/178	6187/0/213	6691/0/235	10682/540/388
Goodness-of-fit on F^2	1.028	1.058	1.024	1.026
Final R indexes [I>=2σ (I)]	R_1 = 0.0381, wR_2 = 0.0728	R_1 = 0.0390, wR_2 = 0.0824	R_1 = 0.0341, wR_2 = 0.0643	R_1 = 0.0637, wR_2 = 0.1575
Final R indexes [all data]	R_1 = 0.0740, wR_2 = 0.0821	R_1 = 0.0660, wR_2 = 0.0912	R_1 = 0.0592, wR_2 = 0.0712	R_1 = 0.0916, wR_2 = 0.1710
Largest diff. peak/hole / e Å^{-3}	0.52/-0.46	0.50/-0.49	0.52/–0.40	1.62/–0.89

[d] Structural details similar to those reported previously in the literature by Ylijoki *et al*.[5]

[e] Structural details comparable to those reported previously in the literature by Hughes and Soares *et al.*[6]

Complex	4.14	4.15
Identifier code	16srv397	16srv402
Empirical formula	$C_{38}H_{32}Co_3I_4O_{0.5}$	$C_{24}H_{31}CoN_3P$
Formula weight	1181.02	451.42
Temperature/K	120	120
Crystal system	orthorhombic	triclinic
Space group	Pbca	P-1
a/Å	13.4110(9)	10.0068(10)
b/Å	18.4429(13)	15.0814(13)
c/Å	29.409(2)	16.1867(15)
α/°	90	68.520(3)
β/°	90	81.181(3)
γ/°	90	81.150(3)
Volume/Å^3	7273.9(9)	2233.6(4)
Z	8	4
ρ_{calc}g/cm^3	2.157	1.342
μ/mm^{-1}	4.776	0.855
F(000)	4456.0	952.0
Crystal size/ mm^3	0.372 × 0.077 × 0.026	0.266 × 0.239 × 0.145
2θ range for data collection/°	4.418 to 57.998	4.636 to 60.134
Index ranges	–18 ≤ h ≤ 18, –25 ≤ k ≤ 25, –40 ≤ l ≤ 40	–14 ≤ h ≤ 14, –21 ≤ k ≤ 21, –22 ≤ l ≤ 22
Reflections collected	121362	38116
Independent reflections	9668 [R_{int} = 0.0766, R_{sigma} = 0.0364]	13037 [R_{int} = 0.0454, R_{sigma} = 0.0653]
Data/restraints/ parameters	9668/17/424	13037/606/583
Goodness-of-fit on F^2	1.069	1.014
Final R indexes [I>=2σ (I)]	R_1 = 0.0319, wR_2 = 0.0564	R_1 = 0.0483, wR_2 = 0.1002
Final R indexes [all data]	R_1 = 0.0527, wR_2 = 0.0622	R_1 = 0.0873, wR_2 = 0.1138
Largest diff. peak/hole / e Å^{-3}	0.87/–0.77	0.76/–0.43

6.2.1. X-Ray crystallographic studies of complexes 4.13 and 4.14

The complexes ($[Ind_2Co]_2[CoCl_4]$) (**4.13**) and ($[Ind_2Co]_2[CoI_4]$. 0.5 THF) (**4.14**) were obtained in salt metathesis reactions between sodium indenide and $CoCl_2$ or CoI_2, respectively (as described in Chapter 4, section 4.4.1.2). The molecular structures of complexes **4.13** and **4.14,** obtained from crystals isolated following recrystallization from THF at −30 °C, are shown in Figure 6.1. As can be seen from Figure 6.1, the unit

cells of the molecular structures of complexes **4.13** and **4.14** contain two molecules of $[Ind_2Co]^+$ alongside one molecule of the relevant Co halide anion $[CoX_4]^{2-}$ (the unit cell for complex **4.14** also contains 0.5 equiv. bound THF, which has been omitted from Figure 6.1 for clarity). The C-C bond distances within the indenyl moieties of complexes **4.13** and **4.14** range between 1.343(5) – 1.455(5) Å, which are distances similar to the analogous lengths of 1.365(5) – 1.460(4) Å reported for Ind_2Co in the literature.[7] In addition, the distances between Co and the centroids of the Cp fragments of the indenyl rings of complexes **4.13** and **4.14** (Table 6.1) are comparable to the corresponding distances of 1.656 – 1.666 Å reported for $[Ind_2Co]_2[Pt(C_6X_5)_4]$ (X = F or Cl) in the literature.[8]

(a) Complex **4.13** ($[Ind_2Co]_2[CoCl_4]$):

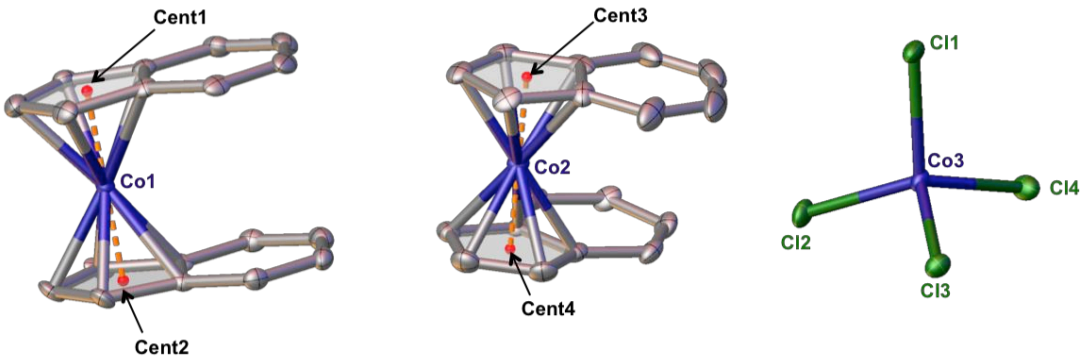

(b) Complex **4.14** ($[Ind_2Co]_2[CoI_4].0.5THF$):

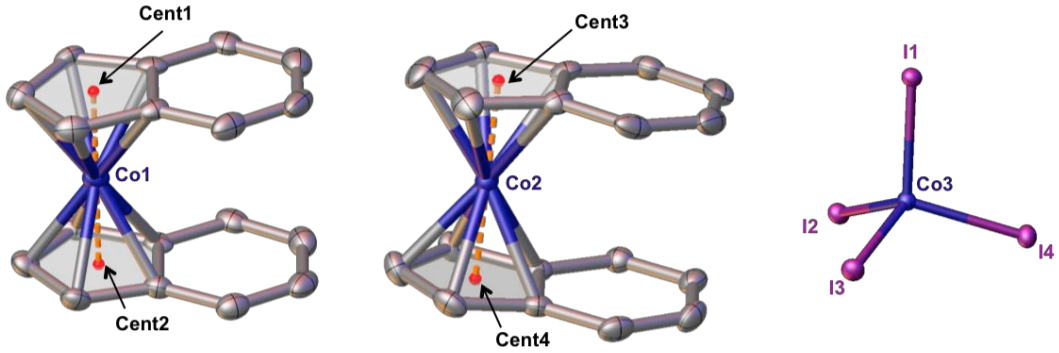

Figure 6.1: Molecular structures of complexes (a) **4.13** and (b) **4.14**, with thermal ellipsoids set at the 50% probability level; H atoms and THF have been omitted for clarity. Computed centroids for Cp rings shown in red with distances from centroid to Co centre represented by dashed orange lines.

Table 6.1: Co-*Cent* distances (Å) for complexes **4.13** and **4.14**, refer to Figure 6.1 for atom labels. *Cent* used to represent computed centroid on Cp rings.

		Complex **4.13**	Complex **4.14**
Co-*Cent* distances (Å)	Co1-*Cent1*	1.654	1.658
	Co1-*Cent2*	1.652	1.657
	Co2-*Cent3*	1.648	1.651
	Co2-*Cent4*	1.647	1.649

In the literature X-ray crystallographic studies of *bis*(indenyl)-containing complexes, four parameters (shown in Figure 6.2) are usually measured in order to assess the indenyl ligand's deviation from planarity, and the extent to which one indenyl ligand is rotated with respect to the second.[7,8] The degree by which the Cp fragment of the indenyl moiety has slipped from an ideal η^5 towards an η^3 coordination mode is quantified by the slip value ($\Delta_{M\text{-}C}$), hinge angle (HA) and fold angle (FA); larger values of these parameters indicating greater disposition towards η^3 *vs.* η^5 coordination. The rotation angle (RA) distinguishes between eclipsed (RA = 0°) and staggered arrangements (RA = 180°) of the indenyl ligands in the *bis*(indenyl) containing complexes (Figure 6.3).

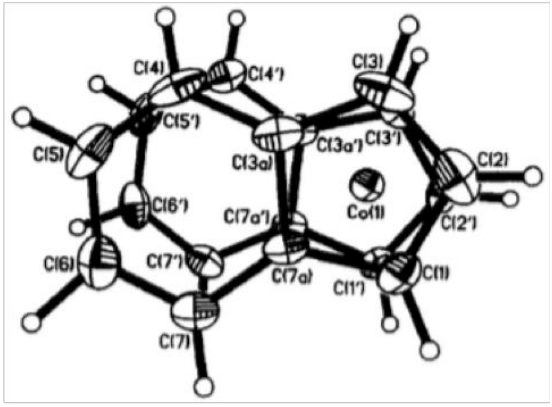

ORTEP representation of Ind_2Co

1. Slip value = $\Delta_{M-C} = \left(\frac{(Co-C3a)+(Co-C7a)}{2}\right) - \left(\frac{(Co-C1)+(Co-C3)}{2}\right)$
2. HA = Hinge angle = angle between planes [C1, C2, C3] and [C1, C3, C3a, C 7a]
3. FA = Fold angle = angle between planes [C1, C2, C3] and [C3a, C4, C5, C6, C7, C7a]
4. RA = Rotation angle = angle between planes [Co, C2, mid C3a,C7a] and [Co, C2', mid C3a',C7a']

Figure 6.2: Crystallographic parameters measured for *bis*(indenyl)-containing complexes in the literature, modified from Westcott *et al.*[7] ORTEP representation of Ind_2Co taken from Westcott *et al.*[7]

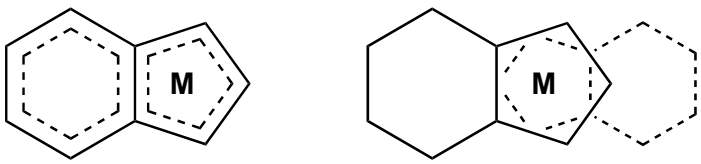

RA = 0° **RA = 180°**

Figure 6.3: Eclipsed and staggered conformations of indenyl ligands in *bis*(indenyl)-containing complexes where **M** = metal and **RA** = rotation angle (see Figure 6.2 for definition), modified from Westcott *et al.*[7]

The values of $\Delta_{M\text{-}C,}$ HA, FA and RA have been determined for the *bis*(indenyl) cobalt cations in complexes **4.13** and **4.14** and are compared to the literature values determined for Ind_2Co and $[Ind_2Co]_2[Pt(C_6X_5)_4]$ (X = F or Cl) in Table 6.2.[7,8] Since the

parameters ($\Delta_{M\text{-}C,}$ HA, FA and RA) of the two crystallographically distinct but chemically equivalent indenyl rings in each of the *bis*(indenyl) cobalt cations in complexes **4.13** and **4.14** are similar, Table 6.2 reports the average parameters calculated for each *bis*(indenyl) cobalt cation. The calculated crystallographic parameters ($\Delta_{M\text{-}C,}$ HA, FA and RA) for complexes **4.13** and **4.14** (Table 6.2) are suggestive of η^5-coordinated indenyl ligands, in eclipsed arrangements with one another in the *bis*(indenyl) cobalt cations. Additionally, the determined values of $\Delta_{M\text{-}C,}$ HA, FA and RA for complexes **4.13** and **4.14** are similar to the literature values for Ind_2Co[7] and $[Ind_2Co]_2[Pt(C_6X_5)_4]$ (X = F or Cl),[8] implying that oxidation of Co (*i.e.* Ind_2Co *vs.* $[Ind_2Co]^+$ in complexes **4.13** and **4.14**) has no impact on the indenyl coordination mode to Co (*i.e.* η^5 *vs.* η^3).

Table 6.2: Comparison of crystallographic parameters measured for complexes **4.13** and **4.14** to analogous parameters of literature complexes {Ind_2Co and $[Ind_2Co]_2[Pt(C_6X_5)_4]$ (X = F or Cl)}. $\Delta_{M\text{-}C}$ = slip value, HA = hinge angle, FA = fold angle and RA = rotation angle; refer to Figure 6.2 for definition of these parameters. [a]From ref. 7. [b]From ref. 8.

Complex	$\Delta_{M\text{-}C}$ (Å)	HA (°)	FA (°)	RA (°)
$[Ind_2Co]_2[CoCl_4]$ (complex **4.13**)	0.056(4), 0.060(3)	1.9(4), 2.7(5)	0.7(3), 0.5(4)	4.1(13), 2.6(14)
$[Ind_2Co]_2[CoI_4]$.0.5THF (complex **4.14**)	0.055(5), 0.055(3)	1.9(4), 2.4(4)	0.4(3), 1.5(3)	2.8(15), 2.5(13)
Ind_2Co[a]	0.119	7.6	6.0	N/A
$[Ind_2Co]_2[Pt(C_6F_5)_4]$[b]	0.060, 0.054	2.5, 3.0	0.6, 2.0	23.1, 25.8
$[Ind_2Co]_2[Pt(C_6Cl_5)_4]$[b]	0.050, 0.064	1.6, 2.9	1.9, 1.4	10.0, 4.9

6.3. Data Tables of Cr/PCN-based Ethylene Oligomerisation Catalysis Runs (Conducted in Chapter 3)

6.3.1. Screening runs of PCN ligands

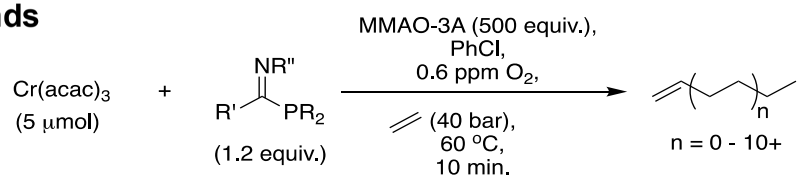

(R and R' = alkyl or aromatic group, R'' = aromatic group)

Scheme 6.1: Conditions used in screening runs of PCN ligands in ethylene oligomerisation catalysis.

Run	Ligand	Activity (Kg/g Cr/h)	Production (Kg/g Cr)	Total product mass (g)	Liquid fraction (wt %)	PE fraction (wt %)	C_4 *{1-C_4}* (wt %)	C_6 *{1-C_6}* (wt %)	C_8 *{1-C_8}* (wt %)	C_{10-14} (wt %)	C_{15+} (wt %)	Total 1-C_6 + 1-C_8 (wt %)
1	**2.1**	115	19	4.97	72	28	0.3 *{65.6}*	66.0 *{94.1}*	33.1 *{99.4}*	0.5	0.0	95.1
2	**2.2**	66	11	2.86	55	45	0.8 *{64.1}*	29.7 *{79.7}*	64.7 *{99.3}*	2.0	2.8	87.9
3	**2.3**	85	14	3.69	36	64	0.1 *{62.1}*	20.0 *{66.2}*	62.2 *{98.6}*	3.9	13.0	74.5
4	**2.4**	173	29	7.50	78	22	0.1 *{100}*	68.9 *{98.7}*	27.7 *{100}*	1.3	2.1	95.7
5	**2.5**	84	14	3.65	63	37	0.1 *{100}*	34.7 *{94.9}*	55.9 *{100}*	1.9	7.4	88.8
6	**2.6**	129	21	5.58	63	37	0.2 *{83.3}*	19.8 *{92.3}*	73.3 *{99.9}*	1.8	5.0	91.5
7	**2.6**	101	17	4.36	66	34	0.2 *{84.8}*	20.5 *{92.5}*	71.6 *{99.9}*	1.4	6.3	90.5
8	**2.7**	136	23	5.91	76	24	0.1 *{100}*	94.8 *{99.3}*	2.4 *{98.6}*	1.0	1.8	96.5
9	**2.8**	51	9	2.23	63	37	0.2 *{100}*	63.1 *{97.2}*	36.5 *{100}*	0.2	0.0	97.8
10	**2.9**	69	12	3.00	74	26	0.3 *{79.1}*	45.7 *{96.6}*	52.9 *{100}*	0.3	0.9	97.0
11	**2.10**	196	33	8.51	95	5	0.1 *{76.4}*	78.8 *{99.2}*	18.4 *{99.5}*	1.2	1.6	96.4
12	**2.10**	241	40	10.42	96	4	0.1 *{79.7}*	77.7 *{99.2}*	19.5 *{100}*	1.3	1.5	96.5
13	**2.11**	204	34	8.82	92	8	0.1 *{100}*	66.1 *{98.8}*	31.0 *{100}*	1.6	1.3	96.3
14	**2.11**	188	31	8.14	92	8	0.1 *{78.6}*	67.8 *{98.7}*	29.3 *{100}*	1.3	1.5	96.2
15	**2.12**	45	8	1.97	41	59	0.8 *{79.1}*	12.9 *{55.9}*	50.4 *{99.6}*	4.7	31.1	57.5
16	**2.13**	99	16	4.29	90	10	0.1 *{100}*	36.9 *{98.2}*	60.5 *{100}*	0.8	1.7	96.7
17	**2.14**	256	43	11.09	90	10	0.1 *{100}*	74.6 *{99.1}*	22.8 *{99.8}*	1.3	1.3	96.7
18	**2.14**	190	32	8.21	87	13	0.1 *{100}*	70.8 *{98.9}*	26.0 *{100}*	1.3	1.8	96.0
19	**2.14**[f]	20	3	0.86	93	7	0.3 *{100}*	66.9 *{95.7}*	15.0 *{100}*	5.9	11.9	79.1

[f] Carried out in the presence of 4 equiv. CO (relative to the ligand).

6.3.2. Screening runs of Cr^{I}-PCN complexes

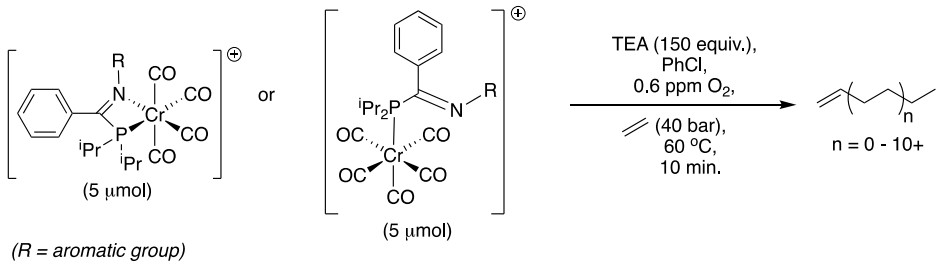

(R = aromatic group)

Scheme 6.2: Conditions used in screening runs of Cr^{I}-PCN complexes in ethylene oligomerisation catalysis.

Run	Cr^{I}-PCN complex	Activator *{equiv.}*	Activity (g/g Cr/h)	Production (g/g Cr)	Total product mass (g)	Liquid fraction (wt %)	PE fraction (wt %)	C_4 *{1-C_4}* (wt %)	C_6 *{1-C_6}* (wt %)	C_8 *{1-C_8}* (wt %)	C_{10-14} (wt %)	C_{15+} (wt %)	Total 1-C_6 + 1-C_8 (wt %)
1	**2.26**	TEA *{150}*	1,209	202	0.05	44	56	50.0 *{26.9}*	13.9 *{100}*	13.3 *{100}*	23.0	0.0	27.3
2	**2.27**	TEA *{150}*	2,492	415	0.11	76	24	22.0 *{11.8}*	9.4 *{100}*	55.7 *{100}*	13.0	0.0	65.0
3	**2.28**	TEA *{150}*	1,569	262	0.07	60	40	24.9 *{15.9}*	18.0 *{100}*	44.0 *{100}*	13.1	0.0	62.0
4	**2.29**	TEA *{150}*	5,329	888	0.23	43	57	12.2 *{100}*	18.3 *{100}*	59.5 *{100}*	10.0	0.0	77.8
5	**2.29**	MMAO-3A *{500}*	1,183	197	0.05	85	15	90.4 *{61.2}*	0.0	0.0	9.6	0.0	0.0
6	**2.30**	TEA *{150}*	385	64	0.02	72	28	63.1 *{34.9}*	0.0	0.0	36.9	0.0	0.0

6.3.3. Screening runs of Cr^{III}-PCN complexes

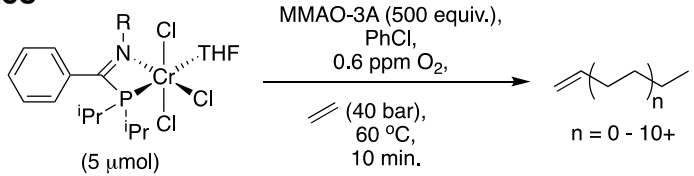

(R = aromatic group)

Scheme 6.3: Conditions used in screening runs of Cr^{III}-PCN complexes in ethylene oligomerisation catalysis.

Run	Cr^{III}-PCN complex	Activity (Kg/g Cr/h)	Production (Kg/g Cr)	Total product mass (g)	Liquid fraction (wt %)	PE fraction (wt %)	C_4 *{1-C_4}* (wt %)	C_6 *{1-C_6}* (wt %)	C_8 *{1-C_8}* (wt %)	C_{10-14} (wt %)	C_{15+} (wt %)	Total 1-C_6 + 1-C_8 (wt %)
1	**2.36**	31	5	1.35	36	64	0.42 *{100}*	24.0 *{81.9}*	55.3 *{100}*	3.8	16.4	75.0
2	**2.37**	43	7	1.85	45	55	0.24 *{100}*	70.7 *{96.3}*	23.0 *{100}*	1.5	4.6	91.1

6.3.4. Larger-scale catalysis runs of Cr-PCN ligands

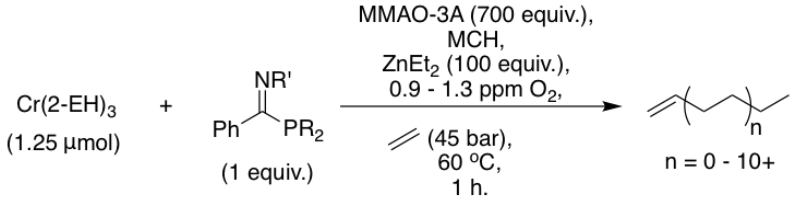

(R= alkyl group and R' = aromatic group)

Scheme 6.4: Conditions used in larger-scale runs of PCN ligands in ethylene oligomerisation catalysis.

Run	Ligand	Activity (Kg/g Cr/h)	Production (Kg/g Cr)	Total product mass (g)	Liquid fraction (wt %)	PE fraction (wt %)	C_4 *{1-C_4}* (wt %)	C_6 *{1-C_6}* (wt %)	C_8 *{1-C_8}* (wt %)	C_{10-14} (wt %)	C_{15+} (wt %)	Total 1-C_6 + 1-C_8 (wt %)
1	**2.1**	1,979	1,979	128.65	95.8	4.2	0.05 *{62.5}*	84.2 *{98.4}*	13.8 *{99.3}*	1.9	0.0	96.6
2	**2.2**	857	873	56.71	95.1	4.9	0.33 *{52.0}*	45.9 *{91.7}*	51.9 *{99.1}*	1.6	0.3	93.5
3	**2.3**	599	599	38.96	85.7	14.3	0.72 *{49.8}*	28.9 *{82.3}*	67.0 *{98.7}*	2.1	1.3	89.9
4	**2.4**	1,686	1,686	109.55	96.4	3.6	0.02 *{83.5}*	82.2 *{99.6}*	15.5 *{99.7}*	2.2	0.0	97.4
5	**2.5**	1,064	1,064	69.13	95.6	4.4	0.04 *{69.4}*	46.5 *{98.8}*	51.4 *{99.8}*	1.9	0.1	97.2
6	**2.6**	886	886	57.58	92.4	7.6	0.08 *{64.3}*	28.1 *{97.4}*	69.5 *{99.8}*	1.9	0.4	96.7
7	**2.7**	3,346	3,346	217.47	98.6	1.4	0.01 *{51.1}*	95.6 *{99.9}*	1.89 *{99.3}*	2.5	0.0	97.3

6.4. Quantification of catalysis products

Samples of a selection of linear α-olefins (including 1-hexene, 1-octene, nonane, decene, 1-dodecene, and 1-octadecene) were analysed by GC-FID in order to identify their retention times. These retention times were used for direct comparison with those of products obtained in ethylene *tri*-/*tetra*-merisation catalysis (discussed in Chapter 3) and 1-butene/1-hexene dimerisation catalysis (discussed in Chapter 4), in order to aid elucidation of linear α-olefins formed in *di*-/*tri*-/*tetra*-merisation catalysis. The calculations used for determining the activity and total mass of catalysis products obtained in *di*-/*tri*-/*tetra*-merisation catalysis are outlined in Equations **6.1** and **6.2**.

Activity = mass of all catalysis products/ mass transition metal/ duration of catalysis run

Equation 6.1: Equation for determining the activity of *di*-/*tri*-/*tetra*-merisation catalysis.

Total mass of catalysis products = mass of liquid fraction + mass of solid product

Equation 6.2: Equation for determining the total mass of catalysis products obtained in *di*-/*tri*-/*tetra*-merisation catalysis.

6.5. List of Seminars Attended

Borenium cations: versatile reagents for borylation of π-nucleophiles
Dr. Mike Ingleson, University of Manchester
29th October 2013

Making polymers swim
Professor Tony Ryan, University of Sheffield
6th November 2013

Designing heterogeneous catalysts for sustainable chemistry
Professor Karen Wilson, Aston University
12th November 2013

Ionic liquids in whole cell biocatalysis
Professor Gill Stephens, University of Nottingham
4th December 2013

Different metals = different products: gold versus platinum in the reaction of allenes with nucleophiles
Dr. Maria Paz Munoz-Herranz, University of East Anglia
22nd January 2014

Cats and Dogma
Professor Guy Lloyd-Jones, University of Edinburgh
12th February 2014

Redox and functionalization reactions of the uranyl ion: in pursuit of transition metal oxo chemistry
Professor Polly Arnold, University of Edinburgh
19th February 2014

Switchable Solvents
Professor Philip Jessop, Queen's University
12th March 2014

From triple bonds to reactive intermediates
Professor Christopher Cummins, Massachusetts Institute of Technology
14th April 2014

Activation of alkynes with $B(C_6F_5)_3$: Intramolecular cyclisation reaction and rearrangements
Dr. Rebecca Melen, University of Toronto
24th April 2014

Controlled polymer synthesis with olefin metathesis catalysts
Professor Robert Grubbs, California Institute of Technology
16th May 2014

The physical chemistry of heterogeneous catalysis – the oxidation of ethylene to ethylene oxide
Professor Ken Waugh, University of Manchester
27th July 2014

Catalysis on the edge
Professor Robert Tooze, Sasol Technology UK
24th September 2014

Durham fluorine meets industry
Professor Graham Sandford, Durham University
24th September 2014

Nanoparticles and *in situ* spectroscopy for understanding syngas conversion catalysis
Dr. Simon Beaumont, Durham University
24th September 2014

Chemicals from waste bio-oils
Professor David Cole-Hamilton, University of St Andrews
24th September 2014

Ionic Mo-, W- and Ru-based olefin metathesis catalysts: access to C-C coupling reactions under biphasic (supported) conditions
Professor Michael Buchmeiser, University of Stuttagart
6th October 2014

From Wadean clusters to functional materials
Professor Catherine Housecroft, University of Basel
15th December 2014

Bond length and bond enthalpy relationships in metal carbonyl clusters
Dr. Andrew Hughes, Durham University
15th December 2014

Bonding in Gold clusters
Professor Michael Mingos, Oxford University
15th December 2014

Recent aspects of the structural chemistry of heterocarboranes
Dr. Alan Welch, Herriot-Watt University
15th December 2014

Structural rules for Boron
Professor Robert Mulvey, University of Strathclyde
15th December 2014

Useful new reactions in organophosphorus chemistry
Professor Declan Gilheany, University of Dublin
13th January 2015

Development of *in situ* methods to study gas and ligand phase heterogeneously catalysed reactions
Professor Chris Hardacre, Queen's University Belfast
28th *January 2015*

Ruthenium and Iridium catalysts equipped with a phosphinesulfate ligand
Dr. Christian Bruneau, Université de Rennes
24th February 2015

Overview of research: Carbon materials, devices, medicine and nanocars
Professor James Tour, Rice University
19th May 2015

Graphene
Professor James Tour, Rice University
20th May 2015

Nanomedicines for stroke, traumatic brain injury, autoimmune diseases and drug delivery
Professor James Tour, Rice University
21st May 2015

Sustainability in industrial chemistry
John Hayler, GlaxoSmithKline
4th November 2015

Transition metal catalysis
Katherine Wheelhouse, GlaxoSmithKline
4th November 2015

Biocatalysis
Kieth Mulholland, AstraZeneca
4th November 2015

Biorenewable feedstocks and chemicals
Jeroen ten Dam, Johnson Matthey
4th November 2015

Sustainability, green chemistry, solvent guide
Helen Sneddon, GlaxoSmithKline
5th November 2015

Sustainable agrochemical manufacturing
George Hodges, Syngenta
5th November 2015

Sustainability in research and development
Matt Grist, AstraZeneca
5th November 2015

New main group metal mediated strategies for ring functionalisation
Professor Eva Hevia, University of Strathclyde
18th November 2015

Using organometallics as catalysts: from drug precursors to little black dresses
Dr. Patrick McGowan, University of Leeds
27th January 2016

Transition metal catalysed borylation of C-H and C-X bonds: synthesis of aryl and alkyl boronates
Professor Todd Marder, Julius-Maximillians-Universität Würzburg
1st February 2016

Recent developments in asymmetric catalysis and total synthesis
Professor Pat Guiry, University College Dublin
17th February 2016

Challenges and opportunities in natural product synthesis
Professor Steven Ley, University of Cambridge
18th May 2016

Synthesis of conjugated polymers for organic electronics: making use of triplet states
Dr. Hugo Bronstein, University College London
19th October 2016

Watching reactions take place at the atomic scale (and learning from them)
Dr. Neeraj Sharma, University of New South Wales, Australia
26th October 2016

Development of gold and palladium catalysed reactions
Dr. Ai-Lan Lee, Herriot Watt University
23rd November 2016

6.6. List of Conferences and Symposia Attended

Dalton 2014
Warwick University, *15th -17th April 2014*

CSCP half-day symposium
Durham University, *24th September 2014*

Ken Wade celebration symposium
Durham University, *15th December 2014*

Postgraduate gala symposium 2015
Durham University, *24th June 2015*
Poster Presentation

Catalysis summer school 2015
University of Liverpool, 20th - *24th July 2015*

RSC main group meeting
Burlington House, *11th September 2015*

Sustainability in industrial chemistry symposium and workshop
Durham University, *4th – 5th November 2015*

13th European workshop on phosphorus chemistry
The Freie Universität Berlin, *4th – 5th November 2015*
Poster presentation and acted as chair for presentation session

Postgraduate gala symposium 2016
Durham University, *15th June 2016*
Oral Presentation

6.7. References

1 O. V. Dolomanov, L. J. Bourhis, R. J. Gildea, J. A. K. Howard and H. Puschmann, *J. Appl. Cryst.*, 2009, **42**, 339–341.
2 G. M. Sheldrick, *Acta Crystallogr. A*, 2008, **64**, 112–122.
3 G. M. Sheldrick, *Acta Crystallogr. A*, 2015, **71**, 3–8.
4 J. E. Radcliffe, PhD Thesis, Durham University, 2015.

5 C. D. Ramful, K. N. Robertson and K. E. O. Ylijoki, *Acta Crystallogr. Sect. E Crystallogr. Commun.*, 2016, **72**, 1301–1304.
6 D. Stinghen, A. L. Rudiger, S. O. K. Giese, G. G. Nunes, J. F. Soares and D. L. Hughes, *Acta Crystallogr. C.*, 2017, **73**, 104–114.
7 S. A. Westcott, A. K. Kakkar, G. Stringer, N. J. Taylor and T. B. Marder, *J. Organomet. Chem.*, 1990, **394**, 777–794.
8 D. Bellamy, N. G. Connelly, G. R. Lewis and A. G. Orpen, *Cryst. Eng. Comm.*, 2002, **4**, 68–79.